UNIVERSITAT DE BARCELONA

Fluxos de partícules i metalls als marges continentals del sud-est de la península Ibèrica

Particle and metal fluxes in the continental margins
of the southeastern Iberian Peninsula

Marta Tarrés Mercader

Marta Tarrés Mercader 2023

Fluxos de partícules i metalls als marges continentals del sud-est de la península Ibèrica

Fluxos de partícules i metalls als marges continentals del sud-est de la península Ibèrica

Particle and metal fluxes in the continental margins of the southeastern Iberian Peninsula

Marta Tarrés Mercader

Memòria de Tesi Doctoral

Programa de doctorat de Ciències del Mar

2023

UNIVERSITAT DE BARCELONA

UNIVERSITAT DE BARCELONA

Fluxos de partícules i metalls als marges continentals del sud-est de la península Ibèrica

Particle and metal fluxes in the continental margins
of the southeastern Iberian Peninsula

Memòria de Tesi Doctoral presentada per

Marta Tarrés Mercader

sota la direcció de

Dr. Miquel Canals i Dra. Anna Sanchez

al Departament de Dinàmica de la Terra i de l'Oceà de la Universitat de Barcelona, dins del programa de doctorat de Ciències del Mar, per optar al grau de Doctor per la Universitat de Barcelona.

Barcelona, 26 de gener de 2024

Doctorand El Director La Directora

Aquesta Tesi ha estat realitzada al Departament de Dinàmica de la Terra i de l'Oceà de la Universitat de Barcelona, dins el Grup de Recerca en Geociències Marines, amb reconeixement de la Generalitat de Catalunya com a Grup de Recerca Consolidat (ref. 2021 SGR 01195). Durant el període d'elaboració de la Tesi la doctoranda ha gaudit d'una beca predoctoral de Formación de Personal Investigador (FPI) del Ministerio de Ciència, Innovación i Universidades (BES-2017-080546). L'estada que la doctoranda realitzà a l'Instituto di Scienze Polari – Consiglio Nazionale delle Ricerche (Bologna, Itàlia) fou finançada pel Ministerio de Ciencia, Innovación y Universidades. La investigació efectuada ha estat finançada pels següents projectes:

NUREIEV: NUevos REtos en la investigación de cañones submarinos: Indicadores del Estado ambiental y Variabilidad espaciotemporal – El papel de los temporales (ref. CTM2013-44598-R). Programa Estatal de I+D+I Orientada a los Retos de la Sociedad, MINECO. 2014-2017.

NUREIEVA: NUevos REtos de Investigacion en el ambiente Extremo de los Vertidos mineros de la Bahía de Portmán: aplicación de tecnologías Avanzadas (ref. CTM2016-75953-C2-1-R). Programa Estatal de I+D+I Orientada a los Retos de la Sociedad, MINECO. 2017-2021.

A la meva mare,
constant recer.

“Geologic processes may be slow,
but they are not beyond our perception.”

-Marcia Bjornerud

Agraïments

Els meus primers agraïments van dirigits als meus directors de Tesi, en Miquel Canals i l'Anna Sanchez. No cal dir que ells són els principals responsables de que la Tesi arribi a bon port. Al Miquel, per la seva expertesa i guia. Has estat sempre disponible quan necessitava un cop de mà. A l'Anna, per el seu esperit crític i educador. El primer dia que vaig arribar al grup, ens vam reunir i vas marcar el rumb a seguir: "Un cop això estigui fet, fes el que et vingui de gust", vas dir. Així he fet. Vull agrair la feina feta als dos, perquè poques vegades les paraules tenen tant de valor com aquelles dirigides a algú que comença a recórrer un camí inexplorat.

També hi ha altres persones amb les quals agraeixo haver compartit aquest camí. Un camí més planer gràcies a elles. Comencem amb tu, Andrea. Vam coincidir en el temps i l'espai, i sort que en vaig tenir! Dius que hem crescut juntes, en els bons moments i en els difícils. No puc estar-hi més d'acord. Coneixe't ha estat una de les millors coses que m'han passat aquests anys a la facultat. Continuo l'agraïment amb en Liam, qui ha viscut amb mi aquesta experiència. Per la serenor que transmets i per les converses de final de Tesi que alliberen.

A tots els companys de les sales 336-337 i laboratoris, als quals agraeixo profundament la seva companyia. A tu, Marc, als companys, Judit, Ester, Albert, Edu, Sergi, Montse, Maria i Maria, i a tots aquells que en vau formar part. A tots els membres del grup de recerca i especialment a en Toni, sempre disposat a escoltar i donar algun que altre consell.

Vet aquí un vegada, a les mateixes sales 336-337, una petita revolució es va produir farà un parell d'anys. Sara i Sara, Mar, Uri, Marta, Luisa, Irene, Dimitris i Guillem. Gràcies per aparèixer de sorpresa i omplir les hores de cerveses i converses. També agraeixo els bons moments viscuts amb aquells companys que venen i van, Cesar, Carlos, Enric, Pol, Julia, i a aquells companys passatgers, Natale i Monica, que deixen empremta.

Les següents paraules estan dedicades als companys de Bologna. Al Tommaso Tesi per haver-me acollit al seu laboratori, a la Gabriela per la seva companyia i, sobretot, a la Francesca per la seva amabilitat.

Si memorem els camins ja recorreguts, val la pena dedicar unes paraules a la geologia. Com molts geòlegs, vaig irrompre en aquesta disciplina més o menys per accident. Gràcies a la geologia recorro camins rals amb persones, de les quals, ja no me n'he separat. Ferran, gràcies per ser-hi.

Deixo els darrers agraïments per a la meva família. Pels meus pares, per ser generosos amb la vida. Per aquells estius que ens portaven, a mi i als meus germans, a buscar fòssils. Pels meus germans, avis, Rita, tiets i cosins i les festes simpàtiques.

Taula de continguts

Acrònims

AOF: *Almeria-Oran Front* (front d'Almeria-Orà).
AW: *Atlantic Water* (Aigua Atlàntica).
BEA: Bon Estat Ambiental.
BSTFA: *bis(trimethylsilyl) trifluoroacetamide* (bis(trimetilsilil) trifluoroacetamida).
CCiT-UB: Centres Científics i Tecnològics de la Universitat de Barcelona.
CF:CS: Constant Flux Constant Sedimentation.
Chl-a: clorofil·la a.
CLIVAR: *Climate and Ocean: Variability, Predictability and Change* (projecte de recerca).
CNR: *Consiglio Nazionale delle Ricerche.*
CO: carboni orgànic (en anglès OC).
CORELAB: Core Analysis Laboratory (Laboratori d'Anàlisi de Testimonis).
CT: carboni total.
CTD: *conductivity, temperature, depth* (conductivitat, temperatura, profunditat; conjunt de sensors)
DAS: descàrregues d'aigües subterrànies.
DISC: *Data and Information Services Centre.*
DTO: Departament de Dinàmica de la Terra i de l'Oceà.
EAG: *Eastern Alboran Gyre* (gir oriental de la mar d'Alborán).
ECO-AFL/FL: environmental characterization optics-fluorometers.
ECO-NTU: *environmental characterization optics-nephelometric turbidity unit*.
EMODnet: European Marine Observation and Data Network
EVLLa: *ethyl vanillin*
FE: factor d'enriquiment (en anglès EF)
GC: *gravity corer* (testificador de gravetat, segons context).
GC: *gas cromatograph* (cromatògraf de gasos, segons context).
GEOS: *Goddard Earth Observing System Model.*
GEOTRACES: *An International Study of the Marine Biogeochemical Cycles of Trace Elements and Isotopes* (projecte de recerca).
GES: *Goddard Earth Science.*
GMAO: *Global Modeling and Assimilation Office.*
ICP-MS: *inductively coupled plasma mass spectrometry* / *spectrometer* (espectrometria / espectròmetre de masses de plasma d'inducció acoblat)
ICP-OES: *inductively coupled plasma optical emission spectroscopy / spectrometer* (espectrometria / espectròmetre d'emissió òptica de plasma d'inducció acoblat).
IEO: Instituto Español de Oceanografía
IRMS: *isotope-ratio mass spectrometry / spectrometer* (espectrometria / espectròmetre de masses de relacions isotòpiques).
ISP: *Istituto di Scienze Polari*.
JGOFS: *Joint Global Ocean Flux Study* (projecte de recerca).
LRA-UAB: *Laboratori de Radioactivitat Ambiental de la Universitat Autònoma de Barcelona* (Environmental Radioactivity Laboratory of the Autonomous University of Barcelona).
LIW: *Levantine Intermediate Water* (Aigua Intermèdia Llevantina).
LRA: Laboratori de Radioactivitat Ambiental (de la Universitat Autònoma de Barcelona).
LS: *laser scanner* (escàner làser).
MAR: mass accumulation rate
MAW: *Modified Atlantic Water* (Aigua Atlàntica Modificada).
MC: *multicorer* (testificador múltiple).
MCA: *multichannel analyzer* (analitzador multicanal).
MC-ICP-MS: *multicollector inductively coupled plasma mass spectrometry* / *spectrometer* (espectrometria / espectròmetre de masses de plasma d'inducció acoblat de multicol·lector)
MERRA: *Moderns-Era Retrospective analysis for Reserach and Applications.*
MIDAS: *Managing Impacts of Deep-seA reSource exploitation* (projecte de recerca).
MO: matèria orgànica (en anglès OM).
MODIS: *Moderate Resolution Imaging Spectrometer.*
MSFD: *Marine Strategy Framework Directive* (Directiva Marc sobre l'Estratègia Marina).
MT: metalls traça (en anglès TM).
m/z: ràtio massa / càrrega.
NASA: *National Aeronautics and Space Administration.*
NBS: *National Bureau of Standards*.
NC: *Northern Current* (Corrent del Nord).
NIST: *National Institute of Standards and Technology*.

NT: nitrogen total.
NUREIEV: *NUevos REtos en la investigación de cañones submarinos: Indicadores del Estado ambiental y Variabilidad espaciotemporal – El papel de los temporales* (projecte de recerca).
NUREIEVA: *NUevos REtos de Investigacion en el ambiente Extremo de los Vertidos mineros de la Bahía de Portmán: aplicación de tecnologías Avanzadas* (projecte de recerca).
OBPG: *Ocean Biology Processing Group.*
Pg: petragram.
PIDS: *polarization intensity differential scattering* (dispersió diferencial per intensitat de polarització)
PPS: *piège à particules séquentielle* (trampa de partícules seqüencial).
PVC: *polyvinyl chloride*.
R/V: *research vessel*
REDEXT: red exterior de boyas (Puertos del Estado).
RSD: *relative standard deviation*.
SRM: *standard reference material*.
SAIH: *Sistema Automático de Información Hidrológica*.
SQG: *Sediment Quality Guidelines*.
SSB: *silicon Surface barrier*
TCMS: *trimethylchlorosilane* (trimetilclorosilà).
TDW: Thyrrhenian Deep Water (Aigua Profunda de la mar Tirrena).
TMF: *total mass flux* (flux de massa total).
TWC: *time weighted content* (contingut ponderat, d'un component o element, segons el temps de mostreig).
TWF: *time weighted flux* (flux ponderat segons el temps de mostreig).
UB: Universitat de Barcelona.
UE: Unió Europea (en anglès EU).
VMS: *Vessel Monitoring System* (Sistema de Monitorització de Vaixells).
WAG: *Western Alboran Gyre* (gir occidental de la mar d'Alborán).
WANA: sèries de vent i onatge procedents de models numèrics (Puertos del Estado).
WET Labs: *Western Environmental Technology Laboratories.*
WIW: *Western Intermediate Water* (Aigua Intermèdia de la Mediterrània Occidental).
WMDW: *Western Mediterranean Deep Water* (Aigua Pro unda de la Mediterrània Occidental).
XRF: X-ray flurescence (fluorescència de raigs X).

Resum

Les partícules que sedimenten en el medi marí tenen un paper clau en el cicle biogeoquímic d'un bon nombre d'elements i, per tant, són essencials per al funcionament de l'ecosistema. L'estudi dels fluxos de partícules permet entendre els processos que controlen la transferència de matèria i dels elements químics associats cap al fons marí, on poden quedar emmagatzemats per llargs períodes de temps. En aquest context, esclarir el transport de partícules als marges continentals, situats entre el continent i la conca profunda, és altament rellevant per millorar el coneixement sobre aitals processos i també per encarar no pas pocs reptes ambientals.

Aquesta Tesi se centra en la dinàmica del transport de partícules sedimentàries als marges continentals dels golfs de Vera i d'Almeria, a la Mediterrània sud-occidental. Aquests marges estan entallats per un seguit de canyons submarins de característiques ben diverses. De tots ells, s'han investigat el canyó d'Escombreras, el sistema Garrucha-Almanzora i el canyó d'Almeria, i també el talús obert i el peu del talús. L'ús d'un conjunt de paràmetres indicatius, com la magnitud dels fluxos, la mida de gra, la composició elemental, i el contingut en metalls (Al, Fe, Ti, Co, Cu, Mn, Ni, Pb i Zn) i As, ha permès caracteritzar les partícules que sedimenten i els sediments del fons marí, i analitzar la dinàmica de les partícules, per determinar finalment els factors que regeixen llur variabilitat espacial i temporal. A aquest efecte, també s'han tingut en compte els forçaments externs, atmosfèrics i oceanogràfics, i les activitats antropogèniques susceptibles de condicionar la composició i el comportament de les partícules. En aquest context, l'ús de traçadors, com els isòtops del carboni i del Pb, i biomarcadors específics, pot ajudar a respondre a algunes preguntes rellevants: (i) Quin és l'origen i la composició de la matèria orgànica en uns marges continentals amb escasses aportacions fluvials, com els investigats? i (ii) Quina és la contribució del dipòsit de residus miners de la badia de Portmán, al sud de Múrcia i, especialment, de la seva extensió submarina, al flux de metalls cap al marge distal?

La recerca efectuada constata que les tempestes, amb un augment de l'onatge i dels corrents, són els principals dinamitzadors del transport de sediments cap al marge profund. L'arribada de material de la plataforma continental resuspès explica, en gran mesura, la variabilitat temporal dels continguts de metalls i As als canyons submarins d'Escombreras i, sobretot, d'Almeria. Les tempestes també poden influir en l'origen i la composició i de la matèria orgànica exportada, com ho mostra el transport de detritus de *Posidonia oceanica* cap al canyó d'Escombreras. Les condicions ambientals abans i durant les tempestes modulen la magnitud i la composició dels fluxos de partícules. Entre aquestes condicions s'hi compten les característiques de la columna d'aigua, les aportacions fluvials i la producció primària. Les especificitats de cada tempesta, com ara la direcció i el règim d'onatge, la velocitat i la direcció dels corrents, i la seva durada, també afecten molt notablement a la remobilització, el transport i l'acumulació de partícules sedimentàries i matèria orgànica, en funció de la seva mida de gra, densitat i forma. Al peu del talús, a 2.500 m de profunditat, la producció primària és el factor principal de control dels fluxos de partícules.

Certs forçaments antropogènics, com la pesca d'arrossegament de fons, també poden afavorir l'exportació de partícules, com s'ha comprovat al sistema de canyons de Garrucha-Almanzora. L'activitat industrial a la franja costanera propera deixa sentir tanmateix els seus efectes sobre la composició dels fluxos de partícules al marge continental profund, com ho demostra el cas concret del canyó d'Escombreras, en que una de les principals vies d'entrada de Pb antropogènic es produiria per la intermediació del transport atmosfèric.

Els resultats obtinguts evidencien que les partícules sedimentàries són vectors de transferència de contaminants metàl·lics cap als canyons submarins i el marge continental profund, en sentit ampli. Aquesta Tesi demostra, per altra banda, la complexitat de les interaccions entre els factors i processos que governen la composició i la dinàmica dels fluxos de partícules i la sedimentació en els marges continentals i les conques pregones adjacents. També és una contribució al coneixement d'una àrea geogràfica encara poc estudiada. Els nous coneixements aportats poden ser útils per a una gestió informada i sostenible de l'ecosistema marí.

Resumen

Las partículas que sedimentan en el medio marino desempeñan un papel crucial en el ciclo biogeoquímico de un buen número de elementos y, por lo tanto, son esenciales para el funcionamiento del ecosistema. El estudio de los flujos de partículas permite entender los procesos que controlan la transferencia de materia y de los elementos químicos asociados hacia el fondo marino, donde pueden quedar almacenados durante largos períodos de tiempo. En este contexto, es clave esclarecer el transporte de partículas a los márgenes continentales, ubicados entre el continente y la cuenca profunda, para mejorar el conocimiento sobre dichos procesos y abordar diversos desafíos ambientales.

Esta Tesis se centra en la dinámica del transporte de partículas sedimentarias en los márgenes continentales de los golfos de Vera y de Almería, en el Mediterráneo suroccidental. Estos márgenes están cortados por una serie de cañones submarinos con características diversas. De todos ellos, se han investigado el cañón de Escombreras, el sistema Garrucha-Almanzora y el cañón de Almería, así como el talud abierto y el pie del talud. El uso de un conjunto de parámetros indicativos, como la magnitud de los flujos, el tamaño de grano, la composición elemental y el contenido de metales (Al, Fe, Ti, Co, Cu, Mn, Ni, Pb y Zn) y As, ha permitido caracterizar las partículas que sedimentan y los sedimentos del fondo marino, y analizar la dinámica de las partículas, para determinar finalmente los factores que rigen su variabilidad espacial y temporal. A este efecto, también se han tenido en cuenta los forzamientos externos, atmosféricos y oceanográficos, así como las actividades antropogénicas susceptibles de condicionar la composición y el comportamiento de las partículas. En este contexto, el uso de trazadores, como los isótopos del carbono y del Pb, y biomarcadores específicos, puede ayudar a responder algunas preguntas relevantes: (i) ¿Cuál es el origen y la composición de la materia orgánica en unos márgenes continentales con escasas aportaciones fluviales, como los investigados? y (ii) ¿Cuál es la contribución del depósito de residuos mineros de la bahía de Portmán, al sur de Murcia y, especialmente, de su extensión submarina, al flujo de metales hacia el margen distal?

La investigación realizada pone de manifiesto que los temporales, con un aumento del oleaje y de las corrientes, son los principales activadores del transporte de sedimentos hacia el margen profundo. La llegada de material de la plataforma continental resuspendido explica, en gran medida, la variabilidad temporal de los contenidos de metales y As en los cañones submarinos de Escombreras y, especialmente, de Almería. Los temporales también pueden influir en el origen y la composición de la materia orgánica exportada, como lo demuestra el transporte de detritus de *Posidonia oceanica* hacia el cañón de Escombreras. Las condiciones ambientales antes y durante las tormentas modulan la magnitud y la composición de los flujos de partículas. Entre estas condiciones se cuentan las características de la columna de agua, las aportaciones fluviales y la producción primaria. Las especificidades de cada tormenta, como la dirección y el régimen de oleaje, la velocidad y la dirección de las corrientes, y su duración, también afectan notablemente a la remobilización, el transporte y la acumulación de partículas sedimentarias y materia orgánica, en función de su tamaño de grano, densidad y forma. En el pie del talud, a 2.500 m de profundidad, la producción primaria es el factor principal de control de los flujos de partículas.

Ciertos forzamientos antropogénicos, como la pesca de arrastre de fondo, también favorecen la exportación de partículas, como se ha comprobado en el sistema de cañones de Garrucha-Almanzora. La actividad industrial en la franja costera cercana también deja sentir sus efectos sobre la composición de los flujos de partículas en el margen continental profundo, como demuestra el caso concreto del cañón de Escombreras, en el que una de las principales vías de entrada de Pb antropogénico se produciría por la intermediación del transporte atmosférico.

Los resultados obtenidos evidencian que las partículas sedimentarias son vectores de transferencia de contaminantes metálicos hacia los cañones submarinos y el margen continental profundo, en sentido amplio. Esta Tesis demuestra, por otra parte, la complejidad de las interacciones entre los factores y procesos que gobiernan la composición y la dinámica de los flujos de partículas y la sedimentación en los márgenes continentales y las cuencas adyacentes. También es una contribución al conocimiento de un área geográfica aún poco estudiada. Los resultados alcanzados pueden ser útiles para una gestión informada y sostenible del ecosistema marino.

Abstract

Sedimentary particles in the marine environment play a crucial role in the biogeochemical cycle of a large number of elements and, therefore, are essential for the functioning of marine ecosystem. The study of particle fluxes allows understanding the processes that control the transfer of matter, and associated chemical elements, down to the seafloor, where they can remain stored for long periods. In this context, it is key to clarify the transport of particles in continental margins, located between the continent and the deep basin, to enhance knowledge of these processes and address various environmental challenges.

This PhD Thesis focuses on the dynamics of sedimentary particle transport in the continental margins of the Vera and Almeria gulfs, in the southwestern Mediterranean Sea. These margins are cut by a number of submarine canyons with distinct characteristics. Specifically, the study encompasses the Escombreras and Almeria canyons, the Garrucha-Almanzora canyon system, and also the open slope and the deep basin. The use of indicative parameters, such as flux magnitude, grain size, elemental composition, and metal content (Al, Fe, Ti, Co, Cu, Mn, Ni, Pb, and Zn) and As, has allowed the characterization of settling particles and seafloor sediments, and analysing the particle dynamics, ultimately determining the factors that govern their spatial and temporal variability. External forcings, atmospheric and oceanographic, as well as anthropogenic activities influencing particle composition and behavior, are also considered. In this frame, the use of tracers like carbon and Pb isotopes, and specific biomarkers, can help answering some relevant questions: (i) Which are the origin and composition of organic matter in continental margins with rare riverine inputs, like the investigated ones? and (ii) Which is the contribution of the Portmán Bay mine tailing deposit, to the south of Murcia province and, especially, of its submarine extension, to metal fluxes towards the distal margin?

The work carried out evidences that storm events, with increased wave height and current speeds, are the main triggers of sediment transport to the deep margin. The arrival of resuspended material from the continental shelf largely explains the temporal variability of metal and As contents in the submarine canyons of Escombreras and, mainly, Almeria. Storms can also influence the origin and composition of exported organic matter, as evidenced by the transport of *Posidonia oceanica* detritus to the Escombreras canyon. Environmental conditions before and during storms modulate the magnitude and composition of particle fluxes. These conditions include water column characteristics, riverine inputs, and primary production. The characteristics of each storm, such as wave direction and regime, current speed and direction, and duration, significantly affect the remobilization, transport, and accumulation of sedimentary particles and organic matter, as a function of their size, density, and shape. At the deep basin, at a depth of 2,500 m, primary production is the main driver of particle fluxes.

Certain anthropogenic forcings, such as bottom trawling, also favour particle export, as observed in the Garrucha-Almanzora canyon system. Industrial activity in the nearby coastal zone also affects the composition of deep continental margin particle fluxes, as demonstrated by the specific case of the Escombreras canyon, where one of the main pathways for anthropogenic Pb entry would occur through atmospheric transport.

The results obtained demonstrate that sedimentary particles act as vectors for the transfer of metal contaminants to submarine canyons and the deep continental margin, broadly speaking. This Thesis also illustrates the complexity of interactions among the factors and processes driving the composition and dynamics of particle fluxes and sedimentation in continental margins and adjacent basins. Also, it is a contribution to the understanding of an understudied geographical area. The results achieved could be useful for and informed and sustainable management of marine ecosystems.

Presentació de la Tesi

Motivació i objectius

Els mars i oceans són reservoris de primer ordre per elements com el carboni, els metalls i els metal·loides, els quals acaben acumulant-se en els sediments marins al llarg de períodes de temps molt dilatats. Les partícules que sedimenten són el principal vector de l'enfonsament de diferents elements i compostos des de la superfície de l'aigua fins el fons marí (Conte et al., 2001) i, per tant, regulen part del cicle d'aquests elements a l'oceà. Aquest procés és essencial per al manteniment de l'equilibri químic de mars i oceans, i per a la preservació de la salut dels ecosistemes marins.

L'estudi dels cicles biogeoquímics de mars i oceans, per sí mateix i en el marc de l'assoliment del seu Bon Estat Ambiental (BEA) (MSFD, 2008), constitueix un camp de recerca actiu d'on en deriven indicadors específics en àmbits tant importants com és la MSFD i altres directives ambientals europees. Està demostrat que l'activitat humana i el canvi climàtic alteren el funcionament dels cicles biogeoquímics, modificant les concentracions i la distribució dels elements químics i provocant desequilibris en els processos que els regulen. Tot i que hi ha la voluntat i la necessitat d'entendre les implicacions dels impactes antropogènics, encara resten per respondre algunes preguntes fonamentals en relació amb la transferència, la dispersió i l'acumulació de metalls i carboni en el medi marí. Per exemple, quins són l'origen i les vies d'entrada de les partícules sedimentàries i els elements químics associats? Com es transporten? Quina mena d'interaccions tenen amb altres matrius ambientals? Com i on es preserven?.

Aquesta Tesi s'emmarca en la recerca multidisciplinària duta a terme durant les darreres dècades als marges continentals de la mar Mediterrània. Diversos estudis s'han focalitzat en la investigació dels ecosistemes marins, de la transferència de matèria i energia des de les zones costaneres fins el marge i la conca profunds —incloent carboni, contaminants diversos i metalls traça—, dels efectes dels forçaments externs meteorològics i climàtics, i del paper dels canyons submarins com a vies preferents de transport d'aigua i sediments. Aquests estudis han mostrat que els cicles biogeoquímics a la mar Mediterrània són el resultat de complexes interaccions entre la terra, l'atmosfera i l'oceà.

El treball que ara teniu a les mans s'ha desenvolupat al marge ibèric sud-oriental, comparativament poc estudiat i amb unes característiques ambientals ben particulars: (i) una descàrrega fluvial escassa i unes aportacions de sediments minses; (ii) un règim micromareal i amb absència d'esdeveniments d'alta energia com els que ocorren, per exemple, al mar Català; (iii) la presència de nombrosos canyons submarins fortament entallats a la plataforma continental i amb capçaleres properes a la línia de costa; i (iv) un seguit de tensions ambientals, entre les quals el dipòsit de residus miners de la badia de Portmán, un dels casos més greus d'impacte ambiental a tota Europa causats per l'abocament de residus miners al medi marí.

La recerca d'aquesta Tesi s'ha dut a terme en el marc de dos projectes finançats pel *Ministerio de Economía y Competitividad*, NUREIEV (*NUevos REtos en la investigación de cañones*

submarinos: Indicadores del Estado ambiental y Variabilidad espaciotemporal – El papel de los temporales) i NUREIEVA (*NUevos REtos de Investigacion en el ambiente Extremo de los Vertidos mineros de la Bahía de Portmán: aplicación de tecnologías Avanzadas*), i d'un projecte finançat per la Comissió Europea dins el Setè Programa Marc, MIDAS (*Managing Impacts of Deep-seA reSource exploitation*).

La Tesi planteja una hipòtesi de partida: en absència de processos de formació i enfonsament d'aigües denses, els temporals exerceixen un control determinant en la transferència de matèria entre el mar costaner i el mar profund i, atès el context en que s'ha desenvolupat, vol (i) esbrinar quines són la magnitud i les característiques composicionals dels fluxos de partícules pel que fa als continguts en metalls (Al, Fe, Ti, Co, Cu, Mn, Ni, Pb, Zn), As, i carboni orgànic (CO); (ii) identificar els processos implicats en la transferència d'aquests elements des del marge continental intern fins el marge extern i la conca pregona; i (iii) escatir quines són les fonts dels metalls i metal·loides que, en forma particulada, sedimenten als golfs de Vera i d'Almeria, amb l'ull posat en el dipòsit de residus miners de la badia de Portmán. Convé assenyalar que l'impacte del dipòsit de Portmán en termes de transferència de metalls traça cap a mar obert és, fins el moment, del tot desconegut.

Organització de la tesi

El contingut de la Tesi es basa en els resultats de 2 articles publicats en revistes indexades i en 2 articles en diferents estadis d'elaboració no publicats a la data de dipòsit. La Tesi s'estructura en 6 capítols:

El **Capítol 1** correspon a la introducció a la temàtica de la Tesi. La seva finalitat és donar una perspectiva general i introduir els temes que es tracten amb més profunditat als capítols de resultats. S'hi presenten les característiques geològiques i oceanogràfiques de la regió d'estudi i es proporciona informació sobre el dipòsit de residus miners de la badia de Portmán.

El **Capítol 2** detalla la metodologia seguida. S'explica l'obtenció de dades i mostres en campanyes oceanogràfiques, així com la instrumentació utilitzada. També es descriuen les anàlisis de laboratori, els protocols seguits i el tractament de les dades.

El **Capítol 3** presenta els resultats obtinguts, i està dividit en 5 subcapítols:

Subcapítol 3.1: article *Particle fluxes in submarine canyons along a sediment-starved continental margin and in the adjacent open slope and basin in the SW Mediterranean Sea*, publicat a la revista *Progress in Oceanography*. Es combinen dades oceanogràfiques, hidrològiques i meteorològiques amb la quantificació i la caracterització dels fluxos de partícules (composició elemental, mida de gra i matèria orgànica) per conèixer els processos transferència involucrats i avaluar llur variabilitat espaciotemporal en ambients de canyó, talús i peu del talús).

Subcapítol 3.2: article *Transport and distributions of naturally and anthropogenically sourced trace metals and Arsenic in submarine canyons*, publicat a la revista *Progress in Oceanography*. S'investiguen les concentracions i la distribució espacial d'un seguit de metalls (Al, Fe, Ti, Co,

Cu, Mn, Ni, Pb, Zn) i d'un metal·loide (As) en els fluxos de partícules i els sediments del fons marí als canyons d'Escombreras, Garrucha-Almanzora i Almeria, i s'interpreten els factors naturals —com ara les tempestes— i antropogènics responsables.

Els resultats d'aquests dos primers articles mostren una clara connexió entre els forçaments naturals i antropogènics i les característiques dels fluxos de partícules, però també posen en relleu les limitacions dels coneixements existents. Per exemple, a l'hora de determinar l'origen de la matèria orgànica (MO) i dels contaminants metàl·lics exportats al marge extern. Aquestes limitacions són especialment rellevants ateses les tensions ambientals i les afectacions sobre els ecosistemes al marge continental de Mazarrón (Baza-Varas, 2023), el qual inclou la badia de Portmán.

Els següents subcapítols es focalitzen en l'origen, les característiques biogeoquímiques i el transport de MO i diversos metalls al canyó submarí d'Escombreras a partir de l'ús de marcadors específics. Convé assenyalar que, entre tots els de l'àrea, el canyó d'Escombreras és el que té la capçalera més propera al dipòsit de residus miners de la badia de Portmán.

Subcapítol 3.3: article en preparació titulat *Across margin export of recalcitrant blue carbon: a study case off SE Iberia*. S'analitzen els continguts en OC i nitrogen (N), els isòtops de carboni i biomarcadors específics derivats de la lignina i la cutina en mostres de partícules en suspensió i sediments del fons marí amb la finalitat de caracteritzar la MO recalcitrant al canyó d'Escombreras, i així poder determinar-ne l'origen i els mecanismes de transport intervinents.

Subcapítol 3.4: article en preparació titulat *Pb and Zn pollution in a submarine canyon: the role of a coastal mine tailings deposit and other potential sources*. S'analitza el contingut de Pb i Zn, i la composició isotòpica del Pb, en els sediments del canyó d'Escombreras. Aitals variables s'utilizen per escatir el paper del dipòsit de residus miners de la badia de Portmán com a font de metalls des d'una perspectiva històrica i fins l'actualitat, així com per a ponderar fonts alternatives.

Subcapítol 3.5: inclou un resum dels resultats dels quatre subcapítols precedents.

El Capítol 4 consisteix en una discussió conjunta dels resultats assolits tenint en compte els objectius inicials.

El Capítol 5 exposa les conclusions del nostre treball i es suggereixen línies d'investigació futures.

Clouen la Tesi les referències bibliogràfiques en el Capítol 6 i un Annex en què es reprodueixen els articles publicats.

Capítol 1

Introducció

Els marges continentals

Fluxos de partícules en el medi marí

- Composició
- Transport, distribució, concentració i preservació

Metalls i metal·loides en el medi marí

- Fonts i formes d'ocurrència
- Rellevància com a contaminants
- Interaccions amb els fluxos de partícules

La mar Mediterrània

- Fisiografia
- Masses d'aigua i circulació general

Els golfs de Vera i Almeria

- Relleu submarí
- Hidrografia
- Fonts de partícules

El dipòsit de residus miners de la badia de Portmán

1.1. Els marges continentals

Des del punt de vista estructural, els marges continentals són les regions submergides dels continents. Per aquesta raó, en algunes llengües hom els anomena també "precontinent". Ocupen un 21% de la superfície total dels oceans (Liu et al., 2010). Els marges continentals passius, com el que ens ocupa, estan formats per tres gran províncies fisiogràfiques: la plataforma continental, entre la línia de costa i l'anomenat cantó o límit de plataforma; el talús continental, amb un pendent més pronunciat que la plataforma, entre el cantó i la base del talús; i el glacis continental, de pendent suau, que s'estén des de la base del talús cap a la conca profunda (Fig. 1.1). Molts marges continentals estan entallats per canyons submarins de característiques diverses. Els canyons submarins són valls encaixades en el talús continental i que poden estendre's cap a la plataforma i el glacis. S'hi acostumen a diferenciar quatre trams: la capçalera, i els cursos superior, intermedi i inferior. Alguns presenten capçaleres molt properes a la línia de costa (Canals et al., 2012; Amblas et al., 2018). Segons alguns càlculs, els canyons submarins ocupen l'11,2% del talús continental a escala global (Harris et al., 2014).

Per les seves característiques morfològiques, per la posició que ocupen en els marges continentals, pel fet de connectar la plataforma amb el marge profund i les conques pregones, i per la seva dinàmica, els canyons submarins són vies preferents per a la transferència de matèria i energia provinents de la plataforma continental, i també en sentit invers, per exemple afavorint l'aflorament d'aigües fondes (Xu et al., 2004; Allen i Durrieu de Madron, 2009). Per les mateixes raons, els canyons submarins són altament rellevants des del punt de vista ecològic, com ho mostren l'alta biodiversitat i l'abundància de recursos vius que acullen (Company et al., 2008; De Leo et al., 2010; Fernandez-Arcaya et al., 2017). És cert també que per les seves característiques i funcionament estan exposats als impactes de les activitats antròpiques, a banda de poder constituir una via per la seva propagació, com ho mostren, per exemple, les abundants concentracions de deixalles i contaminants en alguns d'ells (Palanques et al., 2008; Salvadó et al., 2012, 2017, 2019; Ramirez-Llodra et al., 2013; Tubau et al., 2015; Pierdomenico et al., 2023).

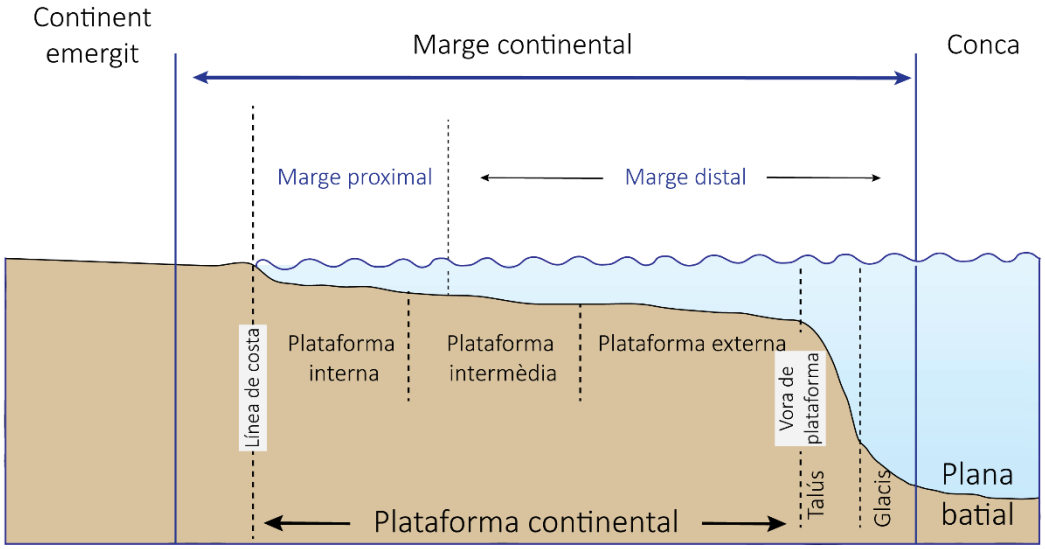

Figura 1.1. Secció i províncies fisiogràfiques d'un marge continental passiu (basat en Liu et al., 2010).

Els marges continentals, tot i representar una proporció relativament petita dels fons marins, tenen un paper fonamental en els cicles del carboni i els metalls traça. No només connecten les àrees somes amb les pregones, sinó que la seva proximitat als principals punts d'entrada de partícules i contaminants d'origen terrestre els converteix en vectors de primera importància per la seva dispersió (Liu et al,. 2010; Geibert et al., 2018). A més, també presenten productivitats elevades, de manera que hom calcula que contribueixen en un 10-30% a la producció primària marina global (Mackenzie et al., 2005). Són, doncs, alhora vies de transmissió i depocentres de partícules, substàncies i elements químics d'origen tant al·lòcton com autòcton (Hedges i Keil, 1995; Atwood et al., 2020). Tanmateix, els corrents marins poden transportar a gran distància part d'aquests materials, amb la intervenció de diversos mecanismes i processos de transport. En aquesta Tesi hom aprofundeix en alguns d'aquests processos, i s'investiga com impacten la variabilitat temporal dels fluxos de partícules.

1.2. Fluxos de partícules en el medi marí

Els oceans contenen una gran quantitat de partícules d'orígens i naturalesa diversos, les quals un cop dipositades al fons marí formen els sediments. Inclouen tant components abiòtics com biòtics, compresos organismes vius i restes d'organismes morts, i poden haver-se format al mar o provenir de les terres emergides per via atmosfèrica o aquàtica, i també per erosió directa de la línia de costa. Hom considera material particulat la fracció que queda retinguda en un filtre de 0,45 µm de diàmetre de porus. Conèixer les propietats, la distribució i la dinàmica de les partícules que hi ha a l'oceà és fonamental per conceptualitzar els cicles biogeoquímics en el medi marí.

1.2.1. Composició

Segons la composició química i l'origen, les partícules que sedimenten en forma de fluxos estan constituïdes per tres fraccions principals: (i) la fracció terrígena (també anomenada detrítica, litogénica, siliciclàstica o silicoclàstica), que prové de fonts externes; (ii) la biogènica, formada a la biosfera marina i no marina; i (iii) l'autigènica, formada *in situ* a la columna d'aigua o els sediments. Les fraccions terrígena i biogènica dominen els fluxos de partícules i els sediments marins (Fig. 1.2), mentre que la fracció autigènica rarament és dominant ni als fluxos ni als sediments. L'excepció són els ambients hidrotermals.

La fracció terrígena té majoritàriament un origen continental i prové de la descomposició de les roques. És introduïda a l'oceà per via fluvial, glacial, atmosfèrica i també hidrotermal. Les dues primeres vies són especialment rellevants als marges continentals. La via fluvial està àmpliament estesa a les latituds baixes, mitjanes i part de les altes. La via glacial només predomina en latituds altes. Per la seva part, la via atmosfèrica introdueix material relativament fi a través de tota la superfície de l'oceà global, tot i que en algunes regions més que en altres. Els constituents principals de la fracció terrígena són els aluminosilicats $(MAlO_2)(SiO_2)_x(H_2O)_y$ (on M^+ normalment és H^+ o Na^+), essent comuns els minerals dels grups de la caolinita, la clorita, la il·lita i la montmoril·lonita, i també silicats, com el quars i els feldspats. També pot incloure altres fases, com ara carbonats detrítics (Müller et al., 2022).

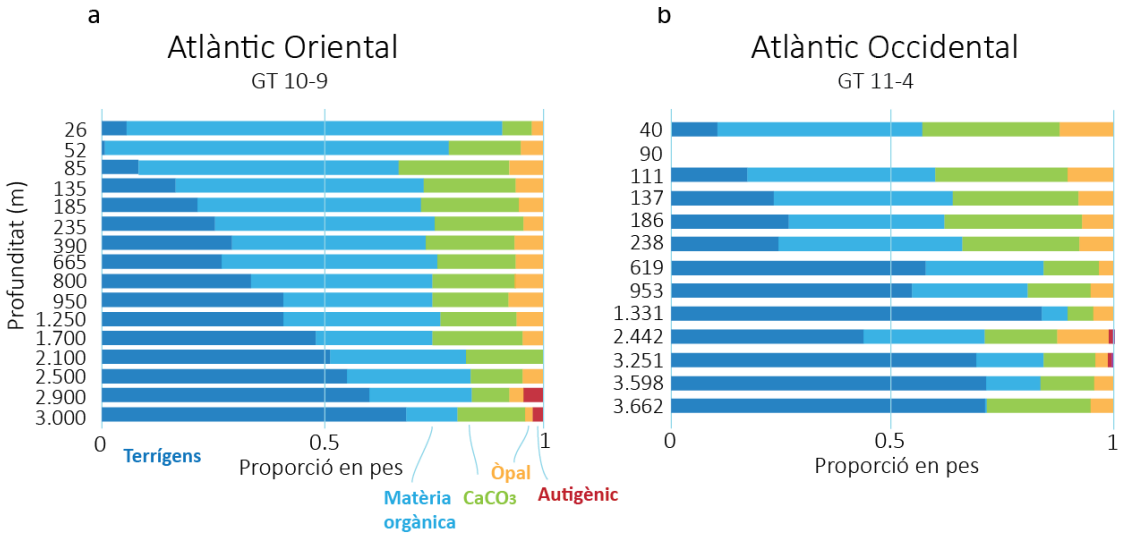

Figura 1.2. Perfils de composició de les partícules (>51 µm) en dos estacions situades a l'est (a) i l'oest (b) de l'oceà Atlàntic (estacions GT10-9/US GEOTRACES North Atlantic Zonal Transect, i GT 11-4/ GEOTRACES North Atlantic Zonal Transect, respectivament) (Lam et al., 2015).

La fracció biogènica està formada per restes d'organismes diversos, incloent les fases inorgàniques de teixits, closques i altres parts esquelètiques. Bona part de la fracció biogènica procedeix del plàncton. El fitoplàncton crea els seus propis constituents orgànics a partir de compostos inorgànics, mentre que el zooplàncton obté l'energia alimentant-se del fitoplàncton. La principal font de components biogènics inorgànics a l'ambient marí són els organismes que

secreten exo- i endosquelets de carbonat de calci ($CaCO_3$) i sílice biogènica (també coneguda com "òpal" i "òpal biogènic") (predominantment, $SiO_2 \cdot nH_2O$). Dins el plàncton, els principals productors d'òpal són les diatomees (fitoplàncton) i els radiolaris (zooplàncton). Encara dins el plàncton, els principals productors de carbonats són els foraminífers (zooplàncton), els cocolitofòrids (fitoplàncton), i els pteròpodes (zooplàncton) que secreten closques d'aragonita. Quan els cocolitofòrids moren, alliberen petits plaques o discs individuals anomenats coccòlits.

La MO en el detritus està composta per restes d'organismes morts, matèria fecal, agregats orgànics i una àmplia varietat de molècules orgàniques. La MO deriva de fonts autòctones, principalment del fitoplàncton mercès a la fotosíntesi, però també hi ha una contribució substancial de fonts al·lòctones. El CO n'és el principal constituent, i s'estima que el transport fluvial introdueix al medi marí aproximadament 0,45 Pg[1] de CO particulat a l'any (Cole et al., 2007).

La caracterització de la MO a l'oceà s'ha basat, en gran mesura, en l'anàlisi de la química elemental, i de components moleculars específics, com ara els lípids, els aminoàcids, els carbohidrats i els pigments, entre altres. La reacció conceptual $CO_2 + H_2O \leftrightarrow CH_2O + O_2$. explica, de forma simplificada, els processos de respiració i fotosíntesi. Tanmateix, la MO és força més complexa, havent-se estimat una composició mitjana de 106C:177H:37O:16N:1P:0.4S per la producció marina primària (Hegdes et al., 2002). A més, per a realitzar la fotosíntesi, les algues necessiten altres macronutrients, com el Si, i també micronutrients, com el Fe, el Cd, el Co, el Cu, el Mn, el Ni i el Zn (Moore et al., 2013). No tota la producció primària marina presenta els valors de l'estequiometria ideal de Redfield. Un exemple són els herbeis de fanerògames marines, que contribueixen a la producció primària en els ambients marins costaners, i presenten elevades ràtios CO/N i CO/P, menys proteïnes i àcids nucleics, i majors continguts de carbohidrats i lignines en la seva estructura (Klap et al., 2000; Trevathan-Tackett et al., 2017).

A mar obert, la composició de la MO de les partícules marines és força uniforme. Això és degut a la predominança de detritus provinents del fitoplàncton i de bactèries, els quals estan constituïts principalment per proteïnes (>50%) (Middelburg, 2019). En canvi, la MO exhibeix un alt grau d'heterogeneïtat als marges continentals, on si afegeixen altres fonts com, per exemple, partícules orgàniques terrestres formades per una barreja heterogènia de components (Goñi et al., 2000; Tesi et al., 2007; Schmidt et al., 2010; Bianchi et al., 2011).

La fracció autigènica està constituïda per fases minerals que precipiten a partir de reaccions inorgàniques, que poden estar induïdes biològicament (Martinez-Ruiz et al., 2020). Entre les fases minerals que formen aquesta fracció hi pot haver oxihidròxids i òxids de Fe i Mn —com $FeOH_3$ i MnO_2—, carbonats, sulfurs —com la pirita—, sulfats —com la barita—, fosfats —com l'apatita— i silicats alterats (Noble, 2012). Les condicions ambientals (temperatura, pressió, pH, Eh), la disponibilitat de reactants (MO) i ions, i l'activitat microbiana poden jugar un paper altament rellevant en la formació d'aquesta fracció.

[1] $1Pg = 10^{15}$ g.

1.2.2. Transport, distribució, concentració i preservació

El transport vertical i els processos advectius (transport lateral) determinen la distribució i la concentració de les partícules a la columna d'aigua. Les partícules en suspensió a la columna d'aigua estan sotmeses a un seguit de processos físics i bioquímics que acaben determinant l'eficiència i la magnitud de la transferència cap al fons marí i, per tant, també dels elements i compostos associats.

El transport vertical de les partícules es produeix en gran mesura per l'acció de la gravetat, i depèn de la seva mida (diàmetre) i densitat (cf. grups funcionals, més amunt), i també de la viscositat de les aigües circumdants. Bona part de la massa de partícules a l'oceà està constituida per partícules de mida petita, des d'una mida sub-micromètrica fins a pocs micròmetres (Lam i Marchal, 2015); així dons, la sedimentació vertical d'aquestes partícules des de la superfície fins al fons marí s'hauria de produir durant centenars o milers d'anys (Taula 1.1). La realitat, però, és que la decantació de les partícules és un procés força més dinàmic. L'agregació de partícules i, en especial, l'agregació de partícules biogèniques —formant l'anomenada "neu marina"[2]—, és un dels principals factors que governen el seu enfonsament dins la columna d'aigua (Fowler i Knauer, 1986). A mesura que les partícules es van agregant —per mecanismes fisicoquímics i biològics, com l'empaquetament en pellets fecals, l'adsorció o la coagulació (Burd, 2013)— i esdevenen més grans, la velocitat de sedimentació augmenta, incrementant així l'eficiència del transport fins al fons marí (Armstrong et al., 2009; Iversen i Ploug, 2010; Smetacek et al., 2012). Per exemple, els fluxos dominats per pellets fecals del zooplàncton assoleixen velocitats de més de 1.000 m d^{-1} (Turner, 2015). En canvi, els processos de fragmentació i remineralització de partícules disminueixen la magnitud dels fluxos cap a indrets més profunds (Weber et al., 2016; Briggs et al., 2020).

Mida de gra	Taxa de sedimentació aproximada m/s	Temps transcorregut per decantar 4 km en la columna d'aigua dies	Distància horitzontal recorreguda amb una corrent de 5 cm/s km
Sorra molt fina (63-125µm)	$9{,}8 \times 10^{-3}$	4,7	20,4
Llim (63-4 µm)	$9{,}8 \times 10^{-5}$	470	2.040
Argila (<4 µm)	$9{,}8 \times 10^{-7}$	47.000	204.000

Taula 1.1. Taxa de sedimentació de les partícules i distància recorreguda. El taxes estan basades en l'assumpció de que les partícules són esfèriques i que presenten una densitat similar al quars. Extret de Duxbury, et al. (2002).

[2] Terme que engloba agregats amorfs de mida relativament gran i origen biològic.

L'advecció transporta les partícules en suspensió dins la columna d'aigua i a prop del fons marí. El transport es produeix mentre la velocitat del corrent sigui suficient per mantenir la partícula en suspensió. El transport lateral de partícules es dona de forma generalitzada als marges continentals, sovint associat amb processos capaços d'erosionar i/o resuspendre els sediments del fons marí, amb la qual cosa aquests contribuiran addicionalment al conjunt (*"pool"*) de partícules en suspensió a la columna d'aigua (Heussner et al., 2006), facilitant així un major transport al llarg del marge continental i més enllà (Puig et al., 2014). En última instància, el conjunt de partícules tendiran a dipositaran al fons marí amb la seva càrrega associada d'elements químics i compostos diversos. El transport advectiu, o lateral, és un procés altament rellevant d'introducció de partícules refractàries cap a l'interior de l'oceà.

De forma general, a mesura que les partícules sedimenten es produeix una disminució de la concentració a la columna d'aigua, essent també comú un increment de la mateixa a prop del fons degut als processos advectius i a la resuspensió (Fig. 1.3a). També canvien les proporcions dels components i elements associats als fluxos (Fig. 1.3b), i la composició del CO (Fig. 1.3c), entre altres variacions (Hedges et al., 1997; Wakeham et al., 1997; Dymond, 1984).

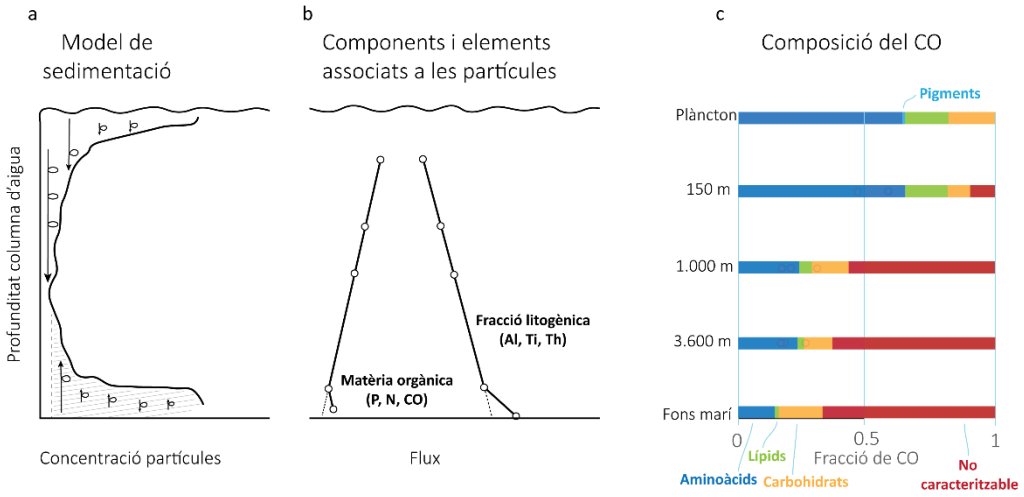

Figura 1.3. (a) Model conceptual de tres capes de la distribució de les partícules en suspensió a la columna d'aigua i els fluxos associats, amb dues fonts principals: un flux primari des de la capa superficial i un flux resuspès des del fons marí (Gardner et al., 1985). (b) Variació vertical dels fluxos dels components i d'alguns elements associats a les partícules en suspensió (Dymond, 1984). (c) Variacions en la composició del CO al llarg de la columna d'aigua (Wakeham et al., 1997).

Un dels aspectes més rellevants del fluxos de partícules és la seva interacció amb el CO. La transformació de les partícules dins la columna d'aigua està directament relacionada amb l'anomenada "bomba biològica del carboni", concepte que incorpora els processos involucrats en la producció, l'enfonsament i la remineralització del carboni en els oceans. En el cas del CO, l'eficiència de la seva exportació depèn de la transferència vertical i del balanç entre els diferents processos que transformen les partícules (Wang i Fennel, 2022). Bona part del CO fixat durant la fotosíntesi (~50 Pg CO) (Middelburg, 2019), i transferit al zooplàncton a través de la cadena tròfica, és reciclat i remineralitzat a la part més superficial de l'oceà. De fem, hom calcula que

només un 20%, aproximadament, del carboni de l'oceà superficial s'escapa de la zona eufòtica (Middelburg, 2019). Els processos de fragmentació i remineralització de les partícules són especialment actius a la zona mesopelàgica (~100-1,000 m) (Fig. 1.4; Lam i Marchal, 2015). Aquests processos comporten la pèrdua de compostos làbils i l'increment relatiu de la fracció del CO no caracteritzable a nivell molecular, causant així la modificació de la composició de la MO (Fig. 1.3c) (Lee et al., 2004). Per altra banda, hi ha diversos mecanismes, com la sorció i la protecció física per formació d'agregats, que afavoreixen la preservació del CO durant l'enfonsament de les partícules (De la Rocha i Passow, 2007). S'estima que cada any s'exporten 5-20 Pg CO cap a l'oceà profund (Henson et al., 2011). De tot aquest material, si fa no fa el 90% haurà estat regenerat abans d'arribar al fons, on se n'acumularà una part a llarg termini, que hom estima en ~ 2 Pg CO (Middelburg, 2019).

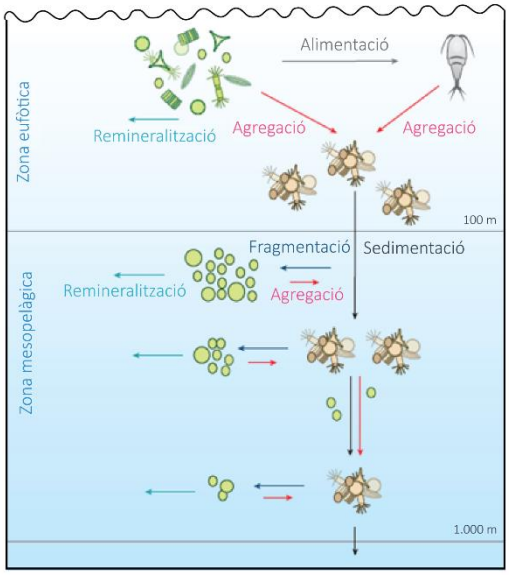

Figura 1.4. Esquema del transport vertical de partícules i CO, i dels processos que modulen l'eficiència de la seva exportació des dels nivells superficials de l'oceà cap als profunds (Lam i Marchal, 2015).

Per altra banda, és habitual que es produeixen diversos cicles de deposició, resuspensió, transport i, de nou, deposició en el fons marí. La preservació de la MO dipositada és afavorida per l'associació amb les partícules minerals —principalment per agregació i sorció—, doncs la mateixa ofereix protecció física front a la degradació oxidativa (Hedges i Keil, 1995; Bruni et al., 2022).

1.3. Metalls i metal·loides en el medi marí

Els metalls i metal·loides són presents de manera natural en el medi marí. Ja s'ha introduït que alguns són essencials per la vida marina atès que intervenen en diverses funcions biològiques (Morel i Price, 2003; Twining i Baines, 2013). Dit d'una altra manera, regulen el cicle del carboni.

Tot i això, en altes concentracions hom els considera contaminants, doncs poden ser tòxics pels organismes marins (Anderson, 2020).

Des de la dècada dels 80 i fins a dia d'avui, la necessitat de comprendre el cicle dels metalls (i metal·loides) en el medi marí ha impulsat nombrosos projectes de recerca, tant d'àmbit europeu com mundial, alguns dels quals de gran abast com JGOFS i CLIVAR. En els últims anys, projectes com GEOTRACES han accelerat el progrés en el coneixement dels cicles dels elements traça i els seus isòtops en el medi marí (Anderson, 2020).

En aquesta Tesi s'investiguen un seguit de metalls (Al, Fe, Ti, Co, Cu, Mn, Ni, Pb i Zn) (d'ara en endavant, MT) i un metal·loide, l'As. S'usa el terme "traça" per emfatitzar que llur concentració a l'oceà és inferior a 0.5 µM (Millero, 2013).

1.3.1. Fonts i formes d'ocurrència

Els metalls que hi ha a l'oceà provenen de fonts diverses, tant naturals —com l'erosió de l'escorça terrestre o les erupcions volcàniques— com antropogèniques. Qualsevol de les fronteres de l'oceà amb la litosfera, l'atmosfera, la hidrosfera, la criosfera i la biosfera constitueix una via potencial d'entrada de metalls i metal·loides (Geibert et al., 2018). Els sediments del fons marí també han estat reconeguts com una font de metalls dissolts a la columna d'aigua (Laës et al., 2007; Noble et al., 2012; Rusiecka et al., 2018).

Una cop dins l'oceà, els metalls interactuen amb els diversos components de les partícules, des dels organismes vius fins els detritus orgànics i minerals. La forma en que es trobi el metall en la matriu aquosa afectarà a la seva reactivitat amb les altres matrius i, per tant, a la seva biodisponibilitat i distribució en la columna d'aigua (Anderson, 2020).

De forma general, els metalls traça es troben en forma divalent (Pb^{2+}, Cu^{2+}, Zn^{2+}, Cd^{2+}), exceptuant les formes oxidades d'alguns metalls, com el Fe III o el Cr III o IV i els oxianions d'alguns metal·loides (per exemple, l'As presenta una valència III o VI depenen de les condicions redox). La majoria de metalls i metal·loides, excloent els alcalins, no estan presents en forma lliure en el medi aquós, sinó que formen complexos estables amb ions inorgànics, com ara el Cl^- o el CO_3^{-2}, i amb compostos orgànics dissolts, com ara lligands o quelats solubles molt estables i molècules orgàniques complexes. Els lligands, en especial els d'origen orgànic, són un grup poc caracteritzat de macromolècules d'orígens ben diversos i juguen un paper important en la biodisponibilitat dels metalls, incrementant o reduint la capacitat dels organismes marins per assimilar-los (Bruland, 1989), i regulant la interacció amb les partícules i llur sedimentació (Rue i Bruland, 1995). Els metalls associats a la fracció particulada poden ocórrer dins l'estructura cristal·lina dels minerals, estar bioassimilats pels organismes, restar retinguts a la interfase aigua-sòlid en forma de (co)precipitats o adsorbits a la superfície dels minerals (Bruland i Lohan, 2004) (Fig. 1.5).

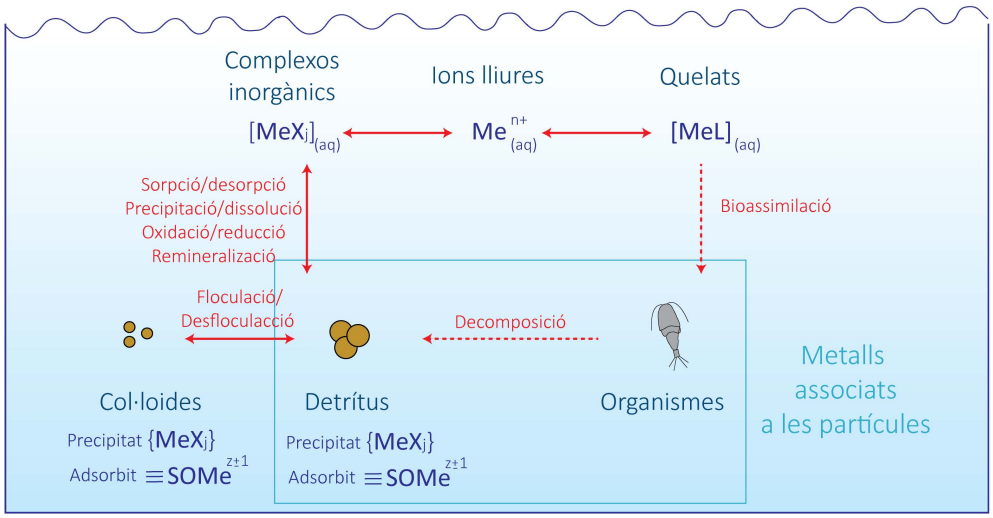

Figura 1.5. Representació esquemàtica de la partició dels metalls traça en diferents compartiments en el medi marí. Me fa referencia a "metall", X indica un lligand inorgànic i L un lligand orgànic (basat en Chester (2002)).

1.3.2. Rellevància com a contaminants

La industrialització dels darrers segles i la globalització de les darreres dècades han contribuït en gran manera a la introducció d'una enorme quantitat i diversitat de productes i elements químics en els ecosistemes del planeta, alterant els valors naturals i generant, per tant, situacions de contaminació notablement esteses. La recerca en contaminació marina s'ha centrat tradicionalment en l'estudi de substàncies i elements considerats perillosos pels organismes i la salut humana (Strain et al., 2022). Una de les conseqüències de la contaminació d'origen múltiple és la formació de barreges complexes de substàncies i elements ben diferents, com POPs, microplastics, productes químics usats en medicina, pesticides, fertilitzants, i també metalls i metal·loides (Dahms, 2014; Pedreira et al., 2018; Azaroff et al., 2020; de Haan et al., 2022; Pell et al., 2021; Liu et al., 2021).

Entre els metalls traça que s'estudien en aquesta Tesi, n'hi alguns (Co, Cu, Ni, Pb, Zn) de gran importància econòmica. Aquesta és la raó per la qual hom els ha extret massivament de l'escorça terrestre, els ha tractat i usat en nombroses aplicacions convertint-los en productes útils, els quals han estat, finalment, descartats al final de la seva vida útil. Al llarg de tot aquest circuit s'han anat alliberant fraccions més o menys elevades d'aquests elements (Taula 1.2). Hi ha múltiples activitats humanes, com ara la mineria, la indústria i l'agricultura, que poden fer augmentar les concentracions de metalls a l'ambient marí, tant per descàrrega directa com a través de la interacció amb altres matrius, com l'atmosfera, les xarxes fluvials i les xarxes de gestió de residus urbans (Landrigan et al., 2020).

Metall/metal·loide	Usos	Fonts de contaminació relacionades
As	Elaboració d'aliatges, pigments, tèxtils, protectors de fusta, pesticides	Mineria, foneries, pesticides, mala gestió de residus
Co	Bateries, dispositius electrònics, ceràmica, pintures, cosmètics	Mineria, foneries, combustió de carbó, mala gestió de residus
Cu	Cables, canonades, pesticides i fertilitzants, dispositius electrònics	Mineria, foneries, pesticides, fertilitzants, mala gestió de residus
Ni	Recobriments, bateries, piles, dispositius electrònics, monedes	Mineria, foneries, combustió de gasolines i gasoils, combustió de carbó, incineració de residus, mala gestió de residus, abocament d'aigües residuals
Pb	Bateries, pigments, municions, revestiment de cables	Mineria, foneries, combustió de gasolines i gasoils, combustió de carbó, insecticides i herbicides, incineració de residus, mala gestió de residus
Zn	Galvanitzats, productes farmacèutics i cosmètics, fertilitzants	Mineria, foneries, combustió de carbó, incineració de residus, mala gestió de residus

Taula 1.2. Usos il·lustratius d'alguns metalls i metal·loides i fonts, productes i activitats associades amb el seu alliberament al medi natural com a contaminants.

1.3.3. Interaccions amb els fluxos de partícules

Tot i no ser components dominants en els fluxos de partícules, els metalls traça s'associen amb les partícules en suspensió, fet que és altament rellevant pel cicle dels mateixos (Lam i Marchal, 2015). Mercès a la seva incorporació a les partícules, els metalls poden ser transportats cap a l'oceà profund a través dels processos de sedimentació. La dissolució dels components terrígens és una font de metalls per la fracció dissolta (Homoky et al., 2016). Els metalls dissolts poden ser utilitzats pels organismes marins, com ara el fitoplàncton, per al seu creixement i reproducció (Twining i Baines, 2013). L'exportació de les partícules en suspensió cap a aigües profundes afavoreix que els elements bioactius (Fe, Cd, Co, Cu, Mn, Ni, Zn) siguin regenerats a formes dissoltes a partir de processos de remineralització (cf. aptat. 1.2.2) (Morel i Price, 2003; Twining i Baines, 2013; Moore et al., 2013). A més, els minerals terrígens i autigènics poden sedimentar metalls i metal·loides (Fe, As, Co, Cu, Mn, Ni, Pb) via un increment de la densitat del llast o per processos de remoció (en anglès, *scavenging* i *co-scavenging*[3]) (Bruland i Lohan, 2004). Aquest

[3] El concepte de *scavening* fa referència a l'acció combinada d'un procés d'adsorció d'un component en una fase sòlida seguit de la decantació o sedimentació de la mateixa (Turekian, 1977).

últim procés encara està poc estudiat (Tagliabue et al., 2016), i hi ha publicacions recents que demostren que és reversible (Lanning et al., 2023).

Tanmateix, la resuspensió i els processos erosius poden retornar els metalls a la columna d'aigua (Kalnejais et al., 2007), mentre els que es troben en fase dissolta a l'aigua de porus degut a la dissolució reductiva poden arribar al fons marí per difusió (Klar et al., 2017). Finalment, i després de llargs períodes de temps, els metalls poden quedar atrapats a les roques que en algun moment varen ésser sediments marins.

1.4. La mar Mediterrània

1.4.1. Fisiografia

La mar Mediterrània és una conca semitancada que cobreix una extensió d'aproximadament $2{,}47 \cdot 10^6$ km^2, representant el 0,7% de la superfície dels oceans. Comunica per el seu extrem occidental amb l'oceà Atlàntic a través del estret de Gibraltar, el qual té una amplada de 14,4 km, i està limitada per tres continents: Àsia, Àfrica i Europa. La mar Mediterrània està formada per dues conques principals, l'occidental i l'oriental, separades per l'estret de Sicília. Cadascuna d'elles conté diverses subconques i mars regionals: mar d'Alborán, mar Balear, mar Liguro-Provençal, mar Tirrena, mar Jònica, mar Adriàtica, mar Egea i mar de Llevant.

Els marges continentals Mediterranis presenten característiques ben diverses. L'amplada de les plataformes continentals és molt variable, amb marges continentals amb una plataforma gairebé inexistent fins a plataformes de 200 km, per exemple, cobrint bona part de la mar Adriàtica. Els talussos presenten morfologies i extensions heterogènies, depenen dels processos tectònics i la acumulació de sediments (Miramontes et al., 2023). Els marges Mediterranis tenen una major densitat de canyons submarins respecte a altres regions del oceà (Harris i Whiteway, 2011). De manera general, els canyons es caracteritzen per ser més dendrítics, de menor àrea i longitud que en altres marges del món (Harris i Macmillan-Lawler, 2015). Per últim, la plana batial cobreix bona part de la superfície de la mar Mediterrània, i presenta àrees caracteritzades per pendents menors d'un grau i àrees dominades per canvis topogràfics, com la presència de monts (en anglès, *seamounts*) (Miramontes et al., 2023).

1.4.2. Masses d'aigua i circulació general

La dinàmica oceanogràfica de la mar Mediterrània està determinada per la circulació termohalina que recorre la conca en sentit antihorari, controlada per l'entrada aigua superficial d'origen atlàntic a través de l'estret de Gibraltar, els vents, l'evaporació, la formació i enfonsament d'aigües denses, i l'entrada d'aigua dolça (Millot i Taupier-Letage, 2005; López-Jurado et al., 2005; Canals et al., 2006; Schroeder et al., 2012; Durrieu de Madron et al., 2013). La Mediterrània està sotmesa a una alta variabilitat, tant espacialment com estacionalment. A grans trets, la circulació està determinada un sistema tricapa, amb tres masses d'aigua estratificades: la superficial, la intermèdia i la profunda (Millot i Taupier-Letage, 2005; Schroeder et al., 2012) (Taula 1.3). L'aigua

atlàntica (AW, de l'anglès *Atlantic Water*) prové de l'oceà Atlàntic i penetra a la Mediterrània a través de l'estret de Gibraltar, estenent-se des de la superfície fins a 150-200 m de profunditat. A mesura que es desplaça per la Mediterrània aquesta aigua es va modificant, augmentant la seva temperatura i salinitat, i passa a anomenar-se aigua atlàntica modificada (MAW, de l'anglès *Modified Atlantic Water*). Les capes intermèdia i profunda estan ocupades per masses d'origen mediterrani. Entre 200 i 600 m se situa l'Aigua Intermèdia Llevantina (LIW, de l'anglès *Levantine Intermediate Water*), formada a la conca oriental, com indica el seu nom, i caracteritzada per una temperatura i una salinitat elevades (Taula 1.3) (Parrilla et al., 1986; Millot i Taupier-Letage, 2005). A l'hivern, a la conca occidental, es forma l'Aigua Intermèdia de la Mediterrània Occidental (WIW, de l'anglès *Western Intermediate Water*), que ocupa la part superior de la capa intermèdia (Vargas-Yáñez et al., 2012). La WIW es forma per pèrdua de calor i evaporació al sector nord de la conca occidental, inclosa la plataforma dels canals balears (Vargas-Yáñez et al., 2012; Vargas-Yáñez et al., 2017). Quan el refredament, l'evaporació i, en definitiva, la densificació de les aigües superficials són especialment intensos es forma l'Aigua Profunda de la Mediterrània Occidental (WMDW, de l'anglès *Western Mediterranean Deep Water*) (Salat et al., 2002), associada a processos de cascadeig (en anglès, *cascading*) d'aigües denses de plataforma i de convecció de mar obert a la regió del golf de Lleó (Canals et al., 2006; Durrieu de Madron et al., 2013). La formació d'aigües denses també té lloc en altres indrets de la Mediterrània, com les mars Tirrena, Adriàtica i Egea (Schroeder et al., 2008; Canals et al., 2009).

Massa d'aigua	Temperatura (°C)	Salinitat (psu)	Referencia
MAW	14-15	36.5-38.3	Millot, 1999
LIW	12.89-12.9	38.47–38.49	
WIW	11.5–13	37.7–38.3	Vargas-Yáñez et al., 2017
WMDW	12.89-12.97	38.47-38.49	

Taula 1.3. Característiques de les principals masses d'aigua de la Mediterrània occidental. MAW: Aigua Atlàntica Modificada. LIW: Aigua Intermèdia Llevantina. WIW: Aigua Intermèdia de la Mediterrània Occidental. WMDW: Aigua Profunda de la Mediterrània Occidental. Les abreviacions dels noms de les masses d'aigua provenen de l'anglès (cf. text principal, més amunt, i Abreviacions).

1.5. Els golfs de Vera i Almeria

La zona d'estudi d'aquesta Tesi està situada al marge sud-oriental ibèric, dins de la Mediterrània occidental. Abraça tres segments, el de Mazarrón al nord i l'est (també conegut com "escarpament de Mazarrón", el de Palomares i la seva continuació cap al sud a la part central, i el d'Almeria al sud i l'oest, ja dins la mar d'Alborán, que és la subconca mediterrània que marca la transició oceanogràfica entre l'oceà Atlàntic i la mar Mediterrània (Fig. 1.6). Els dos primers segments s'inclouen dins el golf de Vera, entès en sentit ampli, mentre que el tercer segment correspon al golf d'Almeria. La distància d'un extrem a l'altre, seguint la isòbata de 200 m és d'aproximadament 307 km.

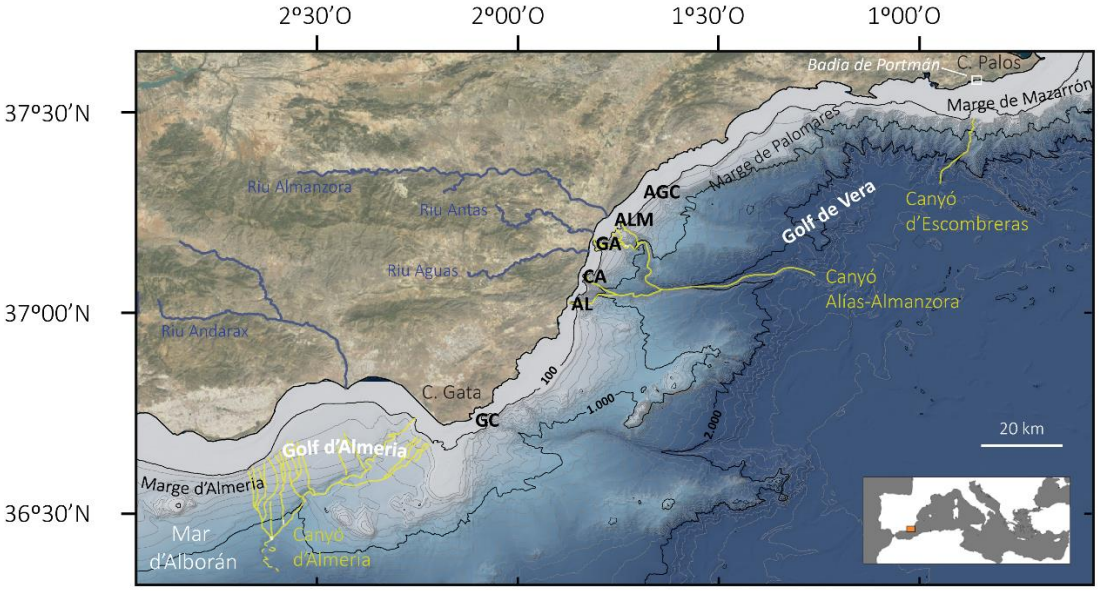

Figura 1.6. Mapa batimètric dels golfs de Vera i d'Almeria on s'indiquen els tres segments de marge continental i el traçat dels tres canyons submarins (en groc) investigats en aquesta Tesi, i talls batimètrics dels marges. En el cas del sistema Alías-Almanzora s'indiquen les branques principals (AL: Alias, CA: Cabrera, GA: Garrucha, i ALM: Almanzora). També s'assenyala la posició de les capçaleres dels canyons d'Águilas (AGC), Cartagena (C) i Gata (GC), així com el traçat del rius principals de la regió i la situació de la badia de Portmán. Batimetria del *Instituto Español de Oceanografía* (IEO).

1.5.1. Relleu submarí

Els tres segments adjacents de marge continental objecte d'aquest estudi són força diferents. El marge de Mazarrón, d'orientació E-O, és molt abrupte i té una plataforma que s'estreny cap a l'oest, des de 13 km a menys de 4 km (Lobo et al., 2014) (Fig. 1.6). El talús està excavat per una xarxa densa de canyons submarins que s'inicien aproximadament a 200 m de profunditat i s'estenen fins al glacis (Acosta et al., 2013). El marge de Palomares, a l'oest de l'anterior, té una orientació general NE-SO (Fig. 1.6). L'ample de la plataforma és de menys de 11 km (Pérez-Hernández, 2014) i el cantó se situa entre 120 i 170 m de fondària. La morfologia del talús és complexa degut a la presència de *seamounts* i canyons submarins, com els d'Águilas, el sistema Alías-Almanzora i el de Gata (Pérez-Hernández et al., 2014; Ercilla et al., 2022). Al marge d'Almeria, al sud, la plataforma té una amplada d'entre 6 i 12 km (García et al., 2006) i el seu límit extern és a 100-120 m de profunditat (Fig. 1.6). La plataforma externa i el talús estan entallats per un seguit de valls submarines que conformen l'anomenat "sistema turbiditic d'Almeria" (en anglès, *Almeria Turbidite System*), que és el més gran del seu tipus a tota la mar d'Alborán (Estrada et al., 1997; García et al., 2006; Vázquez et al., 2015).

Els canyons submarins objecte d'estudi en aquesta Tesi són, en concret i de nord a sud, el canyó d'Escombreras, al marge de Mazarrón, el sistema de canyons Garrucha-Almanzora —que és part del sistema Alías-Almanzora— al marge de Palomares, i el canyó d'Almeria al marge homònim (Fig. 1.6).

El lector podrà trobar més detalls sobre aquests canyons submarins a l'apartat 3.1.2.

1.5.2. Hidrografia

La circulació general de l'àrea d'estudi en sentit ampli està determinada pel flux superficial d'aigües atlàntiques provinents de l'oest, i pel flux intermedi i profund d'aigües mediterrànies procedents de l'est (Fig. 1.7). Al golf de Vera, la circulació superficial està influïda pel Corrent del Nord, que circula paral·lelament a la costa i prové de la Mediterrània nord-occidental. A la mar d'Alborán, el flux d'AW superficial (cf. aptat. 1.4.2) segueix una trajectòria marcadament sinuosa que dona lloc a dos girs anticiclònics no permanents coneguts com a gir occidental i gir oriental (WAG i EAG, de l'anglès *Western Alboran Gyre* i *Eastern Alboran Gyre*, respectivament) (Tintore et al., 1988; Heburn i La Violette, 1990; Millot, 1999). Quan l'AW es troba amb la MAW provinent del nord de la conca occidental es produeix un corrent baroclínic semipermanent conegut com front d'Almeria-Orà (AOF, de l'anglès *Almeria-Oran Front*), el qual s'estén de nord-oest a sud-est des de la costa espanyola fins l'algeriana (Tintore et al., 1988). Des del punt de vista oceanogràfic, hom considera que l'AOF marca el límit oriental de la mar d'Alborán. La seva situació precisa està controlada per la posició geogràfica i la força de l'EAG, formant-se normalment durant el període d'estiu-tardor (Vargas-Yáñez et al., 2002; Renault et al., 2012). Finalment, les masses d'aigua mediterrànies intermèdies i profundes circulen cap a l'estret de Gibraltar seguint el marge continental espanyol (Millot, 1999), tot i que la seva evacuació cap a l'oceà Atlàntic està limitada per l'efecte llindar imposat per la batimetria de l'estret de Gibraltar, molt més som que les parts més pregones de la mar Mediterrània, inclosa la mar d'Alborán (Fig. 1.7). És probable que, degut a aquest efecte, les aigües més pregones que assoleixen la mar d'Alborán recirculin cap a l'est, a diferents nivells i des de diferents indrets, seguint el marge nord-africà.

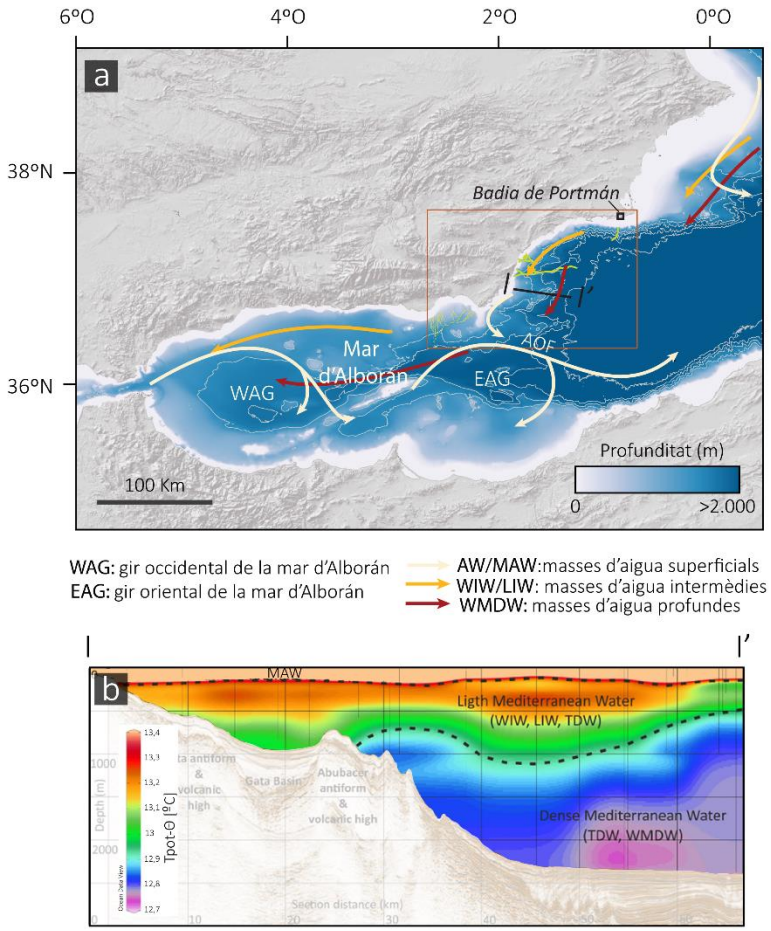

Figura 1.7. (a) Circulació general a la mar d'Alborán i sectors propers a l'est i el nord-est damunt una base batimètrica. (b) Tall hidrogràfic del marge continental de Palomares (golf de Vera) fins la plana batial algeriana (Ercilla et al., 2022). TDW: Aigua Profunda de la mar Tirrena. Pel que fa als acrònims no especificats al peu de figura, vegis el text principal, més amunt, i Abreviacions. Per a més informació sobre les masses d'aigua vegis l'apartat 1.4.2.

1.5.3. Fonts de partícules

L'alta productivitat de la zona d'estudi està estretament lligada a les estructures hidrogràfiques (WAG, EAG i AOF), que en determinen la seva distribució espacial i temporal (Garcia-Gorriz i Carr, 2001). De fet, la mar d'Alboran és considerada una de les regions més productives de la mar Mediterrània (Lazzari et al., 2011). A favor d'aquestes estructures es produeixen afloraments (en anglès, *upwellings*) d'aigües profundes, més fredes i carregades de nutrients, que afavoreixen la producció primària en els nivells superficials. Aquest fenomen és induït pel règim de vents i per les fluctuacions meridionals del corrent en raig de l'Atlàntic (en anglès, *Atlantic Jet*) (Sarhan et al., 2000; Baldacci et al., 2001). S'han descrit, però, altres processos afavoridors de la producció primària, com la desestratificació de les masses d'aigua després de l'estiu (Garcia-Gorriz i Carr, 2001), i l'arribada ocasional de nutrients per descàrrega fluvial (Fabres et al., 2002). S'ha observat que aquests esdeveniments de fertilització i augment subseqüent de la producció primària comporten increments dels fluxos de partícules biogèniques al marge continental i a la conca de Alborán (Fabres et al., 2002; Sanchez-Vidal et al., 2004; Hernández-Almeida et al., 2011).

El clima semiàrid de la regió (< 400 mm yr^{-1}) fa que les descàrregues fluvials siguin puntuals (AEMET, 2011). Aquesta situació és particularment accentuada al marge de Mazarrón, on no hi desguassa cap riu mínimament significatiu. La migradesa de les aportacions de sediment (Lobo et al., 2014) promou la transparència de l'aigua i la formació de extenses praderies de fanerògames a la franja costanera (Maldonado i Zamarreño, 1983). Les principals aportacions terrígenes a l'àrea d'estudi provenen dels rius Almanzora, Antas, Aguas i Alías al marge de Palomares, i del riu Andarax al marge d'Almeria (Fig. 1.6). Presenten un caràcter torrencial, lligat a episodis de tempesta, durant els quals poden transportar-se grans quantitats de sediment que, a l'entrar al mar, generen grans plomalls de partícules suspensió en superfície i també en nivells intermedis i de fons (Liquete et al,. 2005). Aquests episodis es produeixen, sobretot, a la tardor (Fabres et al., 2002), i afavoreixen la formació de petits prodeltes davant les goles (Sanz et al., 2002). La seva influència s'estén a la plataforma continental en sentit més ampli, on s'ha pogut constatar que el transport de sediment està, efectivament, dominat per les tempestes (Lobo et al., 2014; Durán et al., 2018). S'ha comprovat també que una part del sediment pot ésser transportat pels corrents més enllà de la plataforma continental, tant per transport de fons turbulent com en suspensió. Així, al canyó submarí de Garrucha hom hi ha identificat formes del relleu atribuïbles a corrents de terbolesa associades a riuades fortes i episodis de tempesta (Puig et al., 2017). També s'han identificat increments en els fluxos de partícules en el marge continental i a la conca profunda a rel d'aquesta mena d'episodis (Fabres et al., 2002; Sanchez-Vidal et al., 2004).

1.6. El dipòsit de residus miners de la badia de Portmán

La badia de Portmán està situada a la costa de Múrcia, entre la ciutat de Cartagena, a l'oest, i el cap de Palos, a l'est (Fig. 1.8a). Pertany, per tant, al marge de Mazarrón (Fig. 1.6). Actualment, la badia és reblerta per residus miners, l'abocament dels quals provocà un desplaçament de la línia de costa de gairebé 600 m mar endins (Fig. 1.8b). La configuració actual de la badia és, doncs, una herència de l'activitat minera desenvolupada al proper districte miner de Cartagena-La Unión entre 1957 i 1990, i del retreballament per la dinàmica marina dels materials abocats. Els residus provenen de l'explotació a cel obert de dipòsits de sulfurs miocens per a extreure'n Pb i Zn principalment. Fou l'any 1957 quan s'inicià l'abocament directe al mar dels residus generats a la planta de tractament per flotació diferencial "Lavadero Roberto", propera a la costa (Fig. 1.8c). Els residus, enriquits en diversos metalls i metal·loides (Fe, As, Cu, Pb i Zn), van reblir la badia i es van estendre's més d'1,5 km mar endins sobre la plataforma continental adjacent (Oyazun et al., 2013; Cerdà-Domènech, 2020; Baza-Varas et al., 2022), de manera que l'acumulació resultant té una part emergida i una altra, molt més extensa i voluminosa, submergida.

Del dipòsit de la badia de Portmán en sentit estricte encara hi ha relativament poca literatura científica, i especialment sobre l'extensió submergida (Baza-Varas, 2023). Entre els estudis que s'han ocupat de l'estructura superficial del dipòsit, de la seva caracterització geoquímica, dels intercanvis amb l'ambient circumdant, i de la biodisponibilitat de metalls i metal·loides cal citar Cesar et al. (2009), Alorda-Kleinglass et al. (2019), Cerdà-Domènech (2020), Cerdà-Domènech et al. (2020), Baza-Varas (2023), i Baza-Varas et al. (2022 i 2023).

Els residus abocats al mar després del processament de les menes per extreure'n els metalls d'interès, encara contenen valors màxims de 2,755 μg g^{-1} d'As, 1,433 μg g^{-1} de Pb i 1,007 μg g^{-1} de Zn (Baza-Varas et al., 2022). A 55 m de profunditat, prop del límit extern de l'extensió submarina del dipòsit els nivells de metalls són encara considerables, entre 80 i 647 μg g^{-1} de Pb, i entre 98 i 706 μg g^{-1} de Zn (Baza-Varas et al., 2022).

Els nivells superficials de l'extensió marina del dipòsit presenten un gradient espacial en la concentració de metalls, trobant-se les més elevades a prop del punt principal de descàrrega situat a Punta Galera, a la sortida de la badia, cap al sud (Cerdà-Domènech, 2020). Els testimonis de sediment extrets de la plataforma interna enregistren un brusc canvi de fàcies i un increment del contingut de metalls que marca l'inici dels abocaments (Cerdà-Domènech, 2020; Baza-Varas et al., 2022). A partir del cessament dels abocaments, el contingut de metalls i metal·loides va disminuint cap a sostre dels testimonis fins arribar a la capa corresponent al fons marí actual (Baza-Varas, 2022; Cerdà-Domènech, 2020). La part més superior dels residus miners ha estat retreballada per la dinàmica marina des de l'any 1990 fins l'actualitat, la qual cosa ha provocat la resuspensió i el transport selectiu de partícules, així com la formació de dipòsits residuals i de barreja amb materials més recents (Cerdà-Domènech, 2020; Baza-Varas, 2022). Segons Cerdà-Domènech (2020), els centímetres superiors del registre sedimentari, atribuïts al període posterior als abocaments, contribueixen amb menys del 0,05% a la massa total de Pb, Zn i As en el dipòsit de residus, estimat en uns 57 milions de tones (Manteca et al., 2014). El mateix autor assenyala que aproximadament 8,6 km^2 del dipòsit de la plataforma té concentracions elevades de metalls, assolint nivells perillosos d'acord amb les *Sediment Quality Guidelines* (SQG) (Comisión Nacional de Estrategias Marinas, 2015). També observa un flux continu de metalls cap al fons marí, que atribueix a dos possibles processos: (i) l'arribada de partícules des de la part emergida del dipòsit de residus, i (ii) l'extracció de metalls dissolts a la columna d'aigua provinents de descàrregues d'aigües subterrànies (DAS) des de l'interior del dipòsit —tal i com proposen Alorda-Kleinglass et al. (2019)—, amb deposició posterior al fons marí. Per altra banda, l'experiment de resuspensió dels sediments del fons descrit per Bourrin et al. (2021) mostra que les pertorbacions del fons marí generen un increment de les partícules en suspensió i de la concentració de certs metalls (Fe, As i Pb), la qual es manté en el temps durant, al menys, 3 hores després de la pertorbació.

Diversos treballs han estudiat els efectes de l'acumulació de metalls en la biota a l'àrea de Portmán (Auernheimer i Chinchon, 1997; Martínez-Gómez et al., 2012; Llull et al., 2017; Benedicto et al., 2008; Mestre et al., 2017; Cesar et al., 2004, 2009; Gambi et al., 2020). Recentment, Baza-Varas et al. (2022) han descrit la presència de restes de *Posidonia oceanica* en els nivells més inferiors del dipòsit de residus, la qual cosa evidencia l'enterrament ràpid dels herbeis d'aquesta fanerògama marina així que va iniciar-se l'abocament massiu.

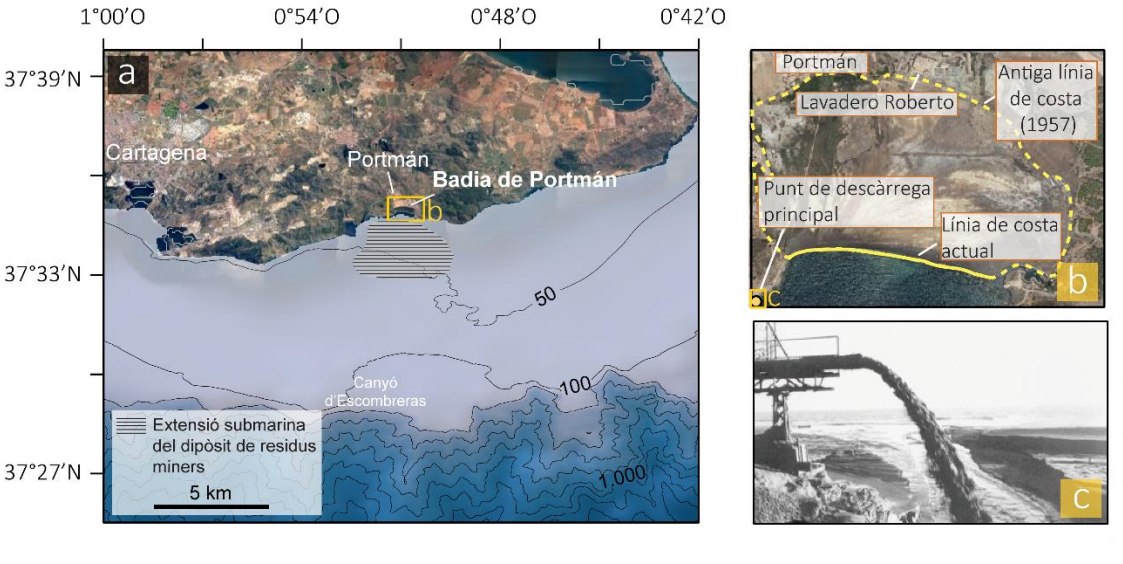

Figura 1.8. (a) Mapa batimètric general de la plataforma continental i de part del talús en les proximitats de la badia de Portmán. S'indica l'àrea aproximada de l'extensió submarina del dipòsit de residus miners de la badia de Portmán, a partir de Cerdà-Domènech (2020) i Baza-Varas (2023). ESC: canyó submarí d'Escombreras. Isòbates en m. (b) Fotografia que mostra el rebliment de la badia de Portmán (part exposada subaèriament). (c) Fotografia de l'abocament de residus mitjançant una canonada a Punta Galera. Les imatges (b) i (c) són del Ilustre Colegio Oficial de Geólogos.

Capítol 2

Metodologia

Adquisició de dades in situ i mostratge

- Realització de perfils hidrogràfics
- Desplegament de línies instrumentades fondejades
- Obtenció de mostres de sediment mitjançant testificador múltiple

Anàlisi de les mostres

- Tractament general
- Mida de gra
- Anàlisi de la composició elemental i del $\delta^{13}C$
- Òpal
- Biomarcadors derivats de la lignina i la cutina
- Metalls i metal·loides
- Composició isotòpica del Pb
- Altres anàlisis

Anàlisi de les dades

Paràmetres ambientals de bases de dades obertes i de sensors remots

2.1. Adquisició de dades in situ i mostratge

L'assoliment dels objectius d'aquesta Tesi passa per estudiar la distribució i la variació temporal dels fluxos de partícules i dels seus constituents principals i elements químics associats. Per aquesta raó, la Tesi es basa en gran mesura en l'anàlisi de partícules obtingudes mitjançant trampes de partícules instal·lades en línies instrumentades fondejades —també anomenades "ancoratges" i "fondejos"— (cf. aptat. 2.1.2). Un dels grans avantatges d'aquesta metodologia és que permet obtenir sèries temporal de les taxes de deposició de les partícules a diferents profunditats. En altres paraules, proporciona informació sobre els patrons temporals dels cicles biogeoquímics. La Tesi també es beneficia de la informació obtinguda a partir de l'anàlisi dels paràmetres fisicoquímics de la columna d'aigua, obtinguts mitjançant perfils hidrogràfics en estacions individuals i al llarg d'un transsecte (cf. aptat. 2.1.1), i del mostreig dels sediments del fons marí (cf. aptat. 2.1.3) (Fig. 2.1).

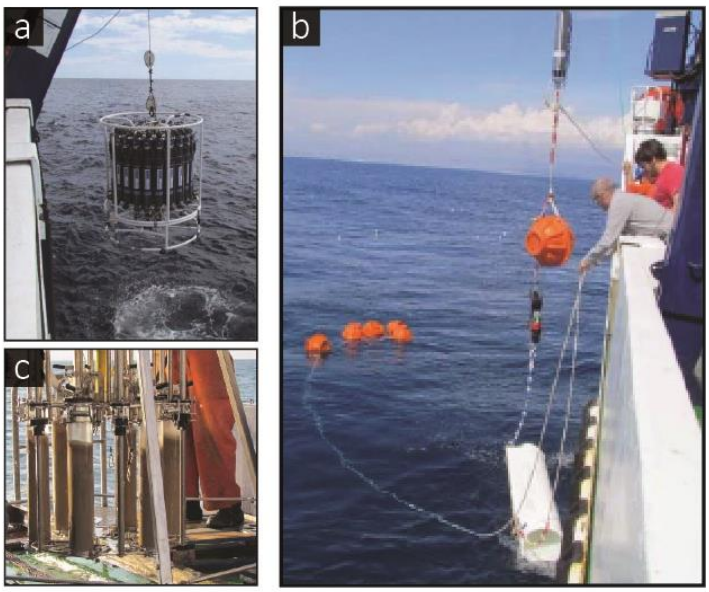

Figura 2.1. Fotografies il·lustratives dels treball efectuats durant la campanya NUREIEV-1. (a) Maniobra de recuperació de la roseta amb el CTD. (b) Maniobra de fondeig d'una línia instrumentada. S'observa una trampa de partícules (cilindre blanc), un correntòmetre (cilindre negre, gris i vermell) i un alliberador acústic (cilindre gris), a més d'un seguit de boies i cordam. (c) Testificador múltiple amb els tubs plens de sediment, a la coberta del vaixell.

El desplegament i la recuperació dels fondejos, la recollida de mostres de sediment i l'adquisició de dades oceanogràfiques s'efectuaren en diverses campanyes oceanogràfiques a bord del B/O Ángeles Alvariño, en el marc dels projectes de recerca NUREIEV i NUREIEVA. Dins el projecte NUREIEV s'efectuaren 3 campanyes: NUREIEV-1 (13-24 març 2015), NUREIEV-2 (29 agost al 5 de setembre 2015) i NUREIEV-3 (del 23 al 30 d'Abril 2016). Pel que fa al projecte NUREIEVA, hem utilitzat dades de la campanya NUREIEVA-MAR 1, efectuada entre el 27 de juny i el 10 de juliol de 2018 (Taules 2.1, 2.2 i 2.3) .

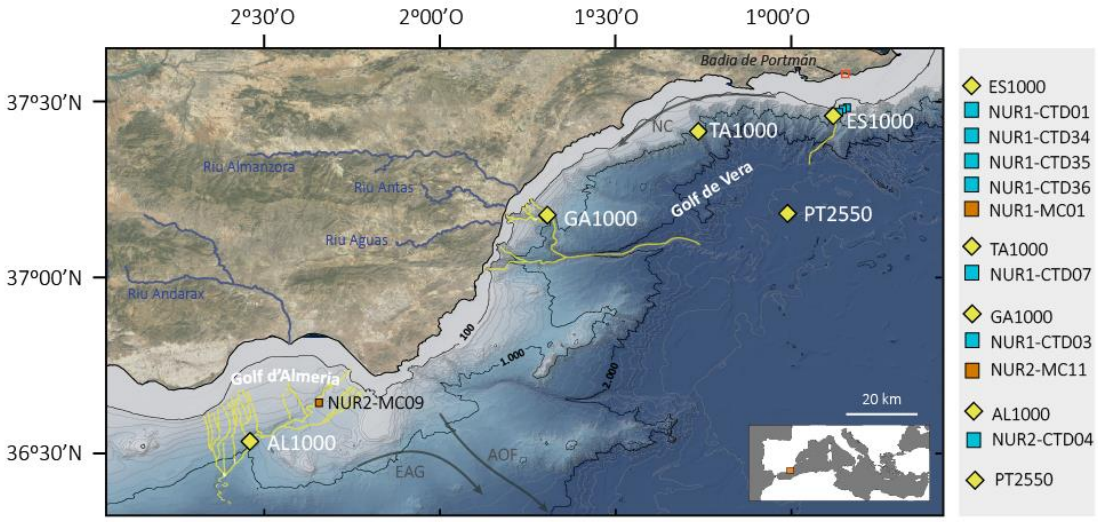

Figura 2.2. Mapa batimètric del golf de Vera i el golf d'Almeria, a la Mediterrània sud-occidental. Es mostra la ubicació dels fondejos (rombes grocs), dels perfils i del transsecte hidrogràfics (quadrats blaus) i dels testimonis de sediment (quadrats taronja). Varies d'aquests mesures i mostreigs queden emmascarats en el mapa pel símbol dels fondejos. Al marge dret de la imatge hi ha una llista de les mesures i mostreigs realitzats a cada estació principal, seguint els codis de color indicats. NUR1 i NUR2 fan referència a la campanya oceanogràfica en que s'efectuà el mostreig o mesura (NUREIEV-1 i NUREIEV-2). CTD fa referència a perfils hidrogràfics (perfils de CTD). M indica testificador múltiple (o *multicorer*). Els valors numèrics a la dreta de les sigles AL, ES, GA, PT i TA corresponen a la profunditat nominal dels fondejos a cadascuna d'aquestes estacions. AL: Almeria. AOF: Front d'Almeria-Orà (*Almeria-Oran Front*). EAG: Gir oriental d'Alborán (*Eastern Alboran Gyre*). ES: Escombreras. GA: Garrucha-Almanzora. NC: Corrent del Nord (*Northern Current*). PT: peu del talús. TA: talús obert. Les fletxes negres mostren, de forma esquemàtica, els elements principals de la circulació regional superficial (cf. aptat. 1.4.1). S'assenyala també el traçat dels canyons submarins investigats i la localització de la badia de Portmán (quadret vermell), d'on s'han obtingut els testimonis de gravetat (GC, *gravity corer*) GC55, GC19 i GC05 (cf. aptat. 2.1.3).

2.1.1. Realització de perfils hidrogràfics

L'instrument utilitzat fou un CTD (de l'anglès *Conductivity, Temperature, Depth*), el qual mesura, justament, i de manera continua i amb alta resolució, els paràmetres indicats durant la realització de perfils verticals descendents i ascendents. Les mesures de conductivitat s'utilitzen per calcular la salinitat de l'aigua. El càlcul de la profunditat s'obté mitjançant un sensor de pressió. La temperatura i la salinitat determinen la densitat de l'aigua i són, per tant, paràmetres essencials per a l'estudiar les masses d'aigua i el seu comportament. Generalment, els CTDs s'instal·len uns suports circulars, o rosetes, portadors d'un seguit d'ampolles per al mostreig seqüencial d'aigua a diferents fondàries. El CTD emprat a les campanyes oceanogràfiques efectuades fou un *Sea-Bird Electronics* model 991. A més dels sensors bàsics duia també un fluorímetre WET Labs ECO-AFL/FL per mesurar la concentració de Chl-a, pigment fotosintètic indicatiu de la producció primària; un sensor d'oxigen dissolt; i un sensor de terbolesa WET Labs ECO-NTU. A diferencia d'altres sensors de terbolesa, com el SeaPoint, el de WET Labs detecta la llum dispersa lateralment a 90º respecte a la llum làser que emet.

Els perfils de CTD utilitzats a la Tesi s'obtingueren durant la campanya NUREIEV-1 (Taula 2.1) a tocar de cadascun dels fondejos (Fig. 2.2). En el cas del fondeig del canyó d'Escombreras (ES1000), i després d'una tempesta, s'efectuà un transsecte de tres perfils que recobrí el curs alt del canyó. A la Tesi hem emprat les dades de conductivitat (salinitat), temperatura, profunditat, fluorimetria i terbolesa obtingudes mercès a la realització d'aquests perfils de CTD.

Codi	Coordenades		Localització	Profunditat (m)	Data de realització	Aptat. resultats
CTD 01	37°27,244' N	0°52,206' O	Canyó d'Escombreras	988	13/03/2015	3.1
CTD 07	37°24,617' N	1°15,408' O	Estació TA1000	963	14/03/2015	3.1
CTD 42	37°10,260' N	1°41,945' O	Sistema Garrucha-Almanzora	1.093	22/03/2015	3.1
CTD 43	36°31,700' N	2°31,943' O	Canyó d'Almeria	986	23/03/2015	3.1
CTD 34	37°28,687' N	0°50,677' O	Canyó dEscombreras	196	20/03/2015	3.1
CTD35	37°28,373' N	0°51,380' O	Canyó d'Escombreras	483	20/03/2015	3.1
CTD37	37°27,660' N	0°52,660' O	Canyó d'Escombreras	760	20/03/2015	3.1

Taula 2.1. Localització i dades dels perfils de CTD realitzats durant la campanya NUREIEV-1 utilitzats en aquesta Tesi. Vegis també la figura 2.2. Els resultats es presenten al subcapítol 3.1 de la Tesi.

2.1.2. Desplegament de línies instrumentades fondejades

Degut a la seva versatilitat, tant pel que fa al seu disseny com a la possibilitat de desplegar-los en indrets molt diversos durant períodes de temps que poden anar des de dies a més d'un any, els fondejos de línies instrumentades han estat àmpliament utilitzats per monitoritzar el medi marí i entendre millor el seu funcionament. Un fondeig consisteix en una línia ancorada al fons marí equipada amb un seguit d'instruments col·locats a diferents profunditats. Un conjunt de boies n'asseguren la flotabilitat dins la columna d'aigua i fan que es mantingui en posició vertical o gairebé. A l'extrem inferior de la línia s'hi enganxa un llast que la manté fixa en la seva posició. Damunt del llast s'instal·la un alliberador acústic, que funciona per control remot i que permet alliberar el fondeig del llast, de manera que tota la línia ascendeix fins la superfície per l'acció de les boies, on hom la recupera. Els fondejos emprats en aquesta Tesi estaven equipats amb trampes de partícules seqüencials i correntòmetres . Cada trampa consistia en un cilíndre equipat amb 12 ampolles per recol·lectar les mostres seqüencialment en el temps mercès a un sistema de programació i un mecanisme de revòlver que permeteren establir intervals temporals predeterminats de rotació i apertura d'una ampolla de mostreig rere l'altra.

En l'estudi dels fluxos de partícules convé tenir en compte algunes consideracions. Baker et al. (1988) ja notaren que l'eficiència de les trampes fondejades disminuïa quan els corrents superaven els 15 cm s^{-1}. Per la seva banda, Gardner et al. (1997) observaren que les trampes fondejades eren força ineficients a l'hora de recol·lectar les partícules transportades per fluxos

advectius. En conseqüència, hom considera que en presència de corrents que ultrapassen un cert llindar de velocitat, la capacitat de les trampes per capturar partícules es redueix apreciablement. Altres fonts d'incertesa a l'hora de determinar els fluxos de partícules i la seva composició poden derivar de la intrusió d'organismes nadadors, de l'alteració de les partícules per processos de degradació un cop recollides, de canvis en l'especiació dels elements, i també de la pèrdua de mostra degut a taxes de sedimentació especialment elevades que provoquen el sobreeiximent de les ampolles de mostreig (Heussner et al., 1990; Buesseler et al., 2007). La ubicació del fondeig, l'interval de mostreig, el monitoratge de les condicions hidrodinàmiques i l'ús de protocols apropiats són determinants per minimitzar biaixos i incerteses.

Per a la realització d'aquesta Tesi s'han desplegat cinc línies instrumentades equipades amb trampes de partícules cilindro-còniques *Technicap PPS3/3* amb una obertura de boca de 0,125 m^2, correntòmetres *Aquadopp Nortek* i alliberadors acústics IXSEA OCEANO 2500 (Fig. 2.3). Tres de les línies van ser fondejades als canyons submarins d'Escombreras, del sistema Garrucha-Almanzora i d'Almeria; la quarta fou situada al talús obert del marge de Palomares; i la cinquena es desplegà al peu del talús, al golf de Vera (Fig. 2.1). Les estacions dels canyons submarins i la del talús obert s'instal·laren a 1,000 m de profunditat aproximadament, mentre que la del peu del talús es col·locà a uns 2,550 m de profunditat.

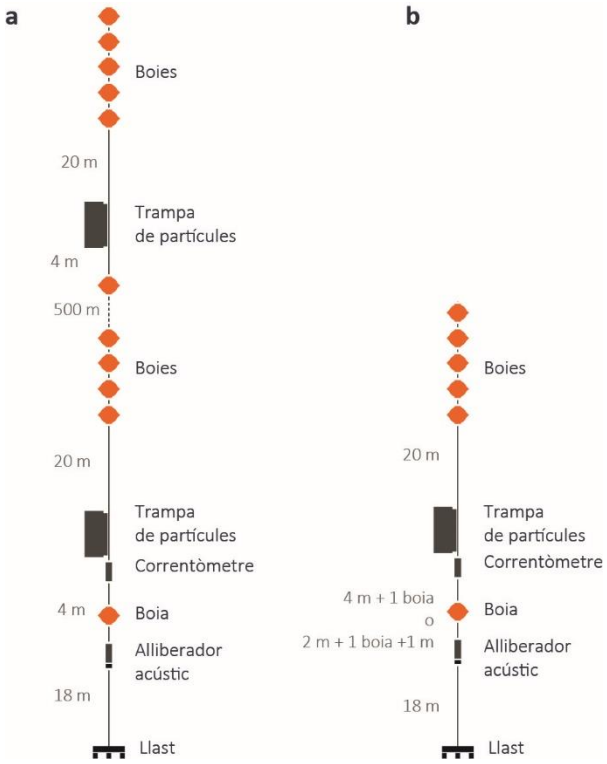

Figura 2.3. Configuració de les línies instrumentades emprades en aquesta Tesi. (a) Configuració llarga, emprada en el fondeig a PT2550. (b) Configuració curta, emprada del aresta de fodejos (Fig. 2.2).

Els fondejos s'instal·laren durant un any, des del mes de març de 2015 fins el mateix mes de 2016, amb una recuperació per manteniment (canvi de bateries i d'ampolles de mostreig) i redesplegament intermèdia al mes 6 (Fig. 2.1b i Taula 2.2). En tots els fondejos hi havia una trampa de partícules a 25 m sobre el fons. En el fondeig llarg de l'estació PT2550 s'hi instal·laà una trampa addicional a 546 m sobre el fons (Fig. 2.3a). Pel que fa a la nomenclatura, les trampes de partícules tenen la mateixa que les línies fondejades corresponents, exceptuant les dues ubicades al peu del talús, que hom anomenà PT2550-S, amb S de som (en anglès, *shallow*), i PT2550-D, amb D de "*deep*" (profunda). Cada trampa de partícules estava equipada amb 12 ampolles de mostreig. Prèviament al seu ús, les ampolles foren netejades amb sabó i HNO_3 (10%) i s'ompliren amb una solució formulada al 5% (v/v) (formaldehid al 37-38% amb aigua de mar filtrada a 0.45 μm) i estabilitzada amb tetraborat de sodi per obtenir un pH 7.5-8. L'interval de mostreig de les trampes es programà de per 7 dies, 16 dies o 1 mes segons el cas.

Les trampes de partícules del canyó d'Almeria, del talús obert i del peu del talús funcionaren correctament durant tot el període de mostreig. Per la seva banda, els sistemes de rotació de les trampes situades al canyó d'Escombreras i al sistema Garrucha-Almanzora experimentaren problemes tècnics durant el segon semestre de desplegament, i només es pogué recuperar part de la sèrie temporal. Concretament, a l'estació ES1000 no es va recuperar cap mostra durant el segon semestre, mentre que a l'estació GA1000 es van recuperar les tres primeres mostres, tot i que la tercera d'elles es descartà degut a que l'ampolla va romandre oberta durant la resta del semestre. En tots els casos, el material recuperat fou emmagatzemat a 4 ºC fins al seu tractament.

Fondeig / trampa	Campanya	Latitud	Longitud	Profunditat del fondeig (m)	Llargada del fondeig (m)	Període de mostreig	Número de mostres
ES1000	NUREIEV 1-3	37°27,309'N	0°52,274'O	985	42	16/3/2015-28/8/2105	12
TA1000	NUREIEV 1-3	37°24,613'N	1°15,394'O	1.003	42	16/3/2015-31/3/2016	24
GA1000	NUREIEV 1-3	37°10,294'N	1°41,968'O	1.100	42	25/3/2015-15/10/2015	14
AL1000	NUREIEV 1-3	36°31,709'N	2°32,003'O	1.000	42	25/3/2015-31/3/2016	24
PT2550-S	NUREIEV 1-3	37°10,635'N	0°59,993'O	2.550	560	16/3/2015-31/3/2016	24
PT2550-D	NUREIEV 1-3	37°10,635'N	0°59,993'O	2.550	560	16/3/2015-31/3/2016	24

Taula 2.2. Metadades dels fondejos instrumentats i de les trampes de partícules desplegades en el marc d'aquesta Tesi. El període complet de mostreig fou de 12 mesos, exceptuant el canyó d'Escombreras, on fou de 6 mesos, i el sistema Garrucha-Almanzora, on fou de 8 mesos. Al fondeig PT2550, "S" indica "som" (*shallow*), referit a la trampa col·locada a 546 m sobre el fons, i "D" indica "*deep*" (profund), referit a la trampa col·locada a 25 m sobre el fons.

Els correntòmetres, situats 2 m sota les trampes properes al fons, permeteren determinar en continu la velocitat i la direcció del corrent, la temperatura i la terbolesa de l'aigua Un fondeig, però, no comptà amb correntòmetre: l'AL1000. Els correntòmetres estaven equipats amb turbidímetres *SeaPoint*, calibrats en unitats de terbolesa de formazina (FTU, de l'anglès *Formazin Turbidity Units*), detecten la llum dispersa a 15º -150º (amb el pic de sensibilitat a 90º) en un volum d'aigua situat entre la finestra del sensor i una distància de 5 cm. L'interval de mostreig dels *SeaPoint* fou de 30 min.

2.1.3. Obtenció de mostres de sediment mitjançant testificador múltiple

El testificador múltiple (MC, de l'anglès *multicorer*) utilitzat fou un *KD Denmark* (Fig. 2.1c i Taula 2.3), el qual permet mostrejar els sediments que recobreixen el fons marí, sempre i quan siguin tous, fins una fondària de 60 cm en el subfons. Estan dissenyats per preservar l'estructura dels sediments i minimitzar la pertorbació dels mateixos durant el mostreig, i també preserven intacta la interfase aigua-sediment. Per tant, proporcionen testimonis curts de molt alta qualitat, a més de la interfase. Incorporen diversos tubs de mostreig, per la qual cosa permeten obtenir en una mateixa operació tants testimonis bessons com tubs duguin.

A la Tesi s'han utilitzat els testimonis múltiples recuperats a tocar de les estacions de fondeig d'Escombreras a mitjans de març del 2015, i del sistema de Garrucha-Almanzora a principis de setembre del 2015, així com un testimoni recuperat al curs alt del canyó d'Almeria (Fig. 2.2). Dels múltiples testimonis obtinguts, un fou submostrejat a intervals seguits de 0,5 cm de gruix fins assolir els 5 cm de fondària, a partir d'on l'interval de mostreig fou d'1 cm fins arribar a la base del testimoni. Les mostres així obtingudes es guardaren en bosses de plàstic dins una càmera frigorífica a 4°C.

Codi	Campanya	Coordenades		Localització	Profunditat (m)	Data d'obtenció	Interval utilitzats (cm)	Aptat. resultats
MC01	NUREIEV 1	37° 27,244' N	0° 52,206' O	Canyó d'Escombreras	1.002	març-15	0-0,5/ 50-51	3.2-3.4
MC11	NUREIEV 2	37° 10,605'N	1° 41,466' O	Sistema Garrucha-Almanzora	1.142	set-15	0-0,5	3.2
MC09	NUREIEV 2	36° 41,064' N	2° 18,885' O	Canyó d'Almeria	407	set-15	40-41	3.2
GC55*	NUREIEVA-MAR 1	37° 34,511' N	0° 51,361' O	Enfora de la badia de Portmán, zona proximal	27	juny-18	87-88	3.4
GC19*	NUREIEVA-MAR 1	37° 34,267' N	0° 51,342' O	Enfora de la badia de Portmán, zona intermèdia	39	juny-18	69-70	3.4
GC05*	NUREIEVA-MAR 1	37° 34,046' N	0° 51,215' O	Enfora de la badia de Portmán, zona intermèdia	42	juny-18	81-82	3.4

Taula 2.3. Metadades dels testimonis recuperats a les campanyes oceanogràfiques NUREIEV-1, NUREIEV-2 i NUREIEVA-MAR 1 utilitzats en aquesta Tesi. *El mostreig de l'extensió submarina del dipòsit de residus miners de la badia de Portmán s'efectuà amb un testificador de gravetat (GC, de l'anglès *gravity corer*) que proporcionà testimonis d'alguns metres de longitud (Baza-Varas, 2023). Com s'indica a la mateixa taula, en aquesta Tesi s'han utilitzat tres submostres de tres testimonis diferents. "Zona proximal"fa referència a l'àrea de la plataforma continental interna més propera al punt de descàrrega de residus miners a la badia de Portmán, és a dir fins a 1,2 km de distància i fins 35 m de fondària, mentre que "zona intermèdia"fa referència a l'àrea de la plataforma continental interna situada a una distància d'1,2 a 1,5 km de l'esmentat punt de descàrrega, dins un rang de profunditats de 35 a 43 m, tot seguint Baza-Varas (2023).

2.2. Anàlisi de les mostres

2.2.1. Tractament general

Les mostres de les trampes de partícules (Taula 2.1) es van processar seguint el protocol descrit per Heussner et al. (1990), amb algunes modificacions. Així, hom extregué els organismes nedadors de mida gran amb una malla de niló d'1 mm i enretirà els de mida menor manualment amb l'ajuda d'una lupa binocular. Posteriorment, per les mostres amb volums elevats, es procedí a obtenir alíquotes de treball amb una bomba peristàltica d'alta precisió. La fracció restant s'emmagatzemà a 4ºC preservada en formaldehid. La submostra de treball fou centrifugada amb aigua ultrapura Milli-Q tres vegades a fi d'extreure de la solució les restes de sal i formol. Finalment, hom liofilitzà i pesà les mostres per determinar-ne la massa. Per la seva banda, les mostres de sediment (Taula 2.3) foren pesades, liofilitzades i pesades de nou, obtenint així la massa total de la mostra i el contingut d'aigua.

2.2.2. Mida de gra

La mida de gra de les partícules és útil per interpretar ambients deposicionals, doncs els paràmetres que hi estan relacionats reflecteixen els processos de transport i els mecanismes de sedimentació (McCave i Hall, 2006; Ferré et al., 2005). A més, diversos estudis han demostrat que la mida de gra de les partícules influeix en l'exportació de MO (Tesi et al., 2010; Pedrosa-Pàmies et al., 2013; Bao et al., 2018) i elements traça (Horowitz i Elrick, 1987).

Les partícules es classifiquen i s'anomenen segons la seva mida en les fraccions argila (< 4 μm), llim (4-63 μm) i sorra (> 63 μm).

Tècnica analítica i procediment

La distribució granulomètrica de les mostres de partícules que sedimenten i dels sediments del canyó d'Escombreras (MC01) es mesurà amb un analitzador de partícules Beckman Coulter LS 230 al Laboratori de Sedimentologia del Departament de Dinàmica de la Terra i de l'Oceà (DTO) de la Universitat de Barcelona (UB). L'única excepció foren les mostres de l'estació de peu del talús PT2550 (Fig. 2.2), les quals no foren analitzades per la poca mostra disponible.

Aquest instrument mesura el percentatge en volum de les partícules de mida compresa entre 0,04 i 2.000 μm partint del principi de que, segons la seva mida, les partícules difracten la llum amb un angle determinat (Agrawal, et al., 1991). Per a l'anàlisi de la mida de gra, el protocol s'inicia amb un atac de les mostres amb 50 ml d'H_2O_2 (10%) un mínim de dos vegades per oxidar la MO i evitar la formació d'agregats. Cada atac va durar un dia, i les mostres s'assecaren després de cada oxidació. Seguidament, hom dividí les mostres en dues submostres, una amb la fracció total i l'altra descarbonatada a fi d'obtenir la distribució granulomètrica de la fracció litogénica. Per eliminar els carbonats, hom afegí 50 ml d'HCl (1M) a la submostra corresponent tantes vegades com fou necessari. Tot seguit, hom centrifugà cada mostra durant 3 min a 5.000 rpm per extreure el sobrenedant. Finalment, hom agregà 50 ml de solució disgregant de polifosfat de sodi als dos grups de submostres, passant-les a continuació i durant unes quantes hores per una

agitadora mecànica per evitar la floculació de les partícules i poder procedir així a l'anàlisi amb el Coulter en condicions òptimes, amb les mostres perfectament disgregades.

Les mesures de Coulter proporcionen informació sobre la distribució granulomètrica de la fracció mineral, però ometen la MO. Això es deu a que, per protocol, cal eliminar la MO per evitar que formi agregats amb la resta de partícules i provoqui un augment enganyós de la mida de gra. Les mostres del canyó d'Escombreras foren examinades amb lupa binocular, observant-se que la fracció sorrenca tenia una contribució significativa de fibres vegetals. A fi d'estimar el contingut de MO a la fracció sorrenca, unes dades incloses en l'apartat 3.3, hom tamisà les mostres amb tamisos d'acer inoxidable de 63 μm, sonificant-les en cas necessari per assolir una millor disgregació.

2.2.3. Anàlisi de la composició elemental i del $\delta^{13}C$

Els continguts de N, CO i carboni total (CT) donen una primera descripció general de la composició del sediments. El contingut de CO respecte del N permet discriminar l'origen de la matèria orgànica en els sediments marins (Hedges et al., 1997). A més, l'estudi del fraccionament isotòpic del carboni ($\delta^{13}C_{CO}$) és útil per discernir els principals constituents de la matèria orgànica (Hedges et al., 1997).

Un element químic pot presentar un nombre variable de neutrons, de manera que als àtoms amb un mateix número de protons i diferent número de neutrons hom els anomena isòtops. El carboni té dos isòtops estables, ^{12}C i ^{13}C, que ocorren naturalment, essent l'isòtop lleuger el més abundant. La diferència en l'abundància relativa dels dos parells d'isòtops ($^{13}C/^{12}C$) es pot mesurar amb una precisió elevada. El $\delta^{13}C_{CO}$ s'expressa com a proporció entre els dos isòtops estables, indicant-ho amb el símbol δ (delta), tot i normalitzant les ràtios isotòpiques per a un material estàndard segons:

$$(‰)\delta^{13}C_{CO} = \left[\frac{\left(\frac{^{13}C}{^{12}C}\right)_{mostra}}{\left(\frac{^{13}C}{^{12}C}\right)_{NBS-19}} - 1\right] x1000 \qquad [2.1]$$

El fraccionament isotòpic s'expressa en tants per mil (‰), i generalment s'usen estàndards homologats i estàndards del laboratori prèviament calibrats amb les homologats. En aquesta tesis s'ha utilitzat l'estàndard NBS-19.

Tècnica analítica i procediment

Els continguts de N, CO i CT de les partícules recollides amb les trampes de partícules es determinaren utilitzant un analitzador elemental model *Elemental Analyser Flash series 1112* (EA) a les instal·lacions dels Centres Científics i Tecnològics (CCiT-UB) de la UB.

En el cas dels sediments del canyó d'Escombreras, es mesurà la ràtio $\delta^{13}C_{CO}$ amb un *Elemental Analyser Thermo Fischer Scientific FLASH 1000* (EA) acoblat a un espectròmetre de masses de relacions isotòpiques (IRMS) *Thermo Fischer Scientific DELTA Q* a les instal·lacions del *Istituto di Scienze Polari del Consiglio Nazionale della Ricerche* (ISP-CNR) de Bolonya, a Itàlia.

L'anàlisi elemental orgànica permet determinar el contingut de N i C mitjançant la combustió de la mostra dins d'un forn a 1.000 °C. Els gasos generats són arrossegats cap a uns reactius per eliminar l'excés d'oxigen i convertir-los en N_2 i CO_2 (Fig. 2.4). Posteriorment, passen a una columna cromatogràfica amb un detector on són quantificats. L'acoblament de l'analitzador elemental amb l'IRMS (Fig. 2.4) permet ionitzar els gasos mitjançant un feix d'electrons. Hom dirigeix mitjançant lents els ions generats i els accelera emprant un voltatge alt fins que travessen un camp magnètic. El voltatge d'acceleració i la força del camp magnètic determinen la trajectòria dels ions (que se separen segons la seva massa), els quals finalment arriben a un detector.

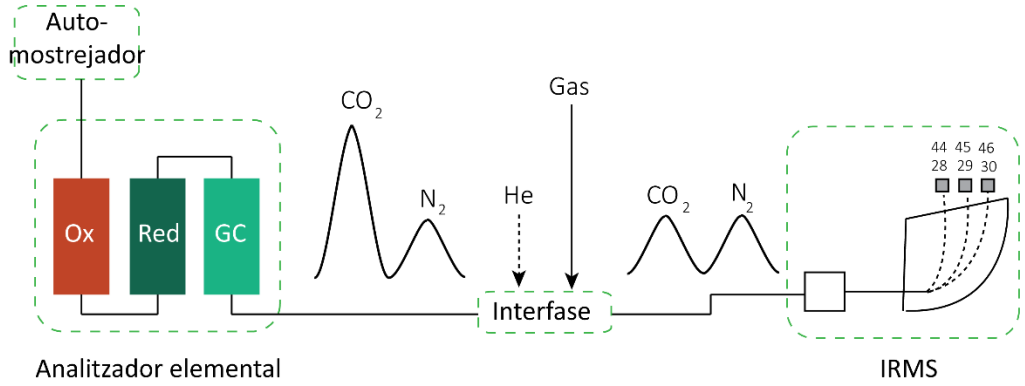

Figura 2.4. Esquema d'un analitzador elemental acoblat a un espectròmetre de masses de relacions isotòpiques (IRMS). Ox: oxidació. Red: Reducció. GC: cromatògraf de gasos. Les xifres de dos dígits damunt el dibuix de l'IRMS fan referència al ràtio m/z (massa/càrrega) dels ions de C i N.

Per determinar el CO les mostres foren descarbonatades dins d'una capsula de Ag a la qual s'afegiren 50 µl de HCl (1M) en tres tongades (10+20+20 µl), assecant-les durant un mínim de 4h a 60ºC després de cada atac fins que cessà l'efervescència. Després de l'últim atac, s'afegí aigua Milli-Q i s'assecaren les mostres. Seguidament, s'addicionà un catalitzador de V_2O_5 i s'embolcallà la mostra fent-ne una boleta. Posteriorment, es tornà a embolcallar amb una càpsula de Sn. Per mesurar el CT hom col·loca igualment la mostra dins d'una càpsula de Sn juntament amb el catalitzador, fent tot seguit la boleta corresponent. Les incerteses analítiques per a la composició elemental foren inferiors a 0,5%, mentre que pel $\delta^{13}C_{CO}$ fou inferior a 0,1 ‰.

2.2.4. Òpal

El contingut d'òpal ($SiO_2 \cdot 0{,}4H_20$) de les partícules recollides amb les trampes de partícules es determinà a partir de l'anàlisi del Si i l'Al per espectrometria d'emissió òptica de plasma d'inducció acoblat (ICP-OES) als CCiT-UB, amb un instrument *Perkin Elmer Optima 8300*.

Cada mostra es vaporitzà en el dispositiu de l'ICP mitjançant un nebulitzador, i es transportà amb argó cap a la torxa de plasma, on l'aerosol a altes temperatures (6.000 – 10.000 °C) la ionitzà. Els ions de dins el plasma emeten radiacions electromagnètiques característiques de cada element. En aquest cas, l'espectròmetre òptic analitzà la longitud d'ona i la freqüència de la radiació electromagnètica emesa a fi de quantificar els continguts de Si i Al.

Aquest mètode requereix d'un factor de correcció, degut a que el Si de la mostra pot provenir tant de sediments biogènics com d'aluminosilicats. Per aplicar aquest factor de correcció cal conèixer la relació Si/Al dels sediments litogènics (Kamatani i Oku, 2000). Atés que la cinètica de dissolució de l'òpal és més ràpida que la dels aluminosilicats, s'efectuen dues digestions. A la primera es lixivien el Si i l'Al procedents de totes dues fraccions, mentre que a la segona, el Si i l'Al provenen només dels aluminosilicats. Ambdues digestions s'efectuaren durant 2h 30' a 90°C amb una solució de Na_2CO_3 (0.5M), assecant la mostra entre la primera i la segona digestió (Fabres et al., 2002). Finalment, les mostres van ser centrifugades i analitzades amb l'ICP-OES.

2.2.5. Biomarcadors derivats de la lignina i la cutina

Els traçadors moleculars, o biomarcadors, s'utilitzen en l'estudi de la composició de la MO, complementant la informació aportada pels marcadors de la composició general. Permeten conèixer l'estat de degradació de la MO i tenen una sensibilitat elevada a l'hora de discernir el seu origen (Hedges et al., 1997).

En aquesta Tesis s'han estudiat diversos components moleculars derivats de la oxidació i hidròlisi de la lignina, un polímer fenòlic present a les parets de les cèl·lules sintetitzat exclusivament per les plantes vasculars (Hedges i Mann, 1979; Hedges et al., 1997). També s'han estudiat àcids carboxílics derivats de la cutina, una macromolècula que és part integral de les cutícules que cobreixen els teixits epitermals de les plantes vasculars (Goñi i Hedges, 1990).

Hom determinà l'abundància de lignina a partir del contingut en diversos monòmers: fenols[4] del grup de la vanil·lina (V, suma de Vd, Vl, Vn), fenols del grup del siringil (S, suma d'Sd, Sl i Sn) i fenols del grup del cinamil (C, suma de Pc i Fd) (vegis denominacions completes i abreviacions a la Taula 2.4). L'abundància de lignina, també referida com Λ_8 quan és normalitza pel CO, es pot calcular a partir de la següent expressió:

$$\Lambda_8 = \sum V + S + C \qquad [2.2]$$

L'abundància de cutina es pot determinar a través de l'anàlisi d'una sèrie d'àcids carboxílics derivats (ω-C16, C16DA, 8,ω-C16, 9,ω-C16, 10,ω-c16, 7-C16DA i 8-C16DA), d'acord amb l'expressió:

$$Cutina = \sum \omega\text{-}C16 + C16DA + x,\omega\text{-}C16 + x\text{-}C16DA \qquad [2.3]$$

A més, també es determinà l'abundància de productes derivats de l'oxidació de l'àcid benzoic (àcid 3,5–dihidroxibenzoic) (Taula 2.4).

[4] Compost orgànic aromàtic amb la molècula formada per una anell de benzè en que un hidroxil ocupa el lloc d'un hidrogen.

Compost	Símbol
Productes de la lignina (monòmers)	
Grup de la vanil·lina (V)	
Vanil·lina	Vl
Acetovanil·lona	Vn
Àcid vanil·lic	Vd
Grup del siringil (S)	
Siringaldehid	Sl
Acetosiringona	Sn
Àcid siringic	Sd
Grup del cinamil (C)	
Àcid trans-p-cumàric	pCd
Àcid ferúlic	Fd
Productes de la cutina	
Àcid 16-gidroxihexadecanoic	ω-C16
Hexadecà-1,16-àcid dioic	C16DA
x, àcid 16-dihididoxihexadecaonic	x,ω-C16 x=8/9/10
x-hidroxihexadecanodioic	x-C16DA x=7/8
Productes de l'àcids benzoic (B)	
Àcid 3,5-dihidroxibenzoic	3,5-Bd

Taula 2.4. Denominació i abreviacions dels biomarcadors analitzats en aquesta Tesi.

Tècnica analítica i procediment

Els continguts de lignina i cutina a les partícules en suspensió i els sediments del canyó d'Escombreras (trampa de partícules ES1000 i testimoni MC01; cf. taules 2.2 i 2.3) es determinaren mitjançant un cromatògraf de gasos (GC) acoblat a un espectròmetre de masses (MS) model GC *Agilent GC 7820 - MSD EI 5977B*) a l'ISP-CNR de Bolonya, a Itàlia (Fig. 2.5).

La preparació de les mostres i el procediment analític és descrit en detall per (Goñi i Montgomery, 2000). Primerament, aproximadament 400 mg de mostra foren oxidats amb CuO en uns vials en condicions bàsiques (6 ml de NaOH [2N] prèviament bombollejat amb N_2). Els reactors es van tancar en una cambra de guants amb atmosfera de N_2, i es van deixar 90 min en un sistema de microones amb pressió controlada a 150ºC. Seguidament, es recuperà el sobrenedant per centrifugació, s'acidificà a pH 1 amb HCl concentrat, i s'extragué amb acetat d'etil. Una vegada l'excés d'aigua fou extreta amb $NaSO_4$, s'evaporà la mostra a 100 ˚C durant aproximadament 1h. Finalment, les mostres es van redissoldre en 300 µl de piridina.

Els productes de la reacció de CuO (grups funcionals carboxil i fenòlics) no es poden detectar directament amb el GC. Els productes foren derivats a partir d'una solució de bis(trimetilsilil) trifluoroacetamida (BSTFA) + 1% trimetilclorosilà (TCMS) abans de la injecció de les mostres en l'instrument.

Un cop injectada, la mostra es volatilitza a alta temperatura, es transfereix a una columna cromatogràfica capil·lar, on els analits (components de la mostra) són transportats amb He al llarg de la columna i separats segons l'adsorció a la columna, la qual depèn de cada component. Les molècules són transferides a l'espectròmetre de masses, on són convertides en ions. Els ions se separen segons la seva relació m/z per l'acció d'un camp magnètic. Tot seguit els ions són transportats fins el detector on es converteixen en senyal elèctric. La quantificació dels productes es va estimar utilitzant els factors de resposta interna d'estàndards (EVLLa i àcid trans-cinàmic).

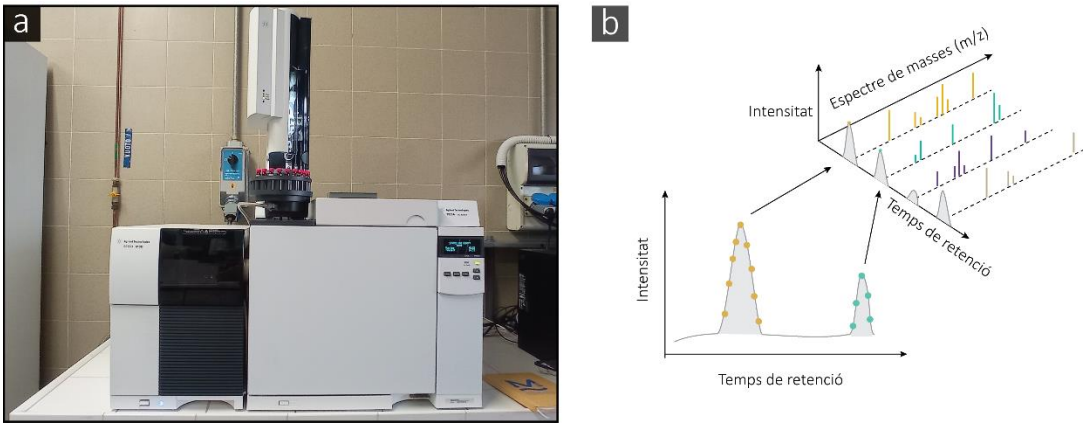

Figura 2.5. (a) Cromatògraf de gasos acoblat a un espectròmetre de masses de l'*Istituto di Scienze Polari* del *Consiglio Nazional delle Ricerche* de Bolonya, emprat per analitzar els biomarcadors en mostres de partícules en suspensió i sediments en el marc d'aquesta Tesi. (b) Esquema d'un cromatograma i l'espectre de masses associat.

2.2.6. Metalls i metal·loides

El contingut en MT a les mostres de les trampes de partícules (ES1000, GA1000 i AL1000) (Taula 2.2) i dels testimonis de sediment MC01, MC11 i MC09 (0,5 cm superiors i dels 0,5 cm inferiors) (Taula 2.3) s'han determinat amb un espectròmetre de masses de plasma d'inducció acoblat (ICP-MS) *Perkin-Elmer Elan-6000* i amb un ICP-OES *Perkin Elmer Optima 8300* als CCiT-UB.

La preparació de les mostres començà per una digestió en un sistema tancat amb 2.5 mL HNO_3 (65%) durant 24 h a 95 ˚C. L'extracte es centrifugà 3 vegades, i el sobrenedant s'extragué i transferí a un matràs de 50 mL, el qual s'enrasà amb HNO_3 (1%), obtenint així la primera solució. La fracció sòlida recuperada de la centrifugació es transferí novament als reactors i s'atacà amb 10 mL HF (40%) durant 24 h a 100ºC. Posteriorment, s'afegiren 2 mL de $HClO_4$ (70%) i s'escalfà al bany de sorra a ~230 ˚C fins l'evaporació de l'àcid. Prèviament a l'evaporació total, s'afegiren 2 mL de HNO_3 (65%) i 1-2 mL H_2O_2 i, a l'evaporar el HNO_3, s'afegiren 2 mL d'$HClO_4$ fins l'evaporació total. El residu es redissolgué amb HNO_3 (65%) i H_2O ultrapura (milli-Q) i es transferí a un matràs de 50 ml, que s'enrasà amb HNO_3 (1%) per obtenir una segona solució. Qualsevol possible contaminació durant el protocol de laboratori es controlà amb blancs, mentre que la precisió s'avaluà amb triplicats. Els valors de la desviació estàndard relativa foren < 5%, exceptuant el Pb (RSD 6,3%) i l'As (RSD 5,4%).

2.2.7. Composició isotòpica del Pb

Els nuclis atòmics dels isòtops no són sempre estables, i alliberen energia emetent partícules i/o radiació electromagnètica, la qual cosa comporta canvis en la composició de protons del nucli atòmic i, per tant, la possible transformació d'un element en un altre.

En aquesta Tesi s'ha estudiat el comportament d'un grup d'isòtops estables que ocorren naturalment: ^{206}Pb (24,1%), ^{207}Pb (22,1%), ^{208}Pb (52,1%) i ^{204}Pb (1,4%). De tots ells, el ^{204}Pb és l'únic no radiogènic, és a dir que no prové d'una cadena de desintegració. Els isòtops estables ^{206}Pb, ^{207}Pb i ^{208}Pb són el producte final de tres cadenes de desintegració, dues de l'urani (^{235}U i ^{238}U) i una del tori (^{232}Th) (Fig. 2.6).

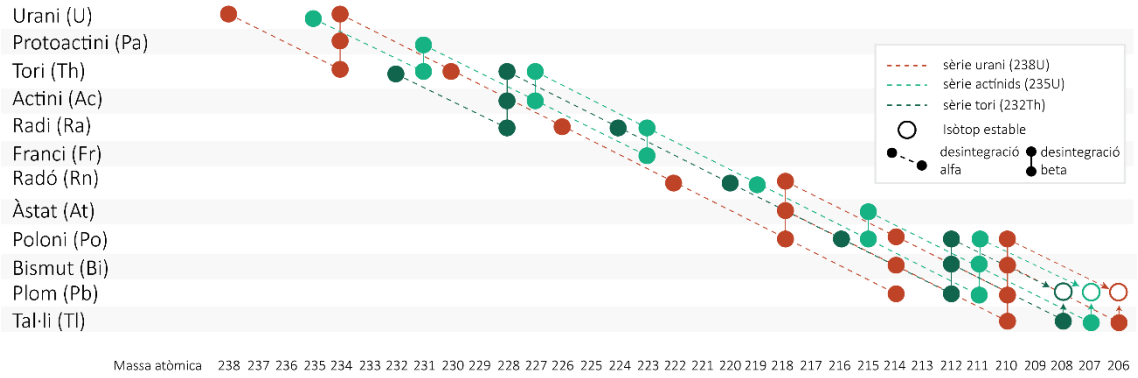

Figura 2.6. Cadenes desintegració de la sèrie de l'^{238}U, l'^{235}U i el ^{232}Th i els seus respectius productes finals. Il·lustra l'emissió de partícules alfa per part dels diferents elements, la qual cosa dona origen a nous elements radioactius emissors de partícules beta negatives, i així successivament.

A les últimes dècades, els isòtops del Pb s'han aplicat com a traçadors de contaminació en estudis mediambientals marins (Álvarez-Iglesias et al., 2012; Noble et al., 2015). De fet, el Pb és possiblement un dels casos més ben estudiats d'alteració de les concentracions naturals en bona part de l'oceà global per causa de les emissions antropogèniques cap a l'atmosfera (Boyle et al., 2014). Els isòtops estables del Pb estan incorporats principalment a l'estructura de la galena, un sulfur de Pb (PbS) que quan cristal·litza accepta el Pb a la seva estructura, però no l'U ni el Th. Als minerals naturals hi ha una gran variabilitat de composicions isotòpiques del Pb (Komárek et al., 2008). La composició isotòpica del Pb en un mineral o una roca dependrà del Pb original, de la quantitat d'U i Th presents, dels processos geològics que fraccionen els diversos isòtops de les cadenes U, Th i fills, i l'edat del dipòsit (Álvarez-Iglesias et al., 2012). Se sap, per altra banda, que la composició isotòpica del Pb no es veu afectada pels processos industrials (Bollhöfer i Rosman, 2001), la qual cosa implica que la composició isotòpica dels minerals de Pb estarà reflectit en la composició del Pb de fonts antropogèniques, com ara els additius de benzines, la combustió del carbó, les industries metal·lúrgiques, les incineradores de residus urbans (Komárek et al., 2008).

Tècnica analítica i procediment

La concentració de Pb i el seu fraccionament isotòpic en mostres de sediment i partícules recollides al canyó Escombreras (testimoni MC01 i trampa de partícules ES1000; cf. taules 2.2 i 2.3), i en tres mostres de l'extensió submergida del dipòsit de residus miners de Portmán (Taula 2.3), s'ha determinat amb un ICP-MS de multicol·lector (MC-ICP-MS) de Nu Instruments-AMETEK als CCiT-UB.

El funcionament de l'MC-ICP-MS és similar al d'un quadrupol, però amb un sistema que permet introduir les mostres a la torxa de plasma en estat sec i reduir les interferències derivades del solvent. Dins l'espectròmetre de masses, els ions són accelerats per un gradient de potencial elèctric i separats per un camp magnètic segons la seva ràtio m/z. Els ions es dirigeixen aleshores cap als col·lectors, on es converteixen en senyals elèctriques, tot i permetent fer vàries mesures a la vegada. La comparació dels voltatges dels diferents col·lectors permet calcular les relacions isotòpiques.

Hom determinà les ràtios: $^{207}Pb/^{206}Pb$, $^{208}Pb/^{206}Pb$, $^{206}Pb/^{204}Pb$, $^{207}Pb/^{204}Pb$ i $^{208}Pb/^{204}Pb$. Les interferències amb altres ions són habituals degut a l'elevada massa dels isòtops de Pb (Komárek et al., 2008), per la qual cosa es van aplicar diverses correccions. La interferència del ^{204}Hg amb el ^{204}Pb fou corregida matemàticament amb el senyal de ^{202}Hg, assumint un valor natural de 0,23007 per a la ràtio $^{204}Hg/^{202}Hg$. A més, per corregir el biaix per cada massa individual, es va utilitzar el Tl ($^{205}Tl/^{203}Tl$) com a estàndard intern de referencia, normalitzant amb un valor de referencia certificat (NIST SRM 981).

La preparació de les mostres es dugué a terme en els CCiT-UB i en el Laboratori d'Isòtops Radiogènics i Ambientals (LIRA) del DTO de la UB, el qual compta amb una classificació general ISO7 de la qualitat d'aire.

El procediment consistí en la digestió total de les mostres i la posterior elució del Pb de la resta d'elements de la matriu. Aquesta separació s'efectuà mitjançant una resina (AG1 X8) a partir de l'intercanvi aniònic amb els ions de la resina que presenten la mateixa càrrega.

S'efectuà una primera digestió total de les mostres amb 2,5 ml HNO_3 (65%) + 10 ml HF (%) + 2 ml $HClO_4$ (%) en un sistema tancat durant 24h a 95ºC. Posteriorment, hom evaporà l'àcid en un bany de sorra, s'afegiren 2 ml $HClO_4$ i es tornà a portar la mostra a sequedat incipient. El residu fou redissolt en 2,5 ml HNO_3 (65%), es transvasà a vials de 0,25 ml i s'evaporà a 120 ˚C. Seguidament, les mostres es redissolgueren en 2 ml HBr (0,7N), es sonificaren durant uns 10 min i es deixaren evaporant en una placa calefactora durant un mínim de 2 h a 100 ˚C. Finalment, hom centrifugà les mostres per extreure'n qualsevol residu sòlid.

La purificació del Pb mitjançant la resina s'efectuà carregant 2 ml de mostra a les columnes amb la resina, prèviament netejades i dutes a condicions ambientals. Un cop introduïda a l'instrument, els anions de la mostra s'intercanviaren amb els de la resina i quedaren retinguts en ella, entre els quals els complexos que el Pb forma amb l'hidrobromur. A continuació s'afegí HBr (0,7N) en tres tandes (1+3+1 ml). Tot seguit, s'addicionaren tres cops 1,2 ml HCl (6N) per elucidar el Pb, el qual es recuperà en un vial net.

Finalment, hom evaporà l'extractat en una placa calefactora a 90 ˚C, i el redissolgué amb 1,4 ml HNO_3 (2%).

2.2.8. Altres anàlisis

2.2.8.1. Datació pel mètode del ^{210}Pb

El radioisòtop ^{210}Pb és present com a producte intermedi de la sèrie de l'urani (Fig. 2.6) amb una vida mitjana de 22,6 anys. La seva vida mitjana permet el seu ús com a datador de sediments recents (≈100 anys).

L'anàlisi del ^{210}Pb del testimoni MC01 (Taula 2.3) s'ha realitzat en col·laboració amb el Laboratori de Radioactivitat Ambiental (LRA) de la Universitat Autònoma de Barcelona. Les activitats totals de ^{210}Pb es van determinar a partir de la mesura del ^{210}Po, un radionúclid producte de la seva desintegració (Sánchez-Cabeza et al., 1998). Després de la digestió de la totalitat de la mostra amb HCl (1M) en discos de plata, l'activitat del ^{210}Po es determinà amb un espectròmetre α amb detectors de silici (SSB) de baix fons. La recuperació del procés fou determinada usant un traçador intern d'activitat coneguda (^{209}Po). Posteriorment, després que el ^{226}Ra assolís l'equilibri secular amb els seus fills de vida curta, es procedí a determinar l'activitat del ^{226}Ra a partir de la mesura de ^{214}Pb per espectrometria Y amb detectors de semiconductor de Ge. El ^{210}Pb base (suportat) es determinà a partir de la mesura del ^{226}Ra. L'excés d'activitat del ^{210}Pb es calculà restant l'activitat del ^{210}Pb base de l'activitat total del ^{210}Pb. La qualitat de l'anàlisi ha fou avaluada amb l'ús de replicats i materials de referència.

2.2.8.2. Determinació no destructiva de la composició elemental

L'aplicació de tècniques no destructives per la caracterització geoquímica de materials ha anat a l'alça les últimes dècades per raons de rapidesa, versatilitat, replicabilitat i resolució (Boyle, 2000). La composició elemental, des de l'Al fins l'U, del testimoni MC01 (Taula 2.3) s'obtingué amb un escàner de fluorescència de raigs X (XRF *core scanner*) de l'empresa Avaatech al Laboratori CORELAB del DTO de la UB. L'escàner compta amb una font de raigs X *Oxford Rhodium* (4-50kV), un detector *Canberra X – Pips 1500 – 1.5* amb una finestra de Be de 125 µm, i un analitzador multicanal *Canberra DSA 1000* (MCA). La mesura es basa en la detecció de les radiacions secundàries emeses pels diferents elements químics després d'excitar-los amb un feix de raigs X. L'expulsió dels electrons de la capa interna de l'àtom deixa un espai buit que és ocupat per altres electrons de capes més externes. La longitud d'ona de la radiació emesa dependrà de la diferència d'energia entre els dos nivells, intern i extern.

El contingut semi-quantitatiu de Fe, As, Cu, Mn, Pb i Zn es determinà directament sobre una secció del testimoni, la superfície de la qual va ser allisada i recoberta amb un film especial *Ultralene X-ray transmission* per evitar la contaminació dels sediments i del propi l'equip de mesura. L'anàlisi s'efectuà amb una resolució de 2 mm. Les condicions d'excitació per als elements amb un pes atòmic entre l'Al i el Fe foren de 10 kV i 1,2 mA amb un temps d'exposició de 10 s. Per als elements entre el Ni i el Pb, les condicions foren de 30 kV i 1,6 mA amb un temps d'exposició de 50 s i un filtre de Pd.

La intensitat dels senyals del Fe, Mn, Pb i Zn es transformar a continguts absoluts d'acord amb la calibració realitzada per Cerdà-Domènech et al. (2020).

2.3. Anàlisi de les dades

Els percentatges de MO i carbonat de calci ($CaCO_3$) s'han calculat seguint les següents equacions:

$$MO = CO\ x\ 2 \quad [2.4]$$

i

$$CaCO_3 = (CT - CO)x\ 8{,}33 \quad [2.5]$$

on 8,33 és la massa molecular del $CaCO_3$ assumint que tot el carboni inorgànic es troba en forma de $CaCO_3$ (Heussner, 1996) (cf. aptat. 2.2.3).

El percentatge d'òpal s'ha calculat seguint les equacions:

$$Si_{bio} = (Si_1 - Al_1) * \left(\frac{Si_2}{Al_2}\right) \quad [2.6]$$

i

$$\grave{O}pal = Si_{bio}x\ 2.4 \quad [2.7]$$

on Si_1 i Al_1 són les concentracions d'aquests elements en el lixiviat de la primera digestió, i Si_2 i Al_2 els de la segona (cf. aptat. 2.2.4). El percentatge d'òpal s'obté multiplicant el Si_{bio} per un factor de 2,4 donat que la silice biogènica dels sediments marins és hidratada amorfa ($SiO_2 \cdot 0{,}4\ H_2O$) (Mortlock i Froelich, 1989).

En aquest cas, la fracció litogénica es calculà assumint que:

$$\%litogènics = 100 - (\%MO + \%CaCO_3 + \%\ \grave{o}pal) \quad [2.8]$$

Per a cada estació de mostreig, es calcularen els fluxos totals de partícules, els dels components principals i els de MT, així com els ponderats en funció de la durada dels intervals de mostreig corresponents.

Els fluxos de massa totals (TMF, de l'anglès *Total Mass Flux*) foren determinats seguint l'equació:

$$TMF\ (g\ m^{-2}d^{-1}) = \frac{Massa\ total\ de\ la\ mostra\ (g)}{0.125\ (m^2) * \text{dies de mostreig}\ (d)} \quad [2.9]$$

Els fluxos ponderats segons el temps de mostreig (TWF, de l'anglès *Time Weighted Fluxes*) es varen obtenir a partir de l'equació:

$$TWF\ (g\ m^{-2}d^{-1}) = \frac{\sum Mi\ (g)}{0.125\ (m^2) * \sum Di\ (d)} \quad [2.10]$$

on M_i és la massa per a cada període de mostreig, 0.125 m^2 és l'àrea de la boca de la trampa i D_i són els dies de mostreig del període corresponent.

Per ponderar els valors segons els períodes de mostreig, hom calculà el contingut ponderat de cada component i MT segons el temps (TWC, de l'anglès *Time Weighted Content*) amb la següent equació:

$$TWC\ (\mu g\ g^{-2}) = \frac{TWF\ (massa\ element)}{TWF\ (massa\ total\ de\ la\ mostra)} \quad [2.11]$$

Hi ha diverses maneres d'estimar la contribució de MT i As antropogènics en els sediments marins. Un enfocament consisteix a calcular els factors d'enriquiment (FE). "Enriquiment" fa referencia a la magnitud amb què les concentracions actuals de metalls en el sediment superen els nivells de fons, sense alteracions causades per l'activitat humana (Birch, 2017). Aquest mètode requereix normalitzar el contingut de MT per a reduir la variabilitat associada a canvis en al mineralogia i la granulometria (Aloupi and Angelidis, 2001).

$$FE = \frac{MT/N}{MT_b/N_b} \quad [2.12]$$

on N indica l'element normalitzador i MT_b i N_b indiquen els valors de fons.

2.4. Paràmetres ambientals de bases de dades obertes i de sensors remots

Les dades metoceanogràfiques (velocitat i direcció del vent, i altura, direcció i període de les onades significatives) foren extretes de l'Agència Estatal de Meteorologia i de la Xarxa de Boies d'Aigües Profundes (REDEXT, Puertos del Estado). Per a obtenir paràmetres precisos de les ones diàries a les capçaleres dels canyons submarins, vàrem utilitzar tres punts de la xarxa WANA, que proporciona sèries temporals de paràmetres del vent i les ones segons la modelització numèrica realitzada per Puertos del Estado en col·laboració amb l'Agència Estatal de Meteorologia.

Els cabals horaris dels rius Andarax i Almanzora s'extragueren de la xarxa SAIH Hidrosur, operada per la Junta d'Andalusia. No hi ha, però, estacions de mesura situades a prop de les desembocadures. Les dades de cabals es completaren amb dades de precipitació de dues estacions meteorològiques situades a la província d'Almeria, de la mateixa font.

Les concentracions mensuals de clorofil·la-a (Chl-a) (mg m^{-3}) i les dades de temperatura superficial del mar (°C), de nivell 3 i amb 4 km de resolució, provenen del *Moderate Resolution Imaging Spectrometer (MODIS)*, en òrbita a la plataforma Aqua. Aquestes dades són processades i distribuïdes pel *Goddard Earth Science (GES) Data and Information Services Centre (DISC)* de la NASA i compten amb el suport de *Ocean Biology Processing Group (OBPG) a efectes de validació*.

La deposició atmosfèrica mensual de partícules s'obtingué del model MERRA-2 produït per la *Global Modeling and Assimilation Office (GMAO)* utilitzant el *Goddard Earth Observing System Model (GEOS)* de la NASA.

L'activitat pesquera ha estat monitoritzada a partir de les dades del Sistema de Monitorització de Vaixells (VMS, de l'anglès *Vessel Monitoring System*), proporcionades per la Secretaria General de Pesca, del Ministeri d'Agricultura, Alimentació i Medi Ambient del govern espanyol. Aquest

sistema proporciona dades regulars de la localització, el rumb i la velocitat dels vaixells de pesca a partir del seu seguiment satal·litari. Des del 2005, és obligatori a la UE per vaixells de més de 12 m d'eslora. Aquestes dades s'utilitzen freqüentment com a indicadors d'esforç pesquer. A fi d'avaluar l'activitat pesquera al voltant de l'estació GA1000 (Fig. 2.1 i Taula 2.1), hom filtrà les dades VMS, retenint només les corresponents a velocitats sostingudes de menys de cinc nusos en un radi de 4 km al voltant de l'estació. S'entén que aquesta velocitat es indicativa d'arrossegadors amb la xarxa calada.

Capítol 3

Resultats

Particle fluxes in submarine canyons along a sediment-starved continental margin and in the adjacent open slope and basin in the SW Mediterranean Sea

Transport and distributions of naturally and anthropogenically sourced trace metals and Arsenic in submarine canyons

Across margin export of recalcitrant blue carbon: a study case off SE Iberia.

Pb and Zn pollution in a submarine canyon: the role of a coastal mine tailings deposit and other potential sources

Resum de resultats

3.1. Particle fluxes in submarine canyons along a sediment-starved continental margin and in the adjacent open slope and basin in the SW Mediterranean Sea

Marta Tarrés[a], Marc Cerdà-Domènech[a], Rut Pedrosa-Pàmies[a,b], Aitor Rumín-Caparrós[a], Antoni Calafat[a], Miquel Canals[a], Anna Sanchez-Vidal[a]*

[a] GRC Geociències Marines, Dept. Dinàmica de la Terra i de l'Oceà, Facultat de Ciències de la Terra, Universitat de Barcelona, 08028 Barcelona, Spain

[b] The Ecosystems Center, Marine Biological Laboratory, Woods Hole, MA, USA

Progress in Oceanography 203 (2022) 102783
Doi: 10.1016/j.pocean.2022.102783

Keywords: particle fluxes, sediment-starved continental margin, submarine canyons, open slope, deep basin, Mediterranean Sea

Abstract Investigating the transfer of particulate matter from the continental shelf to the deep basin is critical to understand the functioning of deep sea ecosystems. In this paper we present novel results on the temporal variability of particle fluxes to the deep in three physiographic domains of a 240 km long margin segment and nearby basin off Murcia and Almeria provinces in the SW Mediterranean Sea, which are submarine canyons forming a rather diverse set (namely Escombreras, Garrucha-Almanzora and Almeria), the adjacent open slope and the deep basin.

This margin is located off one of the driest regions in Europe and, therefore, its study may help understanding how mainland aridity translates into the export of particles to deep margin environments. Five mooring lines equipped with currentmeters, turbidity-meters and sediment traps were deployed for one entire annual cycle, from March 2015 to March 2016. We combine oceanographic, hydrological and meteorological data with grain size and bulk elemental data (organic carbon, opal, $CaCO_3$, lithogenic) from the collected sinking particles to understand what drives particle transfers in such an under-studied setting, and to quantify the resulting fluxes and assess their spatio-temporal variability.

Weighted total mass fluxes in canyons range from 1.64 g $m^{-2}d^{-1}$ in Almeria Canyon to 7.33 g $m^{-2}d^{-1}$ in Garrucha-Almanzora Canyon system, which are rather low values compared to other submarine canyons in the Western Mediterranean Sea. This results from the absence of extreme wind-storm events during the investigated time period combined with the reduced sediment input to the inner shelf by river systems in the study area. Our results also show that wind-storms are the main trigger for off-shelf particle transport to the deep margin, both within submarine canyons and over the open slope. The most significant transfer period is associated to a set of

north-eastern storms in early spring 2015, when the off-shelf transport likely was promoted by storm-induced downwelling. However, the prevailing oceanographic conditions restricts the advection of water down the canyon heads to a few hundred meters, thus promoting a bottom-detached transport of particles seaward. Overall physiography, canyon head incision into the continental shelf and the distance of the canyon head to the shoreline (e.g. very short in Garrucha Canyon) play a key role in particle trapping capability and, therefore, in easing downslope particle transport. Further, bottom trawling activities around the Garrucha-Almanzora Canyon system, feed a nepheloid layer at depths in excess of 400 m, subsequently enhancing particle fluxes throughout the study period. In contrast, maximum particle fluxes in the deep basin respond to seasonal phytoplankton blooms.

Our study shows that particle export from the shallow inner margin to the deep outer margin in sediment-starved settings, even if limited, does occur as dominated by atmosphere and ocean driven short-lived events. However, that export does not reach too far as at several tens of kilometres from the shelf edge advective fluxes are replaced by vertical ones impelled by phytoplankton dynamics.

3.1.1. Introduction

Continental margins are the areas that connect the continent and the deep sea. These areas are where most of the sediments are deposited, and are an important source of material to deep sea ecosystems. Materials supplied by the rivers (and autochthonous biological production) are transferred from the continental shelf to the slope and deep basin, especially in those areas incised by submarine canyons. Submarine canyons are large geomorphic features carved on continental margins that act as preferential conduits for particulate matter export from the continental shelf to the deep margin and basin (Drake and Grosline, 1973; Shepard et al., 1979; Xu et al., 2004; Heussner et al., 2006; Canals et al., 2006; Puig et al., 2014). Canyons are key features for the transfer and sinking, which are often episodic, of organic carbon (OC) and nutrients (Pasqual et al., 2010; Kiriakoulakis et al., 2011; Sanchez-Vidal et al., 2012; Pedrosa-Pàmies et al., 2013), while also facilitating the delivery of litter and chemical pollutants to deep ecosystems (Palanques et al., 2008a; Ramirez-Llodra et al., 2013; Dumas et al., 2014; Tubau et al., 2015).

To date, studies on particle fluxes within submarine canyons around the Iberian Peninsula margins have focused on specific segments such as the North Catalan and Gulf of Lion margins (Heussner et al., 2006; Martín et al., 2006; Durrieu de Madron et al., 2008; Pasqual et al., 2010; Sanchez-Vidal et al., 2012; Canals et al., 2013 and references therein), the Portuguese margin (Schmidt et al., 2001; de Stigter et al., 2007, 2011; Martín et al., 2011), margins of the Western Alboran Sea (Puig et al., 2004b; Palanques et al., 2005) and the Cantabrian margin and neighbouring areas (Heussner et al., 1999; Schmidt et al., 2014; Romero-Romero et al., 2016b; Rumín-Caparrós et al., 2016). These studies illustrate the markedly different behaviour between submarine canyons in the micro-tidal Western Mediterranean Sea and those in the meso-tidal Atlantic Ocean, where high swells are common. Compared to other canyons in the Western Mediterranean Sea and, more generally off Iberia and nearby areas, the sedimentary dynamics

of submarine canyons off south-eastern Spain have been barely investigated (Puig et al., 2017), particularly because of two main reasons: (i) low river discharge resulting in reduced sediment supply to the continental margin; and (ii) lack of high-energy processes other than storms, such as those occurring in other areas, which have subsequently attracted the researchers' interest (e.g. dense shelf water cascading, DSWC, in the NW Mediterranean Sea —see further down—; Canals et al., 2006).

Submarine canyons from the Western Mediterranean Sea exhibit sediment transport interannual variability, reflecting complex interaction between the diverse forcing factors (atmospheric, hydrologic and oceanographic conditions) (Heussner et al., 2006; Palanques et al., 2006a, 2008b; Ogston et al., 2008). It has been documented in the NW Mediterranean region that during major storms sediments deposited on the continental shelf and canyon heads can be remobilized and flushed down-canyon (Canals et al., 2006; Palanques et al., 2006a; Sanchez-Vidal et al., 2012; Pedrosa-Pàmies et al., 2013), triggering large sediment export to the deep margin and basin (Sanchez-Vidal et al., 2012; Puig et al., 2014). Storm-induced downwelling there contributes to the off-shelf transfer of particulate matter, forced by a strong cyclonic circulation and along the coast water convergence during eastern storms (Ulses et al., 2008b; Palanques et al., 2008b; Martín et al., 2013). Another highly relevant process occurring in the NW Mediterranean Sea is DSWC following formation of dense water over the continental shelf and subsequent near-bottom, gravity-driven sinking due to loss of buoyancy. Dense shelf water forms mostly in the Gulf of Lion during favourable winters, characterised by persistent cold and dry northern winds (Durrieu de Madron et al., 2008; Canals et al., 2013). Both dense shelf water formation and cascading present a high degree of interannual variability (Béthoux et al., 2002; Durrieu de Madron et al., 2005). Submarine canyons in the area behave as main conduits for particle-laden cascading waters, which in the absence of submarine canyons can flow downslope anyway until reaching their neutral buoyancy depth (Canals et al., 2006). DSWC occurs in the form of short-lived metoceanographic events deeply impacting the deep ecosystem and associated benthic fauna by supplying large amounts of organic carbon (OC) (Company et al., 2008; Pusceddu et al., 2013). The amount and quality of the sinking particles is modulated by the occurrence of river floods and autochthonous biological production (Guillén et al., 2006; Fabres et al., 2008; Sanchez-Vidal et al., 2013; Lopez-Fernandez et al., 2013a).

Anthropogenic activities also impact the sediment dynamics of submarine canyons. Bottom trawling gear in particular erodes canyon upper flanks (Puig et al., 2012; Martín et al., 2014a), resulting in the remobilization of sediments that are channelized by tributaries (Martín et al., 2014b), ultimately increasing sediment accumulation rates in canyon axes (Paradis et al., 2017).

The non-occurrence of DSWC and the micro-tidal regime in the SW Mediterranean Sea raise the question about the relevance of sediment transfers to the deep margin and basin in this area, while also pointing to the need to quantify the overall fluxes and their composition, including organic matter (OM) contents, to determine possible relationships with specific forcing conditions, and to establish the periodicity of transfer events. These questions become more noteworthy when considering the lack of discharge from river systems during most of the year, severely limiting to rare time periods the supply of terrestrial sediments to the margin (Liquete et al., 2005).

This study focuses on the temporal variability of near-bottom and mid-water particle fluxes and associated oceanographic parameters over one-year in the mid-course of three submarine canyons (Escombreras, Garrucha-Almanzora and Almeria), in the open slope north of Garrucha-Almanzora Canyon, and in the deep basin in the Gulf of Vera, as investigated by means of sediment traps and currentmeters deployed in situ. The aim of the present study is to fill a gap in the knowledge of shelf-to-deep basin mass transfer in the SW Mediterranean Sea and, more generally, in sediment-starved margin segments. The simultaneous study of these three environments (canyons, open slope and deep basin) is also needed to better understand eventual interconnections amongst them.

3.1.2. Overall setting

The study area encompasses the Gulf of Vera to the north and the Gulf of Almeria to the south, in the SW Mediterranean Sea (Fig 3.1). Climate is semi-arid, with low mean annual rainfall (<500 mm yr^{-1}) (AEMET, 2011). In spite of low annual precipitation, involving dry or almost dry streams during most of the year, fast flooding events occur in the region mainly in autumn months (Machado et al., 2011). The main rivers in the area are, in a clockwise direction, Almanzora, Antas, Aguas and Andarax (Fig. 3.1). Almanzora River is the main hydrological system, with a watershed of 2,611 km^2 (Puig et al., 2017), followed by the Andarax River system with 2,160.5 km^2 (Liquete et al., 2005). Both rivers feed delta and prodelta systems (Sanz et al., 2002a; Liquete et al., 2005).

Wind regime in the study area is dominated by NE to SW flux in Cape of Palos and ENE to WSW in Cape of Gata, which may triggers significant wave heights (H_s) of < 5 m with wave periods of 6-7 s (Puig et al., 2017). Less frequent, stronger inter-annual wind events are able to generate 5 m < H_s < 7 m, generally during autumn and winter months. Events triggering major storms with waves between 5 m ≤ H_s < 6 m can occur every 2-3 years, whereas for storms with waves with H_s equal or above 6 m the return period is longer than 13 years (www.puertos.es).

Prevailing surface circulation in the Gulf of Vera is southwards to Cape of Gata. In the neighbouring Alboran Sea the inflow of the Atlantic jet through the Gibraltar Strait forms two main non-permanent anticyclonic gyres, known as the western and eastern Alboran gyres (WAG and EAG, respectively). The encounter of the Mediterranean water from the north and west with the less saline Atlantic Water coming from the Alboran Sea produces a strong baroclinic jet, called Almeria-Oran Front (AOF), which extends in a NW-SE direction from Spanish to Algerian coasts (Tintore et al., 1988). The semi-permanent AOF represents the eastern limit of the Alboran Sea circulation system and is controlled at its eastern edge by the geographic position and strength of the EAG, which usually forms during summer-autumn (Vargas-Yáñez et al., 2002; Renault et al., 2012). Intermediate and deep Mediterranean waters circulate towards the Strait of Gibraltar following the Spanish continental margin (Millot, 1999). Phytoplankton blooms in the study area usually extend from November to March (Garcia-Gorriz and Carr, 2001).

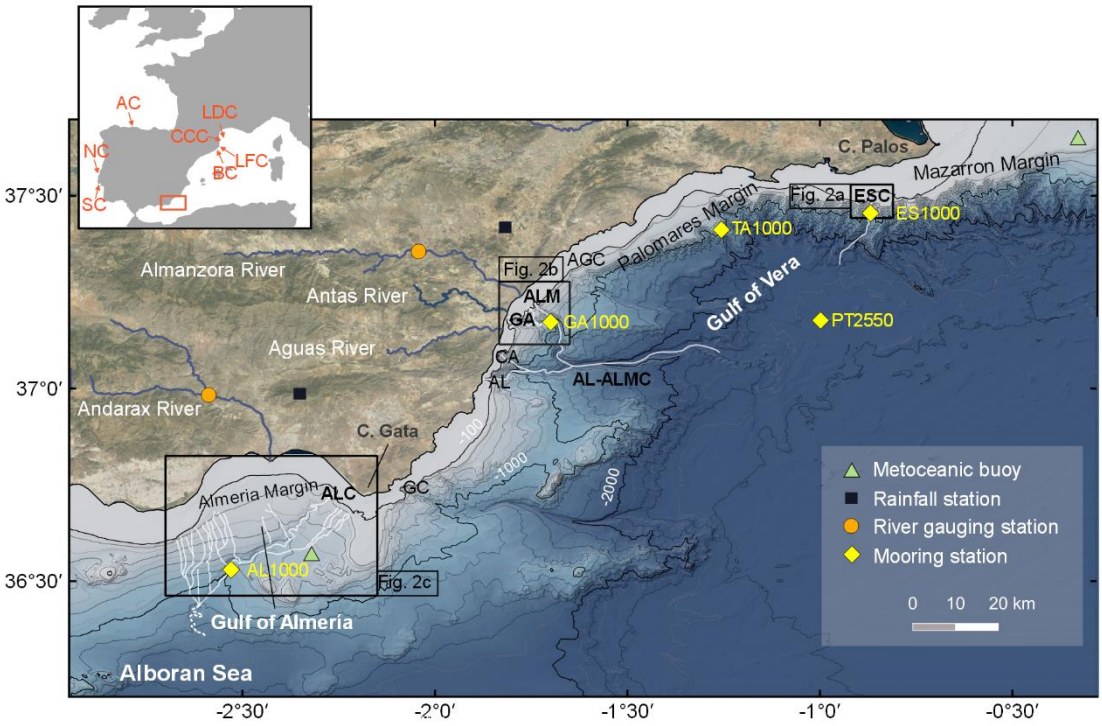

Figure 3.1. Bathymetric map of the gulfs of Vera and Almeria with the main axis of Escombreras (ESC), Alias-Almanzora (AL-ALMC) and Almeria (ALC) canyon systems (white lines). The location of the Alias-Almanzora Canyon tributaries (AL: Alias; CA: Cabrera; GA: Garrucha; ALM: Almanzora) and the Aguilas Canyon (AGC) and the Gata Canyon (GC) are indicated. Yellow diamonds indicate the location of mooring stations. Cape of Palos and Cape of Gata metoceanic buoys (green triangles), rainfall stations (black squares) and river gauging stations (orange dots) are also shown. Black squares show the location of detailed submarine canyon maps in Figure 2. Other submarine canyons referred to in this paper are shown in the inset (LDC: Lacaze-Duthiers Canyon; CCC: Cap de Creus Canyon; LFC: La Fonera Canyon; BC: Blanes Canyon; NC: Nazaré Canyon; SC: Sétubal Canyon; AC: Avilés Canyon.

The study area comprises three margin segments, which are the Mazarron and Palomares margins within the Gulf of Vera, with E-W and NE-SW general orientation, respectively, and the Almeria margin south and west of Cape of Gata (Fig. 3.1). Neogene and Quaternary tectonics have determined the evolution and morphology of these margins (Estrada et al., 1997; Comas et al., 1999; Acosta et al., 2013). Most submarine canyons in the area follow fault systems, some of which are active, as is the case for the Almeria (ALC) and Escombreras (ESC) canyons (Estrada et al., 1997; Gràcia et al., 2006; Acosta et al., 2013; Pérez-Hernández et al., 2014). However, it is uncertain if the faults guiding Alias-Almanzora (AL-ALMC) and Gata (GT) canyon systems (Fig. 3.1) are still active (Gómez de la Peña et al., 2016).

The study area presents a narrow continental shelf (Lobo et al., 2014), which in the Mazarron margin ranges from 13 km to the east to <4 km to the west, to then open to a steep continental slope dominated by multiple short canyons from ~200 m depth downwards (Acosta et al., 2013). The Palomares shelf generally is <11 km wide (Pérez-Hernández et al., 2014), being narrowest in the vicinity of Garrucha Canyon head (GA). The shelf break in the Palomares margin is between 120-170 m depth, and the slope displays a complex morphology due to the presence of several

submarine canyons (Aguilas (AGC), Alias-Almanzora and Gata), and prominent seamounts (Pérez-Hernández et al., 2014). In the Almeria margin, the continental shelf is 6 to 12 km wide (García et al., 2006), with the shelf edge at 100-120 m depth. The main geomorphological features therein are various submarine valleys which conform the Almeria Turbidite System (Estrada et al., 1997; García et al., 2006), which is the largest of its kind in the Alboran Sea (Vázquez et al., 2015).

From north to south and east to west the studied canyons are the N-S oriented single Escombreras Canyon on the Mazarron margin, the W-E Garrucha-Almanzora Canyon system (Fig. 3.2) that is the northern part of the Alías-Almanzora system on the Palomares margin, and the Almeria Canyon on the Almeria margin (Fig. 3.1).

The Escombreras Canyon is more than 20 km long and mostly N-S oriented. It presents a maximum axial gradient of 15º. While the canyon head is convex in shape and it is cut by numerous gullies (Acosta et al., 2013), the lower canyon extends onto the uppermost continental rise where it forms a channel systems (Acosta et al., 2013).

The Alias-Almanzora Canyon system has a total length of 73 km (Pérez-Hernández et al., 2014) and consists of four shelf incised branches entering the Palomares margin. In its northernmost part, the Almanzora Canyon branch (ALM) converges at 1,100 m depth with the Garrucha Canyon branch (GA), resulting in the Garrucha-Almanzora system (following Puig et al., 2017 nomenclature). The Almanzora Canyon extends from 65 m depth off the Almanzora River (Puig et al., 2017) and presents a mean axial slope gradient of 8.6 º and a total length of 8 km. The Garrucha Canyon branch splits in two canyon heads off the Almanzora River prodelta, together with two other main canyon heads further south, located between Antas and Aguas river mouths, opening as closer as 30 m from Garrucha harbor. The southern canyon heads are fed by several small tributary channels that could be tracked up to 7 m depth on the innermost shelf. The Garrucha Canyon branch displays a meandering pattern, with an average axial slope of 5º, for a total length of 15.7 km (Puig et al., 2017). At 1,811 m depth the Garrucha-Almanzora system merges with the southern Alias-Cabrera system, thus forming the Alias-Almanzora system (Pérez-Hernández et al., 2014).

The NE-SW oriented Almeria Canyon is more than 55 km long (García et al., 2006). Its axial gradient ranges between 1.2º and 1.4º, and it is fed by three tributary valley systems (TVS), from west to east, Dalias, Andarax and Gata (Fig. 3.2), which incise the shelf break and converge with the main canyon at 700-1,500, 300 and 650 m, respectively (García et al., 2006). The Dalias TVS covers an area of 300 km^2 with a length of 22 km, but only the Andarax TVS is connected to the Andarax River (García et al., 2006). The Almeria Canyon axis is NE-SW oriented down to 1,200 m depth where it becomes the Almeria Channel feeding a fan lobe system (Cronin et al., 1995; Estrada et al., 1997).

Thus, submarine canyons located in these margin segments are diverse in several aspects, such as size, orientation, with or without shelf incision, individual or with several tributaries and their relation with present day tectonics.

3.1.3. Materials and methods

3.1.3.1. Experimental design

Three mooring lines were deployed along the axis of three submarine canyons at approximately 1,000 m depth: in Escombreras (ES1000), Garrucha-Almanzora (GA1000) and Almeria (AL1000) submarine canyons (Fig. 3.2). Two additional moorings were deployed as control stations, one in the open slope in the Palomares margin (TA1000) and one in the deep basin at 2,550 m depth (PT2550). The moorings were deployed from March 2015 to March 2016, with recovery-redeployment operations at month 6 for maintenance, changing batteries and sampling cups (Table 1). Each mooring was equipped with a Technicap PPS3/3 sequential sediment trap (0.125 m^2, cylindroconical shape) with 12 trap cups with a sample resolution of 7-16 days. The mooring deployed in the deep basin was equipped with two sediment traps: one at mid-water depth (PT2550-S, with "S" standing for "shallower") and the other near the bottom (PT2550-D, with "D" standing for "deeper"). The trap cups were filled with 5% (v/v) formaldehyde solution in 0.45 µm filtered sea water buffered with sodium tetraborate. Aquadopp Nortek current meters with sampling interval of 30 min were placed 2 m below the sediment trap to monitor current velocity, direction, pressure and water temperature. Some currentmeters were equipped with Seapoint turbidity meters, calibrated for Formazin Turbidity Units (FTU), which detect light scattered at 15°-150° (with a sensibility peak at 90°) of a confined volume of five centimetres of the sensor window. Pitch and roll parameters and velocity have been checked to assess that hydrodynamic conditions did not have a detrimental impact on trap verticality and discard a bias in the collection of particle fluxes (Gardner, 1985; Baker et al., 1988; Buesseler et al., 2007).

Mooring station/level	Latitude	Longitude	Mooring depth (m)	Minimum distance from mooring line to coastline (km)	Sampling period	Number of samples
ES1000	37°27.309'N	0°52.274'W	985	14	16/3/2015-28/8/2105	12
TA1000	37°24.613'N	1°15.394'W	1003	16	16/3/2015-31/3/2016	24
GA1000	37°10.294'N	1°41.968'W	1100	10.7	25/3/2015-15/10/2015	14
AL1000	36°31.709'N	2°32.003'W	1000	22	25/3/2015-31/3/2016	24
PT2550-S	37°10.635'N	0°59.993'W	2550	40	16/3/2015-31/3/2016	24
PT2550-D	37°10.635'N	0°59.993'W	2550	40	16/3/2015-31/3/2016	24

Table 3.1. Metadata of mooring lines. Sediment traps were placed 25 mab (m above the bottom) except for PT2550-S level, which was at 546 mab (mid-water deep basin trap). Due to specific technical failures of the rotation system of sediment traps, the complete time series is not available for ES1000 and GA1000 mooring stations. Currentmeters were deployed below each sediment trap excepting in PT2550-S. Each currentmeter was equipped with turbidity meters excepting in AL1000. In PT2550, "S" stands for "shallower" and "D" stands for "deeper" (see further details in the main text).

CTD (Conductivity-Temperature-Depth) profiles were carried out during 13th-23rd March 2015 and 29th August-1st September cruises around each mooring station. Additionally, a transect of 3 CTD casts comprising the outer area of the Mazarron margin and Escombreras Canyon was performed in March 2015 (Fig. 1.2a). The CTD was a SBE 911 equipped with a WET Labs ECO-AFL/FL fluorimeter, a SBE 43 oxygen sensor and a WET Labs ECO-NTU turbidity meter sensor (in Nephelometric Turbidity Units). The turbidimeter measures turbidity from side-scattered light at 90º relative to the laser light.

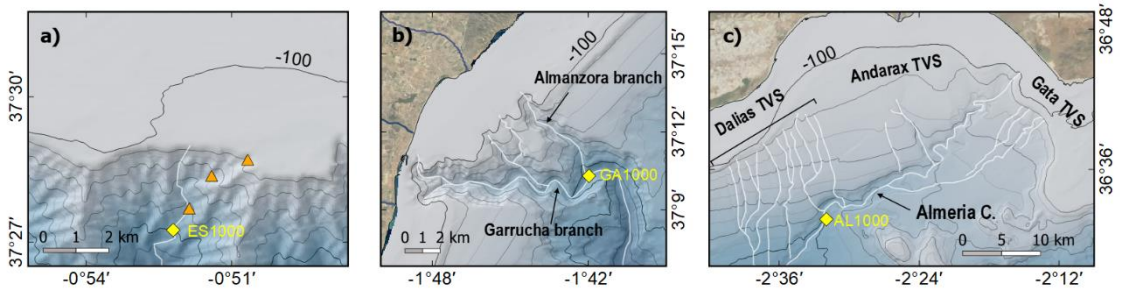

Figure 3.2. Bathymetric maps of the heads of (a) Escombreras Canyon, (b) Garrucha-Almanzora Canyon system, and (c) Almeria Canyon and tributary valley systems (TVS). Yellow diamonds show the location of mooring stations and CTD deployments. Orange triangles illustrate a CTD transect across the outer Mazarron shelf and upper Escombreras Canyon. Yellow diamonds indicate the mooring sites.

3.1.3.2. Sample treatment and analytical procedures

Sediment trap samples were stored in the dark at 2-4 °C, and were processed in the laboratory following a modified protocol from Heussner et al. (1990), as described in Lopez-Fernandez et al. (2013b).

Total Mass Fluxes (TMF) were calculated for each period following next equation:

$$TMF\ (g\ m^{-2}d^{-1}) = \frac{Sample\ dry\ weight\ (g)}{Collection\ area\ (m^2) * sampling\ interval\ (d)} \quad [3.1]$$

Time weighted Fluxes (TWF) represents a weighted average corrected according sampling interval value:

$$TWF\ (g\ m^{-2}d^{-1}) = \frac{\sum Mi\ (g)}{Collection\ area\ (m^2) * \sum Di\ (d)} \quad [3.2]$$

Where: $\mathbf{M_i}$ is the mass of each sample and $\mathbf{D_i}$ is the collection interval days of each sample

The contents of Total Nitrogen (TN), Organic Carbon (OC) and Total Carbon (TC) were determined using an Elemental Analyser EA Flash series 1112 in the Scientific and Technological Centres of the University of Barcelona. Before analysis, samples for OC determination were de-carbonated with repeated additions of 10 µl of HCl (1M) with 3h 60°C drying steps in between until no effervescence was observed. Percentages of organic matter (OM) and calcium carbonate ($CaCO_3$) were calculated following relations:

$$OM = OCx2 \qquad [3.3]$$

and

$$CaCO_3 = (TC-OC)*8.33 \qquad [3.4]$$

where 8.33 is the molecular mass ratio (assuming that all inorganic carbon is in the form of calcium carbonate).

Biogenic Si content was obtained analysing Si and Al with an Inductive Coupled Plasma Optical Emission Spectroscopy (ICP-OES), with a two-step digestion for 2.5 h at 90 ºC with a solution of Na_2CO_3 (0.5 M) following Fabres et al. (2002). Lixiviate Si/Al ratios were used as correction factor to obtain biogenic Si in sediments (Kamatani and Oku, 2000) and multiplied by factor of 2.4 to obtain opal percentage (Mortlock and Froelich, 1989). The opal fraction was determined in the PT2550-S samples, where pelagic sedimentation is expected to be more noticeable. In this case, the lithogenic fraction was calculated assuming that

$$\%lithogenics = 100-(\%OM+\%CaCO_3+\%opal) \qquad [3.5]$$

In the samples collected in the near-bottom traps, discrete analysis indicate a minor opal contribution to total mass. Then, the lithogenic fraction was calculated without considering this fraction.

Grain size analysis of particles were carried out with a Beckman Coulter LS 230 laser diffraction particle size analyser, which measures sizes between 0.04 and 2,000 µm. Prior to analysis, samples were twice oxidized with 50 ml of 10% H_2O_2, drying the samples between each oxidation. Each sample was than divided in two subsamples, one of which was de-carbonated with 50 ml 1M HCl to obtain the grain size distribution of lithogenic particles. Once dry, both fractions were dispersed with 50 ml of 5% sodium polyphosphate solution and placed in a rotary agitating for at least 3 h to prevent particle's flocculation.

3.1.3.3. Metoceanic and human activity records

Metoceanic data (wind velocity and provenance, significant wave height and wave provenance) were obtained from *Agencia Estatal de Meteorología* and *Red de Boyas de Aguas Profundas* (REDEX, *Puertos del Estado*). In this study we used data from the Cabo de Palos buoy (Long. 0.33°W, Lat. 37.65°N), moored in the inner shelf of the northern margin of Gulf of Vera, and the Cabo de Gata buoy (Long. 2.32ºW, Lat. 36.57ºN) near Cape of Gata. In order to obtain accurate daily wave parameters, close to the submarine canyons heads, 3 WANA points were used for this study. The WANA network delivers time series of wind and waves parameters from numerical modelling generated by *Puertos del Estado* in collaboration with *Agencia Estatal de Meteorología*.

Hourly Andarax and Almanzora river discharges were obtained from *Red SAIH Hidrosur*, operated by Junta de Andalucía. Gauging stations are not located near the river mouth. The above data was complemented with rainfall data from two meteorological stations located in the Almeria province, from the same data source.

Monthly chlorophyll-a concentration (Chl-a) (mg m^{-3}) and sea surface temperature (SST) (°C) data were obtained from Moderate Resolution Imaging Spectrometer (MODIS), in orbit on the Aqua platform, using 4 km resolution level 3 binned data. These data are processed and distributed by *NASA Goddard Earth Science (GES) Data and Information Services Centre (DISC)* and supported by the Ocean Biology Processing Group (OBPG).

Fishing activity has been monitored from Vessels Monitoring System (VMS) data provided by *Secretaria General de Pesca*, *Ministerio de Agricultura, Alimentación y Medio Ambiente* of the Spanish Government.

3.1.4. Results

3.1.4.1. Forcing conditions

Beyond major storms with high H_s (cf. section 3.2) the dry or wet character of every storm also is of relevance, as it defines the absence or presence of associated rainfall (Guillén et al., 2006). Indeed, eastern storms are charged with humidity and trigger precipitation by orographic control when encountering the land, conversely to storms coming from mainland, i.e. from the north and west. Rainfall rates are often higher during late summer and autumn, when the evaporation of the relatively warm Mediterranean Sea provides a continuous supply of heat and water vapor, increasing the moisture content at low levels (Hermoso et al., 2021). However, as shown in Figure 3, rainfall does not always translate into an increment of river discharge, since other factors such as infiltration and ground water reserves influence surface runoff and the fluvial response in dry climates such as the one in the study area (Liquete et al., 2005). During the studied period, three main stormy periods occurred (Fig. 3.1.3).

The first period developed in early spring 2015, mainly associated with north-eastern winds and characterized by unstable cold weather with various rainfall episodes. On 17-21th March 2015 the buoys registered a wet northern storm with H_s up to 4.8 m (T_s=6.3 s) in Cape of Palos, exceeding 2 m for 77 h. In Cape of Gata the event had a maximum wave height of 4.2 m and less duration. After the storm, Andarax River registered a slight increase in discharge, with a maximum of 2.2 m^3 s^{-1}. Two other wet storms occurred in April, the first between 6-9th, with a considerable duration of 88 h, was strongest in Cape of Gata with a maximum H_s of 4.5 m (T_s=6.6 s), followed by a milder event on the 12th that was only recorded in Cape of Gata.

The second stormy period took place in autumn months and was characterized by a set of storms accompanied by abundant rainfall episodes, which impacted river discharge during September. On the first of November 2015 a north-eastern storm triggered H_s of 4.2 m at Cape of Gata and 3.9 m at Cape of Palos, lasting 37 h and 28 h, respectively. After the event both gauge stations registered a flood episode of up to 36.1 m^3 s^{-1} in Almanzora River and a less marked increment of 0.7 m^3 s^{-1} in the Andarax River. In late November another storm ($H_s \leq 4$ m) of short duration (13 h) from the southwestern was recorded at the Cape of Gata buoy.

The last stormy period occurred during winter months early in 2016, driven by several strong wind episodes blowing from west and south, accompanied with rather weak rainfall, especially in

the southern part of the study area. A set of events took place in early January, February and March. Near Cape of Palos occurrence and intensity were less, with maximum H_s of 4 m on 12th and 26th February. In Cape of Gata the strongest ones happened on the 7th, 9th and 19th February. In particular, the 9th February storm lasted for 149 h with maximum H_s of 4.8 m and T_s of 6.4 s. The rest of the events during February and March were milder, never surpassing a H_s of 3.7 m.

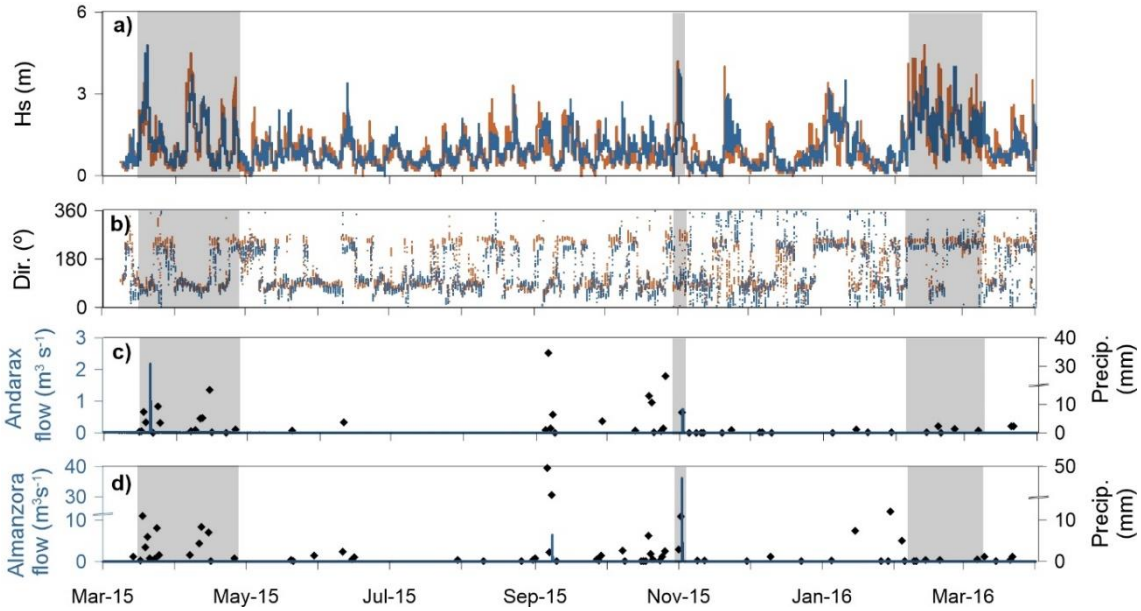

Figure 3.3. Time series of external forcings during the year-round monitoring period from March 2015 to March 2016. (a) Significant wave height (Hs) at Cape of Palos buoy (orange curve) and Cape of Gata buoy (blue curve); the grey vertical stripes highlight the main storm events. (b) Wave provenance in Cape of Palos and Cape of Gata buoys. (c) Andarax River flow (Terque gauging station) and hourly accumulated precipitation (Rambla de Tabernas station). (d) Almanzora River flow (Cantoria gauging station) and hourly accumulated precipitation (Sierra Almagro station).

Concerning primary production, in early spring 2015 a bloom developed close to the coasts (Fig. 3.4), with maximum values up to 0.6 mg m^{-3} in March. Between May and October 2015, oligotrophic conditions prevailed in the study area, with relevant primary production outside the study area, in the south-western Alboran Sea associated to the WAG upwelling zone. An increment of chlorophyll-a at the sea surface occurred from November 2015 to March 2016, restricted to the Alboran Sea during autumn months and extending to the wide Gulf of Vera during winter months in early 2016. This bloom was particularly prominent during January near Cape of Gata and over Mazarron margin, with Chl-a concentration up to 2.7 mg m^{-3}, and low sea surface temperature (SST) near the coast.

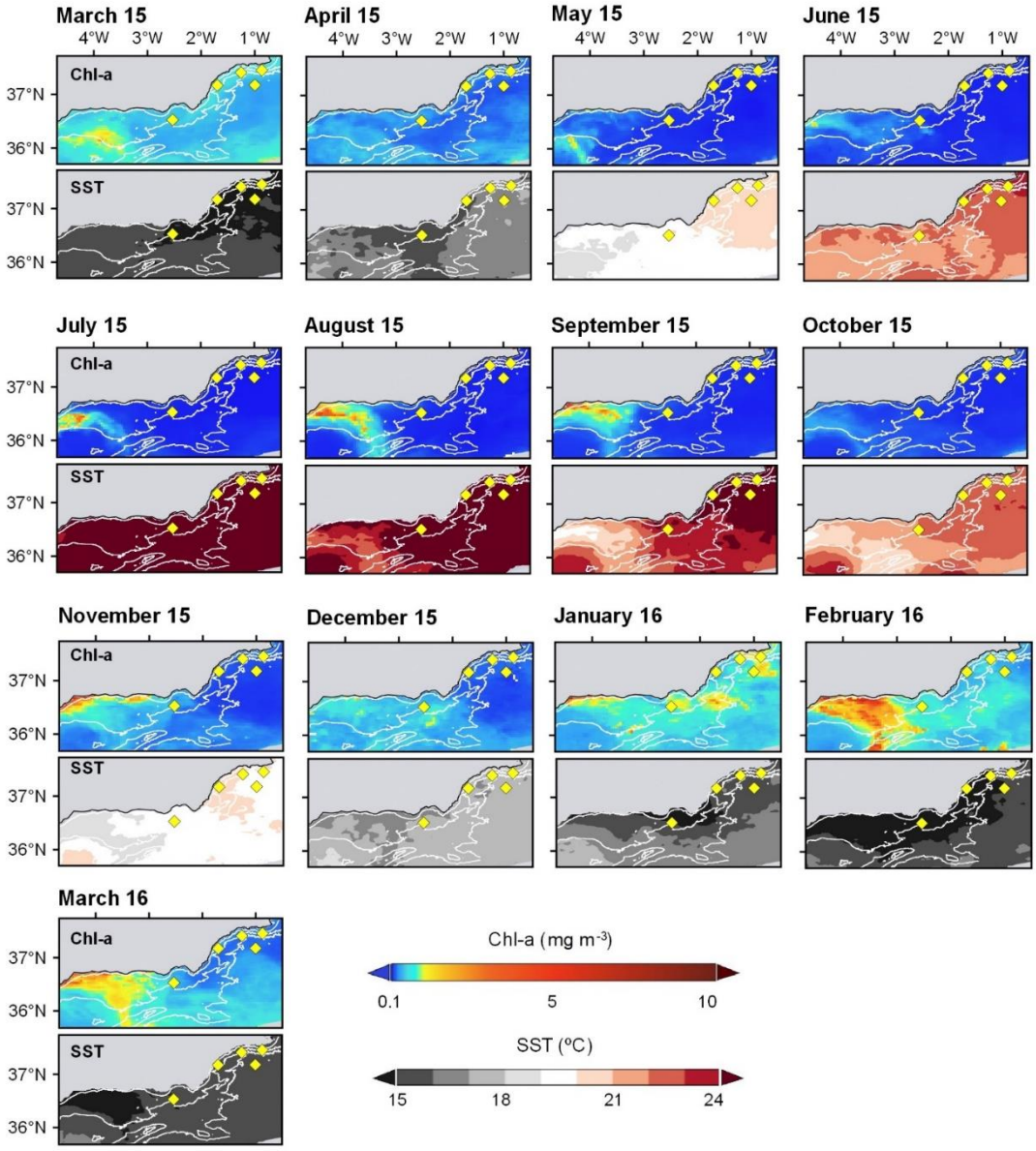

Figure 3.4. Monthly averaged superficial chlorophyll-a concentration maps (mg m^{-3}) and SST (ºC) from March 2015 to March 2016. The yellow diamonds represent the mooring lines.

3.1.4.2. Near bottom currents

Current velocities recorded in all stations did not exceed 20 cm s^{-1}, and only punctually reached more than 10 cm s^{-1} (Fig. 3.5a-d). Currentmeters deployed on the continental margin registered two periods with moderate increments of current speed, first during March-April 2015 and second during February-March 2016, as shown in stations with complete time series. In the deep basin station, the maximum current velocity was recorded at the end of April 2015, up to 19.5 cm s^{-1}, with current pulses coming from continental margin areas located to the north and west of the mooring site.

Current velocity peaks did not coincide with turbidity peaks (Fig. 3.5a-c). The turbidity series generally present low values with subtle increases that did not surpass 3 FTUs, a tendency only disrupted in the Garrucha-Almanzora Canyon. After late July, there was a progressive increase with a peak of 28 FTU at the end of August, followed by a quick decrease until reaching previous values in the last days of August 2015 (Fig. 3.5c). Biofouling is discarded to be the cause of the FTU increment observed in GA1000 because the subsequent flattening of turbidity values is not associated to a current speed increase that eventually could have swept away particles loosely adhered to the sensor.

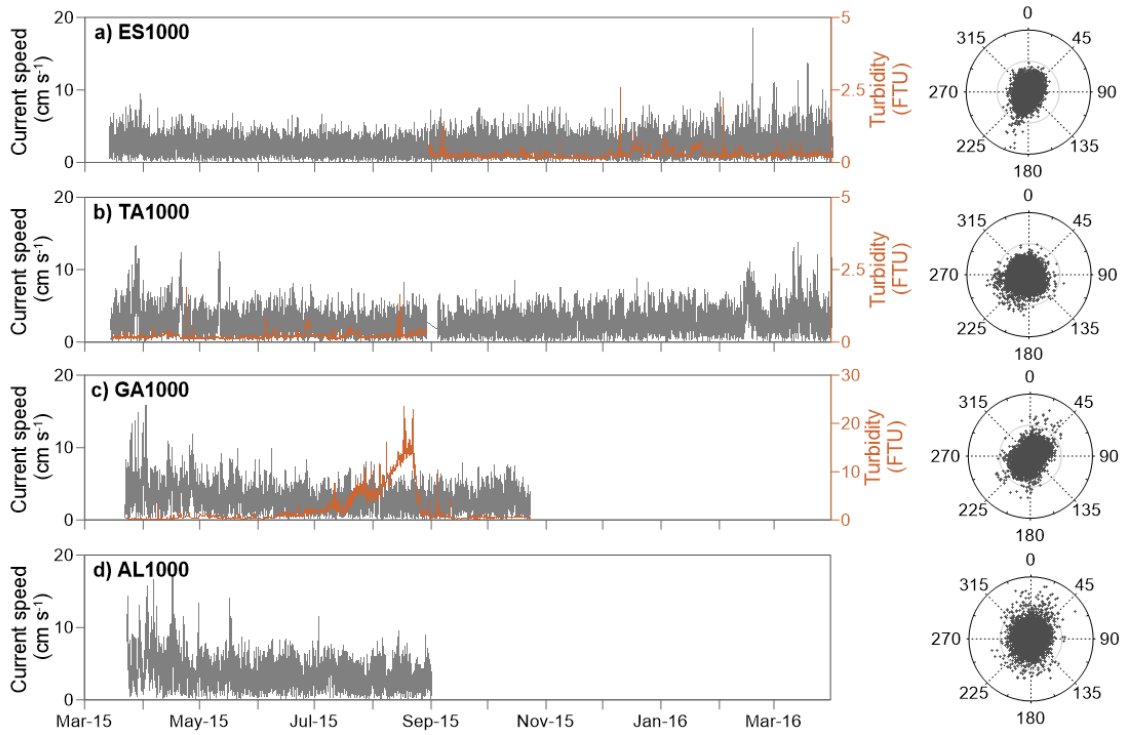

Figure 3.5. Current speed (grey line) and turbidity (orange line) recorded at 20 mab in (a) ES1000, (b) TA1000, (c) GA1000 and (d) AL1000 stations. Polar plots show the direction of currents with the X axis ranging from 0 to 20 cm s^{-1}. FTU: Formazin Turbidity Units.

3.1.4.3. Spatial and temporal variability of total mass fluxes

TMF's in the stations located in the continental margin were one order of magnitude larger than those in the deep basin. Basic statistics (Table 3.2) show a weighted average value (TWF) of 7.33 g m^{-2} d^{-1} in GA1000 whereas the one found in ES1000 is up to 4.80 g m^{-2} d^{-1}. AL1000 presents a lower value than the two previous stations (1.64 g m^{-2} d^{-1}), similar to that obtained in TA1000 (1.90 g m^{-2} d^{-1}). Traps deployed at two levels in the deep basin (PT2550-S and PT2550-D) present TMFs lower than 1 g m^{-2} d^{-1} during all the monitoring period.

TMF values fluctuate considerably throughout the studied period (Fig. 3.6). The maximum values were recorded in March and April 2015. The maximum value was obtained in ES1000, up to 24.96 g m^{-2} d^{-1}, followed by GA1000 (18.15 g m^{-2} d^{-1}), TA1000 (8.37 g m^{-2} d^{-1}) and AL1000 (5.12 g m^{-2} d^{-1}). Two behaviours are noted for the rest of the months. ES1000, AL1000 and TA1000 stations

registered much lower fluxes during the rest of the monitoring period, with a minimal increment during autumn and winter months. In ES1000 station the lack of data prevents us from describing TMFs. Unlike those stations, fluxes recorded in GA1000 fluctuated during spring and summer months, until October. A different behaviour is observed in the deep basin station, with maximum values recorded in April 2015 in PT2550-S and September 2015 in PT2550-D.

Mooring station/sediment trap	TWF	Components (TWC)				Grain size (de-carbonated)		
	g $m^{-2}d^{-1}$	Litho %	CaCO3 %	OM %	Opal %	Clay %	Silt %	Sand %
ES1000	4.80±6.55	60.5±2.7	36.5±3.1	3.0±0.8	-	35.0±2.7	65.0±2.7	null
TA1000	1.90±1.61	60.6±7.3	36.3±8.1	3.1±0.9	-	31.1±6.9	66.9±5.7	2.0±3.7
GA1000	7.33±5.31	62.4±3.2	34.2±3.8	3.4±0.9	-	23.7±4.0	74.0±3.4	2.3±1.2
AL1000	1.64±1.32	72.4±2.1	23.5±2.1	4.1±1.1	-	15.8±5.7	81.2±4.7	3.1±1.7
PT2550-S	0.07±0.12	64.2±10.1	22.7±11.4	5.7±2.9	7.4±5.0	-	-	-
PT2550-D	0.06±0.05	65.0±9.1	29.3±8.8	5.7±2.1	-	-	-	-

Table 3.2. Averaged total weighted flux (TWF), averaged total weighted components (TWC), and grain size of the de-carbonated fraction of samples from each sediment trap. Standard deviation is also shown. Note that the series only cover from March to September 2015 in the GA1000 station and from March to August 2015 in the ES1000 station.

3.1.4.4. Characteristics of settling particles

Main composition

At the canyon and open slope stations the lithogenic fraction is the main component (Table 3.2 and Fig. 3.6), with an averaged content of 72.4% in AL1000, and more similar percentages in the rest of the stations (60.5-65.0%). The averaged $CaCO_3$ content varies from 22.7% in PT2550-S and 36.5% in ES1000. OM percentages are lower in open slope and canyons stations (3.0-4.1%) while higher values have been found in deep basin traps (5.7%). Analyses of some discrete samples from continental margin stations indicate that opal contents are negligible in those stations, with maximum values below 2.5%. In contrast, PT2550-S shows average opal values of 7.4±5.0%.

The molar OC/N ratio is represented in Figure 3.6. Settling particles in GA1000 show values higher than 12 in almost the entire monitoring period, with a maximum of 20.1 in early April. In contrast, values in ES1000 and AL1000 samples are below 12. The OC/N ratio tends to diminish after March and April 2015, except in GA1000 station, which presents high values in August 2015 samples. TA1000 settling particles show the widest range (6.7-20.3), with more extreme values during the second deployment period. Concerning deep basin settling particles, PT2550-S shows lower values than PT2550-D, with an average of 9.0 against 9.8, respectively. In both sediment traps there was a tendency to increase OC/N ratios across the study period, with the exception of punctual PT2550-D samples.

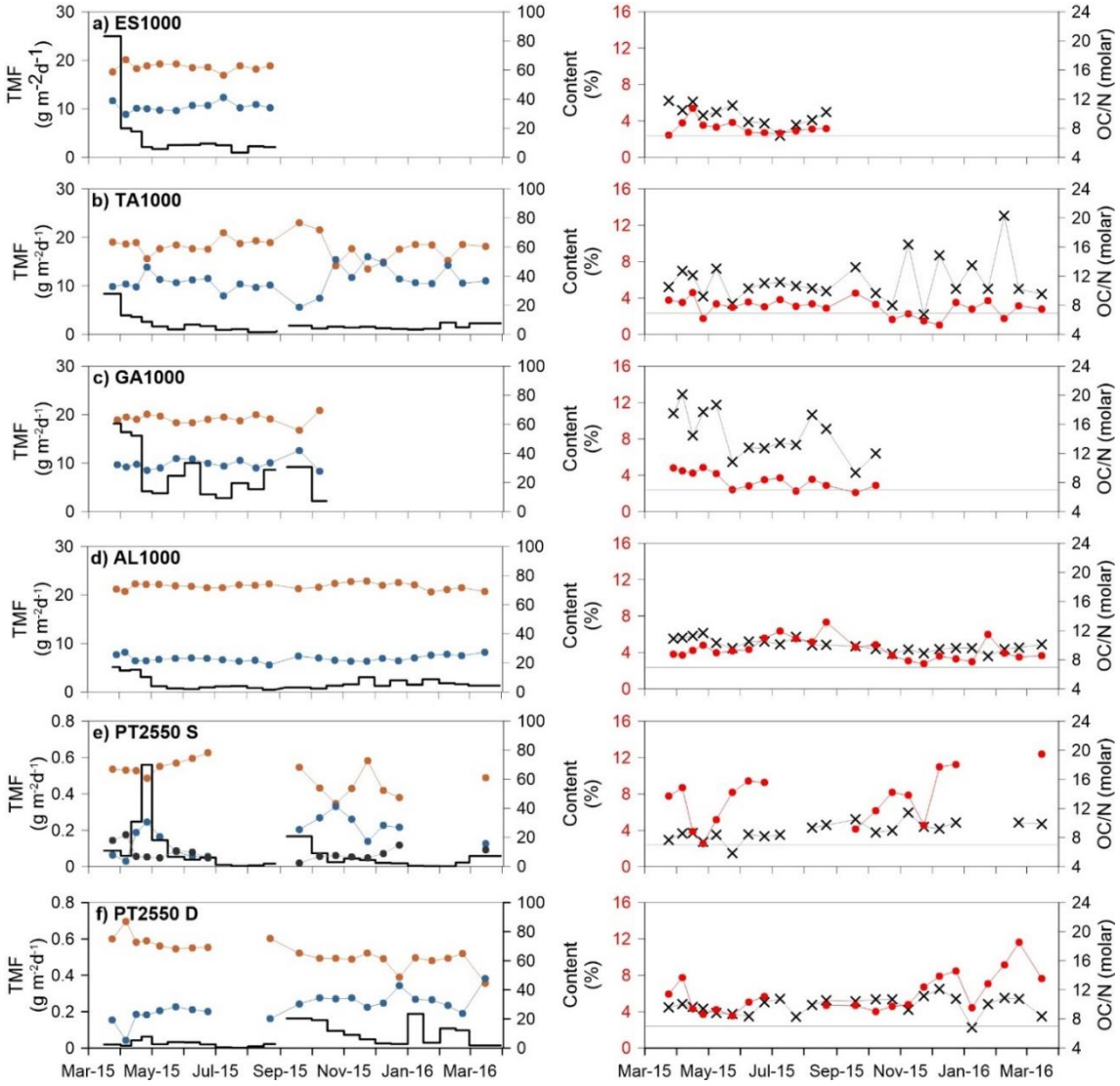

Figure 3.6. Total Mass Fluxes (TMF) in the various traps deployed in mooring stations and percentages of lithogenics (brown line), $CaCO_3$ (blue line), opal (black line) and OM fractions (red line) in station (a) ES1000, (b) TA1000, (c) GA1000, (d) AL1000, (e) PT2550-S and (f) PT2550-D. Black crosses represent OC/N ratios. The grey line separates the OC/N ratios with values higher than 7 from the lower ones. OC/N<7 is considered as indicative of OM from phytoplankton.

Grain size of settling particles

The fine-medium silt fraction dominates de-carbonated samples at all traps and stations (Table 3.2). The finest grains are found in TA1000 and ES1000 settling particles, where the clay fraction averages 31.1% and 35.0%, respectively. GA1000 and AL1000 samples have more silt (74.0% and 81.2%, respectively) and sand fraction (2.3% and 3.1%, respectively). The averaged mean of the particles is coarser in AL1000 (16.2 µm), followed by GA1000 (14.1 µm), TA1000 (12.9 µm) and then ES1000 (9.3 µm).

The average grain size distribution during stormy periods (Fig. 3.3) does not show significant variations (Fig. 3.7). Concerning spring 2015 storms, the main mode was fairly coarse during

March 2015 at ES1000 and AL1000 stations, with means of 11.3 µm and 21.1 µm. In posterior storm events only settling particles collected in TA1000 in early February 2016 show a higher mean (24.5 µm).

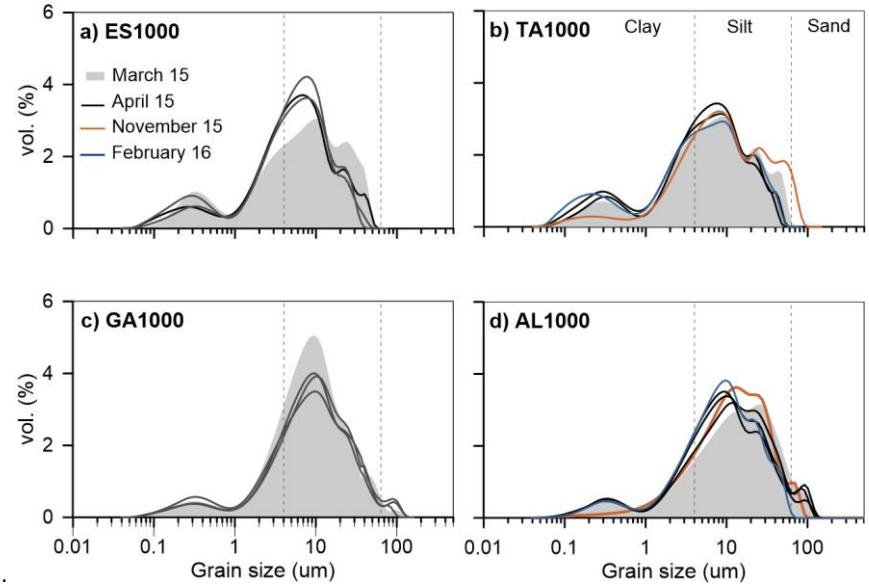

Figure 3.7. Grain size distribution of the lithogenic components during stormy periods in Escombreras, Garrucha, Almeria and open slope sediment traps. The March 2015 sample is represented as shadow grey, April 2015 samples as black lines, early November 2015 as orange lines and early February 2016 as blue lines. The grey vertical dotted lines divide the clay (<4 µm), silt (4-63 µm) (fine-medium silt fraction between 4-40 µm) and sand fractions (63 µm-2 mm).

3.1.4.5. Water column parameters

Suspended particulate matter distribution has been obtained from turbidity meters attached to the CTD in March 2015 and late August 2015 (Fig. 3.8). In March 2015, we observe differences between the CTD casts performed the 13-14th March (TA1000 and ES1000), which show fairly constant turbidity values along the water column around 0.2 NTU, and casts conducted the 20th-23rd March at ES1000 and GA1000 stations, showing an increase of turbidity within continental shelf depths. During that period, the CTD transect along the Escombreras Canyon (Fig. 3.9 c) reveals higher turbidity values (up to 3.74 NTU) near bottom on the outer continental shelf, with turbidity diminished seawards, reaching 1.14 NTU in the last CTD deployed near the ES1000 station. CTD casts near GA1000 station peak at 0.56 NTU, to gradually decrease below the shelf break until reaching values similar to those of the deep basin. Moreover, turbidity values near GA1000 begun increasing again below 400 m depth, extending hundreds of meters down to the bottom, while reaching values up to 0.32 NTU. The CTD cast performed near AL1000 has shown quite constant turbidity values along the water column.

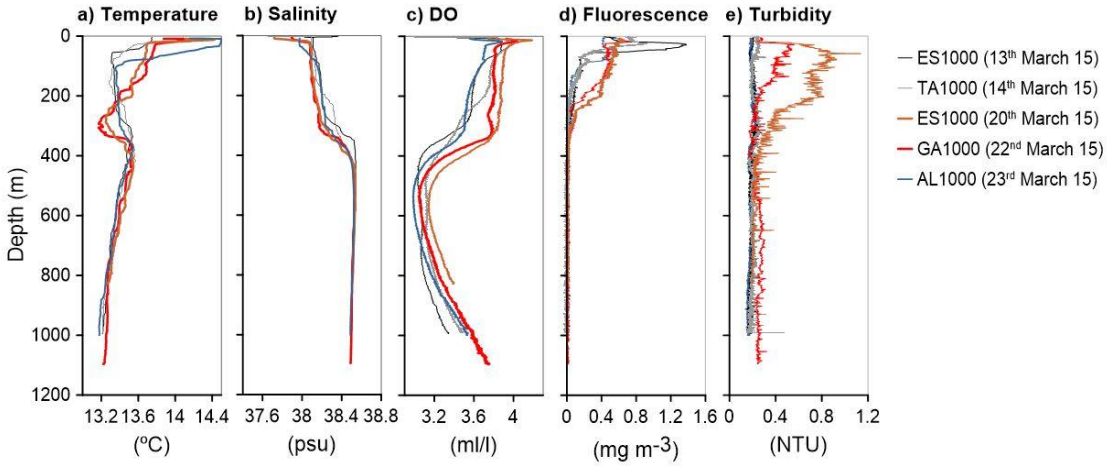

Figure 3.8. Hydrological parameters (potential temperature, salinity, dissolved oxygen (DO), fluorescence and turbidity) from CTD transects during mid-March (pre-storm event; grey tones) and late March 2015 (post-storm event; red, purple and blue colours) at ES1000, TA1000, GA1000 and AL1000 stations. Note that AL1000 station is quite far from the rest of stations (Fig. 3.1).

The hydrological parameters of the upper 1,000 m of the water column also vary notably between the 13-14th and the 20th-23rd March 2015 CTD deployments (Fig. 3.8), as shown by stations ES1000 and TA1000 on one side, and stations GA1000 and ES1000 on the other side. The exception are profiles from AL1000 of the 23rd of March, which are more similar to the ones from ES1000 and TA1000 about 10 days earlier. It should be noted here that AL1000 is quite far from the broad area where the rest of stations are located (Fig. 3.1). Profiles in Figure 8 allow identifying a number of water masses, including a surface layer, a sub-surface layer and the Levantine Intermediate Water (LIW). Most interesting are the 20th and 22nd of March GA1000 and ES1000 profiles, showing surface water mass down to about 200 m with relatively high potential temperature (13.65-13.80 °C) and fairly low salinity (38-38.1 psu), coinciding with a layer-thick fluorescence and, especially, turbidity increase (Fig. 3.8). Below is a sub-surface layer down to 300 m depth, made of almost mixed, colder and oxygen-rich water (minimum temperature of 13.17 °C), less saline (38.15-38.25 psu). Finally, the deeper LIW is indicated by a relative maximum in temperature and a relative minimum of dissolved oxygen. Figure 3.9 a, b, d shows the variation of θ/S and DO seaward over Escombreras Canyon.

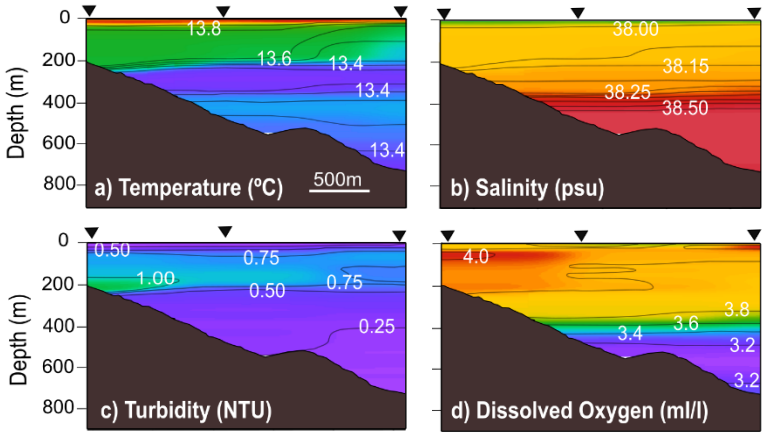

Figure 3.9. Water column properties above the Escombreras Canyon transect after the March 2015 storm: a) Potential temperature (degrees). b) salinity (PSU). c) turbidity (NTU). d) dissolved oxygen (ml/l). The location of CTD casts is shown by the inverted black triangles.

During the late August/early September 2015 cruise, the CTD casts at TA1000 and AL1000 did not show significant differences compared to deep basin values. However, the CTD cast at GA1000 once again presented a turbid layer under 400 m, with a maximum value of 0.37 NTU between 600-750 m and an increase of 0.39 NTU near bottom.

Fluorescence profiles indicate phytoplankton blooms. In mid-March 2015 maximum chlorophyll values were located near the surface with higher values, up to 1.38 mg m^{-3}, over Escombreras Canyon. At the end of March 2015, the fluorescence signal was weaker and distributed along the water column until 250 m depth (Fig. 3.8d). During late summer deployments the fluorescence peak was between 80-90 m depth, with peak values reaching 1.59 mg m^{-3} near GA1000 station, 1.01 mg m^{-3} near TA1000 and 0.75 mg m^{-3} near AL1000.

3.1.5. Discussion

3.1.5.1. Sources of particulate matter

Temporal variability of particle fluxes in continental margins, and in Mediterranean margins in particular, follows deposition and remobilization cycles involving the transfer of matter and energy from the shelf to the slope and deep basin, as pointed out by several authors (Heussner et al., 2006; Ulses et al., 2008b; Palanques et al., 2012; Puig et al., 2014). This leaves an imprint on grain size and the biogeochemical characteristics of the settling particles. Indeed, the grain size of settling particles has been related to lateral transport and sediment sorting (Ferré et al., 2005; Guillén et al., 2006; Sanchez-Vidal et al., 2012; Pedrosa-Pàmies et al., 2013). Also, some biogeochemical parameters are often used as proxies to identify the sources of particle-forming materials. The OC/N ratio in particulate matter is one of these proxies, which allows distinguish between marine and terrestrial OM. Vascular plant–derived OM is typically depleted in nitrogen (molar OC/N ratio > 16), whereas phytoplankton sourced OM shows higher nitrogen contents (molar OC/N ratio < 7) (Goñi and Hedges, 1995). Furthermore, the tendency of vascular plant detritus to preferentially gain N during soil microbial decay may decrease the OC/N ratio from the

originating plants down to 8 (Hedges et al., 1997; Sanchez-Vidal et al., 2013). Therefore, grain size and OC/N ratios allow achieving a rather incisive view of the processes affecting particle fluxes in settings such as the one of the study area.

The grain size distribution of de-carbonated settling particles shows that fine particles dominate in canyons (Table 3.2), in accordance to the calm hydrodynamic conditions during the investigated year-round period. Also, low grain size standard deviation is indicative of fairly stable hydrodynamic conditions at least at the depths where sediment traps were deployed. The lithogenic fraction dominates in all stations, pointing to a high relative contribution of terrestrial inputs along the investigated continental margin. Nonetheless, the terrestrial contribution probably is higher if we take into account that carbonate rocks are abundant in the watersheds feeding the study area, especially to the north. Thus, part of the calculated $CaCO_3$ fraction likely derives from detrital carbonates. As it can be seen in Table 3.2, the mean $CaCO_3$ values in submarine canyons (except Almeria Canyon) and open slope stations are about 11-14% higher than the one in the deep basin mid-water trap, where the highest biogenic contribution could be expected. Fluvial systems are a major source of terrigenous particles for submarine canyons which heads are at short distance from river mouths. These river-sourced particles easily reach mid-canyon segments. Particles settling in the Garrucha-Almanzora Canyon show a clear terrestrial imprint, with OC/N ratios between 9.3 and 20.1 (Fig. 3.6). Lower OC/N ratios are found in settling particles in Almeria (8.5-11.7) and Escombreras (6.9-11.8) canyons. While the lowest values indicate punctual periods of non-degraded marine OC, most ratios found are compatible both with soil degraded OM and mixtures of OM from different origins. Settling particles collected in the open slope show larger heterogeneity of OC/N ratios (6.7 to 20.3). The higher OC/N ratios recorded during autumn and winter months suggest that materials entering the inner shelf through nearby *ramblas* with sporadic discharge events are able to reach the open slope.

The imprint of primary production on settling particles is not always obvious due to the dilution of pelagic marine materials within larger amounts of lithogenic particles carried by advective fluxes from the inner continental margin. Temporal variability of primary production results from shifts in hydrographic conditions throughout the year. Different regimes can be established in the three environments under consideration (i.e. submarine canyons, open slope and deep basin). The seasonal behaviour of settling particles is better recorded in open slope and deep basin samples, with periods where fluxes are dominated by fresh marine OM and biogenic components, which contrasts with prevailing homogeneity in canyon particle samples. Moreover, differences are also evident between near-bottom and mid-water traps in the deep basin (PT2550). Lower OC/N ratios found at mid-water depths compared to those obtained in the near bottom suggest a greater prevalence of pelagic settling at mid-water depth than at near bottom, and the ability of the terrestrial signal to be transferred to the deepest station under scrutiny, at depths larger than 2,000 m. Bottom transport of particulate matter to the deep basin in the western Gulf of Vera has been previously attributed to benthic nepheloid layers detaching from the nearby continental margin (Masque et al., 2003; Sanchez-Vidal et al. 2005).

In March 2015, there was a reinforced primary production along the coastal area, as shown by satellite Chl-a maps (Fig. 3.4). In addition, sub-surface fluorescence in the deep basin showed values between 30 and 80 m deep that were higher than at surface. This is likely connected to

the increase of $CaCO_3$, OM and opal fluxes between late March and May 2015 in the deep basin mid-water station (546 mab) (Fig. 3.6). There is also a variation in the percentages of biogenic components throughout the sampling period, which could be attributed to planktonic community successions. Higher opal and OM percentages are recorded from the end of March to early April, which likely result from diatom-rich phytoplankton blooms (Fabres et al., 2002; Hernández-Almeida et al., 2011). Then OM and opal contributions diminish during the flux peak (559.6 mg m^{-2} d^{-1}) in late April, while the abundance of calcareous particles grows up. High phytoplankton productivity is likely to support the posterior development of zooplankton communities (Hernández-Almeida et al., 2011). This hypothesis fits with the visual inspection of the samples, which allow observing an increment of planktonic foraminifera in that time. Such biogenic imprint is not detected in the deep basin near-bottom trap, suggesting some degree of uncoupling between middle and lower depths.

Between April and October 2015, superficial primary production was restricted to the WAG upwelling, whereas oligotrophy prevailed in the rest of the area (Fig. 3.4). In late summer, fluorescence profiles suggest the presence of a deep chlorophyll maximum (DCM) under the seasonal thermocline, a feature that has been widely observed in other parts of the Mediterranean Sea (Estrada et al., 1993). This is not shown satellite data, as these only illustrate surface pigment contents. Those conditions probably favoured the development of oligotrophic species that contributed to the increment of $CaCO_3$ contents and to higher N values during September in particles settling in the Garrucha-Almanzora Canyon (Fig. 3.6).

In November and December 2015 a widespread phytoplankton bloom occurred in the Gulf of Almeria (Fig. 3.4). Enhanced primary production during this period has been attributed to de-stratification and increased wind speed triggering fertilization events (Garcia-Gorriz and Carr, 2001). Settling particles in Almeria Canyon do not show a biogenic imprint as it could be expected, even though there is a slight decrease of OC/N ratios with respect to previous samples. Concerning the open slope trap in station TA1000, there is a remarkable increment of $CaCO_3$ content (up to 51 and 53% of the total flux during late October and late November 2015, respectively) (Fig. 3.6). An increase of biogenic particles collected in sediment traps could be linked to direct pelagic input from surface blooms or to earlier blooms leading to deposition on the shelf followed by lateral transport (Martín et al., 2006; Bonnin et al., 2008). Nevertheless, it could be assumed that the contribution of pelagic fluxes is significant given the low OC/N ratios measured and the absence of energetic hydrodynamic conditions that could potentially increment advective near-bottom fluxes.

During January and February 2016, the prevalence of westerly winds induces favourable upwelling conditions along the coast (Sarhan et al., 2000; Baldacci et al., 2001). Nutrient-rich cold water tongues promoted pronounced local blooms in January, with superficial blooms concentrating west of Cape of Gata in February 2016 (Fig. 3.4). The arrival of pelagic material this time is detected in settling particles in the Almeria Canyon in late January, characterized by an increment (5.9%) of OM abundance and the lowest measured OC/N ratio (8.5) (Fig. 3.6). In the Gulf of Vera deep basin station, only the near-bottom trap recorded an increase in particle fluxes in early January (188.1 mg m^{-2} d^{-1}) with a low OC/N ratio (6.8). Despite this, the biogenic imprint on the composition of the particles is not evident. Satellite images indicate that the moored trap

is located on the western edge of a highly productive area at the sea surface, thus evidencing that collected particles had been transported by pelagic sedimentation involving both vertical and horizontal motion.

3.1.5.2. The role of oceanographic processes in sedimentary particle transfer

High waves and increased shelf current velocities are the prevalent hydrodynamic responses to strong winds, subsequently increasing bottom shear stress and triggering resuspension and transport of particles across and off-shelf (Guillén et al., 2006; Ulses et al., 2008b; Palanques et al., 2008b; Sanchez-Vidal et al., 2012). Shelf-indented submarine canyons have the ability to intercept shelf sediment transport (Canals et al., 2013). Further, storm characteristics, river inputs and preceding oceanographic conditions determine sediment supply from the shelf to submarine canyons (Fabres et al., 2008; Palanques et al., 2008b; Puig et al., 2014; Rumín-Caparrós et al., 2016). In the study area, storm events were recorded during early spring and autumn 2015 and in winter 2016, as detailed below.

The first storm lashed out from March 17th to 21th during 77 h. Intense north-eastern winds strengthened the advection of water over the Gulf of Vera shelf following the general circulation in the area. 70 h from its start and 17 h after the maximum wave peak, CTD casts were performed around the Escombreras Canyon head, where water column turbidity showed increased values at intermediate depths (Fig. 3.9). This confirms the resuspension of particles due to wave action and their advection from the shelf break. A near-bottom increase of turbidity off the shelf-break was not noticed beyond 1,500 m (Fig. 3.9), indicating that near-bottom downcanyon sediment transport was constrained to the Escombreras Canyon head. The seaward transport of turbid shelf waters was further restricted to the surface layer, over the above-mentioned sub-surface layer of colder water (cf. section 3.1.4.5) that appears in all CTD profiles along the Escombreras Canyon axis (Fig. 3.9) and in the punctual CTD performed in Garrucha-Almanzora Canyon system after the storm (Fig. 3.8). This sub-surface layer could be tentatively related to Winter Intermediate Water (WiW) produced in the western Mediterranean during winter (Millot, 1999 and references therein) or to storm-induced downwelling, or both. Even though a clear WiW hydrological signature is not apparent in θ/S diagrams (Vargas-Yáñez et al., 2017), a WiW warmer than 13 °C was detected south of the Balearic Islands during winter 2015 by Juza et al., (2019). Subsequently, the sub-surface layer in our study area can be interpreted as a WiW intrusion into the Gulf of Vera. It is also worth considering the role that the north-east storm may have played in the arrival of the WiW to our study area, taking into account the change in hydrological structure observed between mid-March (CTDs conducted 2-3 days before the storm) and late-March 2015 (CTDs conducted during and 1 day after the storm) (Fig. 3.8a, b and c). Therefore, our data indicates that the presence of the WiW had a noticeably impact on particle transport into the Escombreras and neighbouring canyons. Such a situation is somehow comparable to the one in canyons of the northern Catalan margin during autumn months, when the seasonal stratification of the water column hinders vertical displacements and restricts the storm-induced downwelling motion to canyon heads (Palanques et al., 2006a, 2008b; Bonnin et al., 2008; Ulses et al., 2008b). However, the spatial resolution of the across-canyon CTD casts in our study is not

adequate to study in detail the interplay between the WiW and downwelling at the upper canyon course.

Accordingly, in the Palomares margin, intense and persistent north-eastern winds may promote coastal downwelling, thus forcing turbid shelf waters to downwell into the heads of Garrucha-Almanzora Canyon system and other canyons nearby. Actually, the role of bottom advective currents in particle transport in the Garrucha-Almanzora Canyon system could be highly relevant, as Puig et al. (2017) found seabed landforms consistent with storm-induced sediment-laden density currents in the canyon heads. However, as noted previously, the presence of pycnoclines may restrict near-bottom suspended transport to the uppermost canyon. Increased downward particle fluxes after a storm may occur when turbid layers pushing offshore isopycnal surfaces loose part of their suspended sediment load (Durrieu de Madron et al., 1990; Langone et al., 2016). This is fully consistent with the lack of enhanced bottom currents at ES1000 station and the low turbidity and bottom current velocities recorded at GA1000 (Fig. 3.5).

The views above are further supported by total mass flux measurements as related to the March 2015 storm (Fig. 3.6). Fluxes up to 24.96 g m^{-2} d^{-1} and 8.37 g m^{-2} d^{-1} were measured in the stations in Escombreras Canyon and the open slope (Fig. 3.6). Sediment traps moored in Garrucha and Almeria canyons opened with 2-3 days of delay with respect to the onset of the storm, recording fluxes up to 18.15 g m^{-2} d^{-1} and 5.12 g m^{-2} d^{-1}, respectively (Fig. 3.6). The last values indicate that the transport event lasted several days while representing minima for particulate matter export. Again, it should be kept in mind that the setting of Almeria Canyon differs from the one of the rest of the investigated canyons.

Storms on the 6th and 12th of April 2015 triggered less particulate matter transport than the previous event according to sediment trap data (Fig. 3.6), likely due to the depletion of unconsolidated, easily resuspendable shelf sediments after the first event, as it would correspond to a sediment-starved marginal setting. Settling particles have higher OC/N ratios in all stations, except in Escombreras Canyon. This could relate to the replenishment of fresh sediments near river mouths during the flooding episode following the storm and subsequent sediment transport, as also observed in the inner shelf off Têt River in the Gulf of Lions (Guillén et al., 2006).

The spring 2015 storms increased the export of particles towards the deep basin all along the continental margin in the study area. However, there are noticeable differences from one margin segment to the other. TMFs recorded in Garrucha-Almanzora Canyon system were at least 1.5 times greater than in Escombreras Canyon, and 3 times greater than in Almeria Canyon, which is close to TA1000. The high values recorded in GA1000 station are linked to canyon heads' configuration, which are strongly indented in to the continental shelf, thus making this canyon system highly sensitive to shelf processes while favouring its interception and funneling capacity of shelf-derived particles. It should be also noted that whereas sediment traps in Garrucha-Almanzora and Escombreras canyons are at similar distance from the coastline (10.7-14.0 km), Almeria Canyon is at twice that distance. Moreover, wave data derived from the WANA model (www.puertos.es) for 2015-2016 near each canyon head document the generation of large waves under prevailing strong northeast winds around Escombreras and Garrucha canyons. Contrastingly, in the Gulf of Almeria only south-western storms are able to generate large waves.

Coastal configuration there, with Cape of Gata promontory to the east likely acting as a shelter against north-eastern storms, leads to the reduction of wave heights, thus lessening the resuspension of bottom sediments that could potentially reach Almeria mid canyon stretch.

During subsequent stormy periods in autumn 2015 and winter 2016, only AL1000 and TA1000 sediment traps remained operational. The 1st and 21th of November 2015 storms were preceded by rainfall episodes. During the first event, H_s increased to 4.2 m and, following the event, Andarax River moderately incremented its discharge to the sea. A rather unusual situation took place during winter months in early 2016, with very low monthly average precipitation with respect to reference values within the same period (AEMET, 2016). The most remarkable storm in those months occurred in February 2016, when southwestern winds blowed during six days triggering a maximum H_s of 4.8 m near Cape of Gata (Fig. 3.3). The impact of the storms on particulate matter fluxes is not visible in either of the two sediment traps, AL1000 and TA1000 (Fig. 3.6). The short duration of the November 2015 events, always less than 37 hours, largely explains the low sediment transfer from the shelf to these mooring stations. Other factors possibly played also a role in the low TMFs during February 2016 storms. The absence of rains during winter months prevented the arrival of new terrestrial material from the river systems to the inner shelf. This factor likely controlled, at least partly, particle fluxes in both stations and especially in the Gulf of Almeria, taking into account the low discharge of Andarax River following autumn storms. Unlike the samples collected during autumn and winter in AL1000, those collected in TA1000 have high OC/N ratios, reaching up to 20.3 in early February (Fig. 3.6). Such high ratios support the arrival of terrestrial material deposited onto the inner shelf during previous floods to the mooring site.

3.1.5.3. The role of anthropogenic activities in sedimentary particle transfer

Studies developed in La Fonera Canyon, in the NW Mediterranean Sea, have shown that the impact of bottom trawling practiced in and around upper submarine canyon reaches is not restricted to those sections, but also affects deeper canyon sections and out of canyon continental rise areas (Palanques et al., 2006b; Puig et al., 2012; Payo-Payo et al., 2017). Detailed monitoring studies have reported sudden sediment gravity flows during summer months triggered by bottom trawling in that area (Palanques et al., 2006b; Puig et al., 2012). Similar situations have been described and / or inferred in and around other submarine canyons both in the Western Mediterranean Sea and beyond, such as Blanes Canyon (Lopez-Fernandez et al., 2013b) in the Catalan margin, Guadiaro Canyon (Palanques et al., 2005) in the Alboran Sea or the Avilés Canyon in Cantabrian margin (Rumín-Caparrós et al., 2016). The Garrucha-Almanzora Canyon system flanks are located at the edge of Verin and Canto Pote fishing grounds, where intensive bottom trawling takes place in the 500-800 m depth range (García-Rodríguez, 2003). Fishing interest for this canyon system relates to quasi-permanent subsurface upwelling conditions (Muñoz et al., 2018) together with its character of terrestrial OC depocenter, which result in fish aggregation and likely enhancement of local biodiversity.

Trawling-induced sediment resuspension probably is the mechanism that feeds the nepheloid layer below 400 m down to the bottom, as observed in late March and late August CTD casts. VMS data show that the majority of fishing vessels operate at 500-650 m of water depth along the canyon rims and adjacent slope, although during June and July they reach deeper regions

around 800 m (Fig. 3.10). The number of vessel data points within a radius of 4 km around the Garrucha-Almanzora Canyon system mooring station increases during July and August (Fig. 3.10a). As a result, CTD turbidity values also augment at depths (600-750 m) slightly deeper than the peak of vessels in operation within the same period (Fig. 3.10b-c) and near the canyon floor. Near-bottom currentmeter measurements show a prominent bottom turbidity increment during summer months followed by a sharp decrease in late August (Fig. 3.5c). The reason for such a drastical diminution of turbidity is not obvious, since hydrodynamic conditions did not appear to change and there was no reduction in fishing activity. It is, however, plausible that the arrival of primary production particles from DCM contributed to the scavenging of suspended particles, which eventually resulted in the minimum OC/N ratio found in settling particles of September 2015 (Fig. 3.6). Unfortunately, the temporal resolution of sediment trap sampling prevents us from assessing in greater detail the interrelations of turbidity with other parameters.

It could be assumed that particles remobilized by bottom trawling come from different places, including the adjacent eastern and western open slope and the canyon flanks. Along slope currents passing over Garrucha Canyon would promote the arrival of particles from the eastern open slope into the canyon, as suggested by the persistent westerly currents recorded by the currentmeter in GA1000. The increase in fishing activity along the upper canyon walls during August 2015 explains the high OC/N ratios found in settling particles during that month (Fig. 3.6), which exceeds the rest of summer samples, and evidences that the material from upper regions is flushed downcanyon.

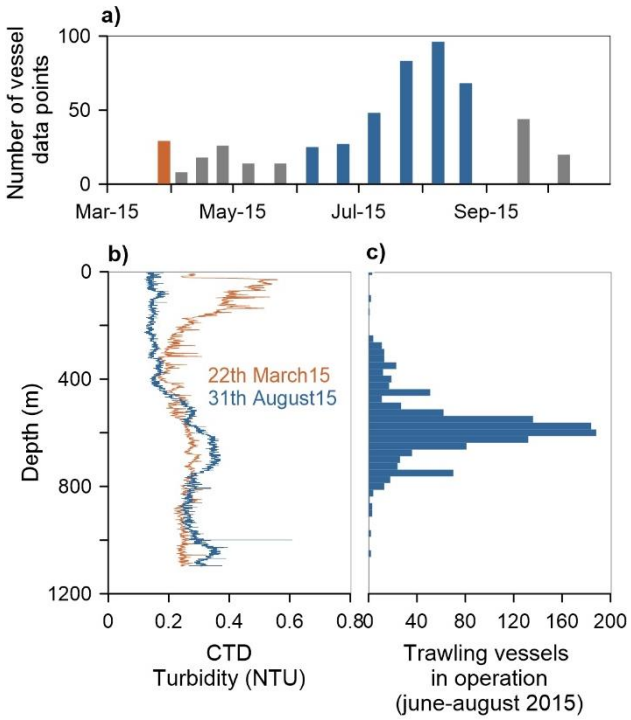

Figure 3.10. (a) Number of VSM data points from fishing vessels within a radius of 4 km around GA1000 sailing at less than 5 knots (i.e. while trawling). (b) CTD turbidity profiles performed in March 2015 (orange) and August 2015 (blue). (c) Operating depth of trawling vessels between June and August within a radius of 4 km from the mooring line.

3.1.5.4. Particle flux comparison with other submarine canyons

The fluxes obtained in Escombreras, Garrucha-Almanzora and Almeria submarine canyons are clearly lower than those observed in other canyons in the Western Mediterranean Sea, and also are in the lowest range of those found in canyons around the entire Iberian Peninsula (i.e. including three submarine canyons in the Atlantic Ocean). This is well illustrated when plotting weighted fluxes calculated in this study against those observed in other canyons (Fig. 3.11). It has to be noted that data from the Atlantic canyons reflect results from canyon reaches that are deeper than those from the Mediterranean Sea, so that it would be reasonable assuming higher fluxes in shallower canyon regions, as pointed by Heussner et al. (2006) for a set of submarine canyons in the Gulf of Lions.

Most submarine canyons in the North Catalan margin have their heads deeply incised in the continental shelf, as marked by small short distances to the shoreline in Figure 3.11, except for Lacaze-Duthiers Canyon. This enables those canyons to trap large volumes of river-delivered sedimentary particles transported by littoral currents. Such trapping effect could be reinforced by specific external forcings and local conditions encompassing metoceanography, physiography, a variety of sedimentary processes and also anthropogenic forcing, as described above (Puig et al., 2014). In the Atlantic Iberian margin, also Nazaré Canyon and to a lesser extent, Setubal Canyon, are deeply incised into the continental shelf with their head at or at short distance from the shoreline.

The low particle fluxes recorded in the studied submarine canyons are highly influenced, first, by the scarcity of river inputs onto the shelf, which is ultimately related to the region's arid climate and weak river discharge. Annual precipitation in the watersheds opening to the investigated continental margin are the lowest in the entire Iberian Peninsula, i.e. less than 500 mm or even less than 300 mm in along most of the coastal area. Precipitation in the watershed feeding the North Catalan margin is always above 600 mm, while in the Cantabrian and Portuguese watersheds opening to the Atlantic Ocean is above 800 mm (AEMET, 2011). Such low particle fluxes in the studied Almeria and Murcia continental margin are also determined by limited shelf to canyon exports due not only to the sediment-starved character of the area but also, and importantly, by the mildness of metoceanic conditions during most of the time, with scarce recurrence of extreme events, including major storms. Such events, bringing high amounts of energy to the system, are instead much more frequent in the North Catalan area and even more in Atlantic regions (Martín et al., 2006; Ulses et al., 2008b; Martín et al., 2011; Sanchez-Vidal et al., 2012; Rumín-Caparrós et al., 2016). Finally, the lack of high-energy oceanographic processes dominating in and off canyon sediment transport in other margins, such as DSWC, does not help in steering shelf to slope particle export in the investigated margin. However, low recurrence, massive transport events may occur in the study area as triggered by strong earthquakes and rare extreme precipitation and flood events (Sánchez-García et al., 2019).

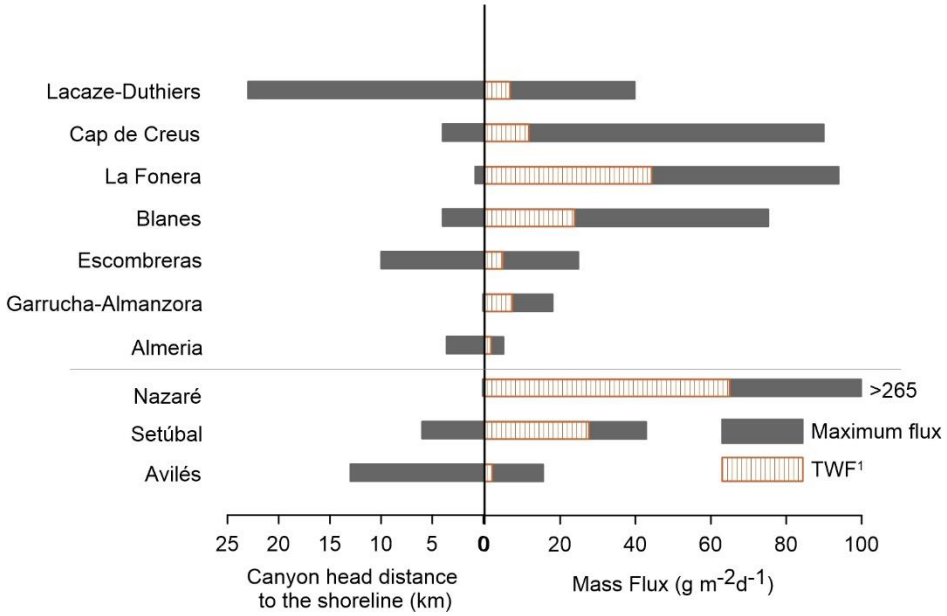

Figure 3.11. Shortest canyon head distance to the shoreline (left) and total weighted fluxes (TWF) and maximum TMF (right) in submarine canyons investigated in this study compared to canyons in the NW Mediterranean Sea: Lacaze-Duthiers at 1,000 m depth (Pasqual et al., 2010), Cap de Creus at 1,000 m depth (Pasqual et al., 2010), La Fonera at 1,200 m depth (Martín et al., 2006) Blanes at 1,200 m depth (Lopez-Fernandez et al., 2013b) and in Atlantic Iberian margins: Nazaré at 1,600 m depth (Martín et al., 2011), Setúbal at 1,324 m depth (de Stigter et al., 2011) and Avilés at 2,000 m depth (Rumín-Caparrós et al., 2016). The horizontal line separates Mediterranean canyons (above) from Atlantic canyons (below). Note that the data on Atlantic canyons correspond to larger water depths than Mediterranean canyons. The location of all those canyons is shown in Figure 3.1. 1: Mean values of TMF have been used it when the TWF was not available.

3.1.6. Conclusions

The analysis of the temporal variability and geochemical properties of particle fluxes provides relevant information on sediment dynamics and particle sources in the sediment-starved Almeria and Murcia continental margin and adjacent deep basin. Our results show that storms are the main trigger of mass transfer from the shallow shelf to the deep slope and basin, enhancing particle fluxes both within submarine canyons and in the open slope. In that respect, the magnitude, direction, associated precipitation and duration of the storms eventually leading to high waves and river discharge events, together with the length of intervals between storm events, are the key factors driving down margin mass transfers. A March 2015 to March 2016 year-round monitoring experiment has shown that most particle export to the deep margin occurred as a result of a set of north-east storms in spring 2015 with noticeable wave heights. During that period, off-shelf export of sediment-laden waters was enhanced due to a storm-induced downwelling process. Also, the detachment of turbid layers from the shelf break and the canyons' floor prompted the transport of particle towards deeper reaches. On the other side, the presence of WiW and an associated pycnocline in the Gulf of Vera restricted the vertical particle transfer to a few hundred meters, as illustrated by an above WiW turbid layer at 200 m depth

spreading from the outer shelf over the Escombreras mid-canyon reach after a storm in March 2015 in the Mazarron margin segment (Fig. 3.1).

While metoceanographic processes appear to dominate sedimentary dynamics in Almeria and Escombreras canyons, at the southern and northern ends of the study area, bottom trawling also impacts particle fluxes inside the Garrucha-Almanzora Canyon system in the middle of the study area. Here, the closeness of various canyon heads to river mouths enhances the transfer of terrestrial OC into this system, which should result in and enhanced fertilization of the area making it attractive for the local fishing industry.

Concerning the deep basin traps (mid-water and near-bottom), particle fluxes are mostly determined by phytoplankton blooms. Advective fluxes coming from the continental margin seem to increment TMFs mostly in the near-bottom trap. In any case, the very low fluxes measured in both mid-water and near-bottom traps indicate that few terrestrial particles reach the deep basin in the Gulf of Vera.

Overall, low particle fluxes are recorded in Escombreras, Garrucha-Almanzora and Almeria canyons compared to other canyons in the Western Mediterranean Sea. The lack of recurrent high-energy oceanographic events and the scarcity of riverine sediment inputs are the most relevant factors conditioning the low TMFs observed in the study area. However, longer and complete temporal series are needed to better establish sediment transfer patterns along the Almeria and Murcia continental margin as well to assess inter-annual variability and the likely system shaking effects of rare major storms in the area.

Acknowledgments We would like to express our gratitude to the many colleagues and technicians and to the crew of RV Ángeles Alvariño for their dedication and help during sea-going work. We also thank M. Guart for her assistance with laboratory analyses. This work was supported by research projects NUREIEV (ref. CTM2013-44598-R) and NUREIEVA (ref. CTM2016-75953-C2-1-R). GRC Geociències Marines is funded by the Catalan Government within its excellence research groups program (ref. 2017 SGR 315). M.Tarrés was supported by a FPI grant from Ministerio de Ciencia, Innovación y Universidades of the Spanish Government.

3.1.7. References

Acosta, J., Fontán, A., Muñoz, A., Muñoz-Martín, A., Rivera, J. et al., 2013. The morpho-tectonic setting of the Southeast margin of Iberia and the adjacent oceanic Algero-Balearic Basin. Marine and Petroleum Geology 45, 17–41. Doi: 10.1016/j.marpetgeo.2013.04.005.

AEMET, 2011. Atlas climático ibérico. Temperatura del aire y precipitación (1971-2000). Agencia Estatal de Meteorología, Ministerio de Medio Ambiente y Medio Rural y Marino, e Instituto de Meteorologia de Portugal.

AEMET, 2016. Avance climatológico mensual febrero 2016. Región de Murcia. Agencia Estatal de Meteorología.

Baker, E.T., Milburn, H.B. and Tennant, D.A., 1988. Field assessment of sediment trap efficiency under varying flow conditions. Journal of Marine Research 46, 573-592. Doi: 10.1357/002224088785113522.

Baldacci, A., Corsini, G., Grasso, R., Manzella, G., Allen, J.T. et al., 2001. A study of the Alboran Sea mesoscale system by means of empirical orthogonal function decomposition of satellite data. Journal of Marine Systems 29, 293-311. Doi: 10.1016/S0924-7963(01)00021-5.

Béthoux, J.P, Durrieu de Madron, X., Nyffeler, F. and Taillez, D., 2002. Deep water in the western Mediterranean: peculiar 1999 and 2000 characteristics, shelf formation hypothesis, variability since 1970 and geochemical inferences. Journal of Marine Systems 33–34, 117–131. Doi: 10.1016/S0924-7963(02)00055-6.

Bonnin, J., Heussner, S., Calafat, A., Fabres, J., Palanque, A. et al., 2008. Comparison of horizontal and downward particle fluxes across canyons of the Gulf of Lions (NW Mediterranean): Meteorological and hydrodynamical forcing. Continental Shelf Research 28, 1957–1970. Doi: 10.1016/j.csr.2008.06.004.

Buesseler, K.O., Antia, A.N., Avan, N., Chen, M., Fowler, S.W. et al., 2007. An assessment of the use of sediment traps for the estimating upper ocean particle fluxes. Journal of Marine Research 65, 345-416. Doi: 10.1357/002224007781567621.

Canals, M., Company, J.B., Martín, D., Sanchez-Vidal, A. and Ramírez-Llorda, E., 2013. Integrated study of Mediterranean deep canyons: novel results and future challenges. Progress in Oceanography 118, 1-27. Doi: 10.1016/j.pocean.2013.09.004.

Canals, M., Puig, P., Durrieu de Madron, X., Heussner, S., Palanques, A. et al., 2006. Flushing submarine canyons. Nature 444 (7117), 354–357. Doi: 10.1038/nature05271.

Comas, M.C., Platt, J.P., Soto, J.I. and Watts, A.B., 1999. The origin and tectonic history of the Alboran Basin: insights from leg 161 results. Proceedings of the Ocean Drilling Program Scientific Results 161, 555-580. Doi: 10.2973/odp.proc.sr.161.262.1999.

Company, J.B., Puig, P., Sarda, F., Palanques, A., Latasa, M. et al., 2008. Climate influence on deep sea populations. PLoS ONE 1, e1431. Doi: 10.1371/journal.pone.0001431.

Cronin, B.T., Kenyon, N.H., Woodside, J., den Bezemer, T., van der Wal, A. et al., 1995. The Almeria Canyon: a meandering channel system on an active margin, Alboran Sea, Western Mediterranean. In: Pickering, K.T., Hiscott, R.N., Kenyon, N.H., Ricci-Lucchi, F., Smith, R.D.A. (Eds.), Atlas of Deep Water Environments: Architectural Style in Turbidite Systems, 84– 88. Doi: 10.1007/978-94-011-1234-5_15.

Drake, D.E. and Gorsline, D.S., 1973. Distribution and transport of suspended particulate matter in Hueneme, Redondo, Newport, and La Jolla submarine canyons, California. Geological Society of America Bulletin 84, 3949–3968. Doi: 10.1130/0016-7606(1973)84<3949:DATOSP>2.0.CO;2.

Dumas, C., Aubert, D., Durrieu de Madron, X., Ludwig, W., Heussner, S. et al., 2014. Storm-induced transfer of particulate trace metals to the deep-sea in the Gulf of Lion (NW Mediterranean Sea). Environmental Geochemistry Health 36, 995-1014. Doi: 10.1007/s10653-014-9614-7.

Durrieu de Madron, X., Nyffeler, F. and Godet, C.H., 1990. Hydrographic structure and nepheloid spatial distribution in the Gulf of Lions continental margin. Continental Shelf Research 10 (9-11), 915-929. Doi: 10.1016/0278-4343(90)90067-V.

Durrieu de Madron, X., Wiberg, P.L. and Puig, P., 2008. Sediment dynamics in the Gulf of Lions: the impact of extreme events. Continental Shelf Research 28, 1867–1876. Doi: 10.1016/j.csr.2008.08.001.

Durrieu de Madron, X., Zervakis, V., Theocharis, A. and Georgopoulos, D., 2005. Comments on "Cascades of dense water around the world ocean". Progress in Oceanography 64, 83–90. Doi: 10.1016/j.pocean.2004.08.004.

Estrada, F., Ercilla, G. and Alonso, B., 1997. Pliocene-Quaternary tectonic-sedimentary evolution of the NE Alboran Sea (SW Mediterranean Sea). Tectonophysics 282, 423– 442. Doi: 10.1016/S0040-1951(97)00227-8.

Estrada, M., Marrasé, C., Latasa, M., Berdalet, E., Delgado, M. et al., 1993. Variability of deep chlorophyll maximum characteristics in the Northwestern Mediterranean. Marine Ecology Progress Series 92, 289-300. Doi: 10.3354/meps092289.

Fabres, J., Calafat, A., Sanchez-Vidal, A., Canals, M. and Heussner, S., 2002. Composition and spatio-temporal variability of particle fluxes in the Western Alboran Gyre, Mediterranean Sea (SW Mediterranean). Journal of Marine Systems 33–34, 431–456. Doi: 10.1016/S0924-7963(02)00070-2.

Fabres, J., Tesi, T., Velez, J., Batista, F., Lee, C. et al., 2008. Seasonal and event-controlled export of organic matter from the shelf towards the Gulf of Lions continental slope. Continental Shelf Research 28, 1971-1983. Doi: 10.1016/j.csr.2008.04.010.

Ferré, B., Guizien, K., Durrieu de Madron, X., Palanques, A., Guillén, J. et al., 2005. Fine-grained sediment dynamics during a strong storm event in the inner-shelf of the Gulf of Lion (NW Mediterranean). Continental Shelf Research 25, 2410-2427. Doi: 10.1016/j.csr.2005.08.017.

Garcia-Gorriz, E. and Carr, M.E., 2001. Physical control of phytoplankton distributions in the Alboran Sea: A numerical and satellite approach. Journal of Geophysical Research 106, 16795-16805. Doi: 10.1029/1999JC000029.

García, M., Alonso, B., Ercilla, G. and Gràcia, E., 2006. The tributary valley systems of the Almeria Canyon (Alboran Sea, SW Mediterranean): Sedimentary architecture. Marine Geology 226, 207-223. Doi: 10.1016/j.margeo.2005.10.002.

García Rodríguez M, 2004. La gamba roja "Aristeus antennatus" (Risso, 1816) (Crustacea, Decapoda): distribución, demografía, crecimiento, reproducción y explotación en el Golfo de

Alicante, Canal de Ibiza y Golfo de Vera. Tesis de la Universidad Complutense de Madrid, Facultad de Ciencias Biológicas, Departamento de Biología Animal I.

Gardner, W.D., 1985. The effect of tilt on sediment trap efficiency. Deep-Sea Research 32 (3), 349–361. Doi: 10.1016/0198-0149(85)90083-4.

Gómez de la Peña, L., Gràcia, E., Muñoz, E., Acosta, J., Gómez-Ballesteros, M. et al., 2016. Geomorphology and Neogene tectonic evolution of the Palomares continental margin (Western Mediterranean). Tectonophysics 689, 25-39. Doi: 10.1016/j.tecto.2016.03.009.

Goñi, M.A. and Hedges, J.I., 1995. Sources and reactivates of marine derived organic matter in coastal sediments as determined by alkaline CuO oxidation. Geochimica et Cosmochimica Acta 59, 2965-2981. Doi: 10.1016/0016-7037(95)00188-3.

Gràcia, E., Pallàs, R., Soto, J.I., Comas, M., Moreno, X. et al., 2006. Active faulting offshore SE Spain (Alboran Sea): Implications for earthquake hazard assessment in the Southern Iberian Margin. Earth and Planetary Science Letters 241, 734–749. Doi: 10.1016/j.epsl.2005.11.009.

Guillén, J., Palanques, A., Puig, P., Durrieu de Madron, X. and Nyffeler, F., 2006. Sediment dynamics during wet and dry storm events on the Têt inner shelf (SW Gulf of Lions). Marine Geology 234, 129–142. Doi: 10.1016/j.margeo.2006.09.018.

Hedges, J.I., Keil, R.G. and Benner R., 1997. What happens to terrestrial organic matter in the ocean? Organic Geochemistry 27, 195-212. Doi: 10.1016/S0146-6380(97)00066-1.

Hermoso, A., Homar, V. and Amengual, A., 2021. The Sequence of Heavy Precipitation and Flash Flooding of 12 and 13 September 2019 in Eastern Spain. Part I: Mesoscale Diagnostic and Sensitivity Analysis of Precipitation. Journal of Hydrometeorology 22 (5), 1117-1138. Doi: 10.1175/JHM-D-20-0182.1.

Hernández-Almeida, I., Bárcena, M.A., Flores, J.A., Sierro, F.J., Sanchez-Vidal, A. et al., 2011. Microplankton response to environmental conditions in the Alboran Sea (Western Mediterranean): One year sediment trap record. Marine Micropaleontology 78, 14-24. Doi: 10.1016/j.marmicro.2010.09.005.

Heussner, S. Durrieu de Madron, X., Radakovitch, O., Beaufort, L., Biscaye, P.E. et al., 1999. Spatial and temporal patterns of downward particle fluxes on the continental slope of the Bay of Biscay (northeastern Atlantic). Deep-Sea Research II 46, 2101-2146. Doi: 10.1016/S0967-0645(99)00057-0.

Heussner, S., Durrieu de Madron, X., Calafat, A., Canals, M., Carbonne, J. et al., 2006. Spatial and temporal variability of downward particle fluxes on a continental slope: lessons from an 8-yr experiment in the Gulf of Lions (NW Mediterranean). Marine Geology 234, 63–92. Doi: 10.1016/j.margeo.2006.09.003.

Heussner, S., Ratti, C. and Carbonne, J., 1990. The PPS 3 time-series sediment trap and the trap sample processing techniques used during the ECOMARGE experiment. Continental Shelf Research 10, 943-958. Doi: 10.1016/0278-4343(90)90069-X.

Juza, M., Escudier, R., Vargas-Yáñez, M., Mourre, B., Heslop, E. et al., 2019. Characterization of changes in Western Intermediate Water properties enabled by an innovative geometry-based detection approach. Journal of Marine Systems 191, 1-12. Doi: 10.1016/j.jmarsys.2018.11.003.

Kamatani, A. and Oku, O., 2000. Measuring biogenic silica in marine sediments. Marine Chemistry 68, 219–229. Doi: 10.1016/S0304-4203(99)00079-1.

Kiriakoulakis, K., Blackbird, S., Ingels, J., Vanreusel, A. and Wolff, G.A., 2011. Organic geochemistry of submarine canyons: The Portuguese Margin. Deep-sea Research II 58, 2477-2488. Doi: 10.1016/j.dsr2.2011.04.010.

Langone, L., Conese, I., Miserocchi, S., Boldrin, A., Bonaldo, D. et al., 2016. Dynamics of particles along thewestern margin of the Southern Adriatic: Processes involved in transferring particulate matter to the deep basin. Marine Geology 375, 28-43. Doi: 10.1016/j.margeo.2015.09.004.

Liquete, C., Arnau, P., Canals, M. and Colas, S., 2005. Mediterranean river systems of Andalusia, southern Spain, and associated deltas: A source to sink approach. Marine Geology 222-223, 471-495. Doi: 10.1016/j.margeo.2005.06.033.

Lobo, F.J., Ercilla, G., Fernández-Salas, L.M. and Gámez, D., 2014. Chapter 11 The Iberian Mediterranean shelves. Geological Society, London, Memoirs 41, 147-170. Doi: 10.1144/M41.11.

Lopez-Fernandez, P., Bianchelli, S., Pusceddu, A., Calafat, A., Danovaro, R. et al., 2013a. Bioavailable compounds in sinking particulate organic matter, Blanes Canyon, NW Mediterranean Sea: Effects of a large storm and sea surface biological processes. Progress in Oceanography 118, 108-121. Doi: 10.1016/j.pocean.2013.07.022.

Lopez-Fernandez, P., Calafat, A., Sanchez-Vidal, A., Canals, M., Flexas, M.M. et al., 2013b. Multiple drivers of particle fluxes in the Blanes submarine canyon and adjacent open slope: results of a year round experiment. Progress in Oceanography 118, 95–107. Doi: 10.1016/j.pocean.2013.07.029.

Machado, M.J., Benito, G., Barriendos, M. and Rodrigo, F.S., 2011. 500 years of rainfall variability and extreme hydrological events in southeastern Spain drylands. Journal of Arid Environtments 75, 1244–1253. Doi: 10.1016/j.jaridenv.2011.02.002.

Martín, J., Durrieu de Madron, X., Puig, P., Bourrin, F., Palanques, A. et al., 2013. Sediment transport along the Cap de Creus Canyon flank during a mild, wet winter. Biogeosciences 10, 3221-3239. Doi: 10.5194/bg-10-3221-2013.

Martín, J., Palanques, A. and Puig, P., 2006. Composition and variability of downward particulate matter fluxes in the Palamós submarine canyon (NW Mediterranean). Journal of Marine Systems 60, 75–97. Doi: 10.1016/j.jmarsys.2005.09.010.

Martín, J., Palanques, A., Vitorino, J., Oliveira, A. and de Stigter, H.C., 2011. Near-bottom particulate matter dynamics in the Nazaré submarine canyon under calm and stormy conditions. Deep-Sea Research II 58, 2388–2400. Doi: 10.1016/j.dsr2.2011.04.004.

Martín, J., Puig, P., Masqué, P., Palanques, A. and Sánchez-Gómez, A., 2014a. Impact of bottom trawling on deep-sea sediment properties along the flanks of a submarine canyon. PLoS ONE 9 (8), e104536. Doi: 10.1371/journal.pone.0104536.

Martín, J., Puig, P., Palanques, A. and Ribó, M., 2014b. Trawling-induced daily sediment resuspension in the flank of a Mediterranean submarine canyon. Deep-Sea Research II 104, 174-183. Doi: 10.1016/j.dsr2.2013.05.036.

Masque, P., Fabres, J., Canals, M., Sanchez-Cabeza, J.A., Sanchez-Vidal, A. et al., 2003. Accumulation rates of major constituents of hemipelagic sediments in the deep Alboran Sea: A centennial perspective of sedimentary dynamics. Marine Geology 193, 207-233. Doi: 10.1016/S0025-3227(02)00593-5.

Millot, C., 1999. Circulation in the Western Mediterranean Sea. Journal of Marine Systems 20, 423–442. Doi: 10.1016/S0924-7963(98)00078-5.

Mortlock, R.A. and Froelich, P.N., 1989. A simple method for the rapid determinations of biogenic opal in pelagic marine sediments. Deep-Sea Research 36 (9), 1415– 1426. Doi: 10.1016/0198-0149(89)90092-7.

Muñoz, M., Reul, A., García-Martínez, M.C., Plaza, F., Bautista, B. et al., 2018. Oceanographic and bathymetric features as the target for pelagic MPA design: A case study on the Cape of Gata. Water 10, 1403. Doi: 10.3390/w10101403.

Ogston, A.S., Drexler, T.M. and Puig, P., 2008. Sediment delivery, resuspension, and transport in two contrasting canyon environments in the southwest Gulf of Lions. Continental Shelf Research 28 (15), 2000–2016. Doi: 10.1016/j.csr.2008.02.012.

Palanques, A., Durrieu de Madron, X., Puig, P., Fabres, J., Guillén, J. et al., 2006a. Suspended sediment fluxes and transport processes in the Gulf of Lions submarine canyons. The role of storms and dense water cascading. Marine Geology 234, 43–61. Doi: 10.1016/j.margeo.2006.09.002.

Palanques, A., El Khatab, M., Puig, P., Masqué, P., Sánchez-Cabeza, J.A. et al., 2005. Downward particle fluxes in the Guadiaro submarine canyon depositional system (north-western Alboran Sea), a river flood dominated system. Marine Geology 220, 23–40. Doi: 10.1016/j.margeo.2005.07.004.

Palanques, A., Guillén, J., Puig, P. and Durrieu de Madron, X., 2008b. Storm-driven shelf-to-canyon suspended sediment transport at the southwestern Gulf of Lions. Continental Shelf Research 28, 1947–1956. Doi: 10.1016/j.csr.2008.03.020.

Palanques, A., Martín, J., Puig, P., Guillén, J., Company, J.B. et al., 2006b. Evidence of sediment gravity flows induced by trawling in the Palamós (Fonera) submarine canyon (northwestern Mediterranean). Deep-Sea Research I 53, 201–214. Doi: 10.1016/j.dsr.2005.10.003.

Palanques, A., Masqué, P., Puig, P., Sanchez-Cabeza, J.A., Frignani, M. et al., 2008a. Anthropogenic trace metals in the sedimentary record of the Llobregat continental shelf and adjacent Foix

Submarine Canyon (northwestern Mediterranean). Marine Geology 248, 213-227. Doi: 10.1016/j.margeo.2007.11.001.

Palanques, A., Puig, P., Durrieu de Madron, X., Sanchez-Vidal, A., Pasqual, C. et al., 2012. Sediment transport to the deep canyons and open-slope of the western Gulf of Lions during the 2006 intense cascading and open-sea convection period. Progress in Oceanography 106, 1–15. Doi: 10.1016/j.pocean.2012.05.002.

Paradis, S., Puig, P., Masqué, P., Juan-Díaz, X., Martín, J. et al., 2017. Bottom-trawling along submarine canyons impacts deep sedimentary regimes. Scientific Reports 7, 43332. Doi: 10.1038/srep43332.

Pasqual, C., Sanchez-Vidal, A., Zuñiga, D., Calafat, A., Canals, M. et al., 2010. Flux and composition of settling particles across the continental margin of the Gulf of Lion: the role of dense shelf water cascading. Biogeosciences 7, 217–231. Doi: 10.5194/bg-7-217-2010.

Payo-Payo, M., Jacinto, R.S., Lastras, G., Rabineau, M., Puig, P. et al., 2017. Numerical modeling of bottom trawling-induced sediment transport and accumulation in La Fonera submarine canyon, northwestern Mediterranean Sea. Marine Geology 386, 107-125. Doi: 10.1016/j.margeo.2017.02.015.

Pedrosa-Pàmies, R., Sanchez-Vidal, A., Calafat, A., Canals, M. and Durán, R., 2013. Impact of storm-induced remobilization on grain size distribution and organic carbon content in sediments from the Blanes Canyon area, NW Mediterranean Sea. Progress in Oceanography 118, 122-136. Doi: 10.1016/j.pocean.2013.07.023.

Pérez-Hernández, S., Comas, M.C. and Escutia, C., 2014. Morphology of turbidite systems within an active continental margin (the Palomares Margin, western Mediterranean). Geomorphology 219, 10–26. Doi: 10.1016/j.geomorph.2014.04.014.

Puig, P., Canals, M., Company, J.B., Martin, J., Amblas, D. et al., 2012. Ploughing the deep sea floor. Nature 489, 286–290. Doi: 10.1038/nature11410

Puig, P., Durán, R., Muñoz, A., Elvira, E. and Guillén, J., 2017. Submarine canyon-head morphologies and inferred sediment transport processes in the Alías-Almanzora canyon system (SW Mediterranean): On the role of the sediment supply. Marine Geology 393, 21-34. Doi: 10.1016/j.margeo.2017.02.009.

Puig, P., Palanques, A., Guillén, J. and El Khatab, M., 2004b. Role of internal waves in the generation of nepheloid layers on the northwestern Alboran slope: implications for continental margin shaping. Journal of Geophysical Research 109, C09011. Doi: 10.1029/2004JC002394.

Puig, P., Palanques, A. and Martín, J., 2014. Contemporary Sediment-Transport Processes in Submarine Canyons. Annual Review of Marine Science 6, 53–77. Doi: 10.1146/annurev-marine-010213-135037.

Pusceddu, A., Mea, M., Canals, M., Heussner, S., Durrieu de Madron, X. et al., 2013: Major consequences of an intense dense shelf water cascading event on deep-sea benthic trophic

conditions and meiofaunal biodiversity. Biogeosciences 10, 2659–2670. Doi: 10.5194/bg-10-2659-2013.

Ramirez-Llodra, E., De Mol, B., Company, J.B., Coll, M. and Sardà, F., 2013. Effects of natural and anthropogenic processes in the distribution of marine litter in the deep Mediterranean Sea. Progress in Oceanography 118, 273-287. Doi: 10.1016/j.pocean.2013.07.027.

Renault, L., Oguz, T., Pascual, A., Vizoso, G. and Tintore, J., 2012. Surface circulation in the Alboran Sea (western Mediterranean) inferred from remotely sensed data. Journal of Geophysical Research 117, C08009. Doi: 10.1029/2011JC007659.

Romero-Romero, S., Molina-Ramírez, A., Höfer, J., Duineveld, G., Rumín-Caparrós, A. et al., 2016b. Seasonal pathways of organic matter within the Avilés submarine canyon: Food web implications. Deep Sea Research Part I: Oceanographic Research Papers 117, 1-10. Doi: 10.1016/j.dsr.2016.09.003.

Rumín-Caparrós, A., Sanchez-Vidal, A., González-Pola, C., Lastras, G., Calafat, A. et al., 2016. Particle fluxes and their drivers in the Avilés submarine canyon and adjacent slope, central Cantabrian margin, Bay of Biscay. Progress in Oceanography 144, 39–61. Doi: 10.1016/j.pocean.2016.03.004.

Sánchez-García, C., Schulte, L., Carvalho, F. and Peña, J.C., 2019. A 500-year flood history of the arid environments of southeastern Spain. The case of the Almanzora River. Global and Planetary Change 181, 102987. Doi: 10.1016/j.gloplacha.2019.102987.

Sanchez-Vidal, A., Canals, M., Calafat, A.M., Lastras, G., Pedrosa-Pàmies, R. et al., 2012. Impacts on the deep-sea ecosystem by a severe coastal storm. PLoS ONE 7 (1), e30395. Doi: 10.1371/journal.pone.0030395.

Sanchez-Vidal, A., Higueras, M., Martí, E., Liquete, C., Calafat, A. et al., 2013. Riverine transport of terrestrial organic matter to the North Catalan margin, NW Mediterranean Sea. Progress in Oceanography 118, 71-80. Doi: 10.1016/j.pocean.2013.07.020.

Sanchez-Vidal, A., Calafat, A., Canals, M., Frigola, J. and Fabres, J., 2005. Particle fluxes and organic carbon balance across the Eastern Alboran Sea (SW Mediterranean Sea). Continental Shelf Research 25, 609-628. Doi: 10.1016/j.csr.2004.11.004.

Sanz, J.L., Hermida, N., Lobato, A.B., Tello, O., Fernández-Salas, L.M. et al., 2002a. Estudio de la Plataforma Continental Española, Hoja MC047-Garrucha-Serie C. Secretaria General de Pesca Marítima e Instituto Español de Oceanografía.

Sarhan, T., García Lafuente, J., Vargas, M., Vargas, J.M. and Plaza, F., 2000. Upwelling mechanisms in the northwestern Alboran Sea. Journal Marine Systems 23, 317–331. Doi: 10.1016/S0924-7963(99)00068-8.

Schmidt, S., de Stigter, H.C. and van Weering, T.C.E., 2001. Enhanced short-term sediment deposition within the Nazaré Canyon, North-East Atlantic. Marine Geology 173 (1-4), 55–67. Doi: 10.1016/S0025-3227(00)00163-8.

Schmidt, S., Howa, H., Diallo, A., Martín, J., Cremer, M. et al., 2014. Recent sediment transport and deposition in the Cap-Ferret Canyon, South-East margin of Bay of Biscay. Deep-Sea Research II 104, 134-144. Doi: 10.1016/j.dsr2.2013.06.004.

Shepard, F.P., Marshall, N.F., McLoughlin, P.A. and Sullivant, G.G., 1979. Currents in Submarine Canyons and Other Seavalleys. AAPG Studies in Geology 8, Tulsa, Oklahoma, 173. Doi: 10.2110/pec.79.27.0085.

de Stigter, H.C., Boer, W., de Jesus Mendes, P.A., Jesus, C.C., Thomsen, L. et al., 2007. Recent sediment transport and deposition in the Nazaré Canyon, Portuguese continental margin. Marine Geology 246 (2-4), 144–164. Doi: 10.1016/j.margeo.2007.04.011.

de Stigter, H.C., Jesus, C.C., Boer, W., Richter, T.O., Costa, A. et al., 2011. Recent sediment transport and deposition in the Lisbon-Setúbal and Cascais submarine canyons, Portuguese continental margin. Deep-Sea Research II 58 (23-24), 2321–2344. Doi: 10.1016/j.dsr2.2011.04.001.

Tintore, J., La Violette, P.E., Blade, I. and Cruzado, A., 1988. A study of an intense density front in the Eastern Alboran Sea: the Almeria-Oran Front. Journal of Physical Oceanography 18, 1384–1397. Doi: 10.1175/1520-0485(1988)018<1384:ASOAID>2.0.CO;2.

Tubau, X., Canal, M., Lastras, G., Rayo, X., Rivera, J. et al., 2015. Marine litter on the floor of deep submarine canyons of the Northwestern Mediterranean Sea: The role of hydrodynamic processes. Progress in Oceanography 134, 379-403. Doi: 10.1016/j.pocean.2015.03.013.

Ulses, C., Estournel, C., Durrieu de Madron, X. and Palanques, A., 2008b. Suspended sediment transport in the Gulf of Lions (NW Mediterranean): impact of extreme storms and floods. Continental Shelf Research 28(15), 2048-2070. Doi: 10.1016/j.csr.2008.01.015.

Vargas-Yáñez, M., Plaza, M., García-Lafuente, J., Sarhan, T., Vargas, J.M. et al., 2002. About the seasonal variability of the Alboran Sea circulation. Journal Marine Systems 35, 229–248. Doi: 10.1016/S0924-7963(02)00128-8.

Vargas-Yáñez, M., García-Martínez, M.C., Moya, F., Balbín, R., López-Jurado, J.L. et al., 2017. Updating temperature and salinity mean values and trends in the Western Mediterranean: The RADMED Project. Progress in Oceanography 157, 27–46. Doi: 10.1016/j.pocean.2017.09.004.

Vázquez, J.T., Ercilla, G., Alonso, B., Juan, C., Rueda, J.L. et al., 2015. Submarine Canyons and related features in the Alboran Sea: continental margins and major isolated reliefs. pp. 183-196 In CIESM Monograph 47 [F. Briand ed.] Submarine canyon dynamics in the Mediterranean and tributary seas- An integrated geological, oceanographic and biological perspective, 232 p. CIESM Publisher, Monaco.

Xu, J.P., Noble, M.A. and Rosenfeld, L.K., 2004. In-situ measurements of velocity structure within turbidity currents. Geophysical Research Letters 31, L09311. Doi: 10.1029/2004GL019718.

www.puertos.es/es-es/oceanografia/Paginas/portus.aspx: Puertos del Estado webpage. From which metoceanographic data have been downloaded.

3.2. Transport and distributions of naturally and anthropogenically sourced trace metals and arsenic in submarine canyons

Marta Tarrés [a], Marc Cerdà-Domènech [a], Rut Pedrosa-Pàmies [a,b], Andrea Baza-Varas [a], Antoni Calafat [a], Anna Sanchez-Vidal [a], Miquel Canals [a,c,d*]

[a] GRC Geociències Marines, Dept. Dinàmica de la Terra i de l'Oceà, Facultat de Ciències de la Terra, Universitat de Barcelona, 08028 Barcelona, Spain

[b] The Ecosystems Center, Marine Biological Laboratory, Woods Hole, MA, USA

[c] Reial Acadèmia de Ciències i Arts de Barcelona (RACAB), La Rambla 115, 08002 Barcelona, Spain

[d] Institut d'Estudis Catalans (IEC), Secció de Ciències i Tecnologia, carrer del Carme 47, 08001 Barcelona, Spain

Progress in Oceanography 218 (2023) 103122
Doi: 10.1016/j.pocean.2023.103122

Keywords: Submarine canyons, Trace metals, Chemical pollutants, Settling particles, Seafloor sediments, SW Mediterranean Sea

Abstract Continental margins play a key role in the cycling of natural and anthropogenic trace metals (TMs) as pathways at the interface between landmasses and deep ocean basins but also as sinks. Knowledge of how short-lived forcings alter the export dynamics of TMs is essential for our understanding of their fate in that setting. Here we report time series of particulate metal fluxes in three submarine canyons —namely Escombreras, Almeria and the Garrucha-Almanzora system— of the South-Western Mediterranean Sea. Our research focuses on combining multi-elemental TMs (Al, Fe, Ti, Co, Cu, Mn, Ni, Pb and Zn) and As (a metalloid) contents of settling particles collected near the bottom by automated particle traps during one year, and seafloor sediment samples from below the traps. We assess the role of storms and bottom trawling in the off-shelf transport of particulate TMs and As, and the natural and anthropogenic contributions of TMs by using enrichment factors (EFs).

The TM export fluxes and composition changed over the study period, from March 2015 to March 2016. TM fluxes increase in early spring 2015 in association with short-lived storm events and during calm months in the Garrucha-Almanzora Canyon system, likely due to sediment resuspension triggered by bottom trawling. In terms of composition, TMs in the sinking fluxes appear to be closely associated with lithogenic (Al, Fe and Ti) and authigenic (Mn) particles' proxies. During storm events, the mass of settling particles in Escombreras and Almeria canyons was impoverished in Al, Fe, As, Co, Cu, Mn and Ni compared to other periods. The Garrucha-Almanzora Canyon system behaves differently as the above-described differences, are not observed there. Moreover, the TM composition of the sediments —with higher contents of Fe, Ti and several other TMs— in this canyon is barely tied to the composition of the settling particles.

Finally, Cu and Zn contents, together with Pb in the northernmost Escombreras Canyon, are best explained by referring to anthropogenic sources. This work provides insights into the profound influence of the natural and anthropogenic forcings controlling the distributions and seasonal dynamics of particulate TMs and As in submarine canyons.

3.2.1. Introduction

Trace metals (Al, Fe, Ti, Co, Cu, Mn, Ni, Pb, and Zn; TMs hereafter) in the marine environment have attracted the interest of researchers due to their critical role in regulating the growth and structure of marine organisms, and their interest as tracers of oceanographic processes, and also as pollutants (Morel and Price, 2003, Twining and Baines, 2013; Jeandel and Vance, 2018). Suspended particles are known by their capability to remove TMs from seawater (Anderson and Hayes, 2015 and references therein). Biological uptake, scavenging onto particle surfaces and precipitation (including bacteria-mediated) incorporate TMs into the particulate phase within the water column (Cowen and Bruland, 1985; Morel and Price, 2003; Anderson, 2020). The cycling of metals is, therefore, driven by sedimentary dynamics controlling the input, production, transformation, transport and accumulation of particles along the water column down to the seafloor. In other words, the distribution of TMs in the ocean is largely regulated by sinking particle fluxes (Huang and Conte, 2009; Kuss et al., 2010; Theodosi et al., 2013; Conte et al., 2019). Within the fluxes, the lithogenic, authigenic (abiotically precipitated) and biogenic fractions are vectors of TMs and As towards the seafloor (Huang and Conte, 2009). In the last years, researchers have employed some individual elements as proxies for mineral phases (e.g., Ba, Fe or Mn for authigenic minerals; Al, Fe or Ti for lithogenic minerals; and P for biogenic minerals, among others) (Sanchez-Vidal et al., 2005; Twining and Baines, 2013; Ohnemus and Lam, 2015; Al-Hashem et al., 2022). Those proxies provide information on transfer vectors and processes involving all other TMs, as elements associated with the same type of particles often exhibit similar distributions (Lee et al., 2018).

Continental margin settings are known as major vectors and suppliers of particulate and dissolved TMs to the deep basins (Lam et al., 2006; Charette et al., 2016; Lemaitre et al., 2020), and also as TMs' sinks (Palanques et al., 2008; Anderson, 2020). Particle transport in continental margins is driven by currents, which eventually can also erode and re-suspend seafloor sediments that will then add to the pool of particles in the water column (Heussner et al., 2006). Ultimately, such particles will be buried with their TMs' load (Geibert, 2018). TM cycling results from a complex interplay of physical and biogeochemical processes and is therefore difficult to understand (Noble et al., 2012). This is well illustrated by high-energy events such as sea storms or dense shelf water cascades (DSWC), which intensify TMs' transport from shallow to deep environments while also enhancing biogeochemical interactions (Hung and Ho, 2014; Dumas et al., 2014; Cossa et al., 2014; Durrieu de Madron et al., 2023). However, beyond the widely recognized key role of continental margins in mediating TMs' transport to the open ocean, significant gaps persist about the distribution of particulate metals and the processes determining their seaward transport, including deep continental margin regions (Palanques et al., 2008; Jesus et al., 2010; Roussiez et al., 2012; Cossa et al., 2014).

Besides, there is clear evidence that anthropogenic TMs have added to natural fluxes along and across continental margin settings and beyond, especially since the mid-nineteenth century (Grousset et al., 1995; Hanebuth et al., 2018), thus contributing to the degradation of the environmental status of our coasts, seas and oceans (Papale et al., 2018; Azaroff et al., 2020). In some places such inputs have been traced back to the Roman Period (Mil-Homens et al., 2016).

This study addresses some of these unknowns in three submarine canyons located off southeast Spain in the Mediterranean Sea (cf. section 3.2.2.1). These canyons connect coastal and shelf environments to the deep-sea (Ross et al., 2009; Puig et al., 2014). This paper is a follow up of a previous one by Tarrés et al. (2022) focusing on the major components of settling particles in the investigated submarine canyons for the same period. In the present paper, we focus on the multi-elemental TM (Al, Fe, Ti, Cu, Co, Mn, Ni, Pb, and Zn) and As (a metalloid) contents in settling particles and assess the processes controlling the dynamics of TMs and As in submarine canyons. By comparing the seafloor sediment composition with particles sinking in the canyons we provide insights into the processes leading TMs to reach canyon floors and their preservation in the sedimentary record. Finally, the calculation of enrichment factors (EFs) allows for estimating the anthropogenic influence on TM fluxes. For the purpose of this paper and for ease of simplicity, from here onwards we will refer to all elements listed above including As as TMs, i. e. those which appear in the relevant environmental matrix with ppm or ppb concentrations. This will include Al and Fe, which according to their concentrations actually appear as TMs in particle fluxes in the water column though not in the analyzed sediments, where they display concentrations of thousands of ppm.

3.2.2. Study area

3.2.2.1. Overall setting

The study area encompasses three margin segments in the SW Mediterranean Sea, namely Mazarron and Palomares, located on the western edge of the Algero-Balearic Sea, and the Almeria one, located on the northeastern border of the Alboran Sea (Fig. 3.12a, b). The continental shelf is narrow (<13 km) (Lobo et al., 2014), with the shelf edge located between 100 and 200 m depth. It is cut by several submarine canyons of small to medium size (Pérez-Hernández et al., 2014), which are smaller and more densely grouped to the north (Acosta et al., 2013). The three submarine canyons here investigated are, from north to south, Escombreras Canyon, Garrucha-Almanzora Canyon system and Almeria Canyon.

Surface circulation is influenced by the Northern Current flowing southward in the Gulf of Vera (Fig. 3.12b) and the entry of Atlantic Water into the Alboran Sea (e.g. Vargas-Yáñez et al., 2002; Macias et al., 2016). The latter forms two gyres known as the Western Alboran Gyre (WAG) and the Eastern Alboran Gyre (EAG). The two flows converge at the Almeria-Oran Front (AOF) from where surface waters are redirected towards the Algerian continental margin (Tintore et al., 1988) (Fig. 3.12b). Intermediate and deep waters flow westwards towards the Strait of Gibraltar (Parrilla et al., 1986; Millot, 1999).

Rivers opening into the study area are dry most of the year due to the semi-arid regional climate. However, short-lived flood events may supply substantial volumes of water, sediment (and also litter) to the coastline. The main rivers in the study area are the Almanzora and Andarax, which discharge in the Gulf of Vera and the Gulf of Almeria, respectively (Fig. 3.12b). Off-shelf transfer of sedimentary particles is driven by storm events triggering high waves and increasing currents velocities over the continental shelf, subsequently resulting in the resuspension of shelf floor sediments (Lobo et al., 2014). Several such stormy periods during the sampling period in this study have been previously documented (Supplementary Fig. 3.1; see further details in Tarrés et al., 2022). Several wet NE storms occurred at the beginning of the study period, i.e. in late March and early April 2015. Storms in the following months were of limited intensity and range. The situation changed in autumn months, when several rainfall episodes led to a noticeable increase in the discharge of Almanzora and Andarax rivers, with the main event in early November 2015. Finally, several SW dry storms took place by the end of the year-round study period.

Sediment transfer into the Garrucha-Almanzora Canyon system is favoured by the overall geomorphic configuration of the margin, with a canyon-incised narrow continental shelf, and the closeness of canyon heads to the mouths of Almanzora River but also Antas and Aguas rivers (Fig. 3.12b) (Puig et al., 2017). Enhanced fluxes recorded during summer months in this canyon system have been attributed to bottom trawling activities in the area (Tarrés et al., 2022).

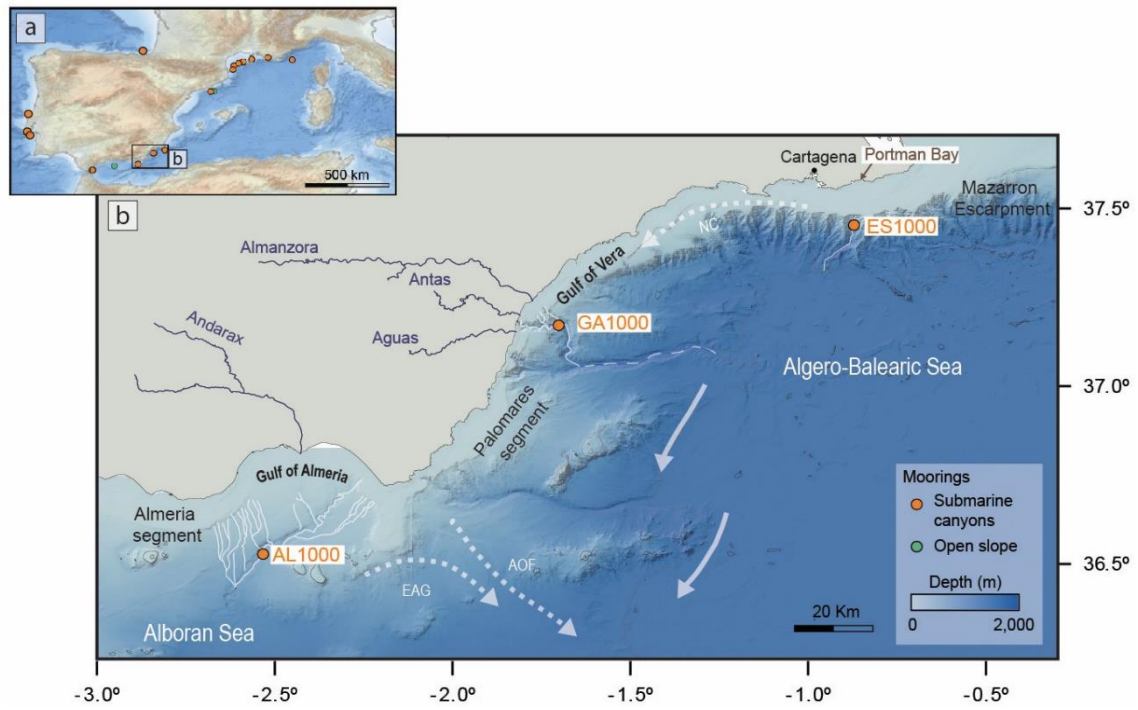

Fig. 3.12. (a) Map of the Western Mediterranean Sea and nearby areas showing places where trace metal contents and fluxes have been measured according to the literature and also from this study (cf. section 4 and Fig. 6). Map after EMODnet (https://emodnet.ec.europa.eu/geoviewer). (b) Shaded relief bathymetry map off SE Spain displaying the location of the mooring lines within the Escombreras Canyon (ES1000), the Garrucha-Almanzora Canyon system (GA1000) and the Almeria Canyon (AL1000). White lines indicate canyon axes including tributaries if present. Discontinuous white line indicates Alias-Almanzora Canyon

axis, when the Garrucha-Almanzora system merges with the southern system. The general surface circulation (discontinuous white arrows) and the intermediate and deep circulation are outlined (continuous white arrows). Main rivers are also shown (blue lines). AOF: Almeria-Oran Front. EAG: Eastern Alboran Gyre. NC: Northern Current. (For interpretation of the references to color in this figure legend, the reader is referred to the web version of this article.)

3.2.2.2. Total mass fluxes

Total mass fluxes (TMF) in the three investigated canyons, including the elemental composition and grain sizes of the particles involved, were described in a previous publication (Tarrés et al., 2022 and references therein). A summary is provided here as background information, including topic specific interpretations wherever judged convenient.

A common feature is that in all three canyons mass fluxes were predominantly composed of lithogenic particles, accounting for approximately 61%, 62%, and 72% in Escombrereras, Garrucha- Almanzora, and Almeria canyons, respectively. The carbonate fraction constituted the second-largest in the fluxes, representing about 37%, 34%, and 24% in the above canyons, respectively. The difference in $CaCO_3$ contents between the two canyons in the Gulf of Vera and Almeria Canyon, further south, was partially attributed to inputs of detrital material containing $CaCO_3$. OM was a small fraction, representing only 3–4% of the TMF in those canyons. The clay and silt fractions dominated the fluxes in all three canyons, with small standard deviations < 4%. This suggested a consistent sorting of the material being transported in suspension towards the distal margin.

Regarding flux magnitudes, Escombreras Canyon —measured from March to August 2015— exhibited two distinct situations. At the beginning of the study period, the trap collected comparatively high fluxes during storm events in March and April 2015 (Fig. 3.13a). Within this time, strong currents led to the resuspension and export of particulate matter from the continental shelf into the neighboring canyons, eased by nepheloid layers. The $CaCO_3$ content increased in March 2015 due to particle resuspension and advection of previously settled biogenic $CaCO_3$ from the shelf. In contrast, minimal fluxes were collected from late April to August, corresponding to calm meteorological and oceanographic conditions.

Mass fluxes in the Garrucha-Almanzora Canyon system —measured from March to September 2015— also peaked during the March and April 2015 storms (Fig. 3.13a). In this canyon system, bottom trawling activities around the canyon generated a nepheloid layer at depths exceeding 400 m, subsequently promoting increased particle fluxes throughout the spring and summer months (Fig. 3.13a). The incision of canyon heads into the continental shelf and the short distance of their heads to river mouths facilitated the transfer of terrestrial organic matter (OM, about 5% of the TMF) during the stormy spring period. Conversely, $CaCO_3$ contents displayed higher values during the summer months, correlating with TMFs. Therefore, such higher contents were not due to lesser dilution within the lithogenic fraction. In terms of particle sizes, there was a coarsening effect after May, with relatively high sand contents (up to 4.5%) for the lithogenic particles, especially in May, late August and September 2015.

Particle fluxes in Almeria Canyon —measured from March 2015 to March 2016— remained consistently low throughout the entire period. Similarly to the other two canyons, higher downward fluxes were observed at the beginning of the study period (Fig. 3.13a), coinciding with spring storm events. Mass fluxes showed a slight increase between November 2015 and January 2016, likely due to short-lived storms and several rainfall episodes that increased water discharge from nearby rivers, especially in early November. By the end of the monitoring period in February-March 2016, dry western storms occurred, which did not enhance downward fluxes at the trap location (Fig. 3.13a). In terms of composition, $CaCO_3$ contents increased during the spring 2015 and winter 2016 storm events, likely due to lateral transport, as previously explained for the Escombreras Canyon. OM presented a more pronounced seasonal pattern, with a higher contribution (about 7%) to mass fluxes during summer months, which can be explained by overall lower mass fluxes. In late January, OM contents increased again to about 6% due to the arrival of biogenic material from surface primary production. In terms of particle sizes, coarser fractions were collected at the beginning of the study period, with the higher sand content (about 6%) coinciding with the March storm. No coarsening trend in the fluxes was noticed during subsequent storms.

3.2.3. Materials and methods

3.2.3.1. Sampling

Sea work was performed during research cruises NUREIEV-1 from 13 to 24 of March 2015, NUREIEV-2 from August 29 to September 5, 2015, and NUREIEV-3 from 23 to 30 of April 2016, onboard R/V Ángeles Alvariño.

Three mooring lines —named ES1000, GA1000 and AL1000, respectively— were deployed along the axis of the Escombreras Canyon, the Garrucha-Almanzora Canyon system and the Almeria Canyon at 985, 1,100 and 1,000 m depth, respectively, from March 2015 to March 2016 (Fig. 3.12b and Supplementary Table 3.1; cf. section 3.2.2.1). Each mooring was equipped with a Technicap PPS3/3 sequential particle trap (aperture 0.125 m^2, cylindroconical shape) with 12 cups at 25 m above the bottom and a sampling interval of 7–16 days. Acid cleaned trap cups were filled with 5% (v/v) formaldehyde solution in 0.45 μm filtered sea water buffered with sodium tetraborate. Within the entire sampling period, only 10 days were devoted to mooring recovery, maintenance and redeployment operations during which there was no sample collection. Failures in the particle trap rotating system of ES1000 and GA1000 stations prevented the collection of samples during the last seven and six months, respectively.

Seabed sediment was collected with a KD Denmark multicorer at 1,002 m depth in the Escombreras Canyon during research cruise NUREIEV-1 in March 2015, and at 1,142 m depth in the Garrucha- Almanzora Canyon system during cruise NUREIEV-2 in September 2015. The sediment cores were subsampled onboard. The cores were sliced every 0.5 cm from the core top down to 5 cm, and every 1 cm from 5 cm to the core bottom. The subsamples thus obtained were stored at 2–4 °C in plastic bags. We used the top 0.5 cm of the cores for our analyses.

3.2.3.2. Sample analysis

The seafloor sediments were freeze-dried and homogenized for later analysis. Trap samples were also freeze-dried after removing the swimmers (i.e., those organisms deemed to have entered alive the traps, Pagès et al., 2007) using a nylon mesh of 1 mm and hand-picking the smallest ones. A high precision peristaltic pump allowed obtaining a working aliquot of each sample, which was then centrifuged with ultrapure water (Milli-Q) to extract the salt and the formaldehyde solution from the trap's cups. Trap sample processing is described in detail in Rumín-Caparrós et al. (2016).

The elemental composition was determined using a Perkin-Elmer Elan-6000 ICP-MS and a Perkin Elmer Optima 8300 ICP-OES at *Centres Científics i Tecnològics de la Universitat de Barcelona* (CCiT-UB). A two-step extraction method was applied for sample digestion. The first step was carried out in a closed digestion system with the goal of avoiding the loss of volatile elements, such as As. The leached elements were then recovered before proceeding with the second step, under open system conditions. The samples were placed in a Teflon reactor closed digestion system with 2.5 mL of HNO_3 (65%) during at least 12 h in a stove at 90 °C. The extract was centrifuged to collect the supernatant and obtain a first solution, thus recovering the leached elements. The solid sample recovered from centrifugation was placed again into a Teflon reactor, and digested with 2.5 mL (65%) HNO_3, 10 mL (40%) HF and 2 mL (70%) $HClO_4$ during at least 12 h in a stove at 90 °C. Then, the Teflon reactor was heated in a sand bath at 250 °C. 2 mL of (65%) HNO_3 and 2 mL of H_2O_2 were added and heated again until total evaporation of the acid volume. When the sample showed incipient dryness, 2 mL $HClO_4$ were added until reaching the total evaporation of the acid. The residue was redissolved in 2 mL HNO_3 and 5 mL of ultrapure water (Milli-Q) to obtain a second solution. Two procedural blanks were analyzed with each sample batch to ensure the lack of contamination during sample processing and analysis. Replicates were routinely performed to determine the uncertainty associated to subsampling heterogeneity and method precision. Relative standard deviation (RSD) was always below 5% for all metals, except for Pb and Ni (~6.5%) and Mn (7.5%). For As, the RSD was 5.4%.

3.2.3.3. Data analysis

Particulate fluxes in the investigated canyons have been previously published in Tarrés et al. (2022) for the same period of time here addressed. Those fluxes allow calculating the annual Time Weighted Fluxes (TWF) of TMs, which represent a weighted average of TMFs corrected according to the number of sampling days:

$$TWF\ (mg\ m^{-2}d^{-1}) = \frac{\sum Mi\ (mg)}{Collection\ area\ (m^2) * \sum Di\ (d)} \quad [3.6]$$

where M_i is the mass per sample and D_i is the total days of collection.

The annual Time Weighted Content (TWC) is calculated for each element to correct sampling interval values, following equation:

$$TWC\ (\mu g\ g^{-2}) = \frac{TWF\ (element\ mass)}{TWF\ (total\ mass)} \quad [3.7]$$

The correlations between variables, including major and trace elements, is evaluated by means of the Pearson's Correlation Coefficient (PCC) for each station, considering $p < 0.05$ as significant. A Principal Component Analysis (PCA) allowed identifying the dominant factors describing the variability of the dataset. PCA variables are the same than for PCC, including OM and $CaCO_3$ main flux components from Tarrés et al. (2022). Lithogenic components were represented by Al, Fe and Ti contents. However, to simplify the dataset, Ti from GA1000 was excluded from the analysis. Biogenic silica was not included given its very minor contribution to the fluxes (Tarrés et al., 2022). AL-I-11 and AL-I-12 samples from AL1000 station were also excluded due to Zn outliers. The dataset was standardized in order to adjust the variance of all variables to the same scale. Data standardization consisted in subtracting the mean of all variables and dividing each one by its standard deviation. It was also conducted on log-transformed contents to improve the normal distribution of the variables (Karageorgis et al., 2009). A Varimax rotation subroutine was performed after the PCA to facilitate the interpretation of the flux components. All statistical analyses have been carried out using the *Statgraphics Centurion* software.

To explore potential statistical differences in TM contents between stations (ES1000, GA1000, and AL1000) and periods within each station (stormy vs. calm periods), we used the Kruskal-Wallis H non-parametric test since normality was not achieved when considering the full dataset. TMs pollution levels are calculated using EFs, which are usually applied to estimate anthropogenic contributions to marine sediments (Birch, 2017). This method requires normalizing metal values to reduce content's variability resulting from natural changes in mineralogy and grain size (Aloupi and Angelidis, 2001; Roussiez et al., 2006). Given the rather diverse particle composition of trap samples, partly due to variations in rock composition inland, a normalization step was applied to compensate for such natural variations. We used Al as the normalizing element as in previous studies (Palanques et al., 2008; Mil-Homens et al., 2013a; Dumas et al., 2014). Pre-industrial background ratios have been estimated from subseafloor sediments in the Almeria and Escombreras canyons, as obtained from ^{210}Pb dating of sediment subsamples at relevant core depths (50–51 cm) from the same location of the Escombreras Canyon sediment trap (unpublished data), which have been extended to the Almeria Canyon (40–41 cm). Whereas in the Garrucha-Almanzora Canyon system this has not been possible since the corresponding multicore reached 15 cm below the seabed only. Therefore, the samples collected in the GA1000 trap were normalized with the subseafloor sediments of the Almeria Canyon given the strong similarity in the mineralogical composition of clay minerals from both canyons. EFs were obtained following equation [3.8] while also considering a threshold of 1.5 as indicative of anthropogenic contributions according to local pre-industrial values (Roussiez et al., 2006):

$$EF = \frac{TM/Al}{TM_b/Al_b} \quad [3.8]$$

where TM and Al refer to TM and Al contents in the sample, respectively, and TM_b and Al_b represent the pre-industrial levels.

3.2.4. Results

3.2.4.1. Trace metal contents in settling particles and fluxes

TM contents in settling particles change from one station to the other (Table 3.3 and Fig. 3.13b). The highest contents correspond to AL1000 station for all elements, as illustrated by As and Al with 19.36 μg g^{-1} and 8.19% peak values, respectively. One exception is the Co, which increases at ES1000 station with 17.42 μg g^{-1}. Minimum values for As, Mn, Ni, Pb and Zn occur at station GA1000, while the lowest ones for Al, Fe, Ti, Cu, and Co appear at ES1000 (Table 3.3).

The highest differences between minimum and maximum TM values occur at AL1000 station, with a remarkable difference for the Mn (from 791.07 to 1,347.46 μg g^{-1}) and the Ti (from 2,790.89 to 3,454.70 μg g^{-1}) relative to the other two stations. However, Co displays the highest variability at ES1000 (from 9.09 to 17.42 μg g^{-1}), while Pb and As do it at GA1000 (from 40.27 to 59.49 μg g^{-1} and from 9.97 to 14.53 μg g^{-1}, respectively) (Table 3.3). Fig. 3.13b shows how TM contents changed during one year (AL1000 station) or half a year (ES1000 and GA1000). In AL1000, some elements reach their highest contents in spring-summer (e.g. Co, Cu, Mn), while others do in late spring-summer and autumn (e.g. Al, Fe, Ti, As, Ni, and Zn). Pb values are rather steady and do not increase at any specific season. The half year records from ES1000 show an increasing trend from March to August 2015 for Co, Cu, Mn and Zn, while Pb is higher during July and August. In the GA1000 station only Al raises throughout most of the period, while other elements diminish during the last months, as shown by As, Co, Cu, Mn, Pb and Zn. In fact, As, Co, Cu and Mn reach their higher concentrations in June. In contrast, Pb and Zn peak during late spring months. Fe correlates well with Mn (r^2 = 0.85; $p < 0.01$) at GA1000, whereas Fe and Ti correlate with Al at ES1000 and AL1000 ($r^2 > 0.78$; $p < 0.01$) (Supplementary Table 3.2).

Our time series shows several TM export events during the investigated period (Fig. 3.13c). A first and most noticeable flux increment, at the beginning of the sampling period, resulted in the highest measured export rates for all elements under consideration, with minimum values for Co up to 0.23, 0.17 and 0.06 mg m^{-2} d^{-1} and maximum values of 1,272.47, 1,000.66 and 349.83 mg m^{-2} d^{-1} for Al at stations ES1000, GA1000 and AL1000, respectively (Table 3.3 and Fig. 3.13c). Minor but consistent increments of all elements were recorded at GA1000 in late May, early June, late August and September 2015 (Fig. 3.13c), which coincided with high turbidity values from 400 m depth down to the bottom at 1,100 m (Tarrés et al., 2022). The early June 2015 peak was noticeable for its comparatively high Cu, Mn, Ni, Pb and Zn export fluxes, whereas As and Co showed values closer to the ones found during the ensuing summer events (Fig. 3.13c). Time series for the following months are available for AL1000 station only. A slight flux increment with maxima ranging between 0.04 and 248.52 mg m^{-2} d^{-1} for Co and Al, respectively, were observed between November 2015 and January 2016. TM fluxes lowered during February and March 2016 (Fig. 3.13c).

Code		ES1000			GA1000			AL1000			SS ES1000	SS GA1000
Depth (m)		985			1,100			1,000			1,002	1,142
Number of samples		12			13			24				
Content	% or µg g^{-1}	Average*	Max	Min	Aver	Max	Min	Average*	Max	Min		
Al	%	5.54	6.60	5.10	5.97	6.42	5.47	7.31	8.19	6.60	5.13	5.66
Fe	%	2.72	3.14	2.54	2.77	2.98	2.62	3.40	3.72	2.98	2.82	3.49
Ti	µg g^{-1}	2,866.65	3,185.58	2,783.64	2,99	3,161.40	2,858.56	3,183.20	3,454.70	2,790.89	2,649.18	3,944.93
As		16.79	18.47	16.18	11.8	14.53	9.97	17.36	19.36	15.40	20.79	13.09
Co		11.41	17.42	9.09	10.2	11.58	9.28	13.55	16.10	12.04	12.36	11.10
Cu		26.24	37.38	22.11	25.6	30.30	22.68	35.34	47.80	31.36	25.00	27.54
Mn		816.99	1,057.47	702.08	563.	686.94	489.12	1,005.10	1,347.46	791.07	2,359.08	664.77
Ni		32.32	37.87	29.55	33.0	36.56	29.06	40.26	45.07	36.56	28.26	33.37
Pb		48.90	56.95	44.48	47.4	59.49	40.27	57.31	60.85	53.02	46.56	61.26
Zn		119.97	135.70	113.12	122.	144.47	107.20	158.08	184.06	144.90	114.12	115.46
Flux**	mg m^{-2} d^{-1}	Average**	Max	Min	Aver	Max	Min	Average**	Max	Min		
Al		266.11	1,272.47	58.00	463.	1,000.66	173.59	119.83	349.83	33.52	-	-
Fe		130.66	633.22	27.94	214.	479.88	82.94	55.81	171.43	15.79	-	-
Ti		13.76	69.76	2.90	23.2	52.90	8.38	5.22	16.36	1.47	-	-
As		0.08	0.40	0.02	0.09	0.23	0.04	0.03	0.09	0.01	-	-
Co		0.05	0.23	0.02	0.08	0.17	0.03	0.02	0.06	0.01	-	-
Cu		0.13	0.55	0.03	0.20	0.49	0.08	0.06	0.16	0.02	-	-
Mn		3.92	17.52	0.99	4.37	10.17	1.91	1.65	4.23	0.52	-	-
Ni		0.16	0.74	0.03	0.26	0.54	0.10	0.07	0.19	0.02	-	-
Pb		0.23	1.20	0.05	0.37	0.88	0.16	0.09	0.31	0.03	-	-
Zn		0.58	2.82	0.12	0.95	2.23	0.36	0.27	0.81	0.11	-	-

Table 3.3. Trace metal contents and fluxes in settling particles and seafloor sediments (SS). AL1000 values correspond to a complete annual cycle, whereas GA1000 and ES1000 values correspond to a half-year period. *: Average metal contents in time-weighted

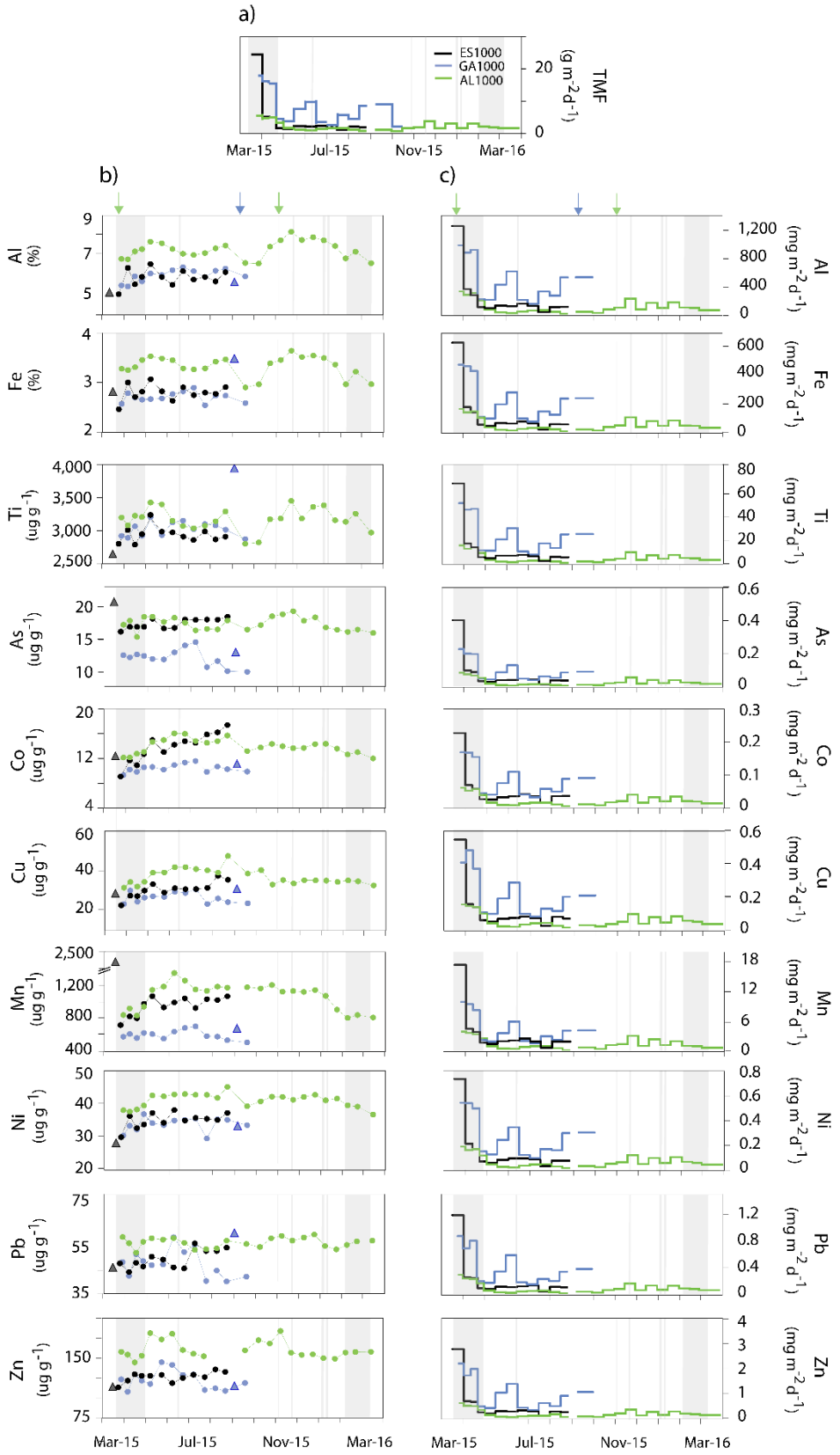

Figure 3.13. Time series of (a) Total mass fluxes in settling particles at stations ES1000 (black line), GA1000 (blue line) and AL1000 (green line) after Tarrés et al. (2022). (b) Trace metal contents —in μg g^{-1} excepting Fe and Al, which are in %— in settling particles (dots) and seafloor sediments (triangles) at stations ES1000

(black dots), GA1000 (blue dots) and AL1000 (green dots). (c) Trace metal fluxes in settling particles. Color codes as in (a). Black and blue triangles indicate trace metal and As contents in seafloor sediments from ES1000 and GA1000, respectively. Grey vertical stripes highlight sea storm events, with two main periods at the beginning and at the end of the study period (cf. Supplementary Figure 3.1 for further details). The arrows above (b) and (c) plots mark river discharge events (green when close to AL1000 and blue when close to GA1000). Note that vertical scales change from one plot to the other.

3.2.4.2. Trace metal contents in seafloor sediments

With few exceptions, TM contents in seafloor sediments are close or very close to the ones in settling particles (Fig. 3.13b). The highest contents of Ti, As, Mn and Pb (20.79, 3,944.93, 2,359.08 and 61.26 μg g^{-1}, respectively) found in this study correspond to sediments (Table 3.3 and Fig. 3.13b). At ES1000, As and Mn contents in sediments were 19% (20.79 vs. 16.79 μg g^{-1}) and 65% (2,359.08 vs. 816.99 μg g^{-1}) higher, respectively, than average contents in sinking particles (Tables 3.3 and 3.4). Sediments collected below GA1000 station show higher Fe (20.7% more), Ti (24.2% more), Mn (15.3% more) and Pb (22.5% more) contents than average contents in settling particles (Tables 3.3 and 3.4). These increments persist after normalizing TMs/Al. Furthermore, the Al-normalized values show moderate increases (<15%) for Co in ES1000, and for As, Co and Cu in GA1000 (Table 3.4).

	Escombreras Canyon		Garrucha-Almanzora Canyon system	
		TMs/Al		TMs/Al
	%	%	%	%
Fe_{xs}	3.7	-	**20.7**	-
Ti_{xs}	-8.2	-	**24.2**	-
$\underline{As}_{xs}$	**19.2**	**25.3**	9.6	**14.3**
$\underline{Co}_{xs}$	-7.6	**14.6**	8.1	**12.9**
$\underline{Cu}_{xs}$	-5.0	2.9	6.9	**11.8**
Mn_{xs}	**65.4**	-	**15.3**	-
$\underline{Ni}_{xs}$	**-14.3**	-5.7	1.0	6.2

Table 3.4. Trace metals and As excess (%) in canyon floor sediments with respect to time weighted contents calculated after settling particles data (both non-normalized and normalized to Al).

3.2.4.3. Outcomes of the multivariate analysis

In the ES1000 station, four components explain 93% of the total variance of the dataset (Fig. 3.14a). Component 1 (53% of the total variance) is characterized by capture majority of individual variance for Co, Cu, Mn (57–77%) and to lesser extent, As, (43%). Component 2 (27% of the total variance) explains most of the variability of lithic elements (Al, Fe, Ti) (51–71%) and also of $CaCO_3$, which displays negative loading. Component 3 (8% of the total variance) is contributed by several TMs (As, Co, Cu, Pb and Zn), and explains most of the variance of Pb (56%) and Zn (85%) and, to lesser extent As (43%). Component 4 (5% of the total variance) describes most of OM variance (70%) and part of Zn variance (22%).

In the GA1000 station, four components explain 90% of the total variance of the dataset (Fig. 3b). Component 1 (49% of the total variance) describes >80% of Cu and Mn variance, and >50% of Fe, As and Co variance. Component 2 (21% of the total variance) describes Al variance (>70%), Fe (31%), Co (42%) and Ni (61%). Component 3 (12% of the total variance) is contributed (>90%) by OM and CaCO3 (negative loadings). Component 4 (8% of the total variance) explains most of Zn variance (91%) and, to a lesser extent, Pb (63%) and As (26%).

In the AL1000 station, three components explain 85% of the total variance of the dataset (Fig. 3.14c). Component 1 (46% of the total variance) reflects most of Co, Cu, Mn and Ni variance (>75%) and to a lesser extent Zn (29%) and OM (24%), with negative loading of $CaCO_3$ (28% of variance). Component 2 (25% of the total variance) greatly explains the variance of Al, Fe, Ti (>80%). As and Ni are also associated to the elements that represent lithogenic minerals, explaining about 20% of their individual variability). This component also captured part of $CaCO_3$ variance (35%), contributing with a negative loading. Component 3 (14%) relates most of Pb (83%) and As and Zn (~55%) variance.

3.2.5. Discussion

3.2.5.1. Intraannual variability of trace metal fluxes

TM export rates in the investigated submarine canyons are comparable to those found in former studies of submarine canyons and open slopes of the Western Mediterranean Basin (Puig et al., 1999; El Khatab, 2006; Heimbürger et al., 2012; Cossa et al., 2014). During the monitored period, the main TM export event into the studied canyons occurred in early spring 2015, concurrently with eastern storms with significant wave heights (Hs) above 4 m (cf. section 3.2.2, Fig. 3.13 and Supplementary Fig. 3.1). During the following calm months, our traps recorded several TMs pulses in the Garrucha-Almanzora Canyon system (Fig. 3.13c), which we attribute to bottom trawling activities on the canyon flanks, as there is no other plausible explanation. A number of studies has shown trawling activities to cause seafloor erosion and sediment resuspension (Martín et al., 2007; Puig et al., 2012; Martín et al., 2014), subsequently modifying the behavior and the biogeochemistry of OM, TMs and other pollutants in the marine environment (Bradshaw et al., 2012; Pusceddu et al., 2014; Paradis et al., 2021; Palanques et al., 2022). After October 2015, only the AL1000 station in the Almeria Canyon remained operational. Slightly higher export fluxes were recorded there between November 2015 and January 2016 after short-lived storms and rainfall episodes, mainly in early November. In short, storms and bottom trawling appear as the main triggers of TM transport events into the investigated submarine canyons.

3.2.5.2. Intraannual variability of trace metal contents in settling particles

Settling particles are vectors for TM export, which are known to be associated with lithogenic, biogenic and authigenic carriers (Huang and Conte, 2009; Conte et al., 2019; Blain et al., 2022). Specific TMs have been used as proxies of particle types, such as Fe, Al and Ti for the lithogenic fraction (Ohnemus and Lam, 2015; Lee et al., 2018), or Fe and Mn for the authigenic fraction (Martín et al., 1983; Cowen and Bruland, 1985; Bruland and Lohan, 2003; Tebo et al., 2004). The

poor correlation between Al and Mn in all our stations (from north to south, r = 0.57 at ES1000, 0.22 at GA1000, and 0.35 at AL1000) supports this view (Supplementary Table 3.2). Fe strongly correlates with Al in the Escombreras and Almeria canyons, with r > 0.91 and p < 0.01 (Supplementary Table 3.2), thus pointing to a lithogenic source and/or shared distributions. On the contrary, in the Garrucha-Almanzora Canyon system there is a poor correlation (r = 0.48) between Fe and Al, but a better Fe correlation with Mn, with r = 0.67 and p < 0.05 (Supplementary Table 3.2). Therefore, Fe contents in the Garrucha-Almanzora Canyon system likely respond to the presence of particle sources other than just lithogenic. In the next subsections, we use the PCA results to assess TMs variability on a canyon by canyon basis.

Escombreras Canyon

The first component in the Escombreras Canyon would reflect an authigenic component, which explains most of the variance of Co, Cu, Mn, Ni and, to a lesser extent, As and Zn, during the six-monthly monitoring period (Fig. 3.14a and Supplementary Table 3.2). The scavenging behavior of these metals onto Mn (oxy)hydroxides (Huang and Conte, 2009) and/or the oxidation of dissolved species leading to the precipitation of oxides (e.g. Co oxides) that behave similarly to Mn oxides (Dulaquais et al., 2017) could explain the above association. Authigenic component scores displayed a clear trend with the minima in March and April, concomitantly with the storm events, with maximum values in summer months. This suggests that variability arises partly from changes in particle sources between the two periods, likely as a result of resuspension over the shelf and subsequent downward transport in the first period, and of disconnection from the shelf and dominating pelagic sedimentation during the second period.

The second component is clearly lithogenic as it describes most of the temporal variance of Al, Fe, Ti and, to a lesser extent, Ni and OM, with modulation by $CaCO_3$ inputs accounting for a negative loading. However, most of the temporal variance of Pb is largely captured within a third component, which is also contributed by other TMs such as As, Co, Cu and Zn, which may derive from anthropogenic sources. This third component displays negative scores in March and April 2015 and positive scores during summer months.

Garrucha-Almanzora Canyon System

We interpret the first component to reflect authigenic Mn and Fe bearing phases, such as oxides and oxidized particle coatings. The PCA results (Fig. 3.14b) and the close correlation of particulate As, Co, Cu and Pb with Mn (from r = 0.68, p < 0.05 for Pb to r = 0.88, p < 0.01 for As), and of Co and Cu with Fe (r > 0.83, p < 0.01) (Supplementary Table 3.2) indicate a joint transport into the canyon. This component depicts strong scores after May, and positive scores during June and early July, when anthropogenic disturbances can be a major driver of TMs transfer into the canyon axis (cf. section 3.2.5.1). Seafloor disturbance is able to release metals from bottom sediments to the water column (Eggleton and Thomas, 2004; Kalnejais et al., 2007; Bancon-Montigny et al., 2019), which then could be re-absorbed onto floating particles following resuspension events (Rusiecka et al., 2018; Al-Hashem et al., 2022).

The negative relationship between TMF and the contents of the above-mentioned TMs (Supplementary Fig. 3.2) suggests that dilution processes could have played a role in the observed temporal fluctuations. Yet, little is known about the role of bottom trawling in the TMs fate and

redistribution (Palanques et al., 2022). Any geographical shift of resuspension area, and/or a change in particle loads and their properties (grain size, composition) or in oxygen content of the bottom water hold the potential to impact metal contents in resuspended particles forming nepheloid layers (Lohan and Bruland, 2008; Palanques et al., 2022) and, therefore, in the sinking fluxes.

The second component describes the lithogenic fraction, explaining most of Al, Ni and, to a lesser extent, Co and Fe variance (31% of individual variance) (Fig. 3.14b). Zn and Pb mostly bivariate together, thus contributing to a fourth component.

Almeria Canyon

The first component primarily reflects the influence of biogenic (OM) and authigenic Mn (oxy)hydroxides, and explains a significant portion of the variance of Co, Cu, Mn, Ni and, to a smaller extent, Zn and OM. Scores associated with this component noticeably increased after April 2015, reaching their maximum during summer months, from where they remained slightly positive until late autumn (Fig. 3.14c). During summer period, the above contributions were not masked by components that otherwise dominate mass fluxes in resuspended material, thus resembling Escombreras Canyon.

The second component is indicative of the lithogenic fraction, and accounts for most of Al, Fe and Ti variance and, to a lower extent, As and Ni. Interestingly, the autumn months displayed stronger positive scores and high Al and Fe contents (Fig. 3.13b), which could relate to the likely arrival to the site of terrestrial material after a November flood of the Andarax River. The enhancement of lithogenic inputs following fluvial discharges in the Alboran Sea has been previously reported (Fabres et al., 2002; Sanchez-Vidal et al., 2004). TM contents were modulated by $CaCO_3$ biogenic inputs (Fig. 3.14c). As mentioned in section 3.2.4.1, $CaCO_3$ inputs into this canyon seem to correspond mostly to pelagic settling from the overlaying water column, with a diminution of the relative abundance of lithogenics during late summer. However, $CaCO_3$ contents were also enhanced by resuspended and laterally advected material during the storm events, at the beginning and the end of the study period (Fig. 3.13b). The two principal components did not account for much of Pb and Zn interannual variability, as observed for the other two canyons (Fig. 3.13c).

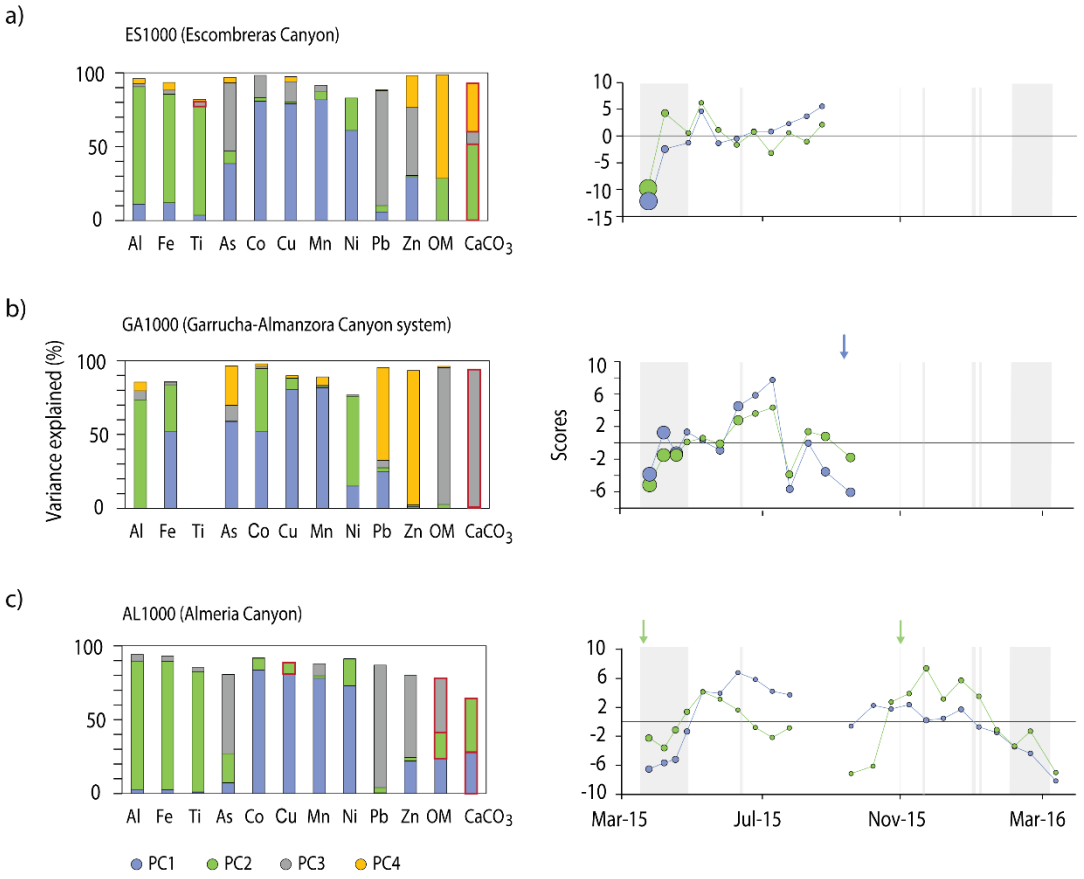

Figure 3.14. Principal Component Analysis (PCA) of settling particles at (a) ES1000 (N=11), (b) GA1000 (N=13) and (c) AL1000 (N=22) mooring stations. Note that some samples have been excluded from analysis due to it including outliers in the dataset. The plots explain de variance (%) for trace metals, organic matter (OM) and $CaCO_3$ after the main components (negative loads are highlighted in red in the corresponding bars of the left side plots), and the temporal variability of the scores for the two principals components (right side plots). Dot size is proportional to mass flux.

Common features amongst canyons

Our results indicate the three investigated canyons share a number of features. Authigenic Mn (oxy)hydroxides played a key role in most of As, Co, Cu, Mn and Ni interannual variance (Fig. 3.14). Particulate Mn contents relate to its predisposition for oxidative precipitation. River discharges, shelf sediment resuspension and diffusion from the seafloor are likely sources of dissolved Mn and Fe into the water column (Marin and Giresse, 2001; Noble et al., 2012; Dulaquais et al., 2017), which can subsequently precipitate onto suspended particles while co-scavenging other dissolved TMs. This would be especially the case of dissolved Mn, which slow kinetic rates of oxidation (Jensen et al., 2020) and easiness to form complexes with organic ligands (Oldham et al., 2017) promote Mn transport to deeper environments (Jensen et al., 2020), such as the Escombreras and Almeria canyons. The width of the continental shelf, together with bottom oxygen concentrations and acting physical processes, can influence the seaward transport of dissolved Mn (Noble et al., 2012). As for the Garrucha-Almanzora Canyon system, our results suggest that Fe oxides also contributed to the authigenic fraction, implying additional processes, such as benthic resuspension as a likely prevalent source of redox sensitive TMs.

The lithogenic contribution to TMs interannual variance was especially relevant for Al, Fe (though less in GA1000 station) and Ti. Nevertheless, it did not account for the variance of most of the other TMs (Fig. 3.14). This could be viewed as surprising as this fraction dominated mass fluxes in all three canyons. Certainly, it was the responsible of most of the temporal variance of Ni and Co in GA1000 (61 and 42% of the total variance, respectively), as observed after PC2 scores (Fig. 3.14b). In contrast, the poor association of TMs with OM (PC3) (Fig. 3.14a) suggests a minor biogenic contribution to TMs export. The near-bottom placement of our sediment traps could have hampered observing potential associations of TMs' export with biological carriers, as the redistribution and dissolution of metals in sinking particles weaken such relationships with depth (Huang and Conte, 2009; Blain et al., 2022). It should be, however, noticed that the statistical analysis in our study tends to highlight the phase to which each TM is mainly associated to, and also that to a greater or lesser extent, most TMs are coupled with multiple types of particles (Huang and Conte, 2009; Conte et al., 2019). Finally, it's worth noting that Pb and Zn's intraannual variation in all three canyons was captured by other components, which likely reflect anthropogenic contributions, possibly from several introductory pathways, including atmospheric deposition, thus further increasing the poor correlation of these metals with the main fractions and the other TMs.

Fig. 3.15 shows a generalized impoverishment of TM contents and metals representing the authigenic and lithogenic fractions (excluding Ti) at the occasion of the spring 2015 and winter 2016 storms in the Escombreras and Almeria canyons. Settling particles from the Garrucha-Almanzora Canyon system exhibited much less marked differences, in terms of TMs contents, between periods with and without storms compared to the other two canyons (Fig. 3.15). The larger compositional shifts between calm and stormy conditions for Zn, Ni, Mn, Fe and Al occur in Almeria Canyon, with e.g. mean values from 1162.4 ± 64.9 down to 848.9 ± 53.5 $\mu g\ g^{-1}$ for Mn. For Co and Cu the larger differences correspond to Escombreras Canyon. For As the step between the two periods —calm vs. stormy— is almost equal in Escombreras and Almeria canyons (Fig. 3.15).

The above suggest that storm events led to the export of resuspended material from the adjacent shelves, which only reached the deep canyon environment during such energetic processes. Both the authigenic Mn oxides and the detrital fractions appeared to be diluted in those laterally advected sediments. Dilution was evident not only in the authigenic fraction but also in the detrital fraction, which dominates the resuspended material on continental margins. An explanation could be that the resuspended material was primarily enriched in $CaCO_3$, as illustrated in Fig. 3.13c and 3.14a, c. This view is in agreement with observations in the northwestern Mediterranean margin during high energy events (Cossa et al., 2014). However, in the investigated canyons we did not observe a correlation between grain size and TMs, which would be largely due to the small variation in the fluxes grain size throughout the monitoring period. While storms may have generated bottom shear stress capable of remobilizing coarse sediments on the shelves, the prevailing currents were likely not sufficient to carry a coarser suspended load till reaching the locations of the mooring stations.

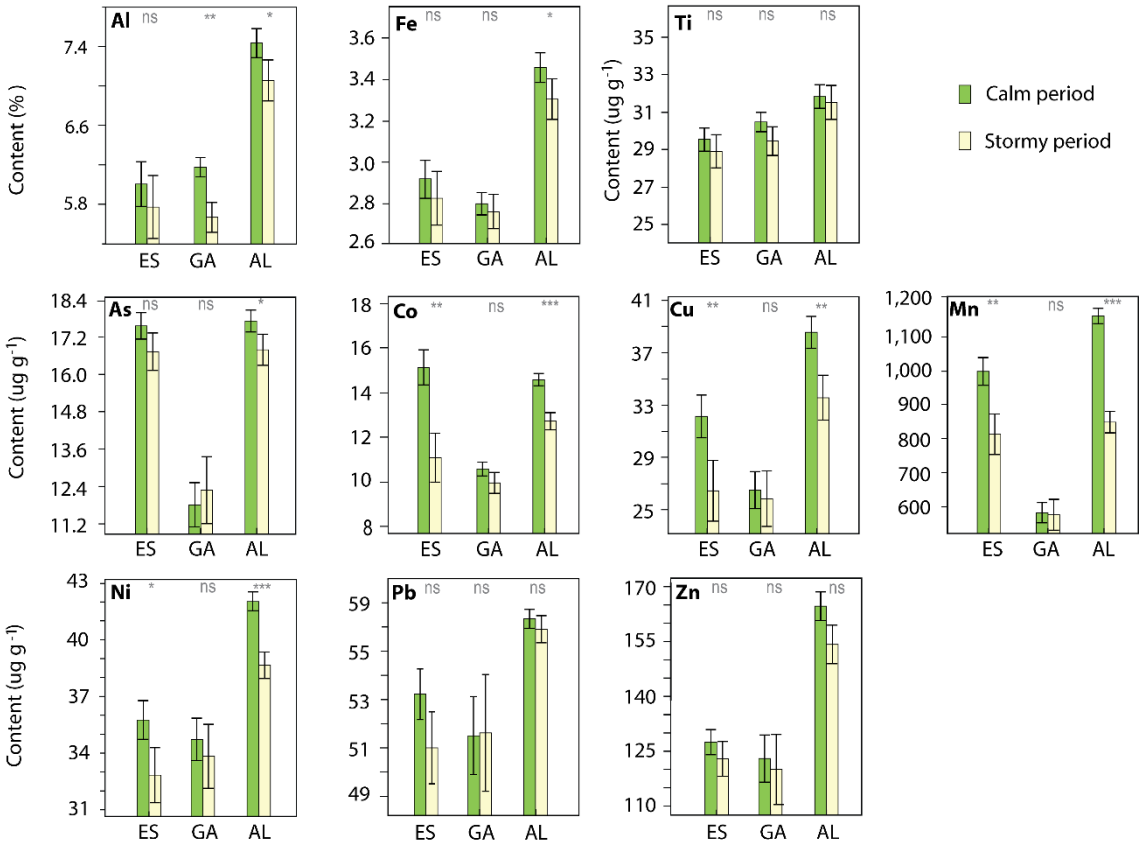

Figure 3.15. Metal contents in settling particles during calm and stormy periods from March 2015 to March 2016 in Escombreras Canyon (ES), Garrucha-Almanzora Canyon system (GA) and Almeria Canyon (AL). Significance of the variance (p-values): *p < 0.05, ** p < 0.01, ***p < 0.001. ns: non-significant.

3.2.5.3. Trace metals distributions in the submarine canyons

We observe regional variations in spatial TMs distributions. The Almeria Canyon commonly displays higher TM contents (Fig. 3.13b) than the Escombreras Canyon and the Garrucha-Almanzora Canyon system to the north. Variance analysis indicates that they are significantly different at a $p < 0.05$ level, except for As and Co from the Escombreras and Almeria stations (see statistical parameters in Table 3.3). The lower contents of detrital $CaCO_3$ in the particles of the margin segment to the south —where Almeria Canyon is located— compared to the northern margin segments (Tarrés et al., 2022) can explain the differences in Al, Fe, Ti and other TM contents. This observation fits with the fact that minerals from terrestrial sources are a relevant constituent of particle standing stocks and bottom sediments in continental marginal settings. This would ultimately relate to inland geology, which determines the composition of the sedimentary particles feeding the continental margin as a result of weathering processes and sediment transport by surface run-off and fluvial discharge.

When normalized to Al, the differences in TM concentrations between sampling stations in the northern and the southern margin segments diminish. This allows grouping the investigated canyons in two clusters: (i) Almeria and Escombreras canyons have high normalized ratios of As, Cu, Co and Mn in settling particles, and (ii) the Garrucha- Almanzora Canyon system has lower

normalized ratios of the previous elements in settling particles. This results from distinct TMs cycling and fate in the Garrucha-Almanzora Canyon system respect the other canyons (cf. section 3.2.5.2).

3.2.5.4. Modification of trace metal contents in canyon floors

So far we have discussed the distributions of TMs in the settling particles. Whereas the ultimate fate for sinking particle fluxes is the seafloor, the bulk composition of bottom sediments often differs from the one of settling particles in the water column, a situation that has been attributed to post-depositional processes, changes of particle sources, and alteration of the primary fluxes in the water column (Tesi et al., 2010; Raiswell, 2011; Heimbürger et al., 2012; Thibault de Chanvalon et al., 2016). We address this issue by comparing the TWC obtained for the study period with the canyon floor sediments of Escombreras Canyon and Garrucha-Almanzora Canyon system. We are obviously aware that even a single centimetre of bottom sediments can encompass years of deposition.

We calculated the TM in excess of seafloor sediments after the TWC of settling particles, both normalized and non-normalized to Al as a proxy for grain size (Table 3.4). The peak value for seafloor excess of Mn (65.4 %) appears at ES1000, while the one for Fe (20.7 %) occurs at GA1000. Such excess Mn and Fe could be associated to early diagenetic processes involving the reduction of Fe-Mn oxides in sub-oxic horizons and the diffusion of the dissolved Fe and Mn towards the sediment–water interface followed by re-precipitation in the redox boundary (Calvert and Price, 1972; Froelich et al., 1979; Marin and Giresse, 2001). After such a cycling in the sediment, resuspension and transport processes could transfer these phases by advection over the seabed (Sanchez-Vidal et al., 2005; Lee et al., 2018), as described in section 3.2.3.2. The excess Ti (24.2%) in surficial sediments of the Garrucha-Almanzora Canyon system compared to Escombreras Canyon (-8.2%) could indicate differential resuspension processes and near-bottom transport from one canyon to the other. It is well known that Ti preferentially concentrates in the coarser fractions of the sediment together with other heavy minerals such as titanomagnetite, ilmenite, augite and rutile (Boyle, 1983). It is plausible that the excess Fe in the Garrucha- Almanzora Canyon system also results from near-bottom processes, as it occurs for some heavy minerals (Dill, 2007).

After normalizing TM concentrations to grain size, the rather similar values (less than ± 10% of excess) for most of them (Table 3.4) suggest that metal excesses in the sediment could be partially explained by differences in grain size. Excesses higher than 25% for As in the Escombreras Canyon floor, and for Pb in the Garrucha-Almanzora Canyon system floor (Table 3.4) could be explained by diagenetic remobilization related to the excess of redox-sensitive Mn. This process would provide a plausible explanation for the distribution of As in Escombreras Canyon (Chaillou et al., 2003), with sulfate reducing bacteria possibly playing a role according to recent findings by Baza-Varas et al. (2023).

Elevated Pb contents in the Garrucha-Almanzora Canyon system can result from in-situ suboxic diagenetic remobilization too (El Houssainy et al., 2020) and/or from reabsorption onto benthic resuspended particles (Rusiecka et al., 2018) and posterior deposition. Additionally, As, Co, Cu

and Mn show moderate increases in bottom sediments. The PCA indicates that the distribution of Cu, Co, As, and Pb in the sediment is linked to the presence of Fe and Mn oxides (Fig. 3.14b). The Garrucha-Almanzora Canyon system apparently being a dynamic setting, with bottom resuspension and lateral advection, is consistent with the observed Ti enrichment of seafloor sediments. Thus, resuspension and near-bottom transport are probably able to modify the geochemical composition of the canyon' floor.

3.2.5.5. The anthropogenic imprint on trace metal contents in deep submarine canyons

The distribution and cycling of TMs in the sediments of the study area and similar settings are likely modified by anthropogenic activities. Increments in TM contents in continental slope environments, including submarine canyons, due to anthropogenic activities have been previously reported (e.g., Palanques et al., 2008; Richter et al., 2009; Jesus et al., 2010; Costa et al., 2011; Mil-Homens et al., 2013b; Cossa et al., 2014; Roussiez et al., 2012; Heimbürger et al., 2012; Azaroff et al., 2020). The EFs approach uses pre-industrial sediments encompassing several years of deposition as normalizers. The estimation of EFs for each individual trap sample could incorporate a bias due to the different time periods represented by the normalizing sediments. This relates to the fact that, after correction for the terrigenous fraction, enrichments could result from several processes that enhance TM concentrations beyond anthropogenic inputs, such as biological uptake or authigenic precipitation (Yiğiterhan et al., 2011). In practice, we have considered TWC > 1.5 as an indicator of anthropogenic inputs, as this value represents the natural variability threshold following Roussiez et al. (2006), Radakovitch et al. (2008), and Jesus et al. (2010). The normalization of metal contents to pre-industrial values reveals a moderate enrichment of Zn and Cu, with mean values of up to 1.7 for Zn in Escombreras Canyon, and 1.5 and 1.6 for Cu in Garrucha-Almanzora Canyon system and Almeria Canyon, respectively (Fig. 3.16). The range of values from 0.75 to 1.5 is normally considered within natural variability (Radakovitch et al., 2008). However, one can note that Pb and Cu almost exceed the natural threshold in Escombreras Canyon, and Zn does the same in the other two canyons. The values obtained for canyon floor sediments tend to be in the interquartile range of the box plot, indicating that the trapped material provides a good record of TM pollutants being buried there. One exception are the metals affected by diagenetic and/or other near-bottom processes as discussed in section 3.2.5.3, which include As and Pb in the ES1000 and GA1000 stations, respectively.

The provinces of Murcia and Almeria experienced a noticeable industrial development during the second half of the 20th century. The region has an intensive farming model, with one of the largest areas in Europe dedicated to greenhouse agriculture along the coastline of the southern margin segment here investigated. Beyond rich agricultural expanses not far from shore, the northern margin segment hosts an important petrochemical industrial complex of Escombreras, which is besides the coastal town of Cartagena and<6 km west of Portman Bay. The complex started its activities in 1950 and since then has experienced several enlargements. Further environmental stressors arise from sewage pipes along the coastline discharging into the sea wastes from industrial activities, ancient ponds and dumping sites filled with industrial and mining wastes, and the traffic of tankers and cargo vessels. Portman Bay actually constitutes one of the

main environmental disasters along the European coastline. This bay was used during>30 years as the dumping site for huge amounts of Pb, Zn, Cu, As and other metals rich mine tailings from the open pit exploitation of sulphide ores (Fig. 3.12) (Baza-Varas et al., 2022, and references therein). Although waste disposal ended in 1990, the mine tailings disposed in the coastal sea remains nowadays. Previous studies have shown high levels of TMs pollution across the modern inner shelf floor off Portman Bay (Alorda- Kleinglass et al., 2019; Cerdà-Domènech et al., 2020), altogether with a diminishing sedimentation rate farther offshore in the tailings deposit itself (Baza-Varas et al., 2022).

Cu contents exceed or are near the pre-industrial threshold in all canyons, which points to a widespread contamination (Fig. 3.16). In other areas, Cu contamination has been mostly related to spillages attributed to the use of fungicides or fertilizers in agriculture (Roussiez et al., 2012; Cossa et al., 2014) or waste water treatment plants (Casadevall et al., 2016). Zn reaches contamination levels only in the Escombreras Canyon (Fig. 3.16), which is the closest to the Escombreras petrochemical complex and to Portman Bay of the three studied canyons. The offshore extension of Portman Bay mine tailings deposit (see Baza-Varas et al., 2023), at about 13 km in straight line from ES1000 (Fig. 3.12), seems a good candidate for Zn and other TMs (Cu and Pb) sourcing to the adjacent continental slope and canyons. Zn enrichment would decrease progressively with increasing distance from Portman's dumping site by mixing with non-enriched particles and dilution. However, we cannot discard other potential sources such as hydrocarbon burning at Escombreras complex or the onshore contaminated sites that could release pollutants able to reach the outer continental margin via atmospheric inputs. In the case of Zn for the rest of canyons, the results of the PCA show that its temporal variation is independent of the rest of the elements, possibly stemming from anthropogenic factors. However, it is associated with Pb, which does not exhibit high EF (Fig. 3.14c).

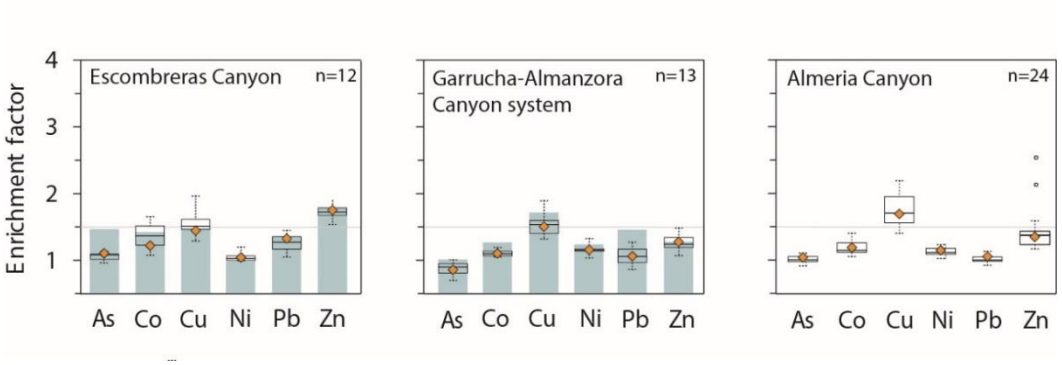

Figure 3.16. Trace metals enrichment factors (EFs) in setting particles in the investigated submarine canyons. The dashed horizontal line represents the natural variability threshold after Roussiez et al. (2006). White dots represent the outliers (in the present case abnormal high values relative to the co-existing data). The orange diamonds illustrate the EFs for TWC whereas the blue grey columns represent EFs in canyon floor sediments. Note that no bottom sediments were available for Almeria Canyon (cf. section 3.2.2.1).

The anthropogenic imprint on submarine canyons in the Iberian Atlantic margin and the SW and NW Mediterranean Sea, in terms of TM enrichment, is illustrated in Fig. 3.17a. Source type, distance from source and transport pathways and their carrying capacity determine which TM

pollutants and amounts may reach the deep continental margin. For instance, the Planier Canyon shows a specific signature due to local inputs from a bauxite treatment plant on the shore (Roussiez et al., 2012). Furthermore, hydrodynamics and sedimentary dynamics in each specific continental margin segment also influence the transference of the TM pollutants, as illustrated by higher Pb values in Atlantic canyon floor sediments (Fig. 3.17a) (Jesus et al., 2010).

The choice of the reference material for the calculation of EFs is critical to correctly assess metal enrichment levels. Fig. 3.17 compares the mean EFs resulting from using pre-industrial sediments as local background. We have also considered in Fig. 3.17 formerly reported TMs enrichments in sediments from different locations and water depths in submarine canyons and open slopes around the Iberian Peninsula and nearby areas against the composition of the upper continental crust (UCC) as obtained from Rudnick and Gao (2003). The values calculated after the UCC global average exceed EFs calculated after the local pre-industrial background, thus illustrating that the use of UCC composition as reference value may result in an inaccurate, exaggerated view of the degree of TM pollution (Fig. 3.17b). This is well illustrated in the Portman area, where there is a natural geochemical anomaly for Pb, Zn and As that directly relates to local geology (López-García et al., 2017). Anthropogenic enrichments are, therefore, seen when local reference values are taken into account.

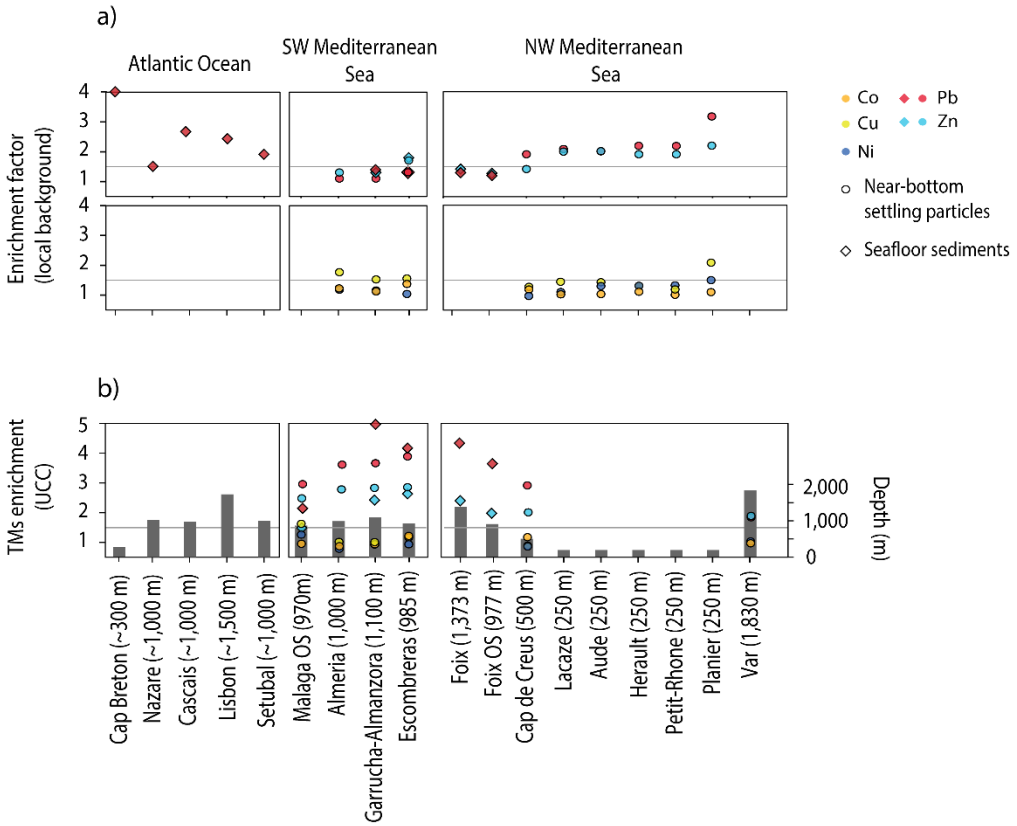

Figure 3.17. Compilation of trace metals (TMs) mean enrichments from submarine canyons and nearby open slopes from Iberian Atlantic and NW Mediterranean continental margins altogether with those from the SW Mediterranean margin, where the investigated canyons lie. (a) Enrichment factors (EFs) calculated with respect to local background pre-industrial values, and (b) enrichment values with respect the Upper

Continental Crust (UCC) global average composition according to Rudnick and Gao (2003). The general location of the canyons in the plot is shown in figure 3.12a. OS: open slope. Malaga OS corresponds to ALB1 station in the Alboran Sea, for which data have not been published previously (see detailed location in Sanchez-Vidal et al., 2005). Water depths in meters are given in brackets for each sampling station. Data are from Azaroff et al. (2020) for Cap Breton Canyon; Jesus et al. (2010) for Nazare, Cascais, Lisbon and Setubal canyons; Palanques et al. (2008) for the Foix Canyon and OS; Cossa et al. (2014) for Cap de Creus Canyon; Roussiez et al. (2012) for Lacaze, Aude, Herault, Petit-Rhone and Planier canyons; and Heimbürger et al. (2012) for Var Canyon. The horizontal lines denote the natural variability threshold after Roussiez et al. (2006).

3.2.6. Conclusions

The transport and sink of TMs in SW Mediterranean submarine canyons depend on a number of physical and biogeochemical processes, and nowadays are also affected by anthropogenic perturbations (i.e. spillage of chemicals used in agriculture, industrial emissions via atmospheric transport, and/or past mining activities). TM contents in downward particle fluxes rely upon the composition and amounts of detrital material reaching the continental margin, on scavenging into Mn oxides, and on anthropogenic inputs. Besides the dominant particulate carriers of TMs described in this study, it is likely that further biological interactions during transport influence TM cycling anyhow. Anthropogenic sources would result in excess Zn in Escombreras Canyon and excess Cu in all the studied canyons. The widespread Cu enrichment suggests a diffuse source such as intensive farming activities in the coastal area and watershed, whereas Zn enrichment in the northern Escombreras Canyon points to local industrial activities. Yet, one possible source could be the export of Zn and other TMs, such as Cu and Pb, from the underwater extension of Portman's mine tailings deposit from sulphide ore exploitation, located at about 13 km from the canyon head. Whereas the shelf edge spillover of TMs and other pollutants is a rather common phenomenon, the calculation of EFs requires a correct choice of the reference materials to be used, prioritizing the local ones.

Storm events enhance downward TM fluxes into the submarine canyons, though concentrations are generally less than in fluxes under calm conditions. This is attributed to a dilution effect of the TMs enriched particles exported during the calm periods within the resuspended shelf material exported during stormy periods. However, seasonal or event-driven changes in sinking fluxes are barely observed in the Garrucha-Almanzora Canyon system, where a more steady TMs export through time has been observed. The content and transport of As, Co, Cu and Pb into the canyon seems to be instead influenced by bottom resuspension and advective transport of Mn and Fe bearing phases, with bottom trawling likely playing a non-negligible role. Further, the rather high Ti and Fe contents in the canyon's floor indicate differential resuspension according to particles' density.

The spreading of bottom trawling points to the need of specific studies to better understand how this activity influences TM fluxes within settling particles in submarine canyons and other deep-sea settings.

Acknowledgements We would like to express our gratitude to the many colleagues and technicians and to the crew of RV Ángeles Alvariño for their support during sea-going work. We

also thank M. Guart and F. Menéndez for their assistance in the lab and J. Martín for his comments on the manuscript. This research was supported by research projects NUREIEV (ref. CTM2013-44598-R) and NUREIEVA (ref. CTM2016-75953-C2-1-R) funded by the Spanish Ministry of Economy and Competitiviness (MINECO), and the Spanish Ministry of Economy, Industry and Competitiviness (MINECO), respectively. GRC Geociències Marines is funded by the Catalan Government within its excellence research groups program (ref. 2021 SGR 01195). M. Tarrés was supported by a FPI grant from the Spanish Ministry of Science and Innovation (MICINN).

3.2.7. References

Acosta, J., Fontán, A., Muñoz, A., Muñoz-Martín, A., Rivera, J. et al., 2013. The morpho-tectonic setting of the Southeast margin of Iberia and the adjacent oceanic Algero-Balearic Basin. Mar. Pet. Geol. 45, 17–41. Doi: 10.1016/j.marpetgeo.2013.04.005.

Anderson, R.F. and Hayes, C.T., 2015. Characterizing marine particles and their impact on biogeochemical cycles in the GEOTRACES program. Prog. Oceanogr. 133, 1-5. Doi: 10.1016/j.pocean.2014.11.010.

Anderson, R. F., 2020. GEOTRACES: Accelerating research on the marine biogeochemical cycles of trace elements and their isotopes. Annu. Rev. Mar. Sci. 12, 9.1–9.37. Doi: 10.1146/annurev-marine-010318-095123

Al-Hashem, A. A., Beck, A. J., Krisch, S., Menzel Barraqueta, J.-L., Steffens, T. et al., 2022. Particulate trace metal sources, cycling, and distributions on the southwest African shelf. Glob. Biogeochem. Cycles, 36, e2022GB007453. Doi: 10.1029/2022GB007453.

Aloupi, M. and Angelidis, M.O., 2001. Normalization to lithium for the assessment of metal contamination in coastal sediment cores from the Aegean Sea. Mar. Environ. Res. 52, 1–12. Doi: 10.1016/S0141-1136(00)00255-5.

Alorda-Kleinglass, A., Garcia-Orellana, J., Rodellas, V., Cerdà-Domènech, M., Tovar-Sánchez, A. et al., 2019. Remobilization of dissolved metals from a coastal mine tailing deposit driven by groundwater discharge and porewater exchange. Sci. Total Environ. 688, 1359-1372. Doi: 10.1016/j.scitotenv.2019.06.224.

Azaroff A., Miossec C., Lanceleur L., Guyoneaud R. and Monperrus M., 2020. Priority and emerging micropollutants distribution from coastal to continental slope sediments: A case study of Capbreton Submarine Canyon (North Atlantic Ocean). Sci. Total Environ. 703, 135057. Doi: 10.1016/j.scitotenv.2019.135057.

Bancon-Montigny, C., Gonzalez, C., Delpoux, S., Avenzac, M., Spinelli, S., Mhadhbi, T., Mejri K., Hlaili, A.S., Pringault, O. (2019). Seasonal changes of chemical contamination in coastal waters during sediment resuspension. Chemosphere 235, 651-661. Doi: 10.1016/j.chemosphere.2019.06.213.

Baza-Varas, A., Canals, M., Frigola, J., Cerdà-Domènech, M., Rodés, N. et al., 2022. Multiproxy Characterization of Sedimentary Facies in a Submarine Sulphide Mine Tailings Dumping Site and Their Environmental Significance: the Study Case of Portmán Bay (SE Spain). Sci. Total Environ. 810, 151183. Doi: 10.1016/j.scitotenv.2021.151183.

Baza-Varas, A., Roqué-Rosella, J., Canals, M., Frigola, J., Cerdà-Domènech, M. et al., 2023. As and S speciation in a submarine sulfide mine tailings deposit and its environmental significance: the

study case of Portmán Bay (SE Spain). Sci. Total Environ. In press. Doi: 10.1016/j.scitotenv.2023.163649.

Birch, G.F., 2017. Determination of sediment metal background concentrations and enrichment in marine environments – A critical review. Sci. Total Environ. 580, 813-831. Doi: 10.1016/j.scitotenv.2016.12.028.

Blain, S., Planquette, H., Obernosterer, I. and Guéneuguès, A. 2022. Vertical Flux of Trace Elements Associated With Lithogenic and Biogenic Carrier Phases in the Southern Ocean. Glob. Biogeochem. Cycles 36, e2022GB007371. Doi: 10.1029/2022GB007371.

Boyle, E. A., 1983. Chemical accumulation variations under the Peru Current during the past 130,000 years. Geophys. Res. 88, 7667- 7680. Doi: 10.1029/JC088iC12p07667.

Bradshaw, C., Tjensvoll, I., Sköld, M., Allan, I.J., Molvaer, J. et al., 2012. Bottom trawling resuspends sediment and releases bioavailable contaminants in a polluted fjord. Environ. Pollut. 170, 232–241. Doi: 10.1016/j.envpol.2012.06.019.

Bruland K.W. and Lohan M.C., 2003. Treatise on geochemistry, Vol. 6. Elsevier, Amsterdam, pp. 23–47. Doi: 10.1016/B0-08-043751-6/06105-3.

Calvert, S.E. and Price, N.B, 1972. Diffusion and reaction profiles of dissolved manganese in the pore waters of marine sediments. Earth Planet. Sci. Lett. 16 (2), 245-249. Doi: 10.1016/0012-821X(72)90197-5.

Casadevall, M., Torres, J., El Aoussimi, A., Carbonell, A., Delgado, E. et al., 2016. Pollutants and parasites in bycatch teleosts from south eastern Spanish Mediterranean's fisheries: concerns relating the foodstuff harnessing. Mar. Pollut. Bull. 104, 182–189. Doi: 10.1016/j.marpolbul.2016.01.040.

Cerdà-Domènech, M., Frigola, J., Sanchez-Vidal, A. and Canals, M., 2020. Calibrating high resolution XRF core scanner data to obtain absolute metal concentrations in highly polluted marine deposits after two case studies off Portmán Bay and Barcelona, Spain. Sci. Total Environ. 717, 134778. Doi: 10.1016/j.scitotenv.2019.134778.

Chaillou, G., Schäfer, J., Anschutz, P., Lavaux, G. and Blanc, G., 2003. The behaviour of arsenic in muddy sediments of The Bay of Biscay (France). Geochim. Cosmochim. Acta 67, No. 16, pp. 2993–3003. Doi: 10.1016/S0016-7037(03)00204-7.

Charette, M.A., Lam, P.J., Lohan, M.C., Kwon, E.Y., Hatje, V. et al., 2016. Coastal ocean and shelf-sea biogeochemical cycling of trace elements and isotopes: lessons learned from GEOTRACES. Phil. Trans. R. Soc. A374: 20160076. Doi: org/10.1098/rsta.2016.0076.

Conte, M.H., Carter, A.M., Koweek, D.A., Huang, S. and Weber, J.C., 2019. The elemental composition of the deep particle flux in the Sargasso Sea. Chem. Geol. 511, 279–313. Doi: 10.1016/j.chemgeo.2018.11.001.

Cossa, D., Buscail, R., Puig, P., Chiffoleau, J.-F., Radakovitch, O. et al., 2014. Origin and accumulation of trace elements in sediments of the northwestern Mediterranean margin. Chem. Geol. 380, 61–73. Doi: 10.1016/j.chemgeo.2014.04.015.

Costa, A.M., Mil-Homens, M., Lebreiro, S.M., Richter, T.O., de Stigter, H. et al., 2011. Origin and transport of trace metals deposited in the canyons off Lisboa and adjacent slopes (Portuguese Margin) in the last century. Mar. Geol. 282, 169–177. Doi: 10.1016/j.margeo.2011.02.007.

Cowen, J.P. and Bruland, K.W., 1985. Deep Sea Res. Part I Oceanogr. Res. Pap. 32 (3), 253-272. Doi: 10.1016/0198-0149(85)90078-0.

Dill, H.G., 2007. Grain morphology of heavy minerals from marine and continental placer deposits, with special reference to Fe–Ti oxides. Sediment. Geol. 198 (1-2), 1-27. Doi: 10.1016/j.sedgeo.2006.11.002.

Dulaquais, G., H. Planquette, S. L'Helguen, M. J., Rijkenberg, A. and Boye, M., 2017. The biogeochemistry of cobalt in the Mediterranean Sea, Glob. Biogeochem. Cycles 31, 377–399. Doi: 10.1002/2016GB005478.

Dumas, C., Aubert, D., Durrieu de Madron, X., Ludwig, W., Heussner, S. et al., 2014. Storm-induced transfer of particulate trace metals to the deep-sea in the Gulf of Lion (NW Mediterranean Sea). Environ. Geochem. Health 36, 995–1014. Doi: 10.1007/s10653-014-9614-7.

Durrieu de Madron, X., Aubert, D., Charrière, B., Kunesch, S., Menniti, C. et al., 2023. Impact of Dense Water Formation on the Transfer of Particles and Trace Metals from the Coast to the Deep in the Northwestern Mediterranean. Water 15, 301. Doi: 10.3390/w15020301.

Eggleton, J. and Thomas, K.V., 2004. A review of factors affecting the release and bioavailability of contaminants during sediment disturbance events. Environ. Int. 30 (7), 973-980. Doi: 10.1016/j.envint.2004.03.001.

El Houssainy, A., Abi-Ghanem, C., Dang, D.H., Mahfouz, C., Omanović, D. et al., 2020. Distribution and diagenesis of trace metals in marine sediments of a coastal Mediterranean area: St Georges Bay (Lebanon). Mar. Pollut. Bull. 155, 111066. Doi: org/10.1016/j.marpolbul.2020.111066.

El Khatab, M., 2006. Dinámica del material sedimentario y de los metales pesados asociados en el margen noroccidental del mar de Alborán. PhD Thesis. Universidad Politécnica de Cataluña, Barcelona, Spain, p.269.

Fabres, J., Calafat, A., Sanchez-Vidal, A., Canals, M. and Heussner, S., 2002. Composition and spatio-temporal variability of particle fluxes in the Western Alboran Gyre, Mediterranean Sea (SW Mediterranean). J. Mar. Syst. 33–34, 431–456. Doi: org/10.1016/S0924-7963(02)00070-2.

Froelich, P.N., Klinkhammer, G.P., Bender, M.L., Luedtke, N.A., Heath, G.R. et al., 1979. Early oxidation of organic matter in pelagic sediments of the eastern equatorial Altantic: suboxic diagenesis. Geochim. Cosmochim. Acta 43, 1075–1090. Doi: 10.1016/0016-7037(79)90095-4.

Geibert, W., 2018. Processes that Regulate Trace Element Distribution in the Ocean. Elements 14, pp. 391–396. Doi: 10.2138/gselements.14.6.3912015.

Grousset, F.E., Quetel C.R., Thomas, B., Donard, O.F.X.., Lambert, C.E. et al., 1995. Anthropogenic vs. lithogenic origins of trace elements (As, Cd, Pb, Rb, Sb, Sc, Sn, Zn) in water column particles: northwestern Mediterranean Sea. Mar. Chem. 48 (3–4), 291-310. Doi: 10.1016/0304-4203(94)00056-J.

Hanebuth, T.J.J., King, M.L., Mendes, I., Lebreiro, S., Lobo, F.J. et al., 2018. Hazard potential of widespread but hidden historic offshore heavy metal (Pb, Zn) contamination (Gulf of Cadiz, Spain). Sci. Total Environ. 637–638, 561–576. Doi: 10.1016/j.scitotenv.2018.04.352.

Heimbürger, L.E., Cossa, D., Thibodeau, B., Khripounoff, A., Mas, V. et al., 2012. Natural and anthropogenic trace metals in sediments of the Ligurian Sea (Northwestern Mediterranean). Chem. Geol. 291, 141–151. Doi: 10.1016/j.chemgeo.2011.10.011.

Heussner, S., Durrieu de Madron, X., Calafat, A., Canals, M., Carbonne, J. et al., 2006. Spatial and temporal variability of downward particle fluxes on a continental slope: lessons from an 8-yr experiment in the Gulf of Lions (NW Mediterranean). Mar. Geol. 234, 63–92. Doi: 10.1016/j.margeo.2006.09.003.

Huang, S. and Conte, M.H., 2009. Source/process apportionment of major and trace elements in sinking particles in the Sargasso sea. Geochim. Cosmochim. Acta 73, 65–90. Doi: 10.1016/j.gca.2008.08.023.

Hung, J.J. and Ho, C.Y., 2014. Typhoon- and earthquake-enhanced concentration and inventory of dissolved and particulate trace metals along two submarine canyons off southwestern Taiwan. Estuar. Coast. Shelf Sci. 136, 179e190. Doi: 10.1016/j.ecss.2013.11.004.

Jeandel, C. and Vance, D., 2018. New tools, new discoveries in marine geochemistry. Elements 14, 379–84. Doi: 10.2138/gselements.14.6.379.

Jensen, L.T., Morton, P., Twining, B.S., Heller, M.I., Hatta, M. et al., 2020. A comparison of marine Fe and Mn cycling: U.S. GEOTRACES GN01 Western Arctic case study. Geochim. Cosmochim. Acta 288, 138–160. Doi: 10.1016/j.gca.2020.08.006.

Jesus, C.C., de Stigter, H.C., Richter, T.O., Boer, W., Mil-Homens, M. et al., 2010. Trace metal enrichments in Portuguese submarine canyons and open slope: anthropogenic impact and links to sedimentary dynamics. Mar. Geol. 271(1–2), 72-83. Doi: 10.1016/j.margeo.2010.01.011.

Kalnejais, L. H., Martin, W. R., Signell, R. P. and Bothner, M. H., 2007. Role of Sediment Resuspension in the Remobilization of Particulate-Phase Metals from Coastal Sediments. Environ. Sci. Technol. 41, 2282-2288. Doi: 10.1021/es061770z.

Karageorgis, A.P., Katsanevakis, S. and Kaberi, H., 2009. Use of Enrichment Factors for the Assessment of Heavy Metal Contamination in the Sediments of Koumoundourou Lake, Greece. Water, Air, and Soil Pollut. 204, 243–258. Doi: 10.1007/s11270-009-0041-9.

Kuss, J., Waniek, J.J., Kremling, K. and Schulz-Bull, D.E., 2010. Seasonality of particle-associated trace element fluxes in the deep northeast Atlantic Ocean. Deep-Sea Res. I 57, 785–796. Doi: 10.1016/j.dsr.2010.04.002.

Lam, P.J., Bishop, J.K.B., Henning, C.C., Marcus, M.A., Waychunas, G.A. et al., 2006. Wintertime phytoplankton bloom in the subarctic Pacific supported by continental margin iron. Glob. Biogeochem. Cycles 20, GB1006. Doi: 10.1029/2005GB002557.

Lee, J.M., Heller, M.I. and Lam, P.J., 2018. Size distribution of particulate trace elements in the U.S. GEOTRACES Eastern Pacific Zonal Transect (GP16). Mar. Chem. 201, 108–123. Doi: 10.1016/j.marchem.2017.09.006.

Lemaitre, N., Planquette, H., Dehairs, F., Planchon, F., Sarthou, G. et al., 2020. Particulate trace element export in the North Atlantic (GEOTRACES GA01 transect, GEOVIDE cruise). ACS Earth Space Chem. 4 (11), 2185–2204. Doi: 10.1021/acsearthspacechem.0c00045.

Lobo, F.J., Ercilla, G., Fernández-Salas, L.M. and Gámez, D., 2014. The Iberian Mediterranean shelves. Geological Society, London, Memoirs 41 (1), 147–170. Doi: 10.1144/M41.11.

Macias, D., Garcia-Gorriz, E. and Stips, A., 2016. The seasonal cycle of the Atlantic Jet dynamics in the Alboran Sea: direct atmospheric forcing versus Mediterranean thermohaline circulation. Ocean Dyn. 66, 137–151. Doi: 10.1007/s10236-015-0914-y.

Marin, B. and Giresse, P., 2001. Particulate manganese and iron in recent sediments of the Gulf of Lions continental margin (north-western Mediterranean Sea): deposition and diagenetic process. Mar. Geol. 172, 147–165. Doi: 10.1016/S0025-3227(00)00124-9.

Martín J.H., Knauer, G.A. and Gordon, R.M., 1983. Silver distribution and fluxes in the North-West Pacific waters. Nature 305, 306-309. Doi: 10.1038/305306a0.

Martín, J., Palanques, A. and Puig, P., 2007. Near-bottom horizontal transfer of particulate matter in the Palamós Submarine Canyon (NW Mediterranean). J. Mar. Res. 65 (2), 193–218. Doi: 10.1357/002224007780882569.

Martín, J., Puig, P., Masqué, P., Palanques, A. and Sánchez-Gómez, A., 2014. Impact of bottom trawling on deep-sea sediment properties along the flanks of a submarine canyon. PLoS ONE 9(8), e104536. Doi: 10.1371/journal.pone.0104536.

Millot, C., 1999. Circulation in the Western Mediterranean Sea. J. Mar. Syst. 20 (1-4), 423–442. Doi: 10.1016/S0924-7963(98)00078-5.

Mil-Homens, M., Blum, J., Canário, J., Caetano, M., Costa, A.M. et al., 2013a. Tracing anthropogenic Hg and Pb input using stable Hg and Pb isotope ratios in sediments of the central Portuguese Margin. Chem. Geol. 336, 62–71. Doi: 10.1016/j.chemgeo.2012.02.018.

Mil-Homens, M., Caetano, M., Costa, A.M., Lebreiro, S., Richter, T. et al., 2013b. Temporal evolution of lead isotope ratios in sediments of the Central Portuguese Margin: A fingerprint of human activities. Mar. Pollut. Bull. 74, 274–284. Doi: 10.1016/j.marpolbul.2013.06.044.

Mil-Homens, M., Vale, C., Naughton, F., Brito, P., Drago, T. et al., 2016. Footprint of roman and modern mining activities in a sediment core from the southwestern Iberian Atlantic shelf. Sci. Total Environ. 571, 1211–1221. Doi: 10.1016/j.scitotenv.2016.07.143.

Morel, F.M.M. and Price, N.M, 2003. The Biogeochemical Cycles of Trace Metals in the Oceans. Science 300, 944–947. Doi: 10.1126/science.1083545.

Noble A.E., Lamborg C.H., Ohnemus D.C., Lam P. J., Goepfert T. J. et al., 2012. Basin-scale inputs of cobalt, iron, and manganese from the Benguela-Angola front to the South Atlantic Ocean. Limnol. Oceanogr. 57(4), 989–1010. Doi: 10.4319/lo.2012.57.4.0989.

Ohnemus, D.C and Lam, P.J., 2015. Cycling of lithogenic marine particles in the US GEOTRACES North Atlantic transect. Deep Sea Res. Part II 116, 283–302. Doi: 10.1016/j.dsr2.2014.11.019.

Oldham, V. E., Miller, M. T., Jensen, L. T. and Luther, G. W., 2017. Revisiting Mn and Fe removal in humic rich estuaries. Geochim. Cosmochim. Acta 209, 267–283. Doi: 10.1016/j.gca.2017.04.001.

Papale, M., Conte, A., Del Core, M., Zito, E., Sprovieri, M. et al., 2018. Heavy-metal resistant microorganisms in sediments from submarine canyons and the adjacent continental slope in the northeastern Ligurian margin (Western Mediterranean Sea). Prog. Oceanogr. 168, 155–168 Doi: 10.1016/j.pocean.2018.09.015.

Pagès, F., Martín, J., Palanques, A., Puig, P. and Gili, J.M., 2007. High occurrence of the elasipodid holothurian Penilpidia ludwigi (von Marenzeller, 1893) in bathyal sediment traps moored in a western Mediterranean submarine canyon. Deep Sea Res. Part I 54, 2170-2180. Doi: 10.1016/j.dsr.2007.09.002.

Palanques, A., Masqué, P., Puig, P., Sanchez-Cabeza, J.A., Frignani, M. et al., 2008. Anthropogenic trace metals in the sedimentary record of the Llobregat continental shelf and adjacent Foix Submarine Canyon (northwestern Mediterranean). Mar. Geol. 248, 213–227. Doi: 10.1016/j.margeo.2007.11.001.

Palanques, A., Paradis, S., Puig, P., Masqué, P. and Lo Iacono, C., 2022. Effects of bottom trawling on trace metal contamination of sediments along the submarine canyons of the Gulf of Palermo (southwestern Mediterranean). Sci. Total Environ. 814, 152658. Doi: 10.1016/j.scitotenv.2021.152658.

Paradis, S., Goñi, M., Masqué, P., Durán, R., Arjona-Camas, M. et al., 2021. Persistence of biogeochemical alterations of deep-sea sediments by bottom trawling. Geophys. Res. Lett. 48, e2020GL091279. Doi: 10.1029/2020GL091279.

Parrilla, G., Kinder, T.H. and Preller, R.H., 1986. Deep and intermediate Mediterranean water in the western Alboran Sea. Deep Sea Res. Part I 33, 55–88. Doi: 10.1016/0198-0149(86)90108-1.

Pérez-Hernández, S., Comas, M.C. and Escutia, C., 2014. Morphology of turbidite systems within an active continental margin (the Palomares Margin, western Mediterranean). Geomorphology 219, 10–26. Doi: 10.1016/j.geomorph.2014.04.014.

Puig, P., Canals, M., Company, J.B., Martin, J., Amblas, D., Lastras, G., Palanques, A., Calafat, A.M. (2012). Ploughing the deep sea floor. Nature 489, 286–290. Doi: 10.1038/nature11410.

Puig, P., Durán, R., Muñoz, A., Elvira, E. and Guillén, J., 2017. Submarine canyon-head morphologies and inferred sediment transport processes in the Alías-Almanzora canyon system (SW Mediterranean): On the role of the sediment supply. Mar. Geol. 393, 21–34. Doi: 10.1016/j.margeo.2017.02.009.

Puig, P., Palanques, A., Sanchez-Cabeza, J.A. and Masque, P., 1999. Heavy metals in particulate matter and sediments in the southern Barcelona sedimentation system (Northwestern Mediterranean). Mar. Chem. 63, 311–329. Doi: 10.1016/S0304-4203(98)00069-3.

Puig, P., Palanques, A. and Martín, J., 2014. Contemporary sediment-transport processes in submarine canyons. Annu. Rev. Mar. Sci. 6, 53–77. Doi: 10.1146/annurev-marine-010213-135037.

Pusceddu, A., Bianchelli, S., Martín, J., Puig, P., Palanques, A. et al., 2014. Chronic and intensive bottom trawling impairs deep-sea biodiversity and ecosystem functioning. Proc. Nat. Acad. Sc. 11 (24), 8861-8866. Doi: 10.1073/pnas.1405454111.

Radakovitch, O., Roussiez, V., Olliver, P., Ludwig, W., Grenz, C. et al., 2008. Input of particulate heavy metals from rivers and associated sedimentary deposits on the Gulf of Lion continental shelf. Estuar. Coast. Shelf Sci. 77, 285-295. Doi: 10.1016/j.ecss.2007.09.028.

Raiswell, R., 2011. Iron transport from the continents to the open ocean: the aging rejuvenation cycle. Elements 7, 101e106. Doi: 10.2113/gselements.7.2.101.

Richter, T.O., de Stigter, H.C., Boer, W., Jesus, C.C. and van Weering, T.C.E., 2009. Dispersal of natural and anthropogenic lead through submarine canyons at the Portuguese margin. Deep. Res. Part I 56, 267–282. Doi: 10.1016/j.dsr.2008.09.006.

Ross, C.B., Gardner, W.D., Richardson, M.J. and Asper, V. L., 2009. Currents and sediment transport in the Mississippi Canyon and effects of Hurricane Georges. Cont. Shelf Res. 29, 1384-1396. Doi: 10.1016/j.csr.2009.03.002.

Roussiez, V., Ludwig, W., Monaco, A., Probst, J.-L., Bouloubassi, I. et al., 2006. Sources and sinks of sediment-bound contaminants in the Gulf of Lions (NW Mediterranean sea): a multi-tracer approach. Cont. Shelf Res. 26, 1843–11857. Doi: 10.1016/j.csr.2006.04.010.

Roussiez, V., Heussner, S., Ludwig, W., Radakovitch, O., Durrieu de Madron, X. et al., 2012. Impact of oceanic floods to particulate metal inputs to coastal and deep sea environments: a case study in the Northwest Mediterranean. Cont. Shelf Res. 45, 15–26. Doi: 10.1016/j.csr.2012.05.012.

Rudnick, R.L. and Gao, S., 2003. In: Rudnick, R.L. (Ed.), Treatise of Geochemistry, 3. Elsevier, Amsterdam, pp. 1–64. Doi: 10.1016/B0-08-043751-6/03016-4.

Rumín-Caparrós, A., Sanchez-Vidal, A., González-Pola, C., Lastras, G., Calafat, A. et al., 2016. Particle fluxes and their drivers in the Avilés submarine canyon and adjacent slope, central Cantabrian margin, Bay of Biscay. Prog. Oceanogr. 144, 39–61. Doi: 10.1016/j.pocean.2016.03.004.

Rusiecka, D., Gledhill, M., Milne, A., Achterberg, E. P., Annett, A. L. et al., 2018. Anthropogenic signatures of lead in the Northeast Atlantic. Geophys. Res. Lett. 45(6), 2734–2743. Doi: 10.1002/2017GL076825.

Sanchez-Vidal, A., Calafat, A., Canals, M. and Fabres, J. 2004. Particle fluxes in the Almeria-Oran front: control by coastal upwelling and sea-surface circulation. J. Mar. Syst. 52, 89-106. Doi: 10.1016/j.jmarsys.2004.01.010.

Sanchez-Vidal, A., Collier, R.W., Calafat, A., Fabres, J. and Canals, M., 2005. Particulate barium fluxes on the continental margin: a study from the Alboran Sea (Western Mediterranean). Mar. Chem. 93 (2–4), 105-117. Doi: 10.1016/j.marchem.2004.07.004.

Tarrés, M., Cerdà-Domènech, M., Pedrosa-Pàmies, R., Rumín-Caparrós, A., Calafat, A. et al., 2022. Particle fluxes in submarine canyons along a sediment-starved continental margin and in the adjacent open slope and basin in the SW Mediterranean Sea. Prog. Oceanogr. 203, 102783. Doi: 10.1016/j.pocean.2022.102783.

Tebo, B. M., Bargar, J. R., Clement, B. G., Dick, G. J., Murray, K. J. et al., 2004. Biogenic manganese oxides: Properties and mechanisms of formation. Annu. Rev. Earth Planet. Sci., 32(1954), 287–328. Doi: 10.1146/annurev.earth.32.101802.120213.

Tesi, T., Puig, A. and Goñi, M.A., 2010. Lateral advection of organic matter in cascading-dominated submarine canyons. Prog. Oceanogr. 84, 185-203. Doi: 10.1016/j.pocean.2009.10.004.

Theodosi, C., Parinos, C., Gogou, A., Kokotos, A., Stavrakakis, S. et al., 2013. Downward fluxes of elemental carbon, metals and polycyclic aromatic hydrocarbons in settling particles from the deep Ionian Sea (NESTOR site), Eastern Mediterranean. Biogeosciences 10, 4449–4464. Doi: 10.5194/bg-10-4449-2013.

Thibault de Chanvalon, A., Metzger, E., Mouret, A., Knoery, J., Chiffoleau, J.F. et al., 2016. Particles transformation in estuaries: Fe, Mn and REE signatures through the Loire Estuary. J. Sea Res. 118, 103e112. Doi: 10.1016/j.seares.2016.11.004.

Tintore, J., La Violette, P.E., Blade, I. and Cruzado, A., 1988. A study of an intense density front in the Eastern Alboran Sea: the Almeria-Oran Front. J. Phys. Oceanogr. 18, 1384–1397. Doi: 10.1175/1520-0485(1988)018<1384:ASOAID>2.0.CO;2.

Twining, B. S. and Baines, S. B., 2013. The trace metal composition of marine phytoplankton. Annu. Rev. Mar. Sci. 5(1), 191–215. Doi: 10.1146/annurev-marine-121211-172322.

Vargas-Yáñez, M., Plaza, F., Garcıá -Lafuente, J., Sarhan, T., Vargas, J.M. et al., 2002. About the seasonal variability of the Alboran Sea circulation. J. Mar. Syst. 35 (3-4), 229–248. Doi: 10.1016/S0924-7963(02)00128-8.

Yiğiterhan, O., Murray, J.W. and Tuğrul, S., 2011. Trace metal composition of suspended particulate matter in the water column of the Black Sea. Mar. Chem. 126, 207–228. Doi: 10.1016/j.marchem.2011.05.006.

https://emodnet.ec.europa.eu/geoviewer/: Interactive map viewer of the EMODnet server [last consulted 18th of April 2023].

3.2.8. Supplementary material

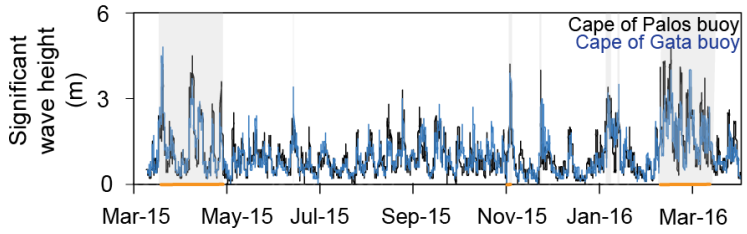

Supplementary Figure 3.1. Forcing conditions in the gulfs of Vera and Almeria, where the investigated submarine canyons are located. Significant wave heights from Cape of Gata and Cape of Palos wavebuoys after Tarrés et al. (2022). Spring 2015 and winter 2016 storms are shown by orange overlays on the lower axis. Grey vertical stripes and lines indicate stormy periods and individual storms, respectively.

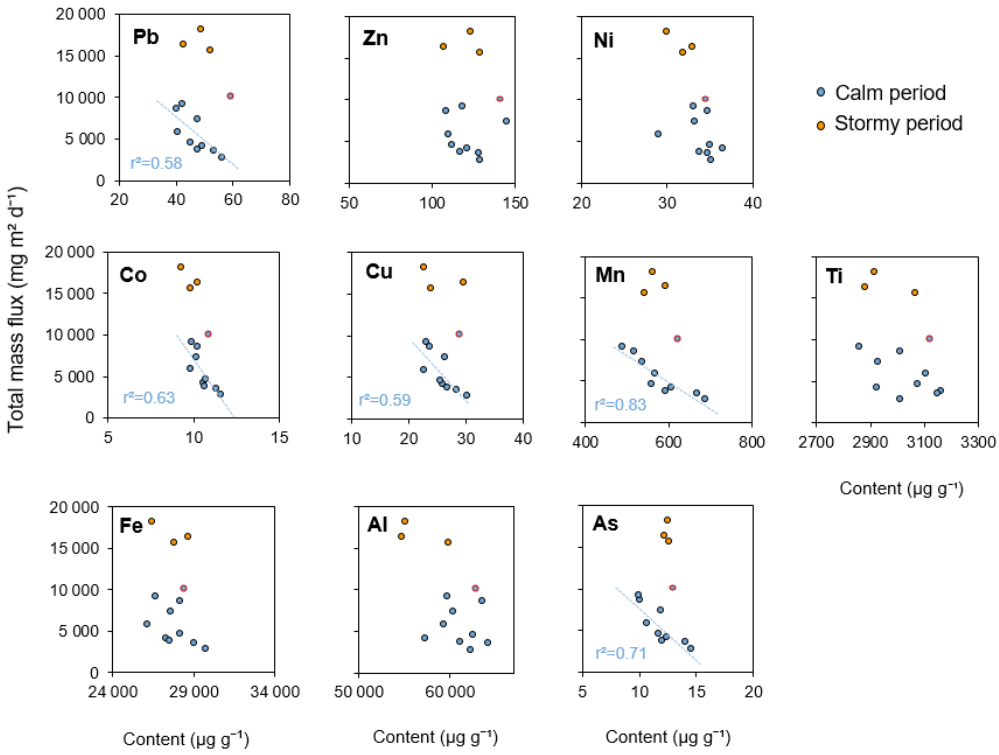

Supplementary Figure 3.2. Correlations between total mass flux values as reported in Tarrés et al. (2022) and TM contents at GA1000 station. Linear regression lines correspond to calm periods data (blue dots), excluding the data concomitant with spring 2015 storms. It has also been excluded sample GA1000-I-7 (red dots). Coefficient of determination (r^2) is referred only when it's significant at $p < 0.05$.

Code	Opening day	Sampling days	Code	Opening day	Sampling days	Code	Opening day	Sampling days
ES1000-I-1	16/03/2015	16	GA-I-1	25/03/2015	7	AL-I-1	25/03/2015	7
ES1000-I-2	01/04/2015	10	GA-I-2	01/04/2015	10	AL-I-2	01/04/2015	10
ES1000-I-3	11/04/2015	10	GA-I-3	11/04/2015	10	AL-I-3	11/04/2015	10
ES1000-I-4	21/04/2015	10	GA-I-4	21/04/2015	10	AL-I-4	21/04/2015	10
ES1000-I-5	01/05/2015	15	GA-I-5	01/05/2015	15	AL-I-5	01/05/2015	15
ES1000-I-6	16/05/2015	16	GA-I-6	16/05/2015	16	AL-I-6	16/05/2015	16
ES1000-I-7	01/06/2015	15	GA-I-7	01/06/2015	15	AL-I-7	01/06/2015	15
ES1000-I-8	16/06/2015	15	GA-I-8	16/06/2015	15	AL-I-8	16/06/2015	15
ES1000-I-9	01/07/2015	15	GA-I-9	01/07/2015	15	AL-I-9	01/07/2015	15
ES1000-I-10	16/07/2015	16	GA-I-10	16/07/2015	16	AL-I-10	16/07/2015	16
ES1000-I-11	01/08/2015	15	GA-I-11	01/08/2015	15	AL-I-11	01/08/2015	15
ES1000-I-12	16/08/2015	12	GA-I-12	16/08/2015	12	AL-I-12	16/08/2015	12
-	-	-	GA-II-1	07/09/2015	24	AL-II-1	07/09/2015	24
-	-	-	-	-	-	AL-II-2	01/10/2015	15
-	-	-	-	-	-	AL-II-3	16/10/2015	16
-	-	-	-	-	-	AL-II-4	01/11/2015	15
-	-	-	-	-	-	AL-II-5	16/11/2015	15
-	-	-	-	-	-	AL-II-6	01/12/2015	15
-	-	-	-	-	-	AL-II-7	16/12/2015	16
-	-	-	-	-	-	AL-II-8	01/01/2016	15
-	-	-	-	-	-	AL-II-9	16/01/2016	16
-	-	-	-	-	-	AL-II-10	01/02/2016	15
-	-	-	-	-	-	AL-II-11	16/02/2016	13
-	-	-	-	-	-	AL-II-12	29/02/2016	31

Supplementary Table 3.1. Sampling dates for each cup of the sediment traps.

	Al	Fe	Ti	As	Co	Cu	Mn	Ni	Pb
(a) ES1000 from March to August 2015 (N=12)									
Al	1								
Fe	0.990*	1							
Ti	0.777*	0.720*	1						
As	0.541	0.547	0.246	1					
Co	0.486	0.484	0.300	0.880*	1				
Cu	0.447	0.480	0.267	0.820*	0.929*	1			
Mn	0.573	0.563	0.489	0.756*	0.927*	0.871*	1		
Ni	0.647	0.610	0.616	0.59	0.740*	0.691	0.730*	1	
Pb	-0.0236	0.010	-0.133	0.696	0.566	0.520	0.337	0.180	1
Zn	0.351	0.419	-0.004	0.664	0.613	0.742*	0.500	0.290	0.613
(b) GA1000 from March to September 2015 (N=13)									
Al	1								
Fe	0.476	1							
Ti	0.665	0.233	1						
As	0.114	0.655	0.268	1					
Co	0.647	0.830*	0.446	0.622	1				
Cu	0.214	0.849*	0.166	0.707*	0.806*	1			
Mn	0.221	0.670	0.403	0.877*	0.792*	0.787*	1		
Ni	0.465	0.642	0.054	0.283	0.752*	0.569	0.375	1	
Pb	0.295	0.523	0.341	0.844*	0.562	0.575	0.682	0.331	1
Zn	0.247	0.224	0.091	0.522	0.256	0.318	0.262	0.146	0.769*
(c) AL1000 from March 2015 to March 2016 (N=24**)									
Al	1								
Fe	0.915*	1							
Ti	0.830*	0.832*	1						
As	0.603*	0.643*	0.440	1					
Co	0.413	0.467	0.226	0.332	1				
Cu	-0.035	0.033	-0.139	0.085	0.784*	1			
Mn	0.347	0.372	0.020	0.502	0.861*	0.676*	1		
Ni	0.566*	0.553*	0.312	0.427	0.909*	0.710*	0.785*	1	
Pb	0.361	0.351	0.354	0.727*	0.08	-0.091	0.213	0.145	1
Zn	0.117	0.117	0.034	0.528	0.441	0.431	0.537	0.385	0.538*

Supplementary Table 3.2. Linear-correlation coefficients (Pearson) for the analysed elements (including the OM content at AL1000 station). Underlined values are significant at $p < 0.05$ and $p < 0.01$. *: Statistics calculated for a number of samples (N) in stations ES1000. GA1000 and AL1000. **: The number of observations for each element is 24 except for Zn. which is 22.

3.3. Across margin export of recalcitrant blue carbon: a study case off SE Iberia

Marta Tarrés[a], Marc Cerdà-Domènech[a], Miquel Canals[a], Anna Sanchez-Vidal[a], Jordi Garcia-Orellana[b,c], Tommaso Tesi[d]

[a] GRC Geociències Marines, Dept. Dinàmica de la Terra i de l'Oceà, Facultat de Ciències de la Terra, Universitat de Barcelona, 08028 Barcelona, Spain

[b] Institut de Ciència i Tecnologia Ambientals (ICTA), Universitat Autònoma de Barcelona, 08193 Bellaterra, Spain

[c] Departament de Física, Universitat Autònoma de Barcelona, 08193 Bellaterra, Spain

[d] Istituto di Scienze Polari, Consiglio Nazionale delle Ricerche ISP-CNR, 40129 Bologna, Italy

Keywords: Particle fluxes, Recalcitrant organic carbon, Lignin phenols, Blue carbon, Submarine canyon, Mediterranean Sea

Abstract This study investigates the origin and characteristics of organic matter (OM) reaching the deep environment in the Escombreras Canyon, situated off the SE Iberian Peninsula. Near-bottom settling particles were collected using a sediment trap moored at approximately 1,000 m depth during the period of March to August 2015. In conjunction, a sediment core was extracted beneath the station. A comprehensive study of settling particles and sediments was conducted, analysing various bulk sedimentological parameters such as grain size, organic carbon (OC) and total nitrogen (NT) content, and $\delta^{13}C$, along with specific biomarkers (lignin phenols, cutin acids and 3,5 –dihydroxybenzoic acid). Additionally, the ^{210}Pb activities in the canyon sediments were determined.

The $\delta^{13}C_{OC}$ values, ranging from -20.02 to -21.87‰, suggest a predominant origin of OC from marine primary production. Lignin and cutin yields exhibit a lower contribution in settling particles OC compared to canyon sediments, with lignin mean values of 0.23 and 0.65 mg /100 mg OC, respectively. The ratios of syringyl and cinnamyl to vanillyl phenols allowed us to identify three primary sources contributing to the recalcitrant OC pool: soil-derived OM, *Posidonia oceanica* detritus (hereafter *P. oceanica*), and pollen. Notably, storm events in March and April 2015 enhanced the lignin and cutin fluxes in the Escombreras canyon. The first event, with a wave height up to 4.8 m, triggered the transfer of large amounts of sediment, OM and *P. oceanica* detritus contained in the sand fraction. In the subsequently milder storm events and the following calm months, we observe a preferential export of soil-derived OM controlled by the sorting of sediments.

The vertical profile of biomarkers indicate an increment in content with increasing depth, suggesting selective preservation in sediments. However, the contributions of *P. oceanica* and soil-derived OM to the sedimentary OC pool also reveal changes, with a lower amount of *P. oceanica* in the topmost sediments. Vertical biomarker profiles exhibit variations, particularly over the last 40 years, coinciding with a series of anthropogenic events and their environmental

consequences. The findings reveal that a portion of coastal blue carbon is transported beyond the continental shelf during sea storm events, and underscores the potential impact of human-related actions on it distribution in deep sea sediments.

3.3.1. Introduction

The fate of organic carbon (OC), a major component of organic matter (OM), in continental margins plays a critical role in the global carbon budget (Liu et al., 2000). High rates of biological productivity and the inputs of land-derived OC can convert continental shelves in major sinks (Hedges and Keil, 1995; Atwood et al., 2020). However, metoceanographic forcings can lead to the export of large quantities of OC towards deeper environments (Masson et al., 2010; Sanchez-Vidal et al., 2012; Selvaraj et al., 2015; Arroyo et al., 2020).

The nature of OM influences crucial aspects such as its preservation efficiency in the marine environment, modulating the removal of carbon from the ocean towards the seafloor and in the marine sediments (Goñi et al., 2000; Aller and Blair, 2004; Burdige, 2007). The use of bulk composition tracers (OC, TN and $\delta^{13}C_{OC}$, amongst other) combined with molecular biomarkers, such as lignin or cutin, has resulted in an improved understanding of the sources of OM, the processes involved in off-shelf export and its ultimate fate in the deep ocean (Hedges and Mann 1979; Goñi et al., 2006; Tesi et al., 2008; Liu et al., 2009). The composition of OM in deep continental margins is highly heterogeneous, as it consists of mixtures of land-delivered inputs carried mainly by rivers (Tesi et al., 2007b; Cathalot et al., 2013) or atmospheric contributions (Pasqual et al., 2011), and autochtonous production. Such OM is subsequently transformed during transport by sediment sorting and biogeochemical processes, further contributing to its differentiation (Tesi et al., 2007a; Bianchi et al., 2007; Liu et al., 2009; Sánchez-García et al., 2009; Sanchez-Vidal et al., 2009).

Research has largely focused on river-influenced continental margins with high sediment inputs, where large volumes of OM in land-sourced constituents can be potentially exported off-shelf (Goñi et al., 2000, 2006; Liu et al., 2009; Tesi et al., 2010; Kiriakoulakis et al., 2011). Yet, the limited sedimentary inputs in some margin systems promote water transparency and the development of coastal seagrass meadows (Maldonado and Zamarreño et al., 1983; Bianchi et al., 1999). Together with tidal marshes and mangroves, seagrass meadows are one of the most efficient carbon trapping ecosystems on Earth (Mcleod et al., 2011; Arias-Ortiz et al., 2018; Serrano et al., 2020), which contain considerable amounts of lignin and other recalcitrant[5] compounds, with amounts depending on the species and characteristics of plant tissues (Klap et al., 2000; Trevathan-Tackett et al., 2017; Kaal et al., 2018). Whereas the role of vegetated coastal habitats in in-situ carbon sequestration has deserved significant attention, the export of “blue carbon” towards the deep margin and basin, and their role as carbon donors to deep-water sediments, have received little consideration (Mateo and Romero, 1997; Bianchi et al., 1999; Dittmar and Lara, 2000; Duarte and Krause-Jensen, 2017; Santos et al., 2021). Indeed, seagrass meadows

[5] Recalcitrant term referred to compounds is commonly used to describe the “quality” of OC (particularly terrestrial OC) as food resources for heterotrophs, emphasizing an OM that is resistant to degradation over time (Bianchi, 2011).

export, on average, 17.8% of their net primary production as particulate OC (Durate and Krause-Jensen, 2017).

The current study aims at assessing the origin and pathways of OC transfer from the continental shelf to the deep margin in a sediment-starved setting with extensive coastal seagrass meadows. More specifically, we address questions such as to what extent recalcitrant OC is transferred to the deep, and in what degree *P. oceanica* litter contribute to the refractory pool in the downward fluxes and associated sediments.

3.3.2. Study area

The study area is part of the Mazarrón continental margin, off SE Spain in the SW Mediterranean Sea. The investigated canyon is incised in the margin segment comprised between Cape Palos, to the east, and Cape Tiñoso, to the west (Fig. 3.18). The margin consists of a westward narrowing continental shelf, from 13 km width offshore Palos Cape to about 2 km off Cape Tiñoso, with (Lobo et al., 2014) the shelf edge located at 80-120 m of water depth (Acosta et al., 2013), followed by an abrupt continental slope (14-31˚ in average) cut by numerous short submarine canyons (< 50 km long) with channel extensions into the continental rise (Acosta et al., 2013) (Fig. 3.18).

The Escombreras Canyon head occurs about 14 km offshore of the coastal mine tailings deposit of Portmán Bay, and about 18 km off the coastal town of Cartagena. The canyon itself extends along more than 20 km, with a convex head indenting the outer shelf at 200 m depth and cut by numerous gullies (Acosta et al., 2013).

The Mazarrón continental margin, and the Palos-Tiñoso segment in particular, receive little sediment supply as no permanent rivers open along the shoreline (Lobo et al., 2014). The scarce sediment input reaching the inner shelf mostly results from ephemeral streams. Sedimentary particles are transported over the shelf and upper slope by southwards flowing geostrophic currents roughly paralleling the shelf edge (Durán et al., 2018), and also by wave action during storms (Lobo et al., 2014; Durán et al., 2018). Swells result from NE-E and SW winds (https://www.puertos.es). A previous study by Tarrés et al. (2022) —to which the reader is referred for further details on environmental conditions in the broader study area— investigated the temporal variability of downward mass fluxes in the deep margin and basin and their characteristics by means of in situ monitoring, elemental composition analyses and grain size measurements.

High water transparency resulting from low sediment input eases the development of rather extensive seagrass meadows along the coastline (Fig. 3.18) (Maldonado and Zamarreño et al., 1983; Ruiz et al., 2015; Baza-Varas, 2023). *Posidonia oceanica* (L.) Delile is the most conspicuous of the four seagrass species in the area, followed by *Cymodocea nodosa*, and then, to a lesser extent and in specific areas, *Zostera noltii* and *Ruppia cirrhosa* (Ruiz et al., 2015). It has been estimated that *P. oceanica* meadows cover over 10,000 ha along the coast of the Murcia province down to 25-30 m of water depth (Fig. 3.18) (Ruiz et al., 2013). Similarly to other regions

worldwide, seagrass meadows in the area have experienced significant regression (Marbá et al., 2014; Ruiz et al., 2015; Telesca et al., 2015).

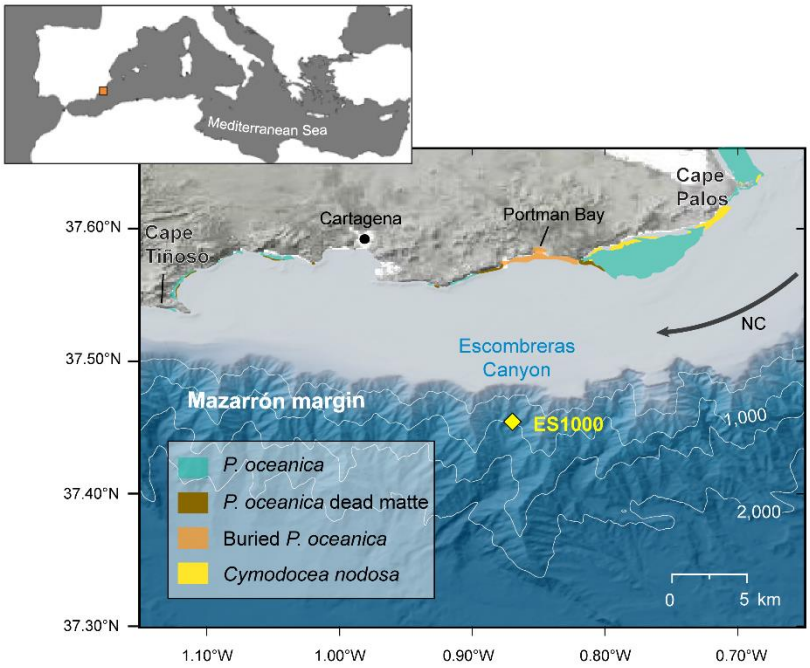

Figure 3.18. Bathymetric map of the Mazarrón margin segment between Cape Palos and Cape Tiñoso, in the SW Mediterranean Sea, with the location of Escombreras Canyon and ES1000 mooring station (yellow dot). *Posidonia oceanica* and *Cymodocea nodosa* meadows are from Ruiz et al. (2015) and from Visor del Sistema de Información Oceanográfico de la Región de Murcia, Comunidades Marinas layer. The extension of *P. oceanica* meadows buried by submarine mine tailings off Portmán Bay is from Baza-Varas (2023). Theoretical surface circulation in the main map (NC: Northern current) and in the framemap are shown.

3.3.3. Methods

3.3.3.1. Sampling

One mooring line equipped with a sequential PPS3 Technicap sediment trap (0.125 m^2, cylindroconical shape) with 12 trap cups was deployed 25 mab in the Escombreras Canyon at 985 m depth (Fig. 3.18), from March 2015 to August 2015, with sampling intervals set at 12-16 days (Table 3.5). The trap cups were filled with 5% (v/v) formaldehyde solution in 0.45 µm filtered sea water buffered with sodium tetraborate. Sediment trap processing is described in detail by Lopez-Fernandez et al. (2013), following a modified protocol from Heussner et al. (1990).

Seafloor sediment samples below the mooring were collected with a KD Denmark multicorer. One of the cores was subsampled every 0.5 cm from 0 to 5 cm core depth, and every 1 cm down to the core bottom at 50 cm depth. The samples were stored in plastic bags in the dark at 2-4ºC until they were freeze-dried. Each sample was weighted before and after freeze-drying.

3.3.3.2. Analytical techniques

Multiple geochemical tracers and biomarkers derived from the oxidation and hydrolysis of lignin and cutin, altogether with grain size parameters and accumulation rates have been used to characterize the settling particles and seafloor sediments, as described below.

Total Nitrogen (TN) and Organic Carbon (OC) and $\delta^{13}C_{OC}$ were prepared weighing 15-30 mg of homogenised sediment in silver capsules. The material was then acidified with a 1.5M HCl solution and subsequently oven-dried at 50°C to eliminate inorganic carbonates. Analyses were carried out with a Thermo Fischer Scientific DELTA Q mass spectrometer coupled with a Thermo Fischer Scientific FLASH 2000 Elemental Analyzer via a Conflo IV (EA-IRMS). OC content is reported as weight % and was used in the quantification of biomarkers concentration. Coefficient of variation for OC and TN was lower than 4% based on replicates of in-house reference material (sediment). $\delta^{13}C_{OC}$ data are reported as conventional delta notation (‰). Standard deviation for $\delta^{13}C_{OC}$ values is better than 0.1‰

Cupric oxide (CuO) oxidation products in settling particles and sediments were determined using an Agilent GC 7820 gas chromatograph coupled with a MSD EI 5977B mass spectrometer in the –above-mentioned lab, following the procedure in Goñi and Montgomery (2000). The CuO reaction products were dissolved in pyridine and derivatized with bis(trimethylsilyl) trifluoroacetamide (BSTFA) + 1% trimethylchlorosilane (TCMS) before injection. We determined a set of monomer compounds resulting from the oxidation of lignin, which include vanillyl phenols (Vd, Vl, Vn), syringyl phenols (Sd, Sl and Sn) and cinnamyl phenols (p-coumaric acid (pCd), and ferulic acid (Fd)). We also analysed hydroxy fatty acids derived from the cutin (ω-C16, C16DA, 8,ω-C16, 9,ω-C16, 10,ω-c16, 7-C16DA and 8-C16DA), and other reaction products of the benzoic acid (3,5 –dihydroxybenzoic acid, 3,5-Bd) (Supplementary Table 3.3). The quantification of the products was estimated by using the internal response factor of standards. Non-lignin products were calculated applying the response factor of *trans*-cinnamic acid. Analytical errors of CuO oxidation products were obtained by conducting replicate analysis. Error was 12.9% for syringyl phenols, 24.4% for vanillyl phenols, 10.7% for cinnamyl phenols, 1.7% for cutin acids and 6.6% for benzoic acids.

Grain size analyses of the sediments was carried out with a Beckman Coulter LS 230 laser diffraction particle size analyser, which measures sizes between 0.04 and 2,000 µm. Prior to analysis, samples were oxidized with H_2O_2 (10%) to remove the OM. A sodium polyphosphate solution was added to prevent particle flocculation. Sediment grains were classified by size classes as sand (63 µm to 2 mm), silt (4-63 µm) and clay (< 4 µm). In addition, sand fraction (< 63 µm) was determined for bulk sediment samples (i.e. without removing the OM). The coarser fraction (> 63 µm) was separated by wet sieving and then oven-dried at 50 ºC.

^{210}Pb activities were determined in selected subsamples of the sediment core at *Laboratori de Radioactivitat Ambiental* (LRA) of *Universitat Autònoma de Barcelona*, through the measurement of its descendant radionuclide ^{210}Po (Sanchez-Cabeza et al., 1998). After total digestion of the samples the ^{210}Po deposited onto silver discs was measured with α–spectrometer equipped with low background silicon surface barrier (SSB) detectors (EG&G Ortec). A spike of ^{209}Po was added as a yield tracer. The ($^{210}Pb_{base}$) was determined through ^{226}Ra measurement with a γ–

spectrometer. Excess ^{210}Pb activities ($^{210}Pb_{xs}$) were determined by subtracting the $^{210}Pb_{base}$ activities from the total ^{210}Pb.

3.3.3.3. Calculations

Sediment mass accumulation rates (MAR) were calculated using the CF:CS model, which assumes a constant $^{210}Pb_{xs}$ flux at the surface of the sediment and a constant sedimentation rate throughout the investigated sediment thickness.

Different OC sources were estimate using a mixing model. Bulk composition parameters ($\delta^{13}C_{OC}$) were combined with molecular biomarkers (lignin content (Λ_8) - OC normalized) to obtain a more accurate assessment (Hedges et al., 1997). The equations followed were:

$$\Lambda_S = \Lambda_1 \times f_1 + \Lambda_2 \times f_2 + \Lambda_3 \times f_3 \quad [3.9]$$

$$\delta^{13}C_S = \delta^{13}C_1 \times f_1 + \delta^{13}C_2 \times f_2 + \delta^{13}C_3 \times f_3 \quad [3.10]$$

$$1 = f_1 + f_2 + f_3 \quad [3.11]$$

Where 1, 2, 3 represent the potential sources and f_1, f_2 and f_3 are they relative contribution

3.3.3.4. Other data sources

Significant wave height (Hs) was obtained from the Cape of Palos buoy (0.33°W and 37.65°N), operated by *Puertos del Estado*. The buoy is located at about 15 km from the Cape of Palos in the continental shelf. Time series of averaged Chl-a contents were obtained from Aqua-MODIS by the NASA Ocean Biogeochemical Model (NOBM). Data on monthly dust deposition (wet+dry) nearby the ES1000 station was obtained from MERRA-2 model produced by the NASA Global Modeling and Assimilation Office (GMAO) using the Goddard Earth Observing System Model (GEOS).

3.3.4. Results

3.3.4.1. Forcing conditions and primary production

During the sampling period, two major north-eastern storms occurred on the 17-21th of March and the 6-9th of April, reaching Hs up to 4.8 m and 3.7 m, respectively (Fig. 3.19a). They were generally associated with rainfall episodes. Mid and late April was characterized by milder storm events. Significant wave heights were of lower intensity (Hs < 3m) and were associated with easterly and westerly winds.

Marine primary production is estimated after the sea surface content of pigment Chlorophyll *a* (Chl-*a*). Enhanced Chl-*a* contents were recorded besides the coastline in March, with peaks of 0.64 mg m^{-3}, whereas low contents (< 0.5 mg m^{-3}) were observed in the following months (Fig. 2b). Atmospheric deposition (wet plus dry) peaked in April, with a monthly average value of about 23 mg m^{-2} d^{-1}. Later months showed a decreasing trend with very low contents from June to August (Fig. 2c).

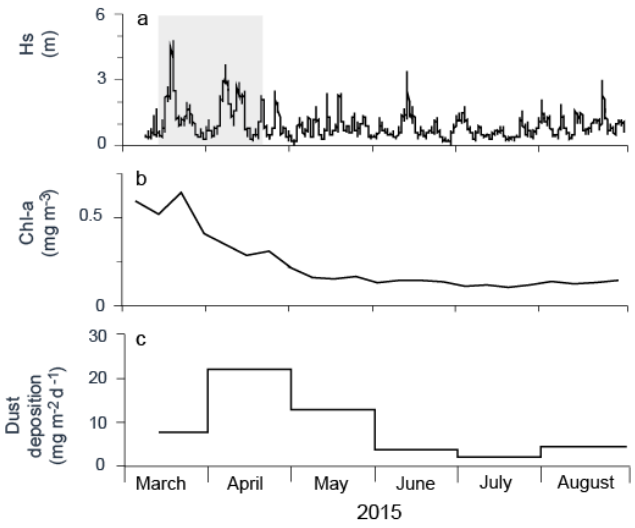

Figure 3.19. Time series of (a) significant wave height (Hs) measured at the Cape of Palos buoy. Major storms are identified in orange. (b) 8-days averaged Chl-a contents and (c) monthly dust deposition (wet+dry) nearby the ES1000 station.

3.3.4.2. Settling particles

The bulk and isotopic composition of settling particles are presented in Table 3.5. $\delta^{13}C_{OC}$ ranged from -22.02 to -23.02‰, with less depleted values mostly at the very beginning of the study period and higher values during the rest of the period, peaking by the end of July. CuO reaction products include those deriving from lignin (S, V, C), cutin acids and precursor 3,5-Bd. The yields of lignin, normalized by OC, showed values ranging from 0.08 to 0.20 mg / 100 mg OC. Lignin-derived phenols (Λ_8) varied from 0.2 to 0.4 mg / 100 mg OC, with only one value above that upper bound (0.45 mg / 100 mg OC for the March sample). All other values above 0.3 mg / 100 mg OC occured in June and July (0.35-0.40 mg / 100 mg OC). Carbon-normalized values of lignin (0.20-0.45 mg lignin / 100 mg OC) were minor that those found in inner shelf areas near river mouths, such as the SW Spain (Sánchez-García et al., 2009) or the western Adriatic Sea (Tesi et al., 2007b). However, they were comparable with those in river-influenced Mediterranean canyons, though in the lower range in the case of canyons in Gulf of Lions (Tesi et al., 2010; Pasqual et al., 2011) and, in particular, similar to those found at about 600 m depth in the Bari Canyon (Tesi et al., 2008). Cutin acids showed a relative peak (0.29 mg / 100 mg OC in March) and a set of values above 0.2 in June and July, with a maximum of 0.33 mg / 100 mg OC in early July. A similar temporal pattern was observed for the 3,5-Bd, with an isolated peak (0.03 mg / 100 mg OC in March) and values with a rounding value of 0.03 between June and July, with a maximum of 0.034 mg / 100 mg OC in early July. CuO oxidation products strongly correlates with each other ($r>0.85$, $p<0.05$), whereas negatively correlates with OC (%) ($r >-0.6$, $p<0.05$) (Supplementary Table 3.4).

The sum of lignin phenols, mass normalized, ranged from 0.039 to 0.067 mg/1g dw, displaying minor values in mid-April and late August, and maximum values in late April. Mass normalitzed cutin acids ranged from 0.029 to 0.052 mg/1g dw. Minimum and maximum values were analysed in mid and late April, respectively, with increased values also found in July.

ID	Cup opening date	Cup closing date	$\delta^{13}C_{OC}$	OC/TN*	S	V	C	Λ_8	Cutin	3,5-Bd	Lignin	Cutin
			‰		mg/100 mg OC	mg/100 mg OC	mg/100 mg OC	mg/100 mg OC	mg/100 mg OC	mg/100 mg OC	mg/1 g dw x10^2	mg/1 g dw x10^2
ES1000-I-1	24/3/2015	1/4/2015	-22.04	11.76	0.15	0.20	0.10	0.45	0.29	0.03	0.55	0.36
ES1000-I-2	6/4/2015	11/4/2015	-22.02	10.50	0.07	0.09	0.05	0.20	0.15	0.01	0.39	0.29
ES1000-I-3	16/4/2015	21/4/2015	-22.33	11.62	0.07	0.09	0.08	0.25	0.19	0.01	0.67	0.52
ES1000-I-4	26/4/2015	1/5/2015	-22.84	9.77	0.09	0.10	0.08	0.28	0.19	0.02	0.49	0.34
ES1000-I-5	8/5/2015	16/5/2015	-22.86	10.19	0.08	0.09	0.09	0.27	0.18	0.02	0.45	0.30
ES1000-I-6	24/5/2015	1/6/2015	-22.44	11.14	0.09	0.09	0.09	0.28	0.21	0.02	0.52	0.40
ES1000-I-7	8/6/2015	16/6/2015	-22.41	8.88	0.11	0.11	0.14	0.36	0.26	0.03	0.48	0.36
ES1000-I-8	23/6/2015	1/7/2015	-22.66	8.68	0.11	0.11	0.13	0.35	0.23	0.03	0.46	0.31
ES1000-I-9	8/7/2015	16/7/2015	-22.50	6.94	0.13	0.14	0.13	0.40	0.33	0.03	0.52	0.43
ES1000-I-10	24/7/2015	1/8/2015	-23.02	8.46	0.12	0.13	0.11	0.36	0.28	0.03	0.51	0.41
ES1000-I-11	8/8/2015	16/8/2015	-22.58	9.10	0.08	0.10	0.09	0.28	0.22	0.02	0.42	0.35
ES1000-I-12	22/8/2015	28/8/2015	-22.50	10.24	0.08	0.09	0.08	0.25	0.19	0.02	0.39	0.30
Mean			-22.52	9.77	0.10	0.11	0.10	0.31	0.23	0.02	0.49	0.36
SD			0.31	1.42	0.02	0.03	0.03	0.07	0.05	0.01	0.08	0.07

Table 3.5. Geochemical parameters of settling particles collected at 25 mab at mooring station ES1000: $\delta^{13}C_{OC}$, TN/OC (molar) and yields of lignin derived phenols oxidation (syringyl —S—, vanillyl —V—, and cinnamyl —C— phenol products), lignin contents, cutin contents and other reaction products contents, such as 3,5-dihydroxybenzoic acid (3,5-Bd). Notice that mass normalized yields values are showed x10^2. *The molar TN/OC ratio is extracted from Tarrés et al. (2022).

3.3.4.3. Seafloor sediments

Key sedimentological and geochemical parameters of the sediment core are shown in Figure 3.20. OM free samples were dominated by the clay and silt size fractions, with very low sand contents (<2% in average, peaking at 5.2%) (Fig. 3.20). Mean silt and clay contents were 48.63 and 49.86 %, respectively, with standard deviations of 3.48 and 3.57%. A higher proportion of sand was found in bulk samples (i.e. without OM removal), with a ~4% in average. Total sand content in bulk sediment was about 3.1 ± 0.25% from 0 to 3 cm core depth to then increase to 5.7 ± 1.3% between 3 and 15 cm core depth. Downcore from that depth sand contents were smaller (3.3±0.9%). Visual inspection of the coarser fraction on the binocular loupe showed abundant vegetal fibres (Supplementary Fig. 3.3).

The average OC content in the sediments was 0.88%, ranging from 0.77 to 1.14% (Fig. 3.20). From the core top to 3.5 cm depth was an increasing trend followed by a rather steady maximum value of about 1.1 % down to about 8.5 cm core depth (Fig. 3.20). Following a few pronounced oscillations between 8.5 and 15.5 cm core depth, OC contents remained rather uniform varying amongst 0.77 and 0.97 %.

$\delta^{13}C_{OC}$ ranged from -20.30 to -21.87‰, with the less depleted values corresponding to intervals with higher TOC contents. Both parameters, OC and $\delta^{13}C_{OC}$ were positively correlated ($r = 0.71$; $p<0.05$) (Supplementary Table 3.5). OC/TN (molar) ratios fluctuated between 7.38 and 10.91 (Fig. 3.20) and were inversely correlated with $\delta^{13}C_{OC}$ ($r = -0.71$; $p<0.05$) (Supplementary Table 3.5).

The ^{210}Pb profile show an exponential decay. Pb supported content was about 32±2 Bq kg^{-1}, and the $^{210}Pb_{xs}$ horizon extended down to ~31.5 cm within the core. $^{210}Pb_{ex}$ concentrations were rather constant between 9.5 and 15.5 cm core depth, which suggest mixed intervals. The representation of $^{210}Pb_{xs}$ versus the accumulated mass (Supplementary Fig. 3.4) shows that two MAR can be estimated in the core: 0.242 g cm^{-2} y^{-1} for the uppermost sediments (0-6.5 cm) and 0.544 g cm^{-2} y^{-1} for the sediments below (6.5-50.5 cm). Average sedimentation rate was 0.348 ± 0.032 g cm^{-2} y^{-1}. To calculate the dates, we assumed constant sedimentation rates (average value). The age model shows that the change of MAR occurred in 1989 ± 2 (Supplementary Fig. 3.4).

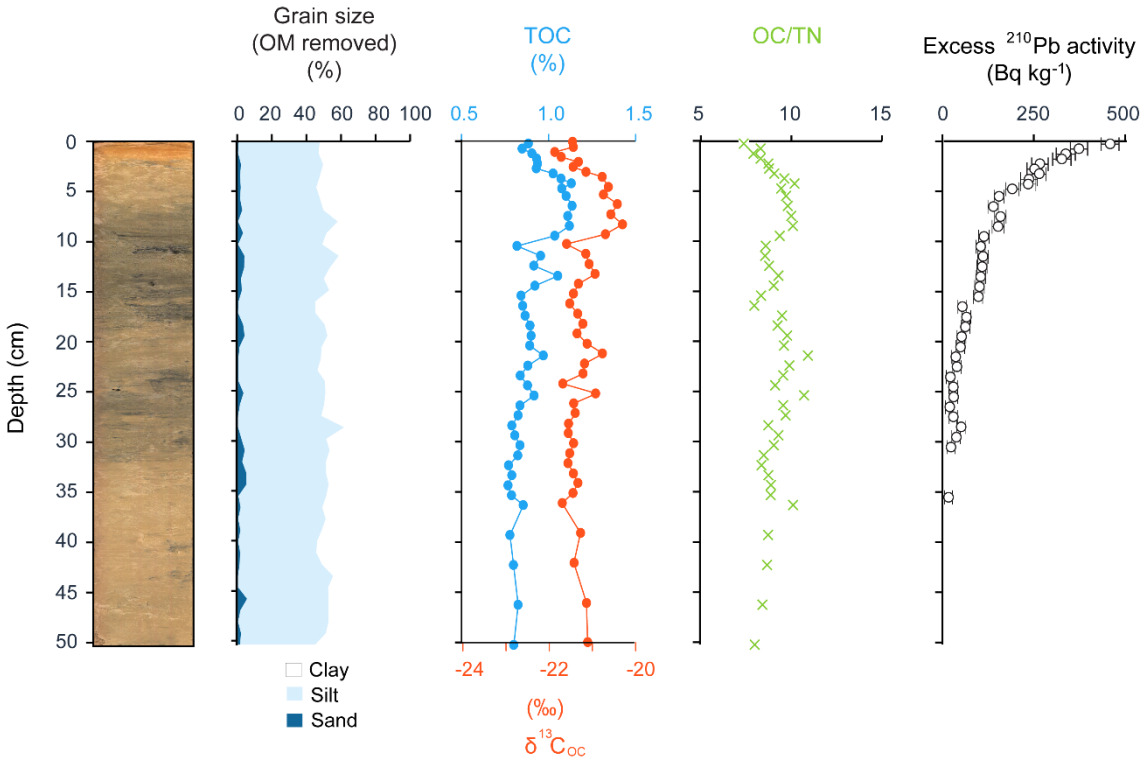

Figure 3.20. Photography of the sediment core from station ES1000 and grain size, total organic carbon (OC), $\delta^{13}C_{OC}$, OC/TN (molar) and excess ^{210}Pb activity profiles.

Lignin yields showed a large variability (0.72-6.61 mg / 100 mg OC), with Λ_8 ranging from 0.40 to 1.08 mg / 100 mg OC, while cutin acids span from 0.27 to 0.61 mg / 100 mg OC. 3,5-Bd ranged from < 0.03 to > 0.06 mg / 100 mg OC. Lignin, cutin and 3,5-Bd profiles exhibited a fluctuating character, with higher contributions in 10.5 cm and in the 39.5-47.5 cm deeper interval (Table 3.6). The CuO reaction products positively correlate between them (Supplementary Table 3.5). The OC deposited into the canyon was enriched in lignin and cutin yields relative to settling particles, as illustrated by mean values of 0.65 mg Λ_8 and 0.37 mg cutin/100 mg OC in sediments and 0.31 mg Λ_8 and 0.23 mg cutin /100 mg OC in settling particles (Tables 3.5 and 3.6). Lignin yields, mass normalized, showed large variability (0.058 ± 0.015 mg/1g dw), whereas cutin yields displayed values of 0.032 ± 0.006 mg/1g dw, being minor respect to the settling particles average values.

Core depth cm	S mg/100 mg OC	V mg/100 mg OC	C mg/100 mg OC	Λ_8 mg/100 mg OC	Cutin mg/100 mg OC	3,5-Bd mg/100 mgOC	Lignin mg/1 g dw x10^2	Cutin mg/1 g dw x10^2
0.25	1.53	2.03	0.72	0.43	0.31	0.04	0.38	0.27
1.25	1.25	1.97	0.86	0.41	0.27	0.03	0.37	0.24
3.25	1.16	1.98	0.86	0.40	0.27	0.04	0.41	0.28
6.5	1.37	2.13	0.88	0.44	0.25	0.03	0.50	0.28
8.5	1.58	3.07	1.16	0.58	0.35	0.03	0.65	0.39
10.5	2.39	4.96	1.60	0.86	0.49	0.04	0.73	0.40
12.5	2.20	3.60	1.37	0.72	0.38	0.04	0.66	0.34
15.5	1.71	2.92	0.86	0.54	0.32	0.04	0.46	0.27
17.5	2.27	3.16	1.50	0.69	0.42	0.05	0.60	0.36
21.5	1.77	3.19	0.99	0.58	0.32	0.03	0.58	0.31
25.5	1.92	3.40	1.23	0.65	0.32	0.04	0.60	0.29
34.5	2.06	3.67	0.95	0.65	0.34	0.04	0.51	0.26
39.5	2.72	5.00	1.90	0.96	0.61	0.04	0.75	0.48
42.5	2.49	4.79	1.25	0.82	0.40	0.05	0.68	0.32
46.5	3.30	6.61	1.38	1.08	0.43	0.07	0.93	0.35
50.5	2.09	3.20	1.23	0.65	0.36	0.04	0.52	0.29
Mean	1.99	3.48	1.17	0.65	0.37	0.04	0.58	0.32
SD	0.57	1.30	0.33	0.20	0.09	0.01	0.15	0.06

Table 3.6. Cupric oxide (CuO) reaction products in sediment core ES1000: S: syringyl. V: vanillyl. C: cinnamyl, Λ_8: lignin, cutin and other reaction products (3,5-Bd: 3,5-dihydroxybenzoic acid). OC: Organic carbon. Notice that mass normalized yields values are showed x10^2.

3.3.5. Discussion

3.3.5.1. Analysis of recalcitrant OC sources

Settling particles are drivers of OC export toward the deep seafloor. Sediment traps have been extensity used to measure particle fluxes allowing investigating OM sources and pathways (Trull et al., 2001; Honjo et al., 2008; Pedrosa-Pamies 2021). $\delta^{13}C$ and $\delta^{15}N$, enable discerning the major constituents of OM in the ocean (Hedges et al., 1997; Goñi et al., 2006; Sanchez-Vidal et al., 2009). Marine algae $\delta^{13}C_{OC}$ values are isotopically heavier (-18 to -22 ‰) (Hedges et al., 1997) than those from terrestrial vascular plants C3 (-25 a -28 ‰) and soil-derived OM. Conversely, seagrass plants C4 display depleted $\delta^{13}C$ values (-12 to -15‰) (Apostolopoulou et al., 2015; Apostolaki et al., 2022). Differences arise from $\delta^{13}C$ values in CO_2 sources for plants and phytoplankton uptake, which is from the atmosphere or dissolved in seawater, respectively, and from fractionation resulting from carbon fixation pathways during photosynthesis (Fry and Sherr, 1989). $\delta^{13}C_{OC}$ values ranging from -22.04 ‰ to -23.02 ‰ suggest that marine phytoplankton was the main source of OM in the downward particle fluxes (Table 3.5).

Nevertheless, lignin-derived phenols and cutin-derived carboxyl acids were detected in all samples, pointing to other sources contributing to OC contents in particle fluxes above Escombreras Canyon (Table 3.5). Lignin and cutin molecules are refractory compounds only produced by vascular plants (Hedges and Mann, 1979; Hedges et al., 1997), which provide

strength and rigidity to their structures (Thevenot et al., 2010). The molecular composition of lignin varies between plant groups (Thevenot et al., 2010). For instance, gymnosperms produce vanillyl phenols but do not synthetize syringyl phenols (Hedges et al., 1997). Also, non-woody tissues have a higher yield of cinnamyl phenols (Hedges and Mann, 1979). The relationship between lignin yields (vs. S/V and C/V ratios) is transferred to terrestrial soils and marine sediments and, consequently, has been used rather extensively to distinguish lignin sources (Hedges and Mann, 1979; Hedges et al., 1997; Prahl et al., 1994; Goñi et al., 2000 Tesi et al., 2007a; Pasqual et al., 2011; Nakakuni et al., 2021).

Plotting S/V against C/V suggests a mixed origin for lignin in settling particles in our study area, with more than two end-members accounting for the lack of linear distribution (Fig. 3.21a). Concerning the settling particles, S/V and C/V ratios showed heterogeneous values (from 0.74 to 0.96 and 0.49 to 1.29, respectively). Most of the settling particle samples exhibited S/V ratio values > 0.8, which is consistent with a relevant contribution of angiosperm soft tissues in the OC pool (Hedges et al., 1997). These materials most likely derived from soil OM given their relatively light $\delta^{13}C_{OC}$ —ranging from -22 to -23 ‰— and low OC/TN values (Table 3.5). In contrast to marine algae, vascular plants have nitrogen-depleted tissues due to the predominance of nitrogen-free molecules, however, they tend to gain nitrogen during microbial decay (Hedges et al., 1997). In addition, several samples were relatively enriched in cinnamyl phenols (C/V > 1.00) (Table 3.5 and Fig. 3.21a). Such values cannot be attributed to leave or needle tissues (Hedges and Mann, 1979). Instead, they are characteristic of pollen, which is also in agreement with high pCd/Fd ratios (Keil et al., 1998; Sheng Hu et al., 1999) (Fig. 3.21b). Finally, two settling particle samples displayed small S/V ratios (0.74-0.78) and are placed in the area of mixture amongst angiosperm soft-tissues field and *P. oceanica* tissues, with syringyl-poorer and vanillyl-richer lignin (Bianchi et al., 1999; Kaal et al., 2018) (Fig. 3.21a). These two samples exhibited the heavier $\delta^{13}C_{OC}$ values (Table 3.5) and variable lignin OC-normalized contents (Fig. 3.21c).

Enrichments in vanillyl phenols and low S/V ratios (0.51-0.75) (Fig. 3.21a and Table 3.6) were observed for the OC deposited into the canyon, suggesting that an important fraction of lignin derived from *P. oceanica* debris OC. *P. oceanica* meadows produce significant amounts of debris from different tissues, part of which can slowly bury with sediments, thus producing the “matte” (Hemminga and Duarte, 2000). In autumn, leaves are shed whereas leaf sheaths remain attached to rhizomes where they can experience abrasion by sand blasting during sea storms. A fraction of the released fibres get entangled amongst themselves altogether with other materials (e.g. small-sized plastics) by water motion and rolling over the bottom, resulting in golf ball-sized soft vegetal fibre balls, also known as aegagropilas, that can get stranded on beaches (Verhille et al., 2017; Sanchez-Vidal et al., 2021; Lefebvre et al. 2023). They can also be exported seaward by currents jointly with individual fibres, providing a large food source from shallow to continental slope depths (Vetter, 1998), while a part is buried in the deep sea (Duarte and Krause-Jensen, 2017). Previous studies have shown that lignin is more abundant in sheaths and rhizomes than in leaves (Klap et al., 2000; Trevathan-Tackett et al., 2017). *P. oceanica* debris in our samples consisted of fibres derived from lignified tissues, such as those in leaf sheaths and rhizomes. The significant variation of particle sizes amongst bulk samples and samples with OM removed for sediment samples indicate that vegetal fibres were enriched in the sand fraction.

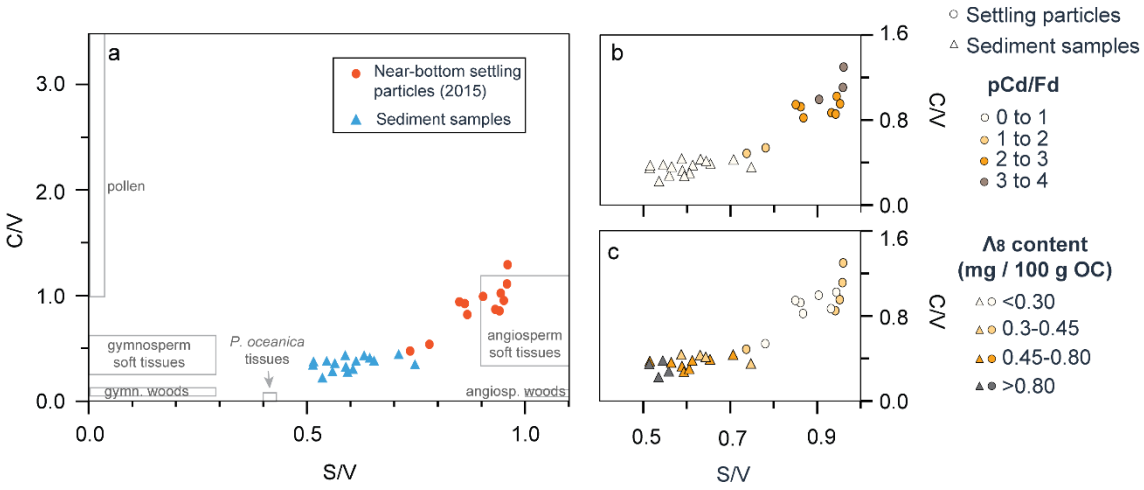

Figure 3.21. (a) Ratios of lignin products cinnamyl phenols / vanillyl phenols (C/V) vs. syringyl phenols / vanillyl phenols (S/V) in settling particles and sediment samples of the Escombreras Canyon. The range of values of potential sources including pollen, gymnosperms, angiosperms, and *Posidonia oceanica* leaf sheaths is indicated after Hedges et al. (1997), Bianchi et al. (1999), Kaal et al. (2018) and Ishiwatari et al. (2006). (b) C/V vs. S/V ratios in our samples as a function of lignin contents normalized by OC. (c) C/V vs. S/V ratios in our samples as a function of depth above or below the seafloor.

In order to better constrain the proportion of OC derived from *P. oceanica* detritus in the fluxes and deposited sediments, we used a three mixing model, considering the contribution of marine phytoplankton, soil-derived OM and *P. oceanica* litter. Despite lignin appeared to primarily derive from three different sources, pollen end-member has been excluded because we didn't find suitable information. We assumed that pollen contribution was negligible in the deposited sediments. Nonetheless, it's important to note that this could potentially lead to an overestimation of the contribution of *P. oceanica* litter in certain trap samples.

The sediments deposited into the canyon were more influenced by OC of *P. oceanica* detritus origin than the settling particles collected in 2015 (OC_{POS}>10% vs OC_{POS}<8%, respectively; for the proposed value of Λ_{SOIL} = 0.7 mg / 100 mg OC) (Fig. 3.22). The composition of the March sample was more similar to the one of the topmost sediments, richer in OC of *P. oceanica* origin (OC_{POS}~9-11%). Low OC_{POS} contributions were found for the rest of the fluxes. Regarding the deposited sediments, the majority of the samples presented a rather stable mixture of both recalcitrant end-members (OC_{Soil} /OC_{Pos} =1.1-1.8), with minor ratios for the 6.5 and 8.5 cm samples, and clearly higher ratios for the topmost sediments (OC_{Soil} /OC_{Pos} =2.0-3.3) (Fig. 3.22 and Supplementary Table 3.6). Finally, recalcitrant compounds predominantly accounted more for the deep sediments horizons, albeit without a clear gradual pattern, likely as a result of degradation processes modulated by complex interrelations amongst multiple physical, chemical and biological factors (Burdige, 2007). The higher relative abundance of OC-normalized lignin and cutin with increasing core depth (Table 3.6) may reflect the loss of labile OM. This is because OM undergoes decomposition in the water column and in seafloor sediments, mainly through redox reactions catalysed by microorganisms (Berner, 1980). Seagrass detritus exhibit a greater storage

efficiency in sediments as they contain degradation-resistant compounds such as lignin (Kawakami, 1980; Klap et al., 2000).

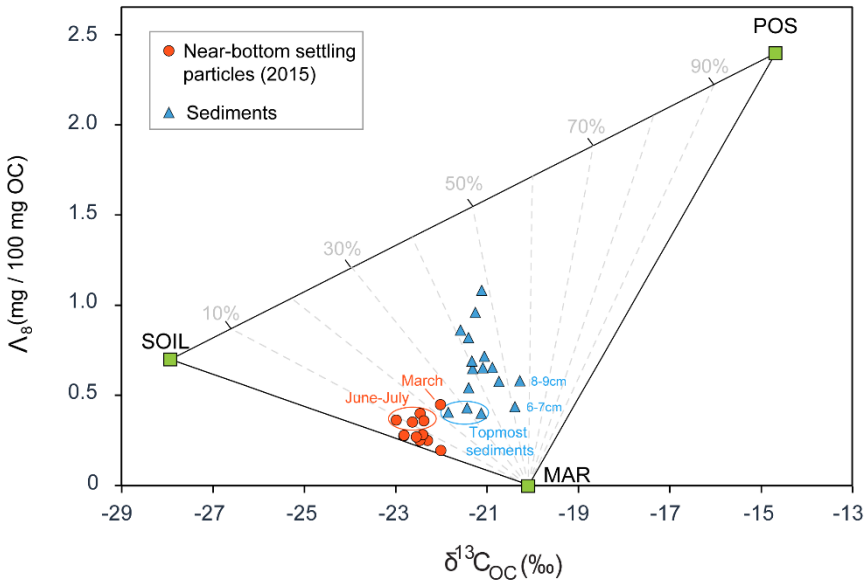

Figure 3.21. $\delta^{13}C$ (‰) vs. Λ_8 (mg / 100 mg OC) plot illustrating the relative abundance of marine phytoplankton (MAR), soil-derived OM (SOIL) and *P. oceanica* litter (POS) in settling particles and canyon floor sediments at Escombreras Canyon. Marine end-member $\delta^{13}C_{OC}$ was chosen from published marine phytoplankton values, measured in the Gulf of Lions, ($\delta^{13}C_{MAR}$ = -20.1‰ (Harmelin-Vivien et al., 2008); Λ_{MAR} = null (Tesi et al., 2008). *P. oceanica* litter in the inner Mazarrón shelf had a signature of $\delta^{13}C_{POS}$ = -14.69‰ (unpublished data), whereas we considered Λ_{POS} = 2.4 mg / 100 mg OC (Bianchi et al., 1999). Terrestrial soil-derived $\delta^{13}C_{OC}$ was chosen on the basis of published values measured in the neighbouring Mar Menor ($\delta^{13}C_{SOIL}$ = -28‰ (Lloret and Marín, 2009). Typical values of degraded OC of forest soils range from 0.5 to 1.8 mg / 100 mg OC (Thevont et al., 2010). In this study, a $\Lambda_8 < 0.75$ is necessary to model the OC mixture. We used Λ_{SOIL} = 0.7 mg / 100 mg OC). Note that the contribution of a pollen end-member has not been estimated, which might cause the contribution of lignin from *P. oceanica* litter to be overestimated in specific trap samples (i.e. potentially those collected in June-July).

3.3.5.2. Delivery of recalcitrant OC

Differences in biomarker characteristics and contents were detected in the settling particles collected throughout the sampling period. S/V ratio exhibited an overall increasing trend from mid-March to August, whereas C/V ratio displayed minor values in mid-March and early April. A relatively high OC-normalized lignin content (up to 0.45 mg / 100 mg OC) (Table 3.5 and Fig. 3.23b), low S/V and C/V ratios and the elevated OC_{POS} (Fig. 3.23c) was found at the beginning of the study period (i.e. late March). During the rest of the period, high S/V ratios (Fig. 3.23c) point to degraded non-woody angiosperms tissues as the main source of lignin, in line with the low OC_{POS} contributions. The 3,5-Bd when it's normalized to vanillyl (3,5-Bd/V) provides information about the degradation state and humification of fresh vascular plant tissues (Houel et al., 2006; Dickens et al., 2007; Sánchez-García et al., 2009). The abundance of 3,5-Bd products has been commonly related with terrestrial OM (Prahl et al., 1994; Tesi et al., 2007a; Dickens et al., 2007),

though they have been also detected in brown microalgae (Goñi and Hedges et al., 1995). In our study area, the positive correlation of 3,5-Bd with lignin ($r=0.88$; $p<0.05$) and cutin ($r=0.90$; $p<0.05$) (Supplementary Table 3.4) indicates its association with recalcitrant compounds. The 3,5-Bd/V ratio increased steadily from March to early July, within an overall range from 0.15 to 0.25 (Fig. 3.23d). Then, it fluctuated slightly till until the end of the sampling period in late August (Fig. 3.23d). The overall increment of the 3,5-Bd/V ratio points to an increasing degradation of OM throughout the study period (Fig. 3.23d).

March and April storm events enhanced wave heights (Fig. 3.19a) and shelf currents thus triggering resuspension and transport of sedimentary particles (Tarrés et al., 2022). In terms of fluxes, the storm events promoted the downslope transport of large volumes of OC (maximum of 302.0 mg OC m^{-2} d^{-1}) (Tarrés et al., 2022) and recalcitrant compounds (maximum of 136.7 mg lignin phenols m^{-2} d^{-1} and 88.8 mg cutin acids m^{-2} d^{-1}) (Fig. 3.23a). The increased content of OC_{POS} in the particle fluxes collected during March, in comparison to the other samples (Fig. 3.22), provides strong evidence that large storm events influence the transport of *P. oceanica* litter and shelf material, as observed in other studies in the Mediterranean Sea (Sanchez-Vidal et al., 2008). Contrastingly, we observed low OC-normalized lignin content in early and mid-April samples (0.20-0.25 mg / 100 mg OC) (Fig. 3.23b and Table 3.5). Those values were likely modulated by marine OC inputs deriving from primary production occurring in the surface (Fig. 3.19b) or by the milder character of the April storms (cf. section 3.3.3.1), because shelf currents were not able to maintain the coarse suspended load until the sediment trap deployment. Indeed, the spatial distribution of vascular plant debris (fragments) has been related to hydrodynamic sorting in other margins such as the Washington coast (Keil et al., 1998) and margin (Prahl et al., 1994), the Cyprus margin (Bianchi et al., 1999), or the western Adriatic Sea (Tesi et al., 2007b). Conversely, in absence of energetic hydrodynamic conditions during most of the sampling period, terrestrial soil derived OM was preferentially transported seaward. The OM incorporation or association with mineral phases (Arndt et al., 2013), especially with fine-grained particles providing mineral protection (Hedges and Keil, 1995), has been proposed to explain the OM transport seaward. Consequently, the transport of OC is influenced by particle sorting processes that operate during the across-shelf transport and beyond (Tesi et al., 2007a; Bianchi et al., 2007; Sánchez-García et al., 2009). Finally, it is worth mentioning that high C/V and pCd/Fd ratios detected in summer months (Fig. 3.23c), and tentatively related to pollen (cf. section 3.3.5.1), point to the contribution of atmospheric inputs. They were noticed in summer months due to the lower dilution within sediments advected from the adjacent shelf.

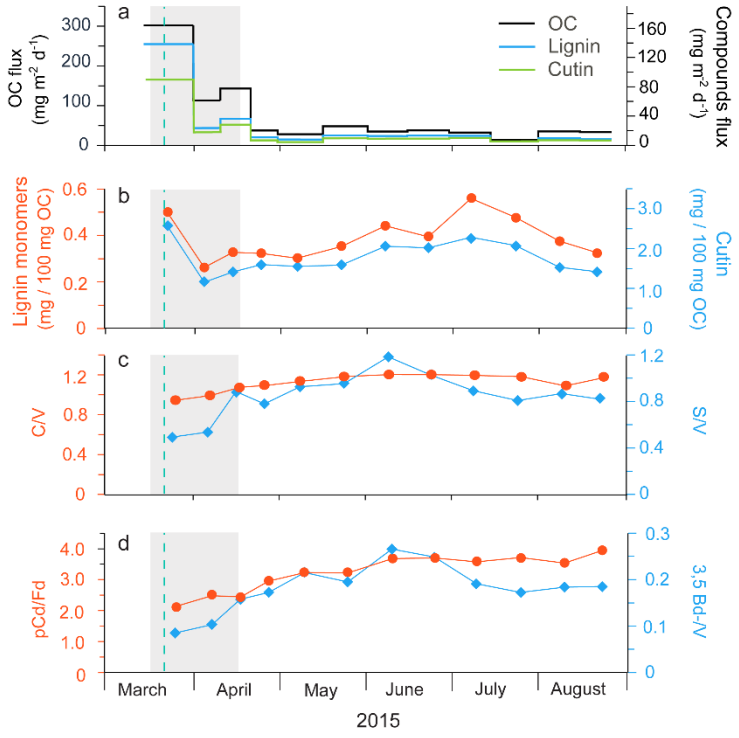

Figure 3.23. Time series of downward OC fluxes and other geochemical parameters in settling particles at Escombreras Canyon. (a) OC and compounds flux (mg m^{-2} d^{-1}). (b) Lignin monomers and cutin products. (c) Composition ratios C/V and S/V. (d) Cinnamyl phenol products ratio (pCd/Fd) and 3,5-dihydroxybenzoic acid normalized to vanillyl ratio (3,5-Bd/V). The grey bands highlight the stormy period at the beginning of the study period. The dashed vertical blue line indicates the Chl-a maximum at the water surface (cf. Fig. 3.19b). OC fluxes from Tarrés et al. (2022).

3.3.5.3. Vertical variations in sediment OC content and origin

The Escombreras canyon middle course (about 1,000 m depth) functions as a sink for fine sediments and OC (Fig. 3.20), as indicated by the relatively high MAR (Supplementary Fig. 3.4). A noticeable decrease of OC content was observed towards the seafloor (from 0.85-0.94% in 0-2.75 cm to 1.03-1.14% in the underlying sediments from 3.25 to 9.5 cm) (Fig.3.20). Based on the age model, the sharp diminish corresponds from 2005 ± 1 to 2015, the year of sediment collection. A Pearson correlation test revealed that the OC content within the top 10 cms positively correlated with the sand fraction in bulk samples ($r=0.77$; $p<0.05$) (Fig. 3.24a), a parameter that is associated with *P. oceanica* detritus. Accordingly, OC content poorly negatively correlated with the clay fraction in OM free samples (Fig. 3.24b). The OC relationship with compositional parameters such as $\delta^{13}C_{OC}$ (‰) and OC/TN ($r=0.91$ and $r=0.94$; $p<0.05$ and $p<0.05$, respectively) (Fig. 3.24c,d) supports this observation. This indicates a close association between the burial of P. *oceanica* detritus and OC content in the uppermost layers of canyon sediments.

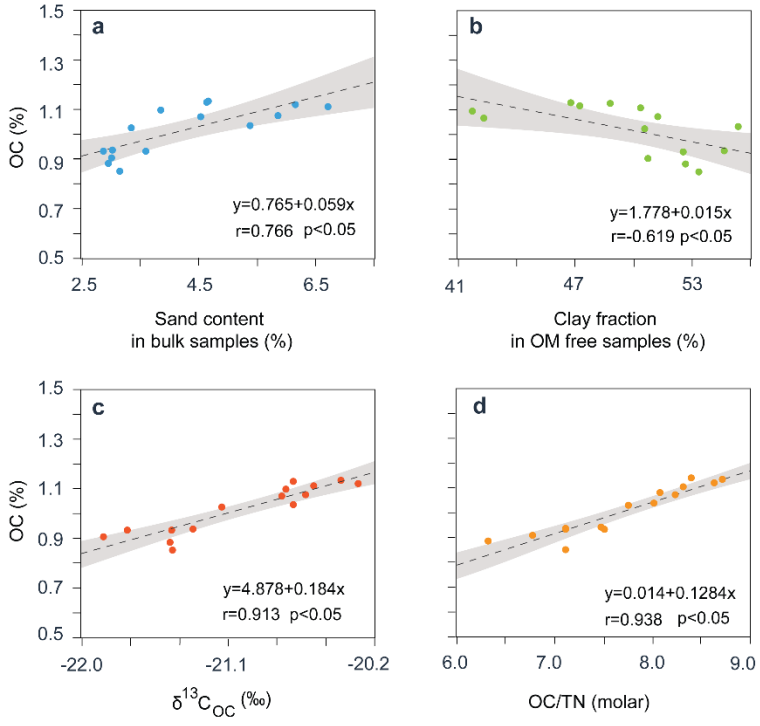

Figure 3.24. Pearson's correlation between organic carbon (OC) contents and OC compositional and sedimentological parameters for the top 10 cm of the Escombreras Canyon sediment core. (a) With sand content in bulk samples. (b) With the clay fraction in organic matter (OM) free samples. (c) With $\delta^{13}C_{OC}$. (d) With OC/TN ratio (molar). OC (y), correlation coefficient (r) and p-value (p) are also provided.

Lignin biomarker ratios could offer additional information about the sources and transformations of OC in sediments. Previous studies on the diagenetic state of lignin relied on transformation of lignin yields such as vanillyl and syringyl acid/aldehyde ratios (Vd/Vl and Sd/Sl), because vanillic acid and syringic acid are more reactive than their aldehydes (Goñi et al., 1993; Opsahl and Benner, 1995; Goñi et al., 1997; Dittmar and Lara, 2000). 3,5-Bd/V ratio has also been used to assess the degree of degradation, as previously stated (cf. section 3.3.5.2). Degradation of lignin has been attributed in particular to white-rot fungi, though several microorganisms can also alter the lignin structure (Goñi et al., 1993; Thevenot et al., 2010 and references therein), thus leading to Vd/Vl > 0.4. In comparison, Vd/Vl in highly altered lignin (i.e. soil-derived) can range from 0.4 to 4 (Goñi et al., 1997). However, high Vd/Vl ratios do not necessarily indicate a high degree of degradation (Dittmar and Lara, 2000). For instance, Bianchi et al. (1999) reported Vd/Vl values equal to 1.88 for *P. oceanica* fresh tissues.

Interestingly, the highest values of vanillyl and syringyl acid/aldehyde ratios (Vd/Vl and Sd/Sl) and the 3,5-Bd/V ratio correspond to the topmost youngest sediments, and showed a rather concave pattern until 17.5 cm, with the minor values at 8.5 cm (Fig. 3.25a). The evolution of these ratios indicates a shift in the degradation state of the lignin preserved in the uppermost sediments, being more degraded at the canyon seafloor. It is unlikely due to OM degradation in-situ (Dittmar and Lara, 2000), but rather it can be the result of preferential deposition of degraded soil OM at the canyon seafloor (Fig. 3.25b,c), in agreement with recalcitrant OC sources estimated following

the ternary mixing model (Fig. 3.22). Therefore, it appears that less amount of *P. oceanica* detritus is funneled into the canyon by currents in recent years.

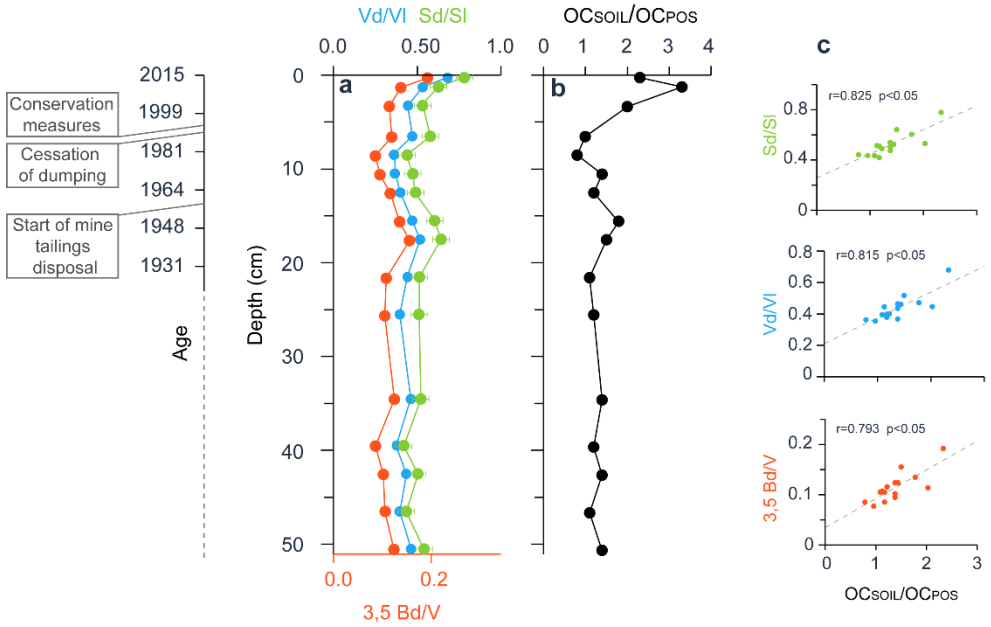

Figure 3.25. Profiles of organic carbon (OC) proxies against age in the sediment core from Escombreras Canyon. Age is derived from excess ^{210}Pb activity measurements (Fig. 3.20) and highlight the main events with environmental consequences in the broader study area (Fig. 3.18): the onset of mine tailings disposal in Portmán Bay (1957) and the cessation of dumping (1990) (Oyarzun et al., 2013; Baza-Varas et al., 2022) and the start of priority habitats protection (Ruiz et al., 2015). (a) Lignin product ratios: 3,5-dihydroxybenzoic acid normalized to vanillyl (3,5-Bd/V), vanillyl acid/aldehyde (Vd/Vl) and syringyl acid/aldehyde (Sd/Sl). (b) OC_{SOIL}/ OC_{POS} ratio derived from mixing model estimations (Fig. 3.22). (c) Pearson's correlation between lignin product ratios and OC_{SOIL}/ OC_{POS}. One sample has been excluded; considering the entire dataset: 0.64<r>0.71 (p<0.05).

3.3.5.4. Human actions affects the export of *Posidonia oceanica* detritus

We have documented that physical forcing's, such as large storm events increasing waves and currents, could stimulate P. *oceanica* detritus export seaward (Figs. 3.22 and 3.23). Hence, a diminution of cross-shelf sediment transport could reduce the supply of *P. oceanica* detritus in the Escombreras Canyon. Nevertheless, the historical time series of Hs do not appear to suggest any significant change in the frequency and intensity of storms in the last 80 years (www.puertosdelestado).

Global losses of seagrass meadows have been largely attributed to human perturbations (de los Santos et al., 2019), but also to extreme meteorological events (Sanchez-Vidal et al., 2012) or climate change (Arias-Ortiz et al., 2018). *P. oceanica* is highly sensitive to water quality loss by eutrophication, salinity variations and pollutant loads, to changes in the local sedimentation/erosion balance, and to direct abrasion by bottom-touching fishing gear and anchoring (Ruiz and Romero 2003; González-Correa et al., 2005; Díaz-Almela and Duarte, 2008;

Ruiz et al., 2009a). The exposure of *P. oceanica* to environmental pressures, both human-induced and natural, can lessen the plant density and coverage (González-Correa et al., 2005; Marbà et al., 2005), and result in a severe depletion of foliar canopy, ultimately leading to a 'dead matte' situation (Apostolaki et al., 2022). However, the consequences of seagrass decline extend far beyond the meadows themselves, as *P. oceanica* detritus facilitate the exchange of OC between marine ecosystems (Heck et al., 2008).

Local threats for *P. oceanica* meadows in the Mazarrón continental margin include boat anchoring, aquiculture facilities, and coastal infrastructures and industries such as mining or the leisure and tourism-related ones (Ruiz and Romero, 2001, 2003; Ruiz et al., 2009b, 2010, 2015; Baza-Vara et al., 2022). The harmful effects of coastal pressures on the inner shelf led to the loss of at least 2.75 km^2 of *P. oceanica* meadows off Portman Bay (Fig. 3.18) (Ruiz et al., 2015) because of persistent water turbidity and direct burial due to the dumping of the mine tailings (Baza-Varas et al., 2022) from 1957 to 1990 (Oyarzun et al., 2013). The loss of *P. oceanica* meadows extension in nearby coastal areas likely resulted in a reduction of the plant debris ready to be exported from source areas in the inner shelf to the broader margin and beyond by marine currents. This is a plausible explanation for the progressive impoverishment of *P. oceanica* detritus in the exported material, especially after the early 2000s (Figs. 3.22, 3.25b). Since the functioning of cross shelf transport in several Mediterranean margins has been observed to be the result of repeated cycles of resuspension and deposition (Heussner et al., 2006; Tesi et al., 2008; Gentil et al., 2022), it is likely that material from the shelf was gradually transferred from the inner to the outer shelf, and finally towards the slope, triggering a temporal decoupling.

Furthermore, conservation and restoration programs have promoted gains in seagrass coverage at European scale in the last years (de los Santos et al., 2019). The seagrass meadows degradation depends on the convergence of several factors, including environmental and anthropogenic in origin. In the Murcia region, priority habitat protection efforts have led to *P. oceanica* meadows now covering an impressive 92.8% of their total area (Ruiz et al., 2015). This covering is attributed to the establishment of artificial reefs in the 1990s, aimed at safeguarding seagrass meadows from the detrimental impacts of trawl fishing (Ruiz et al., 2015). Additionally, significant contributions to this achievement can be attributed to measures implemented in 2006 under the EU Habitats Directive (CE nº 1967/2006) (Ruiz et al., 2015) (Fig. 3.25). Therefore, conservation measures encompassing the control of activities that harm *P. oceanica* meadows looks as another plausible explanation or a complementary factor for the lessening of vegetal litter export far seaward, as recorded at 1,000 m depth in Escombreras Canyon.

3.3.6. Conclusions

The characterization of OC and TN in particle fluxes and sediments in the Escombreras Canyon demonstrates that most OM reaching the canyon floor has a marine origin. However, the presence of enhanced lignin and cutin biomarkers in settling particles and canyon floor sediments further proves the off-shelf export of recalcitrant OC. In this regard, the utilization of lignin phenols together with other biomarkers ratios and $\delta^{13}C_{OC}$ has provided valuable insights on the contribution from recalcitrant OC

Our results demonstrate that part of the blue carbon produced in coastal areas is transferred away off-shelf and deposited in the canyon, where it gets buried. Storm events are the responsables of the major part of the inputs of OM, lignin and other recalcitrant compunds in the Escombreras Canyon. The storm associated waves and currents carry large amounts of material enriched in *P. oceanica* detritus (up to ~10.5% of the OC content) (Supplementary Table 3.6). For the majority of the study period (March-August 2015), under milder storm events and low-energy conditions, the refractory pool was basically composed of soil-derived OM. Under these conditions, the temporal resolution of our study allows us to detect the contribution of pollen, likely introduced through atmospheric deposition.

Canyon sediments exhibited a higher enrichment in lignin and cutin products. The composition of the sedimentary OC was partly influenced by secondary processes promoting the preservation of refractory compounds. However, our results also reveal changes in the relative contribution of soil-derived OM in respect to *P. oceanica* detritus. This shift is potentially linked to fluctuations in the export of *P. oceanica detritus* in recent years. A drastic reduction in seagrass meadows in the adjacent coastal region, due to direct mine waste discharge, could be a predominant factor influencing the decline in *P. oceanica* detritus export. The findings suggest that human activities can significantly influence the overall content, composition, and distribution of OC in deep-sea environments. Nevertheless, further observations are required to comprehensively elucidate the underlying factors that regulate the carbon stock derived from seagrasses in such settings.

Acknowledgements We extend our sincerely gratitude to the crew of RV Ángeles Alvariño for their invaluable support during our sea-based research efforts. We also acknowledge R. Pedrosa-Pàmies, A. Nogarotto and A. Baza-Varas for their laboratory assistance and insightful input on the manuscript. This research received funding from the NUREIEV (ref. CTM2013-44598-R) and NUREIEVA (ref. CTM2016-75953-C2-1-R) projects. Additionally, the GRC Geociències Marines is financially supported by the Catalan Government's excellence research groups program (ref. 2021 SGR 01195), and M. Tarrés received support through an FPI grant from the Spanish Ministry of Science and Innovation

3.3.7. References

Acosta, J., Fontán, A., Muñoz, A., Muñoz-Martín, A., Rivera, J., Uchupi, E., 2013. The morpho-tectonic setting of the Southeast margin of Iberia and the adjacent oceanic Algero-Balearic Basin. Mar. Pet. Geol. 45, 17–41. doi:10.1016/j.marpetgeo.2013.04.005.

Aller, R.C., Blair, N.E., 2004. Early diagenetic remineralization of sedimentary organic C in the Gulf of Papua deltaic complex (Papua New Guinea): net loss of terrestrial C and diagenetic fractionation of C isotopes. Geochim. Cosmochim. Acta 68, 1815e1825. doi:10.1016/j.gca.2003.10.028.

Apostolaki, E.T., Caviglia, L., Santinelli, V., Cundy, A.B., Tramati, C.D., Mazzola, A., Vizzini, S., 2022. The Importance of Dead Seagrass (Posidonia oceanica) Matte as a Biogeochemical Sink. Front. Mar. Sci. 9:861998. doi: 10.3389/fmars.2022.861998.

Apostolopoulou, M.V., Monteyne, E., Krikonis, K., Pavlopoulos K., Roose, P., Dehairs, F., 2015. n-Alkanes and stable C, N isotopic compositions as identifiers of organic matter sources in Posidonia oceanica meadows of Alexandroupolis Gulf, NE Greece. Mar. Pollut. Bull. 99, 346–355. doi:10.1016/j.marpolbul.2015.07.033.

Arias-Ortiz, A., Serrano, O., Masqué, P., Lavery, P.S., Mueller, U., Kendrick, G.A., Rozaimi, M., Esteban, A., Fourqurean, J.W., Marbà, N., Mateo, M.A., Murray, K., Rule, M.J., Duarte, C.M., 2018. A marine heatwave drives massive losses from the world's largest seagrass carbon stocks. Nat. Clim. Change 8, 338–344. doi.org/10.1038/s41558-018-0096-y.

Arndt, Sandra, Jørgensen, B.B., LaRowe, D.E., Middelburg, J.J., Pancost, R., Regnier, P., 2013. Quantifying the degradation of organic matter in marine sediments: A review and synthesis, Earth Science Reviews. doi:10.1016/j.earscirev.2013.02.008

Arroyo, M. C., Shadwick, E. H., Tilbrook, B., Rintoul, S. R., & Kusahara, K., 2020. A continental shelf pump forCO2on the Adélie Land coast, East Antarctica. J. Geophys. Res. Oceans,125, e2020JC016302. doi:10.1029/2020JC016302.

Atwood, T.B, Witt, A., Mayorga, J., Hammill, E., Sala, E., 2020. Global Patterns in Marine Sediment Carbon Stocks. Front. Mar. Sci. 7:165. doi:10.3389/fmars.2020.00165.

Bauer, J., E., Cai, W-J., Raymond, P.A., Bianchi, T.S., Hopkinson, C.S., Regnier, P.A.G., 2013. The changing carbon cycle of the coastal ocean. Nature 504, 61. doi:10.1038/nature12857.

Baza-Varas, A., Canals, M., Frigola, J., Cerdà-Domènech, M., Rodés, N., Tarrés, M., Sanchez-Vidal, A., the NUREIEVA-MAR1 shipboard party, Amblas, D., Rayo, X., Soldevila, E., Rivera, J., Lastras, G., Roqué, J., 2022. Multiproxy Characterization of Sedimentary Facies in a Submarine Sulphide Mine Tailings Dumping Site and Their Environmental Significance: the Study Case of Portmán Bay (SE Spain). Sci. Total Environ. 810, 151183. doi:10.1016/j.scitotenv.2021.151183.

Baza Varas, A., 2023. Aplicación de tecnologías avanzadas para la caracterización del depósito de vertidos mineros de la bahía de Portmán, Murcia (España). Universitat de Barcelona, Tesi Doctoral.

Berner, R.A., 1980. Early Diagenesis: A Theoretical Approach. Princeton University Press, Princeton, 241 p.

Bianchi, T. S., 2011. The role of terrestrially derived organic carbon in the coastal ocean: a changing paradigm and the priming effect. Proc. Natl. Acad. Sci. U.S.A. 108, 19473–19481. doi:10.1073/pnas.1017982108.

Bianchi, T.S., Argyrou, M., Chippett, H.F., 1999. Contribution of vascular-plant carbon to surface sediments across the coastal margin of Cyprus (eastern Mediterranean). Org. Geochem. 30, 287-297. doi:10.1016/S0146-6380(99)00016-9.

Bianchi, T.S., Galler, J.J., Allison, M.A., 2007. Hydrodynamic sorting and transport of terrestrially derived organic carbon in sediments of the Mississippi and Atchafalaya Rivers. Estuar. Coast. Shelf Sci. 73, 211–222. doi:10.1016/j.ecss.2007.01.004.

Burdige, D.J., 2007. Preservation of Organic Matter in Marine Sediments: Controls, Mechanisms, and an Imbalance in Sediment Organic Carbon Budgets? Chem. Rev. 107, 467-485. doi.org/10.1021/cr050347q.

Cathalot, C., Rabouille C., Tisnérat-Laborde N., Toussaint, F., Kerhervé, P., Buscail, R., Loftis, K., Sun, M.-Y., Tronczynski, J., Azoury, S., Lansard, B., Treignier, C., Pastor, L., Tesi, T., 2013. The fate of river organic carbon in coastal areas: A study in the Rhône River delta using multiple isotopic ($\delta^{13}C$, $\Delta^{14}C$) and organic tracers. Geochim. Cosmochim. Acta 118, 33–55. doi:10.1016/j.gca.2013.05.001.

Díaz-Almela E. and Duarte C.M., 2008. Management of Natura 2000 habitats. 1120 **Posidonia* beds (*Posidonion oceanicae*). European Commission

de los Santos, C. B., Krause-Jensen, D., Alcoverro, T., Marbà, N., Duarte, C. M., Katwijk, M. M., Pérez, M., Romero, J., Sánchez-Lizaso, J.L., Roca, G., Jankowska, E., Pérez-Lloréns, J.L., Fournier, J., Montefalcone, M., Pergent, G., Ruiz, J.M., Cabaço, S., Cook, K., Wilkes, R.J., Moy, F.E., Muñoz-Ramos G., Trayter, X., Seglar Arañó, D.J., de Jong, Y. Fernández-Torquemada, I. Auby, I., Vergara, J.J., Santos, R., 2019. Recent trend reversal for declining European seagrass meadows. Nat. Commun. 10, 3356. doi:0.1038/s41467-019-11340-4.

Dickens, A., Gudeman, J.A., Gélinas, Y., Baldock, J.A., Tinner, W., Hu, F.S., Hedges, J.I., 2007. Sources and distribution of CuO-derived benzene carboxylic acids in soils and sediments. Org. Geochem. 38, 1256–1276. doi:10.1016/j.orggeochem.2007.04.004.

Dittmar, T., Lara, R.J., 2001. Molecular evidence for lignin degradation in sulfate reducing mangrove sediments (Amazônia, Brazil). Geochim. Cosmochim. Acta 65, 1403e1414. doi:10.1016/S0016-7037(00)00619-0.

Duarte, C.M. and Krause-Jensen, D., 2017. Export from Seagrass Meadows Contributes to Marine Carbon Sequestration. Front. Mar.Sci.4:13. doi: 10.3389/fmars.2017.00013.

Durán, R., Guillén, J., Rivera, J., Lobo, F. J., Muñoz, A., Fernández-Salas, L. M., and Acosta, J., 2018. Formation, evolution and present-day activity of offshore sand ridges on a narrow, tideless continental shelf with limited sediment supply. Mar. Geol. 397, 93-107. doi:10.1016/j.margeo.2017.11.001.

Fabres, J., Tesi, T., Velez, J., Batista, F., Lee, C., Calafat, A., Heussner, S., Palanques, A., Miserocchi, S., 2008. Seasonal and event-controlled export of organic matter from the shelf towards the Gulf of Lions continental slope. Cont. Shelf Res. 28 (15), 1971–1983. doi: 10.1016/j.csr.2008.04.010.

Fry, B. and Sherr, E.B., 1989. δ13C Measurements as Indicators of Carbon Flow in Marine and Freshwater Ecosystems. In: Rundel, P.W., Ehleringer, J.R., Nagy, K.A. (eds) Stable Isotopes in

Ecological Research. Ecological Studies 68. Springer, New York, NY. doi:10.1007/978-1-4612-3498-2_12.

Gentil, M., Estournel, C., Durrieu de Madron, X., Many, G., Miles, T., Marsaleix, P., Berné, S., Bourrin, F., 2022. Sediment dynamics on the outer-shelf of the Gulf of Lions during an onshore storm: an approach based on acoustic glider and numerical modelling. Continent. Shelf Res. 240, 104721. doi:10.1016/j.csr.2022.104721.

González-Correa, J.M., Bayle, J.T, Sánchez-Lizaso, J.L., Valle, C., Sánchez-Jereza, P., Ruiz., J.M., 2005. Recovery of deep Posidonia oceanica meadows degraded by trawling. J. Exp. Mar. Biol. Ecol. 320, 65–76. doi:10.1016/j.jembe.2004.12.032.

Goñi, M.A. and Hedges, J.I., 1995. Sources and reactivities of marine derived organic matter in coastal sediments as determined by alkaline CuO oxidation. Geochim. Cosmochim. Acta 59, 2965e2981. doi:10.1016/0016-7037(95)00188-3.

Goñi, M.A., Monacci, N., Gisewhite, R., Andrea Ogston, A., Crockett, J., Nittrouer, C., 2006. Distribution and sources of particulate organic matter in the water column and sediments of the Fly River Delta, Gulf of Papua (Papua New Guinea). Estuar. Coast. Shelf Sci. 69, 225e245. doi:10.1016/j.ecss.2006.04.012.

Goñi, M.A. and Montgomery, S., 2000. Alkaline CuO oxidation with a microwave digestion system. Lignin analyses of geochemical samples. Anal. Chem. 72, 3116e3121. doi:10.1021/ac991316w.

Goñi, M.A., Nelson, B., Blanchette, R.A., Hedges, J.I., 1993. Fungal degradation of wood lignins: geochemical perspectives from CuO derived phenolic dimers and monomers. Geochim. Cosmochim. Acta 57, 3985–4002. doi:10.1016/0016-7037(93)90348-Z.

Goñi, M.A., Ruttenberg, K.C., Eglinton, T.I., 1997. Source and contribution of terrigenous organic carbon to surface sediments in the Gulf of Mexico. Nature 389 (6648), 275–278. doi:10.1038/38477.

Goñi, M.A, Yunker, M.B, Macdonald, R.W., Eglinton, T.I., 2000. Distribution and sources of organic biomarkers in arctic sediments from the Mackenzie River and Beaufort Shelf. Mar. Chem. 71, 23–51. doi:10.1016/S0304-4203(00)00037-2.

Harmelin-Vivien, M., Loizeau, V., Mellon, C., Beker, B., Arlhac, D., Bodiguel, X., Ferraton, F., Hermand, R., Philippon, X., Salen-Picard, C., 2008. Comparison of C and N stable isotope ratios between surface particulate organic matter and microphytoplankton in the Gulf of Lions (NW Mediterranean). Cont. Shelf Res. 28, 1911–1919. doi:10.1016/j.csr.2008.03.002.

Hedges, J.I., Keil, R.G., 1995. Sedimentary organic matter preservation: an assessment and speculative synthesis. Mar. Chem. 49, 81–115. doi:10.1016/0304-4203(95)00008-F.

Hedges, J.I., Keil, R.G., Benner, R., 1997. What happens to terrestrial organic matter in the ocean? Org. Geochem. 27, 195e212. doi:10.1016/S0146-6380(97)00066-1.

Hedges, J.I., Mann, D.C., 1979. The lignin geochemistry of marine sediments from the southern Washington coast. Geochim. Cosmochim. Acta 43, 1809e1818. doi:10.1016/0016-7037(79)90029-2.

Heck, K. L. Jr., Carruthers, T. J. B., Duarte, C. M., Hughes, A. R., Kendrick, G., Orth, R., et al., 2008. Trophic transfers from seagrass meadows subsidize diverse marine and terrestrial consumers. Ecosystems 11, 1198–1210. doi:10.1007/s10021-008-9155-y.

Hemminga, M.A., Duarte, C.M., 2000. Seagrass Ecology. Cambridge University Press, Cambridge. doi:10.1017/CBO9780511525551.

Heussner, S., Durrieu de Madron, X., Calafat, A., Canals, M., Carbonne, J., Delsaut, N., Saragoni, G., 2006. Spatial and temporal variability of downward particle fluxes on a continental slope: lessons from an 8-yr experiment in the Gulf of Lions (NW Mediterranean). Mar. Geol. 234 (1-4), 63–92. doi:10.1016/j.margeo.2006.09.003.

Heussner, S., Ratti, C., Carbonne, J., 1990. The PPS 3 time-series sediment trap and the trap sample processing techniques used during the ECOMARGE experiment. Cont. Shelf Res. 10 (9-11), 943–958. doi:10.1016/0278-4343(90)90069-X.

Honjo, S., Manganini, S. J., Krishfield, R. A., Francois, R., 2008. Particulate organic carbon fluxes to the ocean interior and factors controlling the biological pump: A synthesis of global sediment trap programs since 1983, Prog. Oceanogr., 76(3), 217– 285. doi:10.1016/j.pocean.2007.11.003.

Houel, S., Louchouarn, P., Lucotte, M., Canuel, R., Ghaleb, B., 2006. Translocation of soil organic matter following reservoir impoundment in boreal systems: implications for in situ productivity. L&O 51, 1497–1513. doi:10.4319/lo.2006.51.3.1497.

Ishiwatari, R., Yamamoto, S., Shinoyama, S., 2006. Lignin and fatty acid records in Lake Baikal sediments over the last 130 kyr: A comparison with pollen records. Org. Geochem. 37, 1787–1802. doi:10.1016/j.orggeochem.2006.10.005.

Kaal, J., Serrano, O., del Río, J.C., Rencoret, J., 2018. Radically different lignin composition in Posidonia species may link to differences in organic carbon sequestration capacity. Org. Geochem. 124, 247–256. doi.org/10.1016/j.orggeochem.2018.07.017.

Kawakami H., 1980. Degradation of lignin-related aromatics and lignins by several pseudomonads. In: Kirk KT, Takayoshi H, Hou-min C (eds) Lignin biodegradation: microbiology, chemistry, and potential applications, vol II. CRC, Boca Raton, p103.

Kiriakoulakis, K., Blackbird, S., Ingels, J., Vanreusel, A., Wolff, G.A., 2011. Organic geochemistry of submarine canyons: The Portuguese Margin. Deep-Sea Res. II 58 (23-24), 2477–2488. doi:10.1016/j.dsr2.2011.04.010.

Klap, V.A., Hemminga, M.A., Boon, J.J., 2000. Retention of lignin in seagrasses: angiosperms that returned to the sea. Mar. Ecol. Prog. Ser. 194, 1-11.

Liu, K.K., Atkinson, L., Quiñones, R.A., Talaue-McManus, L., 2010. Carbon and Nutrient Fluxes in Continental Margins, Global Change – The IGBP Series, 3. Doi:10.1007/978-3-540-92735-8 1.

Liu, J.T., Hunga, J.J., Lin, H.L., Huh, C.A., Lee, C.L., Hsu, R.T., Huang, Y.W., Chu, J.C., 2009. From suspended particles to strata: The fate of terrestrial substances in the Gaoping (Kaoping) submarine canyon. J. Mar. Syst. 76, 417–432. dio:10.1016/j.jmarsys.2008.01.010.Lefebvre, L., Compère, P., Gobert, S., 2023. The formation of aegagropiles from the Mediterranean seagrass Posidonia oceanica (L.) Delile (1813): plant tissue sources and colonisation by melanised fungal mycelium. Mar. Biol. 170, 19. doi:10.1007/s00227-022-04166-0.

Lloret, J. and Marín, A., 2009. The role of benthic macrophytes and their associated macroinvertebrate community in coastal lagoon resistance to eutrophication. Mar. Pollut. Bull. 58, 1827–1834. doi:10.1016/j.marpolbul.2009.08.001.

Lobo, F.J., Ercilla, G., Fernández-Salas, L.M., Gámez, D., 2014. Chapter 11 The Iberian Mediterranean shelves. Geological Society, London, Memoirs 41 (1), 147–170.

Lopez-Fernandez, P., Calafat, A., Sanchez-Vidal, A., Canals, M., Flexas, M.M., Cateura, J., Company, J.B., 2013b. Multiple drivers of particle fluxes in the Blanes submarine canyon and adjacent open slope: results of a year round experiment. Prog. Oceanogr. 118, 95–107. doi:10.1016/j.pocean.2013.07.029.

Maldonado, A., and Zamarreño, I., 1983. Modelos sedimentarios en las plataformas continentales del Mediterráneo español: factores de control, facies y procesos que rigen su desarrollo. Estudio oceanográfico de la Plataforma Continental. Madrid: Proyecto de Investigacion Cooperatiava Hispano-Norteamericana, p.24-83.

Marbà, N., Durate, C.M., Díaz-Almela, E., Terrados, J., Álvarez, E., Martínez, R., Santiago, R., Gacia, E., Grau, A.M., 2005. Direct Evidence of Imbalanced Shoot Population Dynamics in Seagrass (Posidonia oceanica) the Spanish Mediterranean. Estuaries Vol. 28, No. 1, p. 53-62

Marbà, N., Díaz-Almela, E., Duarte, C. M., 2014. Mediterranean seagrass (Posidonia oceanica) loss between 1842 and 2009. Biol. Conserv. 176, 183–190. doi:10.1016/j.biocon.2014.05.024.

Masson, D.G., Huvenne, V.A.I., de Stigter, H.C., Wolff, G.A., Kiriakoulakis, K., Arzola, R.G., Blackbird, S., 2010. Efficient burial of carbón in a submarine canyon. Geology 38, 831–834. doi: 10.1130/G30895.1.

Mateo, M.A. and Romero, J., 1997. Detritus dynamics in the seagrass Posidonia oceanica: elements for an ecosystem carbon and nutrient budget. Mar Ecol Prog Ser 151:43–53.

McLeod, E., Chmura, G.L., Bouillon, S., Salm, R., Björk, M., Duarte, C.M., Lovelock, C.E., Schlesinger, W.H., Silliman B.R., 2011. A blueprint for blue carbon: Toward an improved understanding of the role of vegetated coastal habitats in sequestering CO2. Front. Ecol. Environ. 9, 552–560. Doi:10.1890/110004.

Masatoshi Nakakuni, M., Watanabe, K., Kaminaka, K., Mizuno, Y., Takehara, K., Kuwae, T., Yamamoto, S., 2021. Seagrass contributes substantially to the sedimentary lignin pool in an estuarine seagrass meadow. Sci. Total Environ. 793, 148488. doi:10.1016/j.scitotenv.2021.148488.

Opsahl, S., Benner, R., 1995. Early diagenesis of vascular plant tissues: lignin and cutin decomposition and biogeochemical implications. Geochim. Cosmochim. Acta 59, 4889–4904. doi:10.1016/0016-7037(95)00348-7.

Oyarzun, R., Manteca Martínez, J. I., López García, J. A., and Carmona, C., 2013. An account of the events that led to full bay infilling with sulfide tailings at Portman (Spain), and the search for "black swans" in a potential land reclamation scenario. Sci. Total Environ. 454(455), 245-249. doi:10.1016/j.scitotenv.2013.03.030.

Pasqual, C., Lee, C., Goñi, M., Tesi, T., Sanchez-Vidal, A., Calafat, A., Canals, M., 2011. Use of organic biomarkers to trace the transport of marine and terrigenous organic matter through the southwestern canyons of the gulf of Lion. Mar. Chem. 126 (1–4), 1-12. doi:10.1016/j.marchem.2011.03.001.

Pedrosa-Pamies R, Parinos C, Sanchez-Vidal A, Calafat A, Canals M, Velaoras D, Mihalopoulos N, Kanakidou M, Lampadariou N and Gogou A., 2021. Atmospheric and Oceanographic Forcing Impact Particle Flux Composition and Carbon Sequestration in the Eastern Mediterranean Sea: A Three-Year Time-Series Study in the Deep Ierapetra Basin. Front. Earth Sci. 9, 591948. doi:10.3389/feart.2021.591948.

Prahl, F.G., Ertel, J.R., Goñi, M.A., Sparrow, M.A., Eversmeyer, B., 1994. Terrestrial organic carbon contributions to sediments on the Washington margin. Geochim. Cosmochim. Acta 58, 3035e3048. doi:10.1016/0016-7037(94)90177-5.

Prahl, F., DeLange, G. J., Scholten, S., Cowie, G. L., 1997. A case of post-depositional aerobic degradation of terrestrial organic matter in turbidite deposits from the Madeira Abyssal Plain. Org. Geochem. 27, 141–152. doi:10.1016/S0146-6380(97)00078-8.

Puig, P., Palanques, A., Martín, J., 2014. Contemporary Sediment-Transport Processes in Submarine Canyons. Ann. Rev. Mar. Sci. 6 (1), 53–77. doi:10.1146/annurev-marine-010213-135037.

Reglamento (CE) 1967/2006, 21 de diciembre de 2006 (ref. DOUE-L-2006-82800).

Ruiz, J.M., Belando Torrentes, M.D., García Muñoz, R., Baulaz, Y., Ramos Segura, A., 2013. Informe anual del proyecto: red de seguimiento Posidonia oceánica de la Región de Murcia (2004-2013). Instituto Español de Oceanografía, Centro Oceanográfico de Murcia, Murcia, 122 pp.

Ruiz, J.M., Guillén, J.E., Ramos Segura, A., Otero, M.M., 2015. Atlas de las praderas marinas de España. IEO/IEL/UICN, Murcia-Alicante-Málaga, 681 pp.

Ruiz J.M., Marco Méndez C., Sánchez Lizaso J.L., 2010. Remote influence of off-shore fish farm waste on Mediterranean seagrass (Posidonia oceanica) meadows. Mar. Environ. Res. 69: 118-126. doi:10.1016/j.marenvres.2009.09.002.

Ruiz, J.M., Marín-Guirao, L., Sandoval-Gil, J.M., 2009. Responses of the Mediterranean seagrass Posidonia oceanica to in situ simulated salinity increase. Bot. Mar. 52 (5), 459–470. doi:10.1515/BOT.2009.051.

Ruiz, J.M. and Romero, J., 2001. Effects of fish farm loadings on seagrass (*Posidonia oceanica*) distribution, growth and photosynthesis. Mar. Pollut. Bull. 42, 749-760. doi:10.1016/S0025-326X(00)00215-0.

Ruiz, J.M. and Romero, J., 2003. Effects of disturbances caused by coastal constructions on spatial structure, growth dynamics and photosynthesis of the seagrass *Posidonia oceanica*. Mar. Pollut. Bull. 46, 1523–1533. doi: 10.1016/j.marpolbul.2003.08.021.

Sanchez-Cabeza, J. A., Masqué, P., Ani-Ragolta, I., 1998. 210Pb and 210Po analysis in sediments and soils by microwave acid digestion. J. Radioanal. Nucl. Chem. 227, 19–22. doi:10.1007/bf02386425.

Sánchez-García, L., de Andrés, J.R., Martín-Rubí, J.A., Louchouarn, P., 2009. Diagenetic state and source characterization of marine sediments from the inner continental shelf of the Gulf of Cádiz (SW Spain), constrained by terrigenous biomarkers. Org. Geochem. 40, 184–194. doi:10.1016/j.orggeochem.2008.11.001.

Sanchez-Vidal, A., Canals, M., Calafat, A.M., Lastras, G., Pedrosa-Pàmies, R., Menéndez, M., Medina, R., Company, J.B., Hereu, B., Romero, J., Alcoverro, T., 2012. Impacts on the Deep-Sea Ecosystem by a Severe Coastal Storm. PLoS ONE 7(1): e30395. doi:10.1371/journal.pone.0030395.

Sanchez-Vidal, A., Canals, M., de Haan, W.P., Romero, J., Veny, M., 2021. Seagrasses provide a novel ecosystem service by trapping marine plastics. Sci. Rep. 11:254 doi:10.1038/s41598-020-79370-3.

Sanchez-Vidal, A., Pasqual, C., Kerherve, P., Calafat, A., Heussner, S., Palanques, A., Durrieu de Madron, X., Canals, M., Puig, P., 2008. Impact of Dense Shelf Water Cascading on settling particles in the Western Mediterranean. Geophys. Res. Lett. 35, L05605.

Sanchez-Vidal, A., Pasqual, C., Kerherve, P., Heussner, S., Calafat, A., Palanques, A., Durrieu de Madron, X., Canals, M., Puig, P., 2009. Across margin export of organic matter by cascading events traced by stable isotopes, northwestern Mediterranean Sea. L&O 54, 1488–1500. doi:10.4319/lo.2009.54.5.1488.

Santos, I. R., Burdige, D. J., Jennerjahn, T. C., Bouillon, S., Cabral, A., Serrano, O.,Wernberg, T., Filbee-Dexter, K., Guimond, J.A., Tamborski, J.J., 2021. The renaissance of Odum's outwelling hypothesis in "Blue Carbon" science. Estuar. Coast. Shelf Sci. 255, 107361. doi: 10.1016/j.ecss.2021.107361.

Selvaraj, k., Lee, T.Y., Yang, J.Y.T., Canuel, E.A., Huang, J.C., Dai, M., Liu, J.T., Kao, S.J., 2015. Stable isotopic and biomarker evidence of terrigenous organic matter export to the deep sea during tropical storms. Mar. Geol. 364, 32-42. doi:10.1016/j.margeo.2015.03.005.

Serrano, O., Rozaimi, M., Lavery, P.S., Smernik, R.J., 2020. Organic chemistry insights for the exceptional soil carbon storage of the seagrass *Posidonia australis*. Estuar. Coast. Shelf Sci. 237, 106662. doi:10.1016/j.ecss.2020.106662.

Sheng Hu, F., Hedges, J.I., Gordon, E.S., Brubaker, L.B., 1999. Lignin biomarkers and pollen in postglacial sediments of an Alaskan lake. Geochim. Cosmochim. Acta 63 (9), 1421–1430. doi:10.1016/S0016-7037(99)00100-3.

Tarrés, M., Cerdà-Domènech, M., Pedrosa-Pàmies, R., Rumín-Caparrós, A., Calafat, A., Canals, M., Sanchez-Vidal, A. (2022). Particle fluxes in submarine canyons along a sediment-starved continental margin and in the adjacent open slope and basin in the SW Mediterranean Sea. Prog. Oceanogr. 203, 102783. doi:10.1016/j.pocean.2022.102783.

Telesca, L., Belluscio, A., Criscoli, A., Ardizzone, G., Apostolaki, E.T., Fraschetti, S., Gristina, M., Knittweis, L., Martin, C.S., Pergent, G., Alagna, A., Badalamenti, F., Garofalo, G., Gerakaris, V., Pace, M.L., Pergent-Martini, C., Salomidi, M., 2015. Seagrass meadows (Posidonia oceanica) distribution and trajectories of change. Sci. Rep. 5, 12505. doi:10.1038/srep12505.

Tesi, T., Puig, P., Palanques, A., Goñi, M.A., 2010. Lateral advection of organic matter in cascading-dominated submarine canyons. Prog. Oceanogr. 84, 185-203. doi:10.1016/j.pocean.2009.10.004.

Tesi T., Miserocchi S., Goni M. A. and Langone L., 2007a. Source, transport and fate of terrestrial organic carbon on the western Mediterranean Sea, Gulf of Lions. France. Mar. Chem. 105, 101–117. doi:10.1016/j.marchem.2007.01.005.

Tesi, T., Miserocchi, S., Goñi, M.A., Langone, L., Boldrin, A., Turchetto, M., 2007b. Organic matter origin and distribution in suspended particulate materials and surficial sediments from the western Adriatic Sea (Italy). Estuar. Coast. Shelf Sci. 73, 431e446. doi:10.1016/j.ecss.2007.02.008.

Tesi. T., Langone, L., Goñi, M.A., Turchetto, M., Miserocchi, S., Boldrin, A., 2008. Source and composition of organic matter in the Bari canyon (Italy): Dense water cascading versus particulate export from the upper ocean. Deep-Sea Res. I 55, 813-831. doi:10.1016/j.dsr.2008.03.007.

Thevenot, M., Dignac, M.F., Rumpel, C., 2010. Fate of lignins in soils: A review. Soil Biol. 42, 1200-1211. doi:10.1016/j.soilbio.2010.03.017.

Trevathan-Tackett, S.M., Macreadie, P.I., Sanderman, J., Baldock, J., Howes, J.M., Ralph, P.J., 2017. A Global Assessment of the Chemical Recalcitrance of Seagrass Tissues: Implications for Long-Term Carbon Sequestration. Front. Plant Sci. 8:925. doi: 10.3389/fpls.2017.00925.

Trull, T. W., Bray, S. G., Manganini, S. J., Honjo, S., François R., 2001. Moored sediment trap measurements of carbon export in the Subantarctic and Polar Frontal zones of the Southern Ocean, south of Australia. J. Geophys. Res. 06 (C12), 31,489-31,509. doi:10.1029/2000JC000308.

Vergara, J.J. and Santos, R., 2019. Recent Trend Reversal for Declining European Seagrass Meadows. Nat. Commun. 10, 3356. doi: 10.1038/s41467-019-11340-4.

Verhille, G., Moulinet, S., Vandenberghe, N., Adda-Bedia, M., Le Gal, P., 2017. Structure and mechanics of aegagropilae fiber network. Proc. Natl. Acad. Sci. 114, 4607–4612. doi:10.1073/pnas.1620688114.

Vetter, E.W., 1998. Population dynamics of a dense assemblage of marine detritivores. J. Exp. Mar. Biol. Ecol. 226 (1), 131-161. doi:10.1016/S0022-0981(97)00246-3.

Global Modeling and Assimilation Office (GMAO) (2015), MERRA-2 tavgM_2d_adg_Nx: 2d,Monthly mean, Time-averaged, Single-Level, Assimilation, Aerosol Diagnostics (extended) V5.12.4, Greenbelt, MD, USA, Goddard Earth Sciences Data and Information Services Center (GES DISC), Accessed: [Data Access Date], 10.5067/RZIK2TV7PP38

SIOM, Servicio de Información Oceanográfica de la Región de Murcia. Descripción oceanográfica del litoral de la Región de Murcia. https://siom-murcia.hub.arcgis.com/

www.puertos.es/es-es/oceanografia/Paginas/portus.aspx: Puertos del Estado webpage. From which Hs data have been downloaded.

3.3.8. Supplementary figures and tables

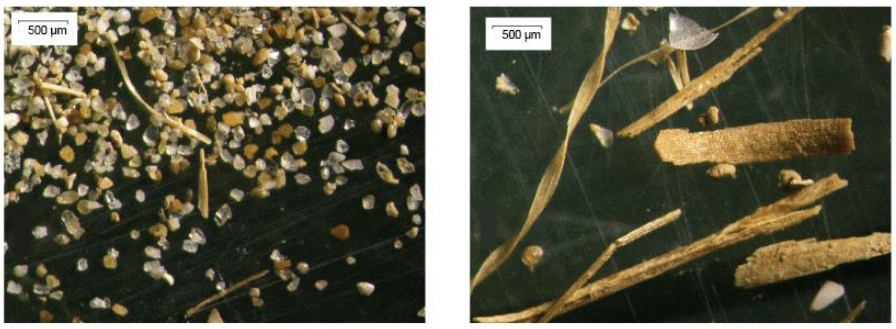

Supplementary Figure 3.3. Plant fibres in sediments observed with a binocular loupe.

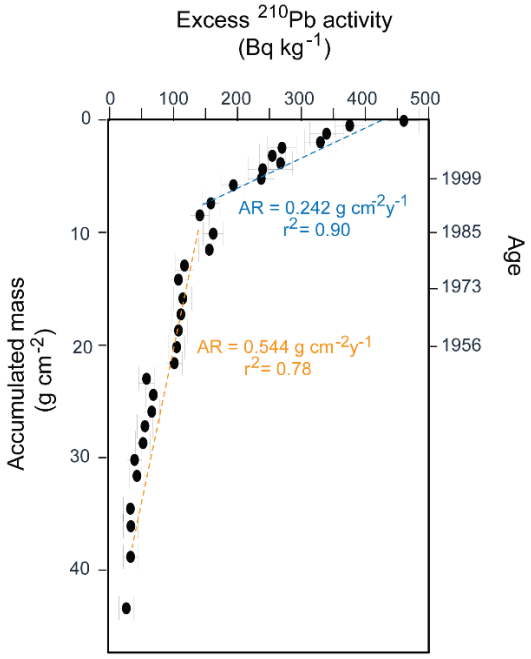

Supplementary Figure 3.4. Sediment core from station ES1000 excess ^{210}Pb activity profile. Two AR trends are considered, one for the uppermost sediments (0-6.5 cm) and a second for the sediments below (6.5-50 cm).

Compound	Symbol
Lignin monomers products (Lig)	
Vanillyl phenol (V)	
Vanillin	Vl
Acetovanillone	Vn
Vanillic acid	Vd
Syringyl phenol (S)	
Syringealdehyde	Sl
Acetosyringone	Sn
Syringic acid	Sd
Cinnamyl phenol (C)	
p-coumaric acid	pCd
Ferulic acid	Fd
Benzoic acids products (B)	
3,5-dihydroxybenzoic acid	3,5-Bd
Cutin products (Cut)	
16-hydroxyhexadecanoic acid	ω-C16
hexadecanedioic acid	C16DA
x,16-dihydroxyhexadecaonic acid	x,ω-C16 x=8/9/10
x-hydroxyhexadecanedioic acid	x-C16DA x=7/8

Supplementary Table 3.3. List of analysed compounds and their respective symbols.

	TN (%)	TOC (%)	d13C (‰)	TN/OC	Cutin	Λ_8	3,5-Bd
TN (%)	1.00						
TOC (%)	**0.78**	1.00					
d13C (‰)	-0.17	0.15	1.00				
TN/OC	0.12	-0.53	-0.41	1.00			
Cutin	-0.32	-0.62	-0.03	0.61	1.00		
Λ_8	-0.55	**-0.70**	-0.01	0.41	**0.92**	1.00	
3,5-Bd	-0.49	**-0.83**	-0.29	0.68	**0.90**	**0.88**	1.00

Supplementary Table 3.4: Correlation coefficient r (Pearson) of settling particles in ES1000. Underlined values in bold are those significant at level $p < 0.05$. Cutin, lignin and 3,5-Bd compounds in (mg/100mg OC).

	TN (%)	TOC (%)	d13C (‰)	TN/OC	Cutin	Lignin	3,5-Bd
TN (%)	1.00						
TOC (%)	0.52	1.00					
$d^{13}C$ (‰)	-0.01	**0.71**	1.00				
TN/OC	0.45	-0.52	**-0.71**	1.00			
Cutin	-0.19	-0.11	0.15	-0.06	1.00		
Lignin	-0.41	-0.28	0.10	-0.12	**0.77**	1.00	
3,5-Bd	-0.32	-0.61	-0.27	0.30	0.30	**0.74**	1.00

Supplementary Table 3.5: Correlation coefficients r (Pearson) for canyon floor sediments in station ES1000. Underlined values in bold are those significant at level $p < 0.05$. Cutin, lignin and 3,5-Bd compounds in (mg/100mg OC).

Trap cup ID	OC_{Pos}	OC_{Marine}	OC_{Soil}	OC_{Soil}/OC_{Pos}	Core depth (cm)	OC_{Pos}	OC_{Marine}	OC_{Soil}	OC_{Soil}/OC_{Pos}
	%	%	%			%	%	%	
ES1000-1	11	58	32	3	0.25	11	65	25	2.3
ES1000-2	1	75	24	>10	1.25	9	63	28	3.3
ES1000-3	3	68	29	>10	3.35	11	68	21	2.0
ES1000-4	1	64	35	>10	6.5	15	71	14	1.0
ES1000-5	1	64	35	>10	8.5	20	64	16	0.8
ES1000-6	2	66	32	>10	10.5	27	36	37	1.4
ES1000-7	-	-	-	-	12.5	23	50	28	1.2
ES1000-8	-	-	-	-	15.5	15	57	28	1.8
ES1000-9	-	-	-	-	17.5	20	50	30	1.5
ES1000-10	-	-	-	-	21.5	18	62	20	1.1
ES1000-11	1	66	33	>10	25.5	21	54	25	1.2
ES1000-12	1	68	31	>10	34.5	20	51	29	1.4
					39.5	31	33	36	1.2
					42.5	25	40	35	1.4
					46.5	34	29	37	1.1
					50.5	20	52	28	1.4

Supplementary Table 3.6. Contribution of *P. oceanica* litter (f_{POS}), marine phytoplankton (f_{MAR}) and soil-derived (f_{SOIL}) organic matter (OM) together with the OC_{SOIL}/ OC_{POS} ratio in settling particles (March-August 2015) and sediments from at Escombreras Canyon.

3.4. Pb and Zn pollution in a submarine canyon: the role of a coastal mine tailings deposit and other potential sources

Marta Tarrés[a], Marc Cerdà-Domènech[a], Andrea Baza-Varas[a], Anna Sanchez-Vidal[a], Miquel Canals[a]

[a] GRC Geociències Marines, Dept. Dinàmica de la Terra i de l'Oceà, Facultat de Ciències de la Terra, Universitat de Barcelona, 08028 Barcelona, Spain

Keywords: trace metals, contaminated sediments, lead isotopes, submarine canyon, Mediterranean Sea

3.4.1. Introduction

Human activities have significantly increased the release of trace metals (TM) into the ocean since the start of the Industrial Revolution (Nriagu, 1996), thus affecting their distribution in the marine environment (i.e. Huang and Conte, 2009; Palanques et al., 2020; Migon et al., 2020; Middag et al., 2022). Metal pollutants enter the ocean through river discharges (Elbaz-Poulichet et al., 2001; Roussiez et al., 2012; Resongles et al., 2015), atmospheric deposition that is able to reach open ocean areas (Sandroni and Migon, 2002; Kumar et al., 2014; Baker and Jickells, 2017), and direct dumping of sewage and other types of waste (Di Leonardo et al., 2008; Ramirez-Llodra et al., 2015; Hanebuth et al., 2018).

One of the most severe environmental catastrophes can result from the deliberate dumping of mine wastes (Koski, 2012). Portmán Bay, in southeast Spain, southwestern Mediterranean Sea, serves as a perfect example of environmental impacts caused by mine waste-dumping in coastal and marine environments. There, from 1957 to 1990, 57 million tons of tailings from open pit sulphide mining were directly discharged into the sea through a pipeline on the coast (Oyarzun et al., 2013; Cerdà-Domènech, 2020).

Results from an environmental assessment of Portmán Bay and the adjacent continental shelf initiated in the early 1980s indicated that the metal-rich waste material were filling the horseshoe-shaped original Portmán Bay, also covering unevenly several square kilometres of the continental (Baños Páez, 2012). Some studies focusing on the underwater extension of the mine tailing deposits have provided valuable insight on the geochemical and physical properties, and the behaviour of fluids within the materials (Alorda-Kleinglass et al., 2019; Cerdà-Domènech et al., 2020; Cerdà-Domènech, 2020; Baza-Varas et al., 2022, 2023). These studies have demonstrated high enrichment levels of Fe, Co, Cu, Pb, Zn and As (a metalloid), which tend to decrease upwards towards a centimetres-thick drape of modern sediments. The sedimentation rates of the dumped tailings where calculated by Baza-Varas et al. (2022), who found that they diminished seawards, which is in agreement with the development of an artificial coastal prism. The estimated sedimentation rates ranged from more than 8 to 12 cm yr^{-1} in the intermediate area (shallower than 25 m of water depth) to less than 1 cm yr^{-1} in more distal locations (at about 3 km from the discharge point and at 53 m of water depth) (Baza-Varas et al., 2022). Reworking

of current seafloor sediments, including the uppermost layers of the tailings deposit, occurs driven by currents and waves, especially during major storm (Cerdà-Domènech, 2020; Baza-Varas, 2023).

In the case of Portmán Bay, no one has been looking to the role of the coastal mine tailings deposit there as a potential source of TM and As for the deep continental margin, neither when dumping was ongoing nor afterwards. This represents an important knowledge gap that is necessary to address given the associated potential environmental implications for the broader offshore area. Consequently, the aim of this work is to assess the potential role of the Portmán Bay mine tailings deposit as a source of metals to the adjacent outer continental margin, namely into the nearby Escombreras submarine canyon. To achieve our goal, we examined the profiles of Pb and Zn contents in a 51 cm long sediment core collected in a strategic location, and used Pb stable isotopes to gain insights on the sources and pathways of anthropogenic Pb inputs into the canyon environment. Sedimentary deposits often are good records of past pollution, subsequently allowing to investigating the pollution history of pollutants in various marine environments (e.g. Hung and Hsu, 2004; Garcia-Orellana et al., 2011; Mil-Homens et al., 2013; Palanques et al., 2020). There are numerous examples illustrating the value of stable isotope ratios to identify the pollutant's sources (e.g. Véron et al., 1994; Ferrand et al., 1999; Ayuso et al., 2013; Mil-Homens et al., 2013; Boyle et al., 2014).

3.4.2. Study area

The study area extends from Portmán Bay, in the Murcia province, southeast of Spain, to the middle reach of Escombreras Canyon, 11 km south of the bay's present shoreline (Fig. 3.26). The continental shelf is 7-13 km wide and finishes in a steep slope at about 100-150 m water depth. At the edge of the shelf are promontories that divide the heads of submarine canyons. The Escombreras Canyon is more than 20 km long, extending onto the uppermost continental rise (Acosta et al., 2013). For further details on the broader study area we refer the reader to Tarrés et al. (2022 and 2023).

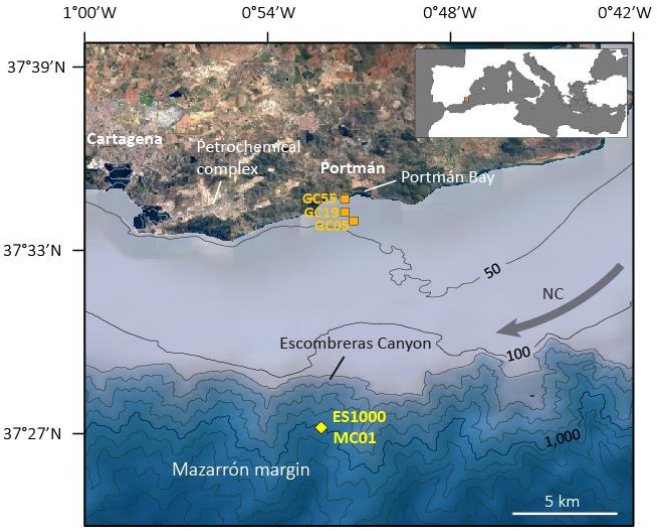

Fig. 3.26: Bathymetric map of a Mazarrón margin segment and the Escombreras Canyon, in the SW Mediterranean Sea. Yellow diamond indicates the location of the mooring station (ES1000) and MC01. Orange squares indicate the location of gravity cores (GC) off Portmán Bay. Theoretical surface circulation (NC: Northern current) is shown.

3.4.3. Methodology

A mooring line equipped with a sequential PPS3 Technicap sediment trap (0.125 m², cylindroconical shape) equipped with 12 trap cups, was deployed at 985 m depth in the Escombreras Canyon (station ES1000). The sampling was performed during the research cruise NUREIEV 1 onboard R/V Ángeles Alvariño. The deployment was planned from March 2015 to March 2016, however, due to a technical failure, the samples collected with the trap cover the period from March 2015 to August 2015. The trap cups were loaded with a 5% (v/v) formaldehyde solution in 0.45 µm filtered seawater buffered with sodium tetraborate. The sediment trap processing methodology is comprehensively detailed by Lopez-Fernandez et al. (2013), following a modified protocol derived from Heussner et al. (1990). More details about the experimental design and particle trap sample processing can be found in Tarrés et al. (2022 and 2023). In the present study we have used two sediment trap samples: ES1000-I-2 (sampling from 1 to 10 April 2015) and ES1000-I-6 (sampling from 16 to 31 May 2015).

The investigated sediment cores were collected at station MC01 (below the mooring ES1000) with a KD Denmark multicorer at 1,002 m depth on the 3rd of March 2015 during the same cruise. One of the various sediment cores obtained was subsampled every 0.5 cm from 0 to 5 cm core depth, and every 1 cm down to the core bottom at 50 cm depth. The subsamples were freeze-dried and homogenized in the laboratory. A second core was stored in a PVC tube for later analysis with an XRF core scanner.

Sediment samples from the submarine mine tailing deposit were acquired with a gravity corer (GC) during the research cruise NUREIEVA-MAR1 (27/06 to 10/07/2018) onboard R/V Ángeles Alvariño. Gravity cores were cut and stored in 1-1.5 length PVC sections at 4-5 °C (Baza-Varas et al., 2022). Three selected cores were used in this study, one recovered close to the

discharge point at 27 m water depth (GC55) and two offshore (GC19 and GC05) at 39 and 42m water depth, respectively. The cores were sliced at 1-cm intervals at the laboratory. Only one centimetre of each sediment core was considered in this study, which were chosen from stratigraphic units corresponding to transitional and massive dumping periods (Baza-Varas et al., 2022).

Trace metals (Fe, Mn, Pb, Zn) in the corresponding sediment core were measured using an Avaatech XRF core scanner at the Corelab laboratory of the Department of Earth and Ocean Dynamics of the University of Barcelona. As and Cu intensity profiles have not been considered because the concentration analysed was lower than the detection limit of the instrument. Before conducting XRF analyses, sections were left at room temperature for 16 hours to minimize water absorption and enhance the XRF signal (Cerdà-Domènech et al., 2020) and were covered with ULTRALENE-SPEX film (4 µm thick). The resolution of XRF measures was set at 2 mm. Excitation conditions for elements with an atomic weight between Al and Fe were configured at 10 kV, 1.0 mA for 10 s. For elements between Ni and Pb, the excitation conditions were set at 30 kV, 1.5 mA with a Pd filter for 50 s.

Some Pb measurements were also close to the detection limit, which involved significant associated errors that were fully taken into account. Uncertainties were less than 2% for Fe, 25% for Mn and 11% for Zn. XRF intensity data in count per second was calibrated to element contents using the linear function defined by Cerdà-Domènech et al. (2020).

Lead quantitative contents and stable isotope ratios were determined with a multicollector inductively coupled plasma mass spectrometer (MC-ICP-MS (from Nu Instruments-AMETEK at *Centres Científics i Tecnològics de la Universitat de Barcelona* (CCiT-UB). The analytical protocol with the total digestion of powdered samples using a mixture of concentrated acids (2.5 ml of HNO_3, 10 ml of HF and 2 ml of $HClO_4$) in a closed system for 24 hours at 95°C. The mixture of acids was then evaporated on a sand bath almost until dryness, and the residue was redissolved in 2 ml of $HClO_4$ and dried again until incipient dryness. The resulting residue was dissolved in 2.5 ml of concentrated HNO_3, transferred into 0.25 ml Teflon vials and evaporated at 120°C. Samples were subsequently dissolved in 2 ml of HBr (0.7N), sonicated for about 10 minutes, and left to evaporate on a hot plate for a minimum of 2 hours at 100°C. Finally, samples were centrifuged to remove any solid residue. 2 ml of sample were afterwards loaded in a column charged with a resin. Before the loading, both the columns and the resin were cleaned and conditioned. Once the sample was introduced into the column, HBr (0.7N) was added in three stages (1+3+1 ml). Next, 1.2 ml of HCl (6N) were added to elute the Pb, which was recovered in a clean vial. This step was repeated 3 times. The extract was evaporated on a hot plate at 90°C and redissolved with 1.4 ml of HNO_3 (2%).

Sediment dating was performed by using ^{210}Pb activities at *Laboratori de Radioactivitat Ambiental de la Universitat Autònoma de Barcelona* (LRA-UAB) (cf. section 3.3). The mean mass accumulation rates (MAR) were inferred from the mean slope of the $^{210}Pb_{xs}$ activitiy profile, using the constant flux: constant sedimentation (CF:CS) model. Sections date were estimated on the basis of average MAR.

3.4.4. Results

3.4.4.1. Age model

The MAR were previously presented in section 3.3 of this Thesis. The profile can be divided in two sections with different sedimentation rates: (i) from the seafloor to 7 cm of the analysed core, characterized by a MAR= 0.242 g cm^{-2} y^{-1}, and (ii) from 7 cm to the bottom of the core, characterized by a MAR=0.544 g cm^{-2} y^{-1}. The average rate was 0.348 ± 0.032 g cm^{-2} y^{-1}. The sedimentation rates increased since 1989 ± 2 (Supplementary Fig. 3.4).

3.4.4.2. Metal contents in sediments

Calibrated XRF core scanner measurements illustrated constant Fe contents (3 ± 0.3 %) along most of the core lenght, with some pronounced spikes pointing to lower contents than the dominating ones at 33.4-34.0, 17.0-17.4 and 10.4-11.4 cm core depth, with 2.6, 2.5 and 1.8%, respectively. There is a sharp increase at the core top (0.5-1.0 cm), peaking at 4.7 % (Fig. 3.27a).

Calibrated XRF core scanner measurements also showed rather stable Mn contents (about 450 µg g^{-1}) along most of the sediment core, except for the top 1 cm, where a sharp increase occurred. Peak values (1,500 µg g^{-1}) were reached at about 0.5 cm core depth (Fig. 3.27a).

Lead contents after calibrated XRF core scanner measurements displayed noticeable shifts, with no clear trends. These oscillations actually correspond to an excess of noise given the closeness to the detection limit defined in the calibration protocol (Cerdà-Domènech et al., 2020) of the values measured (Fig. 3.27a). MC-ICP-MS analyses of discrete sediment samples found the lowest contents (24.4 µg g^{-1}) at the core bottom whereas the highest content (57.1 µg g^{-1}) was identified at 17.5 cm core depth. From there upwards a slightly decreasing trend, down to 34.4 µg g^{-1}, occurred until 6.5 cm core depth. The increasing trend resumed from there upwards till reach 46.6 µg g^{-1} in the seafloor sediments (Table 3.7 and Fig. 3.27 a). .

The Zn profile obtained from calibrated XRF scanner measurements was markedly uneven with an overall upwards increasing tendency. A sharper increase occurred at 18-19 cm. From this depth up to 2 cm core depth values remained in the high range (~120-166 µg g^{-1}) in spite of several oscillations (e.g. between 10.0 and 11.0 cm core depth). The uppermost levels atop of 2 cm core depth displayed a decreasing trend with values in the 73-115 µg g^{-1} range, with seafloor values close to those presented in Tarrés et al. (2023), reaching 116 µg g^{-1} (Fig. 3.27a).

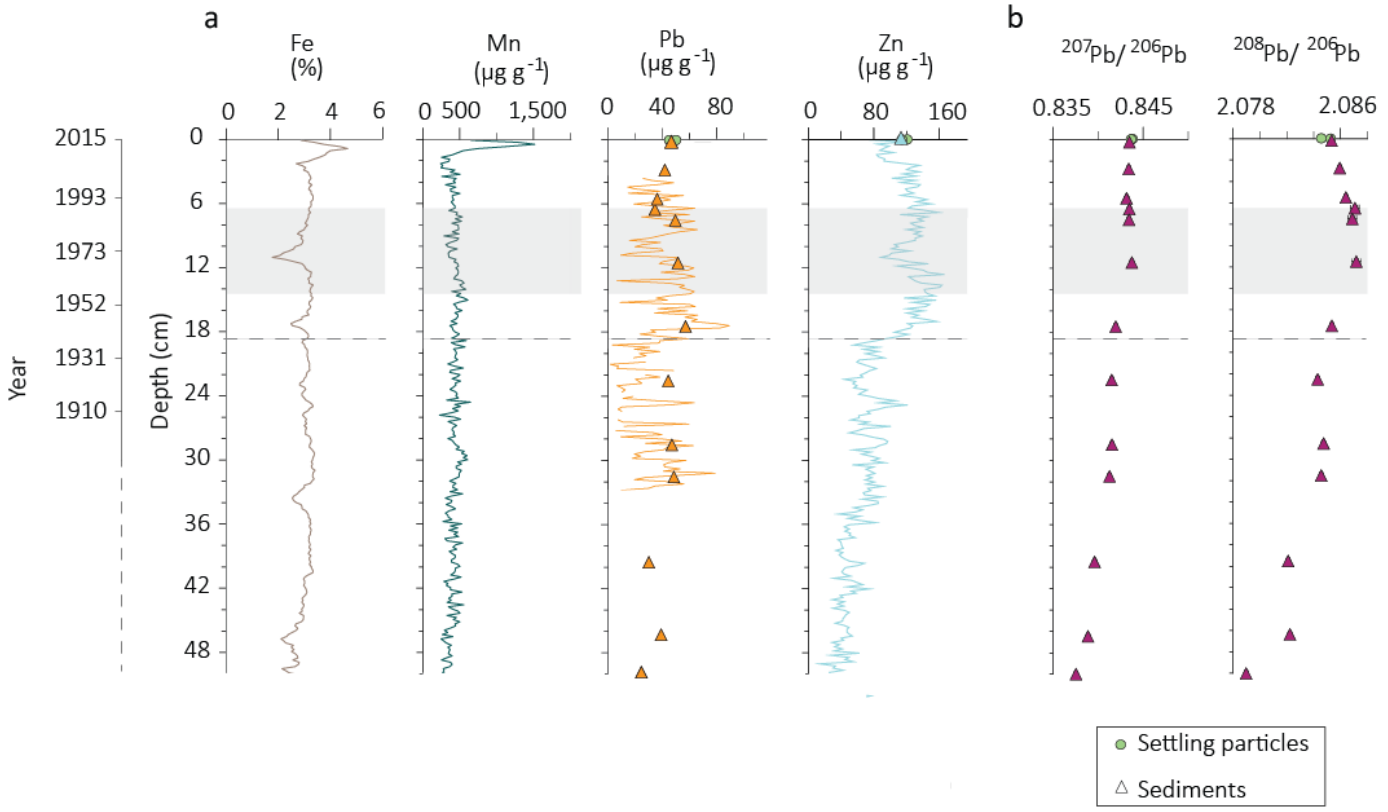

Figure 3.27. (a) Fe, Mn, Pb and Zn profiles in a sediment collected nearby the mooring station ES1000 in the Escombreras Canyon, as obtained after XRF core scanner measurements (continuous coloured lines), together with the results of multicollector inductively coupled plasma mass spectrometry analysis of Pb contents indiscrete sediment samples (triangles). Pb and Zn contents in seafloor sediments (red and green triangles) and settling particles (green circles) from Tarrés et al. (2023) are also shown. **(b)** $^{207}Pb/^{206}Pb$ and $^{208}Pb/^{206}Pb$ ratios in core sediment samples (grey triangles) and settling particles (green circles) from moored particle traps. The grey band shows the mine tailings disposal period (1957-1990) in Portmán Bay. The dashed line shows the increase of Pb and Zn contents during the mid-1940s. The age model shown on the left of the plot was derived from the CF:CS model.

3.4.4.3. Lead isotopic composition

The stable isotope ratios of Pb in the sediments ranged from 0.838 to 0.844 for $^{207}Pb/^{206}Pb$, and 2.079 to 2.085 for $^{208}Pb/^{206}Pb$ (Table 3.7). Both values augmented from the core bottom upwards, peaking at 11.5 cm, 7.5 cm, and 6.5 cm core depth. The $^{207}Pb/^{206}Pb$ ratio was roughly constant in the shallower samples (0-6.5 cm core depth). In contrast, the $^{208}Pb/^{206}Pb$ ratio diminished gradually from 6.5 cm to 0.25 cm, with a value of 2.0853 ± 0.0002 at the canyon floor (Fig. 3.27b). The two settling particle samples displayed $^{207}Pb/^{206}Pb$ ratios very close to those from canyon floor sediments (0.8436-0.8438 ± 0.0001). The ratio $^{208}Pb/^{206}Pb$ also showed values similar to the sediments for sample ES1000-I-6 (2.0853± 0.0002), with sample ES1000-I-2 being slightly less radiogenic (2.0846± 0.0002) (Table 3.7 and Fig. 3.27b).

When normalized for ^{204}Pb, the ratios range from 18.567 to 18.720 for $^{206}Pb/^{204}Pb$, 15.663 to 15.678 for $^{207}Pb/^{204}Pb$, and 38.699 to 38.915 for $^{208}Pb/^{204}Pb$ (Table 3.7).

Pb stable isotope ratios did not exhibit a wide range of values, which is in agreement with those found in other submarine canyons in the western Mediterranean Sea, such as Cap de Creus (Cossa et al., 2014) and Var (Heimbürger et al., 2012), and in the Portuguese margin too (Mil-Homens et al., 2013) (Fig. 3.28). It is to be noted that the total range of variation for both ratios is narrower in Escombreras Canyon than in the other referred canyons for a similar number of samples, i.e. from 15 in the current study to a maximum of 20 in Cascais Canyon at 200 m for $^{207}Pb/^{206}Pb$.

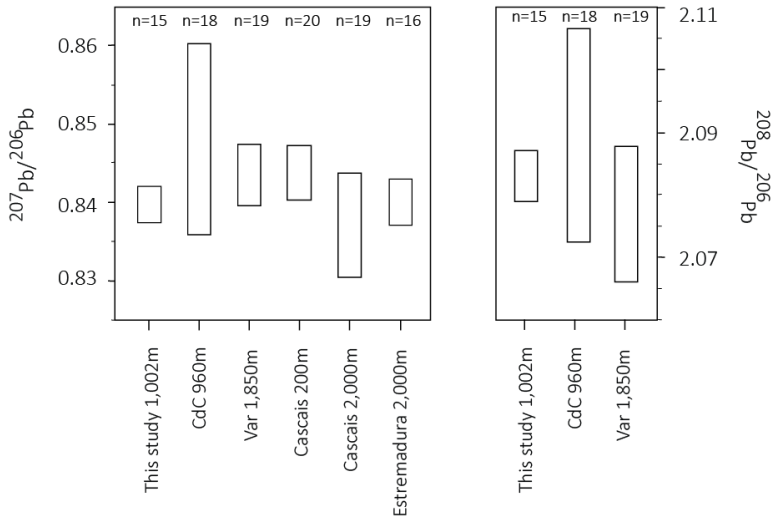

Figure 3.28. Compilation of $^{207}Pb/^{206}Pb$ and $^{208}Pb/^{206}Pb$ ratios in Mediterranean and off Portugal submarine canyons, including Escombreras Canyon, investigated in this study. Data other than the ones in this study are from Cossa et al. (2014), Heimbürger et al. (2012) and Mil-Homens et al. (2013). CdC: Cap de Creus Canyon. n is the number of samples per canyon.

Sample ID	Sample type	Core depth	Pb content (µg kg-1)	$^{207}Pb/^{206}Pb$	±2sd	$^{208}Pb/^{206}Pb$	±2sd	$^{206}Pb/^{204}Pb$	±2sd	$^{207}Pb/^{204}Pb$	±2sd	$^{208}Pb/^{204}Pb$	±2sd
Cruise NUREIEV-I (13 to 24 March 2015)													
ES1000-I-2	Settling particles		44.48*	0.8436	0.0001	20.846	0.0002	185.666	0.0028	156.632	0.0018	386.993	0.0056
ES1000-I-6	Settling particles		49.97*	0.8438	0.0001	20.853	0.0002	185.657	0.0028	156.649	0.0018	387.104	0.0056
MC01 0-0.5	Sediment	0.25	46.56	0.8435	0.0002	20.853	0.0002	185.724	0.0043	156.646	0.0019	387.258	0.0074
MC01 2.5-3	Sediment	2.75	41.80	0.8434	0.0001	20.859	0.0002	185.741	0.0024	156.650	0.0018	387.409	0.0052
MC01 5-6	Sediment	5.5	36.22	0.8432	0.0001	20.864	0.0002	185.808	0.0024	156.663	0.0018	387.634	0.0052
MC01 6-7	Sediment	6.5	34.38	0.8435	0.0002	20.871	0.0003	185.744	0.0020	156.658	0.0031	387.615	0.0070
MC01 7-8	Sediment	7.5	49.41	0.8434	0.0002	20.869	0.0003	185.703	0.0020	156.617	0.0031	387.489	0.0070
MC01 11-12	Sediment	11.5	51.54	0.8437	0.0002	20.872	0.0003	185.662	0.0028	156.641	0.0032	387.464	0.0075
MC01 17-18	Sediment	17.5	57.10	0.8419	0.0001	20.854	0.0001	186.127	0.0022	156.702	0.0018	388.098	0.0050
MC01 22-23	Sediment	22.5	44.32	0.8415	0.0001	20.843	0.0002	186.209	0.0028	156.689	0.0018	388.068	0.0056
MC01 28-29	Sediment	28.5	46.99	0.8415	0.0001	20.847	0.0002	186.208	0.0028	156.693	0.0018	388.146	0.0056
MC01 31-32	Sediment	31.5	48.46	0.8413	0.0001	20.846	0.0002	186.275	0.0028	156.697	0.0018	388.254	0.0056
MC01 39-40	Sediment	39.5	30.21	0.8396	0.0001	20.821	0.0002	186.689	0.0028	156.735	0.0018	388.660	0.0056
MC01 46-47	Sediment	46.5	38.80	0.8389	0.0001	20.822	0.0001	186.890	0.0022	156.769	0.0018	389.103	0.0051
MC01 50-51	Sediment	50.5	24.42	0.8375	0.0001	20.790	0.0002	187.205	0.0032	156.781	0.0018	389.150	0.0060
Cruise NUREIEVA-MAR1 (27 June to 10 July 2018)													
GC55 87-88	Sediment	87.0-88.0	~400**	0.8375	0.0001	20.843	0.0001	187.241	0.0013	156.814	0.0017	390.218	0.0044
GC19 69-70	Sediment	69.0-70.0	~500**	0.8377	0.0001	20.845	0.0001	187.193	0.0013	156.800	0.0017	390.158	0.0044
GC05 81-82	Sediment	81.0-82.0	~200**	0.8376	0.0001	20.844	0.0001	187.228	0.0013	156.825	0.0017	390.203	0.0044

Table 3.7. Metadata (sample ID, sample type and core depth for sediment samples), and results obtained after their analysis for Pb concentrations and stable isotope ratios, together with the associated errors (2sd). *: data from Tarrés et al. (2023). **: data from Baza-Varas (2023). Note that in addition of sediment samples from one of the MC01 cores, three samples from the same number of GC have considered as well.

The three samples from the submarine extension of the mine tailings deposit in Portmán Bay displayed similar Pb stable isotope ratios: 0.8375-0.8377 for $^{207}Pb/^{206}Pb$, and 2.0843-2.0845 for $^{208}Pb/^{206}Pb$, with differences close to the uncertainty of the measurements (±0.0001) (Table 3.7). These values were also close to those measured onshore in the deposits themselves (Müller et al., 2015), and in the ores mined at Emilia I, Emilia II and Navidad open cut mines (Arribas and Tosdal, 1994) (Fig. 3.29).

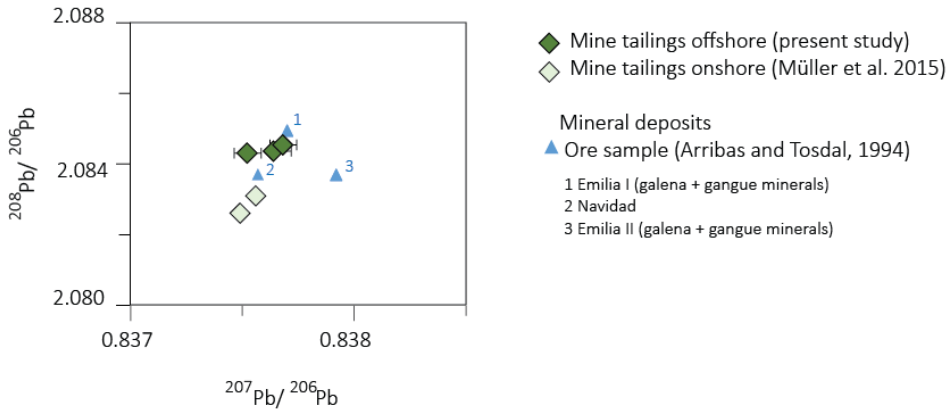

Figure 3.29. $^{207}Pb/^{206}Pb$ and $^{208}Pb/^{206}Pb$ ratios from the submarine extension of the Portmán mine tailings deposit, together with literature data from the onshore deposit (Müller et al., 2015) and the mined ore samples in the Cartagena-La Union mine district (Arribas and Tosdal, 1994).

3.4.5. Discussion

The recorded levels of Pb and Zn in the sediments of Escombreras Canyon, with up to 57.1 µg g^{-1} for Pb and about 160 µg g^{-1} for Zn (Fig. 3.27a), exceed the pre-industrial levels by about 2 and 4-folds, respectively. This evidences that historically the canyon did receive inputs of anthropogenic metals. Indeed, both the particles settling into the canyon —as measured over a 6-months period in 2015— and the canyon floor sediments are moderate enriched in Zn and, to a lesser extent, Pb and Cu (Tarrés et al., 2023). According to the sediments chronology, the increase in Pb and Zn contents in Escombreras Canyon began before the 20th century. However, an obvious increase occurred since the mid-1940s (Fig. 3.27a), i.e. about one decade after the end of the 1936-39 Spanish Civil War, a time marking the onset of modern industrialization in the Cartagena-La Unión area, province of Murcia, which peaked during the 1960s (Andres-Sarasa, 1987). Such a push involved the start of open pit sulphide ore mining in 1945 in the Cartagena-La Unión mining district (Vilar et al., 1985; Andres-Sarasa, 1987; Espejo-Marín et al., 2017) (Table 3.8).

Year	Main industrial activities
1945	Starting of open pit sulphide ore exploitation.
1950	Deployment of the oil refining industry in Cartagena.
1957	Distribution and handling of LPG (storage, filling, and transfer).
1957	Ore processing plant “Lavadero Roberto” in Portmán Bay in operation.
1957	Thermoelectric power plant in 1957.
1960	Zn smelting plant opening in 1960.
1963	Onset of fertilizer industry in 1963.
1966	Modernization of “Santa Lucía” ore smelter facilities in 1966 to obtain Pb-Ag.
1969	Production increase at “Lavadero Roberto” up to 6.000 tons/day.
1980	Further production increase at “Lavadero Roberto” up to 10.000 tons/day.
1990	End of open pit sulphide ore exploitation and closure of “Lavadero Roberto”.
1992	Closure of “Santa Lucía” ore smelter facilities in 1992.
1992	End of part of the production of fertilizers and derivates in 1992 (Enfersa-Cartagena).
1996	Bioethanol production plant in operation in 1996.
1996	Production of strontium salts and derivates starts in 1996.
2001	Leaded gasoline phase-out in EU
2003	Thermoelectric power plant in 2003 starts using natural gas for fueling.
2008	Biodiesel plant in 2008 starts production.
2008	Zn smelting plant in 2008 stops operations.
2021	Leaded gasoline banning in all the Mediterranean region.

Table 3.8. Chronology of the industrialization of the Cartagena-La Unión area after the 1936-39 Spanish Civil War. Key events for the elimination of leaded gasoline are also considered. Naval industry not considered. LPG: liquified petroleum gas. Data compilation from Vilar et al. (1991), Andres-Sarasa (1987), and Espejo-Marín et al. (2017).

Focusing on the sedimentary record within the 1957-1990 period of the mine waste disposal in Portmán Bay, we found that canyon floor sediments exhibited Pb and Zn contents that were one to two orders of magnitude lower than those in the submarine extension of the Portmán deposit according to Cerdà-Domènech (2020) and Baza-Varas et al. (2022). These studies reported values ranging from 50 to 7,300 μg g^{-1} for Zn and 40 to 5,400 μg g^{-1} for Pb, with the highest contents near the discharge point on the coastline and a decreasing gradient in the offshore direction over the inner shelf (Cerdà-Domènech, 2020; Baza-Varas et al,. 2022). This indicates that there was no massive export of contaminated sediments from the Portmán mine tailings coastal deposit to the Escombreras Canyon middle reach.

Stable isotopes can provide insight on the main sources of anthropogenic Pb. Figure 3.30 displays Pb stable isotope ratios ($^{207}Pb/^{206}Pb$ and $^{208}Pb/^{206}Pb$) versus Pb contents. For the entire dataset, Pb isotope ratios appear rather scattered. However, the pre-1950 sediments show a positive correlation with Pb contents ($p<0.05$), with the highest contents associated to more radiogenic values (Fig. 3.30). This suggest a binary mixing between naturally sourced Pb —present in low amounts and with low $^{207}Pb/^{206}Pb$ and $^{208}Pb/^{206}Pb$ ratios— and anthropogenically sourced Pb —present in higher amounts and with a more radiogenic signal. In contrast, the post-1950 subset of samples falls below the pre-1950 regression line and varies within the space, thus suggesting that Pb in these samples derived, in variable proportions, from several anthropogenic sources.

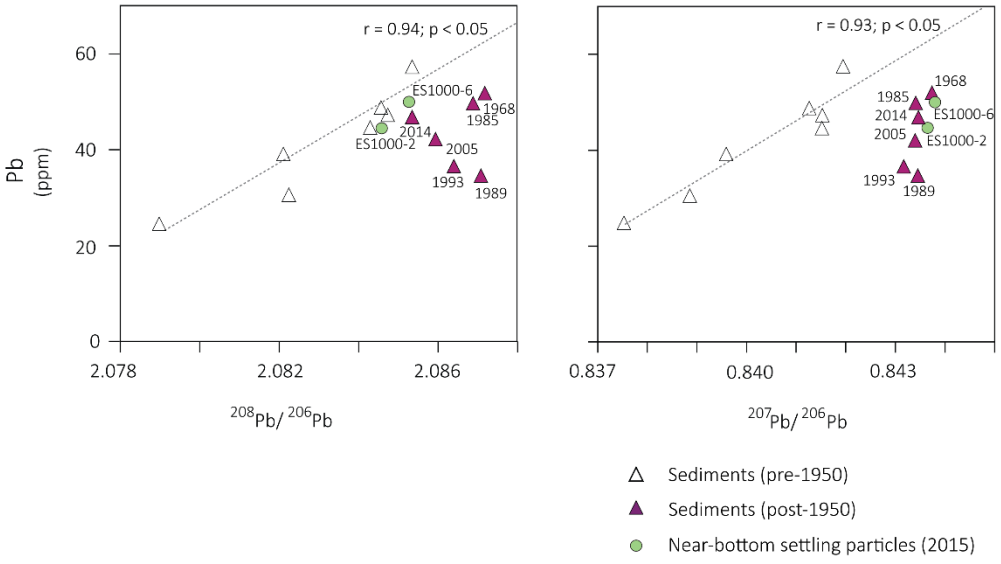

Figure 3.30. Lead stable isotope ratios $^{207}Pb/^{206}Pb$ and $^{208}Pb/^{206}Pb$ versus Pb contents in near-bottom settling particles (green dots) and canyon floor sediments (triangles). Regression lines for pre-1950 sediment samples are also indicated. The year to which every simple corresponds according to the age model is also indicated besides the due symbol.

Figure 3.31 depicts $^{207}Pb/^{206}Pb$ versus $^{208}Pb/^{206}Pb$ ratios, with the results from this study alongside potential sources. Although the limited number of samples available could a priori hamper the temporal assessment of metal sources, especially for the 1957-1990 mine waste dumping period (Oyarzun et al., 2013), the evolution of the ratios reveals a robust temporal pattern.

Sediments dated from 1968 to 1989 present a similar Pb isotope composition, with differences amongst values that are smaller than the analytical error (0.0001) for $^{208}Pb/^{206}Pb$ (Table 3.7). This reflects a rather stable mixture of sources. Sediments deposited after the closure of Lavadero Roberto and the cessation of dumping into the sea in 1990 show a decrease in their radiogenic signature over time (i.e. from 1993 to 2005 to 2014), with low $^{208}Pb/^{206}Pb$ ratios trending towards the isotopic signature of contemporary sources. Such general trend becomes also obvious when considering the sinking particles collected in 2015. Notably, the lowest $^{208}Pb/^{206}Pb$ ratio is observed in the particle trap sample collected in May (Fig. 3.31 and Table 3.7), when the canyon

is disconnected from the coastal area and inner shelf (cf. section 3.3), where the Portmán Bay mine tailings deposit lays.

The isotopic composition of Pb for the natural end-member has been inferred from the deepest sediment sample in the Escombreras Canyon MC01 core, which belongs to the pre-industrial period (Tarrés et al., 2023). The Portmán Bay end-member also represents a local signature, albeit anthropically disposed into the marine environment. $^{207}Pb/^{206}Pb$ ratios are similar to the natural ones found in the canyon, while $^{208}Pb/^{206}Pb$ ratios are slightly higher. The radiogenic composition of the Portmán mine tailings deposit originated a long time back in the geological past, i.e. from metal remobilization events that formed the polymetallic manto-type deposits containing the exploited ores in the Cartagena-La Unión mine district (Manteca and Ovejero, 1992), which were dominated by a Paleozoic metasedimentary source (Arribas and Tosdal, 1994).

The isotopic composition of the sediments accumulated during the period of open pit mining and tailings disposal into the sea (1957-1990) are far from the mixing line between the natural background and the Portmán deposit end-members and are shifted towards higher $^{207}Pb/^{206}Pb$ ratios (Fig. 3.31). Other studies have related the enhancement of $^{207}Pb/^{206}Pb$ ratios in sediments to the contribution of atmospheric aerosols polluted by leaded petrol due to additives such as tetra-ethyl Pb (Ferrand et al., 1999; Komárek et al., 2008; Cossa et al., 2014) or industrial wastes (Richter et al., 2009; Larsen et al., 2012; Cossa et al., 2014; Noble et al., 2015). Thus, it looks likely that the Pb isotopic composition is associated with atmospheric fallout. In the geographic setting of the current study, such enhanced ratios likely relate, at least partly, to industrial activities (Table 3.8) involving different sources, such as oil-refineries, dust releasing open pit mining, ore smelters, or thermoelectric power plants. Indeed, studies carried out near highly polluted areas onshore, such as the Escombreras petrochemical complex (Gabarrón et al., 2017), some mining-impacted areas including Gorguel Bay, just under 2 km west of Portmán Bay, and tailings ponds at short distance from shore (Blondet et al., 2019), reported Pb and Zn enrichments in topsoils and dust. Another likely source of atmospheric Pb in the region was the widespread usage of leaded gasoline, till it was definitively prohibited in the EU in 2001 following several years of progressive reduction (Von Storch et al., 2003). However, in some non-EU Western Mediterranean countries, the use of leaded gasoline did not cease totally till very recent dates, as is the case of Algeria where the last stockpile of leaded gasoline was emptied in a refinery in July 2021 (UNEP, 2021). In broad terms, European gasoline had a composition originating from ore deposits in Australia (the most significant deposit being Broken Hill, characterized by high $^{207}Pb/^{206}Pb$ ratios) (Fig. 3.31a; Komárek et al., 2008). Leaded gasoline was a main contributor to anthropogenic Pb pollution in atmospheric aerosols within Spanish cities (Fig. 3.31a; Bollhöfer and Rosman, 2001).

Since the local atmospheric particulate fallout isotopic signature is unknown, we assume that the isotopic signatures from the European industry are representative of the region where our study area is. Given the wide range of Pb sources, emissions from European industries show mixed values (Komárek et al., 2008 and references therein). Some studies have approached them by using the fly ashes from refuse incinerators (Monna et al., 1997; Hansmann and Köppel, 2000; Richter et al., 2009), as their isotopic composition, with a $^{206}Pb/^{207}Pb$ ratio of 1.149±0.004, is

considered an average for Pb industrial sources (Monna et al., 1997). Three end-member mixing models can be constructed as follows:

$$(^{208}Pb/^{206}Pb)_{sample}=(^{208}Pb/^{206}Pb)_1 \times f_1 + (^{208}Pb/^{206}Pb)_2 \times f_2 +(^{208}Pb/^{206}Pb)_3 \times f_3 \quad [3.12]$$

$$(^{207}Pb/^{206}Pb)_{sample}=(^{207}Pb/^{206}Pb)_1 \times f_1 + (^{207}Pb/^{206}Pb)_2 \times f_2 +(^{207}Pb/^{206}Pb)_3 \times f_3 \quad [3.13]$$

$$f_1+f_2+f_3=1 \quad [3.14]$$

where 1, 2, 3 represent the potential sources and f_1, f_2 and f_3 are their relative contributions.

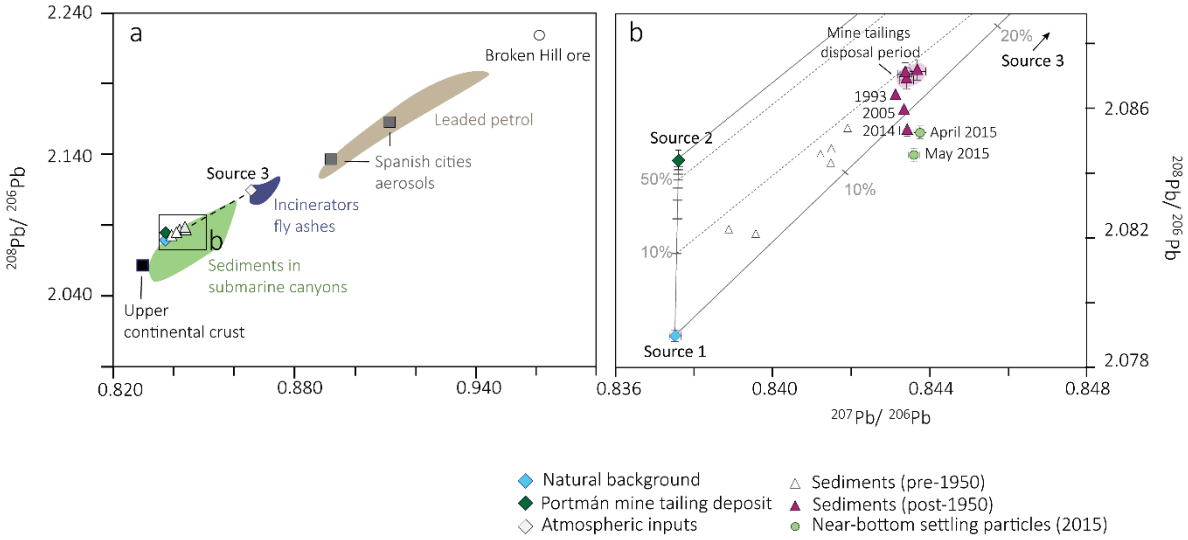

Figure 3.31 (a-b) Lead three-isotope plots for canyon floor sediments and near-bottom settling particles from Escombreras Canyon together with possible end-members: natural background, the mine tailings deposit in Portmán Bay, and atmospheric inputs from industries (namely, incinerators fly ashes following Monna et al., 1997). Literature data on Pb sources are from Millot et al. (2004) for the upper continental crust; Heimbürger et al. (2012), Mil-Homens et al. (2013), Cossa et al. (2014) for sediments from other Mediterranean and Atlantic submarine canyons; Monna et al. (1997), Richter et al. (2009) and references therein for incinerator fly ashes and leaded petrol; Bollhöfer and Rosman (2001) for aerosols in Spain; and Komárek et al. (2008) for the Broken Hill ore. Sediment samples from the mine tailings disposal period in the Escombreras Canyon are embedded in a pink area, whereas sediment and settling particle samples from the post dumping period are within a green area with ages also indicated. The ticks indicate the contribution (in percentage) of the anthropogenic end-members to the resulting mixtures.

Most of our samples fall near the mixing line between the atmospheric and the natural background sources in the three end-members mixing model, whereas the contribution of anthropogenic Pb from the Portmán Bay mine tailings deposit clearly has a smaller weigth than atmospheric inputs (Fig. 3.31b). According to Palanques et al. (2008), this could result from a dilution process of the contaminated sediments after mixing with uncontaminated sediments during across shelf transport towards de submarine canyon. Or it could simply be that currents do not transport particles derived from the inner shelf mine tailings towards the outer shelf and

canyon head. This view is supported by an earlier study by Pauc and Thibault (1976) on sedimentary dynamics in the vicinity of Portmán Bay, which indicated that wave and current directions favoured the redistribution of the tailings to the east along the coast and into the bay itself. The later is strongly supported by evidence, as the original horseshoe-shaped Portmán Bay is completely silted up by the tailings (Fig. 3 in Baza-Varas et al., 2022). It should be also noted that the decrease in $^{208}Pb/^{206}Pb$ ratios was concomitant with a diminishment of sediment accumulation rates in the Escombreras Canyon in 1989 ± 2, i.e. by the end of the dumping period in Portmán Bay. Under these conditions there was less material available for offshore transport by currents. Plumes of suspended particles fed by the dumping of tailings in Portmán Bay have been documented by aerial photography (Baza-Varas, 2023), but to date there was no evidence that such plumes were able to reach the Escombreras Canyon. Consequently, we suggest that suspensate plumes occurring during the 1957-1990 dumping period in Portmán Bay attained Escombreras Canyon at least occasionally, likely in a diluted form. It is also plausible that the nepheloids had lost a substantial part of their Pb loading before arriving at the Escombreras Canyon.

Lead tends to remain in particulate form in seawater under normal conditions (Shen and Boyle, 1988) and settles to the seafloor rather quickly, which favours accumulation near the entry point. A study by Alorda-Kleinglass et al. (2019) concluded that dissolved TM introduced into the coastal sea from the subaerial part of the Portmán tailings deposit rapidly precipitate as iron hydroxides, effectively removing the metals from the water column. In the case of Zn, though it can also bind to sedimentary particles and then to sediments, a higher proportion remains in dissolved form, allowing that metal traveling to greater distances from the dumping site under the action of the prevailing currents before deposition. Therefore, lateral transport can be highly significant for Zn and, possibly, other TM.

A two-vessel bottom trawling experiment over the submarine extension of the mine tailings deposit reported in Bourrin et al. (2021) demonstrated a temporary concentration surge for Fe, As and Pb in the water column particulate load immediately after bottom disturbance. The trawling-induced anomaly persisted for at least 3 hours following the artificial resuspension event. In contrast, Zn contents in water column particles did not change significantly after the resuspension event, which was attributed to its quick dissolution in the water column. Hence, the decoupling between Pb and Zn transfer pathways must be fully taken into account.

The $^{208}Pb/^{206}Pb$ ratios diminishing in recent years (Fig. 3.31b and Fig. 3.27), could also reflect a change in the Pb isotope signatures of the industry, resulting from the stop of mining-derived Pb emissions and dust resuspension in open-pit mine operations, and from better practices in terms of emissions by other Pb-releasing industries (Pacyna et al., 2007), altogether with the supression of leaded gasolines and the associated progressive effect on air qualiy (Migon et al., 2008; Heimbürger et al., 2010). The isotopic composition of sediments after the dumping period differs significantly from that of materials found in the Portman deposit, supporting the idea that most of the Pb comes from the atmospheric inputs. As mentioned before, the experiment conducted by Bourrin et al. (2021) demonstrates a clear connection between Pb and As in water column particles. However, the assessment of particle flux contamination levels in the canyon during 2015 revealed a moderate Pb enrichment

without a corresponding increase in As (Tarrés et al., 2023). This finding strengthens the argument for other transfer pathways.

3.4.6. Conclusions

The results described above allow to conclude that: (i) sediments polluted with Pb and Zn accumulated in Escombreras Canyon from the pre-industrial period, particularly intensifying after the 1940s; (ii) since the start of dumping of mine tailings in Portmán Bay, the accumulation of Pb and Zn in the Escombreras Canyon was rather small compared to the metal levels in the coastal area; (iii) the mining and industry sourced Pb contribution arriving by atmospheric transport to the canyon was certainly more relevant than the one from Portmán Bay; (iv) aerial Pb inputs were likely sourced from various origins, including leaded gasolines, mining-derived Pb emissions and dust resuspension in open-pit mine operations, among others. The decline in this input over time can be attributed to shifts in the region's economic activities and regulatory policies on metal emissions by the EU.

Acknowledgements This work was supported by NUREIEV (ref. CTM2013-44598-R) and NUREIEVA (ref. CTM2016-75953-C2-1-R) projects. We thank the crew of RV Ángeles Alvariño for their invaluable support during our sea-based research efforts. We also thank Dr. E. Paredes and Dra. E. Garcia (Dept. Dinàmica de la Terra i de l'Oceà, UB) and F. Menéndez (CCiT-UB) for their laboratory assistance. Isotopic analyses have been performed at LIRA (UB) and at CCiT-UB. Additionally, the GRC Geociències Marines is financially supported by the Catalan Government's excellence research groups program (ref. 2021 SGR 01195), and M. Tarrés received support through an FPI grant from the Spanish Ministry of Science and Innovation

3.4.7. Bibliography

Acosta, J., Fontán, A., Muñoz, A., Muñoz-Martín, A., Rivera, J. et al., 2013. The morpho-tectonic setting of the Southeast margin of Iberia and the adjacent oceànic Algero-Balearic Basin. Mar. Pet. Geol. 45, 17–41. Doi: 10.1016/j.marpetgeo.2013.04.005.

Alorda-Kleinglass, A., Garcia-Orellana, J., Rodellas, V., Cerdà-Domènech, M., Tovar- Sánchez, A. et al., 2019. Remobilization of dissolved metals from a coastal mine tailing deposit driven by groundwater discharge and porewater exchange. Sci. Total Environ. 688, 1359–1372. Doi: 10.1016/j.scitotenv.2019.06.224.

Andres-Sarasa, J.L., 1987. La industrialización portuaria de Cartagena: su proceso y perspectivas. Anales de Historia Contemporánea, 6, 201-222.

Arribas, A. and Tosdal, R., 1994. Isotopic composition of Pb in ore deposits of the Betic Cordillera, Spain: Origin and relationship to other European deposits. Economic Geology 89, 1074-1093.

Ayuso, R.A., Foley, N.K., Seal II, R.R., Bove, M., Civitillo, D. et al., 2013. Lead isotope evidence for metal dispersal at the Callahan Cu–Zn–Pb mine: Goose Pond tidal estuary, Maine, USA. J. Geochem. Explor. 126–127, 1–22. Doi: 10.1016/j.gexplo.2012.12.013.

Baker, A.R. and Jickells, T.D., 2017. Atmospheric deposition of soluble trace elements along the Atlantic Meridional Transect (AMT). Prog. Oceanogr. 158, 41-51. Doi: 10.1016/j.pocean.2016.10.002.

Baños Páez, P. 2012. Recorrido histórico sobre la degradación de la Bahía de Portmán. Documentos de Trabajo de Sociología Aplicada 1 [consultado en https://revistas.um.es/dtsa/article/view/152751].

Baza-Varas, A., 2023. Aplicación de tecnologías avanzadas para la caracterización del depósito de vertidos mineros de la bahía de Portmán, Murcia (España). Universitat de Barcelona, PhD Thesis, 244 p.

Baza-Varas, A., Canals, M., Frigola, J., Cerdà-Domènech, M., Rodés, N. et al., 2022. Multiproxy characterization of sedimentary facies in a submarine sulphide mine tailings dumping site and their environmental significance: the study case of Portmán Bay (SE Spain). Sci. Total Environ. 810, 151183. Doi: 10.1016/j.scitotenv.2021.151183.

Baza-Varas, A., Roqué-Rosell, J., Canals, M., Frigola, J., Cerdà-Domènech, M. et al., 2023. As and S speciation in a submarine sulfide mine tailings deposit and its environmental significance: The study case of Portmán Bay (SE Spain). Sci. Total Environ. 882, 163649. Doi: 10.1016/j.scitotenv.2023.163649.

Blondet, I., Schreck, E,. Viers, J., Casas, S., Jubany, I. et al., 2019. Atmospheric dust characterisation in the mining district of Cartagena-La Unión, Spain: Air quality and health risks assessment. Sci. Total Environ. 693, 133496. Doi: 10.1016/j.scitotenv.2019.07.302.

Bollhöfer, A. and Rosman, K.J.R., 2000. Isotopic source signatures for atmospheric lead: the Northern Hemisphere. Geochim. Cosmochim. Acta 65, 1727–1740. Doi: 10.1016/S0016-7037(00)00630-X.

Bourrin, F., Uusõue, M., Canals, M., Sanchez-Vidal, A., Aubert, D. et al., 2021. Release of particles and metals into seawater following sediment resuspension of a coastal mine tailings disposal off Portmán Bay, Southern Spain. Environ. Sci. Pollut. Res. 1-18. Doi: 10.1007/s11356-021-14006-1.

Boyle, E.A., Lee, J.M., Echegoyen, Y., Noble, A., Moos, S. et al., 2014. Anthropogenic lead emissions in the ocean: the evolving global experiment. Oceanography 27(1), 69–75. Doi: 10.5670/oceanog.2014.10.

Cerdà i Domènech, M., 2020. Fluxos d'aigua subterrània i concentració de metalls en dipòsits marins costaners contaminats: aproximació metodològica i casos d'estudi a la costa mediterrània de la Península Ibèrica. Universitat de Barcelona, PhD Thesis, p.276. http://hdl.handle.net/10803/672444.

Cerdà-Domènech, M., Frigola, J., Sanchez-Vidal, A. and Canals, M., 2020. Calibrating high resolution XRF core scanner data to obtain absolute metal concentrations in highly polluted marine deposits

after two case studies off Portmán Bay and Barcelona, Spain. Sci. Total Environ. 717, 134778. Doi: 10.1016/j.scitotenv.2019.134778.

Cossa, D., Buscail, R., Puig, P., Chiffoleau, J.F., Radakovitch, O. et al., 2014. Origin and accumulation of trace elements in sediments of the northwestern Mediterranean margin. Chem. Geol. 380, 61–73. doi: 10.1016/j.chemgeo.2014.04.015.

Di Leonardo, R., Bellanca, A., Angelone, M., Leonardi, M. and Neri, R., 2008. Impact of human activities on the central Mediterranean offshore: Evidence from Hg distribution in box-core sediments from the Ionian Sea. Appl. Geochemistry 23, 3756–3766. Doi: 10.1016/j.apgeochem.2008.09.010.

Elbaz-Poulichet, F., Braungardt, C., Achterberg, E., Morley, N., Cossa, D. et al., 2001. Metal biogeochemistry in the Tinto–Odiel rivers (Southern Spain) and in the Gulf of Cadiz: a synthesis of the results of TOROS project. Cont. Shelf Res. 21 (18–19), 1961-1973. Doi: 10.1016/S0278-4343(01)00037-1.

Espejo Marín, C., Serrano Martínez, J.M. and Parra Castaño, A., 2017. La industria de refino del petróleo en Cartagena (España), 1950-2015. Anales de Geografía de la Universidad Complutense, 37 (2), 371–398. Doi: 10.5209/aguc.57730.

Ferrand, J.L., Hamelin, B. and Monaco, A., 1999. Isotopic tracing of anthropogenic Pb inventories and sedimentary fluxes in the Gulf of Lions (NW Mediterranean sea). Cont. Shelf Res.19, 23–47. Doi: 10.1016/S0278-4343(98)00070-3.

Gabarrón, M., Faz, A. and Acosta, J.A., 2017. Effect of different industrial activities on heavy metal concentrations and chemical distribution in topsoil and road dust. Environ. Earth Sci. 76, 129. Doi: 10.1007/s12665-017-6449-4.

Garcia-Orellana, J., Cañas, L., Masqué, P., Obrador, B., Olid, C. et al., 2011. Chronological reconstruction of metal contamination in the Port of Maó (Minorca, Spain). Mar. Pollut. Bull., 62 (8): 1632-40. Doi: 10.1016/j.marpolbul.2011.06.013.

Hanebuth, T.J.J., King, M.L., Mendes, I., Lebreiro, S., Lobo, F.J. et al., 2018. Hazard potential of widespread but hidden historic offshore heavy metal (Pb, Zn) contamination (Gulf of Cadiz, Spain). Sci. Total Environ. 637–638, 561–576. Doi: 10.1016/j.scitotenv.2018.04.352.

Hansmaan, W. and Köppel, V., 2000. Lead-isotopes as tracers of pollutants in soils. Chem. Geol. 171 (1–2), 123-144. Doi: 10.1016/S0009-2541(00)00230-8.

Heimbürger, L.E., Cossa, D., Thibodeau, B., Khripounoff, A., Mas, V. et al,. 2012. Natural and anthropogenic trace metals in sediments of the Ligurian Sea (Northwestern Mediterranean). Chem. Geol. 291, 141–151. Doi: 10.1016/j.chemgeo.2011.10.011.

Heimbürger, L.E., Migon, C., Dufoura, A., Chiffoleau, J.F. and Cossa, D., 2010. Trace metal concentrations in the North-western Mediterranean atmospheric aerosol between 1986 and

2008: Seasonal patterns and decadal trends. Sci. Total Environ. 408 (13), 2629-2638. Doi: 10.1016/j.scitotenv.2010.02.042.

Heussner, S., Ratti, C. and Carbonne, J., 1990. The PPS 3 time-series sediment trap and the trap sample processing techniques used during the ECOMARGE experiment. Cont. Shelf Res. 10 (9-11), 943–958. Doi: 10.1016/0278-4343(90)90069-X.

Huang, S. and Conte, M.H., 2009. Source/process apportionment of major and trace elements in sinking particles in the Sargasso sea. Geochim. Cosmochim. Acta 73, 65–90. Doi: 10.1016/j.gca.2008.08.023.

Hung, J.J. and Hsu, C.L., 2004. Present state and historical changes of trace metal pollution in Kaoping coastal sediments, southwestern Taiwan. Mar. Pollut. Bull.49 (11-12), 986-998. Doi: 10.1016/j.marpolbul.2004.06.028.

Komárek, M., Ettler, V., Chrastný, V. and Mihaljevič, M., 2008. Lead isotopes in environmental sciences: A review. Environ. Int. 34, 562–577. Doi: 10.1016/j.envint.2007.10.005.

Koski, R.A., 2012. Metal dispersion resulting from mining activities in coastal environments: a pathways approach. Oceanography 25 (2), 170–183. Doi: 10. 5670/oceanog.2012.53.

Kumar, A., Abouchami, W., Galer, S.J.G., Garrison, V.H., Williams, E. et al., 2014. A radiogenic isotope tracer study of transatlantic dust transport from Africa to the Caribbean. Atmos. Environ. 82, 130-143. Doi: 10.1016/j.atmosenv.2013.10.021.

Larsen, M.M., Blusztajn, J.S., Andersen, O. and Dahllöf, I., 2012. Lead isotopes in marine surface sediments reveal historical use of leaded fuel. J. Environ. Monit. 14, 2893. Doi: 10.1039/c2em30579h.

Lopez-Fernandez, P., Calafat, A., Sanchez-Vidal, A., Canals, M., Flexas, M.M. et al., 2013. Multiple drivers of particle fluxes in the Blanes submarine canyon and adjacent open slope: results of a year round experiment. Prog. Oceanogr. 118, 95–107. Doi: 10.1016/j.pocean.2013.07.029.

Manteca, J.I. and Ovejero, G., 1992. Los yacimientos Zn, Pb, Ag-Fe del distrito minero de La Unión-Cartagena, Bética Oriental. En: Recursos Minerales de España, Madrid: CSIC, p. 1085-1102. http://hdl.handle.net/10317/443.

Middag, R., Rolison, J.M., George, E., Gerringa, L.J.A., Rijkenberg, M.J.A. et al., 2022. Basin scale distributions of dissolved manganese, nickel, zinc and cadmium in the Mediterranean Sea. Mar. Chem. 238, 104063. Doi: 10.1016/j.marchem.2021.104063.

Migon, C., Heimbürger-Boavida, L.E., Dufour, A., Chiffoleau, J.F. and Cossa, D., 2020. Temporal variability of dissolved trace metals at the DYFAMED time-series station. Northwestern Mediterranean. Marine Chemistry 225, 103846. Doi: 10.1016/j.marchem.2020.103846.

Migon, C., Robin, T., Dufour, A. and Gentili, B., 2008. Decrease of lead concentrations in the Western Mediterranean atmosphere during the last 20 years. Atmos. Environ. 42, 815-21. Doi: 10.1016/j.atmosenv.2007.10.078.

Millot, R., Allègre, C.J., Gaillardet, J. and Roy, S., 2004. Lead isotopic systematics of major river sediments: a new estimate of the Pb isotopic composition of the Upper Continental Crust. Chem. Geol. 203,75–90. Doi: 10.1016/j.chemgeo.2003.09.002.

Mil-Homens, M., Blum, J., Canário, J., Caetano, M., Costa, A.M. et al., 2013. Tracing anthropogenic Hg and Pb input using stable Hg and Pb isotope ratios in sediments of the central Portuguese margin. Chem. Geol. 336, 62–71. Doi: 10.1016/j.chemgeo.2012.02.018.

Monna, F., Lancelot, J., Croudace, I.W., Cundy, A.B. and Lewis, J.T., 1997. Pb isotopic composition of airborne particulate material from France and the southern United Kingdom: implications for Pb pollution sources in urban areas. Environ. Sci. Technol. 31, 2277–2286. Doi: 10.1021/es960870+.

Müller, R,. Brey, G. P., Seitz H.M. and Klein, S., 2015. Lead isotope analyses on Late Republican sling bullets. Archaeol Anthropol Sci. 7, 473–485. Doi: 10.1007/s12520-014-0209-0.

Noble, A.E., Echegoyen-Sanz, Y., Boyle, E.A., Ohnemus, D.C., Lam, P.J. et al., 2015. Dynamic variability of dissolved Pb and Pb isotope composition from the U.S. North Atlantic GEOTRACES transect. Deep-Sea Res. II 116, 208–225. Doi: 10.1016/j.dsr2.2014.11.011.

Nriagu, J.O., 1996. A history of global metal pollution. Science 272 (5259), 223–224. Doi: 10.1126/science.272.5259.223.

Oyarzun, R., Manteca Martínez, J.I., López García, J.A. and Carmona, C., 2013. An account of the events that led to full bay infilling with sulfide tailings at Portman (Spain), and the search for “blackswans” in a potential land reclamation scenario. Sci. Total Environ. 454 (455), 245–249. Doi: 10.1016/j.scitotenv.2013.03.030.

Pacyna, E.G.,Pacyna, J.M., Fudala, J., Strzelecka-Jastrzab, E., Hlawiczka, S. et al., 2007. Current and future emissions of selected heavy metals to the atmosphere from anthropogenic sources in Europe. Atmos. Environ. 41(38), 8557–8566. Doi: 10.1016/j.atmosenv.2007.07.040.

Palanques, A., López, L., Guillén, J. and Puig, P. 2020. Trace metal variability controlled by hydrodynamic processes in a polluted inner shelf environment (Besòs prodelta, NW Mediterranean). Sci. Total Environ. 735, 139482. Doi: 10.1016/j.scitotenv.2020.139482.

Palanques, A., Masqué, P., Puig, P., Sanchez-Cabeza, J.A., Frignani, M. et al., 2008. Anthropogenic trace metals in the sedimentary record of the Llobregat continental shelf and adjacent Foix Submarine Canyon (northwestern Mediterranean). Mar. Geol. 248, 213–227. Doi: 10.1016/j.margeo.2007.11.001.

Pauc, H. and Thibault, M., 1976. L'hydrodynamique et la dynamique des matériaux en suspen sion en baie de Portman (Province de Murcie, Espagne). Bull. BRGM IV (3), 211–221 (12th series).

Ramirez-Llodra, E., Trannum, H.C., Evenset, A., Levin, L.A., Andersson, M. et al., 2015. Submarine and deep-sea mine tailing placements: A review of current practices, environmental issues, natural analogs and knowledge gaps in Norway and internationally. Mar. Pollut. Bull. 97 (1–2), 13-35. Doi: 10.1016/j.marpolbul.2015.05.062.

Resongles, E., Casiot, C., Freydier, R., Le Gall, M., Elbaz-Poulichet, F., 2015. Variation of dissolved and particulate metal(loid) (As, Cd, Pb, Sb, Tl, Zn) concentrations under varying discharge during a Mediterranean flood in a former mining watershed, the Gardon River (France). J. Geochem. Explor. 158, 132–142. Doi: 10.1016/j.gexplo.2015.07.010.

Richter, T.O., de Stigter, H.C., Boer, W., Jesus, C.C. and van Weering, T.C.E., 2009. Dispersal of natural and anthropogenic lead through submarine canyons at the Portuguese margin, Deep-Sea Res. I 56, 267-282. Doi: 10.1016/j.dsr.2008.09.006.

Roussiez, V., Heussner, S., Ludwig, W., Radakovitch, O., Durrieu de Madron, X. et al., 2012. Impact of oceanic floods to particulate metal inputs to coastal and deep sea environments: a case study in the Northwest Mediterranean. Cont. Shelf Res. 45, 15–26. Doi: 10.1016/j.csr.2012.05.012.

Sandroni, V. and Migon, C., 2002. Atmospheric deposition of metallic pollutants over the Ligurian Sea: labile and residual inputs. Chemosphere 47, 753–764. Doi: 10.1016/S0045-6535(01)00337-X.

von Storch, H., Costa-Cabral, M., Hagner, C., Feser, F., Pacyna, J. et al., 2003. Four decades of gasoline lead emissions and control policies in Europe: a retrospective assessment. Sci. Total Environ. 311(1-3), 151–176. Doi: 10.1016/s0048-9697(03)00051-2.

Tarrés, M., Cerdà-Domènech, M., Pedrosa-Pàmies, R., Baza-Varas, A., Calafat, A. et al., 2023. Transport and distributions of naturally and anthropogenically sourced trace metals and Arsenic in submarine canyons. Prog. Oceanogr. 218 (1): 103122. Doi: 10.1016/j.pocean.2023.103122.

Tarrés, M., Cerdà-Domènech, M., Pedrosa-Pàmies, R., Rumín-Caparrós, A., Calafat, A. et al., 2022. Particle fluxes in submarine canyons along a sediment-starved continental margin and in the adjacent open slope and basin in the SW Mediterranean Sea. Prog. Oceanogr. 203, 102783 Doi: 10.1016/j.pocean.2022.102783.

UNEP, 2021. Era of leaded petrol over, eliminating a major threat to human and planetary health. https://www.unep.org/news-and-stories/press-release/era-leadedpetrol-over-eliminating-major-threat-human-and-planetary.

Véron, A.J., Church, T.M., Patterson, C.C. and Flegal, A.R., 1994. Use of stable lead isotopes to characterize the sources of anthropogenic lead in North Atlantic surface waters. Geochim. Cosmochim. Acta 58 (15), 3199–3206. Doi: 10.1016/0016-7037(94)90047-7.

Vilar, J.B., Bruno, P.M.E. and Gutiérrez, J.C.F., 1991. La minería murciana contemporánea (1930-1985). Editum, Universidad de Murcia, p.256.

3.5. Resum de resultats

Els resultats d'aquesta Tesi deriven de l'estudi dels fluxos de partícules i els sediments en ambients de canyó submarí, talús obert i al peu del talús adjacent als golfs de Vera i Almeria. Les dades de fluxos corresponen a un cicle anual sencer, des de març de 2015 fins març de 2016. Els resultats assolits es presenten de forma completa en quatre apartats en al cos de la Tesi (**3.1, 3.2, 3.3 i 3.4**). Tot seguit s'exposa un resum dels resultats més destacats.

Principals resultats del subcapítol 3.1: Condicions ambientals i fluxos de partícules

Pel que fa a la columna d'aigua, es fan paleses les notables diferencies en l'estructura i la terbolesa entre els perfils de mitjans i finals de març de 2015 al golf de Vera, realitzats abans i després d'un temporal. En el transsecte realitzat a finals de març seguint el curs alt del canyó d'Escombreras, els valors més alts de terbolesa (3,74 NTU) s'han trobat prop del fons a la plataforma continental externa, disminuint cap a mar obert fins 1,14 NTU en un CTD proper a l'estació ES1000. En el sistema de canyons de Garrucha-Almanzora, el transsecte hidrogràfic realitzat prop de l'estació GA1000 presenta dos increments, el primer (fins a 0,56 NTU) a profunditats majors de les corresponents al límit de plataforma (200 m) i el segon (assolint 0,32 NTU) per sota dels 400 m, estenent-se centenars de metres fins el fons marí. La capa tèrbola pel davall de 400 m també s'ha enregistrat en el transsecte hidrogràfic realitzat a finals d'agost de 2015.

Els TWF (cf. equació 10) obtinguts van des dels 7,3 ± 5,3 g m^{-2} d^{-1} al sistema de Garrucha-Almanzora fins menys d'1 g m^{-2} d^{-1} a les trampes instal·lades al peu del talús (PT2550), evidenciant una limitada capacitat de transferència del material a grans profunditats. Entremig se situen els valors del canyó d'Escombreras, amb un TWF de 4.8 ± 6.5 g m^{-2} d^{-1}, i els del canyó d'Almeria i el talús obert, de menys de 2 g m^{-2} d^{-1}. Els TMF (cf. equació 9) fluctuen considerablement durant el període d'estudi, corresponent els valors més elevats als mesos de març i abril de 2015 als canyons submarins i al talús obert, coincidint amb varis temporals amb forts vents i onatge. Cal notar, però, que a l'estació GA1000 s'han enregistrat increments en els fluxos durant els mesos d'estiu i tardor, amb valors de 10 g m^{-2} d^{-1} a principis de juny de l'any 2015. En canvi, els fluxos s'incrementen lleugerament a l'estació AL1000 durant els mesos de tardor i principis d'hivern de 2016 després d'enregistrar-se varis episodis de descàrrega fluvial i coincidint amb un augment de la producció primària.

Respecte als components principals dels fluxos, la fracció litogénica llimosa predomina a totes les estacions, amb la proporció més gran al canyó d'Almeria (72,4%) i percentatges lleugerament inferiors a la resta d'estacions (60,5-65,0%). Els carbonats són el segon component en percentatge. Per la seva part, el contingut d'òpal i de MO augmenta a les estacions més allunyades del marge. Les ràtios molars CO/N, amb una forquilla de valors d'entre 6,7 i 20,3, indiquen una contribució de diverses fonts de MO. A més, s'observen diferències notables entre les diferents estacions. Les mostres de l'estació del talús obert (TA1000) i l'estació del sistema Garrucha-Almanzora (GA1000) presenten els valors més elevats.

L'estudi dels fluxos de partícules mostra diferencies notables en les característiques del material que sedimenta en els diferents ambients sedimentaris. A més, la integració de les dades metoceanogràfiques i satel·litàries demostra que les fluctuacions temporals dels fluxos estan estretament relacionades amb els forçaments externs (vent i onatge, descàrrega fluvial i activitats antropogèniques) i la producció primària.

Principals resultats del subcapítol 3.2: Exportació de metalls associats als fluxos de partícules

L'anàlisi del contingut de MT i As dels fluxos als canyons submarins ha permès calcular la magnitud de la massa de metalls i As exportada durant el període de monitoratge. Els resultats demostren que els fluxos de metalls i As segueixen els mateixos patrons de transferència temporal que els TMF. Així dons, la seva variabilitat temporal està bàsicament governada pels mateixos forçaments externs que controlen els TMF. L'estació AL1000 presenta un contingut MT més gran que la resta d'estacions. L'excepció és el Co, més abundant a ES1000. Les diferencies observades entre l'estació ubicada al canyó d'Almeria i les dels canyons del golf de Vera són significatives per diversos MT (Al, Fe, Ti, Cu, Ni, Pb i Zn). S'observa una variabilitat temporal marcada, amb continguts de MT i As menors durant els temporals (març-abril de 2015 i febrer-març de 2016). Les diferències són significatives en els casos de l'Al i el Fe a l'estació AL1000 i de l'As, el Co, el Cu, el Mn i el Ni a les estacions ES1000 i AL1000. En canvi, a GA1000 no s'observen variacions significatives.

L'estudi del contingut de metalls i As en els sediments del fons marí sota les estacions ES1000 i GA1000 evidencia que, amb comptades excepcions, els continguts de MT en els sediments són similars als de les partícules que sedimenten. Els sediments presenten els continguts de Ti, As, Mn i Pb més grans. Més concretament, els sediments recollits sota l'estació ES1000 mostren continguts més elevats d'As i Mn que els fluxos de partícules (contingut mitjà). En canvi, els sediments de sota GA1000 tenen més Fe, Ti, Mn i Pb que no pas els fluxos. Aquests increments persisteixen després de normalitzar per l'Al (MT/Al), i suggereixen l'ocurrència de processos post-deposicionals, l'alteració dels fluxos primaris o un origen diferent dels sediments.

Finalment, s'ha vist que el contingut de certs MT també deriva de fonts antropogèniques. S'ha detectat una alteració de la distribució del Zn i possiblement del Pb i el Cu (propers al llindar dels valors naturals) a l'estació ES1000, i del Cu i possiblement el Zn a les estacions GA1000 i AL1000.

Els resultats d'aquest estudi demostren que les característiques del material que sedimenta i els forçaments externs, però també processos post-deposicionals, són claus per entendre la distribució dels MT i l'As als canyons submarins. A més, s'ha demostrat la transferència de contaminants metàl·lics cap al marge profund.

Principals resultats del subcapítol 3.3: Fonts i transport de matèria orgànica, i carboni orgànic recalcitrant, al canyó d'Escombreras

Els productes de la reacció amb CuO en els fluxos de partícules en l'estació ES1000 es correlacionen positivament entre ells i exhibeixen variacions temporals al llarg del període estudiat. La suma de fenols derivats de la lignina (siringol, S, vanil·lina, V, i cinamols, C) normalitzats per el contingut de CO (Λ_8) és màxima al març de 2015 (0,45 mg / 100 mg de CO), coincidint amb un increment de l'onatge i dels corrents durant un temporal, i amb valors superiors a 0,3 mg / 100 mg de CO només al juny i juliol de 2015. La suma dels àcids carboxílics derivats de la cutina mostren un pic relatiu al març de 2015 (0,29 mg / 100 mg de CO), i valors per sobre de 0,2 al juny i juliol, amb un màxim de 0,33 mg / 100 mg de CO a principis de juliol. Els valors de $\delta^{13}C_{CO}$, les ràtios CO/N i els biomarcadors de la lignina i la cutina palesen contribucions de diverses fonts. A part de CO d'origen marí derivat del fitoplàncton, s'ha identificat la presència de fraccions recalcitrants procedent de plantes vasculars tant d'origen marí com terrestre.

Els sediments del canyó d'Escombreras presenten una taxa d'acumulació mitjana de 0,348 ± 0,032 g cm^{-2} y^{-1}. Els sediments del fons del canyó estan format predominantment per argiles i llims, amb un increment de la fracció grollera a les mostres sense oxidació prèvia de la MO (<2% vs. ~4%). Destaca la presència de fibres vegetals a la fracció més grollera. El contingut mitjà de CO oscil·la entre el 0,77% i l'1,14%, amb una marcada tendència cap a l'augment des del fons marí fins als 4 cm de profunditat en el sediment. El CO dipositat en els sediments del canyó té més lignina i cutina que les partícules que sedimenten, com ho il·lustren els valors mitjans de 0,65 mg Λ_8 i 0,37 mg de cutina/100 mg de CO als sediments, i 0,31 mg Λ_8 i 0,23 mg de cutina/100 mg de CO als fluxos. A més, s'observa un increment del contingut d'aquests biomarcadors a intervals més profunds del testimoni analitzat.

Aquest estudi posa en relleu que el canyó d'Escombreras és un depocentre de sediments fins i de CO, el qual deriva d'una barreja de fonts autòctones i al·lòctones. L'anàlisi dels forçaments externs desenvolupat en els apartats anteriors ha permès identificar els processos que governen la transferència de matèria orgànica provinent de les diverses fonts entre els mesos de març i l'agost de 2015.

Principals resultats del subcapítol 3.4: Transferència de contaminants metàl·lics cap al canyó d'Escombreras

L'estudi de la transferència de contaminants metàl·lics cap al canyó d'Escombreras s'ha centrat en el Pb i el Zn, amb la mirada posada en el dipòsit de residus miners de la badia de Portmán com a possible font principal. Les concentracions de Pb i Zn en els sediments del fons del canyó són prou altes, amb uns màxims entre 2 i 4 vegades més grans que els continguts de la base del testimoni. Per altra banda, els valors observats són entre 1 i 2 ordres de magnitud més petits que a l'extensió submarina del dipòsit miner de la badia de Portmán (Cerdà-Domènech, 2020; Baza-Varas et al, 2022).

Les composicions isotòpiques del Pb en els sediments del canyó mostren una forquilla de variació força estreta, comparable amb la d'altres canyons submarins mediterranis i atlàntics (Heimbürger

et al., 2012; Mil-Homens et al., 2013; Cossa et al., 2014). Les ràtios $^{207}Pb/^{206}Pb$ i $^{208}Pb/^{206}Pb$ dels sediments presenten valors més radiogènics que el valor de base (0,837 i 2,079, respectivament), amb fraccionaments isotòpics entre 0,838 i 0,844, i 2,079 i 2,085, respectivament. Totes dues ràtios augmenten des de la base del testimoni fins a assolir els valors màxims a 11,5 cm, 7,5 cm i 6,5 cm de profunditat, tot i mantenint-se relativament constants als nivells més superficials en el cas de la ràtio $^{207}Pb/^{206}Pb$. En canvi, els valors de $^{208}Pb/^{206}Pb$ exhibeixen una disminució progressiva en direcció al fons marí, fins assolir valors semblants als mesurats en els fluxos de partícules mostrejats a principis d'abril i finals de maig de 2015. La regressió entre el contingut de Pb i les ràtios isotòpiques permet diferenciar dos tipus de sediments, els situats a més profunditat dins el testimoni (pre-1950), receptors de Pb d'una mateixa font antropogènica, i els més superficials (post-1950), receptors de Pb de més d'una font.

Els resultats descrits al subcapítol 3.4 demostren l'arribada de Pb i Zn antropogènic al canyó d'Escombreras des del segle XIX, i també que el contingut de MT en el marge continental profund durant el període d'abocament de residus miners (1957-1990) a la badia de Portmán és substancialment inferior a l'observat en estudis previs a la plataforma continental interna (Cerdà-Domènech, 2020; Baza-Varas et al, 2022). Les dades obtingudes suggereixen que el dipòsit de residus miners de la badia de Portmán no és la font principal del Pb antropogènic que sedimenta al canyó.

Capítol 4

Discussió conjunta

Variabilitat dels fluxos de partícules

Composició dels fluxos de partícules

- Origen i composició de la matèria orgànica
- Metalls en els canyons submarins

Processos sedimentaris

- Efectes dels temporals
- Efectes de la pesca d'arrossegament de fons

Fonts de metalls associats a les partícules que sedimenten i als sediments: el paper del dipòsit de residus miners de la badia de Portmán

En aquest capítol es presenta una discussió conjunta dels resultats del capítol 3, focalitzada en els objectius de la Tesi. Es comparen les característiques dels fluxos de partícules als tres ambients sedimentaris estudiats: canyons submarins, talús obert i peu del talús, i es discuteixen la seva composició i les fonts dels seus constituents, incloent la MO, els MT (Al, Fe, Ti, Co, Cu, Mn, Ni, Pb, Zn) i l'As. També es debat la influència dels temporals i de la pesca d'arrossegament sobre la variabilitat temporal dels fluxos, i, així com la transferència de metalls d'origen antropogènic cap als canyons, i el paper del dipòsit de residus miners de la badia de Portmán com a font de metalls cap al marge continental distal.

4.1. Variabilitat dels fluxos de partícules

L'estudi demostra la transferència actual i en el passat recent de partícules sedimentàries procedents de la plataforma continental fins els cursos intermedis dels canyons submarins i el talús obert investigats, a profunditats properes als 1.000 m.

Els fluxos de partícules presenten una marcada variabilitat espacial, amb valors d'entre 1,64 ± 1,32 i 7,33 ± 5,31 g m^{-2} d^{-1} pel rang batimètric indicat. Un factor que pot explicar part d'aquesta variabilitat és la distància a la línia de costa de les capçaleres i els cursos superiors dels canyons, tenint en compte que els fluxos de massa tendeixen a disminuir mar endins (Antia et al., 1999). Així, els fluxos més baixos s'han detectat al canyó d'Almeria, en que l'estació de mostreig era instal·lada a una distància que doblava la de la resta d'estacions ubicades al marge continental (Fig. 4.1). Un segon factor que podria influir en els fluxos és la configuració de les capçaleres dels canyons submarins. Els fluxos més alts s'han enregistrat al sistema de canyons de Garrucha-Almanzora, amb unes capçaleres ben encaixades a la plataforma continental i, per tant, amb una clara capacitat per interceptar les partícules sedimentàries que circulen al llarg de la plataforma, circumstància que ajuda a canalitzar-les dins els canyons (Canals et al., 2013). Per la seva banda, els fluxos de partícules al peu del talús, lluny ja de la plataforma continental a profunditats de més de 2.000 m, són molt migrats (TWF < 0,1 g m^{-2} d^{-1}).

La fracció litogènica domina la composició dels fluxos a tots els ambients sedimentaris investigats —també al peu de talús. Els continguts més elevats de litogènics s'han mesurat al canyó d'Almeria (72,4 ± 2%), amb valors menors als canyons i al talús obert del golf de Vera (60,5-62,4% de mitjana) (cf. aptat. 3.1). Als canyons i al talús obert del golf de Vera, el contingut relatiu de $CaCO_3$ és més gran que no pas a la conca profunda (Fig. 4.1). Aquest fet es deuria a que la fracció carbonatada no només deriva de la producció primària marina, sinó que també incorpora contribucions de la fracció litogènica (cf. aptat. 3.1), tal i com succeeix en altres marges continentals mediterranis, com el català (Martín et al., 2006) o l'adriàtic (Ravaioli et al., 2013). Al peu del talús els continguts relatius de MO i òpal augmenten (5,7 i 7,4%, respectivament) (Fig. 4.1 i Taula 3.2). Això és degut a una disminució de l'aportació advectiva de partícules sedimentàries cap a la conca profunda, amb la qual cosa la dilució dels components pelàgics és menor. En altres marges continentals mediterranis s'ha observat que el transport advectiu de partícules sedimentàries segueix un patró cíclic de deposició i remobilització des de la plataforma continental cap al talús i la conca profunda (Heussner et al., 2006; Ulses et al., 2008; Palanques

et al., 2012; Puig et al., 2014). Aquesta dinàmica queda reflectida també en la variabilitat temporal dels components principals dels fluxos de partícules. Les partícules que sedimenten als canyons tenen una composició elemental força homogènia, amb un senyal de producció primària no sempre evident. En canvi, al peu del talús, però també al talús obert, la variabilitat temporal en la composició dels fluxos és més patent, amb períodes en que estan dominats per components biogènics i MO marina fresca provinents de la producció primària.

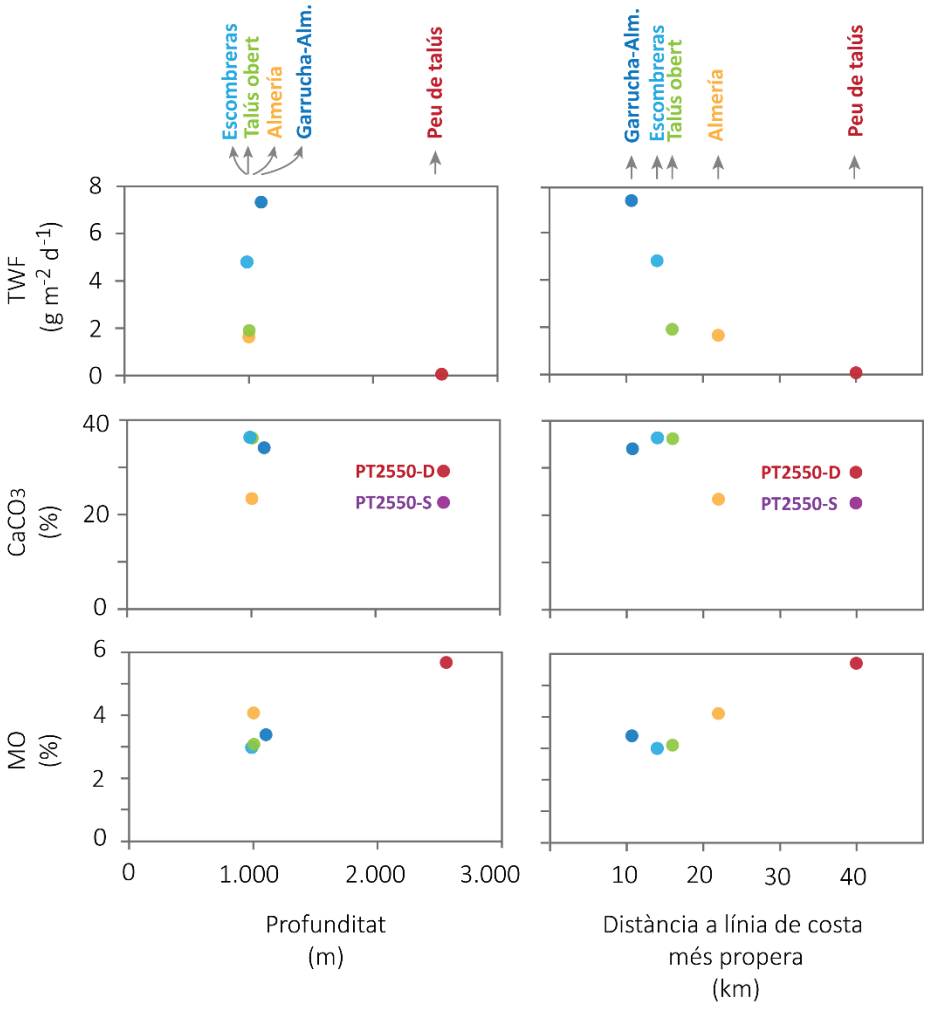

Figura 4.1. Relació de la profunditat i la distància a la línia de costa amb els fluxos ponderats segons el temps de mostreig (TWF), i els continguts de $CaCO_3$ i MO en els ambients sedimentaris de canyó submarí, talús obert i conca profunda. Canyons submarins: Almeria, Escombreras i sistema Garrucha-Almanzora. PT2550-D i PT2550-S fa referència a les trampes de partícules profunda (D) i més soma (S) instal·lades a la línia instrumentada del peu del talús PT2550 (cf. aptat. 2.1).

4.2. Composició dels fluxos de partícules

Un dels principals objectius d'aquesta Tesi és la caracterització dels fluxos de partícules, amb especial interès en el contingut i les característiques de la MO, i el contingut de MT i As.

4.2.1. Origen i composició de la matèria orgànica

Els resultats obtinguts evidencien diferències en l'origen i la composició de la MO que sedimenta en els ambients estudiats. Els canyons estudiats estan situats en marges privats de grans aportacions fluvials. El sistema de canyons de Garrucha-Almanzora i el canyó d'Almeria són els que tenen llurs capçaleres a menor distància de les desembocadures dels rius més significatius de l'àrea d'estudi en sentit ampli (Liquete et al., 2005). Els sistemes fluvials Aguas, Antas i Almanzora (Fig. 3.1) segurament són una font de partícules terrígenes cap al sistema de Garrucha-Almanzora, com ho indiquen les elevades ràtios CO/N (fins 20,1), atribuïbles a una MO provinent de plantes vasculars no degradades, composta típicament per macromolècules pobres en N (CO/N > 16) (Goñi i Hedges, 1995). Les capçaleres del sistema Garrucha-Almanzora estan fortament entallades en la plataforma continental, i entre 7 i 90 m de fondària (Puig et al., 2017). Aquesta circumstància facilitaria la captura de MO d'origen terrestre per les capçaleres de canyó.

També s'han observat ràtios CO/N elevades (fins 20,3) al talús obert a l'oest del canyó d'Escombreras, durant els mesos de tardor i hivern (Fig. 3.6). L'arribada de MO terrestre provindria de rambles efímeres, i seria redistribuïda per l'acció dels corrents i l'onatge. Convé assenyalar, però, que la MO provinent de plantes vasculars marines també presenta ràtios CO/N elevades, tal i com assenyalen diversos estudis (Bianchi et al., 1999; Apostolaki et al., 2022). Aquest fet obliga a introduir un punt de cautela en l'ús d'aquest indicador per determinar les contribucions relatives de MO d'origen terrestre i marí. Cal tenir també en compte que la recerca efectuada ha revelat l'exportació de restes de fanerògames marines més enllà del límit de la plataforma continental cap al marge de Mazarrón profund (cf. aptat. 3.3).

Als canyons d'Escombreras i Almeria les ràtios CO/N presenten un rang de valors restringit (6,9-11,7) (Fig. 3.6). La MO provinent de plantes vasculars té tendència a enriquir-se en N per processos de degradació microbiana mentre és en el sòl, la qual cosa pot fer disminuir fins a 8 la ràtio CO/N (Hedges et al., 1997). A més, el fitoplàncton es caracteritza per alts continguts de N (CO/N fins a 7), tot i que la MO pateix una degradació creixent a mesura que sedimenta, amb una tendència a perdre N en front del CO (Hedges et al., 1997). Així doncs, les ràtios observades suggereixen que els canyons d'Escombreras i d'Almeria reben certes quantitats de MO procedent de sòls terrestres, probablement barrejada amb MO d'altres provinences. Tot i això, durant períodes amb escassa arribada de partícules, la MO d'origen marí provinent de la producció primària pot arribar a prevaldre (CO/N < 7) (Fig. 3.6).

L'estudi combinat del $\delta^{13}C_{CO}$ i de biomarcadors de CO recalcitrant confirmen l'heterogeneïtat de les fonts de MO al canyó d'Escombreras durant els 6 mesos de mostreig dels fluxos de partícules. La major part de la MO exportada a l'eix del canyó és d'origen marí, amb una contribució provinent de la producció primària que representa més del 55% del CO que sedimenta. El contingut de biomarcadors recalcitrants i la relació entre els compostos derivats de la lignina (cf.

aptat. 3.3) indiquen la transferència de MO recalcitrant provinent de fonts terrígenes i marines. La MO recalcitrant d'origen marí exportada prové de detritus de *P. oceanica*, comú en els fons de la plataforma interna de les províncies de Múrcia i Almeria (Ruiz et al., 2015), exceptuant el tram afectat pels abocaments de residus miners de la badia de Portmán (Fig. 3.18) (Baza-Varas et al., 2022). El detritus molt probablement procedeix de les praderes ubicades en la plataforma interna de Mazarrón, les quals arriben a situant-se a 4 km de distància de la línia de costa (Ruiz et al., 2015). El detritus de *P. oceànica* contribueix notablement a la fracció grollera dels sediments i, en general, representa una part petita del CO exportat durant la majoria de mesos. Tot i així, durant períodes puntuals, pot arribar a representar a prop del 11% del CO exportat (Fig. 3.21), evidenciant la transferència de material provinent de la plataforma interna cap a l'eix del canyó. Així doncs, part del CO recalcitrant provindria de l'anomenat "carboni blau costaner" (en anglès *coastal blue carbon*), resultant de la captura de CO_2 atmosfèric per organismes i comunitats costaneres, les quals poden emmagatzemar-lo a llarg termini.

La MO recalcitrant d'origen terrestre prové principalment de teixits d'angiospermes força degradats (present en els sòls de terra ferma). Representa entre el 24 i el 35% del CO que sedimenta al canyó d'Escombreras (Fig. 3.21). La prevalença d'aquesta fracció està associada al transport preferent de partícules de gra fi cap al marge continental profund, especialment durant períodes on imperen condicions hidrodinàmiques poc energètiques a la plataforma. Per últim, els alts valors de les ràtios pCd/Fd i C/V observats durant els mesos de juny i juliol (Fig 3.23c,d)suggereixen la contribució de pol·len (Sheng Hu et al., 1999), coincidint amb fluxos de massa baixos (<3 g m^{-2} d^{-1}) (Fig 3.6). La presència de pol·len palesa l'aportació atmosfèrica de matèria orgànica cap al marge continental profund.

4.2.2. Metalls en els canyons submarins

Els fluxos de partícules juguen un paper crític en l'aportació i la distribució espacial i temporal de MT i del metal·loide As en els marges continentals. Experiments duts a terme amb trampes de sediment en aigües profundes han demostrat l'associació dels MT amb partícules litogèniques, biogèniques i minerals autigènics com els òxids de Mn i els oxy(hydroxids) de Fe (Huang i Conte, 2009; Kuss et al., 2010; Ho et al., 2011; Conte et al., 2019). Mesures al llarg d'un transsecte a través de l'Atlàntic Nord (Lemaitre et al., 2020) mostraren que les partícules litogèniques jugarien un rol molt important en l'exportació de MT en els marges continentals, mentre que els òxids de Fe i Mn serien un vector d'exportació especialment rellevant cap a l'interior de les conques pregones.

Aquesta Tesi millora el coneixement de la distribució de MT i del metal·loide As als canyons submarins del sud-est de la península Ibèrica. S'ha detectat una relació clara entre la variabilitat temporal dels fluxos dels components principals i la dels MT. Els minerals litogènics s'associen amb l'Al, el Fe i el Ti i, al sistema de Garrucha-Almanzora també amb el Ni i el Co. Els oxihidròxids i òxids de Mn (fracció autigènica) s'associen amb As, Co, Cu i Ni i, al sistema de Garrucha-Almanzora també amb Pb. En aquest darrer sistema de canyons, la mateixa fracció autigènica també podria estar associada amb oxihidròxids i òxids de Fe (Fig. 3.14).

En contrast amb altres estudis (Huang i Conte, 2009; Conte et al., 2019), no s'observa una associació significativa entre els MT i els components biogènics, com la MO (Fig. 3.14). No cal descartar, però, una possible associació que podria quedar emmascarada per la predominança d'altres fraccions, com la litogènica. Un altre factor a considerar és el fet que, a mesura que augmenta la profunditat d'aigua, l'associació de la MO amb els elements bioactius s'afebleix degut als processos de remineralització (Huang i Conte, 2009; Blain et al., 2022). En el nostre estudi, les mostres dels fluxos de partícules s'han obtingut, amb la sola excepció de la trampa PT2550-S, a 25 m damunt del fons i a profunditats considerables (Taula 2.1).

Els tres canyons investigats presenten, a més, diferències espacials pel que fa al contingut de metalls en els fluxos de partícules. El canyó d'Almeria presenta continguts significativament més elevats d'Al, Fe, Ti, Cu, Ni, Pb i Zn que els canyons del golf de Vera (cf. aptat. 3.2; Fig. 3.13). Aquesta circumstància es pot explicar, si més no en part, per variacions en la composició de la fracció litogènica transferida als diferents segments del marge continental. Un cop normalitzats els MT pel contingut d'Al, el Mn i altres MT i As associats en els fluxos són significativament més elevats als canyons d'Escombreras i Almeria respecte al sistema de Garrucha-Almanzora (cf. aptat. 3.2). Se sap que el contingut de Mn a la fracció particulada està relacionat amb el transport de Mn dissolt (Jensen et al., 2020; Oldham et al., 2017), el qual està modulat per diversos factors (Noble et al., 2012), amb la seva predisposició a precipitar oxidativament (Lee et al., 2018) i amb els processos que afavoreixen la sedimentació (Bishop i Fleisher, 1987). Tot plegat suggereix que els processos que influeixen el contingut de MT i As associats a la fracció autigènica són diferents en el sistema Garrucha-Almanzora (cf. aptat. 4.3.2). Per últim, i com s'ha palesat en aquesta Tesi, les contribucions antropogèniques també poden afectar als continguts de MT i As.

4.3. Processos sedimentaris

Als canyons submarins i al talús obert dels golfs de Vera i d'Almeria, els fluxos de partícules i dels elements associats presenten una elevada variabilitat temporal tant pel que fa a la seva magnitud com a la seva composició, la qual es pot explicar per la intervenció d'un seguit de processos sedimentaris. En els paràgrafs següents ens centrarem en dos processos majors: els temporals i la pesca d'arrossegament de fons, i els seus efectes. Tanmateix, convé recordar que en a capítol de Resultats (cf. cap. 3) s'han considerat també altres forçaments, com les descàrregues fluvials (cf. aptats. 3.1 i 3.2) i les aportacions atmosfèriques (cf. aptats. 3.2-3.4).

4.3.1. Efectes dels temporals

L'atmosfera i els ecosistemes marins profunds estan connectats per processos d'alta energia impulsats per la dinàmica atmosfèrica, els quals es propaguen des de la costa i la superfície de l'oceà fins fondàries que poden ser molt considerables (Canals et al., 2013). Ho il·lustren els processos de formació d'aigües denses a la superfície i el seu enfonsament posterior cap a les profunditats fins trobar el seu nivell d'equilibri (Canals et al., 2006). La dinàmica atmosfèrica també aixeca l'onatge i accelera els corrents damunt la plataforma continental, la qual cosa sol comportar un increment de la resuspensió i del transport de partícules paral·lelament i

transversal al marge (Guillén et al., 2006; Palanques et al., 2008b; Ulses et al., 2008; Sanchez-Vidal et al., 2012). A la transició entre la plataforma i el talús continentals, els canyons submarins alteren la regularitat del relleu i presenten una alta capacitat per interceptar les partícules sedimentàries que circulen per la plataforma i per transportar-les curs avall (Canals et al., 2006; Palanques et al., 2006a). El període de mesures i mostratge in situ d'aquesta Tesi ha coincidit amb diversos temporals costaners, la qual cosa que ha permès investigar els seus efectes sobre la magnitud i les característiques biogeoquímiques dels fluxos de partícules.

A principis del període d'estudi, l'any 2015, els temporals costaners de finals de març, i de principis i mitjans d'abril, associats a vents del nord-est forts i persistents, produïren un increment de l'onatge, assolint-se alçades d'ona significatives de fins a 4,8 m (cf. aptat. 3.1). L'adquisició de dades de la columna d'aigua 70 hores després del començament del temporal de març, i 17 hores després de l'altura d'onatge màxima, aportà informació valuosa sobre els mecanismes de transport durant aquest temporal concret. L'onatge i els corrents associats a la tempesta produïren la resuspensió dels sediments i un increment de la terbolesa a la plataforma continental. Hi hagué una transferència directa de sediments a prop del fons, restringit a la capçalera del canyó. El transport de sediments cap al marge més distal es produí per un plomall tèrbol superficial (<200 m de profunditat) que s'estengué sobre l'eix del canyó seguint les isopicnes. Al capdamunt de la columna d'aigua s'hi instal·là una capa d'aigua relativament freda (fins 13,7°C) i rica en oxigen, tal i com mostren tots els perfils de CTD obtinguts seguint l'eix del canyó i també l'efectuat al sistema de Garrucha-Almanzora després de la tempesta.

Aquesta situació és d'alguna manera comparable a l'observada als canyons del marge nord-català durant el període d'estratificació estacional de la columna d'aigua i també algunes tardors (Palanques et al., 2006a, 2008b; Bonnin et al., 2008; Ulses et al., 2008). En aquestes condicions, l'increment dels fluxos partícules cap al fons es produeix per la decantació progressiva de la càrrega en suspensió a mesura que els corrents s'atenuaren (Durrieu de Madron et al., 1990; Langone et al., 2016).

Al marge de Palomares (Fig. 1.7), els vents del nord-est associats als temporals de primavera varen promoure amb tota probabilitat la transferència de material des de la plataforma cap al sistema de canyons de Garrucha-Almanzora, semblantment a la situació documentada a la Mediterrània nord-occidental, on una forta circulació ciclònica i la convergència d'aigua al llarg de la costa durant les tempestes de llevant provoca l'enfonsament d'aigües carregades en sediments cap al talús (Ulses et al., 2008; Palanques et al., 2008b; Martín et al., 2013). Tot i així, l'estratificació de la columna d'aigua segurament limità al curs superior d'aquest sistema, o gairebé, el transport de partícules en suspensió a prop del fons.

La remobilització i el transport de partícules sedimentàries durant els temporals de la primavera de 2015 feu augmentar la magnitud dels fluxos de partícules cap al marge mig i distal. Així, es va detectar una intensificació de l'exportació de: (i) MO, tant al curs mig dels canyons com al talús obert (cf. aptat. 3.1; Fig. 4.2); (ii) els components més recalcitrants de la MO al canyó d'Escombreras (cf. aptat. 3.3; Fig. 4.2); i (iii) els metalls i l'As cap a l'interior dels canyons (cf. aptat. 3.2).

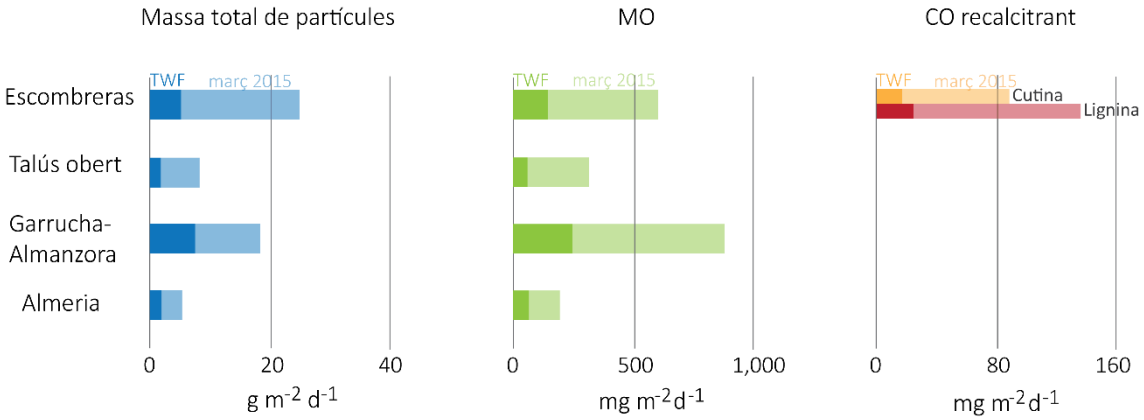

Fig. 4.2: Comparació entre els fluxos ponderats totals segons el temps de mostreig (TWF, tons pujats) i els fluxos recollits durant el període de tempesta de març de 2015 expressats en termes de de massa total de partícules, matèria orgànica (MO) i carboni orgànic (CO) recalcitrant (tons suaus) en els ambients sedimentaris de canyó submarí i talús obert. Canyons submarins: Almeria, Escombreras i sistema Garrucha-Almanzora.

Durant els temporals de març i abril del 2015, s'exportà el 64,7% de la massa total exportada durant els 6 mesos de monitorització del canyó d'Escombreras, dada que demostra fins a quin punt l'acció dels temporals controla la sedimentació al curs mig del canyó. Per la seva banda, en el mateix curt període de temps al sistema de canyons de Garrucha-Almanzora s'exportà el 31,3% de tota la massa exportada en 7 mesos i mig. El menor impacte observat en aquest sistema es podria atribuir a una major recurrència d'esdeveniments de transferència de partícules, desencadenats per altres processos (cf. aptat. 5.3.2). Al canyó d'Almeria, els mateixos episodis representaren el 21,1% de la massa total exportada durant poc més d'un any. Cal tenir en compte, però, que els valors estimats pel sistema de Garrucha-Almanzora i el canyó d'Almeria són els mínims, doncs les trampes corresponents no es van obrir fins 2-3 dies després del començament de la primera tempesta, al mes de març. La configuració de les capçaleres dels canyons i de la línia de costa, la distància entre ambdues i l'amplada de la plataforma són factors que poden influir en el transport particulat a cadascun dels canyons.

Durant els temporals ocorreguts al novembre del 2015 i a l'hivern de 2015-16 no s'observà un increment marcat dels fluxos de partícules al talús obert del marge de Palomares (Figs. 1.7 i 2.1). En el cas del canyó d'Almeria, l'increment sostingut dels fluxos des del novembre de 2015 fins al gener de 2016 estaria fonamentalment associat amb altres forçaments externs i processos (cf. aptat. 3.1). Les característiques específiques de cada tempesta, incloent la direcció, intensitat i persistència del vent, l'onatge i els corrents, a més de la disponibilitat de material en disposició de ser redistribuït, modulen el subministrament de sediments des de la plataforma cap al talús.

Certament, els temporals produeixen canvis en la composició dels *pools* de partícules que sedimenten al marge continental mig, on s'instal·laren la majoria de línies instrumentades. La similitud de la mida de gra de les partícules litogèniques i carbonatades en els canyons submarins durant tot el període d'estudi (cf. aptat. 3.1) indicaria la prevalença de condicions hidrodinàmiques sense grans canvis en el curs mig dels diferents canyons, entorn els 1.000 m de fondària, fruit de la deposició selectiva de fins a mesura que les velocitats dels corrents es van

atenuant amb la profunditat. El canvi més remarcable observat durant un període de tempesta, pel que fa a la mida de gra, és l'increment de la fracció sorrenca durant la tempesta de març de 2015 al canyó d'Almería, amb 4,8% de sorra envers una mitjana del 0,9% durant la resta del període (Fig. 3.7).

Amb tot, és evident que la composició i l'origen de la MO al canyó d'Escombreras estan controlades per la deposició selectiva de partícules sedimentàries durant el transport advectiu. El temporal de març de 2015 va promoure la transferència de detritus groller de *P. oceanica*, els quals assoliren el 10,5% del total de CO sedimentat. En canvi, durant els temporals d'abril de 2015 la contribució als fluxos d'aquesta fracció fou sensiblement inferior (<3%) (Fig. 3.23). Aquests valors més baixos s'explicarien per una menor intensitat de l'onatge i dels corrents (Fig. 3.19), els quals transportarien preferentment MO associada amb les partícules de mida de gra més fina, en comparació amb els fragments vegetals de *P. oceanica* (cf. aptat. 3.3).

Per altra banda, els temporals poden afavorir la redistribució i el transport cap als canyons de material biogènic —diferent de les restes de *P. oceànica*— dipositat a la plataforma, tal i com evidencien els sediments biogènics carbonatats del canyó d'Almeria (cf. aptat. 3.1). Al canyó d'Escombreras, les contribucions més grans de CO procedent del fitoplàncton marí (68-75%) (Fig. 3.21) coincideixen amb els temporals de l'abril de 2015, desencadenats després d'un fort increment de la producció primària a tot el marge continental, amb valors màxims de Chl-a de 0,64 mg m^{-3} sobre l'eix del canyó (Fig. 3.19 i aptat. 3.3). Per últim, si ens fixem en el sistema de canyons de Garrucha-Almanzora, és durant els temporals quan s'observa un major contingut relatiu de MO (Fig. 3.6), tot i el gran volum de material litogènic resuspès. Aquest fet està lligat, probablement, a la transferència de material ric en MO d'origen terrestre des d'indrets propers a les goles fluvials durant les tempestes (cf. aptat. 3.1).

En relació amb els continguts de MT en els fluxos (cf. aptat. 3.2) també s'observen diferencies rellevants segons la situació sigui de temporal o de calma. És destacable la disminució dels continguts de metalls i metal·loides associats amb la fracció autigènica (As, Co, Cu, Mn i Ni) als canyons d'Escombreras i Almeria durant i poc després de les tempestes (Fig. 3.15). Aquest fet es deu molt probablement a l'efecte de dilució d'aquesta fracció dins el *pool* de material resuspès, predominantment litogènic. Tanmateix, al canyó d'Almeria s'ha detectat també una disminució relativa de la fracció litogènica (associada a l'Al i al Fe i, en menor mesura, l'As), que és la predominant en els sediments de les plataformes continentals. L'explicació podria raure en un enriquiment en $CaCO_3$ del material remobilitzat provinent de la plataforma, com ho indica el contingut relatiu de la fracció carbonatada (cf. aptat. 3.1).

4.3.2. Efectes de la pesca d'arrossegament de fons

Superposant-se als processos naturals, certes activitats antropogèniques també poden impactar la dinàmica sedimentària dels marges continentals i els canyons submarins. És conegut que la pesca d'arrossegament de fons erosiona els vessants superiors dels canyons (Puig et al., 2012; Martín et al., 2014a), remobilitzant sediments que alimenten capes nefeloides intermèdies i de fons. Les darreres tendeixen a canalitzar-se per les valls tributàries i pels cursos principals dels canyons (Martín et al., 2014b). Fins i tot es poden generar corrents de gravetat a l'interior dels

canyons durant els mesos de més activitat pesquera (Palanques et al., 2006b; Puig et al., 2012). Tot plegat fa augmentar les taxes d'acumulació als eixos dels canyons en tant que col·lectors principals dels sistemes de drenatge sedimentari dels marges continentals (Paradis et al., 2017). Aquest efecte es pot fer patent fins i tot als trams més profundes dels canyons submarins (Palanques et al., 2006b; Puig et al., 2012; Payo-Payo et al., 2017). Les pertorbacions lligades a la pesca d'arrossegament són més persistents i significatives a fondàries considerables, on l'impacte dels processos naturals capaços de remobilitzar sediments és petit (Martín et al., 2014a). Allà on s'arrossega, especialment a la plataforma continental i al talús superior, tendeix a augmentar la proporció de partícules grolleres en superfície degut al rentat de les fraccions més fines per efecte del propi arrossegament (Martín et al., 2014a), produint-se també un empobriment de les fraccions làbils de la MO (Paradis et al., 2021). En fons fangosos batials, l'arrossegament s'enduu la capa superior de sediments poc compactes, i fa aflorar fangs consolidats més o menys antics (Sultan et al., 2004, 2007).

El sistema de canyons de Garrucha-Almanzora està envoltat de caladors on es practica la pesca d'arrossegament, entre 500 i 800 m de fondària (García-Rodríguez, 2005). Les dades del sistema de monitorització per satèl·lit VMS permeten precisar que la majoria d'arrossegadors operen a profunditats de 500 a 650 m seguint els vessants dels diferents ramals i el talús adjacent. Els mesos de juny i juliol de 2015, però, calen a més profunditat, al voltant dels 800 m. A més, hem observat que el nombre de transmissions de dades VMS des dels pesquers en un radi de 4 km al voltant de la nostra estació d'ancoratge GA1000 augmentà durant els mesos de juliol i agost (Fig. 3.10).

És altament versemblant que la capa nefeloide detectada mitjançant CTD a finals de març i finals d'agost de 2015 al sistema de Garrucha-Almanzora per sota dels 400 m i fins al fons hagués estat causada principalment per la resuspensió de sediments deguda a la pesca d'arrossegament (cf. aptat. 3.1). A més, s'observà un increment pronunciat de la terbolesa també durant els mesos d'estiu, quan l'activitat pesquera és més intensa als voltants i al mateix canyó d'acord amb les dades VMS. Les dades de terbolesa indiquen també una disminució sobtada a finals d'agost de 2015 (Fig. 3.5), sense que haguem trobat una explicació evident, atès que les condicions hidrodinàmiques no semblen haver canviat respecte als mesos precedents, i tampoc hi va haver una reducció de l'activitat pesquera.

L'arribada de quantitats considerables de material (fins 10 g m^2 d^{-1}) a la trampa GA1000 del sistema de Garrucha-Almanzora durant períodes amb poca o nul·la descàrrega fluvial i amb un onatge menor (cf. aptat. 3.1), apunta també a la injecció de sediments resuspesos per causa de la pesca d'arrossegament, la qual esdevindria així un factor de control dels fluxos a l'eix del canyó mig. A més, el material sedimentat durant el mes d'agost presenta unes ràtios CO/N altes (Fig. 3.6), similars a les observades durant el període de tempestes, palesant d'aquesta manera la resuspensió i transferència de material des dels vessants superiors del canyó.

Una característica rellevant dels fluxos recol·lectats en aquest canyó és que entre els mesos d'estiu i els períodes de tempesta no s'observaren diferències significatives en el contingut de Mn i d'altres metalls associats a la fracció autigènica (cf. aptat. 3.2), a diferencia del que s'observa en els altres canyons. Fora del període de tempestes, la correlació negativa entre el contingut de

MT i As i els TMF (Fig. S3.2) suggereix que les fluctuacions temporals observades podrien ésser, en part, degudes a un procés de dilució en el material resuspès. Però un canvi en l'àrea de resuspensió, o un canvi en el contingut de partícules i les seves propietats (mida del gra, composició, entre d'altres) o en el contingut d'oxigen en el fons marí, té el potencial d'influir en el contingut de MT i As de les partícules resuspenses.

Les evidències aplegades fan pensar que les pertorbacions derivades de la pesca d'arrossegament també afecten a la distribució dels MT i l'As. Hi ha, però, pocs estudis en altres indrets que permetin contrastar els resultats obtinguts pel que fa al contingut de MT (vegis, en tot cas, Palanques et al., 2022).

4.4. Fonts dels metalls associats a les partícules que sedimenten i als sediments: el paper del dipòsit de residus miners de la badia de Portmán

Els resultats obtinguts (cf. aptat. 3.2) indiquen que, a l'àrea d'estudi, les partícules que sedimenten són un vector de transport de contaminants metàl·lics cap als canyons. La avaluació dels factors d'enriquiment en els fluxos de partícules indica que el canyó d'Escombreras rep una contribució moderada de Zn i, possiblement, de Pb i Cu antropogènics, pròxims aquests darrers amb valors propers al llindar dels valors naturals. Per la seva part, el sistema de Garrucha-Almanzora i el canyó Almeria reben una contribució moderada de Cu i, possiblement, de Zn. Els valors del canyó d'Escombreras, el més proper al dipòsit de residus miners de la badia de Portmán, podrien ser atribuïbles a transferències des d'aquest dipòsit. Tot i així, el càlcul dels factors d'enriquiment no aporta informació sobre l'origen de la contaminació.

Els sediments del fons marí del canyó d'Escombreras mostren, de manera anàloga als fluxos, un enriquiment en Zn, i en una mesura molt menor, de Cu i Pb, els darrers amb valors igualment propers al llindar natural (Fig. 3.16). Presenten també un enriquiment aparent d'As, el qual seria fruit de processos post-deposicionals, tal i com s'explica a l'apartat 3.2. Els sediments dels 51 cm superiors del testimoni analitzat mostren un increment en el contingut de Pb i Zn a finals de segle XIX, amb un altre increment, força pronunciat, a partir de la dècada de 1940 (cf. aptat. 3.4). Els continguts de Pb i Zn es mantenen elevats a l'interval corresponent al període d'abocament de residus miners al mar (1957-1990) (Fig. 3.27), però aquest valors són entre un i dos ordres de magnitud inferiors als que presenten els materials de l'extensió submarina del propi dipòsit de la badia de Portmán (Cerdà-Domènech et al., 2019; Baza-Varas et al., 2022). Aquesta diferència tan significativa indicaria l'absència d'un transport generalitzat de metalls des de la plataforma fins al talús, on se situa el canyó d'Escombreras.

En conseqüència, les ràtios isotòpiques del Pb de les mostres corresponents al període d'abocament de residus i al període posterior no es poden explicar per una barreja entre el Pb dels residus miners i l'exportat al canyó a l'etapa preindustrial (cf. aptat. 3.4). La composició isotòpica del Pb apunta a una font amb una elevada ràtio $^{207}Pb/^{206}Pb$, semblant al senyal atribuït a la contaminació atmosfèrica causada per l'activitat industrial en sentit ampli (Monna et al., 1997, Komárek et al., 2008), consistent en una barreja d'emissions de fonts diverses, incloent-hi

la resuspensió de pols durant l'explotació minera a cel obert. De fet, les troballes d'aquesta Tesi (cf. aptat. 3.3) evidencien una desconnexió entre el curs mitjà del canyó d'Escombreras i la plataforma interna durant la major part del període estudiat amb les trampes de sediments. Se n'exceptuen alguns períodes puntuals per causa dels temporals. Aquest fet posa en relleu el paper de la deposició atmosfèrica com a via d'entrada de Pb i d'altres contaminants al marge continental.

L'aparentment escassa transferència de metalls des del dipòsit de residus miners de la badia de Portmán fins al marge continental extern també es pot explicar, si més no en part, per la barreja i la dilució de les partícules contaminades amb partícules no contaminats durant el transport al llarg i ample de la plataforma, com també s'ha observat en altres marges mediterranis (Palanques et al., 2008b). També cal comptar amb el paper dels corrents marins que, en lloc d'afavorir la transferència cap a la vora de plataforma i el talús durant el període d'abocament, ajudaren a concentrar els residus en sectors ben proper al punt de descàrrega principal, reblint en conseqüència l'antiga badia de Portmán (Oyarzun et al., 2013; Cerdà-Domènech, 2020; Baza-Varas et al., 2022). Els corrents també poden haver exportat a indrets més allunyats que el canyó d'Escombreras part dels fins que acompanyaren els abocaments. Resta pendent la caracterització de les diverses fonts antropogèniques potencials, en una regió que ha experimentat una evolució considerable del seu teixit industrial en els darrers cent i escaig anys (cf. aptat. 3.4).

Capítol 5

Conclusions

i línies d'investigació futures

En aquesta Tesi s'han estudiat la magnitud i les característiques composicionals dels fluxos de partícules a tres canyons submarins i al talús obert del marge continental dels golfs de Vera i d'Almeria, i a al peu del talús proper. La recollida i l'anàlisi de dades meteorològiques i oceanogràfiques ha permès determinar els processos responsables del transport de partícules sedimentàries, MO, MT (Al, Fe, Ti, Co, Cu, Mn, Ni, Pb, Zn) i As per mediació dels fluxos. També ens hem ocupat de la transferència de contaminants metàl·lics cap als canyons investigats, amb atenció especial al paper del dipòsit de residus miners de la badia de Portmán, a Múrcia, un dels indrets més contaminats de la Mediterrània (Oyarzun et al., 2013).

La intensificació de l'onatge i dels corrents causada per vents forts durant els temporals impulsa l'exportació de sediments, MO, CO, MT i As des de la plataforma continental fins al marge continental profund. El control de la sedimentació al marge continental per l'acció de les tempestes ha quedat palesat per les observacions efectuades i les mostres obtingudes durant la primavera de 2015. S'ha constatat, però, que no tots els temporals desencadenen la mateixa resposta del sistema, ni generen el mateix impacte en els canyons submarins estudiats. Les característiques de cada temporal (és a dir, la direcció i el règim de l'onatge i dels corrents, la seva durada i altres fenòmens associats), la disponibilitat de material, la configuració de la costa el relleu submarí, i la distància de les capçaleres dels canyons submarins a la línia de costa, són factors que modulen la transferència de partícules cap a l'interior dels canyons i més enllà. Quan els temporals tenen lloc en situació d'estratificació de la columna d'aigua, l'advecció cap al marge distal del material resuspès a la plataforma continental es produeix seguint les isopicnes. Mar endins, la sedimentació resulta de la pèrdua progressiva de la càrrega de partícules en suspensió a mesura que els corrents i la turbulència associada s'atenuen.

Al canyó d'Almeria, la variabilitat temporal dels fluxos de partícules a la tardor de 2015 i principis de l'hivern de 2015-16 estigué controlada fonamentalment per la descàrrega fluvial i la producció primària. Durant la tardor, i després d'un període de precipitacions intenses, s'intensificà la transferència de material terrigen, amb un increment de metalls, com l'Al i el Fe, associat. En canvi, a finals de gener de 2016, les partícules transferides presentaven alts continguts de MO, palesant així l'arribada de material procedent de la floració fitoplanctònica registrada al mateix mes.

Al sistema de canyons Garrucha-Almanzora, l'exportació de partícules en suspensió fou constant entre març i octubre de 2015, fins i tot durant els intervals sense forçaments atmosfèrics intensos. Aquesta regularitat dels fluxos de partícules s'ha relacionat amb la pesca d'arrossegament de fons desenvolupada al voltant dels canyons submarins i fins i tot a les seves vessants. L'arrossegament erosiona el fons marí i resuspèn les partícules sedimentàries, les quals aleshores poden ser transportades per efecte de la gravetat i dels corrents locals cap a l'eix del canyó. Possiblement, l'arrossegament i la dinàmica sedimentària que provoca, també són els responsables de l'increment de la terbolesa observat per sota dels 400 m i fins al fons marí.

Els fluxos de partícules als canyons submarins i al talús obert, aproximadament a 1.000 m de profunditat, són més grans que els mesurats al peu del talús, fet que suggereix un intercanvi regular de material entre la plataforma continental i el talús, on estan entallats els

canyons. En canvi, cap a 2.500 m de fondària, els fluxos tenen un caràcter netament pelàgic, i han estat extremadament baixos durant tot el període d'estudi.

La producció primària és una font de partícules, fonamentalment de carbonats, MO i òpal. Les floracions fitoplanctòniques s'han relacionat amb l'aportació de nutrients, amb efectes fertilitzadors, procedents de la descàrrega fluvial i de l'aflorament d'aigües profundes, així com amb episodis de desestratificació de la columna d'aigua. Aquestes situacions fan augmentar l'exportació de material cap a la conca profunda, com s'ha detecta a l'àrea d'estudi durant l'abril de 2015 i l'hivern de 2015-16. En canvi, als canyons no s'ha observat un senyal pelàgic obvi, amb comptades excepcions (cf. aptat. 3.1.5.1.). Les condicions energètiques a la plataforma continental durant els temporals afavoreixen la resuspensió i la transferència de carbonats biogènics i MO cap al marge profund. Tanmateix, no tota la MO d'origen marí transportada durant els temporals procedeix de la floració fitoplanctònica. Una petita porció, que contribueix a les fraccions més recalcitrants i grolleres, consisteix en detritus de *Posidonia oceanica*, un fanerògama que forma herbeis extensos a la plataforma interna, fins uns 40 m de fondària. La transferència d'aquesta fracció grollera depèn de la intensitat dels temporals, i requereix condicions d'onatge i corrents forts.

La fracció terrígena domina la composició dels fluxos de partícules a tots els ambients sedimentaris investigats. Al golf de Vera, aquesta fracció també inclou carbonats. Al canyó d'Escombreras l'arribada de MO d'origen terrestre està associat amb la transferència de material fi per efecte dels corrents i amb la deposició atmosfèrica. Tot i les limitacions existents a l'hora de determinar l'origen de la MO a la resta de canyons investigats, és altament probable que la proximitat de les capçaleres dels canyons del sistema Garrucha-Almanzora a algunes desembocadures fluvials afavoreixi la transferència de MO d'origen terrestre provinent de plantes vasculars cap als seus eixos, principalment durant els temporals.

La distribució dels MT i l'As a les partícules que sedimenten mostrejades a pocs metres damunt del fons està estretament influenciada per la composició de de la fracció terrígena i per la susceptibilitat de certs metalls front als processos de remoció i formació de fases autigèniques a la columna d'aigua, principalment òxids i oxihidròxids de Mn. Els forçaments externs ocasionals no només incrementen l'exportació de MT i As cap als canyons, sinó que en modifiquen el seu contingut en els fluxos de partícules. Així succeeix durant els temporals, quan l'exportació de material resuspès des de la plataforma provoca un efecte de dilució de la fracció autigènica, com s'ha observat als canyons d'Escombreras i d'Almeria. En el cas del canyó d'Almeria també s'ha observat aquest efecte sobre els metalls associats a la fracció litogénica, rica en carbonat biogènic, resuspesa a la plataforma. Per la seva banda, els MT i l'As que sedimenten en el sistema de canyons Garrucha-Almanzora mostren una notable variabilitat temporal, probablement relacionada amb una major complexitat de la dinàmica sedimentaria del canyó, inclosos els efectes de la pesca d'arrossegament de fons que es pràctica al seu voltant.

La distribució del Cu, el Pb i el Zn està vinculada també amb les aportacions antropogèniques, probablement des de de fonts pròximes als mateixos canyons investigats. El càlcul de factors d'enriquiment al canyó d'Escombreras evidencia que tant les partícules que hi sedimenten com els sediments del fons estan contaminats per Zn i, possiblement, per Pb i Cu. Les mesures semi-

quantitatives dels continguts de Pb i Zn en els 51 cm superiors del testimoni analitzat, així com la datació dels sediments pel mètode del ^{201}Pb, demostren que l'increment de les concentracions de metalls s'inicià al segle XIX, mantenint-se en nivells elevats des de la segona meitat del segle XX, coincidint amb el període d'abocament massiu de residus miners a la badia. Tanmateix, l'anàlisi dels isòtops de Pb en mostres del canyó suggereix que el dipòsit de residus de Portmán no fou la font principal de contaminants metàl·lics cap al canyó durant el període esmentat, tot i palesant l'existència d'aportacions atmosfèriques de Pb antropogènic.

Línies d'investigació futures

Els resultats assolits en aquesta Tesi han obert la porta a un conjunt de possibles tasques que podrien ser desenvolupades.

- Els forçaments externs tenen un impacte directe en la redistribució de MT i carboni al llarg del marge continental. Disposar de sèries temporals llargues de fluxos de partícules permetria aprofundir en el paper d'aquests processos, establir el grau de variabilitat interanual i detectar possibles tendències. A més, l'evolució de la composició dels fluxos de partícules a mesura que descendeixen cap al fons marí afecta les taxes d'exportació dels metalls (Huang i Conte, 2009). Així dons, seria interessant monitoritzar els fluxos de partícules a diferents nivells de profunditat de la columna d'aigua per tal d'avaluar com la producció, degradació o alteració biogeoquímica afecten a l'exportació de MT, i indagar en la interrelació dels cicles del carboni i dels MT.

- Les dades revelen que la pràctica de la pesca d'arrosegament de fons prop del sistema Garrucha-Almanzora incrementa la presència de partícules en suspensió dins de l'eix del canyó. Aquestes partícules actuen com a vectors de transport de MT (Laës et al., 2007; Al-Hashem et al., 2022), i per tant, seria molt interessant estudiar la variabilitat temporal i espacial de les capes nefeloides, i dur a terme mostrejos i anàlisis composicionals específiques de les partícules en suspensió.
  Les partícules sovint es classifiquen en dos grups funcionals segons la seva mida (i) la fracció més petita (0,4-53 μm), que es manté en suspensió i constitueix la major part de la massa de les partícules marines, i (ii) la fracció més gran (>53 μm), que s'enfonsa a través de la columna d'aigua i representa la major part dels fluxos de partícules (Lam and Marchal, 2015). Malgrat ser una simplificació, la caracterització geoquímica de les dues fraccions per separat permetria explorar els processos biogeoquímics que regulen part del cicle dels TM d'una manera operativament senzilla (Henderson i Marchal, 2015).

- Els resultats destaquen la presència de CO provinent de restes vegetals de fanerògames marines al canyó d'Escombreras. Aquest CO és depositat i enterrat en el marge extern, una via que tradicionalment no s'ha tingut en compte en les estimacions globals de segrest de carboni dels ecosistemes vegetals costaners (Durate and Krause-Jensen, 2017). L'intercanvi de CO des de la costa fins al marge profund pot ser significatiu en tot el marge sud-est de la península Ibèrica, on les praderes ocupen una àrea extensa d'uns 315 km^2 a les províncies de Múrcia i d'Almeria. El seu paper pot ser especialment rellevant en un marge amb escassa descàrrega fluvial.

-

Capítol 6

Bibliografia

Acosta, J., Fontán, A., Muñoz, A., Muñoz-Martín, A., Rivera, J. et al., 2013. The morpho-tectonic setting of the Southeast margin of Iberia and the adjacent oceànic Algero-Balearic Basin. Mar. Pet. Geol. 45, 17–41. Doi: 10.1016/j.marpetgeo.2013.04.005.

AEMET, 2011. Atlas climático ibérico. Temperatura del aire y precipitación (1971-2000). Agencia Estatal de Meteorología, Ministerio de Medio Ambiente y Medio Rural y Marino, e Instituto de Meteorologia de Portugal.

Agrawal, Y.C., McCave, I.N. i Riley, J.B., 1991. Laser diffraction size analysis, In J.P.M. Syvitski (ed.): Principles, methods, and application of particle size analysis; Cambridge University Press, Cambridge, p. 119-129.

Al-Hashem, A.A., Beck, A.J., Krisch, S., Menzel Barraqueta, J.-L., Steffens, T. et al., 2022. Particulate trace metal sources, cycling, and distributions on the southwest African shelf. Glob. Biogeochem. Cycles 36. Doi: 10.1029/2022GB007453.

Aloupi, M. I Angelidis, M.O., 2001. Normalization to lithium for the assessment of metal contamination in coastal sediment cores from the Aegean Sea. Mar. Environ. Res. 52, 1–12. Doi: 10.1016/S0141-1136(00)00255-5.

Allen, S.E. i Durrieu de Madron, X., 2009. A review of the role of submarine canyons in deep-ocean exchange with the shelf. Ocean Sci. 5, 607–620. Doi: 10.5194/os-5-607-2009.

Alorda-Kleinglass, A., Garcia-Orellana, J., Rodellas, V., Cerdà-Domènech, M., Tovar- Sánchez, A. et al., 2019. Remobilization of dissolved metals from a coastal mine tailing deposit driven by groundwater discharge and porewater exchange. Sci. Total Environ. 688, 1359–1372. Doi: 10.1016/j.scitotenv.2019.06.224.

Álvarez-Iglesias, P., Rubio, B. i Millos, J., 2012. Isotopic identification of natural vs. anthropogenic lead sources in marine sediments from the inner Ría de Vigo (NW Spain). Sci. Total Environ.437, 22-35. Doi: 10.1016/j.scitotenv.2012.07.063.

Amblas, D., Ceramicola, TS., Gerber, T.P., Canals, M., Chiocci, F.L. et al., 2018. Submarine Canyons and Gullies. In: Micallef, A., Krastel, S., Savini, A. (eds) Submarine Geomorphology. Springer Geology. Springer, Cham. Doi: 10.1007/978-3-319-57852-1_14.

Anderson, R.F., 2020. GEOTRACES: Accelerating research on the marine biogeochemical cycles of trace elements and their isotopes. Annu. Rev. Mar. Sci. 12 (1), 49–85. Doi: 10.1146/annurev-marine-010318-095123.

Antia, A.N., von Bodungen, B. I Peinert, R., 1999. Particle flux across the mid-European continental margin. Deep-Sea Res. I 46(12), 1999-2024. Doi: 10.1016/S0967-0637(99)00041-2.

Apostolaki, E.T., Caviglia, L., Santinelli, V., Cundy, A.B., Tramati, C.D. et al., 2022. The Importance of Dead Seagrass (Posidonia oceanica) Matte as a Biogeochemical Sink. Front. Mar. Sci. 9:861998. Doi: 10.3389/fmars.2022.861998.

Armstrong, R. A., Peterson, M. L., Lee, C., i Wakeham, S. G., 2009. Settling velocity spectra and the ballast ratio hypothesis, Deep Sea Res. Part II Top. Stud. Oceanogr. 56, 1470–1478. Doi: 10.1016/j.dsr2.2008.11.032.

Atwood, T.B, Witt, A., Mayorga, J., Hammill, E. i Sala, E., 2020. Global Patterns in Marine Sediment Carbon Stocks. Front. Mar. Sci. 7:165. Doi: 10.3389/fmars.2020.00165.

Auernheimer, C. i Chinchon, S., 1997. Calcareous skeletons of sea urchins as indicators of heavy metals pollution. Portman Bay, Spain. Environ. Geol. 29, 78-83. Doi: 10.1007/s002540050106.

Azaroff, A., Miossec, C., Lanceleur, L., Guyoneaud, R. i Monperrus, M., 2020. Priority and emerging micropollutants distribution from coastal to continental slope sediments: A case study of Capbreton Submarine Canyon (North Atlantic Ocean). Sci. Total Environ. 703, 135057. Doi: 10.1016/j.scitotenv.2019.135057.

Baker, E.T., Milburn, H.B. I Tennant, D.A., 1988. Field assessment of sediment trap efficiency under varying flow conditions. J. Mar. Res. 46 (3), 573–592. Doi: 10.1357/002224088785113522.

Baldacci, A., Corsini, G., Grasso, R., Manzella, G., Allen, J.T. et al., 2001. A study of the Alboran Sea mesoscale system by means of empirical orthogonal function decomposition of satellite data. J. Mar. Syst. 29 (1-4), 293–311. Doi: 10.1016/S0924-7963(01)00021-5.

Bao, R., van der Voort, T. S., Zhao, M., Guo, X., Montluçon, D. B. et al., 2018. Influence of hydrodynamic processes on the fate of sedimentary organic matter on continental margins. Glob. Biogeochem. Cycles, 32. Doi: 10.1029/2018GB005921.

Baza-Varas, A., Canals, M., Frigola, J., Cerdà-Domènech, M., Rodés, N. et al., 2022. Multiproxy characterization of sedimentary facies in a submarine sulphide mine tailings dumping site and their environmental significance: the study case of Portmán Bay (SE Spain). Sci. Total Environ. 810, 151183. Doi: 10.1016/j.scitotenv.2021.151183.

Baza-Varas, A., 2023. Aplicación de tecnologías avanzadas para la caracterización del depósito de vertidos mineros de la bahía de Portmán, Murcia (España). Universitat de Barcelona, PhD Thesis, 244 p.

Baza-Varas, A., Roqué-Rosell, J., Canals, M., Frigola, J., Cerdà-Domènech, M. et al., 2023. As and S speciation in a submarine sulfide mine tailings deposit and its environmental significance: The study case of Portmán Bay (SE Spain). Sci. Total Environ. 882, 163649. Doi: 10.1016/j.scitotenv.2023.163649.

Benedicto, J., Martínez-Gómez, C., Guerrero, J., Jornet, A. i Rodríguez, C., 2008. Contaminación por metales en la bahía de Portmán (Murcia, SE España) 15 años después del cese de las actividades mineras. Cienc Mar 34 (3), 389-398. Doi: 10.7773/cm.v34i3.1391.

Bianchi, T. S., 2011. The role of terrestrially derived organic carbon in the coastal ocean: a changing paradigm and the priming effect. Proc. Natl. Acad. Sci. U.S.A. 108, 19473–19481. Doi: 10.1073/pnas.1017982108.

Bianchi, T.S., Argyrou, M. i Chippett, H.F., 1999. Contribution of vascular-plant carbon to surface sediments across the coastal margin of Cyprus (eastern Mediterranean). Org. Geochem. 30, 287-297. Doi: 10.1016/S0146-6380(99)00016-9.

Birch, G.F., 2017. Determination of sediment metal background concentrations and enrichment in marine environments - A critical review. Sci. Total Environ. 580, 813-831. Doi: 10.1016/j.scitotenv.2016.12.028.

Bishop, J. K. B. i Fleisher, M. Q., 1987. Particulate manganese dynamics in gulf-stream warm-core rings and surrounding waters of the NW Atlantic, Geochim. Cosmochim. Acta 51(10), 2807–2825. Doi: 10.1016/0016-7037(87)90160-8.

Blain, S., Planquette, H., Obernosterer, I. i Guéneuguès, A., 2022. Vertical flux of trace elements associated with lithogenic and biogenic carrier phases in the Southern Ocean. Glob. Biogeochem. Cycles 36. Doi: 10.1029/2022GB007371.

Bonnin, J., Heussner, S., Calafat, A., Fabres, J., Palanques, A. et al., 2008. Comparison of horizontal and downward particle fluxes across canyons of the Gulf of Lions (NW Mediterranean): Meteorological and hydrodynamical forcing. Cont. Shelf Res. 28 (15), 1957–1970. Doi: 10.1016/j.csr.2008.06.004.

Bollhöfer, A. i Rosman, K.J.R., 2000. Isotopic source signatures for atmospheric lead: the Northern Hemisphere. Geochim. Cosmochim. Acta 65, 1727–1740. Doi: 10.1016/S0016-7037(00)00630-X.

Bourrin, F., Uusõue, M., Artigas, M. C., Sanchez-Vidal, A., Aubert, D. et al., 2021. Release of particles and metals into seawater following sediment resuspension of a coastal mine tailings disposal off Portmán Bay, Southern Spain. Environ. Sci. Pollut. Res. 1-18. Doi: 10.1007/s11356-021-14006-1.

Boyle, J.F., 2000. Rapid elemental analysis of sediment samples by isotope source XRF. J. Paleolimnol. 23, 213–221. Doi: 10.1023/A:1008053503694.

Boyle, E.A., Lee, J.M., Echegoyen, Y., Noble, A., Moos, S. et al., 2014. Anthropogenic lead emissions in the ocean: the evolving global experiment. Oceanography 27(1), 69–75. Doi: 10.5670/oceanog.2014.10.

Briggs, N., Dall'Olmo, G I Claustre, H., 2020. Major role of particle fragmentation in regulating biological sequestration of CO2 by the oceans. Science 367 (6479), 791-793. Doi: 10.1126/science.aay1790.

Bruland, 1989. Complexation of zinc by natural organic ligands in the central North Pacific. Limnol. Oceanogr. 34(2), 269-285. Doi: 10.4319/lo.1989.34.2.0269

Bruland, K.W. i Lohan, M.C., 2004. Controls of Trace Metals in Seawater Treatise on Geochemistry, Volume 6. Editor: Henry Elderfield. Executive Editors: Heinrich D. Holland and Karl K. Turekian. pp. 625. ISBN 0-08-043751-6. Elsevier, 2003., p.23-47. Doi: 10.1016/B0-08-043751-6/06105-3.

Bruni, E.T., Blattmann, T.M., Haghipour, N., Louw, D., Lever, M. et al., 2022. Sedimentary Hydrodynamic Processes Under Low-Oxygen Conditions: Implications for Past, Present, and Future Oceans. Front. Earth Sci. 10, 886395. Doi: 10.3389/feart.2022.886395.

Buesseler, K.O., Antia, A.N., Avan, N., Chen, M., Fowler, S.W. et al., 2007. An assessment of the use of sediment traps for the estimating upper ocean particle fluxes. J. Mar. Res. 65, 345–416. Doi: 10.1357/002224007781567621.

Canals, M., Puig, P., Heussner, S., Durrieu de Madron, X., Palanques, A. et al., 2006. Flushing submarine canyons. Nature, 444, 354-357. Doi: 10.1038/nature05271.

Canals, M., Danovaro, R., Heussner, S., Lykousis, V., Puig, P. et al., 2009. Cascades in Mediterranean submarine grand canyons. Oceanography 22 (1), 26-43.

Canals, M., Amblàs, D., Lastras, G., Sànchez-Vidal, A., Calafat, A.M. et al., 2012. Els canyons submarins. Història Natural dels Països Catalans: La Terra a l'Univers, Suplement. Fundació Enciclopèdia Catalana, Barcelona, p. 251-272

Canals, M., Company, J.B., Martín, D., Sanchez-Vidal, A. i Ramírez-Llorda, E., 2013. Integrated study of Mediterranean deep canyons: novel results and future challenges. Prog. Oceanogr. 118, 1–27. Doi: 10.1016/j.pocean.2013.09.004.

Cerdà i Domènech, M., 2020. Fluxos d'aigua subterrània i concentració de metalls en dipòsits marins costaners contaminats: aproximació metodològica i casos d'estudi a la costa mediterrània de la Península Ibèrica. Universitat de Barcelona, PhD Thesis, 276 p. http://hdl.handle.net/10803/672444.

Cerdà-Domènech, M., Frigola, J., Sanchez-Vidal, A. i Canals, M., 2020. Calibrating high resolution XRF core scanner data to obtain absolute metal concentrations in highly polluted marine deposits after two case studies off Portmán Bay and Barcelona, Spain. Sci. Total Environ. 717, 134778. Doi: 10.1016/j.scitotenv.2019.134778.

Cesar, A., Marín, A., Marin-Guirao, L. i Vita, R., 2004. Amphipod and sea urchin tests to assess the toxicity of Mediterranean sediments: The case of Portmán Bay. Sci. Mar. 68 (Suppl. 1), 205-213. Doi: 10.3989/scimar.2004.68s1205.

Cesar, A., Marín, A., Marin-Guirao, L., Vita, R., Lloret, J. et al., 2009. Integrative ecotoxicological assessment of sediment in Portmán Bay (southeast Spain). Ecotoxicol. Environ. Saf. 72 (7), 1832-1841. Doi: 10.1016/j.ecoenv.2008.12.001.

Chester, R., 2002. Marine geochemistry. 2nd ed. Oxford; Blackwell Science. ISBN 0632054328.

Cole, J.J., Prairie, Y.T., Caraco, N.F., McDowell, W.H., Tranvik, L.J. et al., 2007. Plumbing the global carbon cycle: integrating inland waters into the terrestrial carbon budget. Ecosystems 10, 171–84. Doi: 10.1007/s10021-006-9013-8.

Comisión nacional de estrategias Marinas, 2015. Directrices para la caracterización del material dragado y su reubicación en aguas del dominio público marítimo-terrestre. Minist. Agric. Aliment. Y medio Ambient.

Company, J.B., Puig, P., Sardá, F., Palanques, A., Latasa M. et al., 2008. Climate Influence on Deep Sea Populations. PLOS ONE 3(1), e1431. Doi: 10.1371/journal.pone.0001431.

Conte, M.H., Ralph, N i Ross, E., 2001. Seasonal and interannual variability in deep ocean particle fluxes at the Oceanic Flux Program (OFP)/Bermuda Atlantic Time Series (BATS) site in the

western Sargasso Sea near Bermuda. Deep Sea Res.Part I 48(8-9), 1471-1505. Doi: 10.1016/S0967-0645(00)00150-8.

Conte, M.H., Carter, A.M., Koweek, D.A., Huang, S. i Weber, J.C., 2019. The elemental composition of the deep particle flux in the Sargasso Sea. Chem. Geol. 511, 279–313. Doi.org/10.1016/j.chemgeo.2018.11.001.

Cossa, D., Buscail, R., Puig, P., Chiffoleau, J.F., Radakovitch, O. et al., 2014. Origin and accumulation of trace elements in sediments of the northwestern Mediterranean margin. Chem. Geol. 380, 61–73. Doi: 10.1016/j.chemgeo.2014.04.015.

Dahms, H.U., 2014. The grand challenges in marine pollution research. Front. Mar. Sci. 1. Doi: 10.3389/fmars.2014.00009

De la Rocha, C.L i Passow, U., 2007. Factors Influencing the Sinking of POC and the Efficiency of the Biological Carbon Pump. Deep Sea Res. Part II 54(5-7), 639-658. DOI: 10.1016/j.dsr2.2007.01.004.

De Leo, F.C., Smith, C.R., Rowden, A.A., Bowden, D.A. i Clark, M.R., 2010. Submarine canyons: hotspots of benthic biomass and productivity in the deep sea. Proceedings of the Royal Society B, 277(1695), 2783-2792. doi

Durán, R., Guillén, J., Rivera, J., Lobo, F. J., Muñoz, A. et al., 2018. Formation, evolution and present-day activity of offshore sand ridges on a narrow, tideless continental shelf with limited sediment supply. Mar. Geol. 397, 93-107. Doi: 10.1016/j.margeo.2017.11.001.

Duarte, C.M. i Krause-Jensen, D., 2017. Export from Seagrass Meadows Contributes to Marine Carbon Sequestration. Front. Mar.Sci.4:13. Doi: 10.3389/fmars.2017.00013.

Durrieu de Madron, X., Houpert, L., Puig, P., Sanchez-Vidal, A., Testor, P. et al., 2013. Interaction of dense shelf water cascading and open-sea convection in the northwestern Mediterranean during winter 2012. Geophys. Res. Lett. 40, 1379-1385. Doi: 10.1002/grl.50331.

Durrieu de Madron, X., Nyffeler, F. i Godet, C.H., 1990. Hydrographic structure and nepheloid spatial distribution in the Gulf of Lions continental margin. Cont. Shelf Res. 10 (9–11), 915–929. Doi: 10.1016/0278-4343(90)90067-V.

Duxbury, A.B., Duxbury, A.C. i dan Sverdrup, K.A., 2002. Fundamentals of Oceanography, 4th edition. McGraw Hill. New York 344 pp.

Dymond, J., 1984. Sediment traps, particle fluxes, and benthic boundary layer processes, in Global Ocean Flux Study, Proceedings of a Workshop, National Academy Press, Washington, D.C., pp. 260-284.

Ercilla, G., Galindo-Zaldívar, J., Estrada, F., Valencia, J., Juan, C. et al., 2022. Understanding the complex geomorphology of a deep sea area affected by continental tectonic indentation: The case of the Gulf of Vera (Western Mediterranean). Geomorphology 402, 108126. Doi: 10.1016/j.geomorph.2022.108126.

Estrada, F., Ercilla, G. i Alonso, B., 1997. Pliocene-Quaternary tectonic-sedimentary evolution of the NE Alboran Sea (SW Mediterranean Sea). Tectonophysics 282 (1-4), 423–442. Doi: 10.1016/S0040-1951(97)00227-8.

Fabres, J., Calafat, A., Sanchez-Vidal, A., Canals, M. i Heussner, S., 2002. Composition and spatio-temporal variability of particle fluxes in the Western Alboran Gyre, Mediterranean Sea (SW Mediterranean). J. Mar. Syst. 33–34, 431–456. Doi: 10.1016/S0924-7963(02)00070-2.

Fernandez-Arcaya, U., Ramirez-Llodra, E., Aguzzi, J., Allcock, A.L., Davies, J.S. et al., 2017. Ecological Role of Submarine Canyons and Need for Canyon Conservation: A Review. Front. Mar. Sci. 4:5. Doi: 10.3389/fmars.2017.00005.

Ferré, B., Guizien, K., Durrieu de Madron, X., Palanques, A., Guillén, J. et al., 2005. Fine-grained sediment dynamics during a strong storm event in the inner-shelf of the Gulf of Lion (NW Mediterranean). Cont. Shelf Res. 25 (19-20), 2410–2427. Doi: 10.1016/j.csr.2005.08.017.

Fowler, S.W. i Knauer, G.A, 1986. Role of large particles in the transport of elements and organic compounds through the oceanic water column. Prog. Oceanogr. 16, 147-194. Doi: 10.1016/0079-6611(86)90032-7.

Gambi, C., Dell'Anno, A., Corinaldesi, C., Martire, M.L., Musco, L. et al., 2020. Impact of historical contamination on meiofaunal assemblages: the case study of the bagnoli-Coroglio Bay (southern Tyrrhenian Sea). Mar.Environ. Res. 156, 104907. Doi: 10.1016/j.marenvres.2020.104907.

García, M., Alonso, B., Ercilla, G. i Gràcia, E., 2006. The tributary valley systems of the Almeria Canyon (Alboran Sea, SW Mediterranean): Sedimentary architecture. Mar. Geol. 226 (3-4), 207–223. Doi: doi.org/10.1016/j.margeo.2005.10.002.

Garcia-Gorriz, E. i Carr, M.E., 2001. Physical control of phytoplankton distributions in the Alboran Sea: A numerical and satellite approach. J. Geophys. Res. 106 (C8), 16795–16805. Doi: 10.1029/1999JC000029.

García-Rodríguez, M., 2005. La gamba roja "Aristeus antennatus" (Risso, 1816) (Crustacea, Decapoda): distribución, demografía, crecimiento, reproducción y explotación en el Golfo de Alicante, Canal de Ibiza y Golfo de Vera. Tesis de la Universidad Complutense de Madrid, Facultad de Ciencias Biológicas. Departamento de Biología Animal I.

Gardner, W.D., 1985. The effect of tilt on sediment trap efficiency. Deep-Sea Res. 32 (3), 349–361. Doi: 10.1016/0198-0149(85)90083-4.

Gardner, W.D., Biscaye, P.E i Richardson, M.J., 1997. A sediment trap experiment in the vema channel to evaluate the effectof horizontal particle fluxes on measured vertical fluxes. J. Mar. Res. 55(5), 995-1028.

Geibert, W., 2018. Processes that regulate trace element distribution in the ocean. Elements 14, 391–396. Doi: 10.2138/gselements.14.6.3912015.

Goñi, M.A. i Hedges, J.I., 1990. Potential applications of cutin-derived CuO reaction products for discriminating vascular plant sources in natural environaments. Geochim. Cosmochim. Acta. 54 (11), 3073-3081. Doi: 10.1016/0016-7037(90)90123-3.

Goñi, M.A. i Hedges, J.I., 1995. Sources and reactivities of marine derived organic matter in coastal sediments as determined by alkaline CuO oxidation. Geochim. Cosmochim. Acta 59, 2965e2981. Doi: 10.1016/0016-7037(95)00188-3.

Goñi, M.A. i Montgomery, S., 2000. Alkaline CuO oxidation with a microwave digestion system. Lignin analyses of geochemical samples. Anal. Chem. 72, 3116e3121. Doi: 10.1021/ac991316w.

Goñi, M.A., Yunker, M.B., Macdonald, R.W. i Eglinton, T.I., 2000. Distribution and sources of organic biomarkers in arctic sediments from the Mackenzie River and Beaufort Shelf. Mar. Chem. 71, 23-51. Doi: 10.1016/S0304-4203(00)00037-2.

Guillén, J., Bourrin, F., Palanques, A., Durrieu de Madron, X., Puig, P. et al., 2006. Sediment dynamics during wet and dry storm events on the Têt inner shelf (SW Gulf of Lions). Mar. Geol. 234 (1-4), 129–142. Doi: 10.1016/j.margeo.2006.09.018.

de Haan, W.P., Uviedo, O., Ballesteros, M., Canales, I., Curto, X. et al., 2022. Floating microplastic loads in the nearshore revealed through citizen science. Environ. Res. Lett. 17, 045018. Doi: 10.1088/1748-9326/ac5df1.

Harris P.T. i Whiteway, T., 2011. Global distribution of large submarine canyons: Geomorphic differences between active and passive continental margins. Mar. Geol. 285, 69-86. Doi: 10.1016/j.margeo.2011.05.008.

Harris i Macmillan-Lawler, 2015. Geomorphology of Mediterranean submarine canyons in a global context- Results from a multivariate analysis of canyon geomorphic statistics. CIESM 2015. Submarine Canyon Dynamics in the Mediterranean and Tributary Seas. CIESM Workshop Monograph n° 47 [F. Briand, ed.], 232 p., CIESM Publisher, Monaco

Harris, P.T., Macmillan-Lawler, M. Rupp, J. i Baker, E.K., 2014. Geomorphology of the oceans. Mar. Geol. 352, 4-24. Doi: 10.1016/j.margeo.2014.01.011.

Heburn, G.W. i La Violette, P.E., 1990. Variations in the structure of the anticyclonic gyres found in the Alboran Sea. J. Geophys. Res. 95, 1599-1613. Doi: 10.1029/JC095iC02p01599

Hedges, J.I. i Keil, R.G., 1995. Sedimentary organic matter preservation: an assessment and speculative synthesis. Mar. Chem. 49, 81–115. Doi: 10.1016/0304-4203(95)00008-F.

Hedges, J.I., Keil, R.G. i Benner, R., 1997. What happens to terrestrial organic matter in the ocean? Org. Geochem. 27, 195e212. Doi: 10.1016/S0146-6380(97)00066-1.

Hegdes, J.I., Baldock, J.A., Gélinas, Y., Lee, C. Peterson, M.L. et al., 2002. The biochemical and elemental compositions of marine plankton: A NMR perspective." Mar. Chem. 78(1), 47-63. Doi: 10.1016/S0304-4203(02)00009-9.

Hedges, J.I. i Mann, D.C., 1979. The characterization of plant tissues by their lignin oxidation products. Geochim. Cosmochim. Acta 43 (11), 1803-1807. Doi: 10.1016/0016-7037(79)90028-0.

Heimbürger, L.E., Cossa, D., Thibodeau, B., Khripounoff, A., Mas, V. et al., 2012. Natural and anthropogenic trace metals in sediments of the Ligurian Sea (Northwestern Mediterranean). Chem. Geol. 291, 141–151. Doi: 10.1016/j.chemgeo.2011.10.011.

Henson, S. A., Sanders, R., Madsen, E., Morris, P.J., Le Moigne, F. et al., 2011. A reduced estimate of the strength of the ocean's biological carbon pump. Geophys. Res. Lett. 38, 1–5. Doi: 10.1029/2011GL046735.

Henderson, G.M. i Marchal, O., 2015. Recommendations for future measurement and modelling of particles in GEOTRACES and other ocean biogeochemistry programmes. Prog. Oceanogr. 133, 73–78. Doi: 10.1016/j.pocean.2015.01.015.

Hernández-Almeida, I., Bárcena, M.A., Flores, J.A., Sierro, F.J., Sanchez-Vidal, A. et al., 2011. Microplankton response to environmental conditions in the Alboran Sea (Western Mediterranean): One year sediment trap record. Mar. Micropaleontol. 78 (1-2), 14–24. Doi: 10.1016/j.marmicro.2010.09.005.

Heussner, S., Durrieu de Madron, X., Calafat, A., Canals, M., Carbonne, J. et al., 2006. Spatial and temporal variability of downward particle fluxes on a continental slope: lessons from an 8-yr experiment in the Gulf of Lions (NW Mediterranean). Mar. Geol. 234 (1-4), 63–92. Doi.org/10.1016/j.margeo.2006.09.003.

Heussner, S., Calafat, A, I Palanques, A., 1996. Quantitative and qualitative features of particle fluxes in the North-Balearic Basin, EUROMARGE-NB Final Report, Ed. By Canals, M., Casamor, J.L., Cacho, I., Calafat, A.M., Monaco, A., MAST II Program. EC 2, 41-66.

Heussner, S., Ratti, C. i Carbonne, J., 1990. The PPS 3 time-series sediment trap and the trap sample processing techniques used during the ECOMARGE experiment. Cont. Shelf Res. 10 (9-11), 943–958. Doi: 10.1016/0278-4343(90)90069-X.

Ho, T.Y., Chou, W.C., Lin, H.L. i Sheu, D.D., 2011. Trace metal cycling in the deep water of the South China Sea: The composition, sources, and fluxes of sinking particles. Limnol. Oceanogr. 56(4), 1225–1243. Doi: 10.4319/lo.2011.56.4.1225.

Homoky, W.B., Weber, T., Berelson, W.M., Conway, T.M., Henderson, G.M. et al., 2016. Quantifying trace element and isotope fluxes at the ocean–sediment boundary: a review. Phil. Trans. R. Soc. A 374: 20160246. Doi: 10.1098/rsta.2016.0246.

Horowitz, A.J. i Elrick, K.A., 1987. The relation of stream sediment surface area, grain size and composition to trace element chemistry. Applied geochemistry 2 (4), 437-451.

Huang, S. i Conte, M.H., 2009. Source/process apportionment of major and trace elements in sinking particles in the Sargasso sea. Geochim. Cosmochim. Acta 73, 65–90. Doi: 10.1016/j.gca.2008.08.023.

Iversen, M. H. i Ploug, H., 2010. Ballast minerals and the sinking carbon flux in the ocean: carbon-specific respiration rates and sinking velocity of marine snow aggregates. Biogeosciences 7, 2613–2624. Doi: 10.5194/bg-7-2613-2010.

Jensen, L.T., Morton, P., Twining, B.S., Heller, M.I., Hatta, M. et al., 2020. A comparison of marine Fe and Mn cycling: U.S. GEOTRACES GN01 Western Arctic case study. Geochim. Cosmochim. Acta 288, 138–160. Doi: 10.1016/j.gca.2020.08.006.

Kamatani, A. i Oku, O., 2000. Measuring biogenic silica in marine sediments. Mar. Chem. 68 (3), 219–229. Doi: 10.1016/S0304-4203(99)00079-1.

Kalnejais, L.H., Martin, W.R., Signell, R.P. i Bothner, M.H., 2007. Role of sediment resuspension in the remobilization of particulate-phase metals from coastal sediments. Environ. Sci. Tech. 41, 2282–2288. Doi: 10.1021/es061770z.

Klap, V.A., Hemminga, M.A. i Boon, J.J., 2000. Retention of lignin in seagrasses: angiosperms that returned to the sea. Mar. Ecol. Prog. Ser. 194, 1-11.

Klar, J.K., Homoky, W.B., Statham, P.J., Birchill, A.J., Harris, E.L. et al., 2017. Stability of dissolved and soluble Fe(II) in shelf sediment pore waters and release to an oxic water column. Biogeochemistry 135, 49-67. Doi: 10.1007/s10533-017-0309-x.

Komárek, M., Ettler, V., Chrastný, V. i Mihaljevič, M., 2008. Lead isotopes in environmental sciences: A review. Environ. Int. 34, 562–577. Doi: 10.1016/j.envint.2007.10.005.

Kuss, J., Waniek, J.J., Kremling, K. i Schulz-Bull, D.E., 2010. Seasonality of particle associated trace element fluxes in the deep northeast Atlantic Ocean. Deep-Sea Res. I 57, 785–796. Doi: 10.1016/j.dsr.2010.04.002.

Laës, A., Blain, S., Laan, P., Ussher, S. J., Achterberg, E. P. et al., 2007. Sources and transport of dissolved iron and manganese along the continental margin of the Bay of Biscay, Biogeosciences 4, 181–194. Doi: 10.5194/bg-4-181-2007.

Lam, P.J. i Marchal, O., 2015. Insights into Particle Cycling from Thorium and Particle Data Annu. Rev. Mar. Sci. 2015.7:159-184. Doi: 10.1146/annurev-marine-010814-015623.

Lam, P.J., Ohnemus, D.C. i Auro, M.E., 2015. Size-fractionated major particle composition and concentrations from the US GEOTRACES North Atlantic Zonal Transect. Deep Sea Res. Part II 116, 303-320. Doi: 10.1016/j.dsr2.2014.11.020.

Landrigan, P.J., Stegeman, J.J., Fleming, L.E., Allemand, D., Anderson,. D.M. et al., 2020. Human Health and Ocean Pollution. Ann. Glob. Health 86(1), p.151. Doi: 10.5334/aogh.2831.

Langone, L., Conese, I., Miserocchi, S., Boldrin, A., Bonaldo, D. et al., 2016. Dynamics of particles along the western margin of the Southern Adriatic: Processes involved in transferring particulate matter to the deep basin. Mar. Geol. 375, 28–43. Doi: 10.1016/j.margeo.2015.09.004.

Lanning, N. T., Jiang, S., Amaral, V. J., Mateos, K., Steffen, J. M. et al., 2023. Isotopes illustrate vertical transport of anthropogenic Pb by reversible scavenging within Pacific Ocean particle veils. PNAS 120(23), e2219688120. Doi: 10.1073/pnas.2219688120.

Lazzari, P., Solidoro, C., Ibello, V., Salon, S., Teruzzi, A. et al., 2011. Seasonal and inter-annual variability of plankton chlorophyll and primary production in the Mediterranean Sea: a

modelling approach. Biogeosciences Discuss., 8, 5379–5422, 2011. Doi: 10.5194/bgd-8-5379-2011.

Cindy, L., Wakeham, S. i Arnosti, C., 2004. Particulate organic matter in the sea: the composition conundrum. AMBIO: A Journal of the Human Environment 33(8), 565-575. DOI: 10.1639/0044-7447(2004)033[0565:POMITS]2.0.CO;2.

Lee, J.M., Heller, M.I. i Lam, P.J., 2018. Size distribution of particulate trace elements in the U.S. GEOTRACES Eastern Pacific Zonal Transect (GP16). Mar. Chem. 201, 108–123. Doi: 10.1016/j.marchem.2017.09.006.

Liquete, C., Arnau, P., Canals, M. i Colas, S., 2005. Mediterranean river systems of Andalusia, southern Spain, and associated deltas: A source to sink approach. Mar. Geol. 222–223, 471–495. Doi: 10.1016/j.margeo.2005.06.033.

Liu, K.K., Atkinson, L., Quiñones, R. i Talaue-McManus, L. (Eds.), 2010. Carbon and Nutrient Fluxes in Continental Margins: A Global Synthesis Global Change – The IGBP Series Series Editors International Geosphere-Biosphere Programme; The Royal Swedish Academy of Sciences, Stockholm, Sweden. Doi: 10.1007/978-3-540-92735-8.

Liu, M., Xiao, W., Zhang, Q., Yuan, S., Raymond, P.A. 2021. Substantial accumulation of mercury in the deepest parts of the ocean and implications for the environmental mercury cycle. PNAS 118 (51), e2102629118. Doi: 10.1073/pnas.2102629118.

Llull, R. M., Garí, M., Canals, M., Rey-Maquieira, T. i Grimalt, J.O., 2017. Mercury concentrations in lean fish from the Western Mediterranean Sea: dietary exposure and risk assessment in the population of the Balearic Islands. Environ. Res. 158, 16–23. Doi: 10.1016/j.envres.2017.05.033.

Lobo, F.J., Ercilla, G., Fernández-Salas, L.M. i Gámez, D., 2014. Chapter 11 The Iberian Mediterranean shelves. Geological Society, London, Memoirs 41 (1), 147–170. Doi

López-Jurado, J.L., González-Pola, C. i Vélez-Belchí, 2005. Observation of an abrupt disruption of the long-term warming trend at the Balearic Sea, western Mediterranean Sea, in summer 2005. Geophysical Research Letters 32, L24606. Doi:10.1029/2005GL024430.

Mackenzie, F. T., Andersson, A. J., Lerman, A. i Ver, L. M. in The Sea Vol. 13 (eds Robinson, A. R. & Brink, K. H.) 193-225 (Harvard Univ. Press, 2005).

Maldonado, A. i Zamarreño, I., 1983. Modelos sedimentarios en las plataformas continentales del Mediterráneo español: factores de control, facies y procesos que rigen su desarrollo. Estudio oceanográfico de la Plataforma Continental. Madrid: Proyecto de Investigacion Cooperatiava Hispano-Norteamericana, p.24-83.

Manteca, J.I., García, J.Á.L. Oyarzun, R. i Carmona, C., 2014. The beach placer iron deposit of Portman Bay, Murcia, SE Spain: The result of 33 years of tailings disposal (1957–1990) to the Mediterranean seaside. Miner. Deposita 49 (6), 777-783. Doi: 10.1007/s00126-014-0511-x.

Martín, J., Palanques, A. i Puig, P., 2006. Composition and variability of downward particulate matter fluxes in the Palam´os submarine canyon (NW Mediterranean). J. Mar. Syst. 60 (1-2), 75–97. Doi: 10.1016/j.jmarsys.2005.09.010.

Martín, J., Durrieu de Madron, X., Puig, P., Bourrin, F., Palanques, A. et al., 2013. Sediment transport along the Cap de Creus Canyon flank during a mild, wet winter. Biogeosciences 10, 3221–3239. Doi: 10.5194/bg-10-3221-2013.

Martín, J., Puig, P., Masqué, P., Palanques, A. i Sánchez-Gómez, A., 2014a. Impact of Bottom Trawling on Deep-Sea Sediment Properties along the Flanks of a Submarine Canyon. PLOS ONE 9 (8), e104536. Doi: 10.1371/journal.pone.0104536.

Martín, J., Puig, P., Palanques, A. i Ribó, M., 2014b. Trawling-induced daily sediment resuspension in the flank of a Mediterranean submarine canyon. Deep-Sea Res. II 104, 174–183. Doi: 10.1016/j.dsr2.2013.05.036.

Martínez-Gómez, C., Fernández, B., Benedicto, J., Valdés, J., Campillo, J.A. et al., 2012. Health status of red mullets from polluted areas of the Spanish Mediterranean coast, with special reference to Portmán (SE Spain). Mar. Environ. Res. 77, 50-59. Doi: 10.1016/j.marenvres.2012.02.002.

Martinez-Ruiz, F., Paytan, A., Gonzalez Muñoz, M.T., Jroundi, F., Abad, M.M. et al., 2020. Barite Precipitation on Suspended Organic Matter in the Mesopelagic Zone. Front. Earth Sci. 8:567714. Doi:10.3389/feart.2020.567714

McCave, I. N. i Hall, I. R., 2006. Size sorting in marine muds: Processes, pitfalls, and prospects for paleoflow-speed proxies. Geochem., Geophys., Geosyst, 7(10). Doi: 10.1029/2006GC001284.

Mestre, N.C., Rocha, T.L., Canals, M., Cardoso, C., Danovaro, R. et al., 2017. Environmental hazard assessment of a marine mine tailings deposit site and potential implications for deep-sea mining. Environ. Pollut. 228, 169-178. Doi: 10.1016/j.envpol.2017.05.027.

Middelburg, J. J. Marine Carbon Biogeochemistry: A Primer for Earth System Scientists. 1st ed. 2019. Doi: 10.1007/978-3-030-10822-9.

Mil-Homens, M., Blum, J., Canário, J., Caetano, M., Costa, A.M. et al., 2013. Tracing anthropogenic Hg and Pb input using stable Hg and Pb isotope ratios in sediments of the central Portuguese margin. Chem. Geol. 336, 62–71. Doi: 10.1016/j.chemgeo.2012.02.018.

Millero, F.J, 2013. Chemical Oceanography: Composition of the Major Components of Seawater (pp.75-110) CRC Press. Doi: 10.1201/b14753-8.

Millot, C., 1999. Circulation in the Western Mediterranean Sea. J. Mar. Syst. 20 (1-4), 423–442. Doi: 10.1016/S0924-7963(98)00078-5.

Millot, C. i Taupier-Letage, I., 2005. Circulation in the Mediterranean sea. In: Saliot, A. (eds) The Mediterranean Sea. Handbook of Environmental Chemistry, vol. 5K. Springer, Berlin, Heidelberg. Doi: 10.1007/b107143.

Miramontes, E., Déverchère, J., Pellegrini, C., Chiarella i D. Chapter 2 - Mediterranean Sea evolution and present-day physiography, Editor(s): Katrin Schroeder, Jacopo Chiggiato, Oceanography of the Mediterranean Sea, Elsevier, 2023, Pages 13-39, ISBN 9780128236925, Doi: 10.1016/B978-0-12-823692-5.00006-6.

Monna, F., Lancelot, J., Croudace, I.W., Cundy, A.B. i Lewis, J.T., 1997. Pb isotopic composition of airborne particulate material from France and the southern United Kingdom: implications for Pb pollution sources in urban areas. Environ. Sci. Technol. 31, 2277–2286. Doi: 10.1021/es960870+.

Moore, C. M., Mills, M. M., Arrigo, K. R., Berman-Frank, I., Bopp, L. et al., 2013. Processes and patterns of oceanic nutrient limitation. Nat. Geosci. 6(9), 701–710. Doi: 10.1038/Ngeo1765.

Morel, F.M.M. i Price, N.M., 2003. The Biogeochemical Cycles of Trace Metals in the Oceans. Science 300, 944–947. Doi: 10.1126/science.1083545.

MSFD, 2008. Directiva 2008/56/ce del Parlamento Europeo y del Consejo de 17 de junio de 2008 por la que se establece un marco de acción comunitaria para la política del medio marino (Directiva Marc sobre l'Estratègia Marina) (disponible a https://eur-lex.europa.eu/legal-content/EN/TXT/?uri=CELEX%3A32008L0056).

Müller, G., Börker, J., Sluijs, A. i Middelburg, J. J., 2022. Detrital carbonate minerals in Earth's element cycles. Glob. Biogeochem. Cycles. 36, e2021GB007231. Doi: 10.1029/2021GB007231.

Noble, A.E., Lamborg, C.H., Ohnemus, D.C., Lam, P.J., Goepfert, T.J. et al., 2012. Basin-scale inputs of cobalt, iron, and manganese from the Benguela-Angola front to the South Atlantic Ocean. Limnol. Oceanogr. 57 (4), 989–1010. Doi: 10.4319/lo.2012.57.4.0989.

Noble, A.E., Echegoyen-Sanz, Y., Boyle, E.A., Ohnemus, D.C., Lam, P.J. et al., 2015. Dynamic variability of dissolved Pb and Pb isotope composition from the U.S. North Atlantic GEOTRACES transect. Deep-Sea Res. II 116, 208–225. Doi: 10.1016/j.dsr2.2014.11.011.

Oldham, V.E., Miller, M.T., Jensen, L.T. i Luther, G.W., 2017. Revisiting Mn and Fe removal in humic rich estuaries. Geochim. Cosmochim. Acta 209, 267–283. Doi: 10.1016/j.gca.2017.04.001.

Oyarzun, R., Manteca Martínez, J.I., López García, J.A. i Carmona, C., 2013. An account of the events that led to full bay infilling with sulfide tailings at Portman (Spain), and the search for "blackswans" in a potential land reclamation scenario. Sci. Total Environ. 454 (455), 245–249. Doi: 10.1016/j.scitotenv.2013.03.030.

Palanques, A., Durrieu de Madron, X., Puig, P., Fabres, J., Guillén, J. et al., 2006a. Suspended sediment fluxes and transport processes in the Gulf of Lions submarine canyons. The role of storms and dense water cascading. Mar. Geol. 234 (1-4), 43–61. Doi: 10.1016/j.margeo.2006.09.002.

Palanques, A., Guillén, J., Puig, P. i Durrieu de Madron, X., 2008a. Storm-driven shelf-tocanyon suspended sediment transport at the southwestern Gulf of Lions. Cont. Shelf Res. 28 (15), 1947–1956. Doi: 10.1016/j.csr.2008.03.020.

Palanques, A., Martín, J., Puig, P., Guillén, J., Company, J.B. et al., 2006b. Evidence of sediment gravity flows induced by trawling in the Palamós (Fonera) submarine canyon (northwestern Mediterranean). Deep-Sea Res. I 53 (2), 201–214. Doi: 10.1016/j.dsr.2005.10.003.

Palanques, A., Masqué, P., Puig, P., Sanchez-Cabeza, J.A., Frignani, M. et al., 2008b. Anthropogenic trace metals in the sedimentary record of the Llobregat continental shelf and adjacent Foix Submarine Canyon (northwestern Mediterranean). Mar. Geol. 248 (3-4), 213–227. Doi: 10.1016/j.margeo.2007.11.001.

Palanques, A., Puig, P., Durrieu de Madron, X., Sanchez-Vidal, A., Pasqual, C. et al., 2012. Sediment transport to the deep canyons and open-slope of the western Gulf of Lions during the 2006 intense cascading and open-sea convection period. Prog. Oceanogr. 106, 1–15. Doi: 10.1016/j.pocean.2012.05.002.

Palanques, A., Paradis, S., Puig, P., Masqué, P. i Lo Iacono, C., 2022. Effects of bottom trawling on trace metal contamination of sediments along the submarine canyons of the Gulf of Palermo (southwestern Mediterranean). Sci. Total Environ. 814, 152658. Doi: 10.1016/j.scitotenv.2021.152658.

Paradis, S., Puig, P., Masqué, P., Juan-Díaz, X., Martín, J. et al., 2017. Bottom trawling along submarine canyons impacts deep sedimentary regimes. Sci. Rep. 7, 43332. Doi: 10.1038/srep43332.

Paradis, S., Goñi, M., Masqué, P., Durán, R., Arjona-Camas, M. et al., 2021. Persistence of biogeochemical alterations of deep-sea sediments by bottom trawling. Geophys. Res. Lett. 48 Doi: 10.1029/2020GL091279.

Parrilla, G., Kinder, T.H. i Preller, R.H., 1986. Deep and intermediate Mediterranean water in the western Alboran Sea. Deep Sea Res., Part I Oceanogr. Res. Pap. 33, 55–88. Doi: 10.1016/0198-0149(86)90108-1.

Payo-Payo, M., Jacinto, R.S., Lastras, G., Rabineau, M., Puig, P. et al., 2017. Numerical modeling of bottom trawling-induced sediment transport and accumulation in La Fonera submarine canyon, northwestern Mediterranean Sea. Mar. Geol. 386, 107–125. Doi: 10.1016/j.margeo.2017.02.015.

Pedreira, R. M. A., Pahnke, K., Böning, P. i Hatje, V., 2018. Tracking hospital effluent-derived gadolinium in Atlantic coastal waters off Brazil. Water Res. 145, 62–72. Doi: 10.1016/j.watres.2018.08.005.

Pedrosa-Pàmies, R., Sanchez-Vidal, A., Calafat, A., Canals, M. i Durán, R., 2013. Impact of storm-induced remobilization on grain size distribution and organic carbon content in sediments from the Blanes Canyon area, NW Mediterranean Sea. Prog. Oceanogr. 118, 122–136. Doi: 10.1016/j.pocean.2013.07.023.

Pell, R., Tijsseling, L., Goodenough, K., Wall, F., Dehaine, Q. et al., 2021. Towards sustainable extraction of technology materials through integrated approaches. Nat. Rev. Earth Environ. 2, 665–679. Doi: 10.1038/s43017-021-00211-6.

Pérez-Hernández, S., Comas, M.C. i Escutia, C., 2014. Morphology of turbidite systems within an active continental margin (the Palomares Margin, western Mediterranean). Geomorphology 219, 10–26. Doi: 10.1016/j.geomorph.2014.04.014.

Pierdomenico, M., Bernhardt, A., Eggenhuisen, J. T., Clare, M. A. et al., 2023. Transport and accumulation of litter in submarine canyons: A geoscience perspective. Front. Mar. sci. 10, 1224859. Doi: 10.3389/fmars.2023.1224859.

Puig, P., Canals, M., Company, J.B., Martín, J., Amblas, D. et al., 2012. Ploughing the deep sea floor. Nature 489 (7415), 286–289. Doi: 10.1038/nature11410.

Puig, P., Durán, R., Muñoz, A., Elvira, E. i Guillén, J., 2017. Submarine canyon-head morphologies and inferred sediment transport processes in the Alías-Almanzora canyon system (SW Mediterranean): On the role of the sediment supply. Mar. Geol. 393, 21–34. Doi: 10.1016/j.margeo.2017.02.009.

Puig, P., Palanques, A. i Martín, J., 2014. Contemporary sediment-transport processes in submarine canyons. Annu. Rev. Mar. Sci. 6, 53–77. Doi: 10.1146/annurev-marine-010213-135037.

Ramirez-Llodra, E., De Mol, B., Company, J.B., Coll, M. i Sardà, F., 2013. Effects of natural and anthropogenic processes in the distribution of marine litter in the deep Mediterranean Sea. Prog. Oceanogr. 118, 273–287. Doi: 10.1016/j.pocean.2013.07.027.

Ravaioli, M., Alvisi, F. i Vitturi, L. M., 2003. Dolomite as a tracer for sediment transport and deposition on the northwestern Adriatic continental shelf (Adriatic Sea, Italy). Cont. Shelf Res. 23(14-15), 1359-1377. Doi: 10.1016/S0278-4343(03)00121-3.

Renault, L., Oguz, T., Pascual, A., Vizoso, G. i Tintore, J., 2012. Surface circulation in the Alboran Sea (western Mediterranean) inferred from remotely sensed data. J. Geophys. Res. 117, C08009. Doi: 10.1029/2011JC007659.

Rue, E. L. i Bruland, K.W, 1995. Complexation of iron (III) by natural organic ligands in the Central North Pacific as determined by a new competitive ligand equilibration/adsorptive cathodic stripping voltammetric method. Mar. Chem. 50, 117-138. Doi: 10.1016/0304-4203(95)00031-L.

Ruiz, J.M., Guillén, J.E., Ramos Segura, A. i Otero, M.M., 2015. Atlas de las praderas marinas de España. IEO/IEL/UICN, Murcia-Alicante-Málaga, 681 pp.

Rusiecka, D., Gledhill, M., Milne, A., Achterberg, E.P., Annett, A.L. et al., 2018. Anthropogenic signatures of lead in the Northeast Atlantic. Geophys. Res. Lett. 45 (6), 2734–2743. Doi: 10.1002/2017GL076825.

Sanchez-Cabeza, J. A., Masqué, P. i Ani-Ragolta, I., 1998. 210Pb and 210Po analysis in sediments and soils by microwave acid digestion. J. Radioanal. Nucl. Chem. 227, 19–22. Doi: 10.1007/bf02386425.

Sanchez-Vidal, A., Canals, M., Calafat, A.M., Lastras, G., Pedrosa-Pàmies, R. et al., 2012. Impacts on the deep-sea ecosystem by a severe coastal storm. PLoS ONE 7 (1), e30395. Doi: 10.1371/journal.pone.0030395.

Sanchez-Vidal, A., Calafat, A., Canals, M. i Fabres, J., 2004. Particle fluxes in the Almeria-Oran front: control by coastal upwelling and sea-surface circulation. J. Mar. Syst. 52,89–106. Doi: 10.1016/j.jmarsys.2004.01.010.

Sanz, J.L., Hermida, N., Lobato, A.B., Tello, O., Fernández-Salas, L.M. et al., 2002. Estudio de la Plataforma Continental Española, Hoja MC047-Garrucha-Serie C. Secretaria General de Pesca Marítima e Instituto Español de Oceanografía.

Salvadó, J.A., Grimalt, J.O., López, J.F., Palanques, A., Heussner, S. et al., 2012. The role of dense shelf water cascading in the transfer of organochlorine compounds to open marine waters. Environ. Sci. Technol. 46 (5), 2624-2632. Doi: 10.1021/es2038189.

Salvadó, J., López, J., Palanques, A., Heussner, S., Pasqual, C. et al., 2017. Transfer of lipid molecules and polycyclic aromatic hydrocarbons to open marine waters by dense water cascading events. Prog. Oceanogr. 159, 178-194. Doi: 10.1016/j.pocean.2017.10.002.

Salvadó, J.A., Grimalt, J.O., López, J.F., Palanques, A. i Canals, M. 2019. Influence of deep water formation by open-sea convection on the transport of low hydrophobicity organic pollutants in the NW Mediterranean Sea. Sci. Total Environ. 647, 597-605. Doi: 10.1016/j.scitotenv.2018.07.45.

Sarhan, T., García Lafuente, J., Vargas, M., Vargas, J.M i, Plaza, F., 2000. Upwelling mechanisms in the northwestern Alboran Sea. J. Marine Syst. 23, 317–331. Doi: 10.1016/S0924-7963(99)00068-8.

Schmidt, F. Hinrichs, K.U. i Elvert, M., 2010. Sources, transport, and partitioning of organic matter at a highly dynamic continental margin. Mar. Chem. 118, 37-55. Doi: 10.1016/j.marchem.2009.10.003.

Schroeder, K., Ribotti, A., Borghini, M., Sorgente, R., Perilli, A. et al., 2008. An extensive western Mediterranean deep water renewal between 2004 and 2006. Geophys. Res. Lett. 35(18). Doi: 10.1029/2008GL035146.

Schroeder, K., García-Lafuente, J., Josey, S.A., Artale, V. Nardelli, B.B. et al., 2012. Circulation of the Mediterranean Sea and its variability. In P. Lionello (ed.): The climate of the Mediterranean region. Elsevier. Cap. 3, p. 187-256. Doi: 10.1016/C2011-0-06210-5.

Sheng Hu, F., Hedges, J.I., Gordon, E.S. i Brubaker, L.B., 1999. Lignin biomarkers and pollen in postglacial sediments of an Alaskan lake. Geochim. Cosmochim. Acta 63 (9), 1421–1430. Doi: 10.1016/S0016-7037(99)00100-3.

Smetacek, V., Klaas, C., Strass, V., Assmy, P., Montresor, M. et al., 2012. Deep carbon export from a Southern Ocean iron-fertilized diatom bloom, Nature 487, 313–319. Doi: 10.1038/nature11229.

Strain, E.M.A., Lai, R.W.S., White, C.A., Piarulli, S., Leung, K.M.Y. et al., 2022. Editorial: Marine Pollution - Emerging Issues and Challenges. Front. Mar. Sci. 9:918984. Doi: 10.3389/fmars.2022.918984.

Sultan, N., Cochonat, P., Canals, M., Cattaneo, A., Dennielou, B. et al., 2004. Triggering mechanisms of slope instability processes and sediment failures on continental margins: a geotechnical approach. Mar. Geol. 213 (1-4), 291-321. Doi: 10.1016/j.margeo.2004.10.011.

Sultan, N., Gaudin, M., Berne, S., Baztán, J., Canals, M. et al., 2007. Analysis of slope failures in canyon heads: Example from the Gulf of Lions. J. Geophys. Res. 112, F01009. Doi: 10.1029/2005JF000408.

Tagliabue, A., Aumont, O., DeAth, R., Dunne, J. P., Dutkiewicz, S. et al., 2016. How well do global ocean biogeochemistry models simulate dissolved iron distributions? Glob. Biogeochem. Cycles 30(2), 149-174. Doi : 10.1002/2015GB005289.

Tesi, T., Puig, P., Palanques, A. i Goñi, M.A., 2010. Lateral advection of organic matter in cascading-dominated submarine canyons. Prog. Oceanogr. 84, 185-203. Doi: 10.1016/j.pocean.2009.10.004.

Tesi, T., Miserocchi, S., Goñi, M.A. i Langone, L., 2007. Source, transport and fate of terrestrial organic carbon on the western Mediterranean Sea, Gulf of Lions, France. Mar. Chem. 105, 101-117. Doi: 10.1016/j.marchem.2007.01.005.

Tintore, J., La Violette, P.E., Blade, I. i Cruzado, A., 1988. A study of an intense density front in the Eastern Alboran Sea: the Almeria-Oran Front. J. Phys. Oceanogr. 18, 1384–1397. Doi: 10.1175/1520-0485(1988)018<1384:ASOAID>2.0.CO;2.

Trevathan-Tackett, S.M., Macreadie, P.I., Sanderman, J., Baldock, J., Howes, J.M. et al., 2017. A Global Assessment of the Chemical Recalcitrance of Seagrass Tissues: Implications for Long-Term Carbon Sequestration. Front. Plant Sci. 8:925. Doi: 10.3389/fpls.2017.00925.

Tubau, X., Canal, M., Lastras, G., Rayo, X., Rivera, J. et al., 2015. Marine litter on the floor of deep submarine canyons of the Northwestern Mediterranean Sea: The role of hydrodynamic processes. Prog. Oceanogr. 134, 379–403. Doi: 10.1016/j.pocean.2015.03.013.

Turekian, K. K., 1977. The fate of metals in the oceans. Geochim. Cosmochim. Acta 41(8), 1139-1144. Doi: 10.1016/0016-7037(77)90109-0.

Turner, J. T., 2015. Zooplankton fecal pellets, marine snow, phytodetritus and the ocean's biological pump. Prog. Oceanogr. 130, 205–248. Doi: 10.1016/j.pocean.2014.08.005.

Twining, B. S. i Baines, S. B. 2013. The trace metal composition of marine phytoplankton. Annu. Rev. Mar. Sci. 5(1), 191–215. Doi: 10.1146/annurev-marine-121211-172322.

Ulses, C., Estournel, C., Durrieu de Madron, X. i Palanques, A., 2008. Suspended sediment transport in the Gulf of Lions (NW Mediterranean): impact of extreme storms and floods. Cont. Shelf Res. 28 (15), 2048–2070. Doi: 10.1016/j.csr.2008.01.015.

Vargas-Yáñez, M., Plaza, F., García-Lafuente, J., Sarhan, T., Vargas, J.M. et al., 2002. About the seasonal variability of the Alboran Sea circulation. J. Mar. Syst. 35 (3-4), 229–248. Doi: 10.1016/S0924-7963(02)00128-8. J. Mar. Syst. 35, 229– 248.

Vargas-Yáñez, M., Zunino, P., Shroeder, K., López-Jurado, J.L., Plaza, F. et al., 2012. Extreme Western Intermediate Water formation in winter 2010. J. Mar. Syst. 105-108, 52-59. Doi: 10.1016/j.jmarsys.2012.05.010.

Vargas-Yáñez, M., García-Martínez, M.C., Moya, F., Balbín, R., López-Jurado, J.L. et al., 2017. Updating temperature and salinity mean values and trends in the Western Mediterranean: The RADMED Project. Prog. Oceanogr. 157, 27–46. Doi: 10.1016/j.pocean.2017.09.004.

Vázquez, J.T., Ercilla, G., Alonso, B., Juan, C., Rueda, J.L. et al., 2015. Submarine Canyons and related features in the Alboran Sea: continental margins and major isolated reliefs. pp. 183-196 In CIESM Monograph 47 [F. Briand ed.] Submarine canyon dynamics in the Mediterranean and tributary seas-An integrated geological, oceanographic and biological perspective, 232 p. CIESM Publisher, Monaco.

Wakeham, S. G., Lee, C., Hedges, J. I., Hernes, P. J., i Peterson, M. J., 1997. Molecular indicators of diagenetic status in marine organic matter. Geochim. Cosmochi. Acta 61(24), 5363-5369. Doi: 10.1016/S0016-7037(97)00312-.

Wang, B. i Fennel, K., 2022. Biogeochemical-Argo data suggest significant contributions of small particles to the vertical carbon flux in the subpolar North Atlantic. Limnol. Oceanogr. 67(11), 2405-2417. Doi: 10.1002/lno.12209.

Weber, T., Cram, J. A., Leung, S. W., DeVries, T. i Deutsch, C., 2016. Deep ocean nutrients imply large latitudinal variation in particle transfer efficiency. Proc. Natl. Acad. Sci. USA 113, 8606–8611. Doi: 10.1073/pnas.1604414113.

Xu, J.P., Noble, M.A. i Rosenfeld, L.K., 2004. In-situ measurements of velocity structure within turbidity currents. L09311 Geophys. Res. Lett. 31 (9). Doi: 10.1029/2004GL019718.

www.puertos.es/es-es/oceanografia/Paginas/portus.aspx (darrer accés el dia 01/02/22).

www.ieo.es/es_ES/web/ieo/cartografia

Annex

Progress in Oceanography 203 (2022) 102783

Contents lists available at ScienceDirect

Progress in Oceanography

journal homepage: www.elsevier.com/locate/pocean

Particle fluxes in submarine canyons along a sediment-starved continental margin and in the adjacent open slope and basin in the SW Mediterranean Sea

Marta Tarrés [a], Marc Cerdà-Domènech [a], Rut Pedrosa-Pàmies [a,b], Aitor Rumín-Caparrós [a], Antoni Calafat [a], Miquel Canals [a], Anna Sanchez-Vidal [a,*]

[a] GRC Geociències Marines, Dept. Dinàmica de la Terra i de l'Oceà, Facultat de Ciències de la Terra, Universitat de Barcelona, 08028 Barcelona, Spain
[b] The Ecosystems Center, Marine Biological Laboratory, Woods Hole, MA, USA

ARTICLE INFO

Keywords:
Particle fluxes
Sediment-starved continental margin
Submarine canyons
Open slope
Deep basin
Mediterranean Sea

ABSTRACT

Investigating the transfer of particulate matter from the continental shelf to the deep basin is critical to understand the functioning of deep sea ecosystems. In this paper we present novel results on the temporal variability of particle fluxes to the deep in three physiographic domains of a 240 km long margin segment and nearby basin off Murcia and Almeria provinces in the SW Mediterranean Sea, which are submarine canyons forming a rather diverse set (namely Escombreras, Garrucha-Almanzora and Almeria), the adjacent open slope and the deep basin.

This margin is located off one of the driest regions in Europe and, therefore, its study may help understanding how mainland aridity translates into the export of particles to deep margin environments. Five mooring lines equipped with currentmeters, turbidity-meters and sediment traps were deployed for one entire annual cycle, from March 2015 to March 2016. We combine oceanographic, hydrological and meteorological data with grain size and bulk elemental data (organic carbon, opal, $CaCO_3$, lithogenic) from the collected sinking particles to understand what drives particle transfers in such an under-studied setting, and to quantify the resulting fluxes and assess their spatio-temporal variability.

Weighted total mass fluxes in canyons range from 1.64 g m^{-2} d^{-1} in Almeria Canyon to 7.33 g m^{-2} d^{-1} in Garrucha-Almanzora Canyon system, which are rather low values compared to other submarine canyons in the Western Mediterranean Sea. This results from the absence of extreme wind-storm events during the investigated time period combined with the reduced sediment input to the inner shelf by river systems in the study area. Our results also show that wind-storms are the main trigger for off-shelf particle transport to the deep margin, both within submarine canyons and over the open slope. The most significant transfer period is associated to a set of north-eastern storms in early spring 2015, when the off-shelf transport likely was promoted by storm-induced downwelling. However, the prevailing oceanographic conditions restricts the advection of water down the canyon heads to a few hundred meters, thus promoting a bottom-detached transport of particles seaward. Overall physiography, canyon head incision into the continental shelf and the distance of the canyon head to the shoreline (e.g. very short in Garrucha Canyon) play a key role in particle trapping capability and, therefore, in easing downslope particle transport. Further, bottom trawling activities around the Garrucha-Almanzora Canyon system, feed a nepheloid layer at depths in excess of 400 m, subsequently enhancing particle fluxes throughout the study period. In contrast, maximum particle fluxes in the deep basin respond to seasonal phytoplankton blooms.

Our study shows that particle export from the shallow inner margin to the deep outer margin in sediment-starved settings, even if limited, does occur as dominated by atmosphere and ocean driven short-lived events. However, that export does not reach too far as at several tens of kilometres from the shelf edge advective fluxes are replaced by vertical ones impelled by phytoplankton dynamics.

* Corresponding author.
E-mail address: anna.sanchez@ub.edu (A. Sanchez-Vidal).

https://doi.org/10.1016/j.pocean.2022.102783
Received 30 June 2021; Received in revised form 7 January 2022; Accepted 16 March 2022
Available online 24 March 2022

1. Introduction

Continental margins are the areas that connect the continent and the deep sea. These areas are where most of the sediments are deposited, and are an important source of material to deep sea ecosystems. Materials supplied by the rivers (and autochthonous biological production) are transferred from the continental shelf to the slope and deep basin, especially in those areas incised by submarine canyons. Submarine canyons are large geomorphic features carved on continental margins that act as preferential conduits for particulate matter export from the continental shelf to the deep margin and basin (Drake and Gorsline, 1973; Shepard et al., 1979; Xu et al., 2004; Heussner et al., 2006; Canals et al., 2006; Puig et al., 2014). Canyons are key features for the transfer and sinking, which are often episodic, of organic carbon (OC) and nutrients (Pasqual et al., 2010; Kiriakoulakis et al., 2011; Sanchez-Vidal et al., 2012; Pedrosa-Pàmies et al., 2013), while also facilitating the delivery of litter and chemical pollutants to deep ecosystems (Palanques et al., 2008a; Ramirez-Llodra et al., 2013; Dumas et al., 2014; Tubau et al., 2015).

To date, studies on particle fluxes within submarine canyons around the Iberian Peninsula margins have focused on specific segments such as the North Catalan and Gulf of Lion margins (Heussner et al., 2006; Martín et al., 2006; Durrieu de Madron et al., 2008; Pasqual et al., 2010; Sanchez-Vidal et al., 2012; Canals et al., 2013 and references therein), the Portuguese margin (Schmidt et al., 2001; de Stigter et al., 2007, 2011; Martín et al., 2011), margins of the Western Alboran Sea (Puig et al., 2004; Palanques et al., 2005) and the Cantabrian margin and neighbouring areas (Heussner et al., 1999; Schmidt et al., 2014; Romero-Romero et al., 2016; Rumín-Caparrós et al., 2016). These studies illustrate the markedly different behaviour between submarine canyons in the micro-tidal Western Mediterranean Sea and those in the meso-tidal Atlantic Ocean, where high swells are common. Compared to other canyons in the Western Mediterranean Sea and, more generally off Iberia and nearby areas, the sedimentary dynamics of submarine canyons off south-eastern Spain have been barely investigated (Puig et al., 2017), particularly because of two main reasons: (i) low river discharge resulting in reduced sediment supply to the continental margin; and (ii) lack of high-energy processes other than storms, such as those occurring in other areas, which have subsequently attracted the researchers' interest (e.g. dense shelf water cascading, DSWC, in the NW Mediterranean Sea —see further down—; Canals et al., 2006).

Submarine canyons from the Western Mediterranean Sea exhibit sediment transport interannual variability, reflecting complex interaction between the diverse forcing factors (atmospheric, hydrologic and oceanographic conditions) (Heussner et al., 2006; Palanques et al., 2006a, 2008b; Ogston et al., 2008). It has been documented in the NW Mediterranean region that during major storms sediments deposited on the continental shelf and canyon heads can be remobilized and flushed down-canyon (Canals et al., 2006; Palanques et al., 2006a; Sanchez-Vidal et al., 2012; Pedrosa-Pàmies et al., 2013), triggering large sediment export to the deep margin and basin (Sanchez-Vidal et al., 2012; Puig et al., 2014). Storm-induced downwelling there contributes to the off-shelf transfer of particulate matter, forced by a strong cyclonic circulation and along the coast water convergence during eastern storms (Ulses et al., 2008; Palanques et al., 2008b; Martín et al., 2013). Another highly relevant process occurring in the NW Mediterranean Sea is DSWC following formation of dense water over the continental shelf and subsequent near-bottom, gravity-driven sinking due to loss of buoyancy. Dense shelf water forms mostly in the Gulf of Lion during favourable winters, characterised by persistent cold and dry northern winds (Durrieu de Madron et al., 2008; Canals et al., 2013). Both dense shelf water formation and cascading present a high degree of interannual variability (Béthoux et al., 2002; Durrieu de Madron et al., 2005). Submarine canyons in the area behave as main conduits for particle-laden cascading waters, which in the absence of submarine canyons can flow downslope anyway until reaching their neutral buoyancy depth (Canals et al., 2006). DSWC occurs in the form of short-lived metoceanographic events deeply impacting the deep ecosystem and associated benthic fauna by supplying large amounts of organic carbon (OC) (Company et al., 2008; Pusceddu et al., 2013). The amount and quality of the sinking particles is modulated by the occurrence of river floods and autochthonous biological production (Guillén et al., 2006; Fabres et al., 2008; Sanchez-Vidal et al., 2013; Lopez-Fernandez et al., 2013a).

Anthropogenic activities also impact the sediment dynamics of submarine canyons. Bottom trawling gear in particular erodes canyon upper flanks (Puig et al., 2012; Martín et al., 2014a), resulting in the remobilization of sediments that are channelized by tributaries (Martín et al., 2014b), ultimately increasing sediment accumulation rates in canyon axes (Paradis et al., 2017).

The non-occurrence of DSWC and the micro-tidal regime in the SW Mediterranean Sea raise the question about the relevance of sediment transfers to the deep margin and basin in this area, while also pointing to the need to quantify the overall fluxes and their composition, including organic matter (OM) contents, to determine possible relationships with specific forcing conditions, and to establish the periodicity of transfer events. These questions become more noteworthy when considering the lack of discharge from river systems during most of the year, severely limiting to rare time periods the supply of terrestrial sediments to the margin (Liquete et al., 2005).

This study focuses on the temporal variability of near-bottom and mid-water particle fluxes and associated oceanographic parameters over one-year in the mid-course of three submarine canyons (Escombreras, Garrucha-Almanzora and Almeria), in the open slope north of Garrucha-Almanzora Canyon, and in the deep basin in the Gulf of Vera, as investigated by means of sediment traps and currentmeters deployed in situ. The aim of the present study is to fill a gap in the knowledge of shelf-to-deep basin mass transfer in the SW Mediterranean Sea and, more generally, in sediment-starved margin segments. The simultaneous study of these three environments (canyons, open slope and deep basin) is also needed to better understand eventual interconnections amongst them.

2. Overall setting

The study area encompasses the Gulf of Vera to the north and the Gulf of Almeria to the south, in the SW Mediterranean Sea (Fig. 1). Climate is semi-arid, with low mean annual rainfall (<500 mm yr^{-1}) (AEMET, 2011). In spite of low annual precipitation, involving dry or almost dry streams during most of the year, fast flooding events occur in the region mainly in autumn months (Machado et al., 2011). The main rivers in the area are, in a clockwise direction, Almanzora, Antas, Aguas and Andarax (Fig. 1). Almanzora River is the main hydrological system, with a watershed of 2,611 km^2 (Puig et al., 2017), followed by the Andarax River system with 2,160.5 km^2 (Liquete et al., 2005). Both rivers feed delta and prodelta systems (Sanz et al., 2002; Liquete et al., 2005).

Wind regime in the study area is dominated by NE to SW flux in Cape of Palos and ENE to WSW in Cape of Gata, which may triggers significant wave heights (H_s) of < 5 m with wave periods of 6–7 s (Puig et al., 2017). Less frequent, stronger inter-annual wind events are able to generate 5 m < H_s < 7 m, generally during autumn and winter months. Events triggering major storms with waves between 5 m ≤ H_s < 6 m can occur every 2–3 years, whereas for storms with waves with H_s equal or above 6 m the return period is longer than 13 years (https://www.puertos.es).

Prevailing surface circulation in the Gulf of Vera is southwards to Cape of Gata. In the neighbouring Alboran Sea the inflow of the Atlantic jet through the Gibraltar Strait forms two main non-permanent anticyclonic gyres, known as the western and eastern Alboran gyres (WAG and EAG, respectively). The encounter of the Mediterranean water from the north and west with the less saline Atlantic Water coming from the Alboran Sea produces a strong baroclinic jet, called Almeria-Oran Front (AOF), which extends in a NW-SE direction from Spanish to Algerian

coasts (Tintore et al., 1988). The semi-permanent AOF represents the eastern limit of the Alboran Sea circulation system and is controlled at its eastern edge by the geographic position and strength of the EAG, which usually forms during summer-autumn (Vargas-Yáñez et al., 2002; Renault et al., 2012). Intermediate and deep Mediterranean waters circulate towards the Strait of Gibraltar following the Spanish continental margin (Millot, 1999). Phytoplankton blooms in the study area usually extend from November to March (Garcia-Gorriz and Carr, 2001).

The study area comprises three margin segments, which are the Mazarron and Palomares margins within the Gulf of Vera, with E-W and NE-SW general orientation, respectively, and the Almeria margin south and west of Cape of Gata (Fig. 1). Neogene and Quaternary tectonics have determined the evolution and morphology of these margins (Estrada et al., 1997; Comas et al., 1999; Acosta et al., 2013). Most submarine canyons in the area follow fault systems, some of which are active, as is the case for the Almeria (ALC) and Escombreras (ESC) canyons (Estrada et al., 1997; Gràcia et al., 2006; Acosta et al., 2013; Pérez-Hernández et al., 2014). However, it is uncertain if the faults guiding Alias-Almanzora (AL-ALMC) and Gata (GT) canyon systems (Fig. 1) are still active (Gómez de la Peña et al., 2016).

The study area presents a narrow continental shelf (Lobo et al., 2014), which in the Mazarron margin ranges from 13 km to the east to < 4 km to the west, to then open to a steep continental slope dominated by multiple short canyons from ~200 m depth downwards (Acosta et al., 2013). The Palomares shelf generally is < 11 km wide (Pérez-Hernández et al., 2014), being narrowest in the vicinity of Garrucha Canyon head (GA). The shelf break in the Palomares margin is between 120 and 170 m depth, and the slope displays a complex morphology due to the presence of several submarine canyons (Aguilas (AGC), Alias-Almanzora and Gata), and prominent seamounts (Pérez-Hernández et al., 2014). In the Almeria margin, the continental shelf is 6 to 12 km wide (García et al., 2006), with the shelf edge at 100–120 m depth. The main geomorphological features therein are various submarine valleys which conform the Almeria Turbidite System (Estrada et al., 1997; García et al., 2006), which is the largest of its kind in the Alboran Sea (Vázquez et al., 2015).

From north to south and east to west the studied canyons are the N-S oriented single Escombreras Canyon on the Mazarron margin, the W-E Garrucha-Almanzora Canyon system (Fig. 2) that is the northern part of the Alías-Almanzora system on the Palomares margin, and the Almeria Canyon on the Almeria margin (Fig. 1).

The Escombreras Canyon is more than 20 km long and mostly N-S oriented. It presents a maximum axial gradient of 15°. While the canyon head is convex in shape and it is cut by numerous gullies (Acosta et al., 2013), the lower canyon extends onto the uppermost continental rise where it forms a channel systems (Acosta et al., 2013).

The Alias-Almanzora Canyon system has a total length of 73 km (Pérez-Hernández et al., 2014) and consists of four shelf incised branches entering the Palomares margin. In its northernmost part, the Almanzora Canyon branch (ALM) converges at 1,100 m depth with the Garrucha Canyon branch (GA), resulting in the Garrucha-Almanzora system (following Puig et al., 2017 nomenclature). The Almanzora Canyon extends from 65 m depth off the Almanzora River (Puig et al., 2017) and presents a mean axial slope gradient of 8.6 ° and a total length of 8 km. The Garrucha Canyon branch splits in two canyon heads off the Almanzora River prodelta, together with two other main canyon heads further south, located between Antas and Aguas river mouths, opening as closer as 30 m from Garrucha harbor. The southern canyon heads are fed by several small tributary channels that could be tracked up to 7 m depth on the innermost shelf. The Garrucha Canyon branch displays a meandering pattern, with an average axial slope of 5°, for a total length of 15.7 km (Puig et al., 2017). At 1,811 m depth the Garrucha-Almanzora system merges with the southern Alias-Cabrera system, thus forming the Alias-Almanzora system (Pérez-Hernández et al., 2014).

The NE-SW oriented Almeria Canyon is more than 55 km long (García et al., 2006). Its axial gradient ranges between 1.2° and 1.4°, and it is fed by three tributary valley systems (TVS), from west to east, Dalias, Andarax and Gata (Fig. 2), which incise the shelf break and converge with the main canyon at 700–1,500, 300 and 650 m, respectively (García et al., 2006). The Dalias TVS covers an area of 300 km^2 with a length of 22 km, but only the Andarax TVS is connected to the Andarax River (García et al., 2006). The Almeria Canyon axis is NE-SW oriented down to 1,200 m depth where it becomes the Almeria Channel feeding a fan lobe system (Cronin et al., 1995; Estrada et al., 1997).

Thus, submarine canyons located in these margin segments are diverse in several aspects, such as size, orientation, with or without shelf incision, individual or with several tributaries and their relation with present day tectonics.

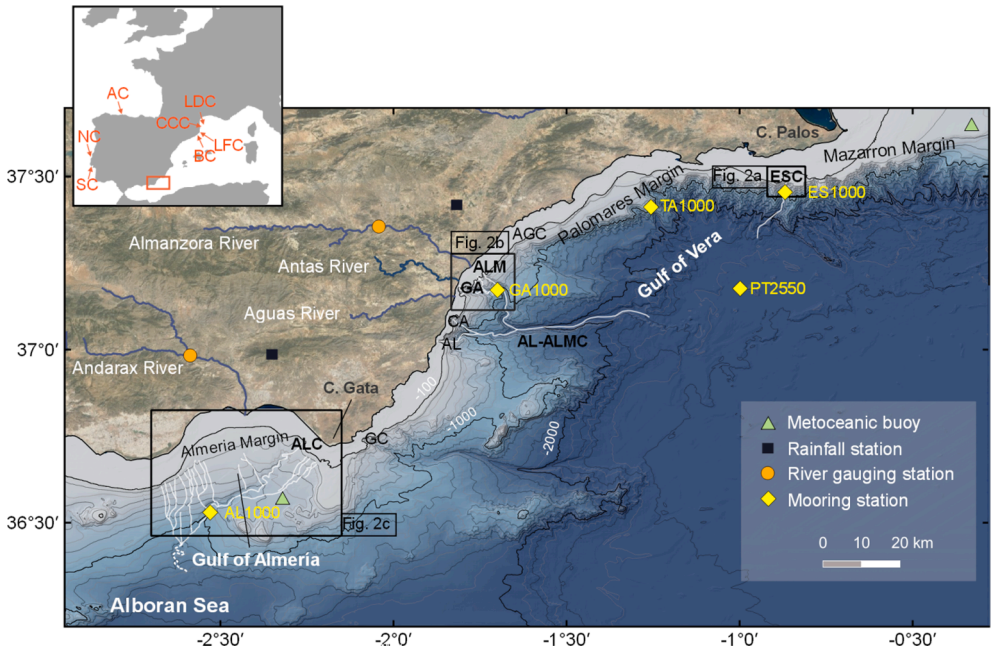

Fig. 1. Bathymetric map of the gulfs of Vera and Almeria with the main axis of Escombreras (ESC), Alias-Almanzora (AL-ALMC) and Almeria (ALC) canyon systems (white lines). The location of the Alias-Almanzora Canyon tributaries (AL: Alias; CA: Cabrera; GA: Garrucha; ALM: Almanzora) and the Aguilas Canyon (AGC) and the Gata Canyon (GC) are indicated. Yellow diamonds indicate the location of mooring stations. Cape of Palos and Cape of Gata metoceanic buoys (green triangles), rainfall stations (black squares) and river gauging stations (orange dots) are also shown. Black squares show the location of detailed submarine canyon maps in Fig. 2. Other submarine canyons referred to in this paper are shown in the inset (LDC: Lacaze-Duthiers Canyon; CCC: Cap de Creus Canyon; LFC: La Fonera Canyon; BC: Blanes Canyon; NC: Nazaré Canyon; SC: Sétubal Canyon; AC: Avilés Canyon.

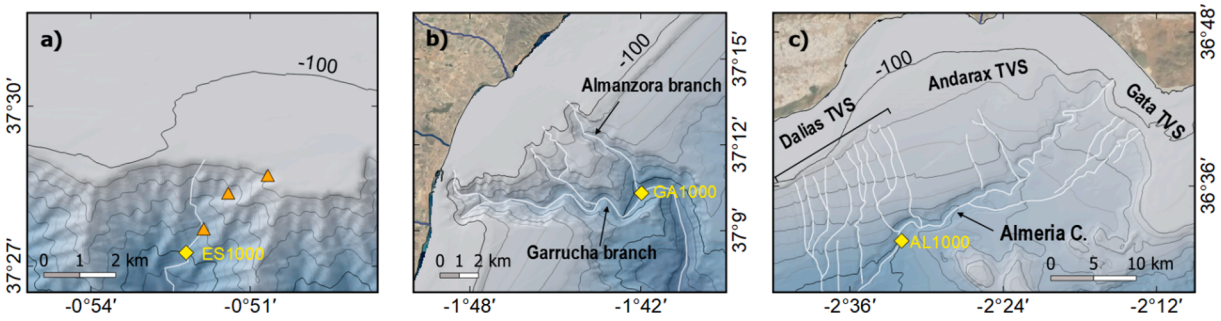

Fig. 2. Bathymetric maps of the heads of (a) Escombreras Canyon, (b) Garrucha-Almanzora Canyon system, and (c) Almeria Canyon and tributary valley systems (TVS). Yellow diamonds show the location of mooring stations and CTD deployments. Orange triangles illustrate a CTD transect across the outer Mazarron shelf and upper Escombreras Canyon. Yellow diamonds indicate the mooring sites.

3. Materials and methods

3.1. Experimental design

Three mooring lines were deployed along the axis of three submarine canyons at approximately 1,000 m depth: in Escombreras (ES1000), Garrucha-Almanzora (GA1000) and Almeria (AL1000) submarine canyons (Fig. 2). Two additional moorings were deployed as control stations, one in the open slope in the Palomares margin (TA1000) and one in the deep basin at 2,550 m depth (PT2550). The moorings were deployed from March 2015 to March 2016, with recovery-redeployment operations at month 6 for maintenance, changing batteries and sampling cups (Table 1). Each mooring was equipped with a Technicap PPS3/3 sequential sediment trap (0.125 m^2, cylindroconical shape) with 12 trap cups with a sample resolution of 7–16 days. The mooring deployed in the deep basin was equipped with two sediment traps: one at mid-water depth (PT2550-S, with "S" standing for "shallower") and the other near the bottom (PT2550-D, with "D" standing for "deeper"). The trap cups were filled with 5% (v/v) formaldehyde solution in 0.45 μm filtered sea water buffered with sodium tetraborate. Aquadopp Nortek current meters with sampling interval of 30 min were placed 2 m below the sediment trap to monitor current velocity, direction, pressure and water temperature. Some currentmeters were equipped with Seapoint turbidity meters, calibrated for Formazin Turbidity Units (FTU), which detect light scattered at 15°-150 ° (with a sensibility peak at 90 °) of a confined volume of five centimetres of the sensor window. Pitch and roll parameters and velocity have been checked to assess that hydrodynamic conditions did not have a detrimental impact on trap verticality and discard a bias in the collection of particle fluxes (Gardner, 1985; Baker et al., 1988; Buesseler et al., 2007).

CTD (Conductivity-Temperature-Depth) profiles were carried out during 13th-23rd March 2015 and 29th August-1st September cruises around each mooring station. Additionally, a transect of 3 CTD casts comprising the outer area of the Mazarron margin and Escombreras Canyon was performed in March 2015 (Fig. 2a). The CTD was a SBE 911 equipped with a WET Labs ECO-AFL/FL fluorimeter, a SBE 43 oxygen sensor and a WET Labs ECO-NTU turbidity meter sensor (in Nephelometric Turbidity Units). The turbidimeter measures turbidity from side-scattered light at 90° relative to the laser light.

3.2. Sample treatment and analytical procedures

Sediment trap samples were stored in the dark at 2–4 °C, and were processed in the laboratory following a modified protocol from Heussner et al. (1990), as described in Lopez-Fernandez et al. (2013b).

Total Mass Fluxes (TMF) were calculated for each period following next equation:

$$TMF\left(gm^{-2}d^{-1}\right) = \frac{Sample\ \ dry\ \ weight(g)}{Collection\ \ area(m^2)*sampling\ \ interval(d)} \quad (1)$$

Time weighted Fluxes (TWF) represents a weighted average corrected according sampling interval value:

$$TWF\ \ \left(gm^{-2}d^{-1}\right) = \frac{\sum M_i(g)}{Collection\ \ area(m^2)*\sum D_i(d)} \quad (2)$$

where: $\mathbf{M_i}$ is the mass of each sample and $\mathbf{D_i}$ is the collection interval days of each sample.

The contents of total Nitrogen (N), Organic Carbon (OC) and Total Carbon (TC) were determined using an Elemental Analyser EA Flash series 1112 in the Scientific and Technological Centres of the University of Barcelona. Before analysis, samples for OC determination were decarbonated with repeated additions of 10 μl of HCl (1 M) with 3 h 60 °C drying steps in between until no effervescence was observed. Percentages of organic matter (OM) and calcium carbonate ($CaCO_3$) were calculated following relations:

$$OM = OCx2 \quad (3)$$

and

Table 1
Metadata of mooring lines. Sediment traps were placed 25 mab (m above the bottom) except for PT2550-S level, which was at 546 mab (mid-water deep basin trap). Due to specific technical failures of the rotation system of sediment traps, the complete time series is not available for ES1000 and GA1000 mooring stations. Currentmeters were deployed below each sediment trap excepting in PT2550-S. Each currentmeter was equipped with turbidity meters excepting in AL1000. In PT2550, "S" stands for "shallower" and "D" stands for "deeper" (see further details in the main text).

Mooring station/ level	Latitude	Longitude	Mooring depth (m)	Minimum distance from mooring line to coastline (km)	Sampling period	Number of samples
ES1000	37°27.309′N	0°52.274′W	985	14	16/3/2015–28/8/2105	12
TA1000	37°24.613′N	1°15.394′W	1003	16	16/3/2015–31/3/2016	24
GA1000	37°10.294′N	1°41.968′W	1100	10.7	25/3/2015–15/10/2015	14
AL1000	36°31.709′N	2°32.003′W	1000	22	25/3/2015–31/3/2016	24
PT2550-S	37°10.635′N	0°59.993′W	2550	40	16/3/2015–31/3/2016	24
PT2550-D	37°10.635′N	0°59.993′W	2550	40	16/3/2015–31/3/2016	24

$$CaCO_3 = (TC - OC)*8.33 \quad (4)$$

where 8.33 is the molecular mass ratio (assuming that all inorganic carbon is in the form of calcium carbonate).

Biogenic Si content was obtained analysing Si and Al with an Inductive Coupled Plasma Optical Emission Spectroscopy (ICP-OES), with a two-step digestion for 2.5 h at 90 °C with a solution of Na_2CO_3 (0.5 M) following Fabres et al. (2002). Lixiviate Si/Al ratios were used as correction factor to obtain biogenic Si in sediments (Kamatani and Oku, 2000) and multiplied by factor of 2.4 to obtain opal percentage (Mortlock and Froelich, 1989). The opal fraction was determined in the PT2550-S samples, where pelagic sedimentation is expected to be more noticeable. In this case, the lithogenic fraction was calculated assuming that.

$$\%\text{lithogenics} = 100 - (\%OM + \%CaCO_3 + \%\text{opal}) \quad (5)$$

In the samples collected in the near-bottom traps, discrete analysis indicate a minor opal contribution to total mass. Then, the lithogenic fraction was calculated without considering this fraction.

Grain size analysis of particles were carried out with a Beckman Coulter LS 230 laser diffraction particle size analyser, which measures sizes between 0.04 and 2,000 μm. Prior to analysis, samples were twice oxidized with 50 ml of 10% H_2O_2, drying the samples between each oxidation. Each sample was than divided in two subsamples, one of which was de-carbonated with 50 ml 1 M HCl to obtain the grain size distribution of lithogenic particles. Once dry, both fractions were dispersed with 50 ml of 5% sodium polyphosphate solution and placed in a rotary agitating for at least 3 h to prevent particle's flocculation.

3.3. Metoceanic and human activity records

Metoceanic data (wind velocity and provenance, significant wave height and wave provenance) were obtained from *Agencia Estatal de Meteorología* and *Red de Boyas de Aguas Profundas* (REDEX, *Puertos del Estado*). In this study we used data from the Cabo de Palos buoy (Long. 0.33°W, Lat. 37.65°N), moored in the inner shelf of the northern margin of Gulf of Vera, and the Cabo de Gata buoy (Long. 2.32°W, Lat. 36.57°N) near Cape of Gata. In order to obtain accurate daily wave parameters close to the submarine canyons heads, 3 WANA points were used for this study. The WANA network delivers time series of wind and waves parameters from numerical modelling generated by *Puertos del Estado* in collaboration with *Agencia Estatal de Meteorología*.

Hourly Andarax and Almanzora river discharges were obtained from *Red SAIH Hidrosur*, operated by Junta de Andalucía. Gauging stations are not located near the river mouth. The above data was complemented with rainfall data from two meteorological stations located in the Almeria province, from the same data source.

Monthly chlorophyll-a concentration (Chl-a) (mg m^{-3}) and sea surface temperature (SST) (°C) data were obtained from Moderate Resolution Imaging Spectrometer (MODIS), in orbit on the Aqua platform, using 4 km resolution level 3 binned data. These data are processed and distributed by *NASA Goddard Earth Science (GES) Data and Information Services Centre (DISC)* and supported by the Ocean Biology Processing Group (OBPG).

Fishing activity has been monitored from Vessels Monitoring System (VMS) data provided by *Secretaria General de Pesca, Ministerio de Agricultura, Alimentación y Medio Ambiente* of the Spanish Government.

4. Results

4.1. Forcing conditions

Beyond major storms with high H_s (cf. section 2) the dry or wet character of every storm also is of relevance, as it defines the absence or presence of associated rainfall (Guillén et al., 2006). Indeed, eastern storms are charged with humidity and trigger precipitation by orographic control when encountering the land, conversely to storms coming from mainland, i.e. from the north and west. Rainfall rates are often higher during late summer and autumn, when the evaporation of the relatively warm Mediterranean Sea provides a continuous supply of heat and water vapor, increasing the moisture content at low levels (Hermoso et al., 2021). However, as shown in Fig. 3, rainfall does not always translate into an increment of river discharge, since other factors such as infiltration and ground water reserves influence surface runoff and the fluvial response in dry climates such as the one in the study area (Liquete et al., 2005). During the studied period, three main stormy periods occurred (Fig. 3).

The first period developed in early spring 2015, mainly associated with north-eastern winds and characterized by unstable cold weather with various rainfall episodes. On 17-21th March 2015 the buoys registered a wet northern storm with H_s up to 4.8 m ($T_s = 6.3$ s) in Cape of Palos, exceeding 2 m for 77 h. In Cape of Gata the event had a maximum wave height of 4.2 m and less duration. After the storm, Andarax River registered a slight increase in discharge, with a maximum of 2.2 m^3 s^{-1}. Two other wet storms occurred in April, the first between 6 and 9th, with a considerable duration of 88 h, was strongest in Cape of Gata with a maximum H_s of 4.5 m ($T_s = 6.6$ s), followed by a milder event on the 12th that was only recorded in Cape of Gata.

The second stormy period took place in autumn months and was characterized by a set of storms accompanied by abundant rainfall episodes, which impacted river discharge during September. On the first of November 2015 a north-eastern storm triggered H_s of 4.2 m at Cape of Gata and 3.9 m at Cape of Palos, lasting 37 h and 28 h, respectively. After the event both gauge stations registered a flood episode of up to 36.1 m^3 s^{-1} in Almanzora River and a less marked increment of 0.7 m^3 s^{-1} in the Andarax River. In late November another storm ($H_s \leq 4$ m) of short duration (13 h) from the southwestern was recorded at the Cape of Gata buoy.

The last stormy period occurred during winter months early in 2016, driven by several strong wind episodes blowing from west and south, accompanied with rather weak rainfall, especially in the southern part of the study area. A set of events took place in early January, February and March. Near Cape of Palos occurrence and intensity were less, with maximum H_s of 4 m on 12th and 26th February. In Cape of Gata the strongest ones happened on the 7th, 9th and 19th February. In particular, the 9th February storm lasted for 149 h with maximum H_s of 4.8 m and T_s of 6.4 s. The rest of the events during February and March were milder, never surpassing a H_s of 3.7 m.

Concerning primary production, in early spring 2015 a bloom developed close to the coasts (Fig. 4), with maximum values up to 0.6 mg m^{-3} in March. Between May and October 2015, oligotrophic conditions prevailed in the study area, with relevant primary production outside the study area, in the south-western Alboran Sea associated to the WAG upwelling zone. An increment of chlorophyll-a at the sea surface occurred from November 2015 to March 2016, restricted to the Alboran Sea during autumn months and extending to the wide Gulf of Vera during winter months in early 2016. This bloom was particularly prominent during January near Cape of Gata and over Mazarron margin, with Chl-a concentration up to 2.7 mg m^{-3}, and low sea surface temperature (SST) near the coast.

4.2. Near bottom currents

Current velocities recorded in all stations did not exceed 20 cm s^{-1}, and only punctually reached more than 10 cm s^{-1} (Fig. 5a-d). Current-meters deployed on the continental margin registered two periods with moderate increments of current speed, first during March-April 2015 and second during February-March 2016, as shown in stations with complete time series. In the deep basin station, the maximum current velocity was recorded at the end of April 2015, up to 19.5 cm s^{-1}, with current pulses coming from continental margin areas located to the north and west of the mooring site.

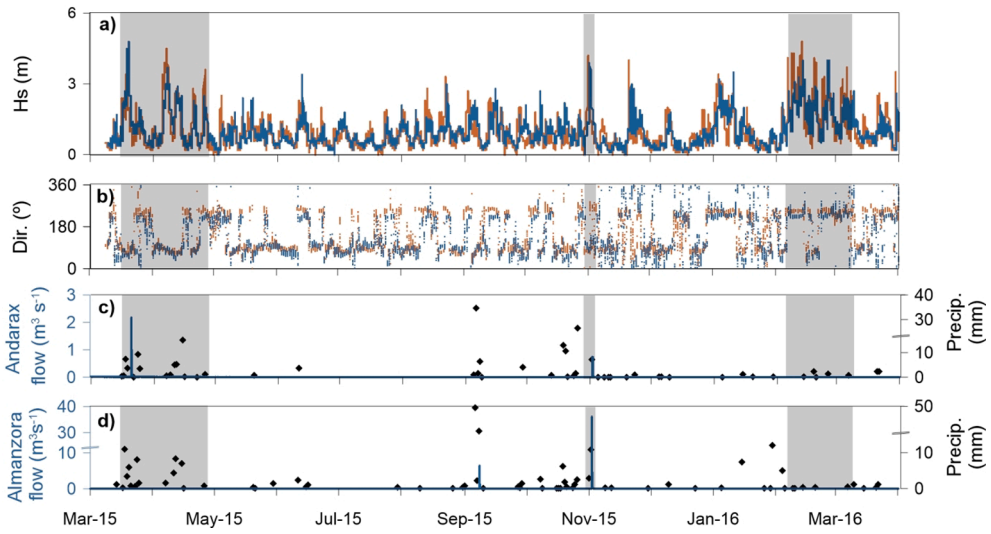

Fig. 3. Time series of external forcings during the year-round monitoring period from March 2015 to March 2016. (a) Significant wave height (Hs) at Cape of Palos buoy (orange curve) and Cape of Gata buoy (blue curve); the grey vertical stripes highlight the main storm events. (b) Wave provenance in Cape of Palos and Cape of Gata buoys. (c) Andarax River flow (Terque gauging station) and hourly accumulated precipitation (Rambla de Tabernas station). (d) Almanzora River flow (Cantoria gauging station) and hourly accumulated precipitation (Sierra Almagro station).

Current velocity peaks did not coincide with turbidity peaks (Fig. 5a-c). The turbidity series generally present low values with subtle increases that did not surpass 3 FTUs, a tendency only disrupted in the Garrucha-Almanzora Canyon. After late July, there was a progressive increase with a peak of 28 FTU at the end of August, followed by a quick decrease until reaching previous values in the last days of August 2015 (Fig. 5c). Biofouling is discarded to be the cause of the FTU increment observed in GA1000 because the subsequent flattening of turbidity values is not associated to a current speed increase that eventually could have swept away particles loosely adhered to the sensor.

4.3. Spatial and temporal variability of total mass fluxes

TMF's in the stations located in the continental margin were one order of magnitude larger than those in the deep basin. Basic statistics (Table 2) show a weighted average value (TWF) of 7.33 g m^{-2} d^{-1} in GA1000 whereas the one found in ES1000 is up to 4.80 g m^{-2} d^{-1}. AL1000 presents a lower value than the two previous stations (1.64 g m^{-2} d^{-1}), similar to that obtained in TA1000 (1.90 g m^{-2} d^{-1}). Traps deployed at two levels in the deep basin (PT2550-S and PT2550-D) present TMFs lower than 1 g m^{-2} d^{-1} during all the monitoring period.

TMF values fluctuate considerably throughout the studied period (Fig. 6). The maximum values were recorded in March and April 2015. The maximum value was obtained in ES1000, up to 24.96 g m^{-2} d^{-1}, followed by GA1000 (18.15 g m^{-2} d^{-1}), TA1000 (8.37 g m^{-2} d^{-1}) and AL1000 (5.12 g m^{-2} d^{-1}). Two behaviours are noted for the rest of the months. ES1000, AL1000 and TA1000 stations registered much lower fluxes during the rest of the monitoring period, with a minimal increment during autumn and winter months. In ES1000 station the lack of data prevents us from describing TMFs. Unlike those stations, fluxes recorded in GA1000 fluctuated during spring and summer months, until October. A different behaviour is observed in the deep basin station, with maximum values recorded in April 2015 in PT2550-S and September 2015 in PT2550-D.

4.4. Characteristics of settling particles

4.4.1. Main composition

At the canyon and open slope stations the lithogenic fraction is the main component (Table 2 and Fig. 6), with an averaged content of 72.4% in AL1000, and more similar percentages in the rest of the stations (60.5–65.0%). The averaged $CaCO_3$ content varies from 22.7% in PT2550-S and 36.5% in ES1000. OM percentages are lower in open slope and canyons stations (3.0–4.1%) while higher values have been found in deep basin traps (5.7%). Analyses of some discrete samples from continental margin stations indicate that opal contents are negligible in those stations, with maximum values below 2.5%. In contrast, PT2550-S shows average opal values of 7.4 ± 5.0%.

The molar OC/N ratio is represented in Fig. 6. Settling particles in GA1000 show values higher than 12 in almost the entire monitoring period, with a maximum of 20.1 in early April. In contrast, values in ES1000 and AL1000 samples are below 12. The OC/N ratio tends to diminish after March and April 2015, except in GA1000 station, which presents high values in August 2015 samples. TA1000 settling particles show the widest range (6.7–20.3), with more extreme values during the second deployment period. Concerning deep basin settling particles, PT2550-S shows lower values than PT2550-D, with an average of 9.0 against 9.8, respectively. In both sediment traps there was a tendency to increase OC/N ratios across the study period, with the exception of punctual PT2550-D samples.

4.4.2. Grain size of settling particles

The fine-medium silt fraction dominates de-carbonated samples at all traps and stations (Table 2). The finest grains are found in TA1000 and ES1000 settling particles, where the clay fraction averages 31.1% and 35.0%, respectively. GA1000 and AL1000 samples have more silt (74.0% and 81.2%, respectively) and sand fraction (2.3% and 3.1%, respectively). The averaged mean of the particles is coarser in AL1000 (16.2 μm), followed by GA1000 (14.1 μm), TA1000 (12.9 μm) and then ES1000 (9.3 μm).

The average grain size distribution during stormy periods (Fig. 3) does not show significant variations (Fig. 7). Concerning spring 2015 storms, the main mode was fairly coarse during March 2015 at ES1000 and AL1000 stations, with means of 11.3 μm and 21.1 μm. In posterior storm events only settling particles collected in TA1000 in early February 2016 show a higher mean (24.5 μm).

4.5. Water column parameters

Suspended particulate matter distribution has been obtained from turbidity meters attached to the CTD in March 2015 and late August 2015 (Fig. 8). In March 2015, we observe differences between the CTD casts performed the 13-14th March (TA1000 and ES1000), which show fairly constant turbidity values along the water column around 0.2 NTU, and casts conducted the 20th-23rd March at ES1000 and GA1000 stations, showing an increase of turbidity within continental shelf depths. During that period, the CTD transect along the Escombreras Canyon (Fig. 9 c) reveals higher turbidity values (up to 3.74 NTU) near bottom

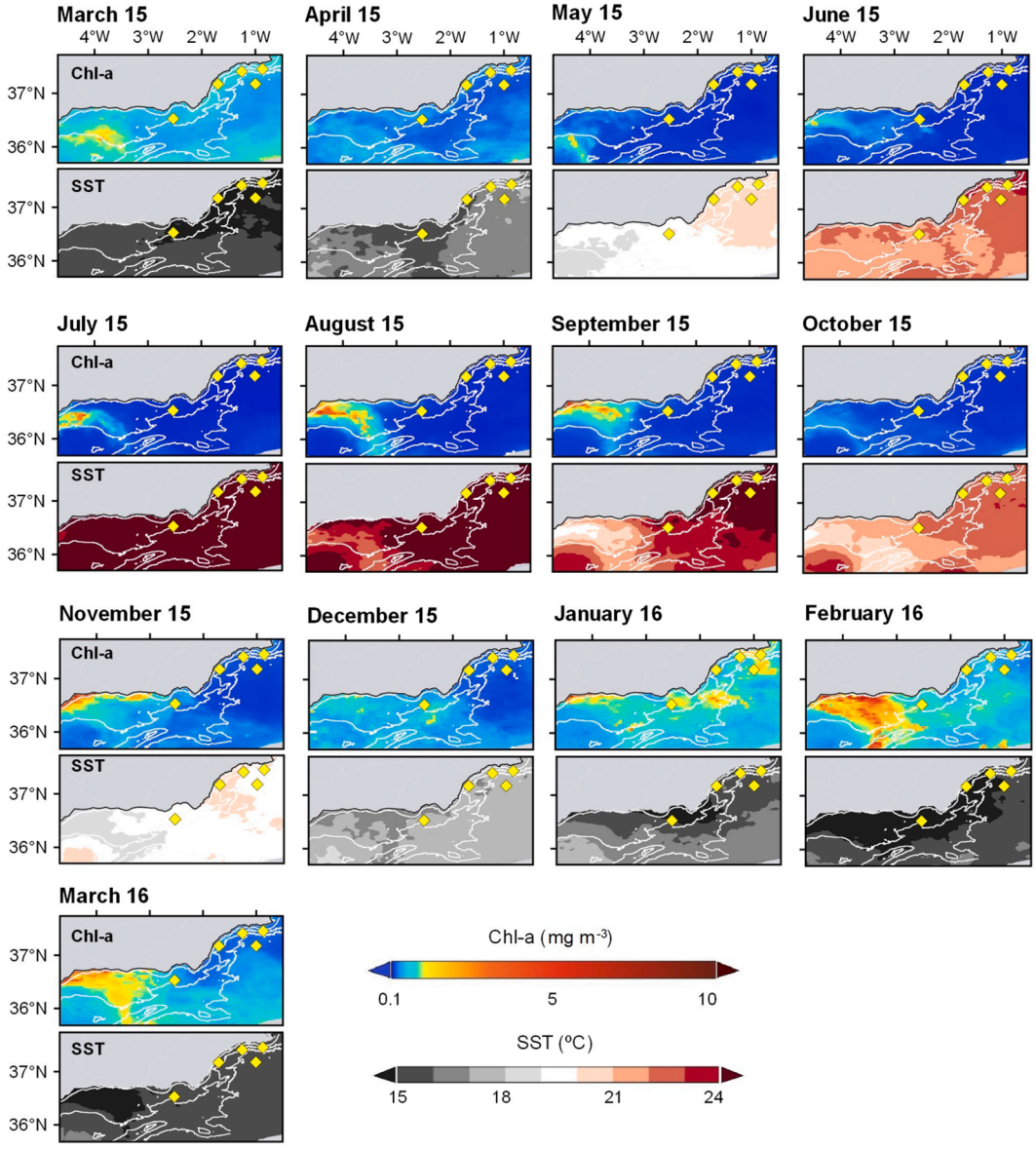

Fig. 4. Monthly averaged superficial chlorophyll-a concentration maps (mg m^{-3}) and SST (°C) from March 2015 to March 2016. The yellow diamonds represent the mooring lines.

on the outer continental shelf, with turbidity diminished seawards, reaching 1.14 NTU in the last CTD deployed near the ES1000 station. CTD casts near GA1000 station peak at 0.56 NTU, to gradually decrease below the shelf break until reaching values similar to those of the deep basin. Moreover, turbidity values near GA1000 begun increasing again below 400 m depth, extending hundreds of meters down to the bottom, while reaching values up to 0.32 NTU. The CTD cast performed near AL1000 has shown quite constant turbidity values along the water column.

The hydrological parameters of the upper 1,000 m of the water column also vary notably between the 13-14th and the 20th-23rd March 2015 CTD deployments (Fig. 8), as shown by stations ES1000 and TA1000 on one side, and stations GA1000 and ES1000 on the other side. The exception are profiles from AL1000 of the 23rd of March, which are more similar to the ones from ES1000 and TA1000 about 10 days earlier. It should be noted here that AL1000 is quite far from the broad area where the rest of stations are located (Fig. 1). Profiles in Fig. 8 allow identifying a number of water masses, including a surface layer, a sub-surface layer and the Levantine Intermediate Water (LIW). Most interesting are the 20th and 22nd of March GA1000 and ES1000 profiles, showing surface water mass down to about 200 m with relatively high potential temperature (13.65–13.80 °C) and fairly low salinity (38–38.1 psu), coinciding with a layer-thick fluorescence and, especially, turbidity increase (Fig. 8). Below is a sub-surface layer down to 300 m depth, made of almost mixed, colder and oxygen-rich water (minimum temperature of 13.17 °C), less saline (38.15–38.25 psu). Finally, the deeper LIW is indicated by a relative maximum in temperature and a relative minimum of dissolved oxygen. Fig. 9 a, b, d shows the variation of θ/S and DO seaward over Escombreras Canyon.

During the late August/early September 2015 cruise, the CTD casts at TA1000 and AL1000 did not show significant differences compared to deep basin values. However, the CTD cast at GA1000 once again presented a turbid layer under 400 m, with a maximum value of 0.37 NTU between 600 and 750 m and an increase of 0.39 NTU near bottom.

Fluorescence profiles indicate phytoplankton blooms. In mid-March 2015 maximum chlorophyll values were located near the surface with higher values, up to 1.38 mg m^{-3}, over Escombreras Canyon. At the end of March 2015, the fluorescence signal was weaker and distributed along the water column until 250 m depth (Fig. 8d). During late summer deployments the fluorescence peak was between 80 and 90 m depth,

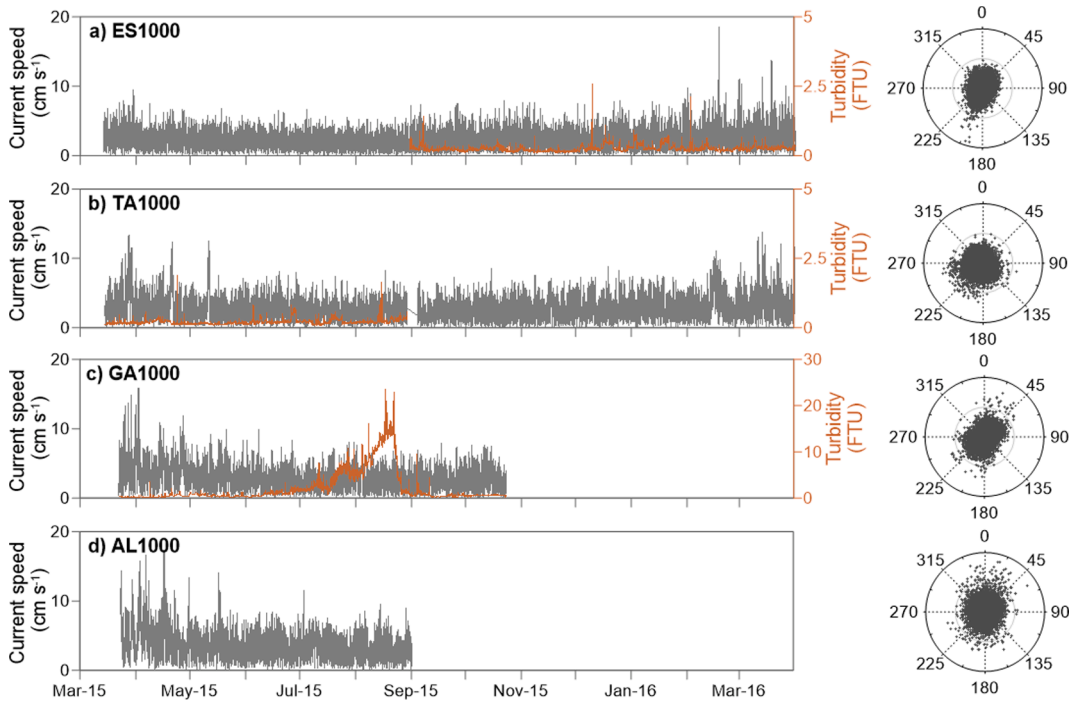

Fig. 5. Current speed (grey line) and turbidity (orange line) recorded at 20 mab in (a) ES1000, (b) TA1000, (c) GA1000 and (d) AL1000 stations. Polar plots show the direction of currents with the X axis ranging from 0 to 20 cm s^{-1}. FTU: Formazin Turbidity Units.

Table 2
Averaged total weighted flux (TWF), averaged total weighted components (TWC), and grain size of the de-carbonated fraction of samples from each sediment trap. Standard deviation is also shown. Note that the series only cover from March to September 2015 in the GA1000 station and from March to August 2015 in the ES1000 station.

Mooring station/sediment trap	TWF g $m^{-2}d^{-1}$	Components (TWC)				Grain size (de-carbonated)		
		Litho %	CaCO3%	OM %	Opal %	Clay %	Silt %	Sand %
ES1000	4.80 ± 6.55	60.5 ± 2.7	36.5 ± 3.1	3.0 ± 0.8	–	35.0 ± 2.7	65.0 ± 2.7	null
TA1000	1.90 ± 1.61	60.6 ± 7.3	36.3 ± 8.1	3.1 ± 0.9	–	31.1 ± 6.9	66.9 ± 5.7	2.0 ± 3.7
GA1000	7.33 ± 5.31	62.4 ± 3.2	34.2 ± 3.8	3.4 ± 0.9	–	23.7 ± 4.0	74.0 ± 3.4	2.3 ± 1.2
AL1000	1.64 ± 1.32	72.4 ± 2.1	23.5 ± 2.1	4.1 ± 1.1	–	15.8 ± 5.7	81.2 ± 4.7	3.1 ± 1.7
PT2550-S	0.07 ± 0.12	64.2 ± 10.1	22.7 ± 11.4	5.7 ± 2.9	7.4 ± 5.0	–	–	–
PT2550-D	0.06 ± 0.05	65.0 ± 9.1	29.3 ± 8.8	5.7 ± 2.1	–	–	–	–

with peak values reaching 1.59 mg m^{-3} near GA1000 station, 1.01 mg m^{-3} near TA1000 and 0.75 mg m^{-3} near AL1000.

5. Discussion

5.1. Sources of particulate matter

Temporal variability of particle fluxes in continental margins, and in Mediterranean margins in particular, follows deposition and remobilization cycles involving the transfer of matter and energy from the shelf to the slope and deep basin, as pointed out by several authors (Heussner et al., 2006; Ulses et al., 2008; Palanques et al., 2012; Puig et al., 2014). This leaves an imprint on grain size and the biogeochemical characteristics of the settling particles. Indeed, the grain size of settling particles has been related to lateral transport and sediment sorting (Ferré et al., 2005; Guillén et al., 2006; Sanchez-Vidal et al., 2012; Pedrosa-Pàmies et al., 2013). Also, some biogeochemical parameters are often used as proxies to identify the sources of particle-forming materials. The OC/N ratio in particulate matter is one of these proxies, which allows distinguish between marine and terrestrial OM. Vascular plant–derived OM is typically depleted in nitrogen (molar OC/N ratio > 16), whereas phytoplankton sourced OM shows higher nitrogen contents (molar OC/N ratio < 7) (Goñi and Hedges, 1995). Furthermore, the tendency of vascular plant detritus to preferentially gain N during soil microbial decay may decrease the OC/N ratio from the originating plants down to 8 (Hedges et al., 1997; Sanchez-Vidal et al., 2013). Therefore, grain size and OC/N ratios allow achieving a rather incisive view of the processes affecting particle fluxes in settings such as the one of the study area.

The grain size distribution of de-carbonated settling particles shows that fine particles dominate in canyons (Table 2), in accordance to the calm hydrodynamic conditions during the investigated year-round period. Also, low grain size standard deviation is indicative of fairly stable hydrodynamic conditions at least at the depths where sediment traps were deployed. The lithogenic fraction dominates in all stations, pointing to a high relative contribution of terrestrial inputs along the investigated continental margin. Nonetheless, the terrestrial contribution probably is higher if we take into account that carbonate rocks are abundant in the watersheds feeding the study area, especially to the north. Thus, part of the calculated $CaCO_3$ fraction likely derives from detrital carbonates. As it can be seen in Table 2, the mean $CaCO_3$ values in submarine canyons (except Almeria Canyon) and open slope stations are about 11–14% higher than the one in the deep basin mid-water trap, where the highest biogenic contribution could be expected. Fluvial systems are a major source of terrigenous particles for submarine canyons which heads are at short distance from river mouths. These river-sourced particles easily reach mid-canyon segments. Particles settling

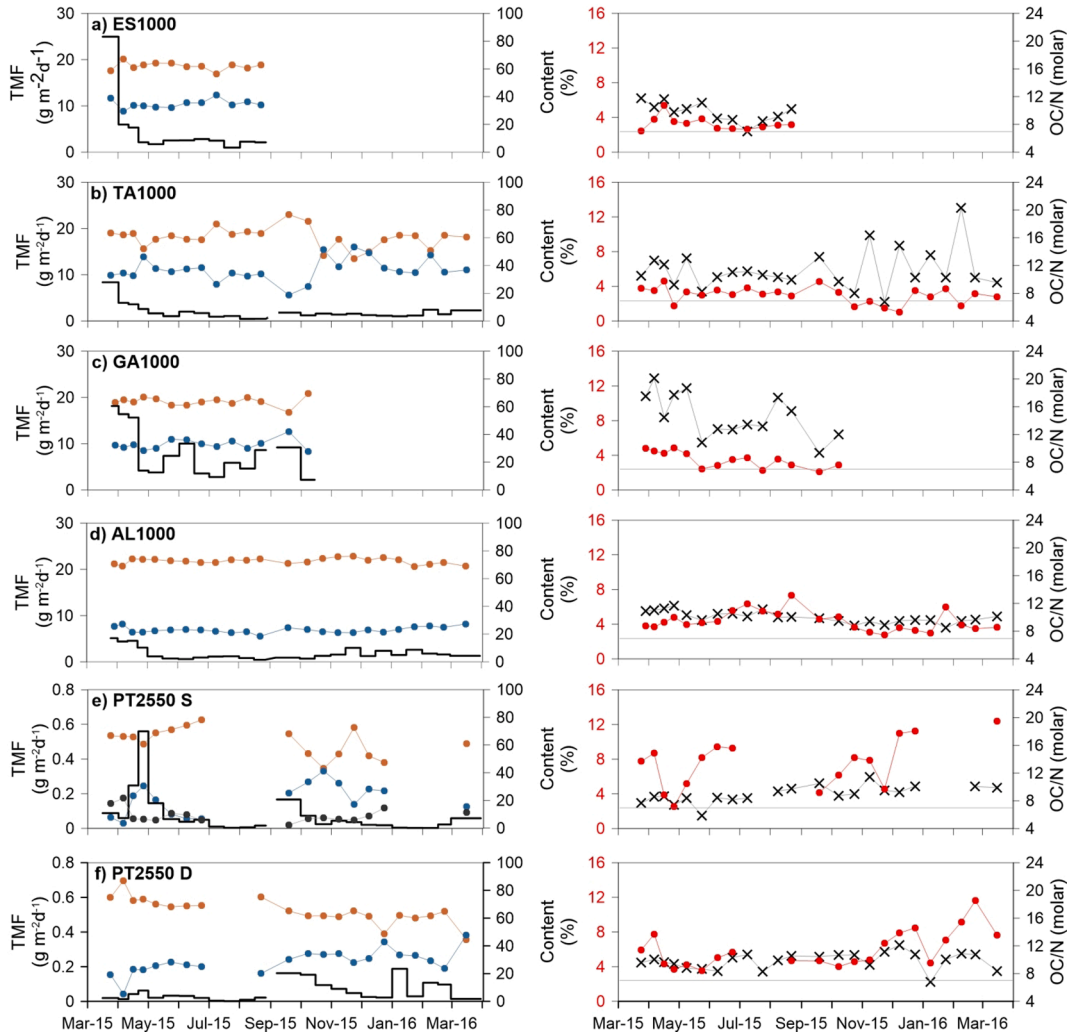

Fig. 6. Total Mass Fluxes (TMF) in the various traps deployed in mooring stations and percentages of lithogenics (brown line), $CaCO_3$ (blue line), opal (black line) and OM fractions (red line) in station (a) ES1000, (b) TA1000, (c) GA1000, (d) AL1000, (e) PT2550-S and (f) PT2550-D. Black crosses represent OC/N ratios. The grey line separates the OC/N ratios with values higher than 7 from the lower ones. OC/N < 7 is considered as indicative of OM from phytoplankton.

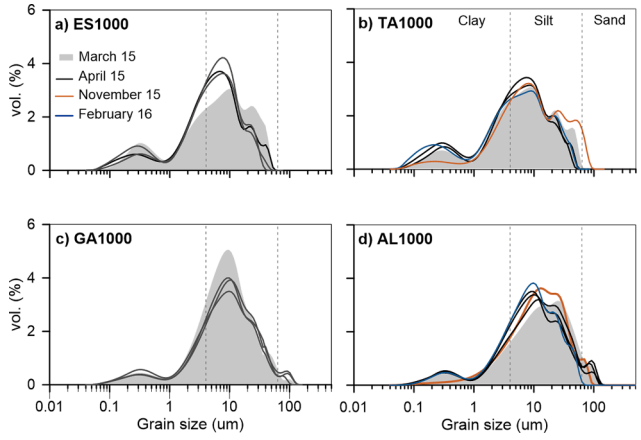

Fig. 7. Grain size distribution of the lithogenic components during stormy periods in Escombreras, Garrucha, Almeria and open slope sediment traps. The March 2015 sample is represented as shadow grey, April 2015 samples as black lines, early November 2015 as orange lines and early February 2016 as blue lines. The grey vertical dotted lines divide the clay (<4 μm), silt (4–63 μm) (fine-medium silt fraction between 4 and 40 μm) and sand fractions (63 μm-2 mm).

in the Garrucha-Almanzora Canyon show a clear terrestrial imprint, with OC/N ratios between 9.3 and 20.1 (Fig. 6). Lower OC/N ratios are found in settling particles in Almeria (8.5–11.7) and Escombreras (6.9–11.8) canyons. While the lowest values indicate punctual periods of non-degraded marine OC, most ratios found are compatible both with soil degraded OM and mixtures of OM from different origins. Settling particles collected in the open slope show larger heterogeneity of OC/N ratios (6.7 to 20.3). The higher OC/N ratios recorded during autumn and winter months suggest that materials entering the inner shelf through nearby *ramblas* with sporadic discharge events are able to reach the open slope.

The imprint of primary production on settling particles is not always obvious due to the dilution of pelagic marine materials within larger amounts of lithogenic particles carried by advective fluxes from the inner continental margin. Temporal variability of primary production results from shifts in hydrographic conditions throughout the year. Different regimes can be established in the three environments under consideration (i.e. submarine canyons, open slope and deep basin). The seasonal behaviour of settling particles is better recorded in open slope and deep basin samples, with periods where fluxes are dominated by fresh marine OM and biogenic components, which contrasts with prevailing homogeneity in canyon particle samples. Moreover, differences are also evident between near-bottom and mid-water traps in the deep basin (PT2550). Lower OC/N ratios found at mid-water depths

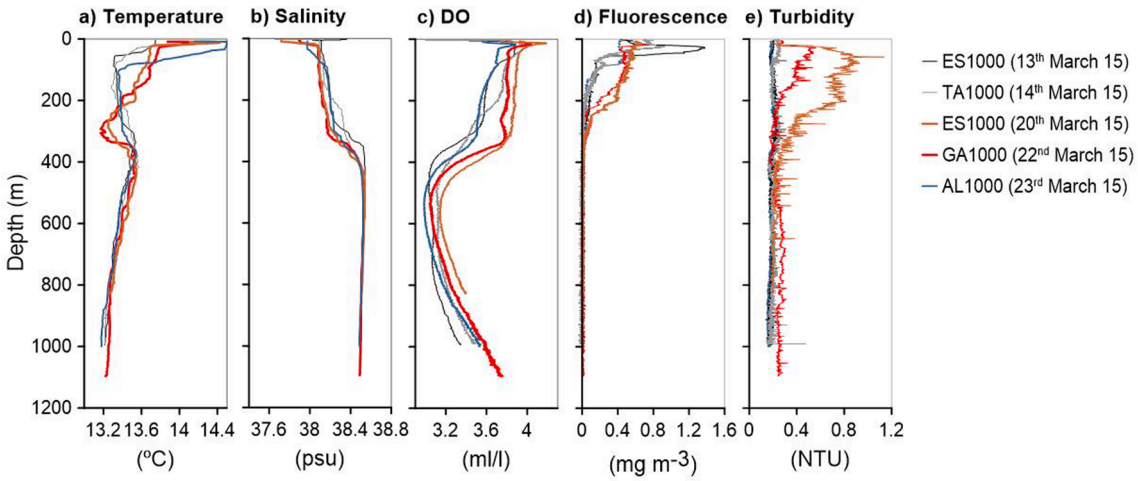

Fig. 8. Hydrological parameters (potential temperature, salinity, dissolved oxygen (DO), fluorescence and turbidity) from CTD transects during mid-March (pre-storm event; grey tones) and late March 2015 (post-storm event; red, purple and blue colours) at ES1000, TA1000, GA1000 and AL1000 stations. Note that AL1000 station is quite far from the rest of stations (Fig. 1).

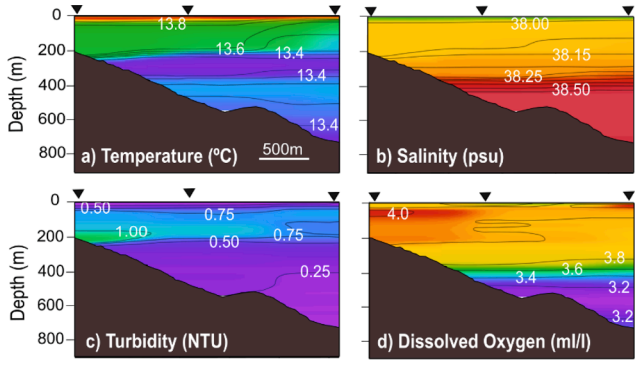

Fig. 9. Water column properties above the Escombreras Canyon transect after the March 2015 storm: a) Potential temperature (degrees). b) salinity (PSU). c) turbidity (NTU). d) dissolved oxygen (ml/l). The location of CTD casts is shown by the inverted black triangles.

compared to those obtained in the near bottom suggest a greater prevalence of pelagic settling at mid-water depth than at near bottom, and the ability of the terrestrial signal to be transferred to the deepest station under scrutiny, at depths larger than 2,000 m. Bottom transport of particulate matter to the deep basin in the western Gulf of Vera has been previously attributed to benthic nepheloid layers detaching from the nearby continental margin (Masqué et al., 2003; Sanchez-Vidal et al., 2005).

In March 2015, there was a reinforced primary production along the coastal area, as shown by satellite Chl-a maps (Fig. 4). In addition, subsurface fluorescence in the deep basin showed values between 30 and 80 m deep that were higher than at surface. This is likely connected to the increase of $CaCO_3$, OM and opal fluxes between late March and May 2015 in the deep basin mid-water station (546 mab) (Fig. 6). There is also a variation in the percentages of biogenic components throughout the sampling period, which could be attributed to planktonic community successions. Higher opal and OM percentages are recorded from the end of March to early April, which likely result from diatom-rich phytoplankton blooms (Fabres et al., 2002; Hernández-Almeida et al., 2011). Then OM and opal contributions diminish during the flux peak (559.6 mg m^{-2} d^{-1}) in late April, while the abundance of calcareous particles grows up. High phytoplankton productivity is likely to support the posterior development of zooplankton communities (Hernández-Almeida et al., 2011). This hypothesis fits with the visual inspection of the samples, which allow observing an increment of planktonic foraminifera in that time. Such biogenic imprint is not detected in the deep basin near-bottom trap, suggesting some degree of uncoupling between middle and lower depths.

Between April and October 2015, superficial primary production was restricted to the WAG upwelling, whereas oligotrophy prevailed in the rest of the area (Fig. 4). In late summer, fluorescence profiles suggest the presence of a deep chlorophyll maximum (DCM) under the seasonal thermocline, a feature that has been widely observed in other parts of the Mediterranean Sea (Estrada et al., 1993). This is not shown satellite data, as these only illustrate surface pigment contents. Those conditions probably favoured the development of oligotrophic species that contributed to the increment of $CaCO_3$ contents and to higher N values during September in particles settling in the Garrucha-Almanzora Canyon (Fig. 6).

In November and December 2015 a widespread phytoplankton bloom occurred in the Gulf of Almeria (Fig. 4). Enhanced primary production during this period has been attributed to de-stratification and increased wind speed triggering fertilization events (Garcia-Gorriz and Carr, 2001). Settling particles in Almeria Canyon do not show a biogenic imprint as it could be expected, even though there is a slight decrease of OC/N ratios with respect to previous samples. Concerning the open slope trap in station TA1000, there is a remarkable increment of $CaCO_3$ content (up to 51 and 53% of the total flux during late October and late November 2015, respectively) (Fig. 6). An increase of biogenic particles collected in sediment traps could be linked to direct pelagic input from surface blooms or to earlier blooms leading to deposition on the shelf followed by lateral transport (Martín et al., 2006; Bonnin et al., 2008). Nevertheless, it could be assumed that the contribution of pelagic fluxes is significant given the low OC/N ratios measured and the absence of energetic hydrodynamic conditions that could potentially increment advective near-bottom fluxes.

During January and February 2016, the prevalence of westerly winds induces favourable upwelling conditions along the coast (Sarhan et al., 2000; Baldacci et al., 2001). Nutrient-rich cold water tongues promoted pronounced local blooms in January, with superficial blooms concentrating west of Cape of Gata in February 2016 (Fig. 4). The arrival of pelagic material this time is detected in settling particles in the Almeria Canyon in late January, characterized by an increment (5.9%) of OM abundance and the lowest measured OC/N ratio (8.5) (Fig. 6). In the Gulf of Vera deep basin station, only the near-bottom trap recorded an increase in particle fluxes in early January (188.1 mg m^{-2} d^{-1}) with a low OC/N ratio (6.8). Despite this, the biogenic imprint on the composition of the particles is not evident. Satellite images indicate that the moored trap is located on the western edge of a highly productive area at

the sea surface, thus evidencing that collected particles had been transported by pelagic sedimentation involving both vertical and horizontal motion.

5.2. The role of oceanographic processes in sedimentary particle transfer

High waves and increased shelf current velocities are the prevalent hydrodynamic responses to strong winds, subsequently increasing bottom shear stress and triggering resuspension and transport of particles across and off-shelf (Guillén et al., 2006; Ulses et al., 2008; Palanques et al., 2008b; Sanchez-Vidal et al., 2012). Shelf-indented submarine canyons have the ability to intercept shelf sediment transport (Canals et al., 2013). Further, storm characteristics, river inputs and preceding oceanographic conditions determine sediment supply from the shelf to submarine canyons (Fabres et al., 2008; Palanques et al., 2008b; Puig et al., 2014; Rumín-Caparrós et al., 2016). In the study area, storm events were recorded during early spring and autumn 2015 and in winter 2016, as detailed below.

The first storm lashed out from March 17th to 21th during 77 h. Intense north-eastern winds strengthened the advection of water over the Gulf of Vera shelf following the general circulation in the area. 70 h from its start and 17 h after the maximum wave peak, CTD casts were performed around the Escombreras Canyon head, where water column turbidity showed increased values at intermediate depths (Fig. 9). This confirms the resuspension of particles due to wave action and their advection from the shelf break. A near-bottom increase of turbidity off the shelf-break was not noticed beyond 1,500 m (Fig. 9), indicating that near-bottom downcanyon sediment transport was constrained to the Escombreras Canyon head. The seaward transport of turbid shelf waters was further restricted to the surface layer, over the above-mentioned sub-surface layer of colder water (cf. section 4.5) that appears in all CTD profiles along the Escombreras Canyon axis (Fig. 9) and in the punctual CTD performed in Garrucha-Almanzora Canyon system after the storm (Fig. 8). This sub-surface layer could be tentatively related to Winter Intermediate Water (WiW) produced in the western Mediterranean during winter (Millot, 1999 and references therein) or to storm-induced downwelling, or both. Even though a clear WiW hydrological signature is not apparent in θ/S diagrams (Vargas-Yáñez et al., 2017), a WiW warmer than 13 °C was detected south of the Balearic Islands during winter 2015 by Juza et al., (2019). Subsequently, the sub-surface layer in our study area can be interpreted as a WiW intrusion into the Gulf of Vera. It is also worth considering the role that the north-east storm may have played in the arrival of the WiW to our study area, taking into account the change in hydrological structure observed between mid-March (CTDs conducted 2–3 days before the storm) and late-March 2015 (CTDs conducted during and 1 day after the storm) (Fig. 8a, b and c). Therefore, our data indicates that the presence of the WiW had a noticeably impact on particle transport into the Escombreras and neighbouring canyons. Such a situation is somehow comparable to the one in canyons of the northern Catalan margin during autumn months, when the seasonal stratification of the water column hinders vertical displacements and restricts the storm-induced downwelling motion to canyon heads (Palanques et al., 2006a, 2008b; Bonnin et al., 2008; Ulses et al., 2008). However, the spatial resolution of the across-canyon CTD casts in our study is not adequate to study in detail the interplay between the WiW and downwelling at the upper canyon course.

Accordingly, in the Palomares margin, intense and persistent north-eastern winds may promote coastal downwelling, thus forcing turbid shelf waters to downwell into the heads of Garrucha-Almanzora Canyon system and other canyons nearby. Actually, the role of bottom advective currents in particle transport in the Garrucha-Almanzora Canyon system could be highly relevant, as Puig et al. (2017) found seabed landforms consistent with storm-induced sediment-laden density currents in the canyon heads. However, as noted previously, the presence of pycnoclines may restrict near-bottom suspended transport to the uppermost canyon. Increased downward particle fluxes after a storm may occur when turbid layers pushing offshore isopycnal surfaces loose part of their suspended sediment load (Durrieu de Madron et al., 1990; Langone et al., 2016). This is fully consistent with the lack of enhanced bottom currents at ES1000 station and the low turbidity and bottom current velocities recorded at GA1000 (Fig. 5).

The views above are further supported by total mass flux measurements as related to the March 2015 storm (Fig. 6). Fluxes up to 24.96 g m^{-2} d^{-1} and 8.37 g m^{-2} d^{-1} were measured in the stations in Escombreras Canyon and the open slope (Fig. 6). Sediment traps moored in Garrucha and Almeria canyons opened with 2–3 days of delay with respect to the onset of the storm, recording fluxes up to 18.15 g m^{-2} d^{-1} and 5.12 g m^{-2} d^{-1}, respectively (Fig. 6). The last values indicate that the transport event lasted several days while representing minima for particulate matter export. Again, it should be kept in mind that the setting of Almeria Canyon differs from the one of the rest of the investigated canyons.

Storms on the 6th and 12th of April 2015 triggered less particulate matter transport than the previous event according to sediment trap data (Fig. 6), likely due to the depletion of unconsolidated, easily resuspendable shelf sediments after the first event, as it would correspond to a sediment-starved marginal setting. Settling particles have higher OC/N ratios in all stations, except in Escombreras Canyon. This could relate to the replenishment of fresh sediments near river mouths during the flooding episode following the storm and subsequent sediment transport, as also observed in the inner shelf off Têt River in the Gulf of Lions (Guillén et al., 2006).

The spring 2015 storms increased the export of particles towards the deep basin all along the continental margin in the study area. However, there are noticeable differences from one margin segment to the other. TMFs recorded in Garrucha-Almanzora Canyon system were at least 1.5 times greater than in Escombreras Canyon, and 3 times greater than in Almeria Canyon, which is close to TA1000. The high values recorded in GA1000 station are linked to canyon heads' configuration, which are strongly indented in to the continental shelf, thus making this canyon system highly sensitive to shelf processes while favouring its interception and funneling capacity of shelf-derived particles. It should be also noted that whereas sediment traps in Garrucha-Almanzora and Escombreras canyons are at similar distance from the coastline (10.7–14.0 km), Almeria Canyon is at twice that distance. Moreover, wave data derived from the WANA model (https://www.puertos.es) for 2015–2016 near each canyon head document the generation of large waves under prevailing strong northeast winds around Escombreras and Garrucha canyons. Contrastingly, in the Gulf of Almeria only south-western storms are able to generate large waves. Coastal configuration there, with Cape of Gata promontory to the east likely acting as a shelter against north-eastern storms, leads to the reduction of wave heights, thus lessening the resuspension of bottom sediments that could potentially reach Almeria mid canyon stretch.

During subsequent stormy periods in autumn 2015 and winter 2016, only AL1000 and TA1000 sediment traps remained operational. The 1st and 21th of November 2015 storms were preceded by rainfall episodes. During the first event, H_s increased to 4.2 m and, following the event, Andarax River moderately incremented its discharge to the sea. A rather unusual situation took place during winter months in early 2016, with very low monthly average precipitation with respect to reference values within the same period (AEMET, 2016). The most remarkable storm in those months occurred in February 2016, when southwestern winds blowed during six days triggering a maximum H_s of 4.8 m near Cape of Gata (Fig. 3). The impact of the storms on particulate matter fluxes is not visible in either of the two sediment traps, AL1000 and TA1000 (Fig. 6). The short duration of the November 2015 events, always <37 h, largely explains the low sediment transfer from the shelf to these mooring stations. Other factors possibly played also a role in the low TMFs during February 2016 storms. The absence of rains during winter months prevented the arrival of new terrestrial material from the river systems to the inner shelf. This factor likely controlled, at least partly, particle fluxes in both stations and especially in the Gulf of Almeria, taking into

account the low discharge of Andarax River following autumn storms. Unlike the samples collected during autumn and winter in AL1000, those collected in TA1000 have high OC/N ratios, reaching up to 20.3 in early February (Fig. 6). Such high ratios support the arrival of terrestrial material deposited onto the inner shelf during previous floods to the mooring site.

5.3. The role of anthropogenic activities in sedimentary particle transfer

Studies developed in La Fonera Canyon, in the NW Mediterranean Sea, have shown that the impact of bottom trawling practiced in and around upper submarine canyon reaches is not restricted to those sections, but also affects deeper canyon sections and out of canyon continental rise areas (Palanques et al., 2006b; Puig et al., 2012; Payo-Payo et al., 2017). Detailed monitoring studies have reported sudden sediment gravity flows during summer months triggered by bottom trawling in that area (Palanques et al., 2006b; Puig et al., 2012). Similar situations have been described and / or inferred in and around other submarine canyons both in the Western Mediterranean Sea and beyond, such as Blanes Canyon (Lopez-Fernandez et al., 2013b) in the Catalan margin, Guadiaro Canyon (Palanques et al., 2005) in the Alboran Sea or the Avilés Canyon in Cantabrian margin (Rumín-Caparrós et al., 2016). The Garrucha-Almanzora Canyon system flanks are located at the edge of Verin and Canto Pote fishing grounds, where intensive bottom trawling takes place in the 500–800 m depth range (García-Rodríguez, 2005). Fishing interest for this canyon system relates to quasi-permanent subsurface upwelling conditions (Muñoz et al., 2018) together with its character of terrestrial OC depocenter, which result in fish aggregation and likely enhancement of local biodiversity.

Trawling-induced sediment resuspension probably is the mechanism that feeds the nepheloid layer below 400 m down to the bottom, as observed in late March and late August CTD casts. VMS data show that the majority of fishing vessels operate at 500–650 m of water depth along the canyon rims and adjacent slope, although during June and July they reach deeper regions around 800 m (Fig. 10). The number of vessel data points within a radius of 4 km around the Garrucha-Almanzora Canyon system mooring station increases during July and August (Fig. 10a). As a result, CTD turbidity values also augment at depths (600–750 m) slightly deeper than the peak of vessels in operation within the same period (Fig. 10b-c) and near the canyon floor. Near-bottom currentmeter measurements show a prominent bottom turbidity increment during summer months followed by a sharp decrease in late August (Fig. 5c). The reason for such a drastical diminution of turbidity is not obvious, since hydrodynamic conditions did not appear to change and there was no reduction in fishing activity. It is, however, plausible that the arrival of primary production particles from DCM contributed to the scavenging of suspended particles, which eventually resulted in the minimum OC/N ratio found in settling particles of September 2015 (Fig. 6). Unfortunately, the temporal resolution of sediment trap sampling prevents us from assessing in greater detail the interrelations of turbidity with other parameters.

It could be assumed that particles remobilized by bottom trawling come from different places, including the adjacent eastern and western open slope and the canyon flanks. Along slope currents passing over Garrucha Canyon would promote the arrival of particles from the eastern open slope into the canyon, as suggested by the persistent westerly currents recorded by the currentmeter in GA1000. The increase in fishing activity along the upper canyon walls during August 2015 explains the high OC/N ratios found in settling particles during that month (Fig. 6), which exceeds the rest of summer samples, and evidences that the material from upper regions is flushed downcanyon.

5.4. Particle flux comparison with other submarine canyons

The fluxes obtained in Escombreras, Garrucha-Almanzora and Almeria submarine canyons are clearly lower than those observed in other canyons in the Western Mediterranean Sea, and also are in the lowest range of those found in canyons around the entire Iberian Peninsula (i.e. including three submarine canyons in the Atlantic Ocean). This is well illustrated when plotting weighted fluxes calculated in this study against those observed in other canyons (Fig. 11). It has to be noted that data from the Atlantic canyons reflect results from canyon reaches that are deeper than those from the Mediterranean Sea, so that it would be reasonable assuming higher fluxes in shallower canyon regions, as pointed by Heussner et al. (2006) for a set of submarine canyons in the Gulf of Lions.

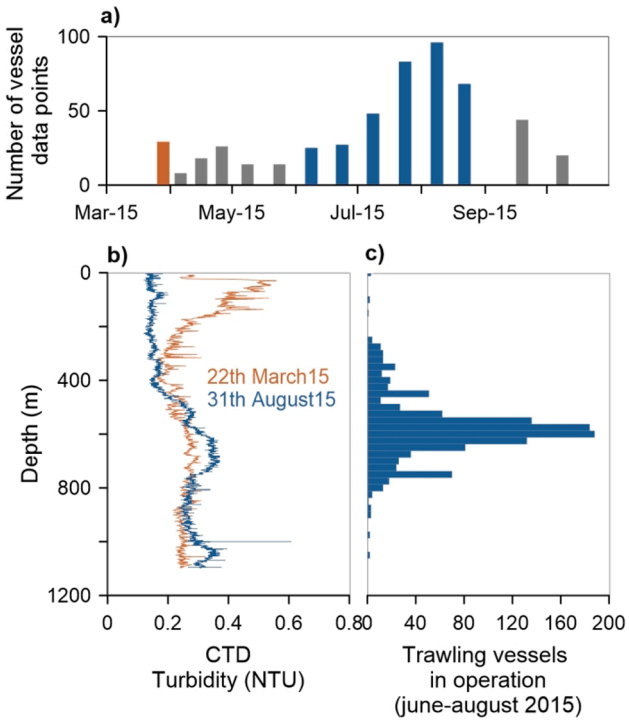

Fig. 10. (a) Number of VSM data points from fishing vessels within a radius of 4 km around GA1000 sailing at<5 knots (i.e. while trawling). (b) CTD turbidity profiles performed in March 2015 (orange) and August 2015 (blue). (c) Operating depth of trawling vessels between June and August within a radius of 4 km from the mooring line.

Most submarine canyons in the North Catalan margin have their heads deeply incised in the continental shelf, as marked by small short distances to the shoreline in Fig. 11, except for Lacaze-Duthiers Canyon. This enables those canyons to trap large volumes of river-delivered sedimentary particles transported by littoral currents. Such trapping effect could be reinforced by specific external forcings and local conditions encompassing metoceanography, physiography, a variety of sedimentary processes and also anthropogenic forcing, as described above (Puig et al., 2014). In the Atlantic Iberian margin, also Nazaré Canyon and to a lesser extent, Setubal Canyon, are deeply incised into the continental shelf with their head at or at short distance from the shoreline.

The low particle fluxes recorded in the studied submarine canyons are highly influenced, first, by the scarcity of river inputs onto the shelf, which is ultimately related to the region's arid climate and weak river discharge. Annual precipitation in the watersheds opening to the investigated continental margin are the lowest in the entire Iberian Peninsula, i.e. <500 mm or even <300 mm in along most of the coastal area. Precipitation in the watershed feeding the North Catalan margin is always above 600 mm, while in the Cantabrian and Portuguese watersheds opening to the Atlantic Ocean is above 800 mm (AEMET, 2011). Such low particle fluxes in the studied Almeria and Murcia continental margin are also determined by limited shelf to canyon exports due not only to the sediment-starved character of the area but also, and

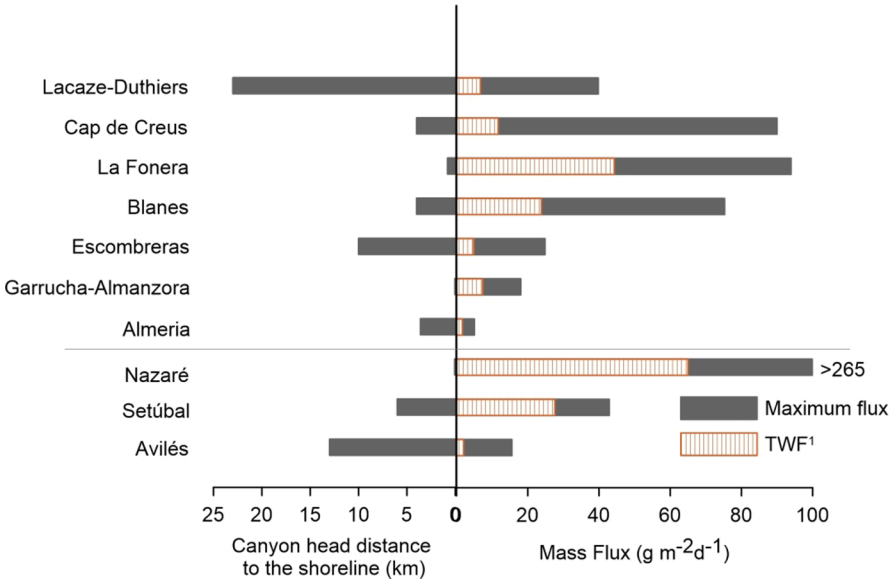

Fig. 11. Shortest canyon head distance to the shoreline (left) and total weighted fluxes (TWF) and maximum TMF (right) in submarine canyons investigated in this study compared to canyons in the NW Mediterranean Sea: Lacaze-Duthiers at 1,000 m depth (Pasqual et al., 2010), Cap de Creus at 1,000 m depth (Pasqual et al., 2010), La Fonera at 1,200 m depth (Martín et al., 2006) Blanes at 1,200 m depth (Lopez-Fernandez et al., 2013b) and in Atlantic Iberian margins: Nazaré at 1,600 m depth (Martín et al., 2011), Setúbal at 1,324 m depth (de Stigter et al., 2011) and Avilés at 2,000 m depth (Rumín-Caparrós et al., 2016). The horizontal line separates Mediterranean canyons (above) from Atlantic canyons (below). Note that the data on Atlantic canyons correspond to larger water depths than Mediterranean canyons. The location of all those canyons is shown in Fig. 1. 1: Mean values of TMF have been used it when the TWF was not available.

importantly, by the mildness of metoceanic conditions during most of the time, with scarce recurrence of extreme events, including major storms. Such events, bringing high amounts of energy to the system, are instead much more frequent in the North Catalan area and even more in Atlantic regions (Martín et al., 2006; Ulses et al., 2008; Martín et al., 2011; Sanchez-Vidal et al., 2012; Rumín-Caparrós et al., 2016). Finally, the lack of high-energy oceanographic processes dominating in and off canyon sediment transport in other margins, such as DSWC, does not help in steering shelf to slope particle export in the investigated margin. However, low recurrence, massive transport events may occur in the study area as triggered by strong earthquakes and rare extreme precipitation and flood events (Sánchez-García et al., 2019).

6. Conclusions

The analysis of the temporal variability and geochemical properties of particle fluxes provides relevant information on sediment dynamics and particle sources in the sediment-starved Almeria and Murcia continental margin and adjacent deep basin. Our results show that storms are the main trigger of mass transfer from the shallow shelf to the deep slope and basin, enhancing particle fluxes both within submarine canyons and in the open slope. In that respect, the magnitude, direction, associated precipitation and duration of the storms eventually leading to high waves and river discharge events, together with the length of intervals between storm events, are the key factors driving down margin mass transfers. A March 2015 to March 2016 year-round monitoring experiment has shown that most particle export to the deep margin occurred as a result of a set of north-east storms in spring 2015 with noticeable wave heights. During that period, off-shelf export of sediment-laden waters was enhanced due to a storm-induced downwelling process. Also, the detachment of turbid layers from the shelf break and the canyons' floor prompted the transport of particle towards deeper reaches. On the other side, the presence of WiW and an associated pycnocline in the Gulf of Vera restricted the vertical particle transfer to a few hundred meters, as illustrated by an above WiW turbid layer at 200 m depth spreading from the outer shelf over the Escombreras mid-canyon reach after a storm in March 2015 in the Mazarron margin segment (Fig. 1).

While metoceanographic processes appear to dominate sedimentary dynamics in Almeria and Escombreras canyons, at the southern and northern ends of the study area, bottom trawling also impacts particle fluxes inside the Garrucha-Almanzora Canyon system in the middle of the study area. Here, the closeness of various canyon heads to river mouths enhances the transfer of terrestrial OC into this system, which should result in and enhanced fertilization of the area making it attractive for the local fishing industry.

Concerning the deep basin traps (mid-water and near-bottom), particle fluxes are mostly determined by phytoplankton blooms. Advective fluxes coming from the continental margin seem to increment TMFs mostly in the near-bottom trap. In any case, the very low fluxes measured in both mid-water and near-bottom traps indicate that few terrestrial particles reach the deep basin in the Gulf of Vera.

Overall, low particle fluxes are recorded in Escombreras, Garrucha-Almanzora and Almeria canyons compared to other canyons in the Western Mediterranean Sea. The lack of recurrent high-energy oceanographic events and the scarcity of riverine sediment inputs are the most relevant factors conditioning the low TMFs observed in the study area. However, longer and complete temporal series are needed to better establish sediment transfer patterns along the Almeria and Murcia continental margin as well to assess inter-annual variability and the likely system shaking effects of rare major storms in the area.

Declaration of Competing Interest

The authors declare that they have no known competing financial interests or personal relationships that could have appeared to influence the work reported in this paper.

Acknowledgements

We would like to express our gratitude to the many colleagues and technicians and to the crew of RV Ángeles Alvariño for their dedication and help during sea-going work. We also thank M. Guart for her assistance with laboratory analyses. This work was supported by research projects NUREIEV (ref. CTM2013-44598-R) and NUREIEVA (ref. CTM2016-75953-C2-1-R). GRC Geociències Marines is funded by the

Catalan Government within its excellence research groups program (ref. 2017 SGR 315). M.Tarrés was supported by a FPI grant from *Ministerio de Ciencia, Innovación y Universidades* of the Spanish Government.

References

Acosta, J., Fontán, A., Muñoz, A., Muñoz-Martín, A., Rivera, J., Uchupi, E., 2013. The morpho-tectonic setting of the Southeast margin of Iberia and the adjacent oceanic Algero-Balearic Basin. Mar. Pet. Geol. 45, 17–41. https://doi.org/10.1016/j.marpetgeo.2013.04.005.

AEMET, 2011. Atlas climático ibérico. Temperatura del aire y precipitación (1971-2000). Agencia Estatal de Meteorología, Ministerio de Medio Ambiente y Medio Rural y Marino, e Instituto de Meteorologia de Portugal.

Aemet, 2016. Avance climatológico mensual febrero 2016. Región de Murcia, Agencia Estatal de Meteorología.

Baker, E.T., Milburn, H.B., Tennant, D.A., 1988. Field assessment of sediment trap efficiency under varying flow conditions. J. Mar. Res. 46 (3), 573–592. https://doi.org/10.1357/002224088785113522.

Baldacci, A., Corsini, G., Grasso, R., Manzella, G., Allen, J.T., Cipollini, P., Guymer, T.H., Snaith, H.M., 2001. A study of the Alboran Sea mesoscale system by means of empirical orthogonal function decomposition of satellite data. J. Mar. Syst. 29 (1-4), 293–311. https://doi.org/10.1016/S0924-7963(01)00021-5.

Béthoux, J.P., Durrieu de Madron, X., Nyffeler, F., Taillez, D., 2002. Deep water in the western Mediterranean: peculiar 1999 and 2000 characteristics, shelf formation hypothesis, variability since 1970 and geochemical inferences. J. Mar. Syst. 33–34, 117–131. https://doi.org/10.1016/S0924-7963(02)00055-6.

Bonnin, J., Heussner, S., Calafat, A., Fabres, J., Palanques, A., Durrieu de Madron, X., Canals, M., Puig, P., Avril, J., Delsaut, N., 2008. Comparison of horizontal and downward particle fluxes across canyons of the Gulf of Lions (NW Mediterranean): Meteorological and hydrodynamical forcing. Cont. Shelf Res. 28 (15), 1957–1970. https://doi.org/10.1016/j.csr.2008.06.004.

Buesseler, K.O., Antia, A.N., Avan, N., Chen, M., Fowler, S.W., Gardner, W.D., Gustafsson, O., Harada, K., Michaels, A.F., Rutgers van der Loeff, M., Sarin, M., Steinberg, D.K., Trull, T., 2007. An assessment of the use of sediment traps for the estimating upper ocean particle fluxes. J. Mar. Res. 65, 345–416. https://doi.org/10.1357/002224007781567621.

Canals, M., Company, J.B., Martín, D., Sanchez-Vidal, A., Ramírez-Llorda, E., 2013. Integrated study of Mediterranean deep canyons: novel results and future challenges. Prog. Oceanogr. 118, 1–27. https://doi.org/10.1016/j.pocean.2013.09.004.

Canals, M., Puig, P., Durrieu de Madron, X., Heussner, S., Palanques, A., Fabres, J., 2006. Flushing submarine canyons. Nature 444 (7117), 354–357. https://doi.org/10.1038/nature05271.

Comas, M.C., Platt, J.P., Soto, J.I., Watts, A.B., 1999. The origin and tectonic history of the Alboran Basin: insights from leg 161 results. Proc. ODP Sci. Results 161, 555–580. https://doi.org/10.2973/odp.proc.sr.161.262.1999.

Company, J.B., Puig, P., Sardà, F., Palanques, A., Latasa, M., Scharek, R., Humphries, S., 2008. Climate influence on deep sea populations. PLoS ONE 3 (1), e1431. https://doi.org/10.1371/journal.pone.0001431.

Cronin, B.T., Kenyon, N.H., Woodside, J., den Bezemer, T., van der Wal, A., Millington, J., Ivanov, M.K., Limonov, A., 1995. The Almeria Canyon: a meandering channel system on an active margin, Alboran Sea, Western Mediterranean. In: Pickering, K. T., Hiscott, R.N., Kenyon, N.H., Ricci-Lucchi, F., Smith, R.D.A. (Eds.), Atlas of Deep Water Environments: Architectural Style in Turbidite Systems, 84– 88. Doi: 10.1007/978-94-011-1234-5_15.

Drake, D.E., Gorsline, D.S., 1973. Distribution and transport of suspended particulate matter in Hueneme, Redondo, Newport, and La Jolla submarine canyons, California. Geol. Soc. Am. Bull. 84, 3949–3968. https://doi.org/10.1130/0016-7606(1973)84<3949:DATOSP>2.0.CO;2.

Dumas, C., Aubert, D., Durrieu de Madron, X., Ludwig, W., Heussner, S., Delsaut, N., Menniti, C., Sotin, C., Buscail, R., 2014. Storm-induced transfer of particulate trace metals to the deep-sea in the Gulf of Lion (NW Mediterranean Sea). Environ. Geochem. Health 36 (5), 995–1014. https://doi.org/10.1007/s10653-014-9614-7.

Durrieu de Madron, X., Nyffeler, F., Godet, C.H., 1990. Hydrographic structure and nepheloid spatial distribution in the Gulf of Lions continental margin. Cont. Shelf Res. 10 (9–11), 915–929. https://doi.org/10.1016/0278-4343(90)90067-V.

Durrieu de Madron, X., Wiberg, P.L., Puig, P., 2008. Sediment dynamics in the Gulf of Lions: the impact of extreme events. Cont. Shelf Res. 28 (15), 1867–1876. https://doi.org/10.1016/j.csr.2008.08.001.

Durrieu de Madron, X., Zervakis, V., Theocharis, A., Georgopoulos, D., 2005. Comments on "Cascades of dense water around the world ocean". Prog. Oceanogr. 64 (1), 83–90. https://doi.org/10.1016/j.pocean.2004.08.004.

Estrada, F., Ercilla, G., Alonso, B., 1997. Pliocene-Quaternary tectonic-sedimentary evolution of the NE Alboran Sea (SW Mediterranean Sea). Tectonophysics 282 (1-4), 423–442. https://doi.org/10.1016/S0040-1951(97)00227-8.

Estrada, M., Marrasé, C., Latasa, M., Berdalet, E., Delgado, M., Riera, T., 1993. Variability of deep chlorophyll maximum characteristics in the Northwestern Mediterranean. Mar. Ecol. Prog. Ser. 92, 289–300. https://doi.org/10.3354/meps092289.

Fabres, J., Calafat, A., Sanchez-Vidal, A., Canals, M., Heussner, S., 2002. Composition and spatio-temporal variability of particle fluxes in the Western Alboran Gyre, Mediterranean Sea (SW Mediterranean). J. Mar. Syst. 33–34, 431–456. https://doi.org/10.1016/S0924-7963(02)00070-2.

Fabres, J., Tesi, T., Velez, J., Batista, F., Lee, C., Calafat, A., Heussner, S., Palanques, A., Miserocchi, S., 2008. Seasonal and event-controlled export of organic matter from the shelf towards the Gulf of Lions continental slope. Cont. Shelf Res. 28 (15), 1971–1983. https://doi.org/10.1016/j.csr.2008.04.010.

Ferré, B., Guizien, K., Durrieu de Madron, X., Palanques, A., Guillén, J., Grémare, A., 2005. Fine-grained sediment dynamics during a strong storm event in the inner-shelf of the Gulf of Lion (NW Mediterranean). Cont. Shelf Res. 25 (19-20), 2410–2427. https://doi.org/10.1016/j.csr.2005.08.017.

Garcia-Gorriz, E., Carr, M.-E., 2001. Physical control of phytoplankton distributions in the Alboran Sea: A numerical and satellite approach. J. Geophys. Res. 106 (C8), 16795–16805. https://doi.org/10.1029/1999JC000029.

García, M., Alonso, B., Ercilla, G., Gràcia, E., 2006. The tributary valley systems of the Almeria Canyon (Alboran Sea, SW Mediterranean): Sedimentary architecture. Mar. Geol. 226 (3-4), 207–223. https://doi.org/10.1016/j.margeo.2005.10.002.

García-Rodríguez, M., 2005. La gamba roja "Aristeus antennatus" (Risso, 1816) (Crustacea, Decapoda): distribución, demografía, crecimiento, reproducción y explotación en el Golfo de Alicante, Canal de Ibiza y Golfo de Vera. Tesis de la Universidad Complutense de Madrid, Facultad de Ciencias Biológicas. Departamento de Biología Animal I.

Gardner, W.D., 1985. The effect of tilt on sediment trap efficiency. Deep-Sea Res. 32 (3), 349–361. https://doi.org/10.1016/0198-0149(85)90083-4.

Gómez de la Peña, L., Gràcia, E., Muñoz, E., Acosta, J., Gómez-Ballesteros, M., Ranero, C. R., Uchipi, E., 2016. Geomorphology and Neogene tectonic evolution of the Palomares continental margin (Western Mediterranean). Tectonophysics 689, 25–39. https://doi.org/10.1016/j.tecto.2016.03.009.

Goñi, M.A., Hedges, J.I., 1995. Sources and reactivates of marine derived organic matter in coastal sediments as determined by alkaline CuO oxidation. Geochim. Cosmochim. Acta 59, 2965–2981. https://doi.org/10.1016/0016-7037(95)00188-3.

Gràcia, E., Pallàs, R., Soto, J.I., Comas, M., Moreno, X., Masana, E., Santanach, P., Diez, S., García, M., Dañobeitia, J., 2006. Active faulting offshore SE Spain (Alboran Sea): Implications for earthquake hazard assessment in the Southern Iberian Margin. Earth Planet. Sci. Lett. 241 (3-4), 734–749. https://doi.org/10.1016/j.epsl.2005.11.009.

Guillén, J., Bourrin, F., Palanques, A., Durrieu de Madron, X., Puig, P., Buscail, R., 2006. Sediment dynamics during wet and dry storm events on the Têt inner shelf (SW Gulf of Lions). Mar. Geol. 234 (1-4), 129–142. https://doi.org/10.1016/j.margeo.2006.09.018.

Hedges, J.I., Keil, R.G., Benner, R., 1997. What happens to terrestrial organic matter in the ocean? Org. Geochem. 27 (5-6), 195–212. https://doi.org/10.1016/S0146-6380(97)00066-1.

Hermoso, A., Homar, V., Amengual, A., 2021. The Sequence of Heavy Precipitation and Flash Flooding of 12 and 13 September 2019 in Eastern Spain. Part I: Mesoscale Diagnostic and Sensitivity Analysis of Precipitation. J. Hydrometeorol. 22 (5), 1117–1138. https://doi.org/10.1175/JHM-D-20-0182.1.

Hernández-Almeida, I., Bárcena, M.A., Flores, J.A., Sierro, F.J., Sanchez-Vidal, A., Calafat, A., 2011. Microplankton response to environmental conditions in the Alboran Sea (Western Mediterranean): One year sediment trap record. Mar. Micropaleontol. 78 (1-2), 14–24. https://doi.org/10.1016/j.marmicro.2010.09.005.

Heussner, S.D., de Madron, X., Radakovitch, O., Beaufort, L., Biscaye, P.E., Carbonne, J., Desault, N., Etcheber, H., Monaco, A., 1999. Spatial and temporal patterns of downward particle fluxes on the continental slope of the Bay of Biscay (northeastern Atlantic). Deep-Sea Res. II 46, 2101–2146. https://doi.org/10.1016/S0967-0645(99)00057-0.

Heussner, S., Durrieu de Madron, X., Calafat, A., Canals, M., Carbonne, J., Delsaut, N., Saragoni, G., 2006. Spatial and temporal variability of downward particle fluxes on a continental slope: lessons from an 8-yr experiment in the Gulf of Lions (NW Mediterranean). Mar. Geol. 234 (1-4), 63–92. https://doi.org/10.1016/j.margeo.2006.09.003.

Heussner, S., Ratti, C., Carbonne, J., 1990. The PPS 3 time-series sediment trap and the trap sample processing techniques used during the ECOMARGE experiment. Cont. Shelf Res. 10 (9-11), 943–958. https://doi.org/10.1016/0278-4343(90)90069-X.

Juza, M., Escudier, R., Vargas-Yáñez, M., Mourre, B., Heslop, E., Allen, J., Tintoré, J., 2019. Characterization of changes in Western Intermediate Water properties enabled by an innovative geometry-based detection approach. J. Mar. Syst. 191, 1–12. https://doi.org/10.1016/j.jmarsys.2018.11.003.

Kamatani, A., Oku, O., 2000. Measuring biogenic silica in marine sediments. Mar. Chem. 68 (3), 219–229. https://doi.org/10.1016/S0304-4203(99)00079-1.

Kiriakoulakis, K., Blackbird, S., Ingels, J., Vanreusel, A., Wolff, G.A., 2011. Organic geochemistry of submarine canyons: The Portuguese Margin. Deep-Sea Res. II 58 (23-24), 2477–2488. https://doi.org/10.1016/j.dsr2.2011.04.010.

Langone, L., Conese, I., Miserocchi, S., Boldrin, A., Bonaldo, D., Carniel, S., Chiggiato, J., Turchetto, M., Borghini, M., Tesi, T., 2016. Dynamics of particles along thewestern margin of the Southern Adriatic: Processes involved in transferring particulate matter to the deep basin. Mar. Geol. 375, 28–43. https://doi.org/10.1016/j.margeo.2015.09.004.

Liquete, C., Arnau, P., Canals, M., Colas, S., 2005. Mediterranean river systems of Andalusia, southern Spain, and associated deltas: A source to sink approach. Mar. Geol. 222–223, 471–495. https://doi.org/10.1016/j.margeo.2005.06.033.

Lobo, F.J., Ercilla, G., Fernández-Salas, L.M., Gámez, D., 2014. Chapter 11 The Iberian Mediterranean shelves. Geological Society, London, Memoirs 41 (1), 147–170.

Lopez-Fernandez, P., Bianchelli, S., Pusceddu, A., Calafat, A., Danovaro, R., Canals, M., 2013a. Bioavailable compounds in sinking particulate organic matter, Blanes Canyon, NW Mediterranean Sea: Effects of a large storm and sea surface biological processes. Prog. Oceanogr. 118, 108–121. https://doi.org/10.1016/j.pocean.2013.07.022.

Lopez-Fernandez, P., Calafat, A., Sanchez-Vidal, A., Canals, M., Flexas, M.M., Cateura, J., Company, J.B., 2013b. Multiple drivers of particle fluxes in the Blanes submarine

canyon and adjacent open slope: results of a year round experiment. Prog. Oceanogr. 118, 95–107. https://doi.org/10.1016/j.pocean.2013.07.029.
Machado, M.J., Benito, G., Barriendos, M., Rodrigo, F.S., 2011. 500 years of rainfall variability and extreme hydrological events in southeastern Spain drylands. J. Arid Environ. 75 (12), 1244–1253. https://doi.org/10.1016/j.jaridenv.2011.02.002.
Martín, J., Durrieu de Madron, X., Puig, P., Bourrin, F., Palanques, A., Houpert, L., Higueras, M., Sanchez-Vidal, A., Calafat, A.M., Canals, M., Heussner, S., Desault, N., Sotin, C., 2013. Sediment transport along the Cap de Creus Canyon flank during a mild, wet winter. Biogeosciences 10, 3221–3239. https://doi.org/10.5194/bg-10-3221-2013.
Martín, J., Palanques, A., Puig, P., 2006. Composition and variability of downward particulate matter fluxes in the Palamós submarine canyon (NW Mediterranean). J. Mar. Syst. 60 (1-2), 75–97. https://doi.org/10.1016/j.jmarsys.2005.09.010.
Martín, J., Palanques, A., Vitorino, J., Oliveira, A., de Stigter, H.C., 2011. Near-bottom particulate matter dynamics in the Nazaré submarine canyon under calm and stormy conditions. Deep-Sea Res. II 58 (23-24), 2388–2400. https://doi.org/10.1016/j.dsr2.2011.04.004.
Martín, J., Puig, P., Masqué, P., Palanques, A., Sánchez-Gómez, A., Vopel, K.C., 2014a. Impact of bottom trawling on deep-sea sediment properties along the flanks of a submarine canyon. PLoS ONE 9 (8), e104536. https://doi.org/10.1371/journal.pone.0104536.
Martín, J., Puig, P., Palanques, A., Ribó, M., 2014b. Trawling-induced daily sediment resuspension in the flank of a Mediterranean submarine canyon. Deep-Sea Res. II 104, 174–183. https://doi.org/10.1016/j.dsr2.2013.05.036.
Masqué, P., Fabres, J., Canals, M., Sanchez-Cabeza, J.A., Sanchez-Vidal, A., Cacho, I., Calafat, A.M., Bruach, J.M., 2003. Accumulation rates of major constituents of hemipelagic sediments in the deep Alboran Sea: A centennial perspective of sedimentary dynamics. Mar. Geol. 193 (3-4), 207–233. https://doi.org/10.1016/S0025-3227(02)00593-5.
Millot, C., 1999. Circulation in the Western Mediterranean Sea. J. Mar. Syst. 20 (1-4), 423–442. https://doi.org/10.1016/S0924-7963(98)00078-5.
Mortlock, R.A., Froelich, P.N., 1989. A simple method for the rapid determinations of biogenic opal in pelagic marine sediments. Deep-Sea Res. 36 (9), 1415–1426. https://doi.org/10.1016/0198-0149(89)90092-7.
Muñoz, M., Reul, A., García-Martínez, M.C., Plaza, F., Bautista, B., Moya, F., Vargas-Yáñez, M., 2018. Oceanographic and bathymetric features as the target for pelagic MPA design: A case study on the Cape of Gata. Water 10, 1403. https://doi.org/10.3390/w10101403.
Ogston, A.S., Drexler, T.M., Puig, P., 2008. Sediment delivery, resuspension, and transport in two contrasting canyon environments in the southwest Gulf of Lions. Cont. Shelf Res. 28 (15), 2000–2016. https://doi.org/10.1016/j.csr.2008.02.012.
Palanques, A., Durrieu de Madron, X., Puig, P., Fabres, J., Guillén, J., Calafat, A., Canals, M., Heussner, S., Bonnin, J., 2006a. Suspended sediment fluxes and transport processes in the Gulf of Lions submarine canyons. The role of storms and dense water cascading. Mar. Geol. 234 (1-4), 43–61. https://doi.org/10.1016/j.margeo.2006.09.002.
Palanques, A., El Khatab, M., Puig, P., Masqué, P., Sánchez-Cabeza, J.A., Isla, E., 2005. Downward particle fluxes in the Guadiaro submarine canyon depositional system (north-western Alboran Sea), a river flood dominated system. Mar. Geol. 220 (1-4), 23–40. https://doi.org/10.1016/j.margeo.2005.07.004.
Palanques, A., Guillén, J., Puig, P., Durrieu de Madron, X., 2008a. Storm-driven shelf-to-canyon suspended sediment transport at the southwestern Gulf of Lions. Cont. Shelf Res. 28 (15), 1947–1956. https://doi.org/10.1016/j.csr.2008.03.020.
Palanques, A., Martín, J., Puig, P., Guillén, J., Company, J.B., Sardà, F., 2006b. Evidence of sediment gravity flows induced by trawling in the Palamós (Fonera) submarine canyon (northwestern Mediterranean). Deep-Sea Res. I 53 (2), 201–214. https://doi.org/10.1016/j.dsr.2005.10.003.
Palanques, A., Masqué, P., Puig, P., Sanchez-Cabeza, J.A., Frignani, M., Alvisi, F., 2008b. Anthropogenic trace metals in the sedimentary record of the Llobregat continental shelf and adjacent Foix Submarine Canyon (northwestern Mediterranean). Mar. Geol. 248 (3-4), 213–227. https://doi.org/10.1016/j.margeo.2007.11.001.
Palanques, A., Puig, P., Durrieu de Madron, X., Sanchez-Vidal, A., Pasqual, C., Martín, J., Calafat, A., Heussner, S., Canals, M., 2012. Sediment transport to the deep canyons and open-slope of the western Gulf of Lions during the 2006 intense cascading and open-sea convection period. Prog. Oceanogr. 106, 1–15. https://doi.org/10.1016/j.pocean.2012.05.002.
Paradis, S., Puig, P., Masqué, P., Juan-Díaz, X., Martín, J., Palanques, A., 2017. Bottom-trawling along submarine canyons impacts deep sedimentary regimes. Sci. Rep. 7, 43332. https://doi.org/10.1038/srep43332.
Pasqual, C., Sanchez-Vidal, A., Zuñiga, D., Calafat, A., Canals, M., Durrieu de Madron, X., Puig, P., Heussner, S., Palanques, A., Delsaut, N., 2010. Flux and composition of settling particles across the continental margin of the Gulf of Lion: the role of dense shelf water cascading. Biogeosciences 7, 217–231. https://doi.org/10.5194/bg-7-217-2010.
Payo-Payo, M., Jacinto, R.S., Lastras, G., Rabineau, M., Puig, P., Martín, J., Canals, M., Sultan, N., 2017. Numerical modeling of bottom trawling-induced sediment transport and accumulation in La Fonera submarine canyon, northwestern Mediterranean Sea. Mar. Geol. 386, 107–125. https://doi.org/10.1016/j.margeo.2017.02.015.
Pedrosa-Pàmies, R., Sanchez-Vidal, A., Calafat, A., Canals, M., Durán, R., 2013. Impact of storm-induced remobilization on grain size distribution and organic carbon content in sediments from the Blanes Canyon area, NW Mediterranean Sea. Prog. Oceanogr. 118, 122–136. https://doi.org/10.1016/j.pocean.2013.07.023.
Pérez-Hernández, S., Comas, M.C., Escutia, C., 2014. Morphology of turbidite systems within an active continental margin (the Palomares Margin, western Mediterranean). Geomorphology 219, 10–26. https://doi.org/10.1016/j.geomorph.2014.04.014.
Puig, P., Canals, M., Company, J.B., Martín, J., Amblas, D., Lastras, G., Palanques, A., Calafat, A.M., 2012. Ploughing the deep sea floor. Nature 489 (7415), 286–289. https://doi.org/10.1038/nature11410.
Puig, P., Durán, R., Muñoz, A., Elvira, E., Guillén, J., 2017. Submarine canyon-head morphologies and inferred sediment transport processes in the Alías-Almanzora canyon system (SW Mediterranean): On the role of the sediment supply. Mar. Geol. 393, 21–34. https://doi.org/10.1016/j.margeo.2017.02.009.
Puig, P., Palanques, A., Guillén, J., El Khatab, M., 2004. Role of internal waves in the generation of nepheloid layers on the northwestern Alboran slope: implications for continental margin shaping. J. Geophys. Res. 109, C09011. https://doi.org/10.1029/2004JC002394.
Puig, P., Palanques, A., Martín, J., 2014. Contemporary Sediment-Transport Processes in Submarine Canyons. Ann. Rev. Mar. Sci. 6 (1), 53–77. https://doi.org/10.1146/annurev-marine-010213-135037.
Pusceddu, A., Mea, M., Canals, M., Heussner, S., Durrieu de Madron, X., Sanchez-Vidal, A., Bianchelli, S., Corinaldesi, C., Dell'Anno, A., Thomsen, L., Danovaro, R., 2013. Major consequences of an intense dense shelf water cascading event on deep-sea benthic trophic conditions and meiofaunal biodiversity. Biogeosciences 10 (4), 2659–2670. https://doi.org/10.5194/bg-10-2659-201310.5194/bg-10-2659-2013-supplement.
Ramirez-Llodra, E., De Mol, B., Company, J.B., Coll, M., Sardà, F., 2013. Effects of natural and anthropogenic processes in the distribution of marine litter in the deep Mediterranean Sea. Prog. Oceanogr. 118, 273–287. https://doi.org/10.1016/j.pocean.2013.07.027.
Renault, L., Oguz, T., Pascual, A., Vizoso, G., Tintore, J., 2012. Surface circulation in the Alboran Sea (western Mediterranean) inferred from remotely sensed data. J. Geophys. Res. 117, C08009. https://doi.org/10.1029/2011JC007659.
Romero-Romero, S., Molina-Ramírez, A., Höfer, J., Duineveld, G., Rumín-Caparrós, A., Sanchez-Vidal, A., Canals, M., Acuña, J.L., 2016. Seasonal pathways of organic matter within the Avilés submarine canyon: Food web implications. Deep Sea Res. Part I 117, 1–10. https://doi.org/10.1016/j.dsr.2016.09.003.
Rumín-Caparrós, A., Sanchez-Vidal, A., González-Pola, C., Lastras, G., Calafat, A., Canals, M., 2016. Particle fluxes and their drivers in the Avilés submarine canyon and adjacent slope, central Cantabrian margin, Bay of Biscay. Prog. Oceanogr. 144, 39–61. https://doi.org/10.1016/j.pocean.2016.03.004.
Sánchez-García, C., Schulte, L., Carvalho, F., Peña, J.C., 2019. A 500-year flood history of the arid environments of southeastern Spain. The case of the Almanzora River. Global Planet. Change 181, 102987. https://doi.org/10.1016/j.gloplacha.2019.102987.
Sanchez-Vidal, A., Canals, M., Calafat, A.M., Lastras, G., Pedrosa-Pàmies, R., Menéndez, M., Medina, R., Company, J.B., Hereu, B., Romero, J., Alcoverro, T., Chin, W.-C., 2012. Impacts on the deep-sea ecosystem by a severe coastal storm. PLoS ONE 7 (1), e30395. https://doi.org/10.1371/journal.pone.0030395.
Sanchez-Vidal, A., Higueras, M., Martí, E., Liquete, C., Calafat, A., Kerhervé, P., Canals, M., 2013. Riverine transport of terrestrial organic matter to the North Catalan margin, NW Mediterranean Sea. Prog. Oceanogr. 118, 71–80. https://doi.org/10.1016/j.pocean.2013.07.020.
Sanchez-Vidal, A., Calafat, A., Canals, M., Frigola, J., Fabres, J., 2005. Particle fluxes and organic carbon balance across the Eastern Alboran Sea (SW Mediterranean Sea). Cont. Shelf Res. 25 (5-6), 609–628. https://doi.org/10.1016/j.csr.2004.11.004.
Sanz, J.L., Hermida, N., Lobato, A.B., Tello, O., Fernández-Salas, L.M., González, J.L., Bécares, M.A., Gómez de Paz, R., Cubero, P., González, F., Muñoz, A., Vaquero, M., Ubiedo, J.M., Contreras, D., Ramos, M., Carreño, F., Pérez, J.I., 2002. Estudio de la Plataforma Continental Española, Hoja MC047-Garrucha-Serie C. Secretaria General de Pesca Marítima e Instituto Español de Oceanografía.
Sarhan, T., García Lafuente, J., Vargas, M., Vargas, J.M., Plaza, F., 2000. Upwelling mechanisms in the northwestern Alboran Sea. J. Marine Syst. 23, 317–331. https://doi.org/10.1016/S0924-7963(99)00068-8.
Schmidt, S., de Stigter, H.C., van Weering, T.C.E., 2001. Enhanced short-term sediment deposition within the Nazaré Canyon, North-East Atlantic. Marine Geol. 173 (1–4), 55–67. https://doi.org/10.1016/S0025-3227(00)00163-8.
Schmidt, S., Howa, H., Diallo, A., Martín, J., Cremer, M., Duros, P., Fontanier, C., Deflandre, B., Metzger, E., Mulder, T., 2014. Recent sediment transport and deposition in the Cap-Ferret Canyon, South-East margin of Bay of Biscay. Deep-Sea Res. II 104, 134–144. https://doi.org/10.1016/j.dsr2.2013.06.004.
Shepard, F.P., Marshall, N.F., McLoughlin, P.A., Sullivant, G.G., 1979. Currents in Submarine Canyons and Other Seavalleys. AAPG Studies in Geology 8, Tulsa, Oklahoma, 173. Doi: 10.2110/pec.79.27.0085.
de Stigter, H.C., Boer, W., de Jesus Mendes, P.A., Jesus, C.C., Thomsen, L., van den Bergh, G.D., van Weering, T.C.E., 2007. Recent sediment transport and deposition in

the Nazaré Canyon, Portuguese continental margin. Marine Geol. 246 (2–4), 144–164. https://doi.org/10.1016/j.margeo.2007.04.011.

de Stigter, H.C., Jesus, C.C., Boer, W., Richter, T.O., Costa, A., van Weering, T.C.E., 2011. Recent sediment transport and deposition in the Lisbon-Setúbal and Cascais submarine canyons. Portuguese continental margin. Deep-Sea Res. II 58 (23–24), 2321–2344. https://doi.org/10.1016/j.dsr2.2011.04.001.

Tintore, J., La Violette, P.E., Blade, I., Cruzado, A., 1988. A study of an intense density front in the Eastern Alboran Sea: the Almeria-Oran Front. J. Phys. Oceanogr. 18, 1384–1397. https://doi.org/10.1175/1520-0485(1988)018<1384:ASOAID>2.0.CO;2.

Tubau, X., Canal, M., Lastras, G., Rayo, X., Rivera, J., Amblas, D., 2015. Marine litter on the floor of deep submarine canyons of the Northwestern Mediterranean Sea: The role of hydrodynamic processes. Prog. Oceanogr. 134, 379–403. https://doi.org/10.1016/j.pocean.2015.03.013.

Ulses, C., Estournel, C., Durrieu de Madron, X., Palanques, A., 2008. Suspended sediment transport in the Gulf of Lions (NW Mediterranean): impact of extreme storms and floods. Cont. Shelf Res. 28 (15), 2048–2070. https://doi.org/10.1016/j.csr.2008.01.015.

Vargas-Yáñez, M., Plaza, F., García-Lafuente, J., Sarhan, T., Vargas, J.M., Vélez-Belchi, P., 2002. About the seasonal variability of the Alboran Sea circulation. J. Mar. Syst. 35 (3-4), 229–248. https://doi.org/10.1016/S0924-7963(02)00128-8.

Vargas-Yáñez, M., García-Martínez, M.C., Moya, F., Balbín, R., López-Jurado, J.L., Serra, M., Zunino, P., Pascual, J., Salat, J., 2017. Updating temperature and salinity mean values and trends in the Western Mediterranean: The RADMED Project. Prog. Oceanogr. 157, 27–46. https://doi.org/10.1016/j.pocean.2017.09.004.

Vázquez, J.T., Ercilla, G., Alonso, B., Juan, C., Rueda, J.L., Palomino, D., Fernández-Salas, L.M., Bárcenas, P., Casas, D., Díaz-del-Río, V., Estrada, F., Farran, M., García, M., González, E., López-Gonzalez, N., El Moumni, B., and Contouriber, Montera and Mower Teams, 2015. Submarine Canyons and related features in the Alboran Sea: continental margins and major isolated reliefs. pp. 183-196 In CIESM Monograph 47 [F. Briand ed.] Submarine canyon dynamics in the Mediterranean and tributary seas-An integrated geological, oceanographic and biological perspective, 232 p. CIESM Publisher, Monaco.

Xu, J.P., Noble, M.A., Rosenfeld, L.K., 2004. In-situ measurements of velocity structure within turbidity currents. L09311 Geophys. Res. Lett. 31 (9). https://doi.org/10.1029/2004GL019718.

www.puertos.es/es-es/oceanografia/Paginas/portus.aspx: Puertos del Estado webpage. From which metoceanographic data have been downloaded.

Progress in Oceanography 218 (2023) 103122

Contents lists available at ScienceDirect

Progress in Oceanography

journal homepage: www.elsevier.com/locate/pocean

Transport and distributions of naturally and anthropogenically sourced trace metals and arsenic in submarine canyons

Marta Tarrés [a], Marc Cerdà-Domènech [a], Rut Pedrosa-Pàmies [a,b], Andrea Baza-Varas [a], Antoni Calafat [a], Anna Sanchez-Vidal [a], Miquel Canals [a,c,d,*]

[a] GRC Geociències Marines, Dept. Dinàmica de la Terra i de l'Oceà, Facultat de Ciències de la Terra, Universitat de Barcelona, 08028 Barcelona, Spain
[b] The Ecosystems Center, Marine Biological Laboratory, Woods Hole, MA, USA
[c] Reial Acadèmia de Ciències i Arts de Barcelona (RACAB), La Rambla 115, 08002 Barcelona, Spain
[d] Institut d'Estudis Catalans (IEC), Secció de Ciències i Tecnologia, carrer del Carme 47, 08001 Barcelona, Spain

ARTICLE INFO

Keywords:
Submarine canyons
Trace metals
Chemical pollutants
Settling particles
Seafloor sediments
SW Mediterranean Sea

ABSTRACT

Continental margins play a key role in the cycling of natural and anthropogenic trace metals (TMs) as pathways at the interface between landmasses and deep ocean basins but also as sinks. Knowledge of how short-lived forcings alter the export dynamics of TMs is essential for our understanding of their fate in that setting. Here we report time series of particulate metal fluxes in three submarine canyons —namely Escombreras, Almeria and the Garrucha-Almanzora system— of the South-Western Mediterranean Sea. Our research focuses on combining multi-elemental TMs (Al, Fe, Ti, Co, Cu, Mn, Ni, Pb and Zn) and As (a metalloid) contents of settling particles collected near the bottom by automated particle traps during one year, and seafloor sediment samples from below the traps. We assess the role of storms and bottom trawling in the off-shelf transport of particulate TMs and As, and the natural and anthropogenic contributions of TMs by using enrichment factors (EFs).

The TM export fluxes and composition changed over the study period, from March 2015 to March 2016. TM fluxes increase in early spring 2015 in association with short-lived storm events and during calm months in the Garrucha-Almanzora Canyon system, likely due to sediment resuspension triggered by bottom trawling. In terms of composition, TMs in the sinking fluxes appear to be closely associated with lithogenic (Al, Fe and Ti) and authigenic (Mn) particles' proxies. During storm events, the mass of settling particles in Escombreras and Almeria canyons was impoverished in Al, Fe, As, Co, Cu, Mn and Ni compared to other periods. The Garrucha-Almanzora Canyon system behaves differently as the above-described differences, are not observed there. Moreover, the TM composition of the sediments —with higher contents of Fe, Ti and several other TMs— in this canyon is barely tied to the composition of the settling particles. Finally, Cu and Zn contents, together with Pb in the northernmost Escombreras Canyon, are best explained by referring to anthropogenic sources. This work provides insights into the profound influence of the natural and anthropogenic forcings controlling the distributions and seasonal dynamics of particulate TMs and As in submarine canyons.

1. Introduction

Trace metals (Al, Fe, Ti, Co, Cu, Mn, Ni, Pb, and Zn; TMs hereafter) in the marine environment have attracted the interest of researchers due to their critical role in regulating the growth and structure of marine organisms, and their interest as tracers of oceanographic processes, and also as pollutants (Morel and Price, 2003, Twining and Baines, 2013; Jeandel and Vance, 2018). Suspended particles are known by their capability to remove TMs from seawater (Anderson and Hayes, 2015 and references therein). Biological uptake, scavenging onto particle surfaces and precipitation (including bacteria-mediated) incorporate TMs into the particulate phase within the water column (Cowen and Bruland, 1985; Morel and Price, 2003; Anderson, 2020). The cycling of metals is, therefore, driven by sedimentary dynamics controlling the input, production, transformation, transport and accumulation of particles along the water column down to the seafloor. In other words, the distribution of TMs in the ocean is largely regulated by sinking particle fluxes (Huang and Conte, 2009; Kuss et al., 2010; Theodosi et al., 2013; Conte et al.,

* Corresponding author.
E-mail address: miquelcanals@ub.edu (M. Canals).

https://doi.org/10.1016/j.pocean.2023.103122
Received 26 April 2023; Received in revised form 1 September 2023; Accepted 5 September 2023
Available online 9 September 2023

2019). Within the fluxes, the lithogenic, authigenic (abiotically precipitated) and biogenic fractions are vectors of TMs and As towards the seafloor (Huang and Conte, 2009). In the last years, researchers have employed some individual elements as proxies for mineral phases (e.g., Ba, Fe or Mn for authigenic minerals; Al, Fe or Ti for lithogenic minerals; and P for biogenic minerals, among others) (Sanchez-Vidal et al., 2005; Twining and Baines, 2013; Ohnemus and Lam, 2015; Al-Hashem et al., 2022). Those proxies provide information on transfer vectors and processes involving all other TMs, as elements associated with the same type of particles often exhibit similar distributions (Lee et al., 2018).

Continental margin settings are known as major vectors and suppliers of particulate and dissolved TMs to the deep basins (Lam et al., 2006; Charette et al., 2016; Lemaitre et al., 2020), and also as TMs' sinks (Palanques et al., 2008; Anderson, 2020). Particle transport in continental margins is driven by currents, which eventually can also erode and re-suspend seafloor sediments that will then add to the pool of particles in the water column (Heussner et al., 2006). Ultimately, such particles will be buried with their TMs' load (Geibert, 2018). TM cycling results from a complex interplay of physical and biogeochemical processes and is therefore difficult to understand (Noble et al., 2012). This is well illustrated by high-energy events such as sea storms or dense shelf water cascades (DSWC), which intensify TMs' transport from shallow to deep environments while also enhancing biogeochemical interactions (Hung and Ho, 2014; Dumas et al., 2014; Cossa et al., 2014; Durrieu de Madron et al., 2023). However, beyond the widely recognized key role of continental margins in mediating TMs' transport to the open ocean, significant gaps persist about the distribution of particulate metals and the processes determining their seaward transport, including deep continental margin regions (Palanques et al., 2008; Jesus et al., 2010; Roussiez et al., 2012; Cossa et al., 2014).

Besides, there is clear evidence that anthropogenic TMs have added to natural fluxes along and across continental margin settings and beyond, especially since the mid-nineteenth century (Grousset et al., 1995; Hanebuth et al., 2018), thus contributing to the degradation of the environmental status of our coasts, seas and oceans (Papale et al., 2018; Azaroff et al., 2020). In some places such inputs have been traced back to the Roman Period (Mil-Homens et al., 2016).

This study addresses some of these unknowns in three submarine canyons located off southeast Spain in the Mediterranean Sea (cf. section 2.1). These canyons connect coastal and shelf environments to the deep-sea (Ross et al., 2009; Puig et al., 2014). This paper is a follow up of a previous one by Tarrés et al. (2022) focusing on the major components of settling particles in the investigated submarine canyons for the same period. In the present paper, we focus on the multi-elemental TM (Al, Fe, Ti, Cu, Co, Mn, Ni, Pb, and Zn) and As (a metalloid) contents in settling particles and assess the processes controlling the dynamics of TMs and As in submarine canyons. By comparing the seafloor sediment composition with particles sinking in the canyons we provide insights into the processes leading TMs to reach canyon floors and their preservation in the sedimentary record. Finally, the calculation of enrichment factors (EFs) allows for estimating the anthropogenic influence on TM fluxes.

For the purpose of this paper and for ease of simplicity, from here onwards we will refer to all elements listed above including As as TMs, i.e. those which appear in the relevant environmental matrix with ppm or ppb concentrations. This will include Al and Fe, which according to their concentrations actually appear as TMs in particle fluxes in the water column though not in the analyzed sediments, where they display concentrations of thousands of ppm.

2. Study area

2.1. Overall setting

The study area encompasses three margin segments in the SW Mediterranean Sea, namely Mazarron and Palomares, located on the western edge of the Algero-Balearic Sea, and the Almeria one, located on the northeastern border of the Alboran Sea (Fig. 1a, b). The continental shelf is narrow (<13 km) (Lobo et al., 2014), with the shelf edge located between 100 and 200 m depth. It is cut by several submarine canyons of small to medium size (Pérez-Hernández et al., 2014), which are smaller and more densely grouped to the north (Acosta et al., 2013). The three submarine canyons here investigated are, from north to south, Escombreras Canyon, Garrucha-Almanzora Canyon system and Almeria Canyon.

Surface circulation is influenced by the Northern Current flowing southward in the Gulf of Vera (Fig. 1b) and the entry of Atlantic Water into the Alboran Sea (e.g. Vargas-Yáñez et al., 2002; Macias et al., 2016). The latter forms two gyres known as the Western Alboran Gyre (WAG) and the Eastern Alboran Gyre (EAG). The two flows converge at the Almeria-Oran Front (AOF) from where surface waters are redirected towards the Algerian continental margin (Tintore et al., 1988) (Fig. 1b). Intermediate and deep waters flow westwards towards the Strait of Gibraltar (Parrilla et al., 1986; Millot, 1999).

Rivers opening into the study area are dry most of the year due to the semi-arid regional climate. However, short-lived flood events may supply substantial volumes of water, sediment (and also litter) to the coastline. The main rivers in the study area are the Almanzora and Andarax, which discharge in the Gulf of Vera and the Gulf of Almeria, respectively (Fig. 1b). Off-shelf transfer of sedimentary particles is driven by storm events triggering high waves and increasing currents velocities over the continental shelf, subsequently resulting in the resuspension of shelf floor sediments (Lobo et al., 2014). Several such stormy periods during the sampling period in this study have been previously documented (Supplementary Fig. 1; see further details in Tarrés et al., 2022). Several wet NE storms occurred at the beginning of the study period, i.e. in late March and early April 2015. Storms in the following months were of limited intensity and range. The situation changed in autumn months, when several rainfall episodes led to a noticeable increase in the discharge of Almanzora and Andarax rivers, with the main event in early November 2015. Finally, several SW dry storms took place by the end of the year-round study period.

Sediment transfer into the Garrucha-Almanzora Canyon system is favoured by the overall geomorphic configuration of the margin, with a canyon-incised narrow continental shelf, and the closeness of canyon heads to the mouths of Almanzora River but also Antas and Aguas rivers (Fig. 1b) (Puig et al., 2017). Enhanced fluxes recorded during summer months in this canyon system have been attributed to bottom trawling activities in the area (Tarrés et al., 2022).

2.2. Total mass fluxes

Total mass fluxes (TMF) in the three investigated canyons, including the elemental composition and grain sizes of the particles involved, were described in a previous publication (Tarrés et al., 2022 and references therein). A summary is provided here as background information, including topic specific interpretations wherever judged convenient.

A common feature is that in all three canyons mass fluxes were predominantly composed of lithogenic particles, accounting for approximately 61%, 62%, and 72% in Escombrereras, Garrucha-Almanzora, and Almeria canyons, respectively. The carbonate fraction constituted the second-largest in the fluxes, representing about 37%, 34%, and 24% in the above canyons, respectively. The difference in $CaCO_3$ contents between the two canyons in the Gulf of Vera and Almeria Canyon, further south, was partially attributed to inputs of detrital material containing $CaCO_3$. OM was a small fraction, representing only 3–4% of the TMF in those canyons. The clay and silt fractions dominated the fluxes in all three canyons, with small standard deviations < 4%. This suggested a consistent sorting of the material being transported in suspension towards the distal margin.

Regarding flux magnitudes, Escombreras Canyon —measured from March to August 2015— exhibited two distinct situations. At the beginning of the study period, the trap collected comparatively high

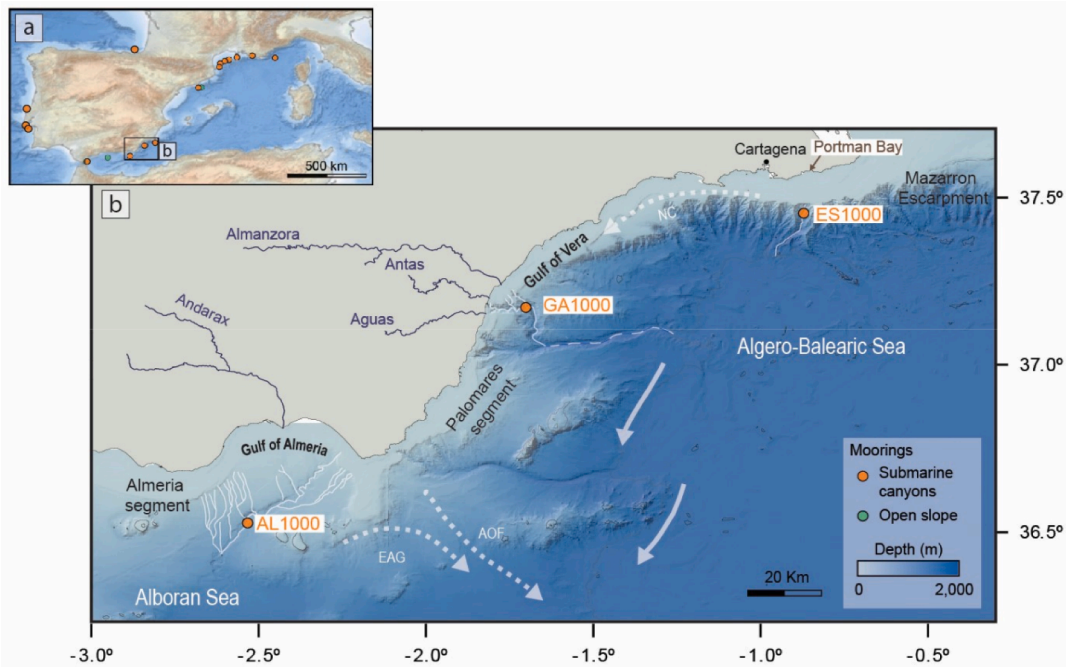

Fig. 1. (a) Map of the Western Mediterranean Sea and nearby areas showing places where trace metal contents and fluxes have been measured according to the literature and also from this study (cf. section 4 and Fig. 6). Map after EMODnet (https://emodnet.ec.europa.eu/geoviewer). (b) Shaded relief bathymetry map off SE Spain displaying the location of the mooring lines within the Escombreras Canyon (ES1000), the Garrucha-Almanzora Canyon system (GA1000) and the Almeria Canyon (AL1000). White lines indicate canyon axes including tributaries if present. Discontinuous white line indicate Alias-Almanzora Canyon axis, when the Garrucha-Almanzora system merges with the southern system. The general surface circulation (discontinuous white arrows) and the intermediate and deep circulation are outlined (continuous white arrows). Main rivers are also shown (blue lines). AOF: Almeria-Oran Front. EAG: Eastern Alboran Gyre. NC: Northern Current. (For interpretation of the references to color in this figure legend, the reader is referred to the web version of this article.)

fluxes during storm events in March and April 2015 (Fig. 2a). Within this time, strong currents led to the resuspension and export of particulate matter from the continental shelf into the neighboring canyons, eased by nepheloid layers. The $CaCO_3$ content increased in March 2015 due to particle resuspension and advection of previously settled biogenic $CaCO_3$ from the shelf. In contrast, minimal fluxes were collected from late April to August, corresponding to calm meteorological and oceanographic conditions.

Mass fluxes in the Garrucha-Almanzora Canyon system —measured from March to September 2015— also peaked during the March and April 2015 storms (Fig. 2a). In this canyon system, bottom trawling activities around the canyon generated a nepheloid layer at depths exceeding 400 m, subsequently promoting increased particle fluxes throughout the spring and summer months (Fig. 2a). The incision of canyon heads into the continental shelf and the short distance of their heads to river mouths facilitated the transfer of terrestrial organic matter (OM, about 5% of the TMF) during the stormy spring period. Conversely, $CaCO_3$ contents displayed higher values during the summer months, correlating with TMFs. Therefore, such higher contents were not due to lesser dilution within the lithogenic fraction. In terms of particle sizes, there was a coarsening effect after May, with relatively high sand contents (up to 4.5%) for the lithogenic particles, especially in May, late August and September 2015.

Particle fluxes in Almeria Canyon —measured from March 2015 to March 2016— remained consistently low throughout the entire period. Similarly to the other two canyons, higher downward fluxes were observed at the beginning of the study period (Fig. 2a), coinciding with spring storm events. Mass fluxes showed a slight increase between November 2015 and January 2016, likely due to short-lived storms and several rainfall episodes that increased water discharge from nearby rivers, especially in early November. By the end of the monitoring period in February-March 2016, dry western storms occurred, which did not enhance downward fluxes at the trap location (Fig. 2a). In terms of composition, $CaCO_3$ contents increased during the spring 2015 and winter 2016 storm events, likely due to lateral transport, as previously explained for the Escombreras Canyon. OM presented a more pronounced seasonal pattern, with a higher contribution (about 7%) to mass fluxes during summer months, which can be explained by overall lower mass fluxes. In late January, OM contents increased again to about 6% due to the arrival of biogenic material from surface primary production. In terms of particle sizes, coarser fractions were collected at the beginning of the study period, with the higher sand content (about 6%) coinciding with the March storm. No coarsening trend in the fluxes was noticed during subsequent storms.

3. Materials and methods

3.1. Sampling

Sea work was performed during research cruises NUREIEV-1 from 13 to 24 of March 2015, NUREIEV-2 from August 29 to September 5, 2015, and NUREIEV-3 from 23 to 30 of April 2016, onboard R/V Ángeles Alvariño.

Three mooring lines —named ES1000, GA1000 and AL1000, respectively— were deployed along the axis of the Escombreras Canyon, the Garrucha-Almanzora Canyon system and the Almeria Canyon at 985, 1,100 and 1,000 m depth, respectively, from March 2015 to March 2016 (Fig. 1b and Supplementary Table 1; cf. section 2.1). Each mooring was equipped with a Technicap PPS3/3 sequential particle trap (aperture 0.125 m^2, cylindroconical shape) with 12 cups at 25 m above the bottom and a sampling interval of 7–16 days. Acid cleaned trap cups were filled with 5% (v/v) formaldehyde solution in 0.45 μm filtered sea water buffered with sodium tetraborate. Within the entire sampling period, only 10 days were devoted to mooring recovery, maintenance and redeployment operations during which there was no sample collection. Failures in the particle trap rotating system of ES1000 and GA1000

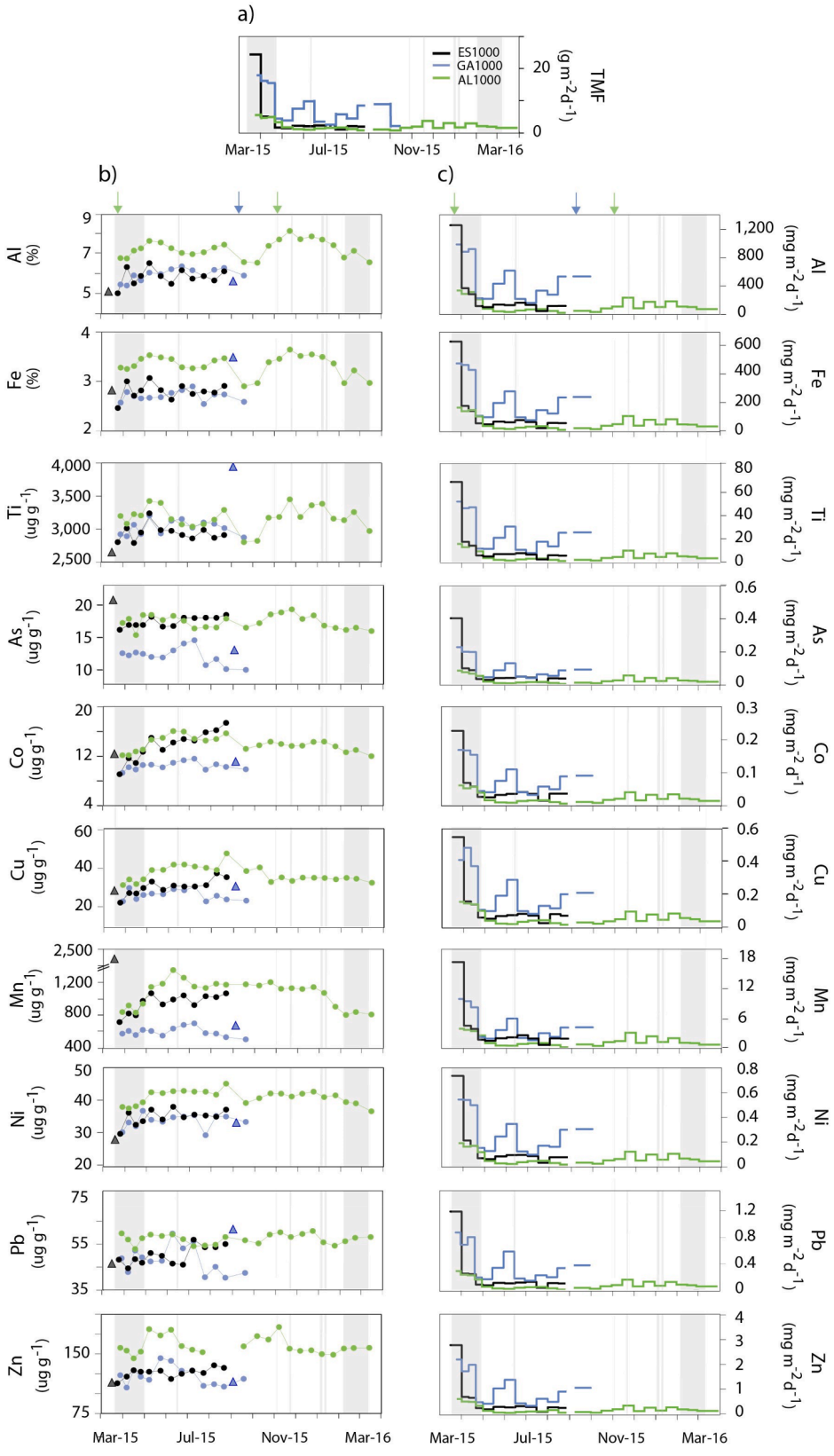

Fig. 2. Time series of (a) Total mass fluxes in settling particles at stations ES1000 (black line), GA1000 (blue line) and AL1000 (green line) after Tarrés et al. (2022). (b) Trace metal contents —in μg g^{-1} excepting Fe and Al, which are in %— in settling particles (dots) and seafloor sediments (triangles) at stations ES1000 (black dots), GA1000 (blue dots) and AL1000 (green dots). (c) Trace metal fluxes in settling particles. Color codes as in (a). Black and blue triangles indicate trace metal and As contents in seafloor sediments from ES1000 and GA1000, respectively. Grey vertical stripes highlight sea storm events, with two main periods at the beginning and at the end of the study period (cf. Supplementary Fig. 1 for further details). The arrows above (b) and (c) plots mark river discharge events (green when close to AL1000 and blue when close to GA1000). Note that vertical scales change from one plot to the other. (For interpretation of the references to color in this figure legend, the reader is referred to the web version of this article.)

stations prevented the collection of samples during the last seven and six months, respectively.

Seabed sediment was collected with a KD Denmark multicorer at 1,002 m depth in the Escombreras Canyon during research cruise NUREIEV-1 in March 2015, and at 1,142 m depth in the Garrucha-Almanzora Canyon system during cruise NUREIEV-2 in September 2015. The sediment cores were subsampled onboard. The cores were sliced every 0.5 cm from the core top down to 5 cm, and every 1 cm from 5 cm to the core bottom. The subsamples thus obtained were stored at 2–4 °C in plastic bags. We used the top 0.5 cm of the cores for our

analyses.

3.2. Sample analysis

The seafloor sediments were freeze-dried and homogenized for later analysis. Trap samples were also freeze-dried after removing the swimmers (i.e., those organisms deemed to have entered alive the traps, Pagès et al., 2007) using a nylon mesh of 1 mm and hand-picking the smallest ones. A high precision peristaltic pump allowed obtaining a working aliquot of each sample, which was then centrifuged with ultrapure water (Milli-Q) to extract the salt and the formaldehyde solution from the trap's cups. Trap sample processing is described in detail in Rumín-Caparrós et al. (2016).

The elemental composition was determined using a Perkin-Elmer Elan-6000 ICP-MS and a Perkin Elmer Optima 8300 ICP-OES at *Centres Científics i Tecnològics de la Universitat de Barcelona* (CCiT-UB). A two-step extraction method was applied for sample digestion. The first step was carried out in a closed digestion system with the goal of avoiding the loss of volatile elements, such as As. The leached elements were then recovered before proceeding with the second step, under open system conditions. The samples were placed in a Teflon reactor closed digestion system with 2.5 mL of HNO_3 (65%) during at least 12 h in a stove at 90 °C. The extract was centrifuged to collect the supernatant and obtain a first solution, thus recovering the leached elements. The solid sample recovered from centrifugation was placed again into a Teflon reactor, and digested with 2.5 mL (65%) HNO_3, 10 mL (40%) HF and 2 mL (70%) $HClO_4$ during at least 12 h in a stove at 90 °C. Then, the Teflon reactor was heated in a sand bath at 250 °C. 2 mL of (65%) HNO_3 and 2 mL of H_2O_2 were added and heated again until total evaporation of the acid volume. When the sample showed incipient dryness, 2 mL $HClO_4$ were added until reaching the total evaporation of the acid. The residue was redissolved in 2 mL HNO_3 and 5 mL of ultrapure water (Milli-Q) to obtain a second solution. Two procedural blanks were analyzed with each sample batch to ensure the lack of contamination during sample processing and analysis. Replicates were routinely performed to determine the uncertainty associated to subsampling heterogeneity and method precision. Relative standard deviation (RSD) was always below 5% for all metals, except for Pb and Ni (~6.5%) and Mn (7.5%). For As, the RSD was 5.4%.

3.3. Data analysis

Particulate fluxes in the investigated canyons have been previously published in Tarrés et al. (2022) for the same period of time here addressed. Those fluxes allow calculating the annual Time Weighted Fluxes (TWF) of TMs, which represent a weighted average of TMFs corrected according to the number of sampling days:

$$TWF\left(mgm^{-2}d^{-1}\right) = \frac{\sum Mi(mg)}{Collectionarea(m^2)^* \sum Di(d)} \quad (1)$$

where M_i is the mass per sample and D_i is the total days of collection.

The annual Time Weighted Content (TWC) is calculated for each element to correct sampling interval values, following equation:

$$TWC\left(\mu g g^{-2}\right) = \frac{TWF(elementmass)}{TWF(totalmass)} \quad (2)$$

The correlations between variables, including major and trace elements, is evaluated by means of the Pearson's Correlation Coefficient (PCC) for each station, considering $p < 0.05$ as significant.

A Principal Component Analysis (PCA) allowed identifying the dominant factors describing the variability of the dataset. PCA variables are the same than for PCC, including OM and $CaCO_3$ main flux components from Tarrés et al. (2022). Lithogenic components were represented by Al, Fe and Ti contents. However, to simplify the dataset, Ti from GA1000 was excluded from the analysis. Biogenic silica was not included given its very minor contribution to the fluxes (Tarrés et al., 2022). AL-I-11 and AL-I-12 samples from AL1000 station were also excluded due to Zn outliers. The dataset was standardized in order to adjust the variance of all variables to the same scale. Data standardization consisted in subtracting the mean of all variables and dividing each one by its standard deviation. It was also conducted on log-transformed contents to improve the normal distribution of the variables (Karageorgis et al., 2009). A Varimax rotation subroutine was performed after the PCA to facilitate the interpretation of the flux components. All statistical analyses have been carried out using the *Statgraphics Centurion* software.

To explore potential statistical differences in TM contents between stations (ES1000, GA1000, and AL1000) and periods within each station (stormy vs. calm periods), we used the Kruskal-Wallis H non-parametric test since normality was not achieved when considering the full dataset. TMs pollution levels are calculated using EFs, which are usually applied to estimate anthropogenic contributions to marine sediments (Birch, 2017). This method requires normalizing metal values to reduce content's variability resulting from natural changes in mineralogy and grain size (Aloupi and Angelidis, 2001; Roussiez et al., 2006). Given the rather diverse particle composition of trap samples, partly due to variations in rock composition inland, a normalization step was applied to compensate for such natural variations. We used Al as the normalizing element as in previous studies (Palanques et al., 2008; Mil-Homens et al., 2013a; Dumas et al., 2014). Pre-industrial background ratios have been estimated from subseafloor sediments in the Almeria and Escombreras canyons, as obtained from ^{210}Pb dating of sediment subsamples at relevant core depths (50–51 cm) from the same location of the Escombreras Canyon sediment trap (unpublished data), which have been extended to the Almeria Canyon (40–41 cm). Whereas in the Garrucha-Almanzora Canyon system this has not been possible since the corresponding multicore reached 15 cm below the seabed only. Therefore, the samples collected in the GA1000 trap were normalized with the subseafloor sediments of the Almeria Canyon given the strong similarity in the mineralogical composition of clay minerals from both canyons. EFs were obtained following equation [3] while also considering a threshold of 1.5 as indicative of anthropogenic contributions according to local pre-industrial values (Roussiez et al., 2006):

$$EF = \frac{TM/Al}{TM_b/Al_b} \quad (3)$$

where TM and Al refer to TM and Al contents in the sample, respectively, and TM_b and Al_b represent the pre-industrial levels.

4. Results

4.1. Trace metal contents in settling particles and fluxes

TM contents in settling particles change from one station to the other (Table 1 and Fig. 2b). The highest contents correspond to AL1000 station for all elements, as illustrated by As and Al with 19.36 μg g^{-1} and 8.19% peak values, respectively. One exception is the Co, which increases at ES1000 station with 17.42 μg g^{-1}. Minimum values for As, Mn, Ni, Pb and Zn occur at station GA1000, while the lowest ones for Al, Fe, Ti, Cu, and Co appear at ES1000 (Table 1).

The highest differences between minimum and maximum TM values occur at AL1000 station, with a remarkable difference for the Mn (from 791.07 to 1,347.46 μg g^{-1}) and the Ti (from 2,790.89 to 3,454.70 μg g^{-1}) relative to the other two stations. However, Co displays the highest variability at ES1000 (from 9.09 to 17.42 μg g^{-1}), while Pb and As do it at GA1000 (from 40.27 to 59.49 μg g^{-1} and from 9.97 to 14.53 μg g^{-1}, respectively) (Table 1). Fig. 2b shows how TM contents changed during one year (AL1000 station) or half a year (ES1000 and GA1000). In AL1000, some elements reach their highest contents in spring-summer (e.g. Co, Cu, Mn), while others do in late spring-summer and autumn (e.g. Al, Fe, Ti, As, Ni, and Zn). Pb values are rather steady and do not

Table 1
Trace metal contents and fluxes in settling particles and seafloor sediments (SS). AL1000 values correspond to a complete annual cycle, whereas GA1000 and ES1000 values correspond to a half-year period. *: Average metal contents in time-weighted content (TWC). **: Average metal fluxes in time-weighted flux (TWF).

Code		**ES1000**			**GA1000**			**AL1000**			**SS ES1000**	**SS GA1000**
Depth (m)		985			1,100			1,000			1,002	1,142
Number of samples		12			13			24				
Content	% or μg g^{-1}	Average*	Max	Min	Average*	Max	Min	Average*	Max	Min		
Al	%	5.54	6.60	5.10	5.97	6.42	5.47	7.31	8.19	6.60	5.13	5.66
Fe	%	2.72	3.14	2.54	2.77	2.98	2.62	3.40	3.72	2.98	2.82	3.49
Ti	μg g^{-1}	2,866.65	3,185.58	2,783.64	2,991.74	3,161.40	2,858.56	3,183.20	3,454.70	2,790.89	2,649.18	3,944.93
As		16.79	18.47	16.18	11.83	14.53	9.97	17.36	19.36	15.40	20.79	13.09
Co		11.41	17.42	9.09	10.21	11.58	9.28	13.55	16.10	12.04	12.36	11.10
Cu		26.24	37.38	22.11	25.65	30.30	22.68	35.34	47.80	31.36	25.00	27.54
Mn		816.99	1,057.47	702.08	563.31	686.94	489.12	1,005.10	1,347.46	791.07	2,359.08	664.77
Ni		32.32	37.87	29.55	33.04	36.56	29.06	40.26	45.07	36.56	28.26	33.37
Pb		48.90	56.95	44.48	47.45	59.49	40.27	57.31	60.85	53.02	46.56	61.26
Zn		119.97	135.70	113.12	122.31	144.47	107.20	158.08	184.06	144.90	114.12	115.46
Flux**	mg m^{-2} d^{-1}	Average**	Max	Min	Average**	Max	Min	Average**	Max	Min		
Al		266.11	1,272.47	58.00	463.65	1,000.66	173.59	119.83	349.83	33.52	–	–
Fe		130.66	633.22	27.94	214.67	479.88	82.94	55.81	171.43	15.79	–	–
Ti		13.76	69.76	2.90	23.22	52.90	8.38	5.22	16.36	1.47	–	–
As		0.08	0.40	0.02	0.09	0.23	0.04	0.03	0.09	0.01	–	–
Co		0.05	0.23	0.02	0.08	0.17	0.03	0.02	0.06	0.01	–	–
Cu		0.13	0.55	0.03	0.20	0.49	0.08	0.06	0.16	0.02	–	–
Mn		3.92	17.52	0.99	4.37	10.17	1.91	1.65	4.23	0.52	–	–
Ni		0.16	0.74	0.03	0.26	0.54	0.10	0.07	0.19	0.02	–	–
Pb		0.23	1.20	0.05	0.37	0.88	0.16	0.09	0.31	0.03	–	–
Zn		0.58	2.82	0.12	0.95	2.23	0.36	0.27	0.81	0.11	–	–

increase at any specific season. The half year records from ES1000 show an increasing trend from March to August 2015 for Co, Cu, Mn and Zn, while Pb is higher during July and August. In the GA1000 station only Al raises throughout most of the period, while other elements diminish during the last months, as shown by As, Co, Cu, Mn, Pb and Zn. In fact, As, Co, Cu and Mn reach their higher concentrations in June. In contrast, Pb and Zn peak during late spring months. Fe correlates well with Mn ($r^2 = 0.85$; $p < 0.01$) at GA1000, whereas Fe and Ti correlate with Al at ES1000 and AL1000 ($r^2 > 0.78$; $p < 0.01$) (Supplementary Table 2).

Our time series shows several TM export events during the investigated period (Fig. 2c). A first and most noticeable flux increment, at the beginning of the sampling period, resulted in the highest measured export rates for all elements under consideration, with minimum values for Co up to 0.23, 0.17 and 0.06 mg m^{-2} d^{-1} and maximum values of 1,272.47, 1,000.66 and 349.83 mg m^{-2} d^{-1} for Al at stations ES1000, GA1000 and AL1000, respectively (Table 1 and Fig. 2c). Minor but consistent increments of all elements were recorded at GA1000 in late May, early June, late August and September 2015 (Fig. 2c), which coincided with high turbidity values from 400 m depth down to the bottom at 1,100 m (Tarrés et al., 2022). The early June 2015 peak was noticeable for its comparatively high Cu, Mn, Ni, Pb and Zn export fluxes, whereas As and Co showed values closer to the ones found during the ensuing summer events (Fig. 2c). Time series for the following months are available for AL1000 station only. A slight flux increment with maxima ranging between 0.04 and 248.52 mg m^2 d^{-1} for Co and Al, respectively, were observed between November 2015 and January 2016. TM fluxes lowered during February and March 2016 (Fig. 2c).

4.2. Trace metal contents in seafloor sediments

With few exceptions, TM contents in seafloor sediments are close or very close to the ones in settling particles (Fig. 2b). The highest contents of Ti, As, Mn and Pb (20.79, 3,944.93, 2,359.08 and 61.26 μg g^{-1}, respectively) found in this study correspond to sediments (Table 1 and Fig. 2b). At ES1000, As and Mn contents in sediments were 19% (20.79 vs. 16.79 μg g^{-1}) and 65% (2,359.08 vs. 816.99 μg g^{-1}) higher, respectively, than average contents in sinking particles (Tables 1 and 2). Sediments collected below GA1000 station show higher Fe (20.7% more), Ti (24.2% more), Mn (15.3% more) and Pb (22.5% more) contents than average contents in settling particles (Tables 1 and 2). These increments persist after normalizing TMs/Al. Furthermore, the Al-normalized values show moderate increases (<15%) for Co in ES1000, and for As, Co and Cu in GA1000 (Table 2).

4.3. Outcomes of the multivariate analysis

In the ES1000 station, four components explain 93% of the total variance of the dataset (Fig. 3a). Component 1 (53% of the total variance) is characterized by capture majority of individual variance for Co, Cu, Mn (57–77%) and to lesser extent, As, (43%). Component 2 (27% of the total variance) explains most of the variability of lithic elements (Al, Fe, Ti) (51–71%) and also of $CaCO_3$, which displays negative loading. Component 3 (8% of the total variance) is contributed by several TMs (As, Co, Cu, Pb and Zn), and explains most of the variance of Pb (56%) and Zn (85%) and, to lesser extent As (43%). Component 4 (5% of the total variance) describes most of OM variance (70%) and part of Zn variance (22%).

In the GA1000 station, four components explain 90% of the total variance of the dataset (Fig. 3b). Component 1 (49% of the total variance) describes>80% of Cu and Mn variance, and>50% of Fe, As and Co

Table 2
Trace metals and As excess (%) in canyon floor sediments with respect to time weighted contents calculated after settling particles data (both non-normalized and normalized to Al).

	Escombreras Canyon		Garrucha-Almanzora Canyon system	
		TMs/Al		TMs/Al
	%	%	%	%
Fe_{xs}	3.7	–	**20.7**	–
Ti_{xs}	−8.2	–	**24.2**	–
As_{xs}	**19.2**	**25.3**	9.6	**14.3**
Co_{xs}	−7.6	**14.6**	8.1	**12.9**
Cu_{xs}	−5.0	2.9	6.9	**11.8**
Mn_{xs}	**65.4**	–	**15.3**	–
Ni_{xs}	**−14.3**	−5.7	1.0	6.2

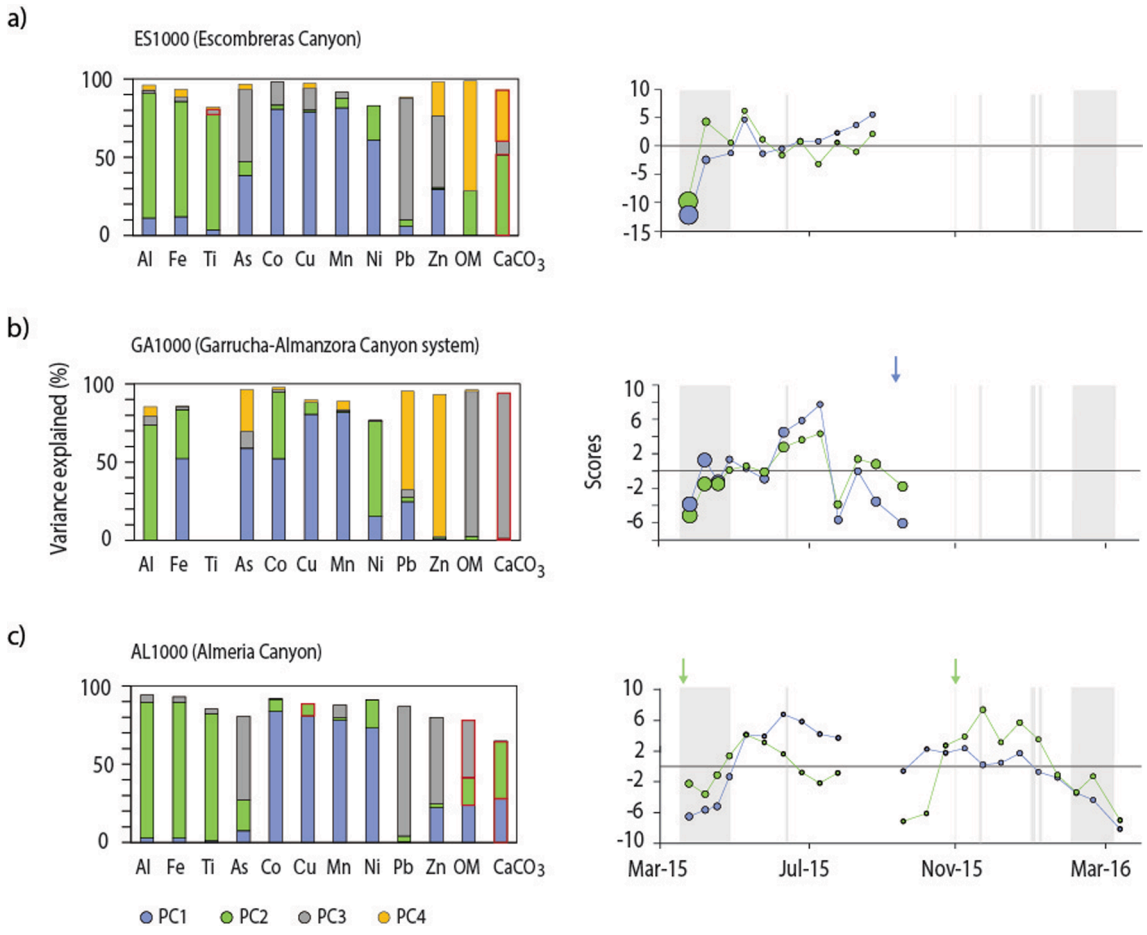

Fig. 3. Principal Component Analysis (PCA) of settling particles at (a) ES1000 (N = 11), (b) GA1000 (N = 13) and (c) AL1000 (N = 22) mooring stations. Note that some samples have been excluded from analysis due to it including outliers in the dataset. The plots explain de variance (%) for trace metals, organic matter (OM) and $CaCO_3$ after the main components (negative loads are highlighted in red in the corresponding bars of the left side plots), and the temporal variability of the scores for the two principals components (right side plots). Dot size is proportional to mass flux. (For interpretation of the references to color in this figure legend, the reader is referred to the web version of this article.)

variance. Component 2 (21% of the total variance) describes Al variance (>70%), Fe (31%), Co (42%) and Ni (61%). Component 3 (12% of the total variance) is contributed (>90%) by OM and $CaCO_3$ (negative loadings). Component 4 (8% of the total variance) explains most of Zn variance (91%) and, to a lesser extent, Pb (63%) and As (26%).

In the AL1000 station, three components explain 85% of the total variance of the dataset (Fig. 3c). Component 1 (46% of the total variance) reflects most of Co, Cu, Mn and Ni variance (>75%) and to a lesser extent Zn (29%) and OM (24%), with negative loading of $CaCO_3$ (28% of variance). Component 2 (25% of the total variance) greatly explains the variance of Al, Fe, Ti (>80%). As and Ni are also associated to the elements that represent lithogenic minerals, explaining about 20% of their individual variability). This component also captured part of $CaCO_3$ variance (35%), contributing with a negative loading. Component 3 (14%) relates most of Pb (83%) and As and Zn (~55%) variance.

5. Discussion

5.1. Intraannual variability of trace metal fluxes

TM export rates in the investigated submarine canyons are comparable to those found in former studies of submarine canyons and open slopes of the Western Mediterranean Basin (Puig et al., 1999; El Khatab, 2006; Heimbürger et al., 2012; Cossa et al., 2014). During the monitored period, the main TM export event into the studied canyons occurred in early spring 2015, concurrently with eastern storms with significant wave heights (Hs) above 4 m (cf. section 2, Fig. 2 and Supplementary Fig. 1). During the following calm months, our traps recorded several TMs pulses in the Garrucha-Almanzora Canyon system (Fig. 2c), which we attribute to bottom trawling activities on the canyon flanks, as there is no other plausible explanation. A number of studies has shown trawling activities to cause seafloor erosion and sediment resuspension (Martín et al., 2007; Puig et al., 2012; Martín et al., 2014), subsequently modifying the behavior and the biogeochemistry of OM, TMs and other pollutants in the marine environment (Bradshaw et al., 2012; Pusceddu et al., 2014; Paradis et al., 2021; Palanques et al., 2022). After October 2015, only the AL1000 station in the Almeria Canyon remained operational. Slightly higher export fluxes were recorded there between November 2015 and January 2016 after short-lived storms and rainfall episodes, mainly in early November. In short, storms and bottom trawling appear as the main triggers of TM transport events into the investigated submarine canyons.

5.2. Intraannual variability of trace metal contents in settling particles

Settling particles are vectors for TM export, which are known to be associated with lithogenic, biogenic and authigenic carriers (Huang and Conte, 2009; Conte et al., 2019; Blain et al., 2022). Specific TMs have been used as proxies of particle types, such as Fe, Al and Ti for the lithogenic fraction (Ohnemus and Lam, 2015; Lee et al., 2018), or Fe and Mn for the authigenic fraction (Martín et al., 1983; Cowen and Bruland, 1985; Bruland and Lohan, 2003; Tebo et al., 2004). The poor correlation

between Al and Mn in all our stations (from north to south, $r = 0.57$ at ES1000, 0.22 at GA1000, and 0.35 at AL1000) supports this view (Supplementary Table 2). Fe strongly correlates with Al in the Escombreras and Almeria canyons, with $r > 0.91$ and $p < 0.01$ (Supplementary Table 2), thus pointing to a lithogenic source and/or shared distributions. On the contrary, in the Garrucha-Almanzora Canyon system there is a poor correlation ($r = 0.48$) between Fe and Al, but a better Fe correlation with Mn, with $r = 0.67$ and $p < 0.05$ (Supplementary Table 2). Therefore, Fe contents in the Garrucha-Almanzora Canyon system likely respond to the presence of particle sources other than just lithogenic.

In the next subsections, we use the PCA results to assess TMs variability on a canyon by canyon basis.

5.2.1. Escombreras Canyon

The first component in the Escombreras Canyon would reflect an authigenic component, which explains most of the variance of Co, Cu, Mn, Ni and, to a lesser extent, As and Zn, during the six-monthly monitoring period (Fig. 3a and Supplementary Table 2). The scavenging behavior of these metals onto Mn (oxy)hydroxides (Huang and Conte, 2009) and/or the oxidation of dissolved species leading to the precipitation of oxides (e.g. Co oxides) that behave similarly to Mn oxides (Dulaquais et al., 2017) could explain the above association. Authigenic component scores displayed a clear trend with the minima in March and April, concomitantly with the storm events, with maximum values in summer months. This suggests that variability arises partly from changes in particle sources between the two periods, likely as a result of resuspension over the shelf and subsequent downward transport in the first period, and of disconnection from the shelf and dominating pelagic sedimentation during the second period.

The second component is clearly lithogenic as it describes most of the temporal variance of Al, Fe, Ti and, to a lesser extent, Ni and OM, with modulation by $CaCO_3$ inputs accounting for a negative loading. However, most of the temporal variance of Pb is largely captured within a third component, which is also contributed by other TMs such as As, Co, Cu and Zn, which may derive from anthropogenic sources. This third component displays negative scores in March and April 2015 and positive scores during summer months.

5.2.2. Garrucha-Almanzora Canyon system

We interpret the first component to reflect authigenic Mn and Fe bearing phases, such as oxides and oxidized particle coatings. The PCA results (Fig. 3b) and the close correlation of particulate As, Co, Cu and Pb with Mn (from $r = 0.68$, $p < 0.05$ for Pb to $r = 0.88$, $p < 0.01$ for As), and of Co and Cu with Fe ($r > 0.83$, $p < 0.01$) (Supplementary Table 2) indicate a joint transport into the canyon. This component depicts strong scores after May, and positive scores during June and early July, when anthropogenic disturbances can be a major driver of TMs transfer into the canyon axis (cf. section 5.1). Seafloor disturbance is able to release metals from bottom sediments to the water column (Eggleton and Thomas, 2004; Kalnejais et al., 2007; Bancon-Montigny et al., 2019), which then could be re-absorbed onto floating particles following resuspension events (Rusiecka et al., 2018; Al-Hashem et al., 2022).

The negative relationship between TMF and the contents of the above-mentioned TMs (Supplementary Fig. 2) suggests that dilution processes could have played a role in the observed temporal fluctuations. Yet, little is known about the role of bottom trawling in the TMs fate and redistribution (Palanques et al., 2022). Any geographical shift of resuspension area, and/or a change in particle loads and their properties (grain size, composition) or in oxygen content of the bottom water hold the potential to impact metal contents in resuspended particles forming nepheloid layers (Lohan and Bruland, 2008; Palanques et al., 2022) and, therefore, in the sinking fluxes.

The second component describes the lithogenic fraction, explaining most of Al, Ni and, to a lesser extent, Co and Fe variance (31% of individual variance) (Fig. 3b). Zn and Pb mostly bivariate together, thus contributing to a fourth component.

5.2.3. Almeria Canyon

The first component primarily reflects the influence of biogenic (OM) and authigenic Mn (oxy)hydroxides, and explains a significant portion of the variance of Co, Cu, Mn, Ni and, to a smaller extent, Zn and OM. Scores associated with this component noticeably increased after April 2015, reaching their maximum during summer months, from where they remained slightly positive until late autumn (Fig. 3c). During summer period, the above contributions were not masked by components that otherwise dominate mass fluxes in resuspended material, thus resembling Escombreras Canyon.

The second component is indicative of the lithogenic fraction, and accounts for most of Al, Fe and Ti variance and, to a lower extent, As and Ni. Interestingly, the autumn months displayed stronger positive scores and high Al and Fe contents (Fig. 2b), which could relate to the likely arrival to the site of terrestrial material after a November flood of the Andarax River. The enhancement of lithogenic inputs following fluvial discharges in the Alboran Sea has been previously reported (Fabres et al., 2002; Sanchez-Vidal et al., 2004). TM contents were modulated by $CaCO_3$ biogenic inputs (Fig. 3c). As mentioned in section 4.1, $CaCO_3$ inputs into this canyon seem to correspond mostly to pelagic settling from the overlaying water column, with a diminution of the relative abundance of lithogenics during late summer. However, $CaCO_3$ contents were also enhanced by resuspended and laterally advected material during the storm events, at the beginning and the end of the study period (Fig. 2b). The two principal components did not account for much of Pb and Zn interannual variability, as observed for the other two canyons (Fig. 3c).

5.2.4. Common features amongst canyons

Our results indicate the three investigated canyons share a number of features. Authigenic Mn (oxy)hydroxides played a key role in most of As, Co, Cu, Mn and Ni interannual variance (Fig. 3). Particulate Mn contents relate to its predisposition for oxidative precipitation. River discharges, shelf sediment resuspension and diffusion from the seafloor are likely sources of dissolved Mn and Fe into the water column (Marin and Giresse, 2001; Noble et al., 2012; Dulaquais et al., 2017), which can subsequently precipitate onto suspended particles while co-scavenging other dissolved TMs. This would be especially the case of dissolved Mn, which slow kinetic rates of oxidation (Jensen et al., 2020) and easiness to form complexes with organic ligands (Oldham et al., 2017) promote Mn transport to deeper environments (Jensen et al., 2020), such as the Escombreras and Almeria canyons. The width of the continental shelf, together with bottom oxygen concentrations and acting physical processes, can influence the seaward transport of dissolved Mn (Noble et al., 2012). As for the Garrucha-Almanzora Canyon system, our results suggest that Fe oxides also contributed to the authigenic fraction, implying additional processes, such as benthic resuspension as a likely prevalent source of redox sensitive TMs.

The lithogenic contribution to TMs interannual variance was especially relevant for Al, Fe (though less in GA1000 station) and Ti. Nevertheless, it did not account for the variance of most of the other TMs (Fig. 3). This could be viewed as surprising as this fraction dominated mass fluxes in all three canyons. Certainly, it was the responsible of most of the temporal variance of Ni and Co in GA1000 (61 and 42% of the total variance, respectively), as observed after PC2 scores (Fig. 3b). In contrast, the poor association of TMs with OM (PC3) (Fig. 3a) suggests a minor biogenic contribution to TMs export. The near-bottom placement of our sediment traps could have hampered observing potential associations of TMs' export with biological carriers, as the redistribution and dissolution of metals in sinking particles weaken such relationships with depth (Huang and Conte, 2009; Blain et al., 2022). It should be, however, noticed that the statistical analysis in our study tends to highlight the phase to which each TM is mainly associated to, and also that to a greater or lesser extent, most TMs are coupled with multiple types of particles (Huang and Conte, 2009; Conte et al., 2019). Finally, it's worth noting that Pb and Zn's intraannual variation in all three canyons was

captured by other components, which likely reflect anthropogenic contributions, possibly from several introductory pathways, including atmospheric deposition, thus further increasing the poor correlation of these metals with the main fractions and the other TMs.

Fig. 4 shows a generalized impoverishment of TM contents and metals representing the authigenic and lithogenic fractions (excluding Ti) at the occasion of the spring 2015 and winter 2016 storms in the Escombreras and Almeria canyons. Settling particles from the Garrucha-Almanzora Canyon system exhibited much less marked differences, in terms of TMs contents, between periods with and without storms compared to the other two canyons (Fig. 4). The larger compositional shifts between calm and stormy conditions for Zn, Ni, Mn, Fe and Al occur in Almeria Canyon, with e.g. mean values from 1162.4 ± 64.9 down to 848.9 ± 53.5 μg g^{-1} for Mn. For Co and Cu the larger differences correspond to Escombreras Canyon. For As the step between the two periods —calm vs. stormy— is almost equal in Escombreras and Almeria canyons (Fig. 4).

The above suggest that storm events led to the export of resuspended material from the adjacent shelves, which only reached the deep canyon environment during such energetic processes. Both the authigenic Mn oxides and the detrital fractions appeared to be diluted in those laterally advected sediments. Dilution was evident not only in the authigenic fraction but also in the detrital fraction, which dominates the resuspended material on continental margins. An explanation could be that the resuspended material was primarily enriched in $CaCO_3$, as illustrated in Fig. 2c and 3a, c. This view is in agreement with observations in the northwestern Mediterranean margin during high energy events (Cossa et al., 2014). However, in the investigated canyons we did not observe a correlation between grain size and TMs, which would be largely due to the small variation in the fluxes grain size throughout the monitoring period. While storms may have generated bottom shear stress capable of remobilizing coarse sediments on the shelves, the prevailing currents were likely not sufficient to carry a coarser suspended load till reaching the locations of the mooring stations.

5.3. Trace metals distributions in the submarine canyons

We observe regional variations in spatial TMs distributions. The Almeria Canyon commonly displays higher TM contents (Fig. 2b) than the Escombreras Canyon and the Garrucha-Almanzora Canyon system to the north. Variance analysis indicates that they are significantly different at a $p < 0.05$ level, except for As and Co from the Escombreras and Almeria stations (see statistical parameters in Table 1). The lower contents of detrital $CaCO_3$ in the particles of the margin segment to the south —where Almeria Canyon is located— compared to the northern margin segments (Tarrés et al., 2022) can explain the differences in Al, Fe, Ti and other TM contents. This observation fits with the fact that minerals from terrestrial sources are a relevant constituent of particle standing stocks and bottom sediments in continental marginal settings. This would ultimately relate to inland geology, which determines the composition of the sedimentary particles feeding the continental margin as a result of weathering processes and sediment transport by surface run-off and fluvial discharge.

When normalized to Al, the differences in TM concentrations between sampling stations in the northern and the southern margin segments diminish. This allows grouping the investigated canyons in two clusters: (i) Almeria and Escombreras canyons have high normalized ratios of As, Cu, Co and Mn in settling particles, and (ii) the Garrucha-Almanzora Canyon system has lower normalized ratios of the previous elements in settling particles. This results from distinct TMs cycling and

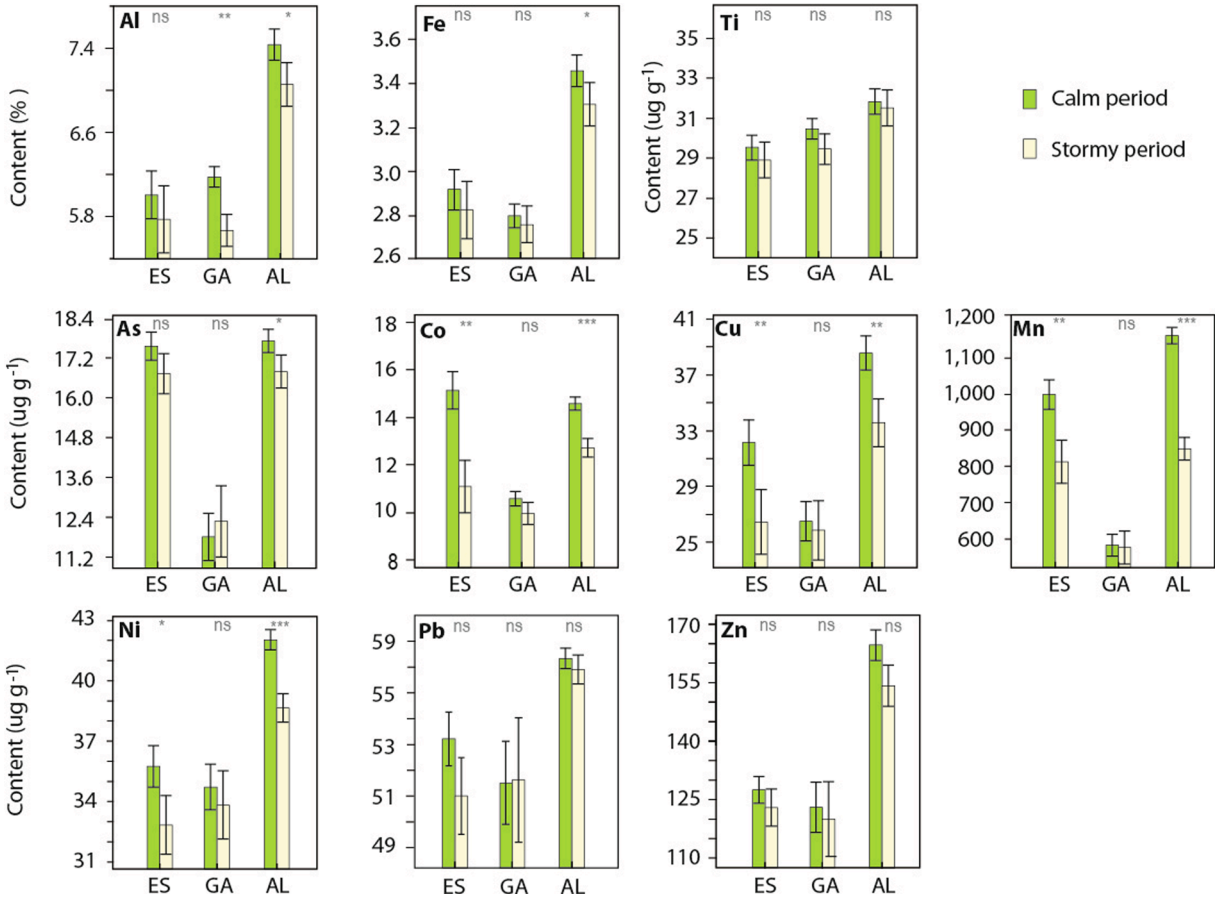

Fig. 4. Metal contents in settling particles during calm and stormy periods from March 2015 to March 2016 in Escombreras Canyon (ES), Garrucha-Almanzora Canyon system (GA) and Almeria Canyon (AL). Significance of the variance (p-values): *$p < 0.05$, ** $p < 0.01$, ***$p < 0.001$. ns: non-significant.

fate in the Garrucha-Almanzora Canyon system respect the other canyons (cf. section 5.2).

5.4. Modification of trace metal contents in canyon floors

So far we have discussed the distributions of TMs in the settling particles. Whereas the ultimate fate for sinking particle fluxes is the seafloor, the bulk composition of bottom sediments often differs from the one of settling particles in the water column, a situation that has been attributed to post-depositional processes, changes of particle sources, and alteration of the primary fluxes in the water column (Tesi et al., 2010; Raiswell, 2011; Heimbürger et al., 2012; Thibault de Chanvalon et al., 2016). We address this issue by comparing the TWC obtained for the study period with the canyon floor sediments of Escombreras Canyon and Garrucha-Almanzora Canyon system. We are obviously aware that even a single centimetre of bottom sediments can encompass years of deposition.

We calculated the TM in excess of seafloor sediments after the TWC of settling particles, both normalized and non-normalized to Al as a proxy for grain size (Table 2). The peak value for seafloor excess of Mn (65.4 %) appears at ES1000, while the one for Fe (20.7 %) occurs at GA1000. Such excess Mn and Fe could be associated to early diagenetic processes involving the reduction of Fe-Mn oxides in sub-oxic horizons and the diffusion of the dissolved Fe and Mn towards the sediment–water interface followed by re-precipitation in the redox boundary (Calvert and Price, 1972; Froelich et al., 1979; Marin and Giresse, 2001). After such a cycling in the sediment, resuspension and transport processes could transfer these phases by advection over the seabed (Sanchez-Vidal et al., 2005; Lee et al., 2018), as described in section 3.2. The excess Ti (24.2%) in surficial sediments of the Garrucha-Almanzora Canyon system compared to Escombreras Canyon (-8.2%) could indicate differential resuspension processes and near-bottom transport from one canyon to the other. It is well known that Ti preferentially concentrates in the coarser fractions of the sediment together with other heavy minerals such as titanomagnetite, ilmenite, augite and rutile (Boyle, 1983). It is plausible that the excess Fe in the Garrucha-Almanzora Canyon system also results from near-bottom processes, as it occurs for some heavy minerals (Dill, 2007).

After normalizing TM concentrations to grain size, the rather similar values (less than ± 10% of excess) for most of them (Table 2) suggest that metal excesses in the sediment could be partially explained by differences in grain size. Excesses higher than 25% for As in the Escombreras Canyon floor, and for Pb in the Garrucha-Almanzora Canyon system floor (Table 2) could be explained by diagenetic remobilization related to the excess of redox-sensitive Mn. This process would provide a plausible explanation for the distribution of As in Escombreras Canyon (Chaillou et al., 2003), with sulfate reducing bacteria possibly playing a role according to recent findings by Baza-Varas et al. (2023). Elevated Pb contents in the Garrucha-Almanzora Canyon system can result from in-situ suboxic diagenetic remobilization too (El Houssainy et al., 2020) and/or from reabsorption onto benthic resuspended particles (Rusiecka et al., 2018) and posterior deposition. Additionally, As, Co, Cu and Mn show moderate increases in bottom sediments. The PCA indicates that the distribution of Cu, Co, As, and Pb in the sediment is linked to the presence of Fe and Mn oxides (Fig. 3b). The Garrucha-Almanzora Canyon system apparently being a dynamic setting, with bottom resuspension and lateral advection, is consistent with the observed Ti enrichment of seafloor sediments. Thus, resuspension and near-bottom transport are probably able to modify the geochemical composition of the canyon' floor.

5.5. The anthropogenic imprint on trace metal contents in deep submarine canyons

The distribution and cycling of TMs in the sediments of the study area and similar settings are likely modified by anthropogenic activities. Increments in TM contents in continental slope environments, including submarine canyons, due to anthropogenic activities have been previously reported (e.g., Palanques et al., 2008; Richter et al., 2009; Jesus et al., 2010; Costa et al., 2011; Mil-Homens et al., 2013b; Cossa et al., 2014; Roussiez et al., 2012; Heimbürger et al., 2012; Azaroff et al., 2020). The EFs approach uses pre-industrial sediments encompassing several years of deposition as normalizers. The estimation of EFs for each individual trap sample could incorporate a bias due to the different time periods represented by the normalizing sediments. This relates to the fact that, after correction for the terrigenous fraction, enrichments could result from several processes that enhance TM concentrations beyond anthropogenic inputs, such as biological uptake or authigenic precipitation (Yiğiterhan et al., 2011). In practice, we have considered TWC > 1.5 as an indicator of anthropogenic inputs, as this value represents the natural variability threshold following Roussiez et al. (2006), Radakovitch et al. (2008), and Jesus et al. (2010). The normalization of metal contents to pre-industrial values reveals a moderate enrichment of Zn and Cu, with mean values of up to 1.7 for Zn in Escombreras Canyon, and 1.5 and 1.6 for Cu in Garrucha-Almanzora Canyon system and Almeria Canyon, respectively (Fig. 5). The range of values from 0.75 to 1.5 is normally considered within natural variability (Radakovitch et al., 2008). However, one can note that Pb and Cu almost exceed the natural threshold in Escombreras Canyon, and Zn does the same in the other two canyons. The values obtained for canyon floor sediments tend to be in the interquartile range of the box plot, indicating that the trapped material provides a good record of TM pollutants being buried there. One exception are the metals affected by diagenetic and/or other near-bottom processes as discussed in section 5.3, which include As and Pb in the ES1000 and GA1000 stations, respectively.

The provinces of Murcia and Almeria experienced a noticeable industrial development during the second half of the 20th century. The region has an intensive farming model, with one of the largest areas in Europe dedicated to greenhouse agriculture along the coastline of the southern margin segment here investigated. Beyond rich agricultural expanses not far from shore, the northern margin segment hosts an important petrochemical industrial complex of Escombreras, which is besides the coastal town of Cartagena and<6 km west of Portman Bay. The complex started its activities in 1950 and since then has experienced several enlargements. Further environmental stressors arise from sewage pipes along the coastline discharging into the sea wastes from industrial activities, ancient ponds and dumping sites filled with industrial and mining wastes, and the traffic of tankers and cargo vessels. Portman Bay actually constitutes one of the main environmental disasters along the European coastline. This bay was used during>30 years as the dumping site for huge amounts of Pb, Zn, Cu, As and other metals rich mine tailings from the open pit exploitation of sulphide ores (Fig. 1) (Baza-Varas et al., 2022, and references therein). Although waste disposal ended in 1990, the mine tailings disposed in the coastal sea remains nowadays. Previous studies have shown high levels of TMs pollution across the modern inner shelf floor off Portman Bay (Alorda-Kleinglass et al., 2019; Cerdà-Domènech et al., 2020), altogether with a diminishing sedimentation rate farther offshore in the tailings deposit itself (Baza-Varas et al., 2022).

Cu contents exceed or are near the pre-industrial threshold in all canyons, which points to a widespread contamination (Fig. 5). In other areas, Cu contamination has been mostly related to spillages attributed to the use of fungicides or fertilizers in agriculture (Roussiez et al., 2012; Cossa et al., 2014) or waste water treatment plants (Casadevall et al., 2016). Zn reaches contamination levels only in the Escombreras Canyon (Fig. 5), which is the closest to the Escombreras petrochemical complex and to Portmán Bay of the three studied canyons. The offshore extension of Portman Bay mine tailings deposit (see Baza-Varas et al., 2023), at about 13 km in straight line from ES1000 (Fig. 1), seems a good candidate for Zn and other TMs (Cu and Pb) sourcing to the adjacent continental slope and canyons. Zn enrichment would decrease progressively with increasing distance from Portman's dumping site by

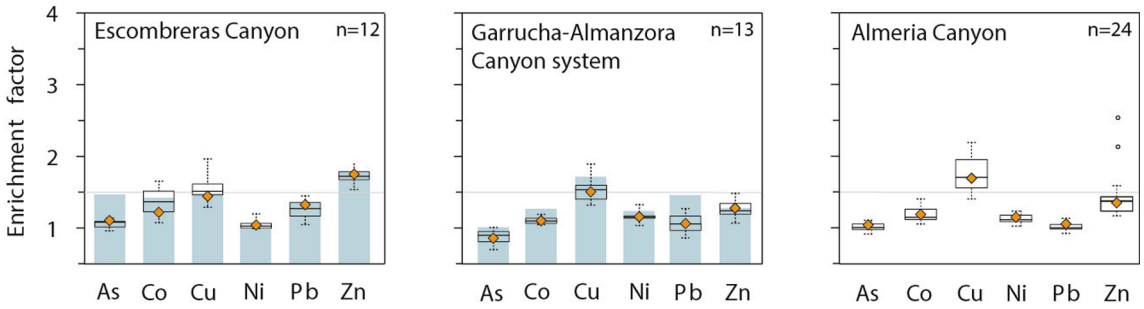

Fig. 5. Trace metals enrichment factors (EFs) in setting particles in the investigated submarine canyons. The dashed horizontal line represents the natural variability threshold after Roussiez et al. (2006). White dots represent the outliers (in the present case abnormal high values relative to the co-existing data). The orange diamonds illustrate the EFs for TWC whereas the blue grey columns represent EFs in canyon floor sediments. Note that no bottom sediments were available for Almeria Canyon (cf. section 2.1). (For interpretation of the references to color in this figure legend, the reader is referred to the web version of this article.)

mixing with non-enriched particles and dilution. However, we cannot discard other potential sources such as hydrocarbon burning at Escombreras complex or the onshore contaminated sites that could release pollutants able to reach the outer continental margin via atmospheric inputs. In the case of Zn for the rest of canyons, the results of the PCA show that its temporal variation is independent of the rest of the elements, possibly stemming from anthropogenic factors. However, it is associated with Pb, which does not exhibit high EF (Fig. 3c).

The anthropogenic imprint on submarine canyons in the Iberian Atlantic margin and the SW and NW Mediterranean Sea, in terms of TM enrichment, is illustrated in Fig. 6a. Source type, distance from source and transport pathways and their carrying capacity determine which TM pollutants and amounts may reach the deep continental margin. For instance, the Planier Canyon shows a specific signature due to local inputs from a bauxite treatment plant on the shore (Roussiez et al., 2012). Furthermore, hydrodynamics and sedimentary dynamics in each specific continental margin segment also influence the transference of the TM pollutants, as illustrated by higher Pb values in Atlantic canyon

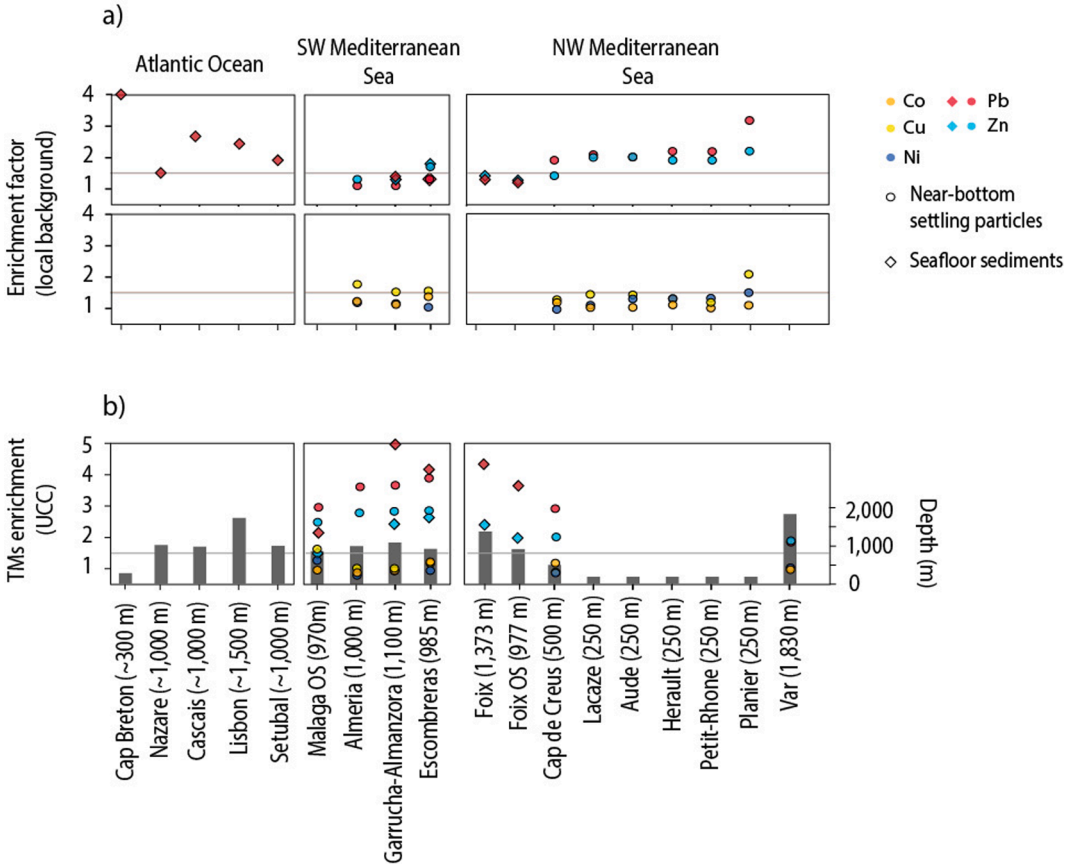

Fig. 6. Compilation of trace metals (TMs) mean enrichments from submarine canyons and nearby open slopes from Iberian Atlantic and NW Mediterranean continental margins altogether with those from the SW Mediterranean margin, where the investigated canyons lie. (a) Enrichment factors (EFs) calculated with respect to local background pre-industrial values, and (b) enrichment values with respect the Upper Continental Crust (UCC) global average composition according to Rudnick and Gao (2003). The general location of the canyons in the plot is shown in Fig. 1a. OS: open slope. Malaga OS corresponds to ALB1 station in the Alboran Sea, for which data have not been published previously (see detailed location in Sanchez-Vidal et al., 2005). Water depths in meters are given in brackets for each sampling station. Data are from Azaroff et al. (2020) for Cap Breton Canyon; Jesus et al. (2010) for Nazare, Cascais, Lisbon and Setubal canyons; Palanques et al. (2008) for the Foix Canyon and OS; Cossa et al. (2014) for Cap de Creus Canyon; Roussiez et al. (2012) for Lacaze, Aude, Herault, Petit-Rhone and Planier canyons; and Heimbürger et al. (2012) for Var Canyon. The horizontal lines denote the natural variability threshold after Roussiez et al. (2006).

floor sediments (Fig. 6a) (Jesus et al., 2010).

The choice of the reference material for the calculation of EFs is critical to correctly assess metal enrichment levels. Fig. 6 compares the mean EFs resulting from using pre-industrial sediments as local background. We have also considered in Fig. 6 formerly reported TMs enrichments in sediments from different locations and water depths in submarine canyons and open slopes around the Iberian Peninsula and nearby areas against the composition of the upper continental crust (UCC) as obtained from Rudnick and Gao (2003). The values calculated after the UCC global average exceed EFs calculated after the local pre-industrial background, thus illustrating that the use of UCC composition as reference value may result in an inaccurate, exaggerated view of the degree of TM pollution (Fig. 6b). This is well illustrated in the Portman area, where there is a natural geochemical anomaly for Pb, Zn and As that directly relates to local geology (López-García et al., 2017). Anthropogenic enrichments are, therefore, seen when local reference values are taken into account.

6. Conclusions

The transport and sink of TMs in SW Mediterranean submarine canyons depend on a number of physical and biogeochemical processes, and nowadays are also affected by anthropogenic perturbations (i.e. spillage of chemicals used in agriculture, industrial emissions via atmospheric transport, and/or past mining activities). TM contents in downward particle fluxes rely upon the composition and amounts of detrital material reaching the continental margin, on scavenging into Mn oxides, and on anthropogenic inputs. Besides the dominant particulate carriers of TMs described in this study, it is likely that further biological interactions during transport influence TM cycling anyhow. Anthropogenic sources would result in excess Zn in Escombreras Canyon and excess Cu in all the studied canyons. The widespread Cu enrichment suggests a diffuse source such as intensive farming activities in the coastal area and watershed, whereas Zn enrichment in the northern Escombreras Canyon points to local industrial activities. Yet, one possible source could be the export of Zn and other TMs, such as Cu and Pb, from the underwater extension of Portman's mine tailings deposit from sulphide ore exploitation, located at about 13 km from the canyon head. Whereas the shelf edge spillover of TMs and other pollutants is a rather common phenomenon, the calculation of EFs requires a correct choice of the reference materials to be used, prioritizing the local ones.

Storm events enhance downward TM fluxes into the submarine canyons, though concentrations are generally less than in fluxes under calm conditions. This is attributed to a dilution effect of the TMs enriched particles exported during the calm periods within the resuspended shelf material exported during stormy periods. However, seasonal or event-driven changes in sinking fluxes are barely observed in the Garrucha-Almanzora Canyon system, where a more steady TMs export through time has been observed. The content and transport of As, Co, Cu and Pb into the canyon seems to be instead influenced by bottom resuspension and advective transport of Mn and Fe bearing phases, with bottom trawling likely playing a non-negligible role. Further, the rather high Ti and Fe contents in the canyon's floor indicate differential resuspension according to particles' density.

The spreading of bottom trawling points to the need of specific studies to better understand how this activity influences TM fluxes within settling particles in submarine canyons and other deep-sea settings.

Declaration of Competing Interest

The authors declare that they have no known competing financial interests or personal relationships that could have appeared to influence the work reported in this paper.

Data availability

Data will be made available on request.

Acknowledgements

We would like to express our gratitude to the many colleagues and technicians and to the crew of RV Ángeles Alvariño for their support during sea-going work. We also thank M. Guart and F. Menéndez for their assistance in the lab and J. Martín for his comments on the manuscript. This research was supported by research projects NUREIEV (ref. CTM2013-44598-R) and NUREIEVA (ref. CTM2016-75953-C2-1-R) funded by the Spanish Ministry of Economy and Competitiviness (MINECO), and the Spanish Ministry of Economy, Industry and Competitiviness (MINECO), respectively. GRC Geociències Marines is funded by the Catalan Government within its excellence research groups program (ref. 2021 SGR 01195). M. Tarrés was supported by a FPI grant from the Spanish Ministry of Science and Innovation (MICINN).

Appendix A. Supplementary material

Supplementary data to this article can be found online at https://doi.org/10.1016/j.pocean.2023.103122.

References

Acosta, J., Fontán, A., Muñoz, A., Muñoz-Martín, A., Rivera, J., Uchupi, E., 2013. The morpho-tectonic setting of the Southeast margin of Iberia and the adjacent oceanic Algero-Balearic Basin. Mar. Pet. Geol. 45, 17–41. https://doi.org/10.1016/j.marpetgeo.2013.04.005.

Al-Hashem, A.A., Beck, A.J., Krisch, S., Menzel Barraqueta, J.-L., Steffens, T., Achterberg, E.P., 2022. Particulate trace metal sources, cycling, and distributions on the southwest African shelf. Glob. Biogeochem. Cycles 36. https://doi.org/10.1029/2022GB007453.

Alorda-Kleinglass, A., Garcia-Orellana, J., Rodellas, V., Cerdà-Domènech, M., Tovar-Sánchez, A., Diego-Feliu, M., Trezzi, G., Sánchez-Quilez, D., Sanchez-Vidal, A., Canals, M., 2019. Remobilization of dissolved metals from a coastal mine tailing deposit driven by groundwater discharge and porewater exchange. Sci. Total Environ. 688, 1359–1372. https://doi.org/10.1016/j.scitotenv.2019.06.224.

Aloupi, M., Angelidis, M.O., 2001. Normalization to lithium for the assessment of metal contamination in coastal sediment cores from the Aegean Sea. Mar. Environ. Res. 52, 1–12. https://doi.org/10.1016/S0141-1136(00)00255-5.

Anderson, R.F., 2020. GEOTRACES: Accelerating research on the marine biogeochemical cycles of trace elements and their isotopes. Annu. Rev. Mar. Sci. 12 (1), 49–85. https://doi.org/10.1146/annurev-marine-010318-095123.

Anderson, R.F., Hayes, C.T., 2015. Characterizing marine particles and their impact on biogeochemical cycles in the GEOTRACES program. Prog. Oceanogr. 133, 1–5. https://doi.org/10.1016/j.pocean.2014.11.010.

Azaroff, A., Miossec, C., Lanceleur, L., Guyoneaud, R., Monperrus, M., 2020. Priority and emerging micropollutants distribution from coastal to continental slope sediments: A case study of Capbreton Submarine Canyon (North Atlantic Ocean). Sci. Total Environ. 703, 135057 https://doi.org/10.1016/j.scitotenv.2019.135057.

Bancon-Montigny, C., Gonzalez, C., Delpoux, S., Avenzac, M., Spinelli, S., Mhadhbi, T., Mejri, K., Hlaili, A.S., Pringault, O., 2019. Seasonal changes of chemical contamination in coastal waters during sediment resuspension. Chemosphere 235, 651–661. https://doi.org/10.1016/j.chemosphere.2019.06.213.

Baza-Varas, A., Canals, M., Frigola, J., Cerdà-Domènech, M., Rodés, N., Tarrés, M., Sanchez-Vidal, A., the NUREIEVA-MAR1 shipboard party, 2022. Multiproxy characterization of sedimentary facies in a submarine sulphide mine tailings dumping site and their environmental significance: the study case of Portmán Bay (SE Spain). Sci. Total Environ. 810, 151183. https://doi.org/10.1016/j.scitotenv.2021.151183.

Baza-Varas, A., Roqué-Rosell, J., Canals, M., Frigola, J., Cerdà-Domènech, M., Sanchez-Vidal, A., Amblàs, D., Campeny, M., Marini, C., 2023. As and S speciation in a submarine sulfide mine tailings deposit and its environmental significance: the study case of Portmán Bay (SE Spain). Sci. Total Environ. 882, 163649. https://doi.org/10.1016/j.scitotenv.2023.163649.

Birch, G.F., 2017. Determination of sediment metal background concentrations and enrichment in marine environments – A critical review. Sci. Total Environ. 580, 813–831. https://doi.org/10.1016/j.scitotenv.2016.12.028.

Blain, S., Planquette, H., Obernosterer, I., Guéneuguès, A., 2022. Vertical flux of trace elements associated with lithogenic and biogenic carrier phases in the Southern Ocean. Glob. Biogeochem. Cycles 36. https://doi.org/10.1029/2022GB007371.

Boyle, E.A., 1983. Chemical accumulation variations under the Peru Current during the past 130,000 years. Geophys. Res. 88, 7667–7680. https://doi.org/10.1029/JC088iC12p07667.

Bradshaw, C., Tjensvoll, I., Sköld, M., Allan, I.J., Molvaer, J., Magnusson, J., Naes, K., Nilsson, H.C., 2012. Bottom trawling resuspends sediment and releases bioavailable

contaminants in a polluted fjord. Environ. Pollut. 170, 232–241. https://doi.org/10.1016/j.envpol.2012.06.019.
Bruland, K.W., Lohan, M.C., 2003. Controls of trace metals in seawater. In: Holland, H. D., Turekian, K.K. (Eds.), Treatise on Geochemistry, Vol. 6. Elsevier, Amsterdam, pp. 23–47. https://doi.org/10.1016/B0-08-043751-6/06105-3.
Calvert, S.E., Price, N.B., 1972. Diffusion and reaction profiles of dissolved manganese in the pore waters of marine sediments. Earth Planet. Sci. Lett. 16 (2), 245–249. https://doi.org/10.1016/0012-821X(72)90197-5.
Casadevall, M., Torres, J., El Aoussimi, A., Carbonell, A., Delgado, E., Sarrà-Alarcón, L., García-Ruíz, C., Esteban, A., Mallol, S., Bellido, J.M., 2016. Pollutants and parasites in bycatch teleosts from south eastern Spanish Mediterranean's fisheries: concerns relating the foodstuff harnessing. Mar. Pollut. Bull. 104, 182–189. https://doi.org/10.1016/j.marpolbul.2016.01.040.
Cerdà-Domènech, M., Frigola, J., Sanchez-Vidal, A., Canals, M., 2020. Calibrating high resolution XRF core scanner data to obtain absolute metal concentrations in highly polluted marine deposits after two case studies off Portmán Bay and Barcelona. Spain. Sci. Total Environ. 717, 134778 https://doi.org/10.1016/j.scitotenv.2019.134778.
Chaillou, G., Schäfer, J., Anschutz, P., Lavaux, G., Blanc, G., 2003. The behaviour of arsenic in muddy sediments of The Bay of Biscay (France). Geochim. Cosmochim. Acta 67 (16), 2993–3003. https://doi.org/10.1016/S0016-7037(03)00204-7.
Charette, M.A., Lam, P.J., Lohan, M.C., Kwon, E.Y., Hatje, V., Jeandel, C., Shiller, A.M., Cutter, G.A., Thomas, A., Boyd, P.W., Homoky, W.B., Milne, A., Thomas, H., Andersson, P.S., Porcelli, D., Tanaka, T., Geibert, W., Dehairs, F., Garcia-Orellana, J., 2016. Coastal ocean and shelf-sea biogeochemical cycling of trace elements and isotopes: lessons learned from GEOTRACES. Philosophical Transactions of the Royal Society A 374, 20160076. https://doi.org/10.1098/rsta.2016.0076.
Conte, M.H., Carter, A.M., Koweek, D.A., Huang, S., Weber, J.C., 2019. The elemental composition of the deep particle flux in the Sargasso Sea. Chem. Geol. 511, 279–313. https://doi.org/10.1016/j.chemgeo.2018.11.001.
Cossa, D., Buscail, R., Puig, P., Chiffoleau, J.-F., Radakovitch, O., Jeanty, G., Heussner, S., 2014. Origin and accumulation of trace elements in sediments of the northwestern Mediterranean margin. Chem. Geol. 380, 61–73. https://doi.org/10.1016/j.chemgeo.2014.04.015.
Costa, A.M., Mil-Homens, M., Lebreiro, S.M., Richter, T.O., de Stigter, H., Boer, W., Trancoso, M.A., Melo, Z., Mouro, F., Mateus, M., Canário, J., Branco, V., Caetano, M., 2011. Origin and transport of trace metals deposited in the canyons off Lisboa and adjacent slopes (Portuguese Margin) in the last century. Mar. Geol. 282, 169–177. https://doi.org/10.1016/j.margeo.2011.02.007.
Cowen, J.P., Bruland, K.W., 1985. Metal deposits associated with bacteria: implications for Fe and Mn marine biogeochemistry. Deep Sea Res. Part I Oceanogr. Res. Pap. 32 (3), 253–272. https://doi.org/10.1016/0198-0149(85)90078-0.
Dill, H.G., 2007. Grain morphology of heavy minerals from marine and continental placer deposits, with special reference to Fe–Ti oxides. Sed. Geol. 198 (1–2), 1–27. https://doi.org/10.1016/j.sedgeo.2006.11.002.
Dulaquais, G., Planquette, H., L'Helguen, S.M.J., Rijkenberg, A., Boye, M., 2017. The biogeochemistry of cobalt in the Mediterranean Sea. Glob. Biogeochem. Cycles 31, 377–399. https://doi.org/10.1002/2016GB005478.
Dumas, C., Aubert, D., Durrieu de Madron, X., Ludwig, W., Heussner, S., Delsaut, N., Menniti, C., Sotin, C., Buscail, R., 2014. Storm-induced transfer of particulate trace metals to the deep-sea in the Gulf of Lion (NW Mediterranean Sea). Environ. Geochem. Health 36, 995–1014. https://doi.org/10.1007/s10653-014-9614-7.
Durrieu de Madron, X., Aubert, D., Charrière, B., Kunesch, S., Menniti, C., Radakovitch, O., Sola, J., 2023. Impact of Dense Water Formation on the Transfer of Particles and Trace Metals from the Coast to the Deep in the Northwestern Mediterranean. Water (15), 301. https://doi.org/10.3390/w15020301.
Eggleton, J., Thomas, K.V., 2004. A review of factors affecting the release and bioavailability of contaminants during sediment disturbance events. Environ. Int. 30 (7), 973–980. https://doi.org/10.1016/j.envint.2004.03.001.
El Houssainy, A., Abi-Ghanem, C., Dang, D.H., Mahfouz, C., Omanović, D., Khalaf, G., Mounier, S., Garnier, C., 2020. Distribution and diagenesis of trace metals in marine sediments of a coastal Mediterranean area: St Georges Bay (Lebanon). Mar. Pollut. Bull. 155, 111066. https://doi.org/10.1016/j.marpolbul.2020.111066.
El Khatab, M., 2006. Dinámica del material sedimentario y de los metales pesados asociados en el margen noroccidental del mar de Alborán. PhD Thesis. Universidad Politécnica de Cataluña, Barcelona, Spain, p. 269.
Fabres, J., Calafat, A., Sanchez-Vidal, A., Canals, M., Heussner, S., 2002. Composition and spatio-temporal variability of particle fluxes in the Western Alboran Gyre, Mediterranean Sea (SW Mediterranean). J. Mar. Syst. 33–34, 431–456.
Froelich, P.N., Klinkhammer, G.P., Bender, M.L., Luedtke, N.A., Heath, G.R., Cullen, D., Dauphin, P., Hammond, D., Hartman, B., 1979. Early oxidation of organic matter in pelagic sediments of the eastern equatorial Altantic: suboxic diagenesis. Geochim. Cosmochim. Acta 43, 1075–1090. https://doi.org/10.1016/0016-7037(79)90095-4.
Geibert, W., 2018. Processes that regulate trace element distribution in the ocean. Elements 14, 391–396. https://doi.org/10.2138/gselements.14.6.3912015.
Grousset, F.E., Quetel, C.R., Thomas, B., Donard, O.F.X., Lambert, C.E., Guillard, F., Monaco, A., 1995. Anthropogenic vs. lithogenic origins of trace elements (As, Cd, Pb, Rb, Sb, Sc, Sn, Zn) in water column particles: northwestern Mediterranean Sea. Mar. Chem. 48 (3–4), 291–310. https://doi.org/10.1016/0304-4203(94)00056-J.
Hanebuth, T.J.J., King, M.L., Mendes, I., Lebreiro, S., Lobo, F.J., Oberle, F.K., Antón, L., Ferreira, P.A., Reguera, M.I., 2018. Hazard potential of widespread but hidden historic offshore heavy metal (Pb, Zn) contamination (Gulf of Cadiz, Spain). Sci. Total Environ. 637–638, 561–576. https://doi.org/10.1016/j.scitotenv.2018.04.352.
Heimbürger, L.-E., Cossa, D., Thibodeau, B., Khripounoff, A., Mas, V., Chiffoleau, J.-F., Schmidt, S., Migon, C., 2012. Natural and anthropogenic trace metals in sediments of the Ligurian Sea (Northwestern Mediterranean). Chem. Geol. 291, 141–151. https://doi.org/10.1016/j.chemgeo.2011.10.011.
Heussner, S., Durrieu de Madron, X., Calafat, A., Canals, M., Carbonne, J., Delsaut, N., Saragoni, G., 2006. Spatial and temporal variability of downward particle fluxes on a continental slope: lessons from an 8-yr experiment in the Gulf of Lions (NW Mediterranean). Mar. Geol. 234, 63–92. https://doi.org/10.1016/j.margeo.2006.09.003.
https://emodnet.ec.europa.eu/geoviewer/: Interactive map viewer of the EMODnet server [last consulted 18th of April 2023].
Huang, S., Conte, M.H., 2009. Source/process apportionment of major and trace elements in sinking particles in the Sargasso sea. Geochim. Cosmochim. Acta 73, 65–90. https://doi.org/10.1016/j.gca.2008.08.023.
Hung, J.J., Ho, C.Y., 2014. Typhoon- and earthquake-enhanced concentration and inventory of dissolved and particulate trace metals along two submarine canyons off southwestern Taiwan. Estuar. Coast. Shelf Sci. 136, 179e190. https://doi.org/10.1016/j.ecss.2013.11.004.
Jeandel, C., Vance, D., 2018. New tools, new discoveries in marine geochemistry. Elements 14, 379–384. https://doi.org/10.2138/gselements.14.6.379.
Jensen, L.T., Morton, P., Twining, B.S., Heller, M.I., Hatta, M., Measures, C.I., John, S., Zhang, R., Pinedo-Gonzalez, P., Sherrell, R.M., Fitzsimmons, J.N., 2020. A comparison of marine Fe and Mn cycling: U.S. GEOTRACES GN01 Western Arctic case study. Geochim. Cosmochim. Acta 288, 138–160. https://doi.org/10.1016/j.gca.2020.08.006.
Jesus, C.C., de Stigter, H.C., Richter, T.O., Boer, W., Mil-Homens, M., Oliveira, A., Rocha, F., 2010. Trace metal enrichments in Portuguese submarine canyons and open slope: anthropogenic impact and links to sedimentary dynamics. Mar. Geol. 271 (1–2), 72–83. https://doi.org/10.1016/j.margeo.2010.01.011.
Kalnejais, L.H., Martin, W.R., Signell, R.P., Bothner, M.H., 2007. Role of sediment resuspension in the remobilization of particulate-phase metals from coastal sediments. Environ. Sci. Tech. 41, 2282–2288. https://doi.org/10.1021/es061770z.
Karageorgis, A.P., Katsanevakis, S., Kaberi, H., 2009. Use of enrichment factors for the assessment of heavy metal contamination in the sediments of Koumoundourou Lake, Greece. Water, Air, Soil Pollut. 204, 243–258. https://doi.org/10.1007/s11270-009-0041-9.
Kuss, J., Waniek, J.J., Kremling, K., Schulz-Bull, D.E. (2010). Seasonality of particle-associated trace element fluxes in the deep northeast Atlantic Ocean. Deep-Sea Res. I 57, 785–796. Doi: 10.1016/j.dsr.2010.04.002.
Lam, P.J., Bishop, J.K.B., Henning, C.C., Marcus, M.A., Waychunas, G.A., Fung, I.Y., 2006. Wintertime phytoplankton bloom in the subarctic Pacific supported by continental margin iron. Glob. Biogeochem. Cycles 20, GB1006. https://doi.org/10.1029/2005GB002557.
Lee, J.M., Heller, M.I., Lam, P.J., 2018. Size distribution of particulate trace elements in the U.S. GEOTRACES Eastern Pacific Zonal Transect (GP16). Mar. Chem. 201, 108–123. https://doi.org/10.1016/j.marchem.2017.09.006.
Lemaitre, N., Planquette, H., Dehairs, F., Planchon, F., Sarthou, G., Gallinari, M., Roig, S., Jeandel, C., Castrillejo, M., 2020. Particulate trace element export in the North Atlantic (GEOTRACES GA01 transect, GEOVIDE cruise). ACS Earth Space Chem. 4 (11), 2185–2204. https://doi.org/10.1021/acsearthspacechem.0c00045.
Lobo, F.J., Ercilla, G., Fernández-Salas, L.M., Gámez, D., 2014. The Iberian Mediterranean shelves. Geol. Soc. Lond. Mem. 41, 147–170. https://doi.org/10.1144/M41.11.
Lohan, M.C., Bruland, K.B., 2008. Elevated Fe(II) and dissolved Fe in hypoxic shelf waters off Oregon and Washington: an enhanced source of iron to coastal upwelling regimes. Environ. Sci. Technol. 42 (17), 6462–6468. https://doi.org/10.1021/es800144j.
López-García, J.A., Oyarzun, R., Lillo, J., Manteca, J.I., Cubas, P., 2017. Geochemical characterization of magnetite and geological setting of the iron oxide ± iron silicate ± iron carbonate rich Pb–Zn sulfides from the La Unión and Mazarrón stratabound deposits (SE Spain). Resour. Geol. 67 (2), 139–157. https://doi.org/10.1111/rge.12124.
Macias, D., Garcia-Gorriz, E., Stips, A., 2016. The seasonal cycle of the Atlantic Jet dynamics in the Alboran Sea: direct atmospheric forcing versus Mediterranean thermohaline circulation. Ocean Dyn. 2016 (66), 137–151. https://doi.org/10.1007/s10236-015-0914-y.
Marin, B., Giresse, P., 2001. Particulate manganese and iron in recent sediments of the Gulf of Lions continental margin (north-western Mediterranean Sea): deposition and diagenetic process. Mar. Geol. 172, 147–165. https://doi.org/10.1016/S0025-3227(00)00124-9.
Martín, J.H., Knauer, G.A., Gordon, R.M., 1983. Silver distribution and fluxes in the North-West Pacific waters. Nature 305, 306–309. https://doi.org/10.1038/305306a0.
Martín, J., Palanques, A., Puig, P., 2007. Near-bottom horizontal transfer of particulate matter in the Palamós Submarine Canyon (NW Mediterranean). J. Mar. Res. 65 (2), 193–218. https://doi.org/10.1357/002224007780882569.
Martín, J., Puig, P., Masqué, P., Palanques, A., Sánchez-Gómez, A., Vopel, K.C., 2014. Impact of bottom trawling on deep-sea sediment properties along the flanks of a submarine canyon. PLoS One 9 (8). https://doi.org/10.1371/journal.pone.0104536.
Mil-Homens, M., Blum, J., Canário, J., Caetano, M., Costa, A.M., Lebreiro, S.M., Trancoso, M., Richter, T., de Stigter, H., Johnson, M., Branco, V., Cesário, R., Mouro, F., Mateus, M., Boer, W., Melo, Z., 2013a. Tracing anthropogenic Hg and Pb input using stable Hg and Pb isotope ratios in sediments of the central Portuguese Margin. Chem. Geol. 336, 62–71. https://doi.org/10.1016/j.chemgeo.2012.02.018.
Mil-Homens, M., Caetano, M., Costa, A.M., Lebreiro, S., Richter, T., de Stigter, H., Trancoso, M.A., Brito, P., 2013b. Temporal evolution of lead isotope ratios in sediments of the Central Portuguese Margin: A fingerprint of human activities. Mar. Pollut. Bull. 74, 274–284. https://doi.org/10.1016/j.marpolbul.2013.06.044.

Mil-Homens, M., Vale, C., Naughton, F., Brito, P., Drago, T., Anes, B., Raimundo, J., Schmidt, S., Caetano, M., 2016. Footprint of roman and modern mining activities in a sediment core from the southwestern Iberian Atlantic shelf. Sci. Total Environ. 571, 1211–1221. https://doi.org/10.1016/j.scitotenv.2016.07.143.

Millot, C., 1999. Circulation in the Western Mediterranean Sea. J. Mar. Syst. 20 (1–4), 423–442. https://doi.org/10.1016/S0924-7963(98)00078-5.

Morel, F.M.M., Price, N.M., 2003. The biogeochemical cycles of trace metals in the oceans. Science 300, 944–947. https://doi.org/10.1126/science.1083545.

Noble, A.E., Lamborg, C.H., Ohnemus, D.C., Lam, P.J., Goepfert, T.J., Measures, C.I., Frame, C.H., Casciotti, K.L., DiTullio, G.R., Jennings, J., Saito, M.A., 2012. Basin-scale inputs of cobalt, iron, and manganese from the Benguela-Angola front to the South Atlantic Ocean. Limnol. Oceanogr. 57 (4), 989–1010. https://doi.org/10.4319/lo.2012.57.4.0989.

Ohnemus, D.C., Lam, P.J., 2015. Cycling of lithogenic marine particles in the US GEOTRACES North Atlantic transect. Deep Sea Res. Part II 116, 283–302. https://doi.org/10.1016/j.dsr2.2014.11.019.

Oldham, V.E., Miller, M.T., Jensen, L.T., Luther, G.W., 2017. Revisiting Mn and Fe removal in humic rich estuaries. Geochim. Cosmochim. Acta 209, 267–283. https://doi.org/10.1016/j.gca.2017.04.001.

Pagès, F., Martín, J., Palanques, A., Puig, P., Gili, J.M., 2007. High occurrence of the elasipodid holothurian Penilpidia ludwigi (von Marenzeller, 1893) in bathyal sediment traps moored in a western Mediterranean submarine canyon. Deep Sea Res. Part I 54, 2170–2180. https://doi.org/10.1016/j.dsr.2007.09.002.

Palanques, A., Masqué, P., Puig, P., Sanchez-Cabeza, J.A., Frignani, M., Alvisi, F., 2008. Anthropogenic trace metals in the sedimentary record of the Llobregat continental shelf and adjacent Foix Submarine Canyon (northwestern Mediterranean). Mar. Geol. 248, 213–227. https://doi.org/10.1016/j.margeo.2007.11.001.

Palanques, A., Paradis, S., Puig, P., Masqué, P., Lo Iacono, C., 2022. Effects of bottom trawling on trace metal contamination of sediments along the submarine canyons of the Gulf of Palermo (southwestern Mediterranean). Sci. Total Environ. 814, 152658 https://doi.org/10.1016/j.scitotenv.2021.152658.

Papale, M., Conte, A., Del Core, M., Zito, E., Sprovieri, M., De Leo, F., Rizzo, C., Urzì, C., De Domenico, E., Luna, G.M., Michaud, L., Lo Giudice, A., 2018. Heavy-metal resistant microorganisms in sediments from submarine canyons and the adjacent continental slope in the northeastern Ligurian margin (Western Mediterranean Sea). Prog. Oceanogr. 168, 155–168. https://doi.org/10.1016/j.pocean.2018.09.015.

Paradis, S., Goñi, M., Masqué, P., Durán, R., Arjona-Camas, M., Palanques, A., Puig, P., 2021. Persistence of biogeochemical alterations of deep-sea sediments by bottom trawling. Geophys. Res. Lett. 48 https://doi.org/10.1029/2020GL091279.

Parrilla, G., Kinder, T.H., Preller, R.H., 1986. Deep and intermediate Mediterranean water in the western Alboran Sea. Deep Sea Res., Part I Oceanogr. Res. Pap. 33, 55–88. https://doi.org/10.1016/0198-0149(86)90108-1.

Pérez-Hernández, S., Comas, M.C., Escutia, C., 2014. Morphology of turbidite systems within an active continental margin (the Palomares Margin, western Mediterranean). Geomorphology 219, 10–26. https://doi.org/10.1016/j.geomorph.2014.04.014.

Puig, P., Palanques, A., Sanchez-Cabeza, J.A., Masque, P., 1999. Heavy metals in particulate matter and sediments in the southern Barcelona sedimentation system (Northwestern Mediterranean). Mar. Chem. 63, 311–329. https://doi.org/10.1016/S0304-4203(98)00069-3.

Puig, P., Canals, M., Company, J.B., Martin, J., Amblas, D., Lastras, G., Palanques, A., Calafat, A.M., 2012. Ploughing the deep sea floor. Nature 489, 286–290. https://doi.org/10.1038/nature11410.

Puig, P., Palanques, A., Martín, J., 2014. Contemporary sediment-transport processes in submarine canyons. Annu. Rev. Mar. Sci. 6, 53–77. https://doi.org/10.1146/annurev-marine-010213-135037.

Puig, P., Durán, R., Muñoz, A., Elvira, E., Guillén, J., 2017. Submarine canyon-head morphologies and inferred sediment transport processes in the Alías-Almanzora canyon system (SW Mediterranean): On the role of the sediment supply. Mar. Geol. 393, 21–34. https://doi.org/10.1016/j.margeo.2017.02.009.

Pusceddu, A., Bianchelli, S., Martín, J., Puig, P., Palanques, A., Masqué, P., Danovaro, R., 2014. Chronic and intensive bottom trawling impairs deep-sea biodiversity and ecosystem functioning. Proc. Nat. Acad. Sc. 11 (24), 8861–8866. https://doi.org/10.1073/pnas.1405454111.

Radakovitch, O., Roussiez, V., Olliver, P., Ludwig, W., Grenz, C., Probst, J.-L., 2008. Input of particulate heavy metals from rivers and associated sedimentary deposits on the Gulf of Lion continental shelf. Estuar. Coast. Shelf Sci. 77, 285–295. https://doi.org/10.1016/j.ecss.2007.09.028.

Raiswell, R., 2011. Iron transport from the continents to the open ocean: the aging rejuvenation cycle. Elements 7, 101e106. https://doi.org/10.2113/gselements.7.2.101.

Richter, T.O., de Stigter, H.C., Boer, W., Jesus, C.C., van Weering, T.C.E., 2009. Dispersal of natural and anthropogenic lead through submarine canyons at the Portuguese margin. Deep. Res. Part I Oceanogr. Res. Pap. 56, 267–282. https://doi.org/10.1016/j.dsr.2008.09.006.

Ross, C.B., Gardner, W.D., Richardson, M.J., Asper, V.L., 2009. Currents and sediment transport in the Mississippi Canyon and effects of Hurricane Georges. Cont. Shelf Res. 29, 1384–1396. https://doi.org/10.1016/j.csr.2009.03.002.

Roussiez, V., Ludwig, W., Monaco, A., Probst, J.-L., Bouloubassi, I., Buscail, R., Saragoni, G., 2006. Sources and sinks of sediment-bound contaminants in the Gulf of Lions (NW Mediterranean sea): a multi-tracer approach. Cont. Shelf Res. 26, 1843–11857. https://doi.org/10.1016/j.csr.2006.04.010.

Roussiez, V., Heussner, S., Ludwig, W., Radakovitch, O., Durrieu de Madron, X., Guieu, C., Probst, J.L., Monaco, A., Delsaut, N., 2012. Impact of oceanic floods to particulate metal inputs to coastal and deep sea environments: a case study in the Northwest Mediterranean. Cont. Shelf Res. 45, 15–26. https://doi.org/10.1016/j.csr.2012.05.012.

Rudnick, R.L., Gao, S., 2003. In: Rudnick, R.L. (Ed.), Treatise of Geochemistry, 3. Elsevier, Amsterdam, pp. 1–64. https://doi.org/10.1016/B0-08-043751-6/03016-4.

Rumín-Caparrós, A., Sanchez-Vidal, A., González-Pola, C., Lastras, G., Calafat, A., Canals, M., 2016. Particle fluxes and their drivers in the Avilés submarine canyon and adjacent slope, central Cantabrian margin, Bay of Biscay. Progr. Oceanogr. 144, 39–61. https://doi.org/10.1016/j.pocean.2016.03.004.

Rusiecka, D., Gledhill, M., Milne, A., Achterberg, E.P., Annett, A.L., Atkinson, S., Birchill, A., Karstensen, J., Lohan, M., Mariez, C., Middag, R., Rolison, J.M., Tanhua, T., Ussher, S., Connelly, D., 2018. Anthropogenic signatures of lead in the Northeast Atlantic. Geophys. Res. Lett. 45 (6), 2734–2743. https://doi.org/10.1002/2017GL076825.

Sanchez-Vidal, A., Calafat, A., Canals, M., Fabres, J., 2004. Particle fluxes in the Almeria-Oran front: control by coastal upwelling and sea-surface circulation. J. Mar. Syst. 52, 89–106. https://doi.org/10.1016/j.jmarsys.2004.01.010.

Sanchez-Vidal, A., Collier, R.W., Calafat, A., Fabres, J., Canals, M., 2005. Particulate barium fluxes on the continental margin: a study from the Alboran Sea (Western Mediterranean). Mar. Chem. 93 (2–4), 105–117. https://doi.org/10.1016/j.marchem.2004.07.004.

Tarrés, M., Cerdà-Domènech, M., Pedrosa-Pàmies, R., Rumín-Caparrós, A., Calafat, A., Canals, M., Sanchez-Vidal, A., 2022. Particle fluxes in submarine canyons along a sediment-starved continental margin and in the adjacent open slope and basin in the SW Mediterranean Sea. Prog. Oceanogr. 203, 102783 https://doi.org/10.1016/j.pocean.2022.102783.

Tebo, B.M., Bargar, J.R., Clement, B.G., Dick, G.J., Murray, K.J., Parker, D., Verity, R., Webb, S.M., 2004. Biogenic manganese oxides: Properties and mechanisms of formation. Annu. Rev. Earth Planet. Sci. 32 (1954), 287–328. https://doi.org/10.1146/annurev.earth.32.101802.120213.

Tesi, T., Puig, P., Palanques, A., Goñi, M.A., 2010. Lateral advection of organic matter in cascading-dominated submarine canyons. Prog. Oceanogr. 84 (3–4), 185–203. https://doi.org/10.1016/j.pocean.2009.10.004.

Theodosi, C., Parinos, C., Gogou, A., Kokotos, A., Stavrakakis, S., Lykousis, V., Hatzianestis, J., Mihalopoulos, N., 2013. Downward fluxes of elemental carbon, metals and polycyclic aromatic hydrocarbons in settling particles from the deep Ionian Sea (NESTOR site), Eastern Mediterranean. Biogeosciences 10, 4449–4464. https://doi.org/10.5194/bg-10-4449-2013.

Thibault de Chanvalon, A., Metzger, E., Mouret, A., Knoery, J., Chiffoleau, J.F., Brach-Papa, C., 2016. Particles transformation in estuaries: Fe, Mn and REE signatures through the Loire Estuary. J. Sea Res. 118, 103e112. https://doi.org/10.1016/j.seares.2016.11.004.

Tintore, J., La Violette, P.E., Blade, I., Cruzado, A., 1988. A study of an intense density front in the Eastern Alboran Sea: the Almeria-Oran Front. J. Phys. Oceanogr. 18, 1384–1397. https://doi.org/10.1175/1520-0485(1988)018<1384:ASOAID>2.0.CO;2.

Twining, B.S., Baines, S.B., 2013. The trace metal composition of marine phytoplankton. Annu. Rev. Mar. Sci. 5 (1), 191–215. https://doi.org/10.1146/annurev-marine-121211-172322.

Vargas-Yáñez, M., Plaza, F., García-Lafuente, J., Sarhan, T., Vargas, J.M., Vélez-Belchi, P., 2002. About the seasonal variability of the Alboran Sea circulation. J. Mar. Syst. 35 (3–4), 229–248. https://doi.org/10.1016/S0924-7963(02)00128-8.

Yiğiterhan, O., Murray, J.W., Tuğrul, S., 2011. Trace metal composition of suspended particulate matter in the water column of the Black Sea. Mar. Chem. 126, 207–228. https://doi.org/10.1016/j.marchem.2011.05.006.